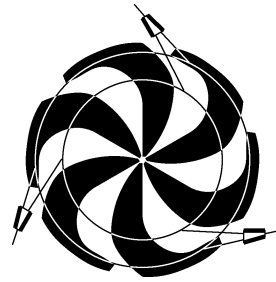


# TRIUMF



## ANNUAL REPORT SCIENTIFIC ACTIVITIES 2001

ISSN 1492-417X

**CANADA'S NATIONAL LABORATORY  
FOR PARTICLE AND NUCLEAR PHYSICS**

OPERATED AS A JOINT VENTURE

MEMBERS:

THE UNIVERSITY OF ALBERTA  
THE UNIVERSITY OF BRITISH COLUMBIA  
CARLETON UNIVERSITY  
SIMON FRASER UNIVERSITY  
THE UNIVERSITY OF VICTORIA

ASSOCIATE MEMBERS:

THE UNIVERSITY OF MANITOBA  
McMASTER UNIVERSITY  
L'UNIVERSITÉ DE MONTRÉAL  
QUEEN'S UNIVERSITY  
THE UNIVERSITY OF REGINA  
THE UNIVERSITY OF TORONTO

UNDER A CONTRIBUTION FROM THE  
NATIONAL RESEARCH COUNCIL OF CANADA

OCTOBER 2002

# TRIUMF

ISSN 1492-417X

ANNUAL REPORT  
SCIENTIFIC ACTIVITIES  
2001

Postal Address:

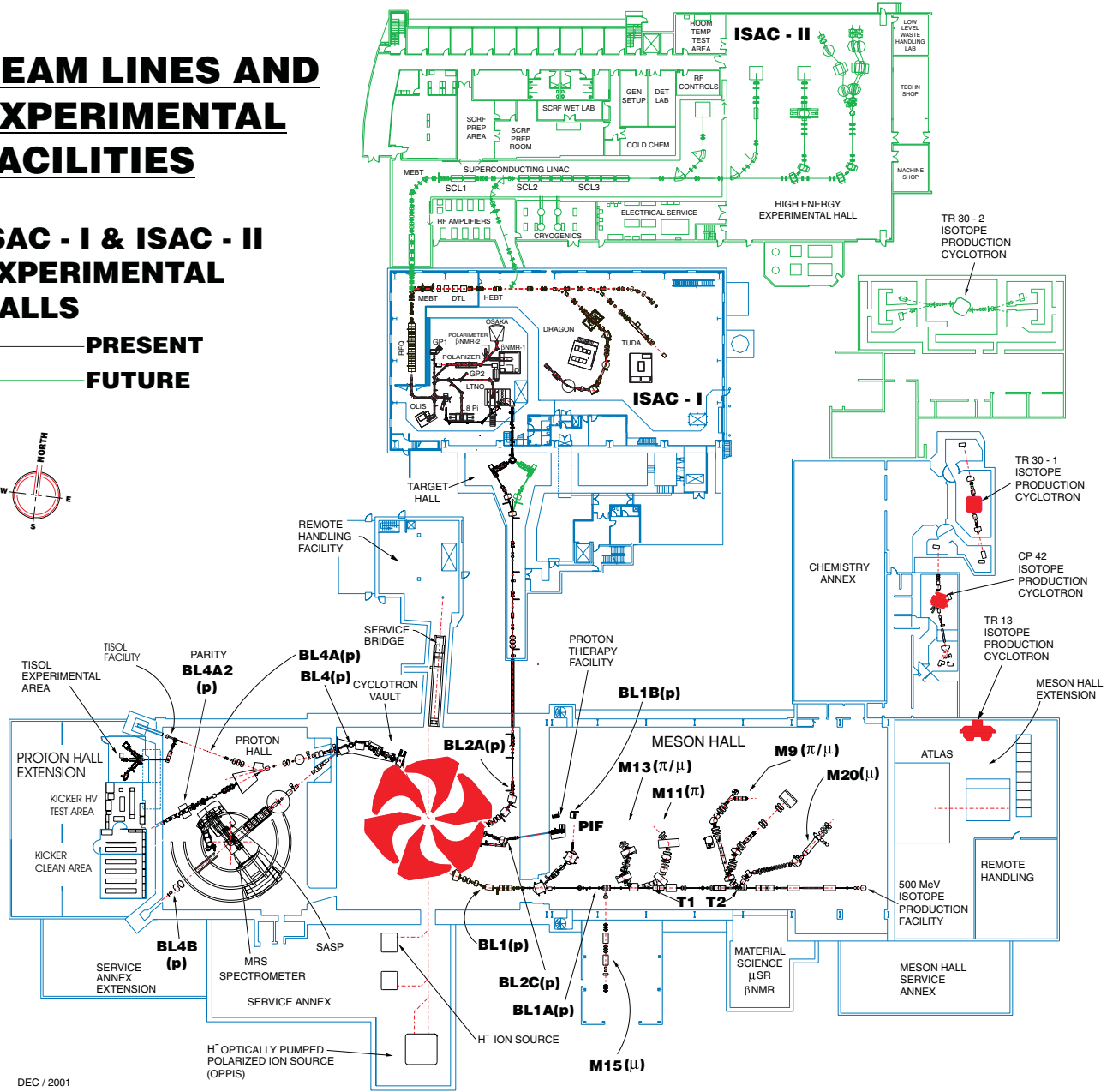
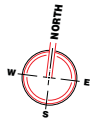
TRIUMF  
Publications Office  
4004 Wesbrook Mall  
Vancouver, BC V6T 2A3  
Canada

<http://www.triumf.ca/annrep>

# BEAM LINES AND EXPERIMENTAL FACILITIES

## ISAC - I & ISAC - II EXPERIMENTAL HALLS

— PRESENT  
— FUTURE



*The contributions on individual experiments in this report are outlines intended to demonstrate the extent of scientific activity at TRIUMF during the past year. The outlines are not publications and often contain preliminary results not intended, or not yet ready, for publication. Material from these reports should not be reproduced or quoted without permission from the authors.*

## FOREWORD

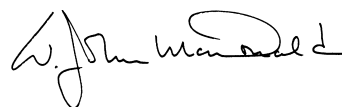
It is with much pleasure that I take the opportunity to report on the activities of the TRIUMF Board of Management. I know that I speak for all of the members of the Board when I say that it is an honour to be associated with this fine organization. We are proud of the extraordinary way that TRIUMF staff have managed to succeed in building and operating new facilities such as ISAC-I, have carried out the program for building ISAC-II, contributed key components for the LHC and ATLAS at CERN, and all the while continuing an exciting program of science in nuclear and astrophysics, precision tests of fundamental processes, medical physics, condensed matter physics, and nuclear chemistry. The growth that has taken place in the transfer of TRIUMF technology to applications that benefit society and aid Canadian industries is an important indicator of the innovative skills and hard work of TRIUMF staff.

Like all successful organizations, TRIUMF relies on many individual contributions. I would be remiss if I did not also explicitly comment on the very able clerical and support staff that do so much to create the working environment that makes it possible for the technical, engineering and scientific staff to function at the high level of excellence they have demonstrated. For example, one cannot help but be struck by the positive comments one hears about a stay in TRIUMF House, the good food provided for a meeting by the cafeteria staff, or the efficient way the business office handles a variety of complex accounts and travel claims. It is clear that TRIUMF's successes have been achieved in large part because so many individual staff, including scientists, engineers, technicians, computer and management professionals as well as secretaries, clerks and other support staff have done their jobs well. I have only touched on a few of the many examples that could be given.

The Board's responsibilities include the appointment of Director, and I had the privilege of chairing the search committee which recommended that Alan Shotter be selected. With the support of the Board, the committee made an early decision to have as open a process as was possible. Accordingly, the community was invited to comment on the process and suggest candidates. Several helpful responses were received and the committee acquired a good list of potential candidates. Once a short list of three excellent candidates was formed, the committee invited, and carefully considered, feedback from inside and outside the community. It then completed the difficult task of forming a recommendation for the Board. The Board, having considered the committee's recommendation, offered the position of Director to Dr. Alan Shotter. Dr. Shotter accepted and took up his duties as Director on September 1, 2001.

As in the past, the Board has been regularly considering matters brought to it from its standing committees: Finance, Personnel, and Safety. Other matters discussed in the past year include communications strategy, university relations, technology transfer and preparations for the next 5-year plan. In order to focus on particular issues the Board has decided that in the future, each of its meetings will have one extended discussion on a specific theme. The objective is to ensure that, over a period of two to three years, the Board would be able to review and make changes as appropriate to all of its key policies.

Before closing, I wish to acknowledge and thank Colin Jones and Alan Astbury. These two people provided wise and sure guidance to accomplish the successful shaping of a new future for TRIUMF following the Government's decision not to build KAON. Canada owes much to both of them for giving us the vision and the reality of a National Laboratory supporting the Canadian particle physics program abroad, and extending the in-house science program with the addition of a world leading radioactive beam facility. I am also personally grateful to Colin for the willing help and sage advice he gives to me as I attempt to follow his example as Board Chair and to Alan for his generosity in helping me during the search for a new Director and for making the transition to Alan Shotter's directorship go so smoothly.



W.J. McDonald  
Chair, Board of Management

TRIUMF was established in 1968 as a laboratory operated by the University of Alberta, the University of British Columbia, Simon Fraser University and the University of Victoria under a contribution agreement from the National Research Council of Canada. The initial consortium has been expanded to include Carleton University as a full member, and the University of Manitoba, McMaster University, the Université de Montréal, Queen's University, the University of Regina and the University of Toronto as associate members. The facility is operated for all Canadian as well as foreign users.

The experimental program is based on a cyclotron which is capable of producing four simultaneous beams of protons, two of which are individually variable in energy from 180–520 MeV, the third from 472–510 MeV, and the fourth between 70 and 110 MeV. The potential for high beam currents – 100  $\mu\text{A}$  at 500 MeV to 300  $\mu\text{A}$  at 400 MeV – qualified this machine as a “meson factory”. The third high intensity beam line feeds the new isotope production facility, ISAC, which started operation in 1998 and qualifies as a second generation radioactive beam facility.

Fields of research include basic science, such as particle physics, nuclear physics, nuclear astrophysics, and condensed matter research, as well as life sciences based primarily on isotope research. There is also a biomedical research facility which uses protons for treatment of ocular melanomae. TRIUMF is providing the Canadian contribution to the Large Hadron Collider at CERN and TRIUMF resources are also available to support the Canadian subatomic program at other laboratories.

The ground for the main facility, located on the UBC campus, was broken in 1970. Assembly of the cyclotron started in 1971. The machine produced its first full-energy beam in 1974 and its full current in 1977.

The laboratory employs approximately 325 staff at the main site in Vancouver and 19 based at the participating universities. The number of university scientists, graduate students and support staff associated with the present scientific program is about 625.

# CONTENTS

INTRODUCTION .....	1
SCIENCE DIVISION .....	3
Introduction and Overview .....	3
Particle Physics .....	5
(Expt. 497) Measurement of the flavour conserving hadronic weak interaction .....	5
(Expt. 614) TWIST – the TRIUMF weak interaction symmetry test .....	11
(Expt. 761) Measurement of parity violation in $pp$ scattering at 221 MeV .....	12
(ATLAS) The ATLAS experiment at the LHC .....	14
(BaBar) The BaBar experiment at the Stanford Linear Accelerator Center .....	21
(BNL 787/949/KOPIO) Measurement of $K \rightarrow \pi\nu\bar{\nu}$ and other rare decays .....	22
(HERMES) The HERMES experiment .....	27
(KEK 246/470) Kaon decay studies .....	30
(TJNAF 00-006) Measurement of the flavour singlet form factors of the proton ( $G\emptyset$ ) .....	32
Nuclear and Atomic Physics .....	38
(Expt. 704) Charge symmetry breaking in $np \rightarrow d\pi^0$ close to threshold .....	38
(Expt. 715) Weak interaction symmetries in $\beta^+$ decay of optically trapped $^{37,38\text{m}}\text{K}$ .....	42
(Expt. 744) A kinematically complete study of $\pi^-p \rightarrow e^+e^-n$ .....	45
(Expt. 778) Low energy $\pi^\pm$ differential cross sections in the Coulomb-nuclear interference region with CHAOS .....	45
(Expt. 801) Studies of multi-phonon states via $\beta$ -decay .....	46
(Expt. 823) Pure Fermi decay in medium mass nuclei .....	47
(Expt. 824) Measurement of the astrophysical rate of the $^{21}\text{Na}(p, \gamma)^{22}\text{Mg}$ reaction .....	49
(Expt. 838) Double radiative capture on pionic hydrogen .....	52
(Expt. 862) Analyzing powers in the $\bar{p}(\pi, \pi\pi)$ reactions with CHAOS .....	52
(Expt. 863) Ground state magnetic moments of $^{75,77,79}\text{Ga}$ (LTNO) .....	53
(Expt. 864) Dibaryon search by double radiative capture on pionic deuterium .....	54
(Expt. 875) MuScat: muon scattering in low $Z$ materials for muon cooling studies .....	55
(Expt. 879) $^{21}\text{Na}(p, p)$ resonant elastic scattering .....	58
Chemistry and Solid-State Physics .....	61
(Expt. 758) Effects of quantum impurities in graphite and in one dimensional spin 1/2 chain CPC .....	61
(Expt. 775) Electron transport in insulators, semiconductors and magnetic materials .....	63
(Expt. 776) Rare-earth materials with disordered spin structures .....	65
(Expt. 782) Non-fermi-liquid behaviour and other novel phenomena in heavy-fermion alloys .....	66
(Expt. 783) Knight shifts in unconventional superconductors: $(\text{U,Th})\text{Be}_{13}$ .....	68
(Expt. 784) Spin dynamics in the two dimensional spin system $\text{SrCu}_2(\text{BO}_3)_2$ .....	69
(Expt. 791) Electronic structure and dynamics of charged muonium centres in semiconductors .....	69
(Expt. 804) Muonium in III-V nitrides .....	70
(Expt. 815/816/817) $\beta$ -NMR .....	72
(Expt. 833) Muon spin relaxation studies on MnSi under applied pressure .....	75
(Expt. 834) $\mu\text{SR}$ study of transverse spin freezing in bond-frustrated magnets .....	75
(Expt. 835) $\mu\text{SR}$ studies in doped HfNiCl superconductors .....	77
(Expt. 842) Mu-substituted free radicals in sub- and supercritical water .....	77
(Expt. 846) Complex order parameter symmetry in $\text{YBa}_2\text{Cu}_3\text{O}_{7-\delta}$ at low $T$ and high magnetic field ....	79
(Expt. 847) Electron-doped high- $T_c$ superconductors .....	80
(Expt. 848) Vortex state of $d$ -wave superconductors investigated by muon spin rotation .....	81
(Expt. 849) Spin structure and magnetic volume fraction of La214 systems .....	82
(Expt. 852) Magnetic phases in geometrically frustrated rare earth pyrochlores .....	83
(Expt. 876) Disordered magnetism near magnetic instabilities in $f$ -electron materials .....	86
(Expt. 883) Muoniated methyl and associated free radicals .....	87
(Expt. 884) $\mu\text{SR}$ studies on magnetic ground state of $S=1/2$ kagomé spin system $\text{Cu}_3\text{V}_2\text{O}_7(\text{OH})_2 \cdot 2\text{H}_2\text{O}$ .....	89
(Expt. 890) Anisotropic Kondo effect in $\text{Ce}_{0.8}\text{La}_{0.2}\text{Al}_3$ ? .....	89

(Expt. 891)	Superconductivity and magnetism in $Ce_nT_mIn_{3n+2m}$ .....	91
(Expt. 894)	Muonium kinetics and free radical formation in solutions of fullerenes .....	92
(Expt. 912)	Formation, structure, and dynamics of muonium in GaAs studied by EF-ALC-RF- $\mu$ SR .....	93
(Expt. 915)	Muonium in semiconductor alloys .....	94
(Expt. 916)	QLCR of diamagnetic muonium states in GaP .....	95
(Expt. 917)	Correlation between magnetism and transport properties of thermoelectric oxides .....	96
Life Sciences .....		98
Introduction .....		98
(Expt. LS0)	PET facilities .....	98
(Expt. LS2)	Synthesis of radiohalogenated carbohydrates for use as imaging agents in PET and SPECT .....	99
(Expt. LS3)	Synthesis of radiopharmaceuticals for positron emission tomography .....	100
(Expt. LS4)	TR13 targets for PET radioisotope production .....	101
(Expt. LS8)	Radiotracers for the physical and biosciences .....	101
(Expt. LS10)	Aptamer imaging agents .....	103
(Expt. LS29)	Production and distribution of FDG (and other tracers) for clinical studies .....	103
(Expt. LS33)	Evaluation and improvement of a dual head coincidence camera .....	103
(Expt. LS35)	Development of $^{18}F$ labelled nitroimidazole PET imaging agents for tissue hypoxia .....	104
(Expt. LS38)	Modelling of the $^{18}F$ -fluorodopa tracer .....	104
(Expt. LS39)	Positron emission profiling (PEP) for pulp and paper fluid dynamic studies .....	106
(Expt. LS42)	Configuration modelling and image reconstruction studies on a depth encoding research tomograph .....	106
(Expt. LS44)	Development of a “formation” (areal density) measurement device for pulp and paper studies .....	107
(Expt. LS46)	Modelling of the dopaminergic system in more severely affected PD patients .....	107
(Expt. LS50)	Antisense imaging nucleic acids for Parkinson’s disease .....	108
(Expt. LS51)	Auger therapy for prostate cancer .....	108
(Expt. LS52)	Comparison of commercial FDG synthesis systems .....	108
(Expt. LS53)	Synthesis of $^{99m}Tc$ and $^{186,188}Re$ sugar derivatives .....	109
Theoretical Program .....		110
Introduction .....		110
The Theory Research Program .....		110
Experimental Facilities .....		118
Proton Irradiation Facility .....		118
Proton Therapy Facility .....		119
$\mu$ SR User Facility .....		119
Beam Lines .....		121
Cryogenic Targets .....		122
Computing Services .....		122
Data Acquisition Systems .....		125
Detector Facility .....		126
GEANT4 .....		127
Scientific Services .....		129
Sudbury Neutrino Observatory .....		131
DRAGON Facility .....		131
$8\pi$ Spectrometer .....		133
Low Temperature Nuclear Orientation at ISAC .....		134
CYCLOTRON OPERATIONS DIVISION .....		136
Introduction .....		136
Beam Production .....		137
Winter Shutdown .....		137
Beam Schedule 99 .....		142
Fall Mini-Shutdown .....		143



Beam Schedule 100 .....	143
Beam Development .....	144
Radio Frequency Systems .....	144
RF Operations .....	144
RF Refurbishing .....	144
RF Support .....	146
Radio Frequency Controls .....	146
Cyclotron .....	146
ISAC .....	146
ISAC-II .....	146
Cyclotron Probes and Diagnostics .....	146
Probes MRO .....	146
Monitor MRO .....	147
Vacuum and Engineering Physics .....	147
Vacuum .....	147
Engineering Physics .....	147
ISIS .....	147
Primary Beam Lines .....	148
BL1A Vault Section .....	148
BL1A West-East Section .....	149
Beam Line 2C Production .....	149
Controls .....	150
CCS Facilities .....	150
Secondary Beam Lines .....	151
Other Systems .....	151
Miscellaneous .....	151
Operational Services .....	151
Remote Handling .....	151
Magnet Power Supplies .....	152
Electrical Engineering Services .....	152
Electrical Systems .....	152
Power Delivery .....	153
Mechanical Systems .....	153
ISAC PROJECT .....	155
Introduction .....	155
ISAC Operations .....	155
Safety and Radiation Control .....	161
Licensing .....	161
Access Control and Radiation Monitoring .....	161
Commissioning .....	161
Remote Handling Group .....	161
Target Modules .....	161
Target Hall .....	161
Hot Cell Facility/Targets .....	162
Remote Crane System .....	162
ISAC Targets and Beams .....	162
Ion Sources for ISAC .....	163
Electron Cyclotron Resonance (ECR) Source .....	163
Off-Line Ion Source (OLIS) .....	163
Charge State Booster (CSB) .....	164
ISAC Polarizer .....	164
Beam Dynamics .....	165
Theory .....	165

Software .....	165
Hardware Designed .....	165
ISAC Controls .....	165
Hardware .....	165
Software .....	166
System and Development Support .....	166
Commissioning and Operation .....	166
RF Systems .....	167
RFQ .....	167
MEBT .....	167
DTL .....	168
HEBT .....	169
ISAC Diagnostics .....	169
Target Diagnostics .....	169
MRO .....	170
Beam Commissioning .....	172
MEBT .....	172
Full DTL Beam Tests .....	172
HEBT .....	174
Beam Delivery .....	175
LEBT .....	176
Mass Separator .....	176
East Target Station .....	177
Services .....	178
Faraday Cage and Electrical Room .....	178
Other Systems .....	178
ISAC Planning .....	178
East Target Station .....	178
Target Conditioning Box .....	179
HEBT .....	179
Low Energy Experiments .....	179
High Energy Experiments .....	179
DRAGON .....	179
ISAC-II .....	179
Contract Administration .....	180
Personnel Resources .....	180
Conventional Facilities and Infrastructures .....	182
Mechanical Services .....	182
Electrical Services .....	182
ISAC-II Conventional Construction .....	184
ISAC-II Accelerator .....	184
Linac Lattice .....	184
Stage 1 Installation .....	185
Stage 2 Installation .....	186
SCRF Developments .....	189
 ACCELERATOR TECHNOLOGY DIVISION .....	 191
Introduction .....	191
Beam Dynamics .....	191
Micro-Bunching at Brookhaven AGS .....	191
Muon Acceleration in an FFAG .....	192
Multi-Turn Simulation of Coherent Betatron Resonance with Space-Charge .....	192
Magnets .....	193
Experiment 614 – TWIST .....	194

Magnet Measurements .....	194
Kickers .....	194
Mechanical Engineering .....	195
ISAC East Target Station .....	195
DRAGON .....	196
Engineering – Other .....	198
Engineering - Victoria .....	199
Engineering - Carleton .....	199
Planning .....	200
ISAC .....	200
Shutdown Activities .....	201
TWIST .....	201
KOPIO Preradiator .....	201
Design Office .....	201
Machine Shop .....	202
Building Program .....	202
Electronics Services .....	202
Overview .....	202
Technical Support .....	202
PC Support .....	203
Electronics Repair Shop – Nucleonics .....	203
High Level Software Support .....	203
Site Communications .....	203
Electronics Shop .....	204
Experimental and Target Support .....	204
Electronics Development .....	204
ISAC Support .....	204
CERN .....	204
Safety Systems .....	204
Miscellaneous .....	204
 CERN COLLABORATION .....	 206
Introduction .....	206
Beam Dynamics .....	206
Coherent Beam-Beam Effects in the LHC .....	206
LHC Collimation .....	207
Resonance-Free LHC Optics .....	207
Controls and Instrumentation .....	207
LHC Orbit System Components .....	207
Magnet Development .....	209
Kicker Magnets .....	209
Thyratron Switch Tanks .....	211
 TECHNOLOGY TRANSFER DIVISION .....	 212
Introduction .....	212
Technology Transfer .....	212
Applied Technology Group .....	212
500 MeV Isotope Production Facility .....	212
CP42 Facility .....	212
TR30 Facility .....	212
ATG Development Projects .....	212
Radioisotope Processing (MDS Nordion) .....	212

ADMINISTRATION DIVISION .....	215
Introduction .....	215
Human Resources and Administration .....	215
Operational Safety .....	215
Licensing .....	215
Training .....	215
Occupational Health and Safety .....	215
Interlocks and Monitoring .....	215
Personnel Dosimetry .....	216
Administration Computing and Communications .....	216
Management Information Systems .....	216
Word Processing Systems .....	216
Telephones .....	216
CONFERENCES, WORKSHOPS AND MEETINGS .....	218
ORGANIZATION .....	224
APPENDICES	
A. Publications .....	228
B. Seminars .....	244
C. Users Groups .....	246
D. Experiment Proposals .....	247
E. Life Sciences Project Proposals .....	261

## INTRODUCTION

The TRIUMF laboratory is Canada's national laboratory for particle and nuclear physics. The mission of the laboratory is to provide in-house world class facilities for specialized areas, provide infrastructure support for Canadian scientists to participate in experiments outside Canada, and to encourage the transfer of technology developed at the laboratory to the commercial sector.

The facilities within the laboratory have been rapidly evolving over the past few years, so the laboratory is now one of the leading world facilities to provide high intensity radioactive beams for a variety of scientific fields. The radioactive ions are produced by spallation reactions using the 500 MeV protons from the main TRIUMF cyclotron. Isotopes are then selected by a mass separator before delivery to the experimenters. These ions of energy several keV/u are used for a variety of studies such as fundamental decay studies, nuclear structure studies, and materials science studies. During this year a milestone was passed with the completion and commissioning of the RFQ and DTL accelerators that can accelerate both stable and unstable ions from 0.15 to 1.5 MeV/u. This energy range is ideal for investigating nuclear reactions of particular relevance to nuclear astrophysics. The accelerator system can accelerate  $1^+$  ions of up to mass 30, but in the future this will be extended to heavier masses for higher charge states with a charge state booster now under construction. During the year another significant milestone was reached with the successful commissioning of the DRAGON and TUDA systems, special apparatus designed to investigate nuclear astrophysics reactions associated with radioactive beams. Both experimental systems undertook successful experimental investigations of the reaction  $^{21}\text{Na}(p, \gamma)^{22}\text{Mg}$ . This particular reaction is of great interest for the investigation of  $^{22}\text{Na}$  production in the galaxy since  $^{22}\text{Na}$  is produced from the decay of  $^{22}\text{Mg}$ .

Now that most of the main components of the first phase of ISAC are nearly all built, the laboratory began to turn its attention to the second phase. This second phase will enhance the energy of radioactive ions to 6.5 MeV/u for masses up to  $A = 150$ . The accelerator complex needed for this will require a new building, the funds for which have been generously provided by the BC provincial government. Construction of this new building will start in January 2002 and should take one year to complete. The accelerator structures associated with this second phase should be ready in the year 2005.

The TRIUMF laboratory over the past few years has made substantial contributions to the LHC accel-

erator at CERN. These contributions have been associated with several discrete projects. One of the major ones in terms of resources has been the design and construction of 52 conventional double beam quadrupole magnets for beam control in the cleaning sections of the main LHC accelerator. These magnets have been a challenge to produce due to the demanding accuracy needed for their function. It is a tribute to all concerned at TRIUMF and the manufacturing company, ALSTOM, that the manufacturing problems have been solved and steady production started towards the end of the year. ATLAS Canada has the responsibility to produce the hadron endcap calorimeter, a component of the ATLAS detector. This project involving TRIUMF and several universities is nearing completion. TRIUMF provides for the management of the project and the clean rooms for assembling the detector modules before they are shipped to CERN for testing.

TRIUMF has and continues to provide general infrastructure support for many Canadian physicists across Canada to enable them to participate in a meaningful way in many experiments outside Canada. By way of example, the inner tracking detector for the BaBar experiment at SLAC was made at TRIUMF. This experiment is now producing exciting new results concerning heavy quark physics, and the Canadian team members through their responsibility for the operation of the inner detector continue to be an essential part of this experiment.

Again TRIUMF is much involved in supporting the  $K$ -meson rare decay experiment at Brookhaven. New results from this experiment are given in this report and, while providing better limits for the branching ratio, the statistical errors are still too large for the results to challenge the standard model; clearly, more data are needed to reduce the statistical errors.

The main 500 MeV cyclotron has worked well during the year. The cyclotron can simultaneously deliver a variety of beams, and has mainly been used during the year either to provide the proton beam for ISAC, or to produce muons for the  $\mu\text{SR}$  program or TWIST. The TWIST experiment aims to measure the physical parameters associated with muon decay to an accuracy that will provide a stringent test of the standard model predictions. This last year saw the full commissioning of all components of the detector and a large superconducting magnet. The  $\mu\text{SR}$  program is an important part of the laboratory's portfolio since the modulation of  $\mu$  decay characteristics in materials provides an excellent probe for various chemistry and materials science investigations. It continues to be a particularly important probe to investigate the magnetic proper-

ties of superconductors and complements the new  $^8\text{Li}$   $\beta$ -NMR facility commissioned at ISAC.

The biological/medical program continues to be an important component of the laboratory portfolio. The main activity centres on the PET technique with TRIUMF providing the essential radioisotopes for this work. Successful grant applications during the year will mean new PET machines will be installed in the near future. In particular, a new micro-PET for small animal experiments will increase the importance and diversity of this research area. Proton irradiation both for cancer therapy treatment and for general irradiation work has continued to be an important activity during the year.

Technical knowledge transfer is an integral part of the mission of many scientific laboratories; TRIUMF is no exception. The highlight of this activity during

the year was MDS Nordion's decision to build a new cyclotron on the TRIUMF site. This \$20M commercial investment for radioisotope production gives testament to the excellent relationship TRIUMF has with MDS Nordion.

In a couple of pages it is difficult to give an overview of all aspects of the laboratory; however, one general statement is that a laboratory is no better than the people within it. That the laboratory continues to run well is a tribute to all staff whether they are scientists, engineers, technicians, or administrative staff. That it has been an excellent, productive year is a tribute to all. Finally, but by no means least, on behalf of all staff I would also like to thank the previous director, Dr. Alan Astbury, who retired during the year, for his many years of hard work.



A. Shotter,  
Director

## SCIENCE DIVISION

### INTRODUCTION AND OVERVIEW

2001 will be remembered at TRIUMF as one of the most successful years in terms of scientific achievements.

The major investments of the last 5 years at ISAC have paid off and both the low energy program and the nuclear astrophysics program with accelerated radioactive beams have produced significant publications. Two other major efforts in particle physics also produced new results; one at TRIUMF with the publication of final results from the parity experiment, the other at the AGS at Brookhaven with the publication of the discovery of a second event from the rare decay  $K^+ \rightarrow \pi^+ \nu \bar{\nu}$ . Finally, one should also acknowledge the major success of the TWIST experiment which took its first data with a complete detector.

Overall, the Science Division reaped the benefits of long years of dedicated effort by TRIUMF staff and collaborators from participating universities.

In ISAC, the low energy part of the program used a large fraction of the beam time in the spring/summer schedule while we were completing and commissioning the facilities using accelerated beams.

The effort connected with our studies of pure Fermi transitions focused this year on determining the contribution of non-analogue transitions to the decay of  $^{74}\text{Rb}$ . The first experiment showed that the superallowed branch was the dominant (>99%) transition. In a second experiment, the transition strength for the non-analogue  $O^+ \rightarrow O^+$  transition was measured to be less than  $3 \times 10^{-4}$ . Now that the  $8\pi$  spectrometer has been recommissioned at ISAC, further studies of the detailed decay scheme will be undertaken.

The low temperature nuclear orientation (LTNO) set-up was used to study the ground state magnetic dipole moment of heavy odd- $A$  Ga isotopes. In a preliminary run, a 15%  $\beta$ -asymmetry was observed for  $^{75}\text{Ga}$ .

The TRINAT group has continued the analysis of data taken in late 2000 on the  $\beta - \nu$  correlation in the decay of  $^{38\text{m}}\text{K}$  atoms trapped by lasers. A preliminary result was given at several conferences and a  $\sim 0.2\%$  final result is expected soon. Also, considerable progress was achieved in establishing methods to polarize trapped potassium atoms (both stable  $^{41}\text{K}$  and  $^{37}\text{K}$ ); >99% polarization was achieved for stable  $^{41}\text{K}$  and should be possible for  $^{37}\text{K}$ . Methods for measuring the absolute value of polarization were also developed.

A major success was achieved with the  $\beta$ -NMR facility. A large polarization for a  $^8\text{Li}$  beam was demonstrated (>70%) and maintained during a week-long data-taking run in which a well-focused  $^8\text{Li}$  beam was

decelerated to less than 1 keV and implanted in pure metallic thin films and in insulator layers in a 3 T magnetic field. The large investment in the polarizer and  $\beta$ -NMR facility is starting to produce interesting physics results.

Also in the low energy area, considerable progress was made to mount two experiments from Osaka University groups. One will study neutron emitting states populated in the  $\beta$ -decay of  $^{11}\text{Li}$  using polarization as a tool to obtain the spin of the decaying states in  $^{11}\text{Be}$  (Expt. 903). The other experiment is studying alignment correlation parameters in  $^{20}\text{Na}$  to extract information on second-class current and meson exchange contributions (Expt. 871).

The beam line to the  $8\pi$  spectrometer has been built and partially commissioned, allowing us to start scheduling experiments in the summer of 2002.

By the summer of 2001, the ISAC accelerator system was ready to accelerate radioactive beams. The initial experiment chosen was to look for the  $^8\text{Li}(\alpha, n)$  cross section at energies of 1 MeV/u or less, with intensities on target (after stripping, acceleration) in the range of a few  $10^8/\text{s}$ . The experiment could not be run in "singles" mode (detecting only the neutron) because of the high counting rate in the neutron plastic counters, while the  $^8\text{Li}$  beam intensity proved to be insufficient to run in coincidence mode ( $n$ , recoil  $^{11}\text{B}$ ) either. A new proposal taking the above limitations into consideration will be developed by the RIKEN group.

The fall running period was mainly devoted to  $^{21}\text{Na}$  beams and both the TUDA and DRAGON teams took advantage of the few  $10^8/\text{s}$  intensities available.

TUDA measured the elastic scattering of  $^{21}\text{Na}$  from hydrogen in a  $\text{CH}_2$  target, establishing the excitation curve between 0.7 and 1.5 MeV (centre of mass energy). Three broad  $s$ -wave resonances were observed. A rapid communication was approved for publication in Phys. Rev. Lett. while much more data are being analyzed in a Ph.D. thesis.

The DRAGON spectrometer was put into action in mid-October. Within 3 shifts, it was demonstrated that this complex instrument was performing as planned with a beam rejection close to calculated levels. The  $^{21}\text{Na}(p, \gamma)$  reaction was then attempted at two resonance energies with beam intensities of  $5 \times 10^8$  ions/s. The 212 keV resonance is important for the production of long-lived  $^{22}\text{Na}$  (2.6 years) in nova and X-ray bursts. This is the first such measurement of its  $\gamma$  strength. The 822 keV resonance is also measured for its value in nuclear structure modelling of the  $^{22}\text{Mg}$  compound nucleus in these reactions.

The success of these initial runs augurs well for the program of nuclear astrophysics measurements at ISAC, for which the facility has been optimized. Both teams, led by J. D'Auria/D. Hutcheon for DRAGON and our director A. Shotter/L. Buchmann for TUDA, are to be congratulated.

In the base program, centred around our beams of pions and muons, the highlight was the first data-taking of muon decay events in the TWIST spectrometer operating at 2 T. During the year, the superconducting coil was fixed, the 52 high precision wire chambers and their associated gas system, analogue and digital electronics, and mechanical assembly were commissioned, and everything came together on November 23 with nice decay positron tracks spiralling in the 2 T field. This represented the culmination of a very large effort by our detector group, the technical staff assembling the spectrometer, and many summer and co-op students, as well as the TWIST team.

Also in the base program, ten years of effort resulted in the publication of the polarization asymmetry in  $p$ - $p$  scattering at 221 MeV from which one can extract the value of the weak coupling constant of the  $\rho$  meson. This result is important for understanding the weak effective interaction of the nucleon and will also have an impact on the asymmetry measurement in  $e$  -  $p$  scattering at TJNAF. These experiments are extremely difficult due to the very weak signal ( $10^{-7}$  level) and were only possible through the dedication of a large team led by the Manitoba group, which has built up a record of credibility in previous measurements of this type.

TRIUMF is also providing infrastructure support for experiments abroad. During the year, a very significant second rare  $K$ -decay event was observed in the BNL E787 experiment at the AGS, confirming the 1997 result, still consistent with the standard model prediction and allowing for a more constrained value of the  $V_{td}$  quark mixing matrix element. Again, in this case, it is the result of a long (18 year) dedicated effort by the Canadian team led by D. Bryman (UBC).

Preparing for the future program at the LHC, the ATLAS groups at TRIUMF and Victoria are well under way to deliver the two hadronic endcap wheels be-

ing assembled at TRIUMF and the associated cryogenic feedthroughs made in Victoria. The focus of activity will now shift to CERN where these devices are going to be fitted into the ATLAS detector.

Focusing also on the future, a Canadian group under A. Konaka's leadership is mounting an effort to join a long baseline neutrino oscillation experiment. So far a collaboration with the JHF-SK program in Japan has been explored, but the option for a similar effort at Fermilab is also contemplated. The very successful Future Opportunities for Neutrino Physics Workshop was held in Victoria in November with 70 attendees, and the most pre-eminent researchers in this exciting field were present.

A proposal to join an effort at the Brookhaven AGS to study  $CP$  violation in the  $K$  system via the neutral rare decay mode  $K^0 \rightarrow \pi^0 \nu \bar{\nu}$  received interim and conditional support from NSERC pending an NSF decision to go ahead with the experiment.

As evident in this Annual Report, the condensed matter community continues to value the superb facilities which have been developed at TRIUMF for  $\mu$ SR users. Even though our maximum muon fluxes are an order of magnitude smaller than those of our competition in PSI, the new state-of-the-art instruments available here maintain our attractiveness in the whole community.

Our life sciences program got a major boost with the funding, through the Canadian Foundation for Innovation, of two new PET cameras; the recently announced funding for an animal camera will open a wide area of research in the medical sciences. This will put pressure on our local team of radiochemists to develop the required tracers for those studies.

In conclusion, TRIUMF is well positioned to play a major role in internationally competitive science projects at the high energy frontier, at the new frontier in nuclear physics with radioactive beams, in precision experiments, in condensed matter, and in the life sciences. Our reach is only limited by our means, not by our vision or our intellect. Our challenge is now to prepare a new five-year plan and convince our funding agencies that we should expand our world-class program for the benefit of Canada.



## PARTICLE PHYSICS

### Experiment 497

#### Measurement of the flavour conserving hadronic weak interaction

(*J. Birchall, S.A. Page, W.T.H. van Oers, Manitoba*)

#### Introduction

The data analysis for the TRIUMF 221 MeV parity violation experiment, Expt. 497, was completed in early 2001 and the results have now been published [Berdoz *et al.*, Phys. Rev. Lett. **87**, 272301 (2001)]. The experiment completed data-taking in 1999 and the complete data set was analyzed during 2000 and 2001, forming the basis of an M.Sc. thesis [J. Bland, “The TRIUMF E497 parity violation experiment in the 221 MeV  $\bar{p}p$  system: a complete analysis of the Feb97, Jul98 and May99 data runs” (University of Manitoba, 2001)]. Whereas previous Annual Reports have presented the results of the 1997, 1998 and 1999 runs separately, the final Expt. 497 result presented here is based on the re-analysis of all the data in a consistent way.

The experiment determines the parity violating longitudinal analyzing power,  $A_z = (\sigma^+ - \sigma^-)/(\sigma^+ + \sigma^-)$ , in  $\bar{p}p$  elastic scattering, where  $\sigma^+$  and  $\sigma^-$  are the scattering cross sections for positive and negative helicity. The measurements were performed in transmission geometry, with beam energy and detector geometries selected to ensure that only parity mixing in the  $^3P_2 - ^1D_2$  partial wave amplitude contributes to the measured parity violating asymmetry [Simonius, Can. J. Phys. **66**, 548 (1988)]. This amplitude has never been studied experimentally, and the possibility is unique to the energy regime accessible with the TRIUMF cyclotron. In the context of the weak meson exchange model [Desplanques *et al.*, Ann. Phys. (N.Y.) **124**, 449 (1980)], our measurement of  $A_z$  provides a direct determination of the weak  $\rho$ -meson-nucleon coupling constant  $h_\rho^{pp} = (h_\rho^0 + h_\rho^1 + h_\rho^2/\sqrt{6})$ . Precision results already obtained by the PSI group at 45 MeV [Kistryn *et al.*, Phys. Rev. Lett. **58**, 1616 (1987)] and the Bonn group at 13.6 MeV [Eversheim *et al.*, Phys. Lett. **B256**, 11 (1991); private communication (1994)] determined essentially the sum  $h_\rho^{pp} + h_\omega^{pp}$ . With the addition of our TRIUMF result at 221 MeV,  $h_\rho^{pp}$  and  $h_\omega^{pp}$  can now be determined separately for the first time.

It is important to have experimentally determined values of the weak meson-nucleon couplings, as theoretical calculations of their values are quite uncertain and the correct values are important in the interpretation of the results of other parity violation experiments. For example, the SAMPLE (MIT Bates) result [Hasty *et al.*, Science **290**, 2117 (2000)] for the electron nucleon axial form factor is very different from calculations. The calculation requires correction for the

nucleon anapole moment, a direct parity violating coupling of the photon to the nucleon. This can be computed in chiral perturbation theory, but one needs to know the weak meson-nucleon couplings.

The TRIUMF measurement will also enhance the usefulness of the  $G_0$  electron proton parity violation experiment at Jefferson Lab. In common with SAMPLE, correction is required for the nucleon anapole moment, which is one contribution to the effective axial form factor required to interpret the  $G_0$  result. Like SAMPLE,  $G_0$  plans to measure the axial form factor with a back angle scattering from deuterium. To the extent that the rho and omega couplings are now determined by experiment, the  $G_0$  axial form factor result will give an independent estimate of the weak pion-nucleon coupling,  $f_\pi^1$ . The most precise value of  $f_\pi^1$  presently comes from the circular polarization of  $\gamma$ -rays from a well known parity mixed doublet in  $^{18}\text{F}$  [Page *et al.*, Phys. Rev. **C35**, 1119 (1987); Bini *et al.*, Phys. Rev. Lett. **55**, 795 (1985)]. The experimental result is quite small compared to theoretical predictions, and Holstein [Can. J. Phys. **66**, 510 (1988)] points out that to get such a small value in a calculation, one must use current algebra quark masses which are about half the original Weinberg values. This would tend to suppress estimates in other processes, including the  $\Delta I = 1/2$  rule. The  $np \rightarrow d\gamma$  experiment at LANL plans a more precise measurement of  $f_\pi^1$ . The  $G_0$  experiment together with the TRIUMF  $pp$  result will provide another piece in the solution of this puzzle.

#### Background

This experiment was first proposed in 1985, funded in 1988, and the beam line was completed in 1994. A major effort to minimize and understand systematic error contributions was required to successfully perform an experiment with this level of precision. Following many years of effort which resulted in the reduction of both the helicity correlated beam modulations  $\Delta x_i$  and the sensitivities  $\frac{\partial A_z}{\partial x_i}$  to these modulations, the first significant data set for Expt. 497 was acquired in February and March of 1997, with a statistical error of  $\pm 0.5 \times 10^{-7}$ , and most systematic errors at or below the  $10^{-7}$  level. That result represented a major milestone for the experiment and formed the basis of the Ph.D. thesis of A.A. Hamian [“The measurement of parity violation in proton-proton scattering at 221 MeV” (University of Manitoba, 1998)]. Data-taking continued in 1998 and 1999, and the final data analysis was complete by early 2001.

## Beam line and instrumentation

In addition to the measuring apparatus itself, the TRIUMF optically pumped polarized ion source (OPPIS), the cyclotron, and the transport beam lines must be considered critical components of the experimental set-up. All these components are illustrated in Fig. 1. A  $5\ \mu\text{A}$  transversely polarized beam is transported to the cyclotron through an approximately 50 m long injection beam line. The ion source Wien filter is tuned to produce vertical polarization at the entrance to the cyclotron. A 200 nA beam at 75–80% vertical polarization is extracted at 221 MeV. Spin precession through a pair of solenoid and dipole magnets results in delivery of a longitudinally polarized beam to the 40 cm liquid hydrogen target, which scatters 4% of the beam. Note that there are two complementary states of the spin transport, so-called “positive helicity” and “negative helicity” beam line tunes, which transport spin-up in the cyclotron into either + or – helicity at the parity apparatus. Half the data are acquired in each of these two beam line tune states, and consistency of the results in the two cases allows limits to be placed on systematic errors associated with the ion source alone, e.g. beam energy modulation, as discussed later in this report.

The custom-built parity instrumentation occupies approximately 10 m of the downstream section of beam line 4A/2 between the last quadrupole magnet and the west wall in the TRIUMF proton hall. Transverse field parallel plate ion chambers, TRIC1 and TRIC2, measure the beam current incident on and transmitted through the target. The parity violation signal is derived from the helicity-correlated analogue signal difference between the beam currents measured by the two TRICs. Upstream of the target are two polarization profile monitors (PPMs) to measure the distributions of transverse polarization  $P_y(x)$  and  $P_x(y)$  across the beam. Two intensity profile monitors (IPMs) measure the intensity distribution of beam current in  $x$  and  $y$  and are coupled to a pair of fast ferrite cored steering magnets (FCSMs) which lock the beam path on the optimum axis through the equipment. An additional IPM, located inside the  $\text{LH}_2$  vacuum enclosure just upstream of the target, is used mainly for beam tuning.

## Data acquisition

The spin of the optically pumped ion source is flipped 40 times per second in a pattern (+ – – + – + + –) or (– + + – + – – +). This pattern makes

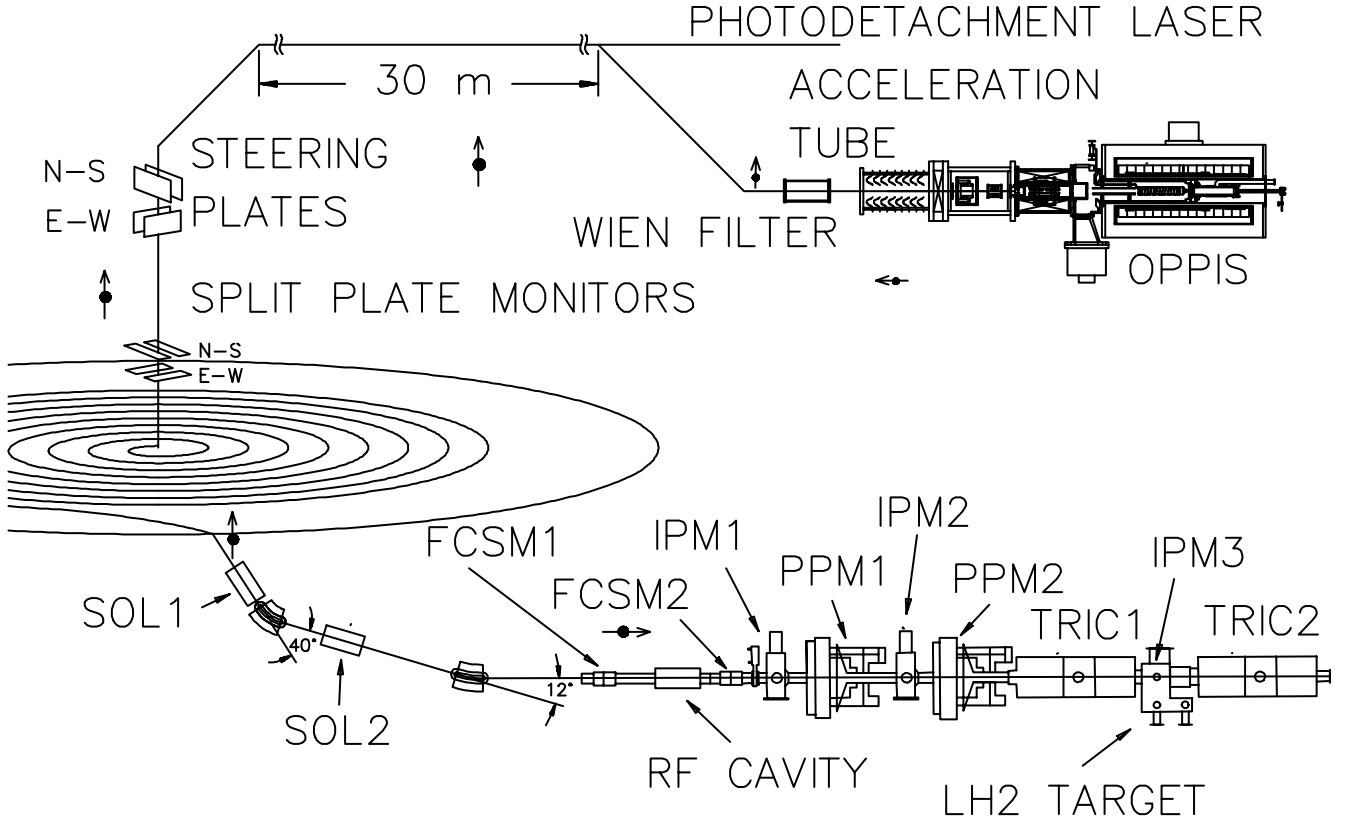


Fig. 1. General layout of TRIUMF parity experiment. (OPPIS: optically pumped polarized ion source; SOL: spin precession solenoid; FCSM: ferrite cored steering magnet; IPM: intensity profile monitor; PPM: polarization profile monitor; TRIC: transverse field ionization chamber.)

us insensitive to linear and quadratic drifts. The initial state of each 8 state (200 ms) group is also made to follow the same (+ - - + - + + -) or (- + + - + - - +) pattern, forming a 64 state “supercycle”. The initial spin state of each supercycle is chosen at random. 20% of the data is taken with all the spin flipping equipment running, but with the pumping lasers blocked with a shutter to guarantee zero polarization. Of this lasers blocked data, half is taken with an artificially enhanced intensity modulation synchronized with the spin flip in order to record our sensitivity to coherent intensity modulation.

The PPMs each have four rotating CH<sub>2</sub> blades, two scanning horizontally and two scanning vertically. The spin flip is synchronized with the rotation of the PPMs such that the polarization profile of the beam is measured during the first part of each spin state. An 8 state “event” hence corresponds to one full 360° rotation of the PPMs and the passage of all 8 blades through the beam. The minimum data set for which a full set of helicity correlated beam properties can be extracted is a 0.4 s “event pair”, as this gives both spin states for each PPM blade. Figure 2 shows the placement of the PPM and main detector (TRIC and IPM) readout intervals during one spin state. The 6.4 ms PPM interval corresponds to a 43 mm scan centred on the beam axis. The TRIC and IPM signals are integrated over exactly 1/60 second to eliminate sensitivity to 60 Hz or harmonics of 60 Hz.

Since the 0.2 s taken for one PPM rotation is exactly 12 cycles of the 60 Hz line, one would expect a given PPM blade to always pass through the beam at the same phase of the 60 Hz line. To prevent this, we introduced a small controlled phase slip. The rate of slip is programmable but, for data-taking, was set to one complete cycle of the 60 Hz line in 18 minutes.

In addition to the regular data-taking runs, we made many dedicated control measurements to measure the sensitivity of our apparatus to various helicity correlated beam properties.

### The data set

The parity data set used in our final analysis was acquired during three major data runs: February–

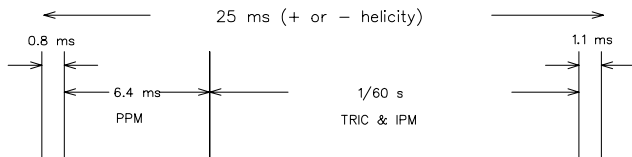


Fig. 2. The placement of detector readout intervals within one spin state. The 6.4 ms PPM interval corresponds to a 43 mm scan centred on the beam axis. The TRIC interval is 1/60 second to eliminate sensitivity to 60 Hz or harmonics of 60 Hz.

March, 1997, July–August, 1998, and May–June, 1999. Statistics for the combined set are:

- 3.8 million event pairs
- 375 runs in positive beam line helicity
- 368 runs in negative beam line helicity
- 80 position modulation runs
- 81 size modulation runs
- 40 energy modulation runs
- 109 neutral axis scans.

The data were grouped into 23 sets, the data in each set sharing the same beam line tune. The top panel in Fig. 3 shows the data from the 23 sets after data obtained under bad running conditions had been cut (see the next section), but before corrections were made for systematic errors. The bottom panel shows the corrected data from which our final result was obtained.

### Reduced data set

During data-taking, every effort was made to maintain the optimum beam conditions (quiet beam, good

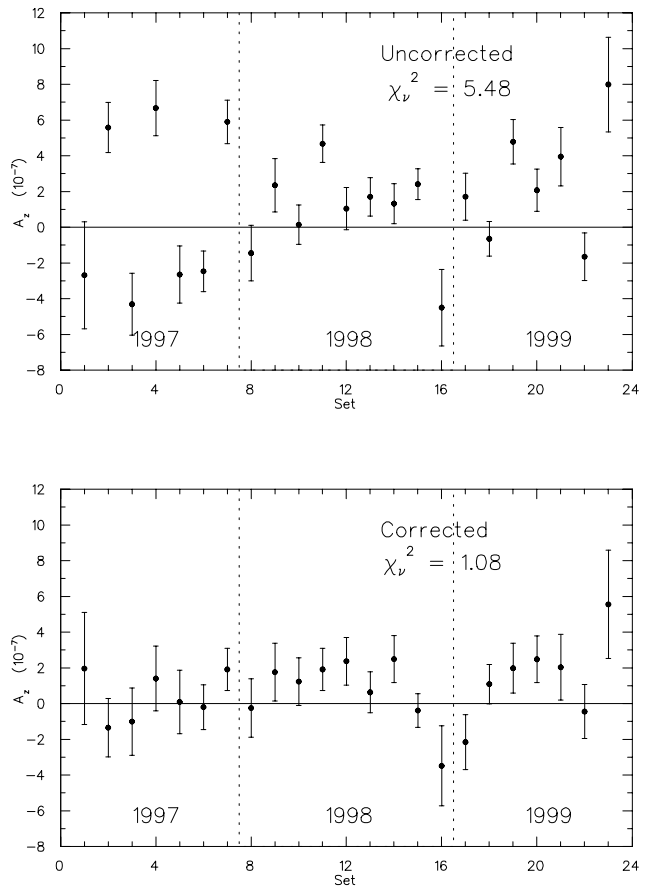


Fig. 3. Experiment 497 data before and after correction. The data are divided into 23 sets of alternating beam line tune. The top panel shows the data after beam quality cuts, but before correction for systematic error. The bottom panel shows the data after correction.

polarization, beam on axis, low transverse polarization, stable position and size, low first moments of transverse polarization, low intensity modulation), and to stop data-taking when these conditions were not met. Nevertheless, some data were taken for which conditions were not ideal. During analysis, 46 runs were first eliminated completely because the signal was anomalously noisy, indicating unstable beam conditions. The remaining data were then subjected to beam quality cuts. The cuts used are summarized in Table I. There are both “hard cuts” at a fixed value of beam parameter and “soft cuts” at  $\pm 3\sigma$  from the mean value. The entire data reduction process reduced the size of the total set by 30%, but significantly improved the quality of the data sample. The  $\chi_v^2$  for the 23 sets went from 11.3 per degree of freedom before the cuts were made to 5.48 after the cuts. The 23 uncorrected data on the top panel of Fig. 3 are from the reduced data set.

Table I. Summary of data reduction cuts. Except for the beam intensity, the centre of the acceptance window for each parameter is the measured centroid of that beam parameter’s distribution. The hard cuts are wide enough to include at least four standard deviations.

Beam parameter	Acceptance window
Neutral axis $x, y$	$\pm 0.3$ mm
Average beam position	$\pm 3\sigma$ (soft)
$\sigma_x, \sigma_y$	$\pm 1.0$ mm
Beam skew	$\pm 0.2$ mm
Intensity	196–204 nA
Intrinsic moments	$\pm 3.0$ mm

### Correction for systematic errors

The parity violating asymmetry,  $A_z$ , is determined from the helicity correlated difference between the signals in the ion chambers (TRICs) located before and after the liquid hydrogen target. Unfortunately, helicity correlated modulations of beam parameters other than helicity can, and usually do, generate a false signal of parity violation. To correct for this, helicity correlated modulations in beam intensity, size, position, transverse polarization, and first moments of transverse polarization are monitored continuously during data-taking. These unwanted modulations are then multiplied by our known sensitivities to these modulations and corrections are applied.

### Coherent intensity modulation

Coherent intensity modulation is measured by the ion chamber (TRIC1) upstream of the target. The sensitivity to this modulation is measured by periods of intentional enhanced ( $\sim 0.1\%$ ) intensity modulation interleaved with the main data-taking.

### Coherent position modulation

Coherent position modulation is measured by two intensity profile monitors (IPMs in Fig. 1) located 1.8 m apart along the beam line. Using two IPMs permits us to measure both tilts and parallel shifts of the beam. The sensitivity to beam motion is measured in separate control measurements during which the beam position is modulated in a variety of ways using the ferrite cored steering magnets (FCSMs).

We parameterize the false analyzing power arising from helicity correlated beam position as

$$\begin{aligned} \Delta A_z = & \left( \frac{\Delta x_1 + \Delta x_2}{2} \right) (a_x x_1 + b_x x_2 + c_x) \\ & + \left( \frac{\Delta x_1 - \Delta x_2}{2} \right) (d_x x_1 + e_x x_2 + f_x) \\ & + \left( \frac{\Delta y_1 + \Delta y_2}{2} \right) (a_y y_1 + b_y y_2 + c_y) \\ & + \left( \frac{\Delta y_1 - \Delta y_2}{2} \right) (d_y y_1 + e_y y_2 + f_y) \end{aligned}$$

where  $\Delta x$  and  $\Delta y$  are the horizontal and vertical helicity correlated beam motion,  $x$  and  $y$  are the beam position and the 1 and 2 subscripts refer to IPM1 and IPM2. The parameters  $a$  to  $f$  are extracted from a fit to the calibration data.

### Coherent beam size modulation

Coherent beam size modulation is also measured by the two IPMs. The sensitivity to beam size is determined by control measurements in which the beam size is intentionally modulated by driving the ferrite cored steering magnets as quadrupoles.

We parameterize the false analyzing power due to beam breathing as

$$\begin{aligned} \Delta A_z = & \alpha_x \sigma_{x_1} \Delta \sigma_{x_1} + \beta_x \sigma_{x_2} \Delta \sigma_{x_2} \\ & + \alpha_y \sigma_{y_1} \Delta \sigma_{y_1} + \beta_y \sigma_{y_2} \Delta \sigma_{y_2} \end{aligned}$$

where  $\sigma$  is the RMS beam size and  $\Delta \sigma$  is the helicity correlated change in beam size. As with position modulation, the parameters are extracted from a fit to the calibration data. Because the beam steers somewhat when the size is modulated, correction for position modulation must be included in the fit.

### Transverse polarization

Transverse polarization is measured by the two polarization profile monitors (PPMs in Fig. 1) located 1.8 m apart along the beam line. The sensitivity to transverse polarization components is measured in a series of “neutral axis scans” in which a vertically polarized beam is scanned horizontally and a horizontally polarized beam is scanned vertically. These calibration scans also determine the beam axis on which we are

insensitive to average transverse polarization components. During data-taking, the beam is held on this neutral axis by a servo system. The false parity violating signal arising from average transverse polarization is proportional to the size of the transverse component multiplied by the distance from the neutral axis – i.e. to the first moment of transverse polarization. In units of  $10^{-7}$  per  $\mu\text{m}$ , the sensitivity to  $\langle y \rangle \langle P_x \rangle$  is 1.9 at PPM1 and  $-2.5$  at PPM2. The sensitivity to  $\langle x \rangle \langle P_y \rangle$  is  $-1.5$  at PPM1 and  $2.0$  at PPM2.

#### Intrinsic first moments of transverse polarization

Intrinsic first moments of transverse polarization are also measured by the PPMs. The first moments,  $\langle x \rangle \langle P_y \rangle$  and  $\langle y \rangle \langle P_x \rangle$ , discussed in the previous section are referred to as extrinsic first moments. They arise when a beam with a net transverse polarization is displaced from the neutral axis, and can be reduced to zero by holding the beam on the neutral axis. By contrast, intrinsic moments,  $\langle x P_y \rangle$  and  $\langle y P_x \rangle$ , result from a distribution of transverse polarization across the beam; they are not changed by moving the beam, and can be large even if the net transverse polarization is zero (for example, the polarization could be up on one side of the beam and down on the other).

Since there are no magnets after the first PPM, the first moments of transverse polarization vary linearly with position along the beam line. Furthermore, for a fixed setting of the upstream beam line magnets, the first moments at PPM1 and PPM2 tend to scale together so that, over a wide range of first moments, the ratio of first moments at PPM1 and PPM2 has a constant value. Since the neutral axis scans show that the first moment sensitivity at PPM1 is of opposite sign to, and 75% of the magnitude of, that at PPM2, it means that if the PPM2 first moment was always 75% of the PPM1 first moment, then the effective sensitivity to first moments would be zero. By adjusting the beam convergence, we attempted to achieve this magic moment ratio, but in the end the cancellation was not perfect and the residual, effective, first moment sensitivity had to be extracted from the data. This could be done either by regressing the first moment ratio from the data and using the sensitivities measured in the neutral axis scans, or by regressing the correlation of  $A_z$  with average first moment directly from the data. This latter method produced the least statistical spread and was the method used.

#### Energy modulation

Energy modulation cannot be measured directly at the parity apparatus. To cancel its effects, we make use of the fact that when the beam line helicity is reversed, the effects of true  $A_z$  reverse, but the effects of energy modulation do not. The 23 sets in Fig. 3 are

taken with alternating beam line helicity. That the  $\chi^2_\nu$  is only 1.08 shows that effects from energy modulation are small. What effects are present will tend to cancel in the final average. In addition to the frequent reversals of beam line helicity, we made frequent measurements of energy modulation at the ion source and of our sensitivity to this modulation. This information was used to include the effects of uncorrected energy modulation in our error budget, as described in more detail in the next section.

#### Method of applying the corrections

The false  $A_z$  arising from a given coherent modulation is found by multiplying the unwanted modulation by the sensitivity to that modulation. We refer to errors from variance of the corrected  $A_z$  distribution as “statistical”. The error quoted is the standard error in the mean of the  $A_z$  distribution. We refer to errors resulting from uncertainties in the sensitivities as “systematic” (even though they are statistical in nature) because an incorrect sensitivity will cause a systematic shift in the mean of the  $A_z$  distribution. There are 23 such distributions, corresponding to 23 beam line tunes of alternating helicity. Figure 3 shows the 23 corrected and uncorrected data sets and Table II summarizes the overall corrections.

To produce the corrected data the following procedure was adopted.

1. The data in each set were grouped into bundles of 10,000 event pairs per bundle.
2. Each bundle was corrected according to the observed coherent modulations (except position and size) for that bundle, giving a corrected  $A_z$  for each bundle. The variance of corrected  $A_z$  values in a set determined an error bar for that set. We call this the “statistical” error. We did not correct for position and size, because the net correction was consistent with zero and when

Table II. Corrections for systematic error. The table shows the average value of each coherent modulation, the false  $A_z$  resulting from that modulation, and the uncertainty resulting from correcting for it.

Property	Average value	$10^7 \Delta A_z$
$A_z^{\text{uncorr}}(10^{-7})$	$1.68 \pm 0.29(\text{stat})$	
$y * P_x(\mu\text{m})$	$-0.1 \pm 0.0$	$-0.01 \pm 0.01$
$x * P_y(\mu\text{m})$	$-0.1 \pm 0.0$	$0.01 \pm 0.03$
$\langle y P_x \rangle(\mu\text{m})$	$1.1 \pm 0.4$	$0.11 \pm 0.01$
$\langle x P_y \rangle(\mu\text{m})$	$-2.1 \pm 0.4$	$0.54 \pm 0.06$
$\Delta I/I(\text{ppm})$	$15 \pm 1$	$0.19 \pm 0.02$
Position + size		$0 \pm 0.10$
$\Delta E(\text{meV})$	7–15	$0.0 \pm 0.12$
Total		$0.84 \pm 0.17(\text{syst})$
$A_z^{\text{corr}}(10^{-7})$	$0.84 \pm 0.29(\text{stat}) \pm 0.17(\text{syst})$	
$\chi^2_\nu$ (23 sets)	1.08	

the corrections were applied they actually increased the residual correlations of  $A_z$  with position and size.

3. The uncertainties in the nil correction for position and size modulation were added in quadrature to each of the 23 sets. We include this in what we report in Table II as “systematic” error.

4. The errors resulting from uncertainties in the various sensitivities were added in quadrature to the corresponding data. The errors on the sensitivities are independent of what is accounted for in step 2, so it is justified to add them in quadrature to get the total error bar on each of the corrected  $A_z$  for the 23 sets. We also include this uncertainty in the “systematic” error in Table II.

5. The  $A_z$  we report is the weighted mean of the 23 data sets with a weight  $1/\text{err}^2$ , where  $\text{err}$  is the “total” error not including energy modulation. It is this total error that is shown in the bottom panel of Fig. 3.

6. As mentioned earlier, the correction for energy modulation is tricky as we could not make a direct measurement of this in the beam line. We do have frequent measures of energy modulation at OPPIS and of  $dA_z/dE_{\text{OPPIS}}$ . These were separate control measurements taken with the pumping lasers blocked. The  $dA_z/dE_{\text{OPPIS}}$  runs were first corrected for all known systematic errors (dominated by  $dI/I$ ), and we assumed that the residual false  $A_z$  was from energy modulation. The energy modulation sensitivities depend on the beam line tune, so we looked at the distribution of measured energy modulation values and  $dA_z/dE_{\text{OPPIS}}$  values for a given beam line tune and estimated a correction and a “worst case” uncertainty in the correction.

7. Corrections were calculated for energy modulation on a year by year basis. 1998 and 1999 required two corrections each, one for each beam line helicity. 1997 needed four corrections, as we had different Wien filter settings as well. Finally, all the energy modulation corrections were combined and one correction was applied to the final  $A_z$ .

8. The energy modulation correction shown in Table II is the net effect of energy modulation over the 1997, 1998 and 1999 runs. The net correction is zero. The  $\pm 0.12$  uncertainty we assign comes from the quadrature sum of the error in energy modulation plus the error in the energy modulation sensitivity. This was not included in the individual error bars for the 23  $A_z$  numbers because we do not know the energy modulation well enough. This means the chi squared for the 23 sets is larger than it really “should” be if we knew the energy modulation error for each of the 23 sets. The fact that  $\chi^2_\nu = 1.08$  without taking this into account indicates that uncorrected energy modulation effects must be small.

We know the  $dA_z/dE$  in the beam line from measurements made using an rf accelerating cavity placed upstream of IPM1 in the beam line. The result of  $(2.9 \pm 0.3) \times 10^{-8} \text{ eV}^{-1}$  agreed well with predictions based on variation of stopping power with energy. Based on this, the  $dA_z/dE_{\text{OPPIS}}$  we measured indicates that the cyclotron amplified  $dE_{\text{OPPIS}}$  by a factor of about 130. This is reasonable because direct measurements we made in beam line 4B indicated a factor of about 100 to 200.

## Results

The overall result for the 23 sets is summarized in Table II in units of  $10^{-7}$ . The uncorrected value of  $A_z$  is  $1.68 \pm 0.29(\text{stat})$ . We estimate that half of the uncorrected  $A_z$  comes from true parity violation and half from the various sources of systematic error as itemized in Table II. After correcting for systematic errors, we find the longitudinal analyzing power to be  $A_z = 0.84 \pm 0.29(\text{stat}) \pm 0.17(\text{syst})$ .

## Conclusion

$A_z$  in  $\bar{p}p$  scattering has already attracted considerable theoretical interest, and many calculations have been made [Driscoll and Miller, Phys. Rev. **C39**, 1951 (1989); *ibid.*, **C40**, 2159 (1989); Grach and Shmatikov, Phys. Lett. **B316**, 467 (1993); Iqbal and Niskanen, Phys. Rev. **C42**, 1872 (1990); Driscoll and Meissner, Phys. Rev. **C41**, 1303 (1990)]. One of the main sources of uncertainty in these calculations is the value of the weak meson-nucleon couplings.

Figure 4 shows the limits on the weak meson-nucleon couplings  $h_\rho^{pp}$  and  $h_\omega^{pp}$  imposed by the low energy results [Kistryn *et al.*, *op. cit.*; Eversheim *et al.*,

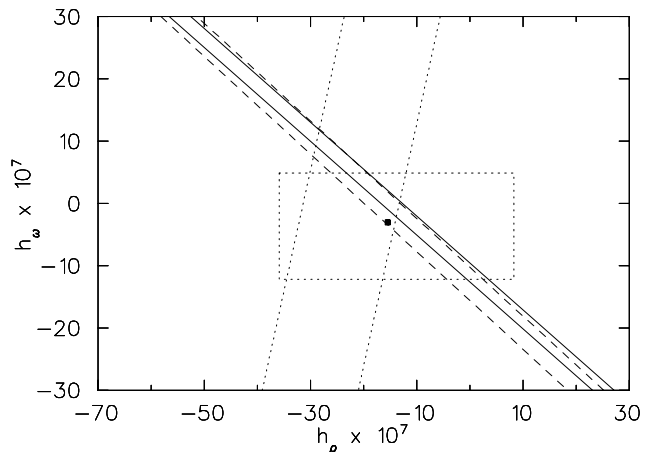


Fig. 4. Current constraints on the weak meson nucleon couplings based on the experimental data and recent calculations by Carlson and Schiavilla. The bands are the constraints imposed by different experiments (Bonn 13.6 MeV, dashed; PSI 45 MeV, solid; TRIUMF 221 MeV, dotted). The filled square and dotted rectangle are the DDH “best guess” and “reasonable range” respectively.

*op. cit.*; private communication (1994)], and the present TRIUMF result. The bands are based on a calculation by Carlson and Schiavilla [private communication (2001)] assuming the Argonne  $v_{18}$  (AV-18) potential [Wirring *et al.*, Phys. Rev. **C51**, 38 (1995)], the Bonn 2000 (CD-Bonn) [Machleidt, Phys. Rev. **C63**, 24001 (2001)] strong interaction coupling constants, and including all partial waves up to  $J = 8$ . One sees that the TRIUMF measurement has greatly reduced the acceptable range of both  $h_{\rho}^{pp}$  and  $h_{\omega}^{pp}$  over what was the case when only the low energy measurements were available.

Better values for the weak meson-nucleon coupling will be valuable in sharpening the theoretical interpretation of upcoming  $ep$  parity violation experiments such as  $G_0$  at Jefferson Lab. By combining the results of several seemingly disparate experiments one can finally hope to get a coherent picture of  $NN$  parity violation and in turn details of the quark content of the proton itself.

### Experiment 614

#### TWIST – the TRIUMF weak interaction symmetry test

(*N.L. Rodning, Alberta*)

While the standard model has been rather successful in describing and predicting diverse phenomena, it is widely regarded as an approximation to a deeper, more fundamental theory. Recent work has renewed excitement in the search for clues to that deeper theory. In particular, the evidence for neutrino oscillations and a possible deviation in  $(g-2)$  for the muon have sparked recent interest.

The TWIST experiment is designed to study the spectrum of positrons from  $\mu^+$  decay with a final precision of 0.01%. This will allow the extraction of the Michel parameters which characterize the spectrum at a precision ranging from approximately 10 to 30 times better than existing work. Work at this precision provides significant sensitivity to possible failures of the standard model.

#### The TWIST spectrometer

The TWIST spectrometer is shown in Fig. 5. The basic elements of the spectrometer include 44 precision planar drift chambers and 12 planar proportional chambers. The drift chambers are used to reconstruct the trajectory of the decay  $e^+$  while the proportional chambers are used to accurately determine the decay time. The planar geometry means that the material seen by the decay particles scales with  $1 \cos(\theta)$ , ensuring reliable corrections for scattering and energy loss.

A polarized muon beam enters from the left and triggers the experiment by leaving a signal in a thin plastic scintillator (not shown). The muon is stopped

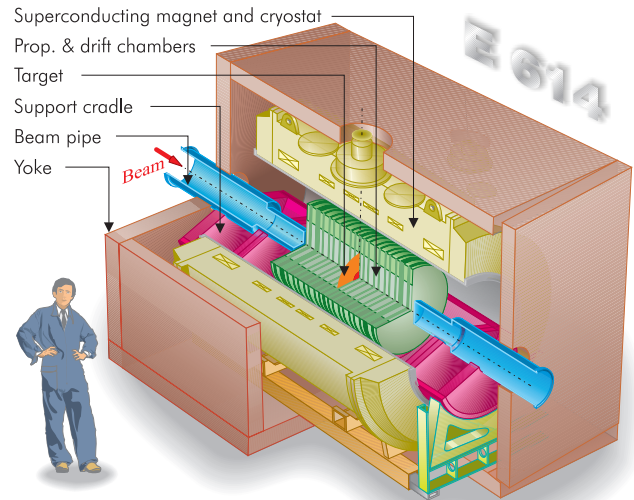


Fig. 5. The TWIST spectrometer.

at the centre of the spectrometer in a thin mylar foil. In the end, metallic targets will be used due to their decreased effect on the muon polarization.

The entire detector is in a highly uniform 2 T magnetic field, provided by a 1 m bore superconducting solenoid and shaped by a 30 ton iron return yoke.

Muons are brought into the spectrometer typically one at a time. Activity in the drift and proportional chambers is recorded for 6  $\mu$ s before, and for 10  $\mu$ s after, the trigger signal.

The entire spectrometer has been built and was studied during an initial commissioning run in November/December, 2001. Fabrication of spare detector planes continues.

#### Hardware performance

The TWIST spectrometer appears to be performing at or beyond expectations. Critical considerations include

- Average geometrical uniformity
- Single cell efficiencies
- Tracking resolution
- Field uniformity
- Depolarization (required for  $P_{\mu}\xi$ ).

#### Average geometrical uniformity

The wires are strung across precision glass rulers at a spacing of 4 mm for the drift planes and 2 mm for the proportional chamber planes. The position of each wire is subsequently mapped using a digital microscope travelling on a precision ruler. For the drift planes, the average spacing matches the design goal to an accuracy of approximately 0.06  $\mu$ m, roughly 30 times better than the design tolerance. Individual wire

positions scatter from their nominal positions with a standard deviation of approximately  $3\ \mu\text{m}$ , or approximately 7 times better than the design specification.

#### Single cell efficiency

A preliminary measurement of the efficiency of the cells yields a value of approximately 99.8% for minimally ionizing particles. The helical tracks of the decay positrons typically involve a large number of hits so that each track is heavily overdetermined and therefore hardware inefficiency is not expected to introduce any tracking ambiguity.

#### Tracking resolution

The determination of the tracking resolution requires that a large number of calibrations be completed and iterated upon. For example, the determination of the decay time is required for the calculation of the drift time. The wires have been strung within the detector planes with high precision, but plane-to-plane variations in position are determined by tracking particles through the detector with zero field. Preliminary values of the calibration parameters provide tracking resolution better than the design specification of  $100\ \mu\text{m}$ .

#### Field uniformity

The magnet cryostat was opened in the summer after evidence indicated that the coils might be moving within the cryostat. Any movement at the millimetre level can lead to large axial forces which increase with additional movement. The cause turned out to be missing structural elements. The magnet was repaired and commissioned to full field in September. The magnet was then used at full field during the November/December beam period, and is scheduled for mapping during March/April, 2002. We anticipate mapping the magnet to a precision of 1 G.

#### Depolarization

A study of the M13 surface muon beam properties was the subject of Robert MacDonald's Master's thesis [University of Alberta, 2001]. The surface muon beam has a polarization of unity if the standard model is valid. Depolarization of the beam can arise from multiple scattering in 1AT1 (the pion production target), from slit edge scattering, and from effects of the beam emittance as the beam crosses the magnet's fringe field. The effects of scattering are not expected to be a problem, but the simulations will require validation using several data sets of  $10^9$  events each. The effects of the beam emittance will be studied during the coming year or more. We are planning to build a time expansion chamber to measure the beam characteristics with minimal disturbance to the beam.

### Experiment 761

#### Measurement of parity violation in $pp$ scattering at 221 MeV

(*J. Birchall, W.T.H. van Oers, Manitoba*)

Experiment 761 is a continuation of Expt. 497 to measure the parity violating longitudinal analyzing power,  $A_z$ , in  $pp$  scattering at 221 MeV. The aim of the experiment is to further reduce the statistical and systematic uncertainties of  $A_z$  so that, when taken together with results from low energy, tight constraints can be placed on the weak meson-nucleon coupling constants  $h_\rho^{pp}$  and  $h_\omega^{pp}$ . Accurate knowledge of these coupling constants is needed, not only to test new calculations of them, but also as input for the analysis of a number of other experiments. For example, the SAMPLE experiment at MIT Bates and  $G\theta$  at Jefferson Lab both need to calculate a correction for the nucleon anapole moment, which represents a parity violating interaction of the photon with a nucleon. Precise knowledge of the weak meson-nucleon coupling constants is needed to perform these calculations. Further details are to be found in the report on Expt. 497 in this Annual Report.

In the past year progress has been made on a number of fronts: the establishment of an enlarged collaboration containing most of the world's experts in performing this type of experiment, refining the aims of the experiment, and improvements to the optically pumped polarized ion source.

#### Expanded parity collaboration, updated goal for Expt. 761

Funds were received from NSERC's International Opportunity Fund to explore the possibility of establishing a wider collaboration. To this end a workshop was held at the University of Bonn, November 8–9, 2001, at which Expt. 761 and other possible parity violation experiments were discussed. Attendees included lead members of the collaborations that made the very precise measurements of  $A_z$  at low energy at Bonn and at PSI, and of the measurement at LANL. Present were experimenters from the universities of Bonn, Erlangen and Cologne, from Forschungszentrum Jülich, LANL, the Institute for Nuclear Research in Moscow, ETH Zürich, from TRIUMF and the University of Manitoba. Discussion was animated and very positive and led to a significant revision of the aims of Expt 761.

It was universally agreed that the goal for Expt. 761 had been too conservative and that we should aim for a combined statistical and systematic error on  $A_z$  reduced by a factor of two to  $0.1 \times 10^{-7}$ . Figure 6 shows the constraints placed on the  $h_\rho^{pp}$  and  $h_\omega^{pp}$  by Expts. 497/761 and the low energy measurements marked "Bonn 13.6 MeV" and "PSI 45 MeV". The "Expt. 497"



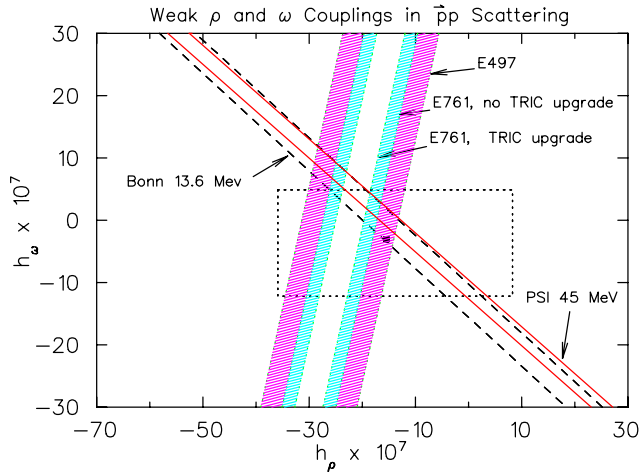


Fig. 6. Constraints on  $h_{\rho}^{pp}$  and  $h_{\omega}^{pp}$  from  $pp$  scattering experiments at low energy and at 221 MeV at TRIUMF.

band shows the present constraint from Expt. 497 data alone. “Expt. 761, no TRIC upgrade” shows the original goal for Expt. 761 running at 200 nA as in Expt. 497. “Expt. 761, TRIC upgrade” shows the constraint from the updated Expt. 761 following discussions in Bonn. It is seen that the revised Expt. 761 will place a constraint on  $h_{\rho}^{pp}$  and  $h_{\omega}^{pp}$  that is of comparable quality to that from the low energy measurements.

The updated goal for Expt. 761 requires a factor of four increase in data. This can be achieved by increasing beam current from 200 to 500 nA and decreasing the non-data-taking overhead. Increasing beam current will necessitate a redesign of the ionization chambers, that at present operate optimally at 200 nA, to improve noise and stability. Changes to the ion chambers include redesign of the corona shields and replacement of the sharp-edged field-shaping electrodes with a smaller number of cylindrical rods to enable the chambers to operate at their designed 20 kV in place of the 8–10 kV used in Expt. 497.

Table III shows contributions to the uncertainties in  $A_z$  from Expt. 497 and the original and updated Expt. 761. Values marked with an asterisk are conservative. They assume no reduction in systematic errors from

Table III. Contributions to uncertainties in  $A_z$  in units of  $10^{-7}$ .

	E497 200 nA	E761 200 nA	E761 500 nA
$A_z^{\text{uncorr}}$ (stat)	1.68	$\pm 0.29$	$\pm 0.20$
Ext. moments	0	$\pm 0.03$	0
Int. moments	0.65	$\pm 0.06$	0
$\Delta I/I$	0.19	$\pm 0.02$	$\pm 0.02^*$
$\Delta E$	0	$\pm 0.12$	$\pm 0.09^*$
Position + size	0	$\pm 0.10$	$\pm 0.07^*$
$A_z^{\text{corr}}$	0.84	$\pm 0.34$	$\pm 0.23$
			$\pm 0.11^*$

improvements made to the ion source which should significantly reduce modulations of beam properties on spin flip. The last column assumes 130 days of running at 500 nA with a reduction of data-taking overhead from a factor of five to a factor of three. Additional time will be required to commission the upgraded ion chambers and the fully-instrumented current-mode polarimeters.

### Upgrades to the optically pumped ion source

Slight differences in beam properties from OPPIS on spin flip translate into changes in beam energy and current extracted from the cyclotron, which generate false parity signals. A number of upgrades have been made to OPPIS to increase current and eliminate troublesome changes of beam properties on spin flip.

#### New sodium ionizer

The new ionizer cell has a sodium jet, which is better at confining the sodium vapour than the old design. This means that the apertures can be made larger, thus preventing secondary electron emission, and the cell can be biased to  $-15$  kV. The advantage of biasing the cell is that the  $H^-$  beam is accelerated as it leaves the cell, which will suppress changes of beam properties on spin flip. In addition, the reduced beam emittance at the higher beam energy will improve matching into the injection beam line to the cyclotron, and should increase the available current by a factor of 2 or 3. This would allow the source to be run at the same time as ISAC, without the bunchers which cause large beam modulations. Independent of ISAC, the source can be run in a lower current mode, with better optical pumping and polarization saturation of the rubidium vapour and therefore decreased current modulation.

#### New microwave generator power supply

The old power supply had considerable downtime in the last two parity runs. At RHIC a new power supply was built by Russian engineers that produces a much more stable voltage, resulting in reduced intensity fluctuations. Unlike the old supply, it also meets the warranty requirements for the new microwave tubes for the ECR dissociator.

#### Lasers

As the source of all helicity-correlated modulations, the lasers are critical to the experiment. OPPIS has had one titanium sapphire (TiS) probe laser to measure polarization and two TiS lasers for optical pumping of rubidium vapour, one of which is shared with the  $\beta$ -NMR set-up. It is planned to replace the present two standing-wave TiS optical pumping lasers with a single 6 W TiS ring laser. The TiS ring laser operates in travelling wave mode without standing waves and will exhibit less spatial mode change on spin flip. A double

etalon system with two counter-rotating etalons will further reduce spatial changes, and hence further reduce changes of beam properties on spin flip.

### The ATLAS experiment at the LHC

(C. Oram, TRIUMF)

As described in detail in the 1996 Annual Report, ATLAS is building a general purpose  $pp$  detector which is designed to exploit the full discovery potential of the Large Hadron Collider (LHC) at CERN. The TRIUMF group is responsible for the engineering of the hadronic endcap calorimeter (HEC), and the feedthroughs for the endcap cryostat. For the HEC, this year has seen the continuation of module production and the final stages of the manufacture of the wheel assembly equipment. This year the TRIUMF HEC group has had two visitors from China as part of its close collaboration with a Chinese group. This group is a three university cluster of Nanjing University, USTC Hefei, and Shangdong University.

#### Physics goals

The present theoretical understanding of elementary particles is in the context of the standard model. The standard model is a remarkably successful model, providing predictions which have been consistently confirmed by experiment for over two decades. Its agreement with experimental results, to enormous accuracy in some cases, makes it the most accurately verified model in science. Of the many elementary particles contained in the standard model, only the Higgs remains to be discovered. The central goal of ATLAS is the search for the Higgs particle.

There are good theoretical reasons to believe that the discovery of the Higgs will at least contain hints of, and more likely direct evidence of, what lies beyond the standard model. If the Higgs is composite, its existence requires as yet unknown ultra-strong forces. If it is elementary, it would be the only spinless particle to be discovered so far. There is a theoretical “naturalness” problem for the masses of spinless particles. In the standard model, which is a highly nonlinear dynamical system, the elementary particles tend to take on the heaviest of all possible mass scales which in such a model are at inaccessible energies and inconsistent with other requirements of the model. All other particles discovered thus far have natural mechanisms, such as gauge and chiral symmetries, for protecting their masses so that they can lie in the observable range. For the Higgs particle, there is no such symmetry in the present model. The only theoretical scenarios which leave the Higgs particle light enough to observe are hypothetical ones, either technicolour or supersymmetry, both radical departures from the present structure

of the standard model. If Higgs is seen at LHC, one of these scenarios should be seen at the same time.

Particle theory has progressed enormously over the last few decades with many appealing scenarios for physics beyond the standard model. The most likely of these is supersymmetry and the boldest of these is superstring theory. These theories are intimately related and are both radical ideas which promise a new conceptual framework for understanding elementary particles. Though far from being complete theories so far, there are superstring models which resemble the standard model in their low energy limit. These models have a great appeal as they contain a unification of fundamental forces which includes gravity. They have already had substantial impact on gravitational physics where, for example, in addition to the long sought reconciliation of gravity with quantum mechanics, they have been used to derive a fundamental understanding of black hole thermodynamics. Superstring theory is still in its infancy, but progress has been dramatic and the promise of great things to come has captured the imagination of a substantial fraction of the world’s theoretical particle physicists.

The present theoretical view is that the conventional grand unification of the strong, weak and electromagnetic forces can only work in the supersymmetric extension of the standard model. In that model, the grand unified energy scale is only two decades below the Planck scale, the ultimate energy where spacetime itself has quantum fluctuations. It is not out of the realm of imagination that, at energy scales where supersymmetry would be observed, evidence for an ultimate theory of everything, at least everything that can exist once spacetime is formed, is within human grasp.

Experiments at the LHC, where the ATLAS detector will take data, will probe the energy region where the Higgs particle, possibly supersymmetry, or other structures will be visible. This will be the first experimental probe of an energy region where fundamentally new physics is expected to occur in many years. There is every reason to believe that the results will be among the most dramatic ever.

#### Basic ATLAS design considerations

The most prominent issue for the LHC is the quest for the origin of the spontaneous symmetry-breaking mechanism in the electroweak sector of the standard model (SM). This is related to one of the most fundamental questions of physics: What is the origin of the different particle masses? New direct experimental insight is required to answer this question.

One of the possible manifestations of the spontaneous symmetry-breaking mechanism could be the existence of a SM Higgs boson ( $H$ ), or of a family of Higgs particles ( $H^\pm$ ,  $h$ ,  $H$  and  $A$ ) when considering the min-

imal supersymmetric extension of the standard model (MSSM). The Higgs search is therefore used as a first benchmark for the detector optimization. For the SM Higgs, the detector has to be sensitive to the following processes ( $\ell = e$  or  $\mu$ ) in order to cover the full mass range above the discovery limit set by the final LEP operation in the fall of 2000 (see Fig. 7):

$H \rightarrow b\bar{b}$  from  $WH$ ,  $ZH$  and  $t\bar{t}H$  using a  $\ell^\pm$  and  $b$ -tagging,  
mass range  $80 < m_H < 100$  GeV;

$H \rightarrow \gamma\gamma$   
mass range  $90 < m_H < 150$  GeV;

$H \rightarrow WW^* \rightarrow \ell^\pm\nu\ell^\pm\nu$   
mass range  $150 < m_H < 200$  GeV;

$H \rightarrow ZZ^* \rightarrow 4\ell^\pm$   
mass range  $130 \text{ GeV} < m_H < 2m_Z$ ;

$H \rightarrow ZZ \rightarrow 4\ell^\pm, 2\ell^\pm + 2\nu$   
mass range  $m_H > 2m_Z$ ;

$H \rightarrow WW, ZZ \rightarrow l^\pm\nu + 2 \text{ jets}, 2\ell^\pm + 2 \text{ jets}$   
from  $WW, ZZ$  fusion using tagging of forward jets for  $m_H$  up to about 1 TeV.

In addition to signatures similar to these, the MSSM Higgs searches also require sensitivity to processes such as:

$$\begin{aligned} A \rightarrow \tau^+\tau^- &\rightarrow e\mu + \nu\text{'s} \\ &\rightarrow \ell^\pm + \text{hadrons} + \nu\text{'s}; \\ H^\pm &\rightarrow \tau^\pm\nu \text{ from } t\bar{t} \rightarrow H^\pm W^\mp b\bar{b} \text{ and using} \\ &\ell^\pm \text{ tag and } b\text{-tagging} \\ &\rightarrow 2 \text{ jets}. \end{aligned}$$

The observable cross sections for most of these processes are small over a large part of the mass range to be explored at the LHC. Hence it is important to operate at high luminosity, and to maximize the detectable rates above backgrounds by high-resolution measurements of electrons, photons, and muons.

### Canada's participation in ATLAS

The Canadian group consists of 29 grant eligible physicists from TRIUMF, University of Alberta, Carleton University, UBC, IPP, Université de Montréal, UQAM, Simon Fraser University, University of Toronto, University of Victoria, and York University. We are strongly involved in three construction projects centred around detecting hadrons in the endcap region: the hadronic endcap project, the hadronic portion of the forward calorimeter project, and the pipeline electronics for calorimetry. In addition we are committed as part of our common project contribution to providing the feedthroughs for the two endcap cryostats. TRIUMF is directly involved in all these projects, and in the trigger and physics simulations.

### The hadronic endcap project

The hadronic endcap calorimeter (HEC) is a liquid argon sampling calorimeter with copper absorbers [ATLAS Collab., ATLAS Liquid Argon Technical Design Report, December 15 (1996)]. A concise overview of this design was provided in the 1996 TRIUMF Annual Report. An artist's impression of a module can be seen in Fig. 8.

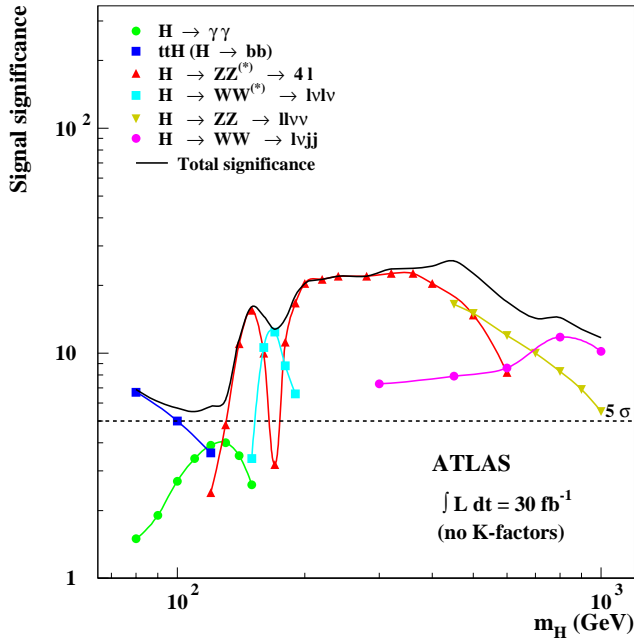


Fig. 7. Expected significance in ATLAS of the standard model Higgs boson signal, as a function of the Higgs mass, for an integrated luminosity of  $10^5 \text{ pb}^{-1}$  for several decay channels.

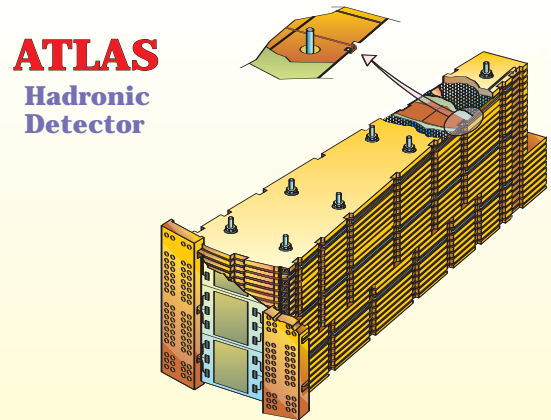


Fig. 8. Artist's impression of a hadronic endcap module.

### Hadronic endcap module production

This year the major scheduled milestone was the series module production of one complete endcap, consisting of 2 wheels. By the end of the year the TRIUMF group was 70% complete on module production. The copper machining facility at the University of Alberta completed all machining for the Canadian contribution during the summer of 2001, and then moved on to helping the European group finish their allocation in a timely manner.

### Test beam measurements of the hadronic endcap modules

Two test beam periods on the CERN H6 beam line this year have tested the performance of the series production modules of the calorimeter. The H6 beam line provides beams from 20 to 180 GeV. Analysis of the data shows the response is the same as in previous years. This data-taking successfully completes the quality control tests of an eighth of our series modules. A NIM paper has been submitted detailing the stand-alone behaviour of the calorimeter with pions, muons, and electrons. These measurements have been discussed in previous TRIUMF Annual Reports so we omit any details here and refer those interested to the NIM paper. To be ready for ATLAS, further test beam measurements with the other calorimeters in the endcap region “EM EndCap” and “Forward” are planned in the coming years.

In ATLAS the operating parameters for the liquid argon calorimeter will differ from those used and accessible in test beam measurements. The ATLAS system is based on the use of subcooled liquid argon, and the pressure is defined by the hydrostatic pressure at a given position in the endcap cryostat and the operating over pressure at the top surface of the liquid argon. To transfer calibration constants and signal shape parameters from the test beam results to ATLAS, the pressure and temperature effects have to be well understood. These dependencies have been studied during the summer of 2001 in beam tests at CERN using 119 GeV electrons.

To understand the temperature variation, the electron’s signal was measured at a variety of argon temperatures and beam impact positions in the calorimeter. The temperature range accessible in the test beam cryostat was about 3 K. Figure 9 shows the dependence of the electron drift time, across the 1.8 mm readout gaps, on the liquid argon temperature. The data points are the measurements of the beam test. Also shown is the expected temperature range in ATLAS and the linear extrapolation of the data. Figure 10 shows the dependence of the primary signal current on the liquid argon temperature. Again the data are shown with a linear extrapolation into the ATLAS operating region. In

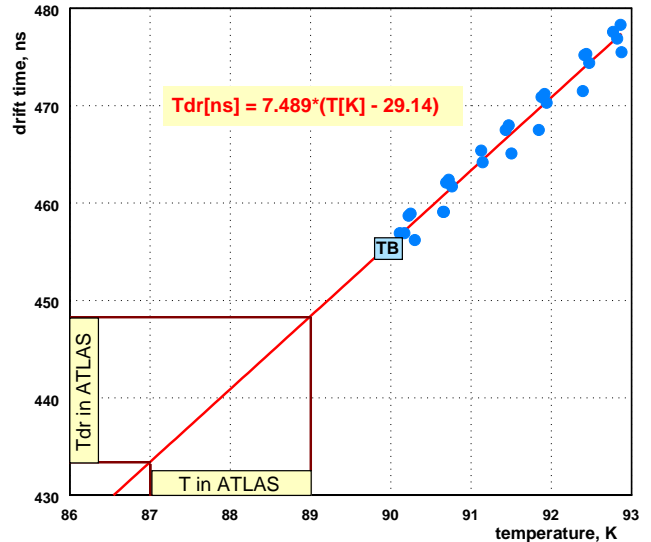


Fig. 9. Temperature dependence of drift time.

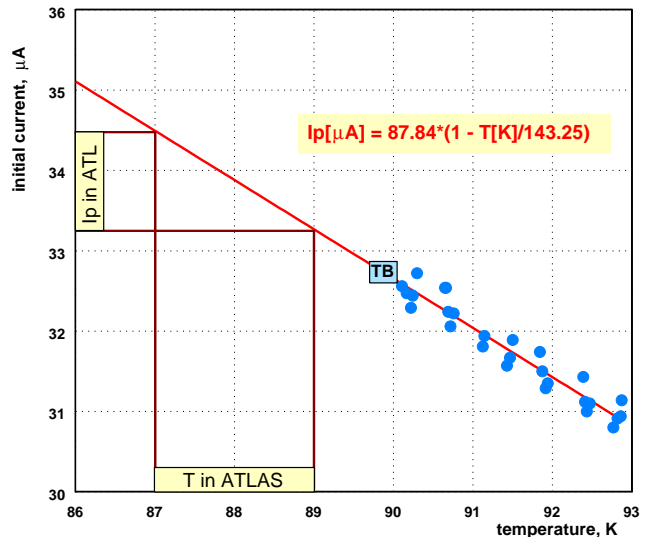


Fig. 10. Temperature dependence of primary current signal.

ATLAS we thus expect about 3.6% larger signals than in the beam test.

### Preparations for wheel assembly at CERN

32 modules of the HEC form a wheel. There are two wheels at each end of ATLAS, so we must construct 128 modules into four wheels. The equipment to undertake this is a Canadian responsibility. These four wheels and the two wheels of the EM calorimeter, which go in the same calorimeter, are assembled in the horizontal orientation. Hence each wheel, which weighs about 90 tonnes, must be taken from its assembly table, rotated to the vertical and moved to the cryostat. This translation and rotation of equipment is a Canadian responsibility. The engineering was undertaken by



Fig. 11. Wheel assembly tooling on truck outside manufacturing plant in Ontario.



Fig. 12. Wheel rotation tooling inside manufacturing plant in Ontario.



Fig. 13. Wheel rotation tooling and assembly table inside manufacturing plant in Ontario.

a collaboration between Alberta and TRIUMF personnel. The production of the equipment was in Canadian industry. Figure 11 shows a portion of this equipment being transported between manufacturer sites in Ontario in late fall. Figures 12 and 13 show views of some of the equipment assembled at the manufacturing site.

### **The ATLAS endcap signal feedthroughs**

*(M. Lefebvre, Victoria)*

The TRIUMF group is responsible for the engineering of the HEC and contributes to the production of high density cryogenic signal feedthroughs for both endcap cryostats. The feedthroughs are critical to the success of ATLAS. They are being built and tested at the University of Victoria by TRIUMF and Victoria staff. The endcap signal feedthroughs are currently scheduled to be installed on the two endcap cryostats during two periods starting approximately March, 2002 and October, 2002. At the end of 2001, approximately 1.5 months remained until the completion of this 7 year project. As this is the first time the endcap signal feedthrough project is covered in significant details in a TRIUMF Annual Report, the most important aspects of the project are reviewed.

### **Responsibilities, management and reviews**

The ATLAS collaboration has determined that some components of the detector can be regarded as contributions in kind to the Common Fund; these are known as Common Fund Projects. The endcap signal feedthroughs are part of the Canadian group contribution to the Common Fund. The Canadian group is responsible for the assembly, testing, and commissioning of the ATLAS endcap signal feedthroughs, as well as participation in their installation on the cryostats. The design of the feedthrough was made in collaboration with the Brookhaven National Laboratory (BNL), which is responsible for the production of the barrel cryostat signal feedthroughs.

A Canadian involvement in the endcap signal feedthroughs was already proposed in 1995. From the \$12.2 M Major Installation Grant awarded to ATLAS in the 1997–98 competition, a total of \$4.28 M is earmarked for the endcap signal feedthrough project. Considerable effort has been spent developing the management tools needed for successful completion of the project. Documents describing in detail the feedthrough design, the assembly procedures, the test procedures, the procurement plan, the quality assurance plan, and the material traceability are available. The administrative structure needed for duty exemption for goods for re-export has been set up in Victoria.

ATLAS reviews of the feedthrough project were held at BNL on June 12–13, 1997, and at CERN

on October 13–15, 1997, and October 2, 1998. The feedthrough Production Readiness Review (PRR) took place at CERN on January 29, 1999, where the green light was given for the procurement of the glass technology pin carriers. Status reports were presented at three NSERC ATLAS Reviews (TRIUMF, January 9, 2000, October 19, 2000 and December 14, 2001).

### Overview of the project

The ATLAS liquid argon calorimetry is composed of a barrel section and two endcap sections. Each endcap cryostat contains an electromagnetic calorimeter, two wheels of one HEC, and a forward calorimeter. The calorimeter signal and calibration lines are routed to the outside of each endcap cryostat via 25 feedthrough assemblies arranged approximately equally spaced in azimuth. The low voltage needed to operate the endcap hadronic calorimeter preamplifiers, which are located in the cold region, are also supplied via the signal feedthroughs as well as various monitoring lines.

The specifications that drove the technical design of the feedthrough assembly are quite complex. They involve geometrical and space constraints in the cryostat design, physical limitations on the space which is allocated to the feedthroughs, signal transmission quality, vacuum integrity, heat loss considerations, access possibilities, installation, reliability, and cost issues.

The design is based on gold plated conductive pins insulated and sealed by glass inserts in a stainless steel carrier. The carriers are then welded into the cold and ambient (temperature) flanges. A total of 1920 signal and calibration lines per feedthrough assembly is required in the chosen design. The ambient and cold flanges are connected by a bellows to isolate the feedthrough vacuum from the cryostat inter-vessel vacuum. The cold flange is attached to a transition piece, known as a funnel, which is welded to the cryostat via a bi-metallic joint. The electrical signals are brought from the calorimeter to the cold flange by coaxial kapton cables; these are called pigtail cables. Cables located in the vacuum between the cold and the ambient flange, i.e. inside the bellows, carry the signals through the cryostat wall; these are called vacuum cables. For each endcap, four feedthrough assemblies also carry the low voltage for the HEC preamplifiers. Figure 14 shows an overview drawing of one endcap signal feedthrough.

### Project set-up

The project set-up comprises the hardware and software required for the production of the feedthrough assemblies. The most important items are the leak test station, the electric test station, and the assembly jigs.

#### Leak test station

The selected glass technology for the signal feedthrough is mature and has shown good results in

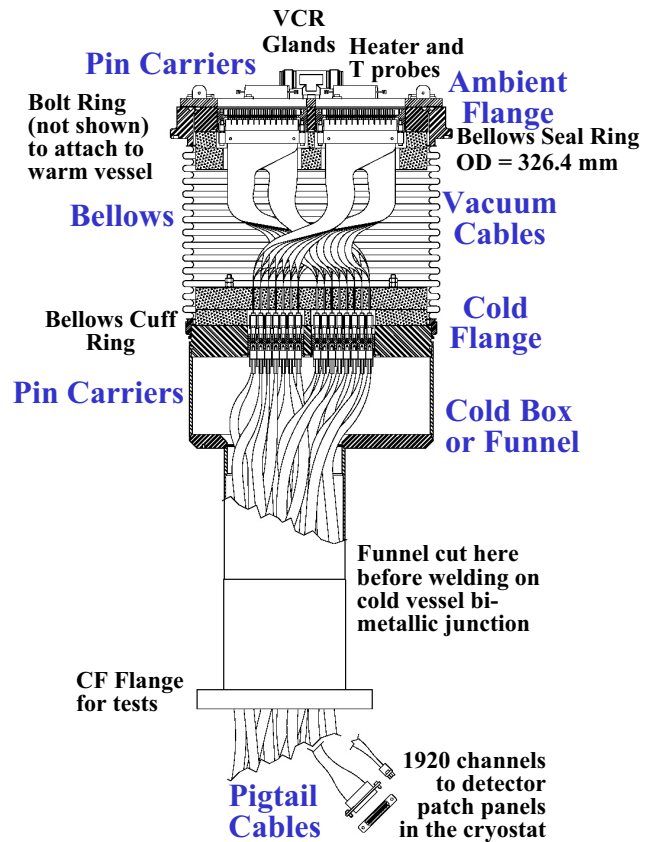


Fig. 14. Overview drawing of one endcap signal feedthrough, identifying its most important components.

applications that require high reliability under extreme temperature and pressure conditions. Still, the application considered here is pushing technology to its limits in order to reach the required density. The failure rate that we can tolerate is essentially zero over 20 years of operation. Since access to the various feedthrough assembly parts will be limited, a detailed and comprehensive testing procedure is vital.

Following the experience acquired at BNL, we have designed and assembled a leak test station that allows warm and cold leak tests to be performed in a controlled way. A precision of  $1 \times 10^{-9}$  atm.cc/s is required and has been achieved. The station is based on a helium leak checker, a residual gas analyzer and various pressure and temperature probes that service a warm test station for feedthrough assembly components, and a cold test station for full assemblies. Measurements are read by a PC based LabView DAQ system developed in Victoria. This test station is fully operational.

#### Electric test station

The feedthrough cables are used to carry analogue signals from the cryostats to the outside world, as well as calibration signals into the cryostats. Because of the fast shaping, the signal integrity is a major concern.

The grounding and shielding must be of good quality to avoid signal deterioration.

We have developed the electric test station needed to certify the electrical integrity of the signal feedthroughs. This station provides automated measurements of cable resistance, impedance and cross-talk. It uses, among other components, a network analyzer for detailed transient tests, a purpose built channel scanner developed in Orsay and assembled at UBC, and a purpose built channel multiplexer developed at UBC. Measurements are read by a PC based LabView DAQ system developed in Victoria. The instrumentation for testing the low voltage distribution for the HEC feedthrough units has also been developed. This test station is fully operational.

#### **Assembly jigs**

Each feedthrough assembly is too heavy to be handled manually. Assembly jigs and related hoists have been developed and built to allow the various phases of the assembly to be performed. In particular, the proper relative orientation of the flanges is ensured by the jigs' design.

#### **Prototyping**

Since 1997, our group has produced a full scale model, and purchased or produced prototypes of the various components of a feedthrough assembly. These were vital to the finalization of the design, the assembly procedures, including the welds, and the choice of suppliers. We have then used prototype parts to construct a feedthrough assembly with a dismountable flange-bellows interface. This prototype, which can easily be reconfigured, has been extensively used for the study of convective thermal loss and the study of leak and electric test procedures. We have also constructed a mechanical prototype to allow the cryostat team to perform various installation tests.

#### **Final design**

Contributions to the design of feedthrough assembly components through finite element analyses (FEA) were initiated early in 1996. These analyses, performed by Terry Hodges (TRIUMF), include detailed FEA of the mechanical stresses and deformation for the cold and ambient flanges, equipped with pin carriers, for various design options. Further mechanical stress analyses were performed for the funnel and the bi-metallic joint. These led to design guidelines suitable for both the barrel and endcap feedthrough assemblies. FEA studies of the flange temperature validate the plan to heat the ambient flange via resistors, and prescribe a maximum cooling rate for a safe cold testing of the equipped flanges. A detailed design of the ambient flange heater plate system has been finalized in 2000.

## **Procurement of components**

### **Vacuum cables**

The development of signal vacuum cables in Canada was successfully completed in 1998. Prototype assemblies have been designed and constructed in Canada in collaboration with CRPP and STC. These cable assemblies have been sent for tests to the BNL and LAL/Orsay laboratories. One cable has been irradiated in Grenoble in July, 1998 and successfully inspected and tested in Victoria. The performance of these prototypes was very encouraging. A series pre-production of 100 cables was launched at STC late in 1998, and received in the spring of 1999. These cables were extensively tested and found to perform as required. Meanwhile the BNL team has chosen FCI-BERG as the supplier of the barrel feedthrough vacuum cables. Following a Request For Quote sent to both FCI-BERG and STC for the endcap feedthrough signal vacuum cables, our group also opted for FCI-BERG as suppliers. We have now received all 1750 vacuum cables.

Special vacuum cables have been developed for the distribution of the HEC low voltage. Detailed tests with a complete low voltage HEC chain have been performed in Victoria in October, 1999. We have ordered and received all 40 HEC low voltage vacuum cables from Axon.

### **Pigtail cables**

The development of the pigtail cables was part of a larger effort to develop signal and calibration cables for the whole of the LAr readout chain. The pigtail cables for the endcap signal feedthrough are also part of the Canadian Common Fund contribution. They are purchased through Orsay, along with the other ATLAS LAr cables, from Axon. A Memorandum of Understanding for the procurement of the endcap pigtail cables has been signed by Orsay and ATLAS-Canada. A detailed procurement schedule has been developed, and reception of pigtails in Victoria is now (at year-end) 74% complete. Reception is expected to be completed early in 2002.

### **Pin carriers**

Extensive and detailed tests comparing the ceramic and glass pin carrier technologies were made in 1997 and 1998. Both technologies were found to be suitable for our project. A glass technology pin carrier was welded to a test flange in Canada and subjected to a burst test in CERN. It was found not to be affected by a pressure of up to 250 bar. The green light was given at the PRR to purchase glass technology pin carriers made of low inclusion 304L stainless steel. The order was placed in June, 1999. Procurement problems with

the low inclusion stainless steel caused approximately six months' delay. Further delays occurred when the procured steel proved to be unsuitable for hermetic seal use. After extensive studies and tests, coordinated by Tom Muller (BNL) and the manufacturer, a source of suitable stainless steel was found. Pin carrier production resumed in February, 2001. We have now (at year-end) received 77% of the required pin carriers. Reception is expected to be completed early in 2002.

#### Other components

Other components (bellows, flanges, funnels, VCR T-glands and heater plate parts) are all in stock.

#### Assembly and installation

A total of 50 feedthrough assemblies plus 5 spares must be produced (see Fig. 15). From the experience gained with the prototype construction and tests and with the production of the first assemblies, a detailed assembly procedure, quality plan and quality assurance plan have been developed and refined. These include the description of the testing of components from their arrival in Victoria through the completion of feedthrough units. Complete material traceability is ensured through the use of detailed traveller sheets.

The funnel and cold flange of each feedthrough assembly are part of the cryostat pressure vessel. An officially licensed company is doing the welding and extensive testing to conform to accepted welding code. Special test sections of a feedthrough assembly have been made for TIS (CERN Safety Group) tests. Final TIS approval of our welding plan has been obtained.

The shipment of feedthrough assemblies to CERN is done by air freight. Shipping crate construction follows the feedthrough assembly production. Upon arrival at CERN, each feedthrough assembly is subjected to an ambient temperature leak test and a basic electrical test. We are responsible for these tests. The



Fig. 15. Vacuum cables being installed on a feedthrough by Paul Birney (TRIUMF) at the University of Victoria.

required testing equipment was commissioned at CERN in October, 2001, when the first feedthrough assemblies arrived at CERN.

The installation of the feedthrough assemblies on the cryostat is a delicate and complex operation. Although the feedthrough installation is not a Canadian responsibility, our group is expected to actively assist during the operation. In particular, given the softness of the pins, members of our team will manually connect the so-called warm cables that join the outside of the ambient flange to the electronics crate baseplane. Each feedthrough assembly, once welded on the cryostat, must also be electrically tested. Furthermore, we must assist during the leak testing of the cryostat.

#### Project schedule

The current ATLAS schedule indicates that the endcap cryostats will be ready for feedthrough integration approximately in March, 2002 and October, 2002. The endcap signal feedthrough project is on track with the ATLAS schedule. As of the end of 2001, 23 feedthrough assemblies have been produced and tested, and 21 are at CERN. An average production rate of 3 assemblies per month, including tests, is expected (a peak production rate of 3 assemblies in 22 days was achieved). It is expected that Canada's involvement in the feedthrough installation will end during 2003 with the connection of the warm cables to the ambient flange.

#### Canadian participants in ATLAS

Investigators: J. McDonald, J. Pinfold, M. Vincter (Alberta); D. Gingrich, P.W. Green (Alberta/TRIUMF); J. Armitage, M. Dixit, G. Oakham (Carleton); P. Depommier, C. Leroy, J.-P. Martin (Montréal); G. Azuelos (Montréal/TRIUMF); G. Couture (Montréal/UQAM); M.C. Vetterli (SFU/TRIUMF); D.C. Bailey, R.S. Orr, P. Sineruo, W. Trischuk (Toronto); P. Krieger, J.F. Martin (Toronto/IPP); M. Losty, C. Oram (TRIUMF); D. Axen (UBC); A. Astbury, R. Keeler, M. Lefebvre (Victoria); R. McPherson, R. Sobie (Victoria/IPP); S. Bhadra (York).

Collaborators: S. Liu, R. Soluk, S. Wheeler (Alberta); B. Caron (Alberta/TRIUMF); M. Khakhzad (Carleton); R. Mehdiyev (Montréal); Kyung Kwang Joo (Toronto); S. Chekulaev, H. Stenzel, M. Wielers (TRIUMF); M. Fincke-Keeler, N. Kanaya (Victoria).

Graduate students: N. Buchanan, L. Chen, C. Cojocaru, B. Dowler, J. de Jong, R. McDonald, Wei-Yuan Ting (Alberta); G. Belanger, B. Williams (Carleton); P.H. Beauchemin, G. Fubiani, M.H. Genest, C. Lebel, R. Mazini, F. Marullo, P. Roy (Montréal); K. Martens (Toronto); M. Dobbs, T. Ince, V. Singh (Victoria).



## The BaBar experiment at the Stanford Linear Accelerator Center

(C. Hearty, UBC)

### Introduction

BaBar is an experiment to study the electroweak sector of particle physics using  $B$  mesons produced at the high-luminosity  $e^+e^-$  collider PEP-II. The primary physics goal is to observe and quantify  $CP$  violation in  $B$  mesons, but more generally, it is to test the standard model description of electroweak physics and to look for new physics beyond the standard model. The charged weak force is described by the CKM matrix in the standard model, and the central physics goals of BaBar are often described in terms of overconstraining the “unitarity triangle”, a geometrical representation of the CKM matrix. In particular, a non-zero angle in the unitarity triangle would imply  $CP$  violation.

The BaBar detector was designed, constructed and assembled prior to the start of the first data run in October, 1999. The current data run started in January, 2001 and will continue until summer, 2002. The drift chamber, one of six major detector systems, was constructed at TRIUMF. It is performing well: the observed mass resolution for  $J/\psi$  mesons decaying to muon pairs is  $12.3 \pm 0.3 \text{ MeV}/c^2$ , consistent with the value of  $12.0 \pm 0.1 \text{ MeV}/c^2$  predicted by simulation (Fig. 16).

### Observation of $CP$ violation in $B$ mesons

2001 was a productive year for BaBar, with numerous interesting physics results. The most exciting of these is the first observation of  $CP$  violation in  $B$  mesons. This measurement compares the decay rates

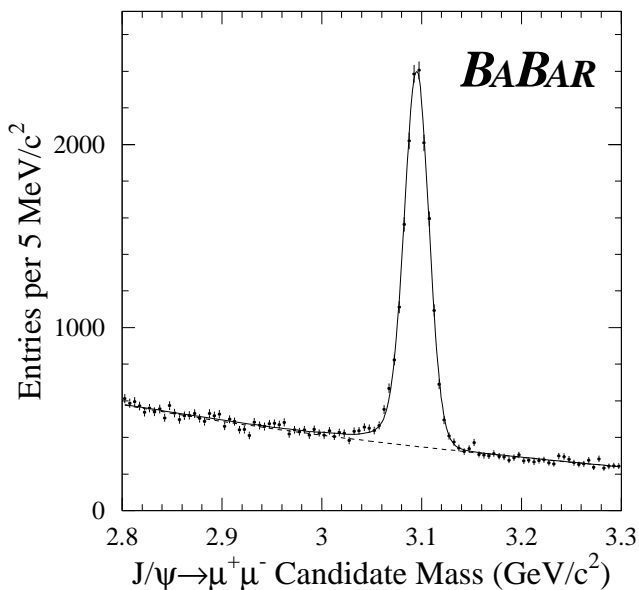


Fig. 16.  $J/\psi$  mesons reconstructed in BaBar via decay to a muon pair.

of  $B^0$  and  $\bar{B}^0$  mesons to  $CP$  eigenstates, where the rates would be identical if  $CP$  were a good symmetry of nature.  $B$  mesons at BaBar are produced in  $B^+B^-$  or  $B^0\bar{B}^0$  pairs in the decay of an  $\Upsilon(4S)$  resonance. The events useful in the asymmetry analysis are those in which one  $B^0$  meson decays to a  $CP$  eigenstate, such as  $J/\psi K_S$ , and the other decays in such a way that it can be “tagged”. Tagging consists of partially reconstructing the decay products for the purpose of detecting whether the original meson was a  $B^0$  or a  $\bar{B}^0$ .

The most recent results use a sample of 62 million  $\Upsilon(4S)$  decays recorded in  $56 \text{ fb}^{-1}$  of data. A total of 1848  $B^0$  meson candidates are reconstructed in the following final states:  $J/\psi K_S$ ,  $J/\psi K_L$ ,  $\psi(2S)K_S$ ,  $\chi_{c1}K_S$  and  $J/\psi K^{*0}$ , with an average purity of 80%. This total includes only those events in which the other  $B^0$  has been tagged. The effective tagging efficiency (including the dilution of the signal due to incorrect tagging) is 25%.

The asymmetry between  $B^0$  and  $\bar{B}^0$  is illustrated in Fig. 17. The corresponding measurement of the unitarity triangle is  $\sin 2\beta = 0.75 \pm 0.09$  (statistical)  $\pm 0.04$  (systematic). This clearly demonstrates the violation of  $CP$  in the  $B$  system.

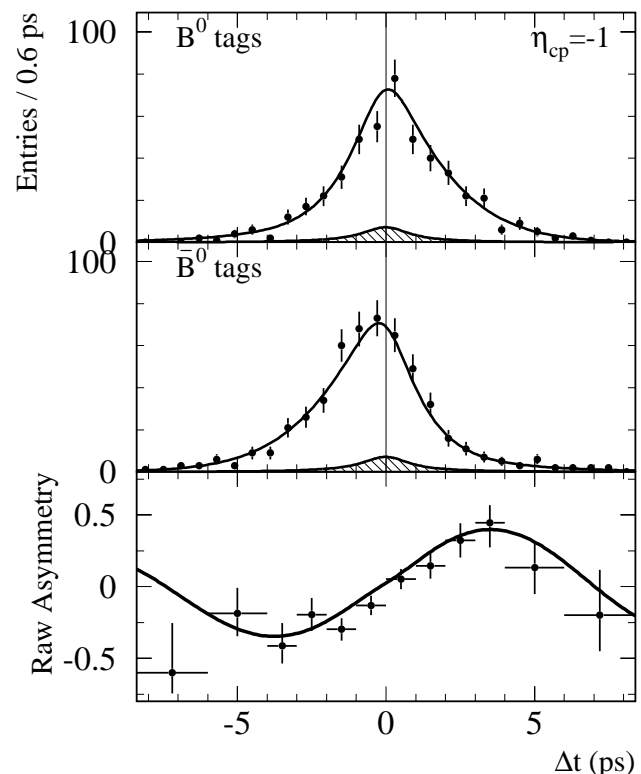


Fig. 17. Number of  $CP$  final state candidates (top) with a  $B^0$  tag  $N_{B^0}$ , (middle) with a  $\bar{B}^0$  tag  $N_{\bar{B}^0}$ , and (bottom) the raw asymmetry  $(N_{B^0} - N_{\bar{B}^0}) / (N_{B^0} + N_{\bar{B}^0})$ , as functions of the time difference between the signal and tag decay.

## Activities of the local group

The local group has led the analysis for two publications in 2001. One analysis was the first observation of the direct production of  $J/\psi$  mesons in  $e^+e^-$  annihilation. These mesons were distinguished from the much more copious production in  $B$  decay by using data recorded at energies below the threshold for  $B\bar{B}$  production, and by using  $J/\psi$  mesons with momentum higher than kinematically possible for  $B$  decay. This analysis has helped illuminate the production mechanisms of heavy quarkonia, such as non-relativistic QCD.

The second paper determined the branching fractions of the  $\psi(2S)$  to  $e^+e^-$  and  $\mu^+\mu^-$ . The  $\psi(S)$  mesons are widely used in reconstructing  $B$  mesons, and the previous precisions of these quantities were a limiting factor in a number of analyses.

The group has more recently started collaborating with colleagues at the University of Victoria on a search for the as-yet undiscovered decay  $B \rightarrow K\nu\bar{\nu}$ . This is a rare, flavour-changing neutral current process that occurs via loops in the standard model. It is a theoretically clean process with a rate that is sensitive to supersymmetry or other physics beyond the standard model.

## Outlook

The success of BaBar is due largely to the success of PEP-II, which has consistently delivered luminosity above the design value. In 2001, for example, BaBar recorded  $39.5 \text{ fb}^{-1}$  of data, compared to a design value of  $30 \text{ fb}^{-1}$ . This trend is anticipated to continue. The high luminosity will permit BaBar to determine a second angle of the unitarity triangle and to accurately measure the length of its sides. It will also permit a wide range of searches for rare  $B$  decays, possibly exposing new physics.

## BNL E787/949/KOPIO

### Measurement of $K \rightarrow \pi\nu\bar{\nu}$ and other rare decays

(D. Bryman, UBC)

The rare kaon decays  $K^+ \rightarrow \pi^+\nu\bar{\nu}$  and  $K_L^0 \rightarrow \pi^0\nu\bar{\nu}$  offer unique opportunities to scrutinize higher order phenomena associated with quark mixing and charge-parity ( $CP$ ) non-invariance. Initial data from Experiment E787 at Brookhaven National Laboratory (BNL) yielded the first evidence for the  $K^+ \rightarrow \pi^+\nu\bar{\nu}$  decay. This year the final result from E787 was reported [Adler *et al.*, Phys. Rev. Lett. **88**, in press] based on the full data set which doubled the previously reported sensitivity. The branching ratio remains consistent with the standard model (SM) expectation.

To fully explore the possibility of new physics, or to make a precise measurement of the  $t-d$  quark coupling

$|V_{td}|$ , requires a new measurement capable of a single event sensitivity of  $B(K^+ \rightarrow \pi^+\nu\bar{\nu}) = (8-14) \times 10^{-12}$ , roughly an order of magnitude below the SM prediction. Substantial upgrades to the E787 detector system have been made during the past two years in preparation for a continued experiment, E949, aimed at reaching this sensitivity. In 2001, E949 commenced with a brief engineering run starting in September. The Alternating Gradient Synchrotron (AGS) will be operated for E949 in conjunction with its role as injector to the Relativistic Heavy Ion Collider (RHIC). Injection is planned roughly twice per day, leaving more than 20 hours per day available for AGS slow extracted beam. With the completion of E949, the possibility of an inconsistency with the SM prediction of  $B(K^+ \rightarrow \pi^+\nu\bar{\nu})$  will be fully explored, or the important top-down quark mixing parameter will be determined to a precision of 15-30% if the SM expectation is confirmed.

Despite an enormous worldwide effort in  $B$  physics, it has become evident that the  $K$  sector can yield the single most incisive measurement in the study of direct  $CP$  violation through a measurement of the branching ratio for  $K_L^0 \rightarrow \pi^0\nu\bar{\nu}$ . In the context of the SM  $B(K_L^0 \rightarrow \pi^0\nu\bar{\nu})$  is a unique quantity which directly measures the common area of the CKM unitarity triangles, i.e. the physical parameter that characterizes all  $CP$  violation phenomena, or, alternately, the height of the triangle. Measurements of both  $B(K_L^0 \rightarrow \pi^0\nu\bar{\nu})$  and  $B(K^+ \rightarrow \pi^+\nu\bar{\nu})$  will allow the unitarity triangle to be precisely reconstructed from  $K$  decay information alone. Thus, a complete picture of standard model  $CP$  violation in the  $K$  system will result and a comparison with comparably precise measurements anticipated from the  $B$  sector will be enabled.

The challenges of measuring  $B(K_L^0 \rightarrow \pi^0\nu\bar{\nu})$ , expected to occur at  $3 \times 10^{-11}$ , have been taken up by the KOPIO collaboration. KOPIO will employ a low energy, time structured  $K_L^0$  beam from the BNL AGS to allow determination of the incident kaon momentum. The goal of KOPIO is to obtain about 50 events with a signal to background ratio of at least 2:1. This will yield a statistical uncertainty in the measurement of the area of the CKM unitarity triangle of less than 10%. KOPIO is presently in an R&D phase.

## Final results from E787

The decay  $K^+ \rightarrow \pi^+\nu\bar{\nu}$  is very sensitive to the magnitude of the coupling of top to down quarks,  $V_{td}$ , in the Cabibbo-Kobayashi-Maskawa quark mixing matrix. In the context of the standard model (SM), the predicted branching ratio is  $B(K^+ \rightarrow \pi^+\nu\bar{\nu}) = 0.75 \pm 0.29 \times 10^{-10}$  [Buras, preprint hep-ph/0101336 (2001); Buras and Fleischer, preprint hep-ph/0104238 (2001); Buchalla and Buras, Nucl. Phys. **B548**, 309

(1999)]. In the earlier E787 study, a single event consistent with the decay  $K^+ \rightarrow \pi^+ \nu \bar{\nu}$  at a branching ratio of  $B(K^+ \rightarrow \pi^+ \nu \bar{\nu}) = 1.5_{-1.2}^{+3.5} \times 10^{-10}$  was found [Adler *et al.*, Phys. Rev. Lett. **84**, 3768 (2000) and Phys. Rev. Lett. **79**, 2204 (1997)].

The observable signature for  $K^+ \rightarrow \pi^+ \nu \bar{\nu}$  decay from kaons at rest involves only the  $\pi^+$  track and  $\pi^+$  decay products. Major background sources include the two-body decays  $K^+ \rightarrow \mu^+ \nu_\mu$  ( $K_{\mu 2}$ ) and  $K^+ \rightarrow \pi^+ \pi^0$  ( $K_{\pi 2}$ ), pions scattered from the beam, and  $K^+$  charge exchange (CEX) reactions resulting in decays  $K_L^0 \rightarrow \pi^+ l^- \bar{\nu}_l$ , where  $l = e$  or  $\mu$ . In order to make an unambiguous measurement of  $B(K^+ \rightarrow \pi^+ \nu \bar{\nu})$ , it is advantageous to suppress all backgrounds well below the signal level.

The additional data discussed here were acquired during the 1998 run of the AGS. The kaons were stopped in a scintillating fibre target used for kaon and pion tracking. Measurements of the momentum ( $P$ ), range ( $R$ ), and kinetic energy ( $E$ ) of charged decay products were made using the target, a central drift chamber, and a cylindrical range stack (RS) with two layers of tracking chambers embedded in it, all within a 1 T solenoidal magnetic field. The  $\pi^+ \rightarrow \mu^+ \rightarrow e^+$  decay sequence from pions which came to rest in the RS was observed using 500 MHz transient digitizers. Photons were detected in a nearly  $4\pi$  14-radiation-length-thick calorimeter array of either lead/scintillator sandwich or undoped CsI crystals.

To be accepted as a  $K^+ \rightarrow \pi^+ \nu \bar{\nu}$  candidate, a decay particle must be positively identified as a  $\pi^+$  by comparing  $P$ ,  $R$ , and  $E$  measurements, and by observation of the  $\pi^+ \rightarrow \mu^+ \rightarrow e^+$  decay sequence. Events containing other decay products including photons or beam particles were eliminated by detectors covering  $4\pi$  sr. The search was restricted to the measured momentum region  $211 < P < 229$  MeV/ $c$  between the  $K_{\mu 2}$  and  $K_{\pi 2}$  peaks. The maximum pion momentum from  $K^+ \rightarrow \pi^+ \nu \bar{\nu}$  decays at rest is 227 MeV/ $c$ .

Some new aspects of the analysis of the 1998 data set include applications of neural network techniques in the particle identification process and incorporation of improved routines to detect large angle scattering of particles in the range stack. In the 1998 exposure, the effective number of kaon stops was  $N_{K^+} = 2.7 \times 10^{12}$ , approximately 82% as large as all previous E787 data sets, and the acceptance was determined to be  $0.173 \pm 0.005 \pm 0.009\%$  giving a single event sensitivity of  $2.14 \times 10^{-10}$ .

The data analysis obtained detailed estimates of all backgrounds prior to examining the pre-determined signal region. In order to evaluate observed events, the parameter space of observables was subdivided into 7500 bins with differing levels of expected backgrounds.

To confirm the background estimates, the selection criteria were relaxed to allow about 14 times higher background, and all bins except those in the final signal region were examined. Two events were observed, in agreement with the number of expected background events  $\sum_{i=487}^{7500} b_i = 0.9 \pm 0.7$  for this region.

The signal region was defined to include the first 486 bins and was not examined until the final step in the analysis procedure. For the 1998 data set, the final candidate selection requirements were similar to those used previously, although more stringent track reconstruction criteria were imposed. Following the background study, the signal region was examined yielding one candidate event (event C). The kinematic values are  $P = 213.8 \pm 2.7$  MeV/ $c$ ,  $R = 33.9 \pm 1.2$  cm (in equivalent cm of scintillator), and  $E = 117.1 \pm 3.6$  MeV. A display of this event is shown in Fig. 18. Close inspection of Event C indicates that it is consistent with being due to  $K^+ \rightarrow \pi^+ \nu \bar{\nu}$  decay.

The combined result for E787 data taken between 1995 and 1998 is shown in Fig. 19, the range vs. kinetic energy of events surviving all other cuts. In Fig. 19 the box represents the signal region in which two events, A(1995) and C(1998) appear. Using a likelihood ratio technique [Junk, Nucl. Instrum. Methods **A434**, 435 (1999)] to determine the best estimate of the branch-

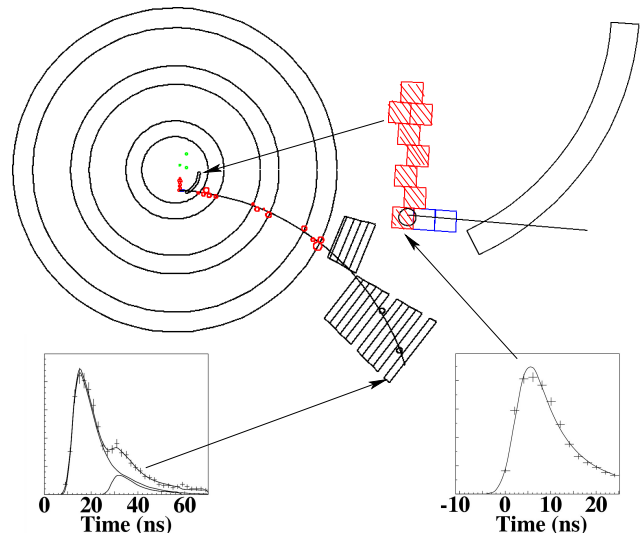


Fig. 18. Display of candidate event C. On the top left is the end view of the detector showing the track in the target, the drift chamber, and the range stack. On the top right is a blow-up of the track in the target, where the hatched squares represent target fibres hit by the  $K^+$  and the open squares indicate those hit by the  $\pi^+$ ; a trigger scintillator that was hit is also shown. The lower right-hand box shows the digitized signal in the target fibre where the kaon stopped, indicating no additional activity. The pulse was sampled every 2 ns (crosses) and the solid line is a fit. The lower left-hand box shows the digitized  $\pi \rightarrow \mu$  decay signal in the scintillator where the pion stopped. The curves are fits for the first, second and combined pulses.

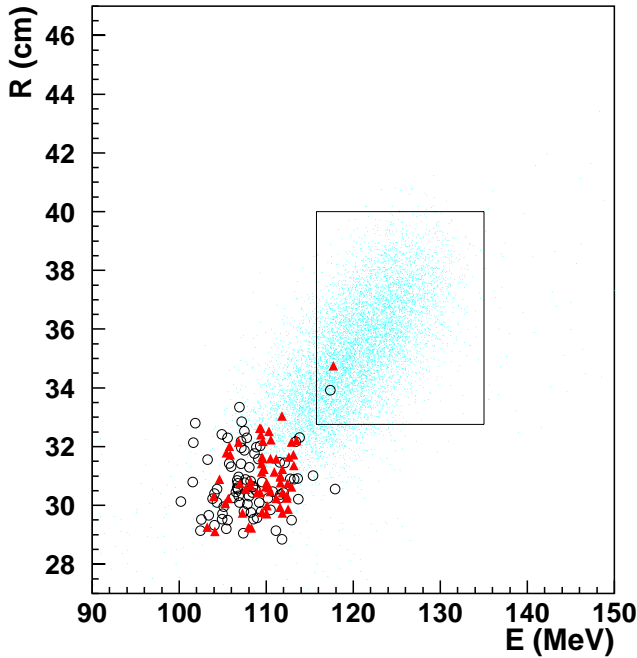


Fig. 19. Range vs. energy plot of the final sample. The circles are for the 1998 data and the triangles are for the 1995-97 data set. The group of events around  $E = 108$  MeV is due to the  $K\pi_2$  background. The simulated distribution of expected events from  $K^+ \rightarrow \pi^+\nu\bar{\nu}$  is indicated by dots.

ing ratio based on two observed events with their associated signal-to-background estimates, the determined acceptance, the number of  $K^+$  incident on the target, and the expected background levels, the result is  $B(K^+ \rightarrow \pi^+\nu\bar{\nu}) = 1.57_{-0.82}^{+1.75} \times 10^{-10}$  (68% C.L.). This result would be consistent with being due entirely to background only at the level of 0.02%.

Bounds obtained on  $|V_{td}|$  from  $B(K^+ \rightarrow \pi^+\nu\bar{\nu})$  are  $0.007 < |V_{td}| < 0.030$  (68% C.L.) or  $0.0051 < |V_{td}| < 0.033$  (90% C.L.) and do not require knowledge of  $V_{ub}$  or  $\epsilon_K$ . Alternatively, one can extract corresponding limits on the quantity  $|\lambda_t|$  ( $\lambda_t \equiv V_{ts}^* V_{td}$ ):  $2.9 \times 10^{-4} < |\lambda_t| < 1.2 \times 10^{-3}$ . In addition, the bounds  $-0.88 \times 10^{-3} < Re(\lambda_t) < 1.2 \times 10^{-3}$  can be obtained. For  $Im(\lambda_t)$ , an upper limit of  $Im(\lambda_t) < 1.1 \times 10^{-3}$  (90% C.L.) is found. The bounds on  $\lambda_t$  are derived without reference to the  $B$  system or to measurements of  $\epsilon_K$  or  $\epsilon'/\epsilon$ , and are of particular interest because  $Im(\lambda_t)$  is proportional to the area of the unitarity triangle.

The limit found in the search for decays of the form  $K^+ \rightarrow \pi^+ X^0$ , where  $X^0$  is a neutral weakly interacting massless particle [Wilczek, Phys. Rev. Lett. **49**, 1549 (1982)], is  $B(K^+ \rightarrow \pi^+ X^0) < 0.59 \times 10^{-10}$  (90% C.L.), based on zero events observed in a  $\pm 2\sigma$  region around the pion kinematic endpoint.

Progress has also been made to access the region below the  $K\pi_2$  peak. A complete analysis of data taken in 1996 has been performed at BNL leading to a back-

ground of  $1.0 \pm 0.5$  events expected at a sensitivity level of approximately  $10^{-9}$ , roughly an order of magnitude below the previous E787 results. Final results are in preparation for publication [Adler *et al.*, e-print archive: hep-ex/0201037].

E787 has also studied numerous other rare  $K$  and  $\pi$  decays and performed searches for many as-yet unobserved processes. In 2001 and late 2000, results were reported for the first high statistics measurement of the direct emission component of the radiative decay  $K^+ \rightarrow \pi^+\pi^0\gamma$  [Adler *et al.*, Phys. Rev. Lett. **85**, 4856 (2000)], as well as searches for the decays  $K^+ \rightarrow \pi^+\gamma$  [Adler *et al.*, Phys. Rev. **D** (in press)] and  $K^+ \rightarrow \pi^+\pi^0\nu\bar{\nu}$  [Adler *et al.*, Phys. Rev. **D63**, 032004 (2001)].

### E949

E949 is based on incremental upgrades to the techniques and technology of E787. Since E949 is expected to be the primary (or only) AGS user, the proton beam on target is intended to have an intensity of  $65 \times 10^{12}$  in a 4 s spill, giving a duty factor of 64%. This translates into an effective luminosity improvement of 56% over previous running conditions while keeping instantaneous rates at the same level. E949 running with higher instantaneous rates will also be attempted to increase the sensitivity.

Enhancements to the detector included improvements to the range stack inner layers and trigger counters (manufactured in Russia), elements of the photon veto systems, upgrade of the trigger system, and improvements to the data acquisition system for higher rates.

For E949, the TRIUMF group constructed a new set of more highly segmented beam counters in order to achieve improved spatial resolution where the incoming particle enters the target, and improved photon vetoing efficiency for photons coming back along the beam line. In E787 the escape of these photons was a major contributor to the overall photon detection inefficiency. The total number of hodoscope elements was doubled and re-designed to improve the  $X - Y$  spatial resolution. Each hodoscope element is read out by 3 wavelength shifting (WLS) double-clad 1 mm diameter fibres. In addition, a new “ring veto” will allow the detection and vetoing of particles which enter counter B4 near its outside edge.

In order to improve photon detection efficiency, the 3-radiation-length ( $X_0$ ) thick lead glass detector used in E787 has been replaced by a copper/scintillator sandwich active degrader (AD) of larger diameter. This detector consists of 40 layers of 2.2 mm thick copper interposed with 2 mm thick scintillator to give a total thickness of  $6.3 X_0$ . The scintillators are split into 12 azimuthal segments. Each segment is read out via

WLS fibres. The 12-fold segmentation was chosen to minimize the likelihood that a photon signal would be hidden by the much larger pulse deposited by an incoming kaon. Further photon detection is provided by a new upstream photon veto (UPV) counter located in front of the entrance to the magnet. This detector is a  $3 X_0$  lead/scintillator sandwich, also read out by WLS fibres with an aperture to allow the incident kaon beam to pass through without interacting.

The TRIUMF-built central drift chamber (UTC) was repaired to improve cathode foil signals which were affected by deteriorating foil-connector joints due to micro-cracks in the conductive epoxy. A longstanding problem associated with the cathode charge measurement system, caused by ADCs malfunctioning due to a tiny wrong-polarity undershoot from large pulses, was addressed by replacing the 768 pre-amplifiers and post-amplifier/discriminator electronics. As an additional benefit, the noise level in the ADC measurements dropped by a factor of 2–3, and improvements in the  $z$ -position resolution were obtained. In addition, we modified the anode front end electronics (1152 channels) to improve the signal transmission.

Several of the limited-streamer mode straw tube detectors (RSSC) required repair and a new electronics front end system was implemented to improve the performance of the  $z$ -coordinate measurement used to suppress backgrounds from scattered muons. The poor resolution was due to low pulse height time-walk effects and a new preamplifier-dual-discriminator front end system was designed and constructed. Tests indicate improvements in resolution by a factor of three to about 1.5 cm. This improved performance of the RSSCs will translate into much improved muon background rejection in E949.

The TRIUMF group participated substantially in many other E949 upgrade projects. Since the TRIUMF group maintains the E787/E949 software systems, major upgrades of the primary analysis shell were implemented to accommodate new hardware systems.

For the E949 engineering run in September–October, 2001, most of the upgrade elements were in place and commissioned. An 8–12 week data run is scheduled to begin in February, 2002.

## KOPIO

The KOPIO experiment is designed to observe and measure the rate of the decay  $K_L^0 \rightarrow \pi^0 \nu \bar{\nu}$  by observing a large sample of clean events. This goal will allow the SM  $CP$  violation parameter,  $\eta$ , to be determined to 15% accuracy with minimal contributions from background or systematic effects.

In the KOPIO design, a  $500 \mu\text{sr}$  solid angle neutral beam is extracted at  $45^\circ$  to produce a “soft”  $K_L$  spectrum peaked at  $0.65 \text{ GeV}/c$ ; kaons in the range from

about  $0.5 \text{ GeV}/c$  to  $1.3 \text{ GeV}/c$  will be used. Downstream of the final beam collimator is a 3.5 m long decay region which is surrounded by the main detector. Approximately 16% of the kaons decay, yielding a decay rate of about 25 MHz. The beam region is evacuated to a level of  $10^{-7}$  torr to suppress neutron induced  $\pi^0$  production. The decay region is surrounded by an efficient Pb/scintillator photon detector which serves to veto photons and charged particles. In the forward detection region the primary photon detector system, illustrated in Fig. 20, consists of two sections: a fine grained preradiator (PR) in which the photons are converted, followed by an  $18 X_0$  calorimeter in which the remaining energy of the photon shower is measured. The PR functions to measure the photon positions and directions accurately in order to allow reconstruction of the  $K_L$  decay vertex, while also contributing to sufficient energy resolution. The calorimeter is constructed using Pb/scintillator layers. In the barrel and upstream regions, a Pb/scintillator combination will also be used to obtain high veto efficiency. Downstream of the main  $\pi^0$  detector, a beam hole photon counter (“beam catcher”) consists of Čerenkov detectors designed to be insensitive to neutrons.

The Canadian group’s main hardware contribution to KOPIO is the PR detector system which consists of 64  $0.03 X_0$  layers (total effective thickness of  $2 X_0$ ), each with plastic scintillator, metal converter and dual-coordinate drift chambers. The requirements include a photon angular resolution of approximately 25 mr, a photon conversion efficiency of about 0.7 ( $2.0 X_0$ ), a good measurement of the deposited energy, and as short as possible linear extent so as to limit shower size at the calorimeter.

The principle employed is to measure the positions and angles of the first  $e^+e^-$  pair following photon conversion in a series of thin converter/detector modules. Each PR module consists of an inactive converter material, a dual coordinate drift chamber (anode wires and cathode strips) and a scintillator. The chambers provide the position measurements and the scintillation counters are used for triggering, timing, and energy loss measurement. To keep multiple Coulomb scattering at the 25 mr level the PR layers are thin ( $\leq 0.034 X_0$ ), are separated by about 1 cm, and have position resolution of between 150 and 200  $\mu\text{m}$ . In addition, the energy deposited in the preradiator will be measured with sufficient precision to allow the full energy measurement (including the PR and the calorimeter) to be better than  $3.0\%/\sqrt{E}$  (GeV).

This method of measuring the photon directions has been confirmed experimentally by KOPIO in a proof-of-principle measurement in a tagged photon beam at BNL LEGS, and the expected angular

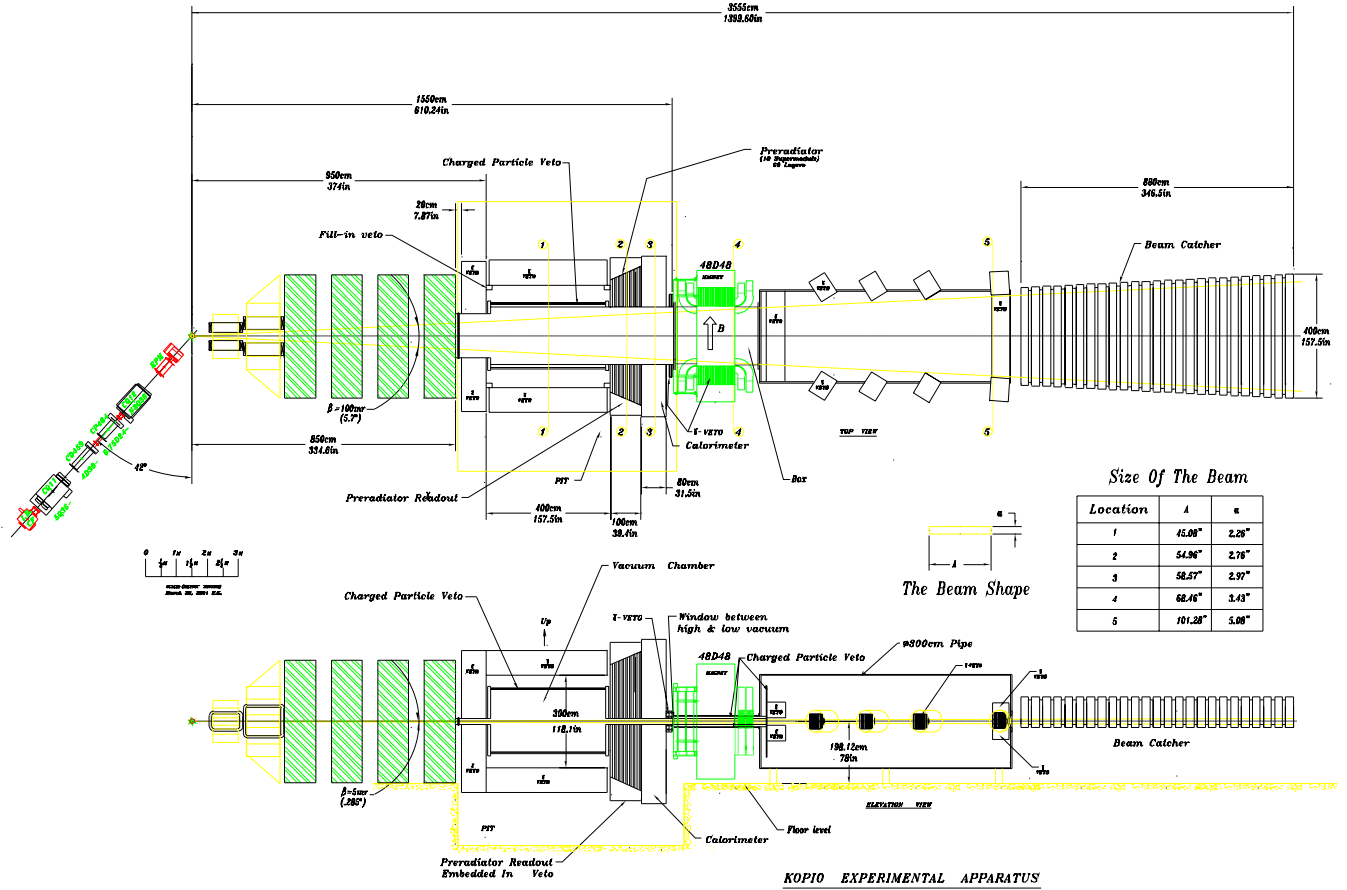


Fig. 20.  $K_L^0 \rightarrow \pi^0 \nu \bar{\nu}$  detector.

resolution for photons was determined by GEANT simulation with 3.4%  $X_0$  per layer and assuming 150  $\mu\text{m}$  position resolution for the measurements of  $e^+e^-$  pairs.

Several chamber prototypes are being constructed. Five small (8 cm  $\times$  15 cm) chambers were fabricated to test the basic cell design and construction technique mentioned above. These gave the expected level of performance. The maximum drift time using an Ar/ethane mixture was measured to be 70 ns with full efficiency. For  $\text{CF}_4$ /isobutane mixtures, we expect 35 ns maximum drift. These chambers were assembled in a stack to study tracking properties using different chamber parameters. Two larger (30 cm  $\times$  30 cm) chambers were also constructed and are being readied for testing.

Other chamber structures will be full length devices in each of the anode and cathode dimensions (200 cm  $\times$  20 cm) primarily for electronics development. The next step will be chambers approximately 50 cm  $\times$  50 cm in size to be used in stacks of eight to test the tracking and energy measurement performance in test beams at TRIUMF and BNL LEGS using pre-production electronics. The final prototype will be a full size pre-production model.

The anodes and cathodes of each preradiator layer will be read out and digitized individually at the chamber; only digitized information will be taken from the chamber area. The electronics is designed to be a fully pipelined dead-timeless system. The analogue electronics for the cathode strips contains a charge amplifier, shaper, and a 10-bit 40 MHz A/D converter followed by a programmable logic device which includes memory, peak detection (to represent the charge integral), pedestal subtraction, data sparsification and readout. The timing electronics employs a fast amplifier and a discriminator followed by a time-memory-cell VLSI chip. We are investigating the use of several ASICs designed for ATLAS and CMS.

The scintillator planes interposed between the chambers will be read out in strips using wavelength shifting fibres. The fibres will be oriented to read alternating coordinates in vertical, horizontal and diagonal directions. The latter will be used to help resolve multiple hits on the other two planes. The scintillator planes also extend beyond the preradiator wirechamber dimensions to provide a veto halo for photons whose showers are not fully contained in the preradiator/calorimeter.

The scintillator planes need to be of highly uniform thickness and flatness in order to also serve as a vital structural element supporting the wire chambers. The possibility of using extrusion techniques to manufacture “planks” which can be bonded together into the large planes is being investigated.

### The HERMES experiment

(C.A. Miller, S. Yen, TRIUMF; M.C. Vetterli, SFU/TRIUMF; M.G. Vincet, Alberta)

The HERMES experiment has been recording data for 6 years, investigating primarily the spin structure of the nucleon, but also a rich variety of other topics in QCD physics. The unique capabilities of the experiment include a pure nuclear-polarized atomic gas target in a 27.5 GeV stored polarized electron beam. The spectrometer has acceptance sufficient to detect hadrons associated with the scattered electron, with complete hadron identification by a dual-radiator ring-imaging Čerenkov detector. An extensive data set has been accumulated, which is under continuing analysis. The final results are expected to achieve the main goals set out in the original proposal. Simulations based on the preliminary results indicate that the flavour separation of the polarized quark distributions will be complete, with sensitivity to even a  $\bar{u}/\bar{d}$  sea flavour asymmetry at a precision that can distinguish between model predictions. These preliminary results are expected to be released in early 2002. In the meantime, several new HERMES results have appeared in both polarized and unpolarized QCD physics, many benefiting from the much thicker unpolarized gas targets that are now used near the end of every HERA beam fill.

### Beam spin transfer to $\Lambda$ 's

It has been proposed that one could obtain additional information on the polarized quark distributions in the baryons of the spin 1/2 octet through the production of  $\Lambda$  hyperons in polarized deep-inelastic lepton scattering. By measuring the polarization of the  $\Lambda$ 's that are likely to have originated from the struck quark (so-called “current fragmentation”), the longitudinal spin transfer  $D_{LL}^{\Lambda}$  can be determined. This quantity is defined as the fraction of the virtual photon polarization transferred to the  $\Lambda$ . In the naive quark parton model (QPM) the spin of the  $\Lambda$  is entirely due to the strange quark, and the up and down quark polarizations are zero. On the other hand, assuming SU(3) flavour symmetry, the up, down and strange quark distributions (and fragmentation functions) for the  $\Lambda$  can be related to those in the proton. If existing data on hyperon decays and polarized structure functions of the nucleon are interpreted in the framework of SU(3) symmetry, the first moments of the polarized up and

down quark distributions in the  $\Lambda$  can be estimated to be about  $-0.2$  each. If one assumes in addition that quark helicity is conserved in the fragmentation process, one obtains this same negative value for the expected spin transfer from a struck up or down quark to the  $\Lambda$ . A measurement of the spin transfer thus has the potential to provide information on the spin structure of the  $\Lambda$  hyperon.

Longitudinal spin transfer in  $\Lambda$  production has previously been studied at the  $Z^0$  pole at LEP. In the standard model, strange quarks (or quarks of charge  $-1/3$  in general) produced via  $Z^0$  decays have an average polarization of  $-0.91$ . Both the ALEPH and OPAL collaborations have reported a measurement of the  $\Lambda$  polarization of about  $-0.3$  for  $z > 0.3$ . (Here,  $z$  is the fraction of the available energy carried by the  $\Lambda$ .) These data are consistent with the naive constituent quark model, but their interpretation is not unique as all three light quark flavours contributed significantly to the production of  $\Lambda$  hyperons, with the strange quark playing the dominant role. By contrast,  $\Lambda$  production in deep-inelastic lepton scattering is dominated by scattering on up quarks. Hence such experiments with a polarized lepton beam provide a means to distinguish between the various models of the  $\Lambda$  spin structure, and to investigate further the degree of helicity conservation in the fragmentation process.

The polarization of  $\Lambda$  hyperons can be measured via the weak decay channel  $\Lambda \rightarrow p\pi^-$ , through the angular correlation of the final state. HERMES has extracted about  $10^4$   $\Lambda$  events from the 1999/2000 data sets. In the current fragmentation region, where the Feynman  $x_F$  variable is positive, the spin transfer is found to be consistent with zero:  $D_{LL}^{\Lambda} = 0.04 \pm 0.08(\text{stat}) \pm 0.03(\text{syst})$ , again supporting the naive quark model. On the other hand, other experiments in the target fragmentation region ( $x_F < 0$ ) result in negative values, as shown compared to the HERMES data in Fig. 21. The neutrino results suggest a mechanism in which the spin of  $s\bar{s}$  pairs pre-existing in the target anticorrelates with the spin of the struck quark.

### Quark-hadron duality

When protons are probed by electrons at energies large compared to the proton mass with correspondingly large 4-momentum transfers ( $-Q^2$ ), the scattering probability (summarized in the structure function  $F_2(W^2, Q^2)$  where  $W$  is the invariant mass of the initial photon nucleon system) is rather simple. It exhibits the well known property of scale invariance where  $F_2 \sim F_2(W^2/Q^2)$ , with small corrections that are well understood from perturbative QCD. The magnitude of  $F_2(W^2/Q^2)$  is proportional to the sum of the squares of the parton (quark and antiquark) charges.

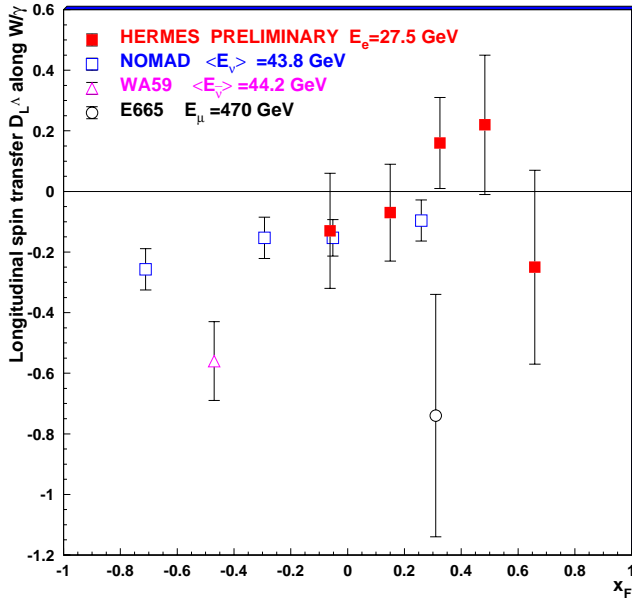


Fig. 21. Longitudinal spin transfer  $D_{LL}^{\Lambda}$ , from the lepton beam to the detected  $\Lambda$ , from HERMES (filled symbols) and other experiments (empty symbols).

Before the advent of QCD, Bloom and Gilman discovered an empirical property of the data, namely that the electroproduction of  $N^*$ 's at lower energies and momentum transfers averages smoothly around the scaling curve measured at large momentum transfers. During the subsequent three decades, and especially following the advent of quantum chromodynamics, this enigma has received considerable theoretical attention. The literature has primarily focused on understanding how the  $Q^2$  dependence of resonance excitation can conspire to mimic the  $x' \sim \frac{Q^2}{W^2+Q^2}$  dependence of the deep-inelastic data.

Recent precise unpolarized data from Jefferson Lab have shown that this duality is observed for both proton and neutron targets, at least for spin averaged scattering. This has sparked a renewed interest in the origin of low energy duality, and in the circumstances whereby  $F_2(x')$  – whose magnitude is in proportion to the sum of the squares of the (quark and antiquark) constituent charges – can in general match with the excitation of individual resonances which is driven by the coherently summed square of constituent charges. HERMES has recently released the first experimental evidence for the validity of duality for spin degrees of freedom. Longitudinally polarized positrons were inelastically scattered from longitudinally polarized protons, with values of  $Q^2$  between 1.2 and 12  $\text{GeV}/c^2$  and values of  $W$  between 1 and 2  $\text{GeV}$ . Figure 22 shows the double-spin asymmetry of the cross section in this nucleon resonance domain, compared to the existing world data for the same observable measured in deep-inelastic scattering at larger  $Q^2$  but at the same values

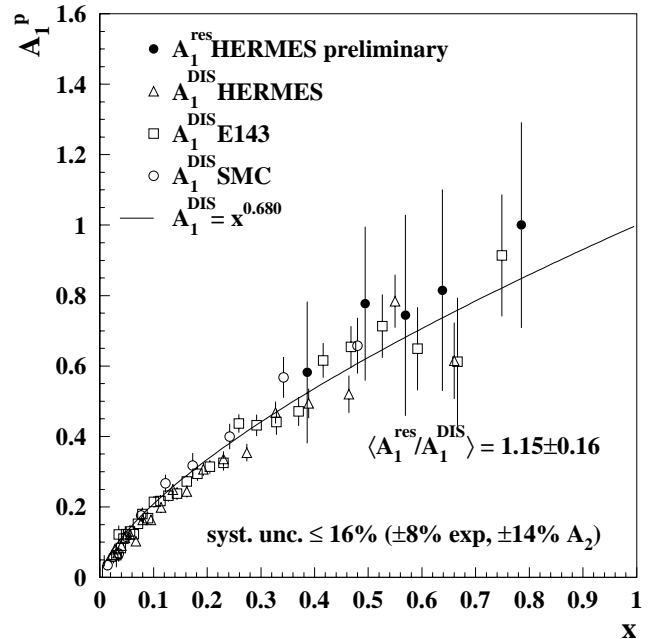


Fig. 22. Photo-absorption spin asymmetries  $A_1$  as a function of  $x$  measured in the resonance region (filled circles). The error bars represent the statistical uncertainties; the systematic uncertainty is about 16%. The empty symbols are previous results obtained in the DIS region, and the curve represents a phenomenological fit to DIS data at  $x > 0.03$ .

of the Björken scaling variable  $x$ . Unlike earlier such resonance asymmetries from SLAC at lower values of  $Q^2$ , these are found to be consistent with the DIS asymmetries. This implies that the description of asymmetries in terms of quark degrees of freedom applies also in the resonance region, for  $Q^2 > 1.6 \text{ GeV}/c^2$ .

#### Fragmentation functions

Much of the HERMES spin physics program depends on *semi*-inclusive DIS measurements, in which the detection of a hadron produced by fragmentation of the struck quark serves to “tag” the flavour of that quark. The interpretation of these data in turn depends on our knowledge of the fragmentation functions that describe the probabilities that a quark of a particular flavour will fragment to a particular type and charge state of hadron. There exists a large set of data on fragmentation functions, as well as phenomenological QCD-motivated parametrizations and Monte Carlo models that well represent these data. However, most of these data were measured at energies higher than the beam energy used by HERMES. Therefore, it is important to confirm that the fragmentation process is well understood also at this lower beam energy.

HERMES has recently published a study of the multiplicities of both charged and neutral pions produced in DIS. Multiplicities are closely related to fragmentation functions – they differ only due to breaking



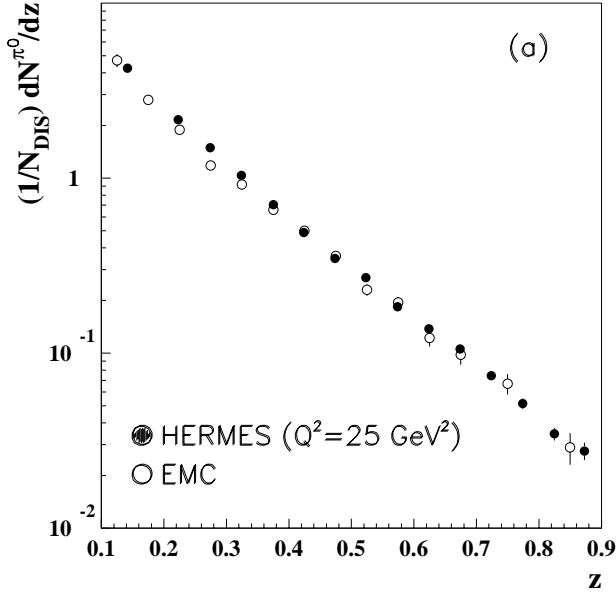


Fig. 23. Multiplicities for neutral pions from the HERMES and EMC experiments. The HERMES results have been evolved to  $Q^2 = 25 \text{ GeV}^2$  using the NLO QCD model of Kniehl, Kramer and Pötter [2000]. Only statistical uncertainties are shown. The systematic uncertainties are 9% for HERMES and  $\leq 13\%$  for EMC.

of isospin symmetry ( $D_u^\pi = D_d^\pi$ , where  $\pi$  represents the sum of positive and negative pions) and the contributions of the strange quark. Figure 23 shows a comparison of the multiplicities of neutral pions measured by the HERMES and EMC experiments at energies that differ by about an order of magnitude. The HERMES results have been evolved to  $Q^2 = 25 \text{ GeV}^2$  using a NLO QCD model that unifies all of the world data on fragmentation functions. The level of agreement is remarkable. It is less so in the case of charged pions, but in this case only actual fragmentation functions are available from EMC, precluding a direct comparison.

#### Transverse momenta of hadrons from DIS

By studying the average transverse momenta  $\langle P_\perp \rangle$  of hadrons produced by fragmentation of a quark that has absorbed an energetic virtual photon, it is possible to extract information about both the distribution in the primordial momentum component of quarks in the target nucleon transverse to its (infinite) momentum, and the transverse momentum produced in the fragmentation process. It is possible to disentangle these two contributions because that from the target tends to dominate at large values of  $z$  (the fraction of the energy of the virtual photon transferred to the hadron), indicating that the hadron probably emerged early in the fragmentation process before its direction was thereby smeared, while that from fragmentation appears at lower values of  $z$  where the hadron probably emerged after a larger number of fragmenting interactions. HERMES has recently released such

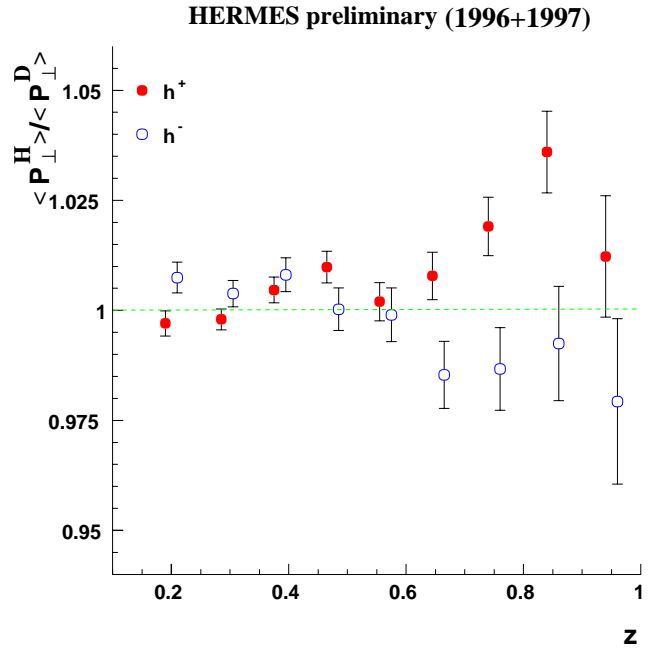
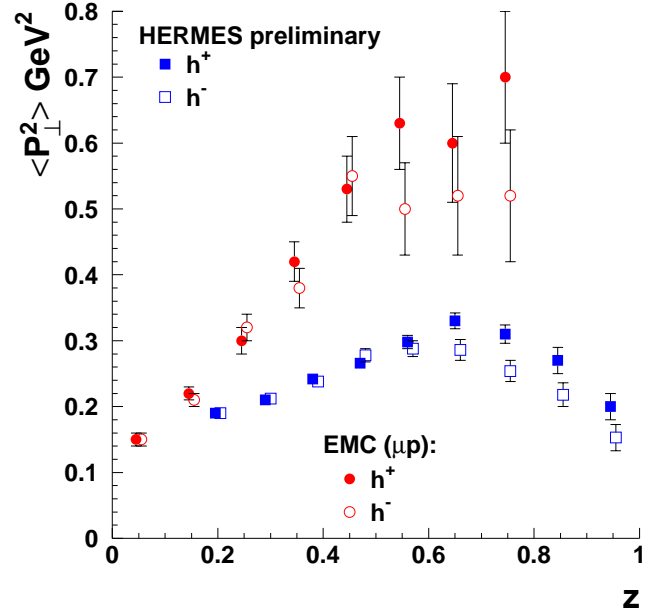


Fig. 24. The dependence of the mean square momentum component of electroproduced hadrons transverse to the direction of the virtual photon, as a function of the fraction of the photon's energy carried by the hadron. The top frame shows data from the hydrogen target, while the bottom frame shows the ratio of values for hydrogen to those for deuterium.

data with sufficient statistical precision to clearly reveal a new phenomenon. Figure 24 (top) shows these results for  $\langle P_\perp^2 \rangle$  as a function of  $z$ , compared to earlier measurements from the EMC measurement at much higher energy. It is intriguing that the change of slope at large  $z$  depends on the sign of the hadron charge. Some of this effect may be due to a flavour dependence of the primordial momentum of the quarks in the

target. Up quark dominance arising from the square of the charge ratios  $(+2/3)^2$  versus  $(-1/3)^2$  appearing in the photoabsorption cross sections implies that positive hadrons are predominantly produced from up quarks, while negative hadrons are produced from a more equal balance of up and down. Hence the data imply that up quarks have larger primordial  $P_1$ . This is supported by the dependence on the isospin of the nucleon target, shown in Fig. 24 (bottom).

Unanticipated discoveries revealed by the existing HERMES data, together with recent dramatic theoretical progress in the understanding of QCD bound states through the exploitation of exclusive reactions, have inspired a revitalized experimental program for HERMES. This program has been approved by the DESY Programme Review Committee (PRC), leading to a promise by DESY that HERMES can run at HERA through 2006. First on this agenda is a measurement of transversity – the last unmeasured leading-twist structure function of the nucleon. In preparation for this, during the 9-month long shutdown of the HERA accelerator in 2001 for the Luminosity Upgrade, a transversely-polarized atomic gas target has been installed, and is now operational. The spectrometer is also ready, including a new silicon tracker close to the target – the “A Wheels”. Among other advantages, this tracker will greatly enhance the acceptance for decay products of  $\Lambda$  hyperons, whose self-analyzing polarization carries information about the polarizations of target quarks.

The HERMES Collaboration is still building for the future. Reflecting the intense current interest in unambiguously identifying exclusive processes, the DESY PRC has now approved a proposal to construct a new recoil detector to provide large acceptance for low energy recoil target nucleons from such reactions. It is planned to be ready for running in 2004. Most of the funding is now in place. Also, the Collaboration has been strengthened by the addition of several new institutes. These include Giessen, Glasgow, IHEP Protvino, Warsaw, and soon Beijing. The Canadian group has recently welcomed two new research associates, who are focusing on extracting more physics results from the wealth of HERMES data.

### KEK Expt. 246 and 470 (Japan-Russia-Canada-Korea-U.S.A. Collaboration)

#### Kaon decay studies

(*M.D. Hasinoff, UBC; J.A. Macdonald, B. Shin, TRIUMF*)

The apparatus that was constructed at the KEK 12 GeV Proton Synchrotron (PS) for the search for  $T$ -violation in the transverse polarization ( $P_T$ ) of muons in  $K^+ \rightarrow \pi^0 \mu^+ \nu_\mu$  ( $K_{\mu 3}^+$ ) decay is also well suited to precision studies of other kaon decay modes. The

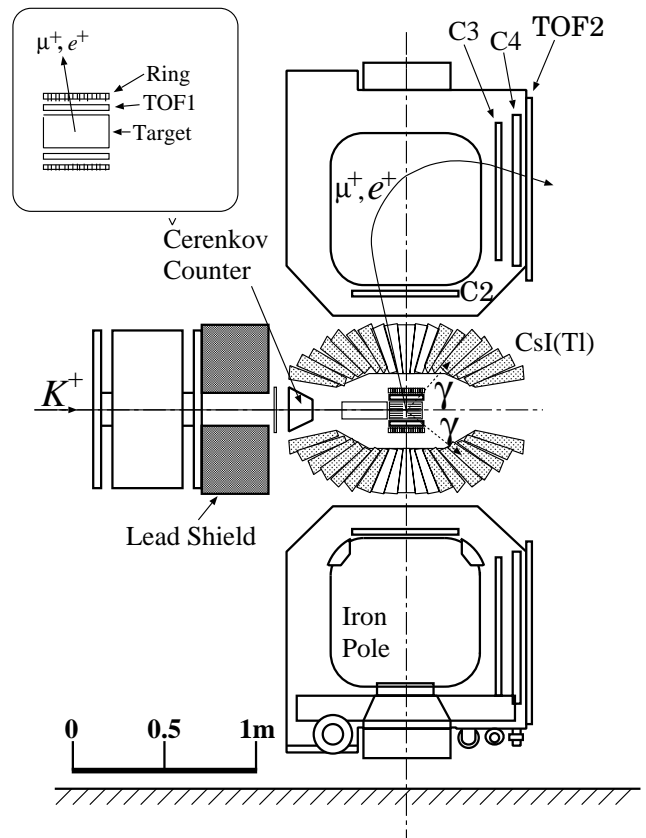


Fig. 25. Cross sectional side view of the detector, not showing the  $\mu$  polarimeter which is located to the immediate right of TOF2. Assembly detail of the central region is shown in the inset.

detector, shown in Fig. 25, consists of an active scintillating-fibre target which serves as a kaon stopper and vertex detector, a CsI(Tl) calorimeter system which detects photons including  $\pi^0$  decay, and a superconducting toroidal magnet spectrometer system to analyze and select  $\mu^+$ 's,  $e^+$ 's, and  $\pi^+$ 's. A muon polarimeter system, not shown in Fig. 25, is located at the quasi-focal planes of the toroidal magnet gaps. The complete kinematics from stopped  $K$ -decay can be reconstructed from the charged track obtained in the target, ring scintillators and spectrometer tracking chambers, and from photons and  $\pi^0$ 's in the photon detector array.

The  $T$ -violation search has been described in previous Annual Reports and the final data-taking was completed in 2000. During 2001 analysis effort was directed at the total data set taken since 1996. About two thirds of the data, through 1998, has yielded a result consistent with the standard model expectation of no  $T$ -violation. However, the inclusion of the data from the later runs has not been completed since they were taken under sufficiently different conditions that several systematic effects have required additional study.

Analysis of  $K_{\ell 3}$  decays, where  $\ell = \mu$  or  $e$ , was carried out in 2001. A reanalysis [Levchenko *et al.*, Proc. 3rd Int. Conf. on Nonaccelerator New Physics (NAN-Pino 01), Dubna, June 19–23, 2001, hep-ex/0111048] of our  $K_{e3}$  decay data was carried out in order to attempt to reduce the errors further and thus improve the test for non-standard model scalar and tensor components in the electroweak form factors.

The most general Lorentz invariant form of the matrix element of  $K_{e3}$  decay can be written as

$$M \propto f_+(q^2)(P_K + P_{\pi^0})^\lambda \bar{u}_e \gamma_\lambda (1 - \gamma_5) u_\nu \\ + f_-(q^2) m_l \bar{u}_e (1 - \gamma_5) u_\nu + 2m_K f_S \bar{u}_e (1 - \gamma_5) u_\nu \\ + (2f_T/m_K)(P_K)^\lambda (P_{\pi^0})^\mu \bar{u}_e \sigma_{\lambda\mu} (1 - \gamma_5) u_\nu,$$

where  $f_\pm(q^2)$ ,  $f_S$  and  $f_T$  are the vector, scalar and tensor form factors,  $P_K$  and  $P_\pi$  are four-momenta of the  $K^+$  and  $\pi^0$ . The vector form factors  $f_\pm(q^2)$  are assumed to be linearly dependent on the momentum transfer squared  $q^2 = (P_K - P_\pi)^2$  and they can be represented by the equation  $f_\pm(q^2) = f_\pm(0)(1 \pm \lambda_\pm(q^2/m_{\pi^0}^2))$ . Because of the small mass of the positron, the part of the matrix element that depends on  $f_-(q^2)$  is negligible and there are just three free parameters of the theory:  $\lambda_+$ ,  $f_S$  and  $f_T$ . Within the standard model (SM), due to  $W$ -boson exchange, no terms other than those of a pure vector nature are expected. A possible contribution to  $f_S$  and  $f_T$  from electroweak radiative corrections is negligibly small and, therefore, non-zero values of  $f_S$  and  $f_T$  would signal new physics beyond the SM. Our first result [Shimizu *et al.*, Phys. Lett. **B495**, 33 (2000)] was unable to confirm previously reported non-zero values.

Compared to the first analysis, improvements in reconstruction of the charged particle track were made. In the new analysis, information about the kaon stopping position from the target ( $x, y$ ) and ring counter ( $z$ ) was included in the momentum reconstruction routine. The reconstruction of the  $\pi^0$  kinematics was also improved by using tighter time windows in the CsI and improved calibration. The Monte Carlo routines more accurately described the kaon stopping distribution in the target and the electromagnetic shower leakage effects in the CsI. This allowed us to use all CsI crystals for reconstruction of the  $\pi^0$ , resulting in approximately a factor of four increase in acceptance.

Within the standard model the only parameter to be obtained is  $\lambda_+$ . It can be extracted in a model-independent way from the  $q^2$  dependence of  $f_+$ . For extraction of all three parameters  $\lambda_+$ ,  $f_S$  and  $f_T$ , the Dalitz distribution fit was performed using the  $P_{e^+}$ ,  $\theta_{\pi^0 e^+}$  variables. The angle between the pion and positron,  $\theta_{\pi^0 e^+}$ , was preferred instead of pion energy  $E_{\pi^0}$  in order to reduce a systematic error related to the energy leakage in the electromagnetic calorimeter.

The values obtained for  $\lambda_+$ , and the scalar and tensor form factors are

$$\lambda_+ = 0.0278 \pm 0.0017(\text{stat}) \pm 0.0015(\text{syst}) \\ f_S = 0.0040 \pm 0.0160(\text{stat}) \pm 0.0067(\text{syst}) \\ f_T = 0.019 \pm 0.080(\text{stat}) \pm 0.038(\text{syst}).$$

The statistical errors have been improved by a factor of 1.5 and systematic errors for  $\lambda_+$ ,  $f_S$  and  $f_T$  were reduced by the factors 2.0, 2.1 and 2.4, respectively, compared to our previous result. This result is in agreement with the standard model prediction and there is no evidence for a deviation from zero for the values of scalar and tensor form factors.

In another analysis [Horie *et al.*, Phys. Lett. **B513**, 311 (2001)] the  $K^+ \rightarrow \pi^0 \mu^+ \nu$  ( $K_{\mu 3}$ ) events, which were collected simultaneously, were analyzed to determine the ratio of the  $K_{\mu 3}$  and  $K_{e3}$  decay widths  $\Gamma(K_{\mu 3})/\Gamma(K_{e3})$ .

Assuming that only the  $V - A$  interaction contributes to the  $K_{\ell 3}$  decay, the decay amplitude can be described by the two dimensionless form factors  $f_+(q^2)$  and  $f_0(q^2)$ , defined above, which are functions of the momentum transferred to the leptons  $q^2 = (P_K - P_{\pi^0})^2$  where  $P_K$  and  $P_{\pi^0}$  are the four momenta of the  $K^+$  and  $\pi^0$ , respectively. Assuming  $\mu - e$  universality, the form factors for  $K_{\mu 3}$  and  $K_{e3}$  decays are identical and  $\Gamma(K_{\mu 3})/\Gamma(K_{e3})$  can be written as,

$$\Gamma(K_{\mu 3})/\Gamma(K_{e3}) = 0.6457 - 0.1531\lambda_+ + 1.5646\lambda_0 + \text{H.O.}$$

If the  $\lambda_+$  value derived from the  $K_{e3}$  analysis is assumed, the  $\lambda_0$  parameter can be obtained.

Data were taken at two spectrometer fields, 0.65 and 0.90 T, in order to study systematic effects. In the analysis  $K_{\mu 3}$  and  $K_{e3}$  events were selected by time-of-flight of  $\mu^+$ 's and  $e^+$ 's through the spectrometer, and the  $\pi^0$ 's were identified from exactly two photon clusters in the CsI calorimeter.

In order to obtain the detector acceptance and estimate the background fraction, a Monte Carlo simulation was carried out for both the charged particle measurement in the spectrometer and the  $\pi^0$  measurement in the CsI(Tl) detector. The initial Dalitz distributions were generated with the values of  $\lambda_+ = 0.0278$  and the current world average  $\lambda_0 = 0.006$ , while the Dalitz distribution of  $K_{e3}$  decay is insensitive to the  $\lambda_0$  parameter. The simulation data were analyzed in the same manner as the experimental sample.

The results obtained in this work are:

$$\Gamma(K_{\mu 3})/\Gamma(K_{e3}) = 0.671 \pm 0.007(\text{stat}) \pm 0.008(\text{syst}), \\ \lambda_0 = 0.019 \pm 0.005(\text{stat}) \pm 0.004(\text{syst}).$$

The value of  $\lambda_0$  obtained is consistent with that from  $K_{\mu 3}$  Dalitz plot analyses [Whitman *et al.*, Phys. Rev.

**D21**, 652 (1980); Artemov *et al.*, Phys. of Atomic and Nuclei **60**, 2023 (1997)], which supports the validity of  $\mu-e$  universality. If the assumption of  $\mu-e$  universality is removed and values of  $\lambda_+^\mu$ ,  $\lambda_+^e$ , and  $\lambda_0$  are taken from other work, then the result for  $\Gamma(K_{\mu 3})/\Gamma(K_{e 3})$  can be used to obtain the ratio of weak coupling constants  $g_\mu f_+^\mu(0)/g_e f_+^e(0) = 0.971 \pm 0.019$ , which is consistent with unity.

Finally, in October, 2001, the last beam time with the apparatus was used to study the radiative  $K\pi_2$  decay,  $K^+ \rightarrow \pi^+\pi^0\gamma$ . For this run, additional photon veto counters were added to detect photons escaping through the muon holes in the CsI(Tl) calorimeter. This decay channel is unique. The direct photon emission from the vertex is easy to observe because the internal bremsstrahlung contribution is suppressed by the  $\Delta I = 1/2$  rule. This direct emission is dominated by the chiral anomaly of magnetic transitions and the decay amplitude can be analyzed in terms of chiral perturbation theory (ChPT). This measurement can potentially confirm and extend the recent result from BNL E787 [Adler *et al.*, Phys. Rev. Lett. **85**, 4856 (2000)] by virtue of its high kinematic resolution, and its capability to reach the lower  $\pi^+$  energy region where the direct photon emission is more important. Analysis of these data is currently in progress.

**TJNAF Experiment E00-006**  
**Measurement of the flavour singlet form factors of the proton ( $G\emptyset$ )**

(*W.T.H. van Oers, Manitoba*)

The structure of the nucleon at low energies in terms of the quark and gluon degrees of freedom is not well understood. The  $G\emptyset$  experiment aims to measure two proton ground state matrix elements which are sensitive to point-like strange quarks and hence to the quark-antiquark sea in the proton. The matrix elements of interest are the elastic scattering vector weak neutral current charge and magnetic form factors,  $G_E^Z$  and  $G_M^Z$ , respectively. These can be extracted from a set of parity violating electron-proton scattering measurements. If one assumes a relationship between the proton and neutron structure in that the proton and neutron differ only by the interchange of up and down quarks, i.e., isospin symmetry, the strange quark (as well as the up and down quark) contribution to the charge and magnetic form factors of the nucleon can be determined. This would result from taking appropriate linear combinations of the weak neutral form factors and their electromagnetic counterparts.

Determinations of both the charge and magnetic strange quark form factors are of fundamental interest, as these would constitute the first direct evidence of the quark sea in low energy observables. It is the objective of the  $G\emptyset$  experiment to determine these contributions

to the proton form factors at the few per cent level. Observations at high energy suggest that the strange quarks carry about half as much momentum as the up and down quarks in the sea. It is important to determine both the role of the quark sea and the relevance of strange quarks at low energy where there are voids in understanding the theory of the strong interaction (quantum chromodynamics, QCD). Even if the strange quark contributions are found to be below the level of sensitivity of the experiment, upper limit determinations at this level are as valuable as non-zero results. The matrix elements  $G_E^Z$  and  $G_M^Z$  are also relevant to discussions of the Ellis-Jaffe sum rule and the pion-nucleon sigma term; there is uncertainty in both of these about the strange quark contributions. The  $G\emptyset$  experiment will allow the determination of the strange contributions to the proton charge and magnetic form factors in a more straightforward manner.

In the  $G\emptyset$  experiment parity violating longitudinal analyzing powers will be measured in electron-proton scattering in the range  $0.1 \leq Q^2 \leq 1.0 \text{ GeV}^2$  at both forward and backward angles. The longitudinal analyzing power is defined as

$$A_z = (1/P) \frac{[\sigma^+(\theta) - \sigma^-(\theta)]}{[\sigma^+(\theta) + \sigma^-(\theta)]}$$

where  $P$  is the polarization of the incident electron beam and the + and - superscripts indicate the helicity state. Making pairs of measurements at forward and backward angles will allow the separation of  $G_E^Z$  and  $G_M^Z$ . Predicted longitudinal analyzing powers range from about  $(-3 \text{ to } 35) \times 10^{-6}$ ; it is planned to measure the longitudinal analyzing powers with statistical uncertainties of  $\Delta A/A = 5\%$  and systematic uncertainties related to helicity correlated effects of  $\Delta A/A \leq 2.5 \times 10^{-7}$ . In the first phase of the experiment longitudinal analyzing powers will be measured concurrently at seven values of the momentum transfer in the range  $0.1 \leq Q^2 \leq 1.0 \text{ GeV}^2$ . It now appears highly probable that by the time of data-taking for the  $G\emptyset$  experiment (starting in 2002) higher beam polarizations ( $\sim 70\%$ ) will be available at the reduced beam pulse frequency of 31 MHz, decreasing considerably the original estimate of 700 hours for the first phase of the experiment. However, it must be realized that the length of the experiment is in part governed by making rather elaborate control measurements to determine the corrections that have to be made to the measured asymmetries and to assess systematic errors. In the second phase of the experiment each subsequent backward angle analyzing power measurement would require from one half to one month of running time. The results of the SAMPLE experiment at the MIT-Bates Laboratory have shown the importance of mea-

asuring the axial form factor corrections, since these appear to be quite different from the theoretical predictions. Therefore, companion measurements of quasi-elastic scattering from deuterium will also be made at the backward angles. With these measurements, the effective axial current of the nucleon will also be determined. This current includes effects from the effective axial coupling of the photon to the nucleon or anapole moment, which are relevant also in other processes, e.g., parity violating Moller scattering and atomic parity violation.

### The $G0$ collaboration

The  $G0$  experiment will be carried out in Hall C at TJNAF by a collaboration of scientists from Canada, France, Georgia, and the United States, with funding provided through NSERC (Canada), IN2P3 (France), and DOE/NSF (US).

### Canadian contributions

The Canadian members of the  $G0$  collaboration, based at the universities of Manitoba and Northern British Columbia, and TRIUMF, have been asked to:

- (i) develop and produce specialized photomultiplier tube bases for the main detector arrays;
- (ii) design, build, and commission an automated magnetic field measuring apparatus complete with its own data acquisition system;
- (iii) prototype and produce the cryostat exit detector arrays for the backward angle measurements;
- (iv) prototype and produce the aerogel Čerenkov arrays for background rejection in the backward angle measurements;
- (v) coordinate the implementation of TJNAF built beam monitors and control apparatus with TRIUMF built parity type electronics;
- (vi) provide design and implementation support for the liquid hydrogen target slow controls system;
- (vii) manage the coordination and scheduling of resources for  $G0$  engineering runs at TJNAF.

Considerable progress has been made in the design and production of the subsystems listed above, many of which are now operational.

### The $G0$ main detector array

The heart of the  $G0$  detection system is a spectrometer which consists of an eight-sector toroidal magnet with an array of scintillation detectors located at the focal surface of each sector (see Fig. 26). Since data will not be acquired in event-by-event mode in this experiment, and since the scintillator arrays are the only detectors to measure the scattered particles in the forward angle mode, the performance of these focal-plane detectors (FPD) is of critical importance. The timing and pulse shape characteristics of this system must be

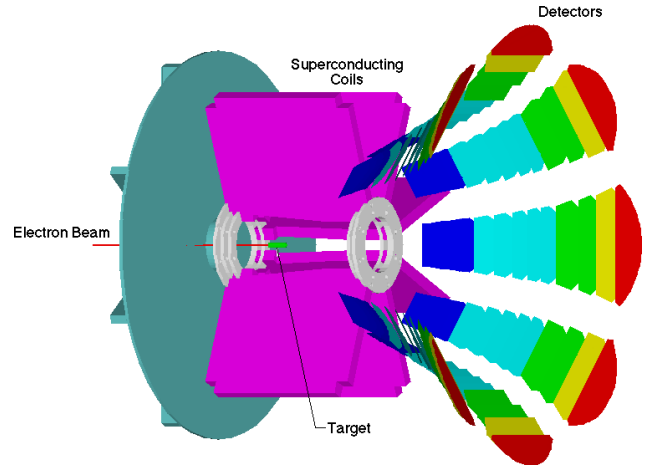


Fig. 26. View of the  $G0$  superconducting toroidal spectrometer with one sector and the housing removed.

fine-tuned at the hardware level as it will not be possible to reconstruct individual events. Furthermore, the rates associated with many of the FPD elements will be quite high (1 MHz) and the photon yield(s) will have a large dynamic range. As such, special demands will be made on the photomultiplier tubes (PMT) and especially on their associated divider/base circuit. Work on the design, development, and production of the  $G0$  bases began at TRIUMF in 1997. Several iterations of prototype high-rates bases were constructed and tested in late 1997 and early 1998. In the summer of 1998, 12 final prototype bases were constructed and delivered to TJNAF for tests with the first set of prototype FPDs, and fabrication of the production bases began. With the help of summer students (funded partly through the TRIUMF Summer Students program and partly through the  $G0$  NSERC grant), the fabrication of the electrical components for all of the production bases was completed in 1998. The design of the mechanical housing for the PMT-base subsystem depended on the final design of the FPD support structure and, after much effort resolving subsystem integration issues, the final design for the PMT-base housing assembly was completed in late 1998. The fabrication and assembly of the mechanical housings and integration of the electrical components was completed over the summer of 1999 (again with the help of summer students at TRIUMF). Final testing of the completed bases was carried out in late fall, 1999, and shipment of all the bases (300 units) to TJNAF occurred at the end of calendar year 1999. Integration of this subsystem with the FPD arrays and the DAQ electronics was completed at TJNAF in 2000 and 2001 during the final assembly of the FPD system. Presently, all of the FPDs are fully instrumented and undergoing tests of the detector chain (scintillator/PMT-base/electronics/DAQ/analysis) in Hall C using cosmics and beam background.

### Magnetic verification of the $G\emptyset$ spectrometer

An automated field measuring apparatus is being used to provide a magnetic verification of the  $G\emptyset$  superconducting toroid by determining the locations of a pre-specified set of magnetic reference points. These reference points correspond to the zero-crossing locations of specific field components at selected points of symmetry around the toroidal magnet. This measurement is carried out by scanning a predefined set of contour lines, and determining where specific field components reverse sign. The system must be capable of providing a position determination of  $\pm 0.2$  mm and a field determination of  $\pm 0.2$  G. Considerable effort has gone into the design, construction and commissioning of this magnetic field measuring apparatus or magnetic verification device at TRIUMF, the University of Manitoba and UNBC. The device consists of a programmable gantry with full 3D motion anywhere within a  $4\text{ m} \times 4\text{ m} \times 2\text{ m}$  volume, and a set of high precision Hall probes mounted at the end of a probe boom on the gantry (see Fig. 27). Procurement of parts commenced in early 2000, and final assembly and testing began in late spring 2000 at TRIUMF. The

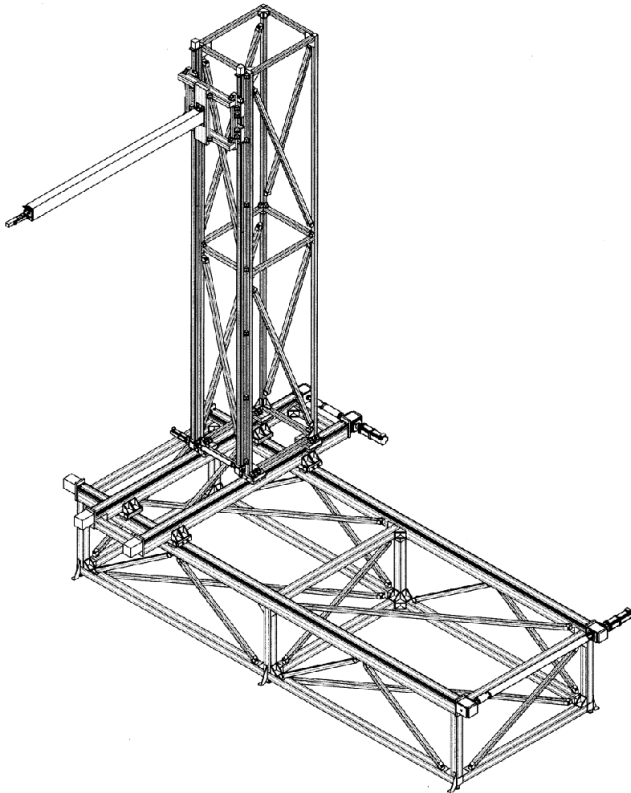


Fig. 27. Layout of the magnetic verification device, which consists of a programmable gantry (capable of full 3D motion anywhere within a  $4\text{ m} \times 4\text{ m} \times 2\text{ m}$  volume) with a set of high precision Hall probes, temperature, inclination, and photo sensors mounted at the end of a probe boom on the gantry.

magnetic verification device was completed in mid-summer, 2000 and transported to the University of Illinois to carry out the magnet measurements. Over the past year, much effort has gone into commissioning this device and upgrading the motion control and data acquisition software. In the spring of 2001, a series of measurements were carried out with the magnet energized at low currents. The magnetic verification device yielded remarkably consistent results and indicated that the final measurements, with the superconducting magnet at high current, should be straightforward. After many months of effort to cool the magnet coils, the  $G\emptyset$  spectrometer made the transition to superconducting mode in late 2001 (December). At this point, the magnet was energized at high currents and two complete sets of magnetic field verification scans were carried out. These data are presently being analyzed and preliminary results will be available shortly. Shown in Fig. 28 is the magnetic verification device and the  $G\emptyset$  superconducting spectrometer. Although this magnetic verification device was designed, tested, and built by the Canadian subgroup at TRIUMF and the universities of Manitoba and Northern B.C., it should be noted that funding for hardware components of this subsystem has been provided via NSF funding for

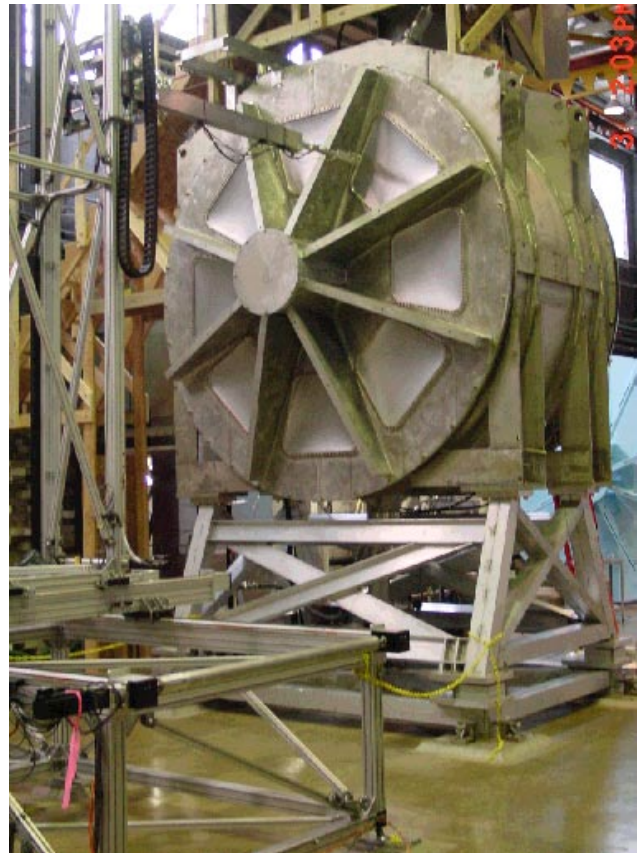


Fig. 28. The magnetic verification apparatus and  $G\emptyset$  superconducting magnet at UIUC.

$G\theta$  through the University of Illinois. Infrastructure support, however, has been provided by TRIUMF and the Universities of Manitoba and Northern B.C.

### The cryostat exit detector array

For the backward angle measurements during the second phase of the  $G\theta$  experiment, the addition of a second array of scintillation detectors, located near the spectrometer cryostat exit windows, will be required in order to discriminate the elastically from the inelastically scattered electrons. The geometry of these cryostat exit detector (CED) arrays (see Fig. 29) has been studied in detail and a reference design was completed in the spring of 1999. With the resident expertise at TRIUMF in producing high quality scintillation detectors and lightguides, the Canadian subgroup was asked to play the main role in the prototyping and production of the CEDs. A set of prototypes was built at TRIUMF and delivered to Louisiana Tech University for further studies in early summer, 1999. Results from these studies indicate that the reference design and the prototype detectors will meet the specification requirements for the CED arrays. Production of a full set of dummy CED prototypes was then completed at TRIUMF in 2000, to aid in the design of the CED scintillator support structure. After finalizing the CED design, fabrication of the production versions of the CED arrays started at TRIUMF in late 2000. In fall 2001, the full 8 sets of CED scintillators were completed and delivered to TJNAF. Presently, fabrication of the helical-bending and transition lightguides for the CEDs is under way at TRIUMF, and a first set should be available for final assembly tests in spring, 2002. The CEDs will make use of the same photomultiplier tubes and specialized TRIUMF/ $G\theta$  bases as the FPDs.

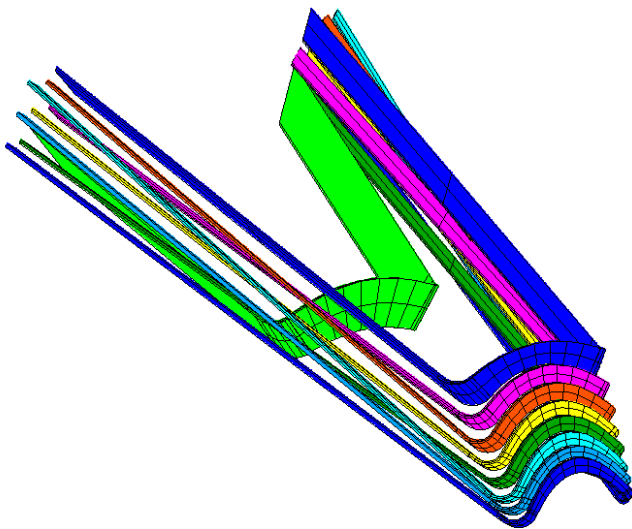


Fig. 29. Geometry of the cryostat exit detector (CED) array for a single octant.

### Aerogel Čerenkov array

Monte Carlo simulation results have shown that backgrounds from negative pions will be problematic for the second phase backward angle measurements. Recent efforts of the  $G\theta$  Simulation subgroup have focused on characterizing this  $\pi^-$  background and providing options regarding the design of an additional set of detectors to reject the background pions. The  $G\theta$  Canadian and French subgroups have been asked to undertake the construction of this crucial set of additional detectors, which will be made up of arrays of aerogel Čerenkov counters. Over the past year, much effort has gone into the design of this detector array and its support structure. A conceptual design (see Fig. 30) has been evolved into a first prototype (see Fig. 31) at TRIUMF and has undergone tests with both cosmics and beam. In December, 2001, a test run was conducted in the M11 area. Two Čerenkov detectors, one built at TRIUMF and one built at Caltech, were placed in the M11 beam along with three scintillators to establish a trigger on the incident beam particles. The two Čerenkov detector light boxes were similar in size but somewhat different in shape and total light diffusion volume. Data were collected at 120, 200, 300, 350, and 400 MeV/ $c$ ; the maximum momentum of the  $G\theta$   $\pi^-$ 's is 400 MeV/ $c$ . At these momenta the electrons have a high velocity and should always produce Čerenkov light while the pions have

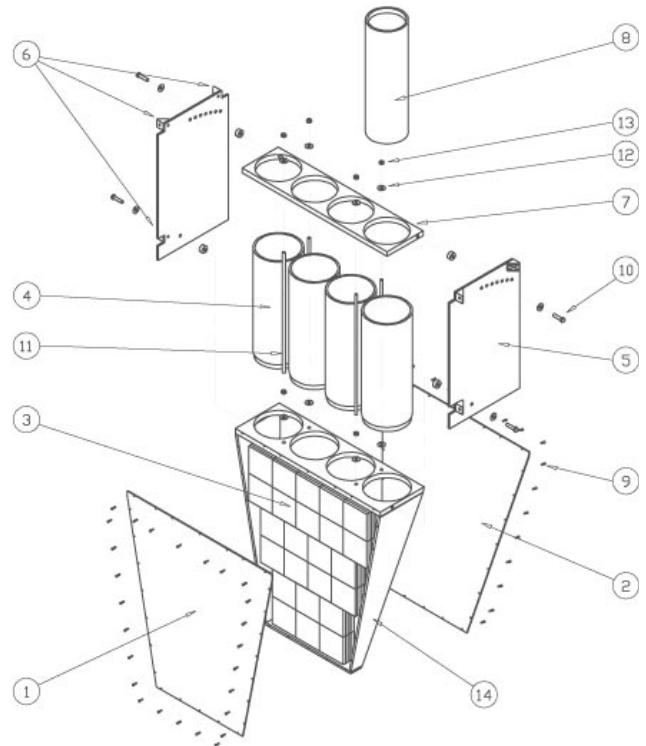


Fig. 30. Conceptual layout of the aerogel Čerenkov veto detector for a single octant.



Fig. 31. Prototype aerogel Čerenkov detector at TRIUMF.

a velocity below the Čerenkov threshold. The light yield and timing spread were studied as a function of beam momenta, position and angle of incidence. Preliminary results indicate some differences between the boxes and variation in the light yield with both position and angle. These results are presently being studied with Monte Carlo techniques, and further testing with cosmics is under way. Depending on the results of these studies, a second iteration prototype may be used in further in-beam tests in M11, planned for summer, 2002. Shown in Fig. 32 is a conceptual illustration of the  $G0$  backward angle configuration with the superconducting magnet, the 3 detector arrays (FPD, CED, Čerenkov) in each of the 8 sectors, and their respective support structures.

#### Beam monitors and parity electronics

Five sets of XYQ monitors will be required in order to measure the beam current and trajectory at several critical locations. A beam current sensitivity of  $\pm 4 \times 10^{-5}$  measured in a 33 ms integration-time sample will be required to monitor and correct for possible helicity correlated intensity modulations. For the beam position monitors (BPMs), a spatial resolution of better than 25  $\mu\text{m}$  at an integration time of 33 ms will be required. Some of the beam current and position

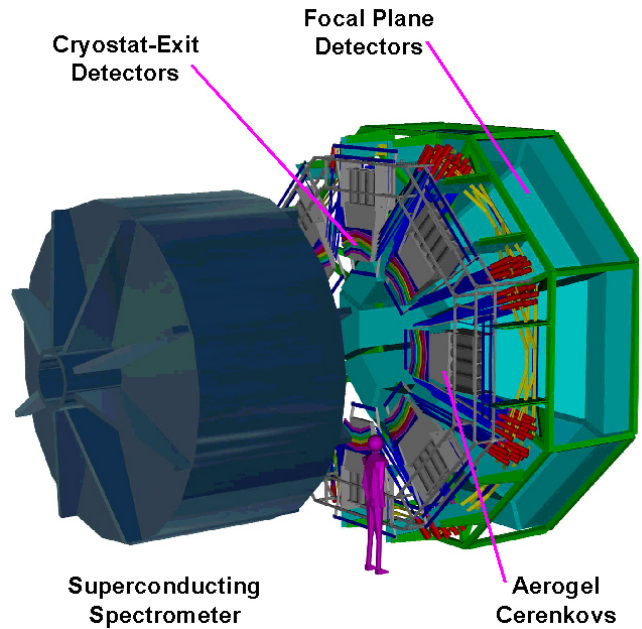


Fig. 32. Conceptual layout of the  $G0$  backward angle configuration.

monitors were tested during an engineering run in July 1997 at TJNAF. The run was organized by members of the  $G0$  Canadian subgroup and personnel from TJNAF (Hall C), with much of the parity type electronics provided by the Canadian subgroup. Helicity correlated properties of the TJNAF polarized electron beam and noise characteristics of some of the beam monitors were successfully measured. Analysis of the data indicates that the beam current and position monitors will meet the specification requirements listed above. Further test beam time is planned for the future. To read out the analogue signals from the beam current and position monitors, and to provide feedback control signals, specialized parity type electronics is required for the  $G0$  experiment. Much of this electronics, such as precision analogue subtractors/dividers and precision voltage-to-frequency converters, has already been designed and used by members of the Canadian subgroup in their parity experiments at TRIUMF. Modifications, driven by  $G0$  requirements, were made to some of these modules and they were operated successfully at the July, 1997 engineering run at TJNAF, as mentioned above. Since that time, several voltage-to-frequency converters of the TRIUMF/parity variety have been requested by TJNAF for the  $G0$  experiment. Construction of these 32-channel precision V-to-Fs was completed at TRIUMF and delivery made to TJNAF in early 1998. With the successful implementation of these first sets of converters, a second set of V-to-F modules was requested by TJNAF in summer, 1999. This second set of V-to-F modules was again constructed at TRIUMF and delivered to TJNAF in



fall, 1999. A third set of V-to-F modules was requested and delivered to TJNAF in 2000. It is anticipated that several more sets of V-to-F modules, as well as other specialized parity type electronics modules, will be required by the  $G\theta$  collaboration over the next few years, as the experiment moves into the commissioning and data-taking phase.

#### **Slow controls for cryogenic target system**

The  $G\theta$  experiment will use a 20 cm long liquid hydrogen ( $\text{LH}_2$ ) target connected to a cryogenic loop to recirculate and cool the liquid. This target will operate at 20 K and 25 psia, and the heat deposited by the 40  $\mu\text{A}$  electron beam will be carried away from the hydrogen by a compressed He gas heat exchanger. The main components of the target system are a pump for circulating the target fluid in a closed cryogenic loop, a heat exchanger, the target cell, and a manifold to direct the fluid flow down the centre of the target cell. A gas handling system is employed to provide gas to the target, the He coolant to the heat exchanger, and to evacuate the region surrounding the target. The state of the target (temperatures, pressures, position, etc.) and the gas handling system (valve settings) is monitored/controlled by what is called the slow controls system. This system sounds alarms when operating conditions become improper, monitors beam current and maintains a constant heat load on the target. The control system also records the target state at regular intervals to log files. The Canadian subgroup has been providing design and implementation support for the liquid hydrogen target slow controls system. Specifically, the responsibilities include: (a) participation in MEDM monitoring and control screens design; (b) installation and integration into the system of the Joule-Thompson valve controller to control the flow of the He coolant; (c) testing of target and He coolant temperature sensors; (d) participation in the pressure transducer calibration and target motion testing/calibration; and (e) configuration and management of the channel archiver software which logs and plots the target data. Members of the Canadian subgroup have taken part in the test cooldowns of the target and are also involved in the design of the  $G\theta$

main screen software which displays the experiment and system status.

#### **$G\theta$ engineering runs**

Several engineering runs have been carried out by the  $G\theta$  collaboration to study (a) the helicity correlated properties of the TJNAF polarized electron beam and the noise characteristics of the Hall C beam line monitors (July, 1997); and (b) the neutron background and energy spectrum in the vicinity of the  $G\theta$  detector system (December, 1999). Both these efforts were coordinated by members of the Canadian subgroup and personnel from TJNAF (Hall C) with much of the equipment provided by the Canadian subgroup. Presently, as construction of the first-phase forward-angle mode of the  $G\theta$  experiment nears completion, the individually complex systems comprising the experiment must be integrated into one overall system. To accomplish this, the collaboration will undertake a number of engineering runs to test the functionality of these systems and identify deficiencies. These engineering runs will ultimately test the interaction of the complete system, which includes the data acquisition system, detectors, analysis software, and magnet and target controls. Members of the Canadian subgroup, together with the University of New Mexico subgroup, have planned and detailed the requirements and benchmarks of the engineering runs. Coordination and scheduling of resources for the engineering runs is being managed by members of the  $G\theta$  Canadian subgroup. The goals of the engineering runs are: commission and test the individual systems; schedule and verify mechanical assembly of sub-assemblies; integrate the systems to establish the fundamental detector and DAQ operation(s); identify and correct deficiencies and system conflicts; test and verify that the composite system is capable of parity violation asymmetry measurements.

Canadian subgroup of the  $G\theta$  collaboration: J. Birchall, J. Chiang, B. Chow, W.R. Falk, M. Hasselfeld, A. Horning, L. Lee, S.A. Page, W.D. Ramsay, A. Rauf, G. Rutledge, M. Steeds, W.T.H. van Oers (Manitoba); E. Korkmaz, T. Porcelli (Northern British Columbia); C.A. Davis (TRIUMF).

## NUCLEAR AND ATOMIC PHYSICS

### Experiment 704

#### Charge symmetry breaking in $np \rightarrow d\pi^0$ close to threshold

(A.K. Opper, Ohio; E. Korkmaz, UNBC)

Experiment 704 expects to have final results from its high precision measurement of charge symmetry breaking in the strong interaction completed by mid-2002. The observable of interest is the forward-backward asymmetry ( $A_{fb}$ ) in  $np \rightarrow d\pi^0$ , which must be zero in the centre of mass if charge symmetry is conserved and has a predicted value that ranges between  $(-35 \rightarrow +70) \times 10^{-4}$  [Niskanen, Few-Body Systems **26**, 241 (1999); van Kolck *et al.*, Phys. Lett. **B493**, 65 (2000)] depending on the strengths of the various contributions. The forward-backward asymmetry is defined as

$$A_{fb}(\theta) \equiv \frac{\sigma(\theta) - \sigma(\pi - \theta)}{\sigma(\theta) + \sigma(\pi - \theta)}$$

with the relevant contributions being the neutron-proton mass difference ( $\delta$ ), exchange of an isospin mixed  $\eta - \pi$  meson, and the effect of the  $d u$  quark mass difference on pion nucleon scattering.

The experiment was carried out with a 279.5 MeV neutron beam, a liquid hydrogen target, and the SASP spectrometer positioned at  $0^\circ$ . With these kinematics, and the large acceptance of SASP, the full deuteron distribution was detected in one setting of the spectrometer, thereby eliminating many systematic uncertainties. Measurements of  $np$  elastic scattering with incident neutron beams that fill the same target space and produce protons that span the momentum distribution of the  $np \rightarrow d\pi^0$  reaction provide a stringent test of the acceptance description of the spectrometer. With over seven million  $np \rightarrow d\pi^0$  events and six million  $np$  elastic events, the statistical uncertainty of this measurement is  $5 \times 10^{-4}$ . The anticipated systematic uncertainty is  $7 \times 10^{-4}$ , as indicated in Fig. 33.

#### Data analysis

Experiment 704 production data were analyzed in four successive passes: (1) detector calibration; (2) beam direction determination in the SASP-centric front end wire chamber coordinate system; (3) final extraction of the deuteron kinematic locus (see Fig. 34); and (4) efficiency determination. In addition to extracting the kinematic locus and detector efficiencies, the last pass of analysis also produced a filtered data set of 8 words/event (four target variables and four focal plane variables) for all good locus events. The filtered data set of  $\sim 200$  Mbytes can be resorted and analyzed in one hour on a Linux box. The final

Integrated  $A_{fb}$  for different neutron lab energies

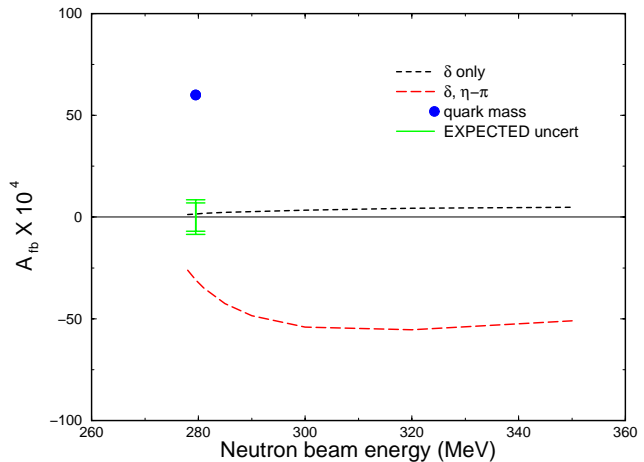


Fig. 33. Calculated contributions to  $A_{fb}$  and anticipated uncertainties.

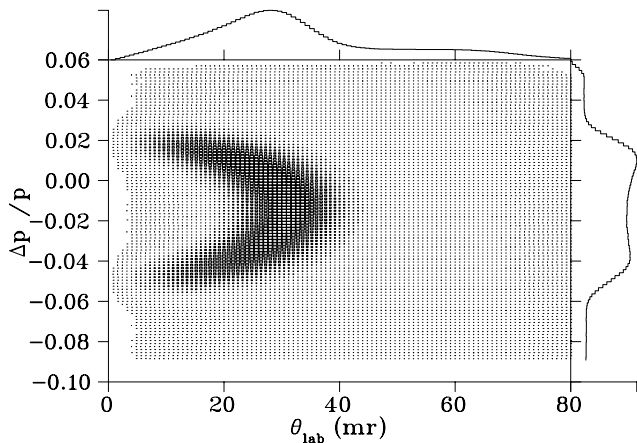


Fig. 34. Kinematic locus of all  $np \rightarrow d\pi^0$  data.

analysis of the  $np \rightarrow d\pi^0$  data took approximately two months and was finished at the end of September, 2000.

#### Extraction of $A_{fb}$

The data have the accumulated effects of multiple scattering, energy loss, and other physical processes which make extracting  $A_{fb}$  directly from the locus impossible. As such, Monte Carlo techniques are used to extract the angle integrated  $A_{fb}$ . Close to threshold the  $np \rightarrow d\pi^0$  cross section in the centre of mass frame is given by:

$$\frac{d\sigma}{d\Omega} = A_0 + A_1 P_1(\cos(\theta)) + A_2 P_2(\cos(\theta)),$$

where  $P_i$  are Legendre polynomials,  $\theta$  is the centre of mass scattering angle [Hutcheon *et al.*, Nucl. Phys. **A535**, 618 (1991)]. The presence of charge symmetry

breaking will be reflected in the  $A_1$  term as it is odd in terms of  $\cos\theta$ . The angle integrated form of  $A_{fb}$  is given by

$$A_{fb} = \frac{1}{2}A_1/A_0.$$

Thus, determining the value of  $A_1$ , which minimizes the  $\chi^2$  of the fit between the real and simulated data, determines  $A_{fb}$ .

Due to the strong sensitivity of  $A_{fb}$  to the central momentum of the spectrometer ( $p_0$ ), the LH<sub>2</sub> target thickness, and the average energy of the primary beam ( $T_{\text{beam}}$ ), the simulation must span a four dimensional space defined by these three experimental parameters and  $A_1/A_0$ . This procedure requires generating simulations at the nominal values, plus a canonical step, and minus a canonical step for each parameter. With a four dimensional parameter space needing to be covered, this means 81 (i.e.  $3^4$ ) independent simulations must be generated. The comparison of data to these simulations produces a four dimensional  $\chi^2$  space and the values of the four parameters that give a global minimum of that  $\chi^2$  space determine the value of  $A_1/A_0$  and consequently  $A_{fb}$ .

### Simulation

The simulation is based on GEANT and begins with a proton beam incident on a <sup>7</sup>Li target to reproduce the energy loss effects in that target. The model of the equipment is in agreement with the best known blueprints, “as-built drawings”, and recent measurements. The SASP dipole field used in the simulation is a map of that magnet at 875 A, scaled up to the running current of 905 A. Data were acquired in 19 different periods spanning two years and the simulation “schedules in” measured detector efficiencies, scintillator thresholds, and missing wires in a manner consistent with the actual running periods. The simulation also allows the target thickness and average beam energy to vary for each of the data-taking periods.

To reduce the possibility of psychological bias in matching simulation to data, a “black box” subroutine has been added to the simulation. This routine adds a (hidden) offset to the  $A_1/A_0$  asymmetry parameter used to set up the  $np \rightarrow d\pi^0$  generator in the simulation. After selecting the value for the offset, a member of the collaboration not involved in simulation development compiled the subroutine on all simulation farms, mailed the source code to two people outside the collaboration, and deleted the source code.

### Hadronic losses

Deuteron reaction losses, which account for 1–2% of all deuteron events, have a significant momentum

dependence over the 8% momentum range of the experiment. Reactions on carbon are the dominant processes and include significant contributions from both elastic and reaction processes. Including these processes in the simulation required that these processes be parametrized from the world’s data on deuteron elastic and reaction cross sections from hydrogen and carbon [Auce *et al.*, Phys. Rev. **C53**, 2919 (1996); Saturne, Nucl. Phys. **A464**, 717 (1987); Okamura *et al.*, Phys. Rev. **C58**, 2180 (1998); Baumer *et al.*, Phys. Rev. **C63**, 037601 (2001)]. As such, the systematic uncertainty in  $A_{fb}$  associated with the deuteron hadronic losses is a function of the uncertainties in the world’s data. Due to complexities in the simulation, the systematic uncertainty in  $A_{fb}$  associated with the deuteron hadronic losses could not easily be deduced directly from the parametrization of the deuteron hadronic processes in the simulation. Instead, an estimate of the false asymmetry introduced by deuteron hadronic processes was obtained by comparing the change in simulation output with the hadronic processes being turned on and off. The ratio of these outputs is referred to as  $R$  and is a function of the deuteron momentum. Assuming a simple relationship for the momentum dependence of the hadronic processes, a linear function:

$$R(\delta) = a + b\delta$$

is fit to the ratio with  $a = 0.9365 \pm 0.005$  and  $b = 0.13 \pm 0.02$ . With the exclusion of deuteron hadronic losses, it is assumed that the deuteron locus is spread over a momentum interval of  $(2\Delta)$  for which the count density ( $C$ ) is constant.

Incorporating hadronic processes into the reaction should produce a count density ( $C'$ ) which is proportional to the change in count ratio:

$$C' = C(a + b\delta).$$

Integrating  $C'$  from  $-\Delta$  to 0 (0 to  $\Delta$ ) gives the number of backward (forward) going deuterons and inserting these into  $A_{fb}$  gives the change in  $A_{fb}$  as:

$$A_{fb} = \frac{b\Delta}{2a}.$$

Using the values found for  $a$  and  $b$ , the false asymmetry introduced by the energy dependence in the total cross section was found to be 0.28% when comparing reaction losses on and off in the simulation. With the uncertainty in the energy dependence of the cross section being approximately 30 mb in 539 mb, the systematic uncertainty in  $A_{fb}$  is in the order of 0.016%.

### Model of SASP acceptance

The acceptance of SASP is a complicated function of the position and angle at which the deuteron is produced and its momentum ( $X_i$ ,  $\theta_i$ ,  $Y_i$ ,  $\phi_i$ , and  $\delta$ ). Describing this acceptance properly requires an accurate model of the magnetic fields in SASP because (1) deuterons can collide with interior surfaces of SASP and be lost from the locus, and (2) the reconstructed momentum variable, which is a function of the focal plane variables  $X_f$  and  $\theta_f$ , may be distorted in a momentum dependent way by an inaccurate model.

The  $np$  elastic scattering data provide the best means to determine the acceptance in that the incident beam of this reaction fills the target parameter space in a way that is similar to that of the  $np \rightarrow d\pi^0$  reaction. To investigate momentum dependent effects, projections of  $Y_i$  and  $\phi_i$  have been made for slices in  $X_i$  and  $\theta_i$  and ratios of these distributions made for data vs. GEANT and for the  $-4\%$  vs.  $+4\%$  momentum sets. The basic features of these ratios are understood in terms of the focusing action of the SASP entrance quads, Q1 and Q2. These features appear in both data and GEANT, but GEANT does not accurately represent the shoulder region where the acceptance in  $\phi_i$  begins to fall. Consequently, we have determined cuts which exclude those portions of the acceptance that cannot be adequately modelled. These cuts are on target position and angle and define regions of uniform acceptance. Much effort was directed at developing a method to find the flat acceptance range in an automated and unbiased manner.

### Systematic uncertainties and error budget

Simulation vs. simulation comparisons were carried out to determine how strongly the experimental parameters are correlated with  $A_1/A_0$ . For each parameter this involved simulating kinematic locus scatter plots for a  $3 \times 3$  grid of the experimental parameter vs.  $A_1/A_0$ , calculating the  $\chi^2$  of those nine plots when compared to a plot simulated with nominal values, and fitting the  $\chi^2$  space. The correlation of  $A_1/A_0$  with the experimental parameter was then obtained from the error matrix based on the curvature of the  $\chi^2$  space. Combining this correlation with the uncertainty in the parameter gives the systematic uncertainty of  $A_1/A_0$  due to that experimental parameter. Note that the uncertainty in the parameter comes from a separate determination and not from the  $\chi^2$  minimization.

These studies quantified the expected strong sensitivity of  $A_1/A_0$  to  $p_0$ , the LH<sub>2</sub> target thickness, and  $T_{\text{beam}}$ . The only way to reduce the systematic effects of these parameters on  $A_1/A_0$  is to reduce the uncertainties of these parameters. This was done by letting these three parameters and  $A_1/A_0$  vary freely and de-

termining the values which minimize the  $\chi^2$  of the fit between data and the simulation. With the whole kinematic locus constraining the fit, the uncertainties in the parameters were greatly reduced. As mentioned above, this procedure required generating simulations at three different values for each parameter. The curvature of the resulting 4D  $\chi^2$  space gave the set of sensitivities and uncertainties shown in Table IV.

Table IV. Systematic uncertainties from the main grid.

Parameter	Sensitivity	Uncertainty	$\Delta A_1/A_0$
$p_0$	42.9%/%	$\pm 0.0015\%$	0.066%
LH <sub>2</sub>	1.2%/mm	$\pm 0.043$ mm	0.052%
$T_{\text{beam}}$	-7.22%/MeV	$\pm 0.0012$ MeV	-0.0087%

The systematic uncertainty in  $A_1/A_0$  resulting from adding the above uncertainties in quadrature is  $8.5 \times 10^{-4}$ ; this yields a systematic uncertainty in  $A_{fb}$  of  $4.3 \times 10^{-4}$ . The overall error budget, based on simulation vs. simulation studies and the 4D parameter space is given in Table V.

Table V. Error budget.

	Uncertainty $A_{fb}$ ( $10^{-4}$ )
FEV threshold	2.5
FEC separation	2.5
Li target position	2.5
$A_2/A_0$	2
Deuteron losses	1.5
Efficiencies	1.5
$\sigma(T)$	1
Neutron angle	1
Background	1
FET threshold	0.5
Fit	4.3
Total systematics	7.1
Statistics	5
Total uncertainty	9

### Verification of acceptance model

The  $np$  elastic scattering data have been used to determine the regions of target space and angle which yield a flat acceptance for the SASP spectrometer. As mentioned above, this reaction is the best way to identify these regions as the incident beam of this reaction fills the target parameter space in a way that is similar to that of the  $np \rightarrow d\pi^0$  reaction. In a robust test of the uniformity of the acceptance,  $A_1/A_0$  was extracted for various subsets of the target space.

Table VI. Stability of  $A_1/A_0$  for target subspaces; first simulation set.

$X_i$ $Y_i$	Angular	$\Delta(A_1/A_0)$ ( $10^{-4}$ )
standard $\pm 2$ cm	standard	0
standard	8 mr tighter	$2 \pm 14$
$r < 2$ cm	standard	$-6.5 \pm 14$
$r < 1$ cm	standard	$-22.7 \pm 24$
$\pm 1$ cm	standard	$-23.4 \pm 21$
$\pm 0.66$ cm	standard	$2.6 \pm 32$
standard	$\phi_1$	$34.6 \pm 27$
standard	$\phi_2$	$32.6 \pm 23$
standard	$\phi_3$	$-44.4 \pm 38$
standard	$\phi_4$	$-28.4 \pm 24$
bottom	standard	$-102.2 \pm 19$
top	standard	$83.7 \pm 18$
left	standard	$5.6 \pm 19$
right	standard	$-16.7 \pm 18$

Initially the results of this study, shown in Table VI, indicated that the extracted value of  $A_1/A_0$  is stable over the acceptance subspaces. However, the last set of subspaces to be analyzed uncovered a surprising difference in  $A_1/A_0$  for the top and bottom subspaces. The source of this discrepancy was an inconsistency between the front end trigger scintillator (FET) thicknesses used in the simulation and their true thicknesses. The FET is a pair of scintillators, one above the other, to reduce sagging of the PMTs when exposed to the high rates of this experiment,  $\sim 5$  MHz. A major project undertaken in 2000 was the verification of the description of the equipment in the simulation; this involved remeasuring much of the equipment. Logbook entries from that project give the top scintillator thickness as 0.159 cm and that of the bottom scintillator as 0.170 cm. The simulation naively used the average of these, which meant that the energy loss of the deuterons as they passed through the FET scintillators was incorrect. With the strong sensitivity of  $A_1/A_0$  to energy (see Table IV), a false  $A_{fb}$  was systematically introduced into the simulation.

After correcting the FET scintillator thicknesses, a new set of 81 simulations was generated covering the 4D parameter space. Generating a new set of simulations requires 1100 cpu-days on a Linux box. When done on the four Linux clusters available to us, this takes about four weeks of live time. This new set of simulations showed much better agreement of  $A_1/A_0$  for the different acceptance subspaces, however, the values of the other three parameters at the global minimum were not stable for the top and bottom halves of the acceptance (see Table VII). While the different acceptance subspaces give consistent values of  $A_1/A_0$ , the

Table VII. Stability of the four free parameters for target subspaces; second simulation set.

	$\Delta(A_1/A_0)$ ( $10^{-4}$ )	LH <sub>2</sub> (mm)	$p_0$ (MeV/c)	$T_{\text{beam}}$ (MeV)
std	$0 \pm 14$	$0.72 \pm 0.05$	$0.425 \pm 0.013$	$0.072 \pm 0.001$
b	$-9 \pm 20$	$0.35 \pm 0.07$	$0.645 \pm 0.019$	$0.118 \pm 0.002$
t	$2 \pm 19$	$1.02 \pm 0.07$	$0.237 \pm 0.018$	$0.031 \pm 0.002$
l	$-5 \pm 20$	$0.74 \pm 0.07$	$0.343 \pm 0.019$	$0.068 \pm 0.002$
r	$2 \pm 19$	$0.72 \pm 0.07$	$0.496 \pm 0.018$	$0.075 \pm 0.002$

std = standard; b = bottom; t = top; l = left; r = right

inconsistency of the other parameters of the fit suggests that a feature of the acceptance is still not understood.

### Final steps

In looking for the problem with the acceptance, another inconsistency between the simulation description of the FET scintillators and the true scintillators was discovered. The gap between the upper and lower halves of the FET was centred at  $X_i = 0.152$  cm, but was positioned in the simulation at  $X_i = -0.173$  cm. This mismatch yielded a region 0.325 cm high in which the energy loss in the FET was not calculated correctly by the simulation. The mismatch has been corrected and the agreement in simulation and data gap positions can be seen in Fig. 35.

It is unlikely that the gap mismatch alone could cause the inconsistencies seen in  $p_0$ , LH<sub>2</sub> thickness, and  $T_{\text{beam}}$  for the different acceptance subspaces. Before investing the cpu time to generate a new set of simulations with the corrected gap position, we are working to eliminate any other systematic effects.

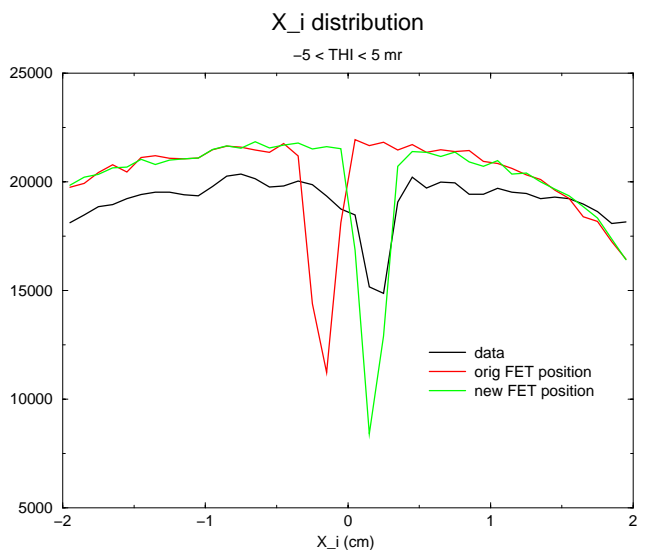


Fig. 35.  $X_i$  position of FET gap;  $-5 \text{ mr} < \phi_i < 5 \text{ mr}$ .

## Experiment 715

### Weak interaction symmetries in $\beta^+$ decay of optically trapped $^{37,38}\text{mK}$

(J.A. Behr, TRIUMF; K.P. Jackson, TRIUMF/SFU)

The experimental progress of the TRIUMF neutral atom trap program in the last year will all be summarized in this section of the Annual Report.

Data taken in fall, 2000 for the  $\beta^+-\nu$  correlation measurement in the  $0^+ \rightarrow 0^+$  pure Fermi decay of  $^{38}\text{mK}$  are still under analysis. From these data, limits have been set on the admixture of possible heavy (0.7–3.8 MeV) neutrinos with the electron neutrino, producing a Ph.D. thesis and an imminent publication. The status of these experiments will be briefly summarized here.

The spin-polarized program has completed analysis of the test  $^{37}\text{K}$  data taken in November, 2000. In the off-line lab, nuclear vector polarization of stable  $^{41}\text{K}$  has now reached sufficient quality to schedule a test run right-handed current search in  $^{37}\text{K}$  in the next running period. A possible polarization systematic, a subtle atomic physics effect called “coherent population trapping”, has been identified and eliminated. Its careful characterization is now being prepared for publication, and explored as a possible spectroscopy technique on the radioactives.

The December, 2001 EEC approved two new shorter-term experiments which will also be summarized here. Experiment 925, isospin mixing in  $^{36}\text{Ar}$  via spin-polarized observable in  $^{36}\text{K}$   $\beta^+$  decay, will test the nuclear structure calculations needed to extract  $V_{ud}$  from Fermi strength data. Experiment 926, measurement of charge radius and  $\beta^+$  decay Q-value of laser-trapped  $^{74}\text{Rb}$ , will also produce a small contribution to the understanding of  $V_{ud}$ .

### $^{38}\text{mK}$ $\beta^+$ -recoil coincidence experiments

#### Search for scalar interactions in $\beta^+-\nu$ correlation in $^{38}\text{mK}$

For details of the apparatus, the fall, 2000 data set, and a table of dominant systematic errors, see last year’s Annual Report.

To reach the low systematic errors projected, it has been necessary to include the  $\beta^+-\nu$  correlation geometry within a GEANT simulation in order to include small effects due to the  $\beta^+$ ’s scattering from the walls. We have shown in the past how we can separate such  $\beta^+$  recoil coincidences from the true events by kinematic cuts – mostly the time of flight of the recoils – if the  $\beta^+$ ’s scatter off materials on the other side of the trap from the  $\beta^+$  telescope. However, if the  $\beta^+$  hits the “collimator” near the  $\beta^+$  telescope before scattering into it (see Fig. 36), this cannot be excluded kinematically. We find we must

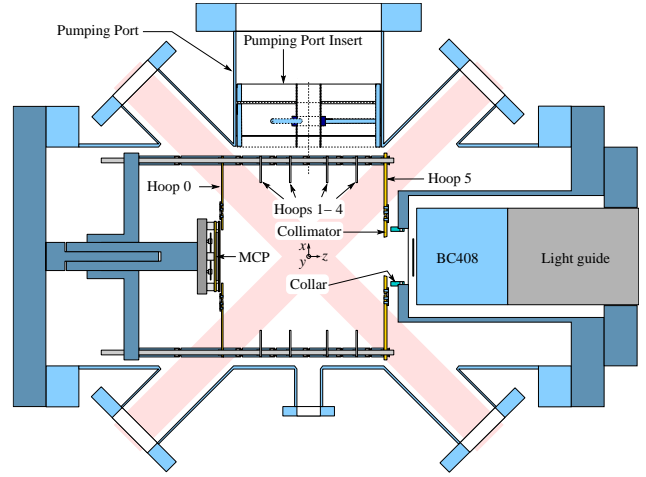


Fig. 36. Top view of present detection trap.

include this scattering to correctly account for the magnitude of the tail of the  $\beta^+$  response function deduced from the  $\text{Ar}^0$  recoil coincidences. This constitutes good indirect evidence of the effect and gives us confidence in the GEANT simulations.

This effect, and other similar scattering effects, produce very small systematic errors in the  $\beta^+-\nu$  correlation coefficient  $a$ . However, including these effects has been necessary to reach the good confidence levels recently achieved for the fits to the TOF spectra. As was known before, it is impractical to fit the data directly to the full GEANT simulation, because of computation time. Therefore much effort has been expended in producing a Monte Carlo that indirectly includes the GEANT scattering effects without compromising accuracy.

Radiative corrections, mostly from the emission of hard photons produced in the creation of the  $\beta^+$ , are now being indirectly included in the simulations using methods and calculations provided by F. Glück. This should be adequate at the present level of accuracy.

### Massive $\nu$ admixture search

We have set 90% C.L. limits of  $\leq 6 \times 10^{-3}$  on the admixture of  $\nu$ ’s having mass 0.7–3.8 MeV with the  $\nu_e$  produced in  $\beta^+$  decay. We search for extra TOF peaks in the recoil spectra using maximum likelihood techniques. To achieve this sensitivity, all the position information from the recoil and  $\beta^+$  detectors, as well as the  $\beta^+$  energy, is used to reduce the kinematic broadening of the TOF spectra. These are the best direct limits in this mass region for  $\nu$ ’s (as opposed to  $\bar{\nu}$ ’s, where  $\leq 2 \times 10^{-3}$  was achieved in  $^{20}\text{F}$   $\beta^-$  energy spectrum shape measurements [Deutsch *et al.*, Nucl. Phys. **A518**, 149 (1990)]). There are better indirect limits from the TRIUMF  $\pi \rightarrow e\nu_e$  branching ratio [Britton *et al.*, Phys. Rev. Lett. **68**, 3000 (1992)], but this can in principle also be

affected by other new physics. Admixtures with neutrinos in this mass region would affect big bang nucleosynthesis, and can be produced in extra dimension models. M. Trinczek has completed his Ph.D., and we will be submitting a paper for publication shortly.

#### $^{74}\text{Rb}$ charge radius and Q-value

Using the same apparatus and Ti:S laser, we can in principle also trap  $I=0$   $^{74}\text{Rb}$ , which is the isobaric analogue of  $^{74}\text{Kr}$ . The  $ft$  value of its decay is being studied at TRIUMF and ISOLDE to contribute to CVC and CKM matrix unitarity tests, in a system at higher  $Z$  where isospin breaking effects are expected to be larger.

The charge radius is a required input (in the approach used by Towner and Hardy) for the radial wavefunction mismatch correction, the larger of the isospin breaking corrections to the pure Fermi  $ft$  values. States with mixed oblate and prolate  $0^+$  configurations with different dynamic deformation have been shown to occur in even-even nuclei in this mass region, e.g.  $^{74}\text{Kr}$ . The difference in dynamic deformation of these configurations is large enough to generate charge radii differences of as large as 0.04 fm or 1.0%, producing a potentially significant uncertainty in the isospin breaking calculations.

The Q-value of  $^{74}\text{Rb}$  decay is needed for the  $ft$  determination. Once the optimum trap frequency (hence the isotope shift and charge radius) is determined, we hope to determine by our standard  $\beta^+$ -recoil coincidence methods the recoil momentum spectrum, from which the Q-value can be deduced. The fastest Kr recoils have momentum  $p_{\max} \approx \sqrt{Q^2 + m_\beta^2} \approx Q$ . For a Fermi decay this is a sharply determined function.  $^{74}\text{Rb}$  can be photoionized to determine the trap size and position. By reconstructing the recoil momentum – i.e. not simply taking the recoil TOF – we can narrow the peak and increase the sensitivity. We could reach  $\approx 20$  keV accuracy in modest beam time, limited by our knowledge of the electric field. The best existing value is 19 keV from ISOLTRAP measurements of the  $^{74}\text{Rb}$  mass; 2 keV is eventually needed to achieve 0.1% error in  $ft$ .

#### Spin-polarized measurements for right-handed current search

##### $^{37}\text{K}$ test run

Here we detail the outcome of the November, 2000  $^{37}\text{K}$  polarization tests. Higher polarization has since been achieved and is discussed below.

The polarization scheme presented in the past was partially implemented, in time to make detector tests. The scheme presented has been: 1) turn off trap laser beams and  $B$  field; 2) polarize atoms in  $X$  direction with optical pumping beam; 3) count; 4) turn on trap to re-confine atoms; 5) repeat.

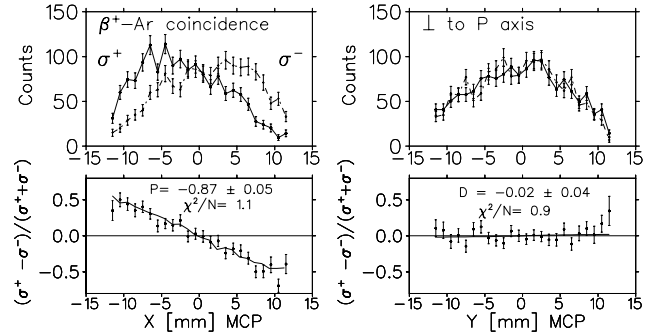


Fig. 37. Asymmetry in MCP position for  $\beta^+$ -Ar coincidences. This asymmetry is dominated by  $B_\nu$ .

The asymmetries in the  $X$  and  $Y$  MCP directions are shown in Fig. 37. A clear large asymmetry in the  $\hat{x}$  direction is generated; unfortunately, a much smaller but still finite unwanted  $\hat{y}$  asymmetry also exists. The symmetry axis was rotated in the analysis to zero the  $\hat{y}$  asymmetry. Assuming the standard model, the recoil asymmetry implies that  $(87 \pm 5)\%$  nuclear vector polarization was achieved. (The simple atomic probes for  $^{41}\text{K}$  in this geometry indicated between 80 and 90% polarization.) A similar polarization is implied by recoil singles data (not shown). If the polarization were known, the recoil asymmetry in coincidence with  $\beta^+$ 's is dominated by the  $\nu$  asymmetry  $B_\nu$  in this geometry.

##### $^{41}\text{K}$ 99% polarization

We have since achieved much higher polarization of stable  $^{41}\text{K}$ , largely by learning to turn off the trap quadrupole  $B$  field, and by improvements in the circular polarization quality of the light. When we optically pump the atoms with a circularly polarized beam tuned to the  $4S_{1/2} \rightarrow 4P_{1/2}$  “D1” transition, where the ground and excited state angular momenta are the same, the absorption of the beam vanishes when the atoms reach  $M_F = F$ . Then both the atoms and the nuclei are fully polarized. The vanishing of the fluorescence as a function of time is demonstrated in Fig. 38. Detailed rate equation and optical Bloch equation models then imply that  $P \geq 0.99$ .

Fluorescence also can vanish via “coherent population trapping”, a delicate quantum mechanical effect where the light field couples  $m_F=0$  ground states of some of the atoms into coherent superpositions that

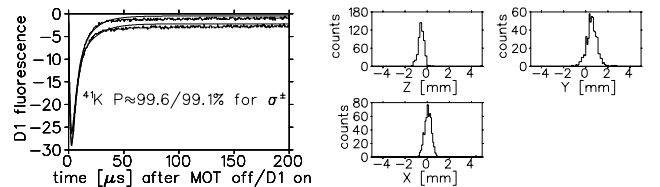


Fig. 38. Left: fluorescence from optical pumping. Right: photoionized  $^{38m}\text{K}$  radioactive atom cloud.

do not absorb light, so the atoms are not polarized. The effect is simple to destroy by detuning the laser frequency splitting to more than 100 kHz from the hyperfine ground state splitting. This technique yields remarkably narrow linewidths for an optically driven transition; 10 kHz at our laser powers, with a few Hz achieved elsewhere. We are investigating the possible utility of this technique for  $^{36}\text{K}$  and  $^{35}\text{K}$  ground state hyperfine splitting measurements. We have characterized the phenomenon and will attempt to publish in an atomic physics journal.

### Probing the polarization: non-resonant photoionization

The remaining challenge is to develop direct probes to accurately measure  $P$  and the nuclear tensor alignment, both of which are needed for the  $\beta^+$  decay experiments. The fluorescence curve must be absolutely calibrated using the large signals from  $^{41}\text{K}$  atoms, to minimize reliance on atomic physics calculations. Then the fluorescence curve must be measured for  $^{37}\text{K}$ , and hopefully  $^{36}\text{K}$ , during the measurements. We trap  $\approx 1000$   $^{37}\text{K}$  atoms, too few for direct fluorescence measurements to be feasible. We have demonstrated a much more sensitive technique, using a nitrogen laser to photoionize the  $^{38\text{m}}\text{K}$  radioactive atoms (Fig. 38). The ions are then accelerated to the MCP in the electric field. The 337 nm light from the nitrogen laser is sufficient for one-step photoionization from the first excited state of the atoms, not from the ground state. So the photoionization rate is a direct probe of the excited-state population, or the residual non-perfect polarization for the polarized experiments with the  $D1$  light on. This presents the unique prospect of monitoring the polarization of the same atoms that are decaying without disturbing their polarization.

We have replaced the present unreliable low-power laser, borrowed from TRIUMF's detector facility, with an economical 355 nm tripled diode-pumped Nd:YAG, a higher-power laser needed to make the fluorescence time curve measurement viable for the small number of  $^{37}\text{K}$  and  $^{36}\text{K}$  atoms. In addition, we have a 266 nm laser which can photoionize the atoms from their ground state.

### $^{36}\text{K}$ polarized observables for isospin mixing

We intend to measure in the next scheduling period the isospin mixing between the first two  $I^\pi = 2^+$  excited states of  $^{36}\text{Ar}$  and the lowest  $2^+$   $T = 1$  "isobaric analogue" state. We will measure spin-polarized  $^{36}\text{K}$   $\beta$  decay observables. The main purpose is to help test isospin mixing models in the  $s, d$ -shell needed for determination of the superallowed Fermi strength (and hence CKM matrix unitarity), as the calculation's methodology is the same.

We will measure the  $\beta$  asymmetry,  $A_\beta$ , and neutrino asymmetry,  $B_\nu$ . Deviations of these from the value of  $1/3$  and  $-1/3$  for  $2^+ \rightarrow 2^+$  pure Gamow-Teller transitions are very sensitive to isospin mixing admixtures [Schuermans *et al.*, Nucl. Phys. **A672**, 89 (2000)]. The prediction from the isospin mixing methodology performed by Towner is such that  $A_\beta$  is expected to be 0.29 and 0.18 for the two states. The large effect should enable a measurement of the isospin mixing amplitudes to an accuracy of 20% or better. This would be competitive with the best measurements of isospin mixing admixtures to date [Hagberg *et al.*, Phys. Rev. Lett. **73**, 396 (1994)], from branching ratios of  $0^+$  nuclei to non-analogue transitions, all of which are confined to the  $f, p$ -shell.

We have concluded that this is a good first experiment to do with these methods because a measurement with knowledge of the polarization to 3%, and 1% in other systematic errors, will produce a useful result (as opposed to the 0.1% total systematic errors we will need to reach in  $^{37}\text{K}$ ).

### Planned upgrades

The  $^{36}\text{K}$  measurement relies on development of polarization methods,  $\beta^+$  detectors, UHV-compatible optical pumping beam mirrors, and other techniques being developed for the approved  $^{37}\text{K}$  parity violation measurements.

Two scintillators will be added to existing ports at  $30^\circ$  to the push beam (Fig. 39). These will be back-to-back with respect to the polarization direction, to minimize systematic errors in the  $A_\beta$  measurement. We plan for each of these to be a phoswich, using plastic scintillator for a fast  $\Delta E$  and  $\text{CaF}_2(\text{Eu})$  for the slow ( $0.96 \mu\text{s}$  decay time) E detector.

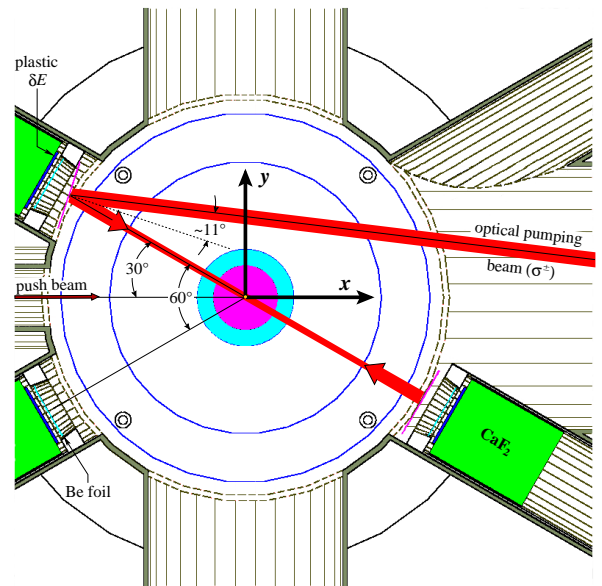


Fig. 39. 2-D side view of planned geometry.



The higher-density  $\text{CaF}_2$  ( $3.16 \text{ g/cm}^3$ ) allows the 9.8 MeV endpoint  $\beta^+$  to be contained with a manageable increase in backscatter probability compared to plastic scintillator. We plan to transport the optical pumping light with commercially available multilayer dielectric mirrors mounted on thin substrates (0.1 mm) to minimize  $\beta^+$  energy loss and angle straggling. A matched pair of mirrors with cancelling angles is necessary to avoid circular polarization distortion from the phase between S and P reflection, and we have demonstrated this technique. We have shown we can switch the trap quadrupole field off quickly enough in the presence of the stainless steel detection chamber.

More laser power is being added to the collection trap, using an existing standing-wave Ti:S and our  $\text{Ar}^+$  laser retrieved from the parity violating proton scattering experiment. This has increased the trapping efficiency for  $^{41}\text{K}$  by a factor of 2, but in a configuration where insufficient frequency stability has been attained. We are converting this to a ring geometry that should enable better frequency locking.

#### Experiment 744

##### A kinematically complete study of $\pi^- p \rightarrow e^+ e^- n$

(*M.A. Kovash, Kentucky*)

Radiative pair production,  $\pi^- p \rightarrow e^+ e^- n$ , has been shown to be a sensitive probe of the axial structure of the nucleon when studied at low pion energy. Calculations show that at a fixed pion momentum of 160 MeV/c, the shape of the  $q^2$  distribution near its endpoint directly follows the nucleon axial form factor. Accurate measurements of this  $q^2$  distribution can then be used to determine the first moment of the form factor, the axial radius. Experimentally, the value of  $q^2$  can be determined, event by event, by reconstruction from the measured electron and positron momenta. The goal of Expt. 744 is to use the large-acceptance RMC spectrometer to measure the  $q^2$  distribution for radiative pair production at a pion momentum of 160 MeV/c, and, from these data, determine the nucleon axial radius.

During the past year a major milestone in this project has been achieved with the completion of a specially designed liquid hydrogen target. The hydrogen cell and vacuum chamber were developed to minimize the energy loss and straggling of electrons exiting the sides of the cell, while maintaining a large overall target thickness to the beam. Importantly, the target's cantilevered design allows unobstructed detection of electrons over the full range of azimuthal angles. During first beam tests in December, the target, which includes new control, filling and safety systems, was successfully operated without incident.

Due to the small diameter of the target cell, 6 cm, a

significant fraction of the pion beam at the focus of the M9A channel falls outside the hydrogen region. Pions which miss the hydrogen affect the cross section normalization, and may produce significant backgrounds if they strike the relatively thick target flanges. In order to track each incident pion into the target region, we have proposed installing MWPCs into the channel at a location directly upstream of the entrance to the RMC spectrometer. Detailed simulations of this geometry are currently under way, but in the interim the wire chambers have been refurbished and chamber mounting hardware has been installed in the channel.

Our previous preliminary radiative pair production data taken with a solid  $\text{CH}_2$  target indicate that the observed shape of the  $q^2$  distribution is significantly affected by the energy spread of the pion beam within the target cell. The two most important factors affecting beam energy spread are the irreducible energy acceptance of the channel, and the energy loss of the pion beam in the target assembly. We have proposed to measure the distribution of pion momenta within the hydrogen cell by observing the distribution of momenta of forward-going neutrons from pion charge exchange,  $\pi^- p \rightarrow \pi^0 n$ . A time-of-flight distribution of cex neutrons directly determines the distribution of incident pion momenta.

To this end, we have made a first attempt at searching for cex neutrons using a new thin scintillation detector with fast timing and neutron-gamma discrimination capabilities. The detector was mounted at a distance of 3 m from the target cell, and TOF spectra were recorded for neutron triggers. The observed distribution shows a large background contribution (the detector was unshielded for this test), but also a distinct feature which is consistent with both the kinematics of charge exchange as well as the expected energy spread of the pion beam. While these first results are encouraging, clearly much work remains to be done to develop this into a reliable diagnostic tool.

#### Experiment 778

##### Low energy $\pi^\pm$ differential cross sections in the Coulomb-nuclear interference region with CHAOS

(*E.L. Mathie, Regina*)

In Expt. 778 the CHAOS collaboration has focused on forward angle  $\pi^+ p$  ( $\pi^- p$ ) elastic scattering at low energies. In this angular region there is a dramatic destructive (constructive) interference between the Coulomb scattering and  $\pi^+ p$  ( $\pi^- p$ ) hadronic scattering. These data contribute to the broad goals of testing the predictions of chiral-perturbation theory, and determination of the parameters of this fundamental theory. Analyses of  $\pi N$  scattering including this in-

terference region are expected to impact upon the determinations of the  $\pi N$  scattering-amplitudes and the  $\pi N$   $\Sigma$ -term.

Traditionally measurements in this angular range are complicated by the presence of a halo of muons arising from pions which decay upstream of the detectors. In this experiment a segment of the usual CHAOS CFT array was removed to enable use of a larger, external, array which was positioned to distinguish between pions and muons detected at small angles. The information from this auxiliary array (“The Stack”) is interpreted using a neural net. The training or calibrating of the neural net required a whole series of runs at a number of energies around each pion scattering data set energy. In these calibrations, runs with both the whole beam (pions with decay muons) and muon beam (selected by time of flight) were made with the beam passing through each stack counter.

Another distinguishing feature of the experiment was the custom built, planar liquid hydrogen target. In this target a buffer region of hydrogen gas was used to keep the liquid hydrogen thickness uniform across the whole beam width.

The first data for Expt. 778 were obtained in 1999, however, most of the data were obtained in a series of runs throughout 2000. In total some 4.7 TB of data were recorded for seven incident pion energies between 57 MeV (using beam line M11), down to 15 MeV (using M13). Data at 39 MeV were collected using both M13 and M11. In addition, data were collected for the large angle regions of  $\pi^+p$  elastic scattering at 67 MeV.

Since early 2001, the collaboration has been working on the analysis of the data, beginning with analysis of the neural net training data and a very large scale skimming effort. The experimental trigger included rather a large number of muons arising from pion decays in the vicinity of the target, which were removed in the skimming using track information (specifically the momentum versus track angle). In addition, considerable progress was made throughout the year in using the neural net decisions to distinguish between these muons and the pions of interest, scattered to small angles.

It is clear that Monte Carlo simulation of the foreground and background processes is quite important in, for example, determination of the CHAOS and Stack acceptances. The standard GEANT3 based simulation package, CHAOSSIM, was modified in 2001 to incorporate the details of the planar liquid hydrogen target geometry and materials. This plays a particularly important role in the large angle portion of the data, where two structural pillars in the target inhibit scattered pions from reaching the trigger detectors in specific angular regions.

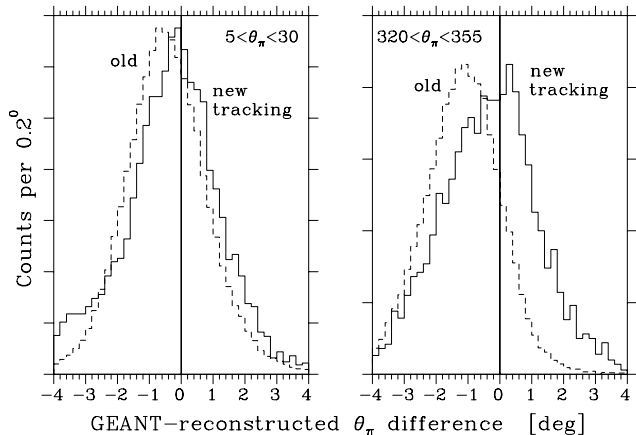


Fig. 40. Histograms of the GEANT-simulated pion scattering angle with the reconstructed value from our analysis using conventional (dashed line) and newly implemented GEANE-based algorithms (solid line) for the most forward scattered particles.

In the forward angle region accurate scattering angle determination is very important because the cross sections vary extremely rapidly. In order to optimize the CHAOS scattering angle resolution, a new track fitting scheme based upon GEANE has been implemented. In this scheme the GEANT representation of all of the detectors (already developed for the Monte Carlo) is used to determine particle energy loss along the track. Generally this algorithm provides a better momentum, scattering angle and vertex determination, shown in Fig. 40.

Analysis of Expt. 778 continues in 2002.

### Experiment 801 Studies of multi-phonon states via $\beta$ -decay (*R.F. Casten, Yale*)

The aim of Expt. 801 is to investigate the collective phonon and multi-phonon structure of low-lying intrinsic excitations in rotational nuclei.  $\beta$ -decay from a low-spin parent is an effective method for the population of low-spin members of these bands. Accurate measurement of low-intensity  $\gamma$ -ray transitions is of central importance in the interpretation of these excitations. The use of a compact configuration of large-volume Ge detectors, for efficient  $\gamma$ - $\gamma$  coincidence spectroscopy, coupled with the high intensity and high isotopic purity beams available at ISAC, provides a much higher sensitivity than was available in the previous generation of experiments.

An experiment to study  $^{162}\text{Er}$  was carried out in 2000 at the ISAC GPS  $\beta$ -decay end station. The  $^{162}\text{Er}$  nuclei were populated through the  $\beta$ -decay of  $^{162}\text{Yb}$  and studied through  $\gamma$ -ray spectroscopy. (The details of this experiment are described in the 2000 Annual Report.)

This nucleus is of special interest since the  $2^+$  member of the  $K^\pi = 0_2^+$  band (at 1171 keV) is reported to decay with collective strength to the ground state band, and so this excitation would seem a likely candidate for being a  $\beta$ -vibration: The  $B(E2; 2_{K=0}^+ \rightarrow 0_g^+)$  strength [Ronningen *et al.*, Phys. Rev. **C26**, 97 (1982)] corresponds to a squared intrinsic matrix element  $|\langle K^\pi = 0_2^+ | E2 | K^\pi = 0_g^+ \rangle|^2 = 8.0(15)$  W.u., which is comparable to the largest such values in the rare earth region and fully half as large as for the  $\gamma$ -vibrational excitation in this nucleus. The literature values [de Boer *et al.*, Nucl. Phys. **A236**, 349 (1974)] for the relative  $B(E2)$  strengths of the transitions depopulating this level ( $2_{K=0}^+ \rightarrow 0_g^+, 2_g^+, 4_g^+$ ), however, deviate from the Alaga rules by nearly an order of magnitude. These anomalous results have precluded any simple interpretation of the intrinsic structure of the  $K^\pi = 0_2^+$  excitation in  $^{162}\text{Er}$  and have called the validity of a pure rotational interpretation of this excitation into doubt.

The present measurements of the decay properties of the  $K^\pi = 0_2^+$  excitation (Fig. 41) substantially revise the  $\gamma$ -ray branching data. The relative intensities of the transitions depopulating the  $2_{K=0}^+$  level can be obtained in a straightforward fashion from spectra gated upon transitions feeding the  $2_{K=0}^+$  level (Fig. 42). With the newly measured intensities, the  $B(E2)$  values for

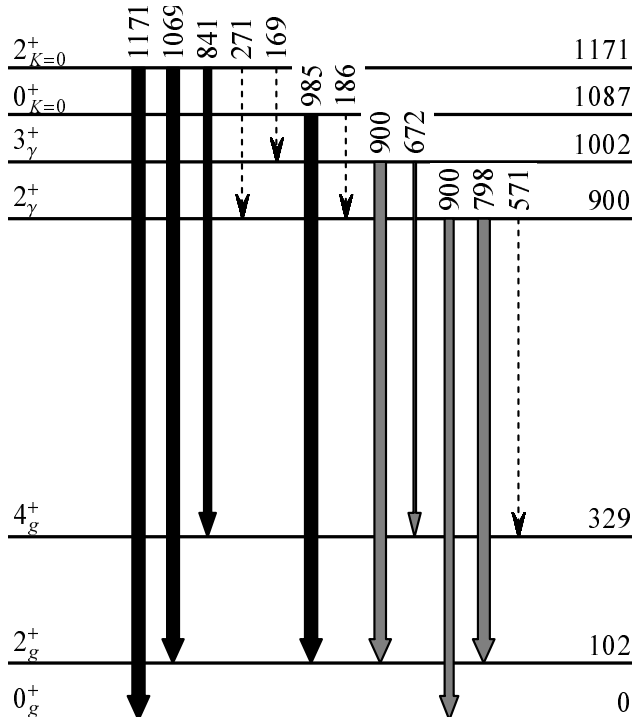


Fig. 41. Decay scheme for the low-spin members of the ground,  $\gamma$ , and  $K^\pi = 0_2^+$  bands in  $^{162}\text{Er}$  obtained from the present work. Arrow widths are proportional to  $\gamma$ -ray intensity, normalized to the strongest transition from each level. Unobserved transitions for which intensity limits were obtained are indicated by dashed arrows.

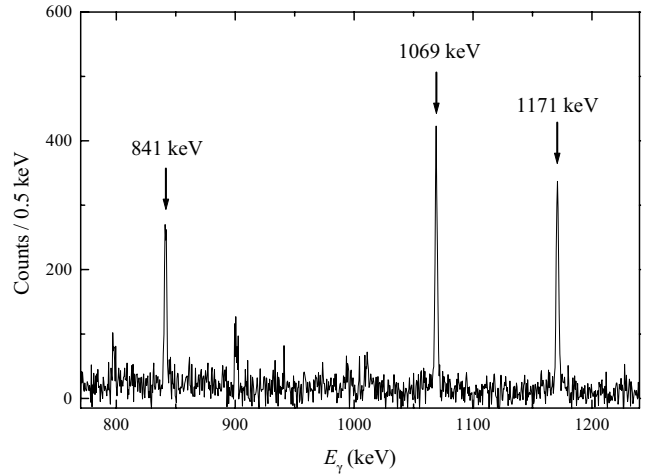


Fig. 42. Composite spectrum gated upon transitions feeding the  $2_{K=0}^+$  level at 1171 keV, showing the 841, 1069, and 1171 keV branches from this level.

the branches from the  $2_{K=0}^+$  level are found to be in reasonably good agreement with the Alaga rules. The measured  $B(E2; 2_{K=0}^+ \rightarrow 4_g^+)/B(E2; 2_{K=0}^+ \rightarrow 0_g^+)$  ratio is 3.1(2). The deviation of this from the Alaga value of 2.6 can be attributed to relatively minor mixing effects; in contrast, the literature ratio of 20(15) would have pointed towards extreme mixing of the  $K^\pi = 0^+$  band with other bands or a breakdown of the rotational picture. The present results suggest the  $K = 0_2^+$  excitation in  $^{162}\text{Er}$  is now a viable candidate for a  $\beta$ -vibrational excitation.

The only other low-lying  $K^\pi = 0^+$  excitation in  $^{162}\text{Er}$  identified in the literature is based upon a spin assignment of  $(0^+)$  for a level at 1420 keV. This excitation, from its reported decay properties, would have been of interest as a possible two- $\gamma$ -phonon excitation candidate. The present coincidence data, however, show the existence of a weak 418 keV transition from the level at 1420 keV to the  $3^+$  member of the  $\gamma$  band. The existence of such a transition is inconsistent with a  $0^+$  assignment for the level. A tentative spin assignment of  $2^-$ , based upon the level's decay properties, is reasonable in the context of the octupole excitation systematics for the region.

This work was supported by the US DOE under grants DE-FG02-91ER-40609 and DE-FG02-88ER-40417.

### Experiment 823 Pure Fermi decay in medium mass nuclei (G.C. Ball, TRIUMF)

Precise measurements of the intensities for super-allowed Fermi  $0^+ \rightarrow 0^+$   $\beta$  decays have provided a demanding test of the CVC hypothesis at the level of  $3 \times 10^{-4}$  and also led to a result in disagreement with unitarity (at the 98% confidence level) for the CKM

matrix [Towner and Hardy, WEIN'98 (World Scientific, Singapore, 1999) p. 318]. Since this would have profound implications for the minimal standard model, it is essential to address possible “trivial” explanations for this apparent non-unitarity, such as uncertainties in the theoretical isospin symmetry-breaking correction. Uncertainties in the calculated Coulomb corrections can be studied by extending the precision  $\beta$  decay measurements to heavier ( $A \geq 62$ ,  $T_z = 0$ ) odd-odd nuclei where these corrections are predicted to be much larger [Ormand and Brown, Phys. Rev. **C52**, 2455 (1995)]. The primary goal of the Expt. 823 experimental program is to measure the half-lives and branching ratios for the superallowed  $\beta$  decay of these radioactive nuclei produced at ISAC. The early measurements have focused on  $^{74}\text{Rb}$  (see 1999 and 2000 Annual Reports).

### High precision $\beta$ decay branching ratio measurements for $^{74}\text{Rb}$

Since the  $Q_{\text{EC}}$  values are large for the heavier  $T_z = 0$  nuclei, there are a large number of excited  $(0,1)^+$  states in the daughter nucleus that could be populated by  $\beta$  decay. This so-called “pandemonium effect” [Hardy *et al.*, Phys. Lett. **B17**, 107 (1977)] could confound an accurate determination of the superallowed transitions if these highly excited states in the daughter nucleus decay directly to the ground state. These measurements are also demanding because of the short half-lives ( $< 100$  ms) and limited beam intensities. Two experiments were carried out at ISAC in 2000–2001 to search for allowed non-analogue transitions in the  $\beta$  decay of  $^{74}\text{Rb}$  to excited  $(0,1)^+$  states in  $^{74}\text{Kr}$ . The first experiment was carried out using a technique similar to that described previously [Hagberg *et al.*, Nucl. Phys. **A571**, 555 (1994)]. In this case, a fast tape transport system was used to collect and move the  $^{74}\text{Rb}$  samples out of the vacuum chamber and position them between two plastic scintillator paddles each backed by a large ( $\sim 80\%$ ) HPGe detector mounted collinearly (see the 2000 Annual Report for a more complete description of this experiment). One difficulty in this measurement was the background coming from the decay of  $^{74}\text{Ga}$ , a long-lived ( $t_{1/2} = 8.12$  ms) contaminant beam which determined the limit for detecting very weak high-energy  $\gamma$ -rays from the  $\beta$  decay of  $^{74}\text{Rb}$ . However, weak Gamow-Teller/Fermi decays to one or more high-lying levels in  $^{74}\text{Kr}$  were observed by their depopulation through the known first excited  $2^+$  level at 456 keV. This result indicates that the superallowed branch is the dominant transition ( $> 99\%$ ), similar to those observed previously for odd-odd  $T_z = 0$  superallowed decays.

The determination of the transition strengths for non-analogue  $0^+ \rightarrow 0^+$  decays provides a critical test of the model predictions for the isospin mixing compo-

nent of the Coulomb correction for superallowed  $\beta$  decays. Recently, in-beam experiments [Chandler *et al.*, **C56**, R2924 (1997); Becker *et al.*, Eur. Phys. J. **A4**, 103 (1999)] have revealed the existence of a low-lying, isomeric  $0_2^+$  level in  $^{74}\text{Kr}$  at 508 keV which decays primarily by an electric monopole transition to the ground state of  $^{74}\text{Kr}$ . A preliminary experiment to search for the  $\beta$  decay of  $^{74}\text{Rb}$  to this excited  $0_2^+$  level was carried out in May–June, 2000 at a new target station, GP2, provided by TRIUMF. In this measurement the  $^{74}\text{Rb}$  atoms were implanted into a 6 mm wide mylar tape of a moving tape transport system that operated in vacuum. The collection point was viewed by two large plastic scintillation counters (one thin  $\Delta E$  counter and one thick E counter) to detect positrons, three LN-cooled Si(Li) diodes for the detection of conversion electrons and an ( $\sim 80\%$ ) HPGe detector for  $\gamma$ -rays. Both Si(Li)-plastic and Ge-plastic coincidence data were recorded (see the 2000 Annual Report for a more complete description of this preliminary experiment). Before the production run in May, a number of improvements in the experimental hardware were made including: 1) the installation of a wider (13 mm) tape transport system to ensure that all of the implanted activity is deposited on the tape; 2) the fabrication of a hollow light guide for the thin  $\Delta E$  scintillator which resulted in a factor of three reduction in 511 keV  $\gamma$ -rays in the  $\beta$ -coincident HPGe spectrum; and 3) the three Si(Li) detectors were replaced by two Si(Li) detectors mounted symmetrically above and below the tape collection spot to improve the conversion electron detection efficiency. Plans to operate the mass separator in the high-resolution mode to significantly reduce the isobaric contaminant  $^{74}\text{Ga}$  could not be carried out because of difficulties with the ISAC target ion source. Nevertheless, the quality of the production run data was improved substantially over that obtained in the preliminary run. Data analysis is still in progress.

Weak transitions were observed in the Si(Li) spectra at 39 and 495 keV corresponding to the decay of the 508 keV level to the ground state and first excited  $2^+$  level in  $^{74}\text{Kr}$  (see Fig. 43). In addition,  $^{74}\text{Rb}$   $\beta$ -delayed  $\gamma$ -rays were observed at 456, 1198, 1233 and 4244 keV (see Fig. 44). These results are in disagreement with a recent ISOLDE measurement [Oinonen *et al.*, Phys. Lett. **511B**, 145 (2001)] which observed the 495 keV electron transition at about the same intensity but did not observe any  $\gamma$ -rays. Our data have been incorporated into the partial decay scheme shown in Fig. 45. The upper limit for the non-analogue  $\beta$  decay branch ( $< 3 \times 10^{-4}$ ) is far smaller than previously predicted [Ormand and Brown, *op. cit.*] Recently, shell model calculations have been carried out that included the promotion of two particles to the  $g$ - $d$  shell [Towner and

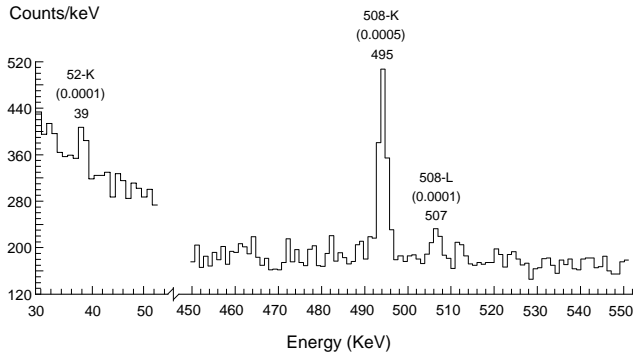


Fig. 43. Parts of the  $\beta$ -coincident KeV conversion electron spectrum measured with the Si(Li) diodes. The numbers in parentheses represent the approximate intensities of the transitions per  $^{74}\text{Rb}$  decay.

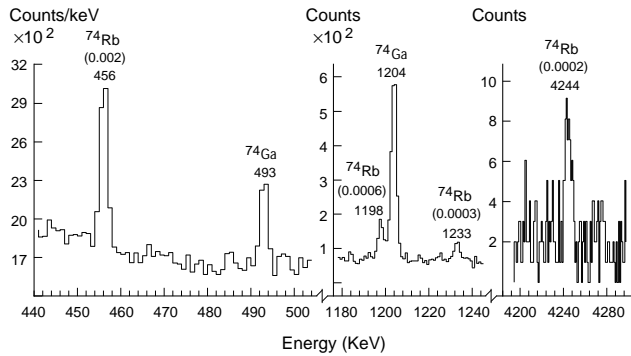


Fig. 44. Parts of the  $\beta$ -coincident  $\gamma$ -ray spectrum measured with HPGe detector. Numbers in parentheses represent the approximate intensities of the transitions per  $^{74}\text{Rb}$  decay.

Hardy, private communication and to be published]. In this model space, with an adjustment of the effective interaction, it was possible to get the first excited  $0^+$  state at  $\sim 0.5$  MeV in  $^{74}\text{Kr}$  with a small branching ratio consistent with the present data. These same calculations also predict that a large number of excited  $1^+$  states are populated at 4–6 MeV excitation in  $^{74}\text{Kr}$  with five levels carrying three-quarters of the total decay strength of  $\sim 0.9\%$ . The calculations also indicate that about half of the decay strength from these  $1^+$  levels feeds the first excited  $2^+$  level, while 24% and 16% directly feed the ground and first excited  $0^+$  states, respectively. While these predictions are qualitatively in agreement with experiment, further theoretical and experimental studies are needed. In particular, detailed spectroscopy measurements using the reconfigured  $8\pi$  spectrometer are planned [Svensson *et al.*, TRIUMF Expt. 909].

### Outlook

During the coming year the objectives are: 1) to complete the analysis of the precision branching ratio measurement for the decay of  $^{74}\text{Rb}$  and submit a paper for publication and 2) to measure the transition strength of the non-analogue  $0^+ \rightarrow 0^+$  branch in  $^{38\text{m}}\text{K}$ .

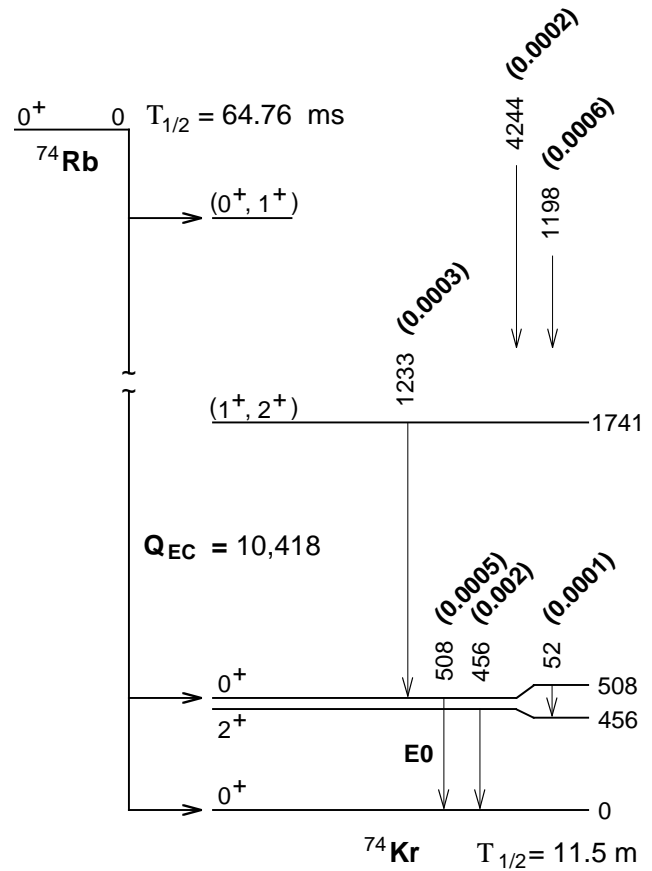


Fig. 45. The  $^{74}\text{Rb}$  decay scheme. The numbers in parentheses are approximate intensities of the transitions per  $^{74}\text{Rb}$  decay.

### Experiment 824

#### Measurement of the astrophysical rate of the $^{21}\text{Na}(p, \gamma)^{22}\text{Mg}$ reaction

(*J.M. D'Auria, SFU*)

Experiment 824 has initiated the data-taking phase using the new DRAGON facility in 2001. The objective of this experiment is to measure, with a precision of 20% or better, the astrophysical rate of the reaction  $^{21}\text{Na}(p, \gamma)^{22}\text{Mg}$  at explosive stellar temperatures. This reaction is thought to play a key role in the production and destruction of the long-lived isotope  $^{22}\text{Na}$  during nova and X-ray bursts. Unsuccessful searches in the universe for the observation of its unique decay  $\gamma$ -ray using  $\gamma$ -ray observatories in such cataclysmic events have indicated that present nova models require improvement. In the energy region of interest such radiative proton capture reactions are governed primarily by narrow resonances, requiring direct and indirect studies to elucidate.

This experiment is performed on the new DRAGON facility (see the Experimental Facilities section of this Annual Report) just installed on the HEBT-2 beam line at ISAC. The system consists of

a windowless gas target in which Expt. 824 uses hydrogen gas, surrounded by a BGO gamma detector array, a recoil mass separator to separate the rare reaction products from the relatively more intense beam particles, and a focal plane detection system to detect the separated reaction products. The focal plane detection system can be either a simple charged particle detector such as a silicon strip detector, or a more sophisticated package consisting of a micro channel plate/electron system to produce a start signal and a large volume ionization chamber with front end, parallel plate avalanche counter to provide an energy and a stop signal.

In the gas target a distribution of charge states is created of both the beam and the reaction products. The charge state of interest is then selected in the first dipole of DRAGON (MD1). In earlier studies the charge distribution of low energy heavy ions resulting from passage through a gas system was studied [W. Liu, M.Sc. thesis (Simon Fraser University, 2001)]. Table VIII presents a summary of some of these data obtained using the DRAGON windowless gas target and also taken using a similar system at the University of Naples.

The reaction products are then separated from the beam particles using the first electrostatic dipole unit, ED1, taking advantage of the small energy difference ( $\approx 4.5\%$ ). In the second stage of DRAGON, a second separation stage using further magnetic and electrostatic elements is then performed. Around the gas target, an array of 29 BGO gamma detectors is positioned to observe the prompt reaction gammas ( $E \geq 2$  MeV in this study) both singly and in coincidence; this can provide an additional factor to further suppress beam background in the recoil detector.

Further discussion on the operation of DRAGON and details of the system can be found on pg. 131 of this Annual Report.

Over the course of the last 12 months the following studies were undertaken as part of the preparation for data-taking. The commissioning of DRAGON was initiated using the  $^{15}\text{N}(p, \alpha\gamma)^{12}\text{C}$  and  $^{21}\text{Ne}(p, \gamma)^{22}\text{Na}$  reactions. The former was used to determine the pressure/density profile in the windowless gas target (see pg. 132, Fig. 124 of this Annual Report) and the latter reaction was used both to test the operation of the entire system as well as to provide an initial estimate of its transmission.

In the  $^{21}\text{Ne}(p, \gamma)^{22}\text{Na}$  reaction, resonances with  $E_{\text{cm}} = 258.3/259.3$  and  $732.7$  keV were studied. The measured resonance strengths ( $\omega\gamma$ ) were within one standard deviation of literature values. In these studies a double sided, silicon strip (16 + 16 strips) detector (DSSSD) was used to detect the separated recoils

and the gamma array was used to provide a coincident signal with the prompt reaction gammas.

A radioactive beam with intensities up to  $5 \times 10^8/\text{s}$  was made available from the ISAC system to initiate measurements of the  $^{21}\text{Na}(p, \gamma)^{22}\text{Mg}$  reaction in inverse kinematics. Using a hydrogen target thickness of about  $4 \times 10^{18}$  atoms/cm<sup>2</sup>, prompt reaction gammas were detected with the BGO gamma array, and separated reaction products detected with the DSSSD. Figure 46 displays a composite spectrum collected for two different runs. Initially, a high charge state (11+) of the  $^{21}\text{Na}$  beam was transmitted through DRAGON and used to calibrate the DSSSD. Following this, the  $^{22}\text{Mg}$  recoils (5+ charge state) from the  $^{21}\text{Ne}(p, \gamma)^{22}\text{Na}$  reaction were transmitted to the DSSSD. The lower peaks in the spectrum arise from an alpha calibration source.

Over a series of runs a special diagnostic to minimize the amount of beam spill into the gamma array around the target was developed and efforts taken to optimize the beam transmission and minimize the background radiation into the array.

Yield measurements (recording singles and coincident gamma signals simultaneously) were performed by scanning the beam energy around the known state reported previously in  $^{22}\text{Mg}$  at  $E_{\text{cm}} = 212$  keV, and, in addition, scanning in energy a strong resonance observed at  $E_{\text{cm}} \approx 822$  keV. These data are still under analysis. Further study of the operational performance of the entire DRAGON facility is presently in progress.

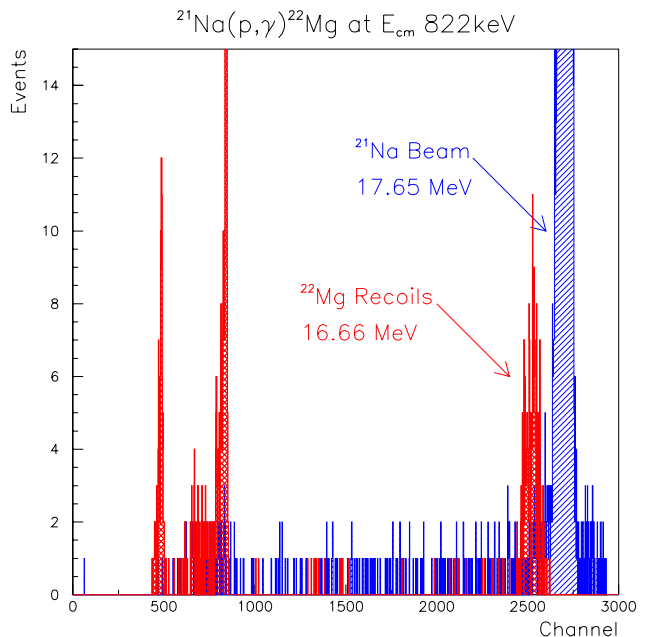


Fig. 46. Composite figure from two separate runs of reaction recoils and the  $^{21}\text{Na}$  beam (11+). See text.

Table VIII. Experimental equilibrium charge state fractions (%), where \* and † refer to data from University of Naples and DRAGON measurements, respectively.

	E(MeV/u)	$q_{in}$	n(1+)	n(2+)	n(3+)	n(4+)	n(5+)
$^{15}\text{N}+\text{H}_2^\dagger$	0.435	4+				$3.70 \pm 0.22$	$34.32 \pm 0.90$
$^{16}\text{O}+\text{H}_2^*$	0.138	2+,3+,4+	$10.46 \pm 0.56$	$43.30 \pm 1.21$	$38.99 \pm 1.18$	$7.01 \pm 0.46$	$0.33 \pm 0.05$
$^{16}\text{O}+\text{H}_2^*$	0.200	3+,4+,5+		$17.59 \pm 0.71$	$48.78 \pm 1.21$	$30.17 \pm 1.05$	$3.41 \pm 0.27$
$^{16}\text{O}+\text{H}_2^*$	0.325	3+,5+		$1.10 \pm 0.09$	$13.41 \pm 0.56$	$47.59 \pm 1.22$	$34.19 \pm 1.13$
$^{16}\text{O}+\text{H}_2^\dagger$	0.325	4+			$7.37 \pm 0.41$	$50.07 \pm 0.94$	$37.51 \pm 0.91$
$^{16}\text{O}+\text{H}_2^*$	0.500	4+			$0.50 \pm 0.06$	$10.00 \pm 0.44$	$44.50 \pm 1.27$
$^{16}\text{O}+\text{H}_2^\dagger$	0.500	4+			$0.35 \pm 0.04$	$9.89 \pm 0.54$	$41.88 \pm 0.95$
$^{16}\text{O}+\text{H}_2^*$	0.588	3+			$0.11 \pm 0.02$	$3.50 \pm 0.29$	$32.23 \pm 1.17$
$^{16}\text{O}+\text{H}_2^\dagger$	0.800	4+				$0.36 \pm 0.04$	$8.93 \pm 0.51$
$^{23}\text{Na}+\text{H}_2^*$	0.200	3+,5+,6+		$7.39 \pm 0.49$	$42.51 \pm 1.21$	$40.78 \pm 1.20$	$8.72 \pm 0.57$
$^{23}\text{Na}+\text{H}_2^*$	0.374	4+,6+			$1.01 \pm 0.11$	$13.25 \pm 0.54$	$40.90 \pm 1.15$
$^{23}\text{Na}+\text{H}_2^*$	0.478	4+,7+			$0.10 \pm 0.02$	$2.18 \pm 0.15$	$16.74 \pm 0.66$
$^{24}\text{Mg}+\text{H}_2^\dagger$	0.200	6+			$36.17 \pm 0.88$	$48.72 \pm 0.94$	$14.03 \pm 0.44$
$^{24}\text{Mg}+\text{H}_2^\dagger$	0.500	6+				$0.66 \pm 0.08$	$8.29 \pm 0.40$
$^{24}\text{Mg}+\text{H}_2^\dagger$	0.800	6+					
$^{16}\text{O}+\text{He}^*$	0.138	2+,3+,4+	$20.78 \pm 0.79$	$44.96 \pm 1.18$	$27.69 \pm 0.97$	$6.31 \pm 0.35$	$0.26 \pm 0.04$
$^{16}\text{O}+\text{He}^*$	0.200	3+,4+,5+	$0.02 \pm 0.003$	$33.04 \pm 1.10$	$46.31 \pm 1.22$	$18.64 \pm 0.74$	$1.92 \pm 0.15$
$^{16}\text{O}+\text{He}^*$	0.325	3+,5+		$7.90 \pm 0.43$	$34.48 \pm 1.10$	$42.28 \pm 1.17$	$14.61 \pm 0.59$
$^{16}\text{O}+\text{He}^*$	0.371	3+		$4.82 \pm 0.27$	$25.56 \pm 0.93$	$47.21 \pm 1.47$	$20.31 \pm 0.78$
$^{16}\text{O}+\text{He}^*$	0.588	3+			$3.90 \pm 0.22$	$24.45 \pm 0.90$	$47.52 \pm 1.19$
$^{16}\text{O}+\text{He}^*$	0.750	6+				$9.00 \pm 0.59$	$37.38 \pm 1.19$
$^{16}\text{O}+\text{He}^*$	0.875	5+					$29.88 \pm 1.11$

Table VIII. Continued.

	E(MeV/u)	$q_{in}$	n(6+)	n(7+)	n(8+)	n(9+)	n(10+)
$^{15}\text{N}+\text{H}_2^\dagger$	0.435	4+	$57.57 \pm 0.95$	$4.41 \pm 0.26$			
$^{16}\text{O}+\text{H}_2^*$	0.138	2+,3+,4+					
$^{16}\text{O}+\text{H}_2^*$	0.200	3+,4+,5+	$0.05 \pm 0.01$				
$^{16}\text{O}+\text{H}_2^*$	0.325	3+,5+	$3.71 \pm 0.29$				
$^{16}\text{O}+\text{H}_2^\dagger$	0.325	4+	$5.05 \pm 0.35$				
$^{16}\text{O}+\text{H}_2^*$	0.500	4+	$43.50 \pm 1.26$	$1.50 \pm 0.09$			
$^{16}\text{O}+\text{H}_2^\dagger$	0.500	4+	$46.77 \pm 0.96$	$1.11 \pm 0.07$			
$^{16}\text{O}+\text{H}_2^*$	0.588	3+	$59.85 \pm 1.24$	$4.31 \pm 0.30$			
$^{16}\text{O}+\text{H}_2^\dagger$	0.800	4+	$65.81 \pm 0.84$	$23.78 \pm 0.72$	$1.12 \pm 0.14$		
$^{23}\text{Na}+\text{H}_2^*$	0.200	3+,5+,6+	$0.60 \pm 0.07$				
$^{23}\text{Na}+\text{H}_2^*$	0.374	4+,6+	$34.69 \pm 1.09$	$9.44 \pm 0.50$	$0.71 \pm 0.08$		
$^{23}\text{Na}+\text{H}_2^*$	0.478	4+,7+	$40.18 \pm 1.14$	$32.81 \pm 1.06$	$7.50 \pm 0.48$	$0.49 \pm 0.08$	
$^{24}\text{Mg}+\text{H}_2^\dagger$	0.200	6+	$1.07 \pm 0.06$	$0.01 \pm 0.001$			
$^{24}\text{Mg}+\text{H}_2^\dagger$	0.500	6+	$30.45 \pm 0.76$	$40.81 \pm 0.85$	$17.66 \pm 0.51$	$2.13 \pm 0.12$	
$^{24}\text{Mg}+\text{H}_2^\dagger$	0.800	6+	$1.40 \pm 0.08$	$10.51 \pm 0.33$	$41.64 \pm 0.89$	$37.78 \pm 0.86$	$8.67 \pm 0.42$
$^{16}\text{O}+\text{He}^*$	0.138	2+,3+,4+					
$^{16}\text{O}+\text{He}^*$	0.200	3+,4+,5+	$0.07 \pm 0.01$				
$^{16}\text{O}+\text{He}^*$	0.325	3+,5+	$0.73 \pm 0.08$				
$^{16}\text{O}+\text{He}^*$	0.371	3+	$2.10 \pm 0.12$				
$^{16}\text{O}+\text{He}^*$	0.588	3+	$23.31 \pm 0.87$	$0.82 \pm 0.09$			
$^{16}\text{O}+\text{He}^*$	0.750	6+	$48.11 \pm 1.25$	$5.51 \pm 0.31$			
$^{16}\text{O}+\text{He}^*$	0.875	5+	$59.44 \pm 1.22$	$10.68 \pm 0.59$			

**Experiment 838**  
**Double radiative capture on pionic hydrogen**  
*(RMC Collaboration)*

Negative pions stopped in hydrogen form pionic hydrogen atoms. These atoms can disintegrate via several modes that include the well known processes of charge exchange  $\pi^-p \rightarrow \pi^0n$ , radiative capture  $\pi^-p \rightarrow \gamma n$ , and pair production  $\pi^-p \rightarrow e^+e^-n$ .

However, for pionic hydrogen an additional mode of capture is predicted by theory

$$\pi^-p \rightarrow \gamma\gamma n.$$

The predicted branching ratio is  $5.1 \times 10^{-5}$ , with a mechanism that is dominated by the annihilation of the stopped, real  $\pi^-$  on a soft, virtual  $\pi^+$ , i.e.  $\pi\pi \rightarrow \gamma\gamma$ . It thereby offers a novel window on the  $\pi\pi \rightarrow \gamma\gamma$  vertex and the proton's pion field.

In Expt. 838, using the RMC spectrometer on the M9A beam line, we have conducted the first measurement of double radiative capture on pionic hydrogen. Incoming pions were counted in a plastic scintillator telescope and stopped in a liquid hydrogen target. Outgoing photons were detected by pair production in a cylindrical Pb converter and electron-positron tracking in cylindrical multiwire and drift chambers. We employed a two-photon trigger based on the hit multiplicities and the hit topologies in the trigger scintillator rings and the drift chamber cells.

The major backgrounds were real  $\gamma\text{-}\gamma$  coincidences arising from  $\pi^0 \rightarrow \gamma\gamma$  decay and accidental  $\gamma\text{-}\gamma$  coincidences arising from simultaneous  $\pi^-$  stops. To reject the  $\pi^0$  background we imposed a photon opening angle cut of  $\cos\theta > -0.1$ , and to reject the multi- $\pi$  background we imposed a beam telescope amplitude cut. This yielded a total of 544 events from double radiative capture on pionic hydrogen.

After accounting for the number of stopped pions and the acceptance of the RMC detector we obtained a branching ratio for double radiative capture on pionic hydrogen of  $(3.08 \pm 0.13(\text{stat.}) \pm 0.31(\text{syst.})) \times 10^{-5}$ . A comparison of the corresponding photon opening angle distributions from experiment and theory is shown in Fig. 47. Our measured branching ratio and opening angle distributions are in reasonable agreement with the theoretical predictions. In particular our result supports the theoretical prediction of a dominant  $\pi\pi$  annihilation mechanism.

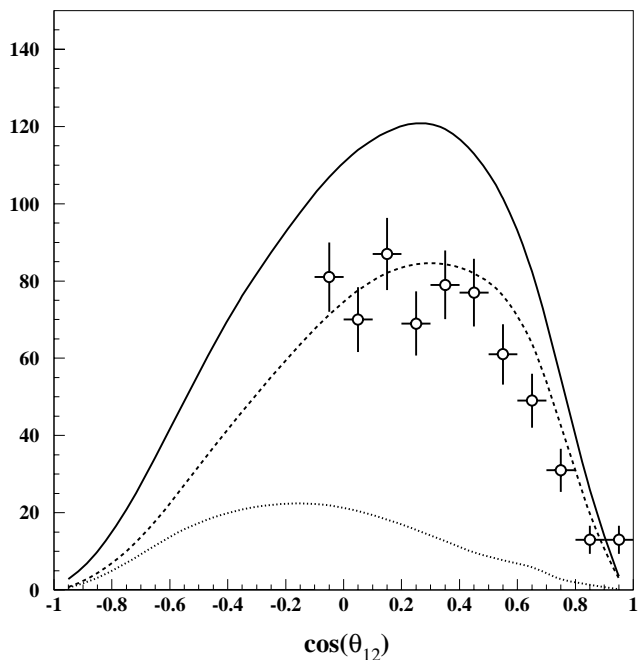


Fig. 47. Comparison of the opening angle distribution from the experimental data and the theoretical calculation. For theory the dashed curve is the  $\pi\pi$  annihilation process, the dotted curve is the  $NN$  bremsstrahlung process, and the solid curve is the full calculation. These curves are convoluted with the response function of the RMC spectrometer.

**Experiment 862**  
**Analyzing powers in the  $\vec{p}(\pi, \pi\pi)$  reactions with CHAOS**  
*(E.L. Mathie, Regina)*

Chiral perturbation theory (ChPT) is considered the most important effective field theory applied at low energies. Some argue that ChPT is QCD at low energies. Experimental descriptions of interactions involving pions and nucleons provide important tests of ChPT. To date, applications of ChPT for the pion induced pion production reactions have only been tested by total and differential cross sections. In his M.Sc. thesis, K. Babcock has argued that total cross sections do not provide adequate constraints to uniquely determine the parameters of the theory, the low energy constants (LEC). In Fig. 48 a number of statistically equivalent fits to total cross sections are shown. In addition it remains possible that third order theory may be insufficient to describe the details of the differential cross section distribution, which were not successfully fit. Polarization dependent quantities offer independent constraints from total and differential cross sections, and it is hoped determination of such quantities may help to address the question of convergence of the theory at third order, and hopefully to determine values for the low energy constants (LEC) of the theory, which must come from experiment.



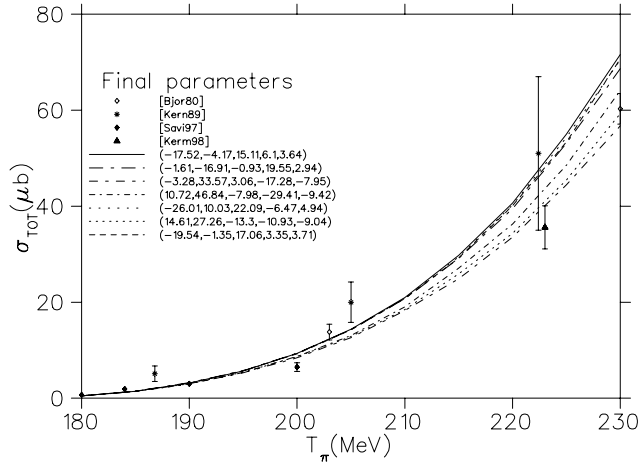


Fig. 48. The total cross sections for  $p(\pi^-, \pi^+ \pi^-)n$  vs. incident kinetic energy with a variety of equivalent fitted distributions [Babcock, 2001]. The values of the LECs for each fit are shown in the legend.

In Expt. 862, the first measurements of the asymmetry  $A$  in the  $\bar{p}(\pi, \pi\pi)$  reactions will be obtained. The CHAOS spectrometer will be used to observe the incident and outgoing charged particles after interaction in the CHAOS polarized proton target (CPPT), which was previously used in Expt. 560. This asymmetry is defined in terms of the differential cross sections  $\sigma^+$  ( $\sigma^-$ ) for positive (negative) target polarization according to

$$A = \frac{1}{P_{\text{tgt}}} \frac{\sigma^+ - \sigma^-}{\sigma^+ + \sigma^-}$$

where  $P_{\text{tgt}}$  refers to the magnitude of target polarization and  $\sigma$  refers to any one of several differential cross sections which may be determined. In earlier CHAOS experiments, such as Expt. 624, it has been demonstrated that the differential distributions for  $(\pi, \pi\pi)$  reactions can be expressed in terms of: the square of the dipion invariant mass,  $M_{\pi\pi}^2$ ; the square of the momentum transfer to the nucleon,  $t$ ; and the angle between the two final state pions in the dipion system. The fourth kinematical variable,  $x$  (the angle between the dipion and the plane defined by the incident pion and outgoing nucleon), is not well covered in the CHAOS acceptance and hence must be modelled.

The most recently completed CHAOS experiment, Expt. 778, required a unique small scattering angle configuration in which part of the spectrometer was not utilized. In addition, during the two years of operating Expt. 778, significant improvements were made to the data acquisition system, including the replacement of a programable hardware second level trigger with software (VME) equivalent trigger. It was thus necessary for the CHAOS collaboration to begin Expt. 862 with a lengthy recommissioning of the spectrometer during May and June, 2001 in order to recommission the full

horizontal angle acceptance of the spectrometer and adapt the software triggers to the pion production experiment. At the same time all of the detectors were retuned and a major reorganization of the spectrometer electronics was accomplished.

The procedure to use the CPPT in CHAOS involves polarizing the target in an external, high homogeneity solenoid; transporting the target with an internal polarization holding field into the spectrometer; and then using the spectrometer field to maintain the frozen target polarization throughout the reaction studies. The decay of the target polarization is a strong function of the CHAOS field. In our pion elastic scattering experiments, the CHAOS field was higher than what was used in the earlier  $p(\pi, \pi\pi)$  studies, so the recommissioning run included considerable running with  $\text{CH}_2$  targets to investigate the effect of operating at a higher field on the acceptance. These results are being analyzed, and will help determine the detailed goals for running in 2002.

The improvements in triggering and data acquisition rate meant that triggers caused by a pion and proton in the final state, which were rejected in our earlier  $(\pi, \pi\pi)$  experiments by a high momentum cut, could now be accepted. In an effort to make use of this additional capability, an investigation of the feasibility of triggering on for example,  $p(\pi^-, \pi^- p)\pi^0$ , was undertaken. Although the reaction could be identified, it is unlikely that sufficient statistics above background could be obtained within the running constraints of Expt. 862 to realize the additional goal of determining an analyzing power for this channel.

Unfortunately, TRIUMF was unable to recommission the CPPT in time for running in 2001, so data runs were necessarily postponed until 2002. Work was, however, begun on the target with new control software and upgrades to the pumping systems. Operation of Expt. 862 continues in 2002.

### Experiment 863

#### Ground state magnetic moments of $^{75,77,79}\text{Ga}$ (LTNO)

(P. Mantica, MSU)

The focus of Expt. 863 is to study the evolution of the single-particle structure of medium-mass nuclides above  $^{28}\text{Ni}$  toward the  $N = 50$  shell closure. A well-known shape transition from spherical to moderate deformation ( $\beta_2 \approx 0.2$ ) occurs in the neutron-rich  $^{31}\text{Ga}$  and  $^{32}\text{Ge}$  isotopes between  $N = 40 - 42$ . Since the ground state magnetic dipole moment can serve as a sensitive probe of the nuclear ground state wavefunction, the experimental determination of the magnetic moments of heavy, odd- $A$  Ga isotopes can address the extent to which quadrupole deformation persists toward  $N = 50$ .

A low-energy beam of  $^{75}\text{Ga}$  was produced at the TRIUMF-ISAC facility using a surface ion source equipped with a Ta production target. An average proton beam current of  $20\ \mu\text{A}$  was maintained on the Ta target. The  $^{75}\text{Ga}$  nuclei were implanted into an iron foil mounted on a cold finger inside the  $^3\text{He}/^4\text{He}$  dilution refrigerator. No evidence of other  $A = 75$  isobar contaminants was observed in the low-energy radioactive beam.

The nuclear orientation of  $^{75}\text{Ga}$  was monitored by measuring the angular distribution of  $\beta$  particles emitted from the radioactive parent ( $T_{1/2}(^{75}\text{Ga}) = 126\ \text{s}$ ). Two plastic scintillator  $\Delta E$ - $E$  telescopes were placed at  $0^\circ$  and  $180^\circ$  relative to the external magnetic field provided by a superconducting split-coil magnet surrounding the  $^{75}\text{Ga}$  implantation position. The detectors were mounted external to the dilution refrigerator cryostat, 10.3 cm from the centrepoint of the implantation foil. The energies of the  $^{75}\text{Ga}$   $\beta$  particles,  $Q_\beta(\text{max}) = 3.4\ \text{MeV}$ , are sufficient to ensure that a large fraction of these particles pass through the thin cryostat walls. Three Ge detectors were also placed around the sample position at  $0^\circ$ ,  $90^\circ$ , and  $180^\circ$  relative to the external magnetic field. These detectors were used to monitor the  $\gamma$ -rays emitted from the  $^{60}\text{Co}/\text{Fe}$  thermometer placed on the cold finger to monitor the temperature of the sample. The Ge detectors were also used to monitor the  $^{75}\text{Ga}$   $\gamma$ -ray activity.

Warm ( $T > 1\ \text{K}$ ) and cold ( $T < 15\ \text{mK}$ ) data were collected at an external magnetic field of 0.2 T to determine the fractional polarization of the implanted  $^{75}\text{Ga}$  sample. The observed  $\beta$  particle asymmetry was 15%. To confirm polarization of the  $^{75}\text{Ga}$  sample, the external field was reversed, and a corresponding

reversal of the  $\beta$  particle asymmetry was observed. These data are shown in Fig. 49.

Radio frequency scans over the range 85 to 175 MHz were completed. This range covers g-factor values between 1.0 and 2.1 for  $^{75}\text{Ga}$ , taking the known hyperfine field of Ga in iron to be  $-11.0(3)\ \text{T}$ . These data are currently under analysis.

### Experiment 864

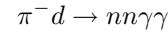
#### Dibaryon search by double radiative capture on pionic deuterium

(RMC Collaboration)

At present the deuteron is the only established particle with a baryon number  $B = 2$ . However, a large number of theoretical predictions for additional dibaryons have been published in the literature. Obviously the experimental discovery of another dibaryon would provide new insight into meson-baryon and quark-gluon dynamics at the GeV scale.

A recent claim for dibaryon production in proton-proton double bremsstrahlung reaction  $pp \rightarrow pp\gamma\gamma$  has been published by the Di2 $\gamma$  collaboration at the JINR phasetron. Specifically, they reported an intriguing double-peaked structure in the energy spectrum of the coincident  $\gamma$ -ray events from the  $pp \rightarrow pp\gamma\gamma$  reaction. They attributed the structure to the  $d^*$  dibaryon of mass  $1959 \pm 6\ \text{MeV}$  and width  $\leq 8\ \text{MeV}$ , which was first produced via the two-body process  $pp \rightarrow d^*\gamma$  and then decayed via the three-body process  $d^* \rightarrow pp\gamma$ .

Recently Gerasimov suggested that double radiative capture on pionic deuterium



is an excellent candidate for the further investigation of the dibaryon's existence. In the equation, the  $d^*$  dibaryon is first produced via radiative capture  $\pi^- d \rightarrow d^*\gamma$  and then disintegrates via radiative decay  $d^* \rightarrow nn\gamma$ . Using a simple model, Gerasimov estimated that the branching ratio for the  $d^*$ -mediated process may be as large as a few tenths of one per cent. This yield would exceed by 100 times the expected two-photon branching ratio for non-resonant double radiative capture.

In Expt. 864, using the RMC spectrometer on the M9A beam line, we have performed a dedicated search for dibaryon production via double radiative capture on pionic deuterium. Incoming pions were counted in a plastic scintillator beam telescope and stopped in a liquid deuterium target. The outgoing photons were detected by pair production in a cylindrical lead converter and electron-positron tracking in a cylindrical

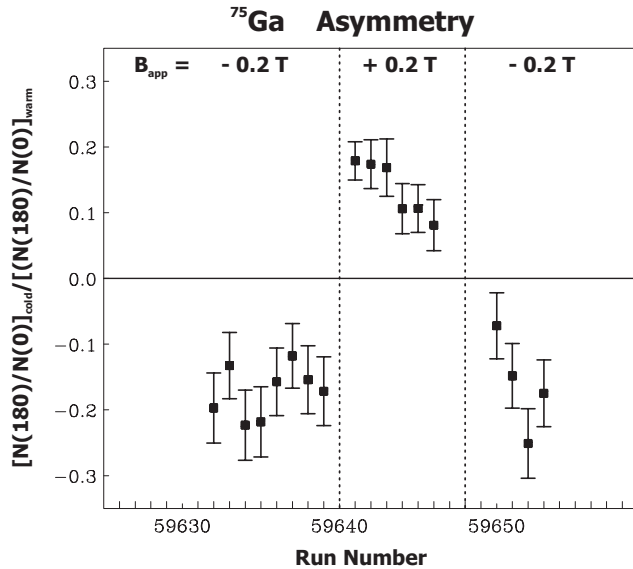


Fig. 49. Change in asymmetry as a function of applied magnetic field for  $\beta$  particles emitted from  $^{75}\text{Ga}$ .

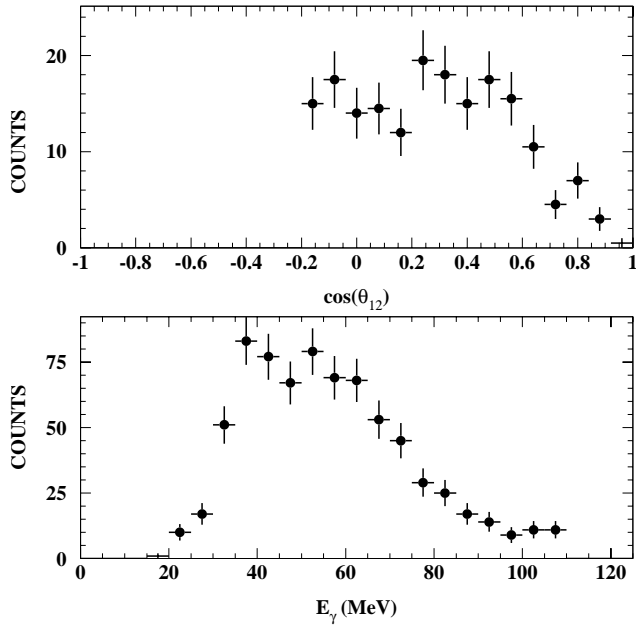


Fig. 50. The measured photon opening angle (top) and individual energy (bottom) spectra from double radiative capture on pionic deuterium.

drift chamber. An axial magnetic field was employed for momentum analysis and concentric plastic scintillator rings were employed for fast triggering.

The measured photon opening angle and individual energy spectra of the 386 recorded two-photon events from pionic deuterium are shown in Fig. 50. These spectra are entirely consistent with non-resonant double radiative capture. The expected signature of dibaryon events, i.e. a monoenergetic peak from the production process  $\pi^- d \rightarrow \gamma d^*$  and a three-body continuum from the decay process  $d^* \rightarrow \gamma nn$ , is not seen.

After correcting for the number of pion stops and the acceptance of the RMC detector we obtained a branching ratio upper limit on  $d^*$  production in  $\pi^- d$  capture of  $BR < 1.5 \times 10^{-6}$  (90% C.L.) for  $d^*$  masses of 1920–1980 MeV and  $d^*$  widths of  $< 10$  MeV. In particular we observed no evidence for a dibaryon of mass 1956 MeV and narrow width as claimed by Khrykin *et al.* Our upper limit on dibaryon production is several orders of magnitude below the yield estimate of Gerasimov.

### Experiment 875

#### MuScat: muon scattering in low $Z$ materials for muon cooling studies

(*R. Edgecock, RAL; K. Nagamine, RIKEN*)

As explained in the 2000 Annual Report, MuScat is making a precise measurement of the multiple scattering of muons in the momentum range 150–200 MeV/ $c$ . This measurement is of great importance to studies of ionization cooling, the process proposed for cooling muons for both a neutrino factory and a muon

collider [MUCOOL Collab., Fermilab Proposal P904 (1998)]. Due to the complexity of the cooling process and the fact that ionization cooling has never been demonstrated to work, MuScat is only the first of potentially three cooling experiments. The second of these is likely to be an upgrade of MuScat to measure the other physics processes of ionization cooling. This could form the subject of another proposal to TRIUMF. The last, the international muon ionization cooling experiment (MICE), will be a test of a prototype of the cooling channel for a neutrino factory. This will be a major experiment. The cooling section is likely to consist of eight 200 MHz rf cavities, eight superconducting solenoids and three liquid hydrogen absorbers each about 400 mm thick and 300 mm in diameter. This will be surrounded by two instrumentation sections, consisting of scintillating fibres similar to those to be used for MuScat (see below) contained in superconducting solenoids. There will also be time-of-flight counters and an electron identifier which could be very similar to the TINA calorimeter.

The layout of MuScat during the 2000 run is shown in Fig. 51. The most upstream parts were a veto shield and veto scintillator to eliminate beam halo. These were followed by the first trigger counter, which also acted as the TOF start. This is built from two fingers of scintillator, each 1 mm thick, 28 mm long and 3 mm high. These overlap by 20 mm in length and 3 mm in height. The timing resolution is about 250 ps. The TOF stop came from the following rf bucket of the cyclotron. This is almost a square-wave of length 1.9 ns, the smearing of the edges corresponding to a resolution of about 500 ps.

This trigger scintillator was followed by a 1 m long vacuum tube containing the collimation system. This consisted of a 40 mm thick lead block at the front and a 160 mm lead block at the back, plus 4 intermediate blocks each 10 mm thick. The first block had a slit 20 mm long by 2 mm high cut in it, while the slot in the second block was tapered to prevent large angle scatters off the internal face. With this arrangement,

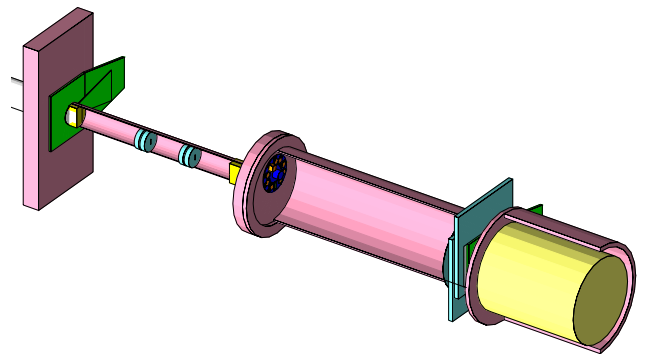


Fig. 51. The layout of the MuScat experiment in 2000, shown from below.

the scattering distribution was measured vertically, in the narrow direction of the slot. The second dimension was longer to increase the particle intensity.

The vacuum tube was connected to the main vacuum vessel, which contained the solid targets. In 2000, lithium, beryllium, carbon, aluminum and iron targets were used. They were mounted on a target wheel that could be controlled from outside the vacuum so it was unnecessary to break this each time a target was changed. The wheel had ten slots, the last of which had no target mounted and was used to measure the intrinsic properties of the beam.

The tracking detectors used were delay-line chambers. These are multi-wire proportional chambers with two cathode planes and one anode plane. Each chamber gives 2-dimensional readout, but with better resolution from the cathode plane perpendicular to the anode plane,  $\sim 0.6$  mm compared to 1–2 mm. Rather than each wire being readout, the number of electronics channels required is reduced by recording only two signals from each plane. These are time values, giving the position along the delay-line from which the signal originated. As shown in Fig. 51, three of these chambers were used, each 300 mm by 300 mm in size. The most important of these was the first, which was orientated such that the dimension with the better resolution was vertical. It was approximately 1 m from the target wheel. Between the second and third chambers was the second trigger scintillator.

The final part of the detector was MINA, a NaI calorimeter of 360 mm diameter and 360 mm depth [Waltham *et al.*, Nucl. Instrum. Methods **A256**, 91 (1987)]. It has a measured energy resolution (fwhm) of 5.2% at 90 MeV with an energy dependence of  $E^{-0.55}$ . It was used for both a muon energy measurement and additional pion/muon separation.

During 2001, a number of improvements were made for a second run in 2002, based on the experience gained in 2000. These improvements are described in the following sections.

### Detectors

The delay-line chambers used for the first run of MuScat were found to have a rapid and non-uniform loss in efficiency during the running period (see the 2000 Annual Report). As a result, it was decided to replace these with three new chambers built from scintillating fibres. These consist of two offset planes of 1 mm thick fibres in each dimension, to give a uniform efficiency and two dimensional readout. Two of the chambers, which are 30 cm by 30 cm, are shown under construction in Fig. 52. There is a total of 1024 fibres per chamber. Unlike the delay-line chambers, they will be mounted inside the vacuum to remove all material between them and the targets.

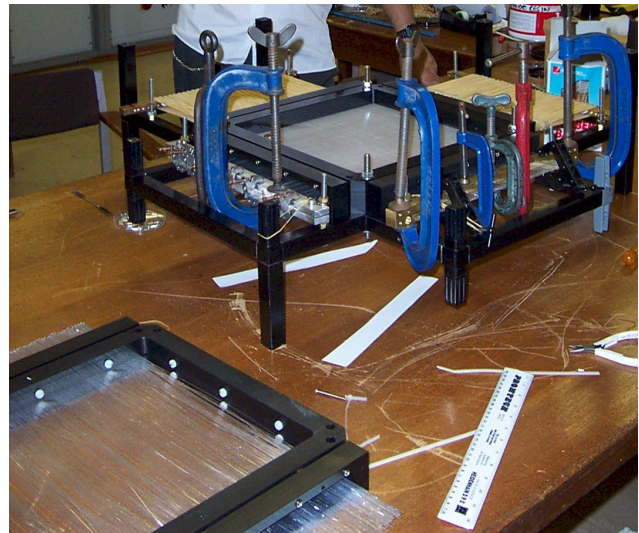


Fig. 52. Two new scintillating fibre detectors shown under construction at Imperial College, London.

The light from the scintillating fibres is transmitted to photomultipliers using clear fibres. The PMTs used are Hamamatsu R5900 L16s (see <http://cat1.hpk.co.jp/Eng/catalog/ETC/R5900U-L16.TPMH1146E06.pdf>) and contain 16 anodes, each 16 mm long and 0.8 mm wide. An array of 16 by 16 clear fibres is formed to match these anodes, thus giving a 16-fold multiplexing. To ensure that signals can be de-convoluted, the scintillating fibres are read out at both ends and the PMTs at each end are rotated by  $90^\circ$  with respect to each other. The PMTs sit outside the vacuum vessel and the fibre arrays form the vacuum seal. Tests show that the leak rate from these is sufficiently small to allow a vacuum of less than  $10^{-6}$  torr.

Purpose built front-end sample and hold electronics are used to readout the PMTs. The analogue signals from this are digitized using an ADC mounted on a card in one of the DAQ computers.

At year end, all the chambers and the 24 clear fibre arrays have been built. These are currently being inserted into the connectors that match them to the scintillating fibres. All the readout electronics are also complete. One chamber has been tested in an accelerator beam. Figure 53 shows the signals from this chamber, converted into the number of photoelectrons seen. A cosmic ray rig is being built to continue the chamber testing.

### Collimation system

The performance of the collimation system in 2000 is shown in Fig. 54, with a number of software cuts applied, including tracking back to the target region, to minimize background. Although this is adequate for the aims of MuScat, it was decided to reduce both the

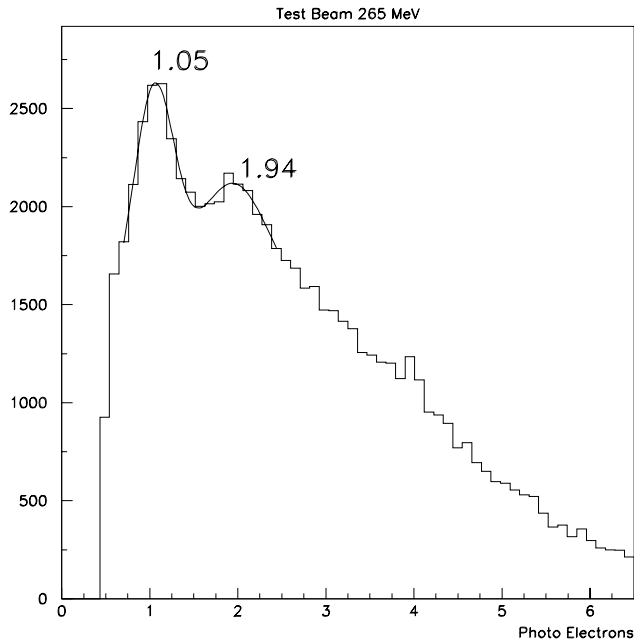


Fig. 53. Signals from a scintillating fibre detector using a 265 MeV/c mainly pion beam. A calibration has been applied which is believed to convert the signal into photoelectrons. Fits made indicate that the first two peaks do correspond to one and two photoelectrons, respectively.

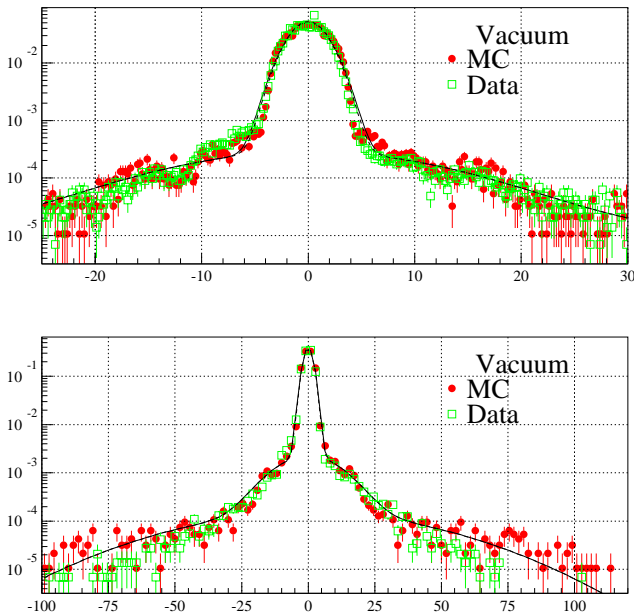


Fig. 54. The distribution of hits in the most upstream delay-line chamber without a target. The open squares are data from 2000 and the closed circles are MC predictions. The lines are the result of the fit of three Gaussians. The bottom plot shows the hits from  $\pm 100$  mm, while the top is zoomed to  $-25$  to  $+30$  mm.

width of the peak and the size of the tails of the no target scattering distribution for 2002. This has been done by moving the existing collimator disks in the collimator tube to the ends, two to each, to increase the

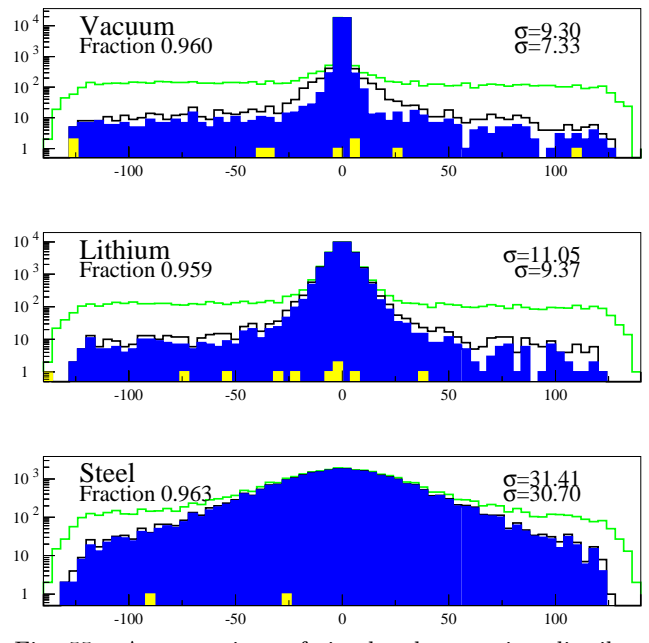


Fig. 55. A comparison of simulated scattering distributions with no target, 10 mm of lithium and 2 mm of iron using the old and new collimation systems. In each case, the upper line is the old collimation system, with no software cuts, the middle line is the new system and the dark shaded area is the new system using the active collimator. The light shaded blocks are from decays in flight.

thickness of the 40 mm and 160 mm thick end collimators. The disks have been replaced by another four, each 10 mm thick, but with 2 cm radius holes through the centre. As well as reducing the penetration through the collimators, this dramatically reduces large angle scatters off the internal faces of all the collimators. The large angle scatters will be further reduced by wrapping the collimator tube with 6 mm thick lead sheet and doubling the thickness of the front flange of the main vacuum vessel. Finally, an active collimator is being added to the front face of the 160 mm collimator block. This is being done by placing small blocks of scintillator above and below the slit of the collimator. This will eliminate particles that just clip this edge of the collimator. These improvements are demonstrated in Fig. 55.

### Targets

In the 2000 run, nine different solid targets were used, mounted on the ten hole target wheel. The tenth hole was used for measuring the intrinsic distribution of the beam. For the run in 2002, a twelve hole wheel has been created. This will allow nine targets of the same type as in 2000 to be used, but thicker to allow for the use of a higher beam energy than originally expected. In addition, one target from 2000 will be re-used, to have a comparison with the previous data. Finally, it is hoped to use a lithium hydride target, if a solid piece of the required size can be obtained.

However, the main change compared to 2000 will be two liquid hydrogen targets, one 100 mm thick and the other 150 mm. These have been built by the Cryogenics group at TRIUMF. Two thicknesses are to be measured to make it easier to de-convolute the effects of the target windows.

### Vacuum vessel

Due to the new scintillating fibre detectors and the liquid hydrogen targets, a new main vacuum vessel has been built. This vessel has a large port for the LH2 targets and larger diameter section at the end for mounting the three detectors and providing ports for the clear fibre bundles to be connected to the PMTs. In addition, there is an expansion length to be inserted when the LH2 targets are used to maintain the same distance between the middle of these and the solid targets. The vessel has been tested to the vacuum level required for the LH2 targets and pressure tested to the required safety standards.

In addition, a new stand has been built to hold the new vacuum vessel. This has also been made long and strong enough to support MINA. The mounting mechanism has been improved to allow easier alignment of the experiment.

The final change to the experiment is a larger trigger scintillator at the back of the experiment to cover the full active area of the detectors.

### Experiment 879

#### $^{21}\text{Na}(p,p)$ resonant elastic scattering

(*C. Ruiz, Edinburgh*)

This experiment used a newly available radioactive  $^{21}\text{Na}$  beam at TRIUMF's ISAC facility to study the resonant elastic scattering of  $^{21}\text{Na}$  on protons, with the intention of determining states in the compound nucleus system  $^{22}\text{Mg}$ .

$^{21}\text{Na}$  ( $T_{1/2} = 22.49$  s) beams of energies between 0.5 and 1.56 MeV/nucleon were accelerated through the ISAC-DTL and transported via the HEBT line to the TUDA particle scattering facility (TUDA collaboration: TRIUMF, University of Edinburgh, University of York). Here, highly segmented axially-symmetric LEDA silicon detector arrays were used to detect the recoil protons scattered from various thicknesses of  $\text{CH}_2$  targets. The energy loss of the incident  $^{21}\text{Na}$  through the thick  $\text{CH}_2$  targets (between  $250 \mu\text{g}/\text{cm}^2$  and  $50 \mu\text{g}/\text{cm}^2$ ) enabled the detection of protons from a range of centre-of-mass scattering energies. Therefore a range of corresponding excitation energies in the compound nucleus system can be studied.

The maximum  $^{21}\text{Na}$  beam intensities achieved were of the order  $5 \times 10^8$  particles/s, however, data acquisition constraints forced the use of a lower intensity

during the main experiment. The intensities used (typically  $5 \times 10^7$  particles/s) enabled the collection of spectra with high statistics over a short period of time. Three broad  $s$ -wave resonances in the centre-of-mass region between 0.7 and 1.5 MeV were identified, and an ongoing analysis of the data may yet reveal more. The data obtained will provide useful information on the  $T=1, A=22$  mirror system, and may also contribute to the detailed understanding of the astrophysically important  $^{21}\text{Na}(p,\gamma)^{22}\text{Mg}$  reaction.

### The experimental set-up

The TUDA facility was designed as an all-purpose particle scattering facility, providing up to 512 channels of particle detection, and a range of possible target types and positions. TUDA is particularly suited to resonant elastic scattering experiments due to the highly segmented nature of the detectors, enabling detection of recoil protons over a range of different centre-of-mass angles with high statistics. Not only can excitation functions be determined over the centre-of-mass energy range, but angular distributions can be determined providing vital information on the spin and parity of the resonant states.

In this experiment, two LEDA detectors were used at 20 cm and 62.8 cm from the target position, covering lab angles of  $4.552^\circ$ – $11.687^\circ$  and  $14.036^\circ$ – $33.004^\circ$  respectively. These correspond to a centre-of-mass energy range of approximately  $156.6^\circ$ – $170.9^\circ$  and  $114.0^\circ$ – $151.9^\circ$ , enough to determine angular distributions for strong  $p$ -waves, for example. Each LEDA detector comprises eight azimuthal sectors with sixteen annular strips at different angles.

Both LEDA detectors were shielded with a thin mylar film to prevent the scattered  $^{21}\text{Na}$  and recoil  $^{12}\text{C}$

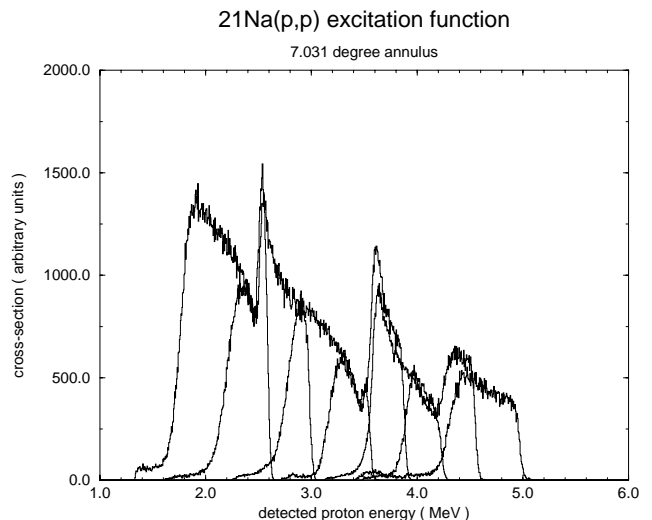


Fig. 56. Thick target proton spectra at beam energies of 880, 990, 1144, 1240, 1340, 1440 and 1560 keV/nucleon, for one annulus of a LEDA detector.

from the CH<sub>2</sub> targets from hitting the silicon. One of the eight azimuthal sectors was left uncovered by the mylar, and its corresponding electronics set at a lower gain to allow the collection of eight heavy-ion spectra for the purpose of normalization.

The centre-of-mass energy scan for a 250 μg/cm<sup>2</sup> target is approximately 200 keV. Thus, beam energies were chosen so that each thick target run would overlap substantially with the previous one, enabling target edge effects to be rejected in the final excitation function. An example of the overlapping thick target spectra for one angle can be seen in Fig. 56.

#### Data reduction and preliminary results

The data were normalized by the beam via the detected <sup>21</sup>Na in the low gain sector. The cross section was evaluated over the angular range of each strip and the energy range of the thick target to provide an accurate estimate of the number of incident <sup>21</sup>Na ions. The data were also normalized to the amount of hydrogen

in the CH<sub>2</sub> targets, which tends to deplete over time exposed to the beam, by a similar method involving the proton spectra obtained in the low gain sector. The normalization factors were then applied to each thick target spectrum, and the edges of each spectrum cut off to exclude target edge effects. The resulting data were concatenated, examples of which can be seen in Fig. 57.

Elastic scattering of <sup>21</sup>Ne+p was also performed over several known resonances for the purpose of energy calibration of the <sup>21</sup>Na data. This will be combined with a calibration from the target edges using the known beam energies.

In Fig. 57, the two spectra at largest angles show a discontinuity in the excitation functions caused by different thicknesses of mylar used for the different beam energies on the LEDA detector at 20 cm. Also, the straggling of the protons in the thick target and mylar, combined with the kinematic spread due to the

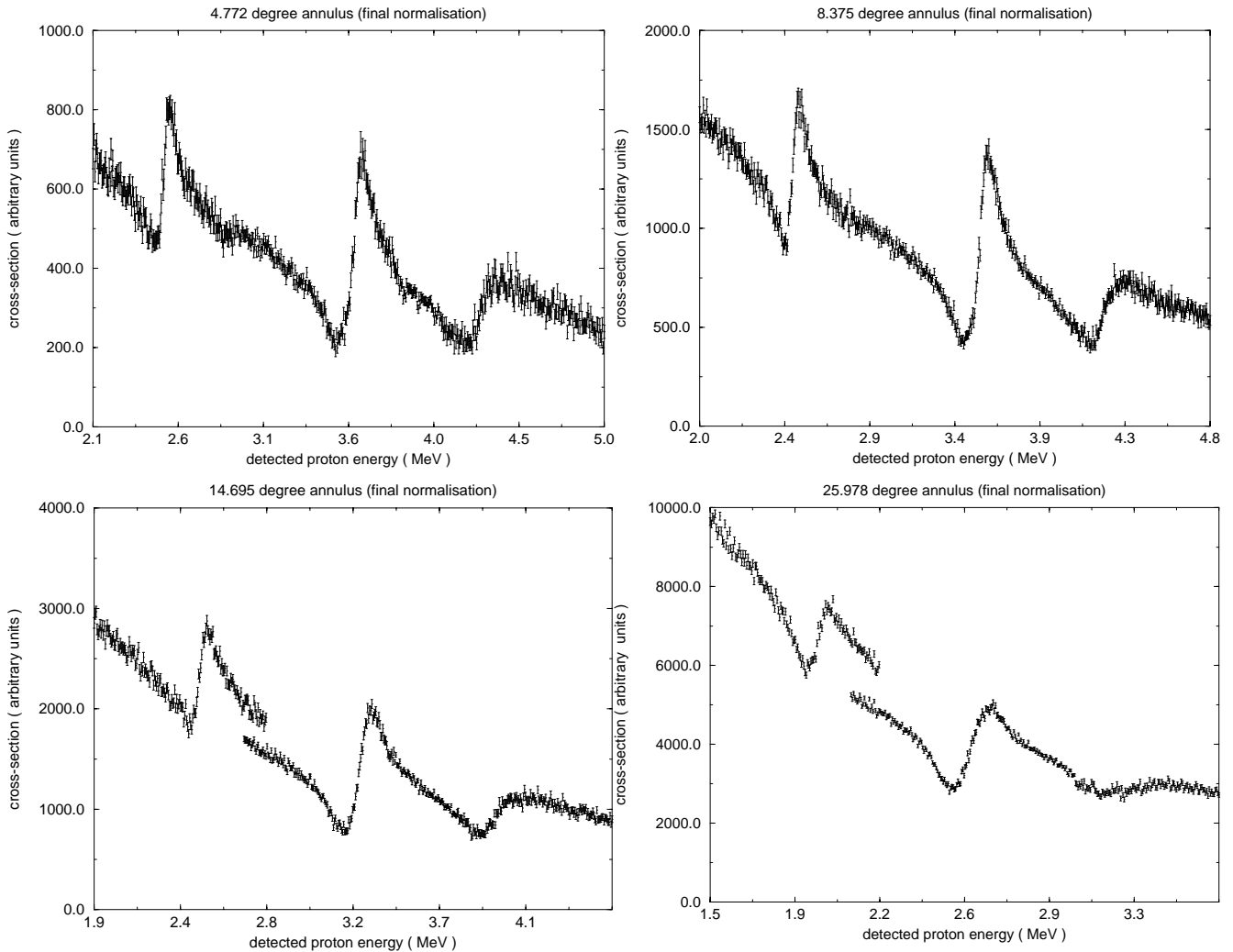


Fig. 57. <sup>21</sup>Na+p excitation functions for a selection of the 32 separate angles.

angular opening of each detector strip, causes the excitation function to be convoluted, as can be seen from the higher angle spectra. At present a Monte Carlo simulation is under construction to determine the size and type of convolution required for a fit to these spectra.

An R-matrix fit for all angles is required to determine accurately the widths and resonance energies of the observed states. A preliminary R-matrix fit for the smallest angle data has been performed and the results have been submitted for publication.

### **Concluding remarks**

The first radioactive beam experiment performed at ISAC using the TUDA particle scattering facility has been successfully completed, and an ongoing data analysis is under way. Preliminary results have been submitted for publication. It is expected that the final results will have been submitted for full publication by the end of 2002. The analysis of the data will form the major part of the thesis of C. Ruiz, University of Edinburgh.



**Experiment 758**
**Effects of quantum impurities in graphite and in one dimensional spin 1/2 chain CPC**

(R.F. Kieft, UBC/TRIUMF; J. Chakhalian, UBC)

**Graphite**

The purpose of these experiments is to test theoretical predictions on the effects of quantum impurities. The electronic and magnetic properties of an isolated positively charged impurity in a degenerate electron gas have been the subject of numerous theoretical studies [van Dyke, Nucl. Mater. **67-70**, 533 (1978); Lane and Cloney, *ibid.*, 582; Popovic and Scott, Phys. Rev. **B5**, 2109 (1972); Zaremba *et al.*, J. Physics **F7**, 1763 (1977); Jena and Singwi, Phys. Rev. **B17**, 3518 (1978)] because of its fundamental importance. Interesting quantum critical phenomena occur when gapless bulk magnetic excitations interact with a single charge impurity. The most well-known example is the Kondo effect in normal metals where a particularly large modification of the local susceptibility in the vicinity of the impurity occurs at low  $T$ .

In order to verify the theories, we have studied the local electronic structure for muons implanted in HOPG graphite by means of the muon Knight shift measurements from 3 K to 900 K. The measured Knight shift in graphite is unusually large and temperature dependent which indicates the formation of a local moment (see Fig. 58).

This is in contrast to normal metals where the Knight shifts are small and scale with the Pauli susceptibility. The isotropic part of the Knight shift is much larger than the dipolar part and rises with temperature as shown in Fig. 59. We have interpreted these results in terms of a local model where the spin density is predominantly on the neighbouring carbons, which is

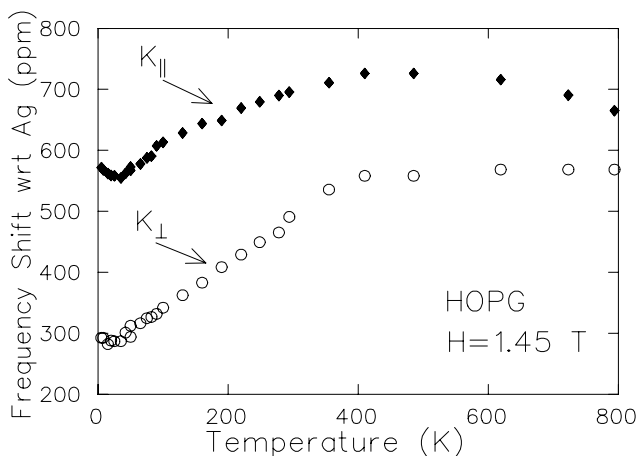


Fig. 58. Shift in muon precession frequency in HOPG relative to Ag as a function of temperature in an applied magnetic field of 1.45 T.

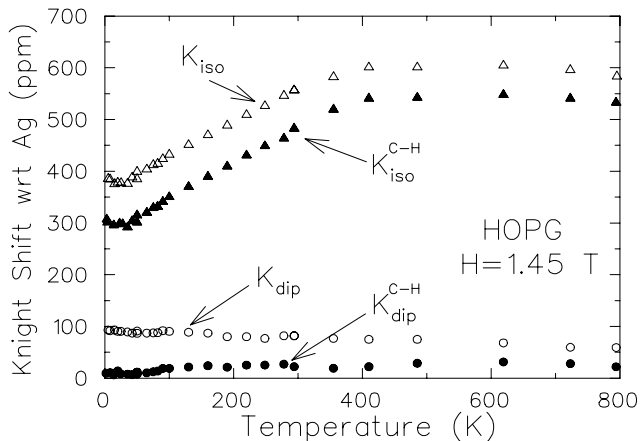


Fig. 59. Temperature dependence of the isotropic  $\mathcal{K}_{\text{iso}}$  and axial or dipolar  $\mathcal{K}_{\text{dip}}$  parts of the muon Knight shift in graphite. The filled circles and triangles represent the corrected value of the Knight shift assuming that a muon is at the C-H bond distance from a carbon atom. The open circles and triangles represent the corrected Knight shift assuming that  $\mu^+$  is in the interplane position.

similar to what is observed in some semiconductors (e.g. GaAs). This is also consistent with recent molecular orbital calculation for hydrogen on a single graphite sheet [Cox *et al.*, J. Phys. Cond. Matter **13**, 2169 (2001)].

The increase in the isotropic part of the Knight shift, which measures the contact interaction, indicates that the local electronic structure changes with temperature. At very low temperatures the observed upturn in  $\mathcal{K}_{\parallel}$  is attributed to the bulk susceptibility, which is influenced by the De Haas-van Alphen effect at low  $T$ .

In addition, the measured muon spin relaxation rate  $1/T_1$  is unusually large and deviates from the Korringa relation for metals (see Fig. 60).

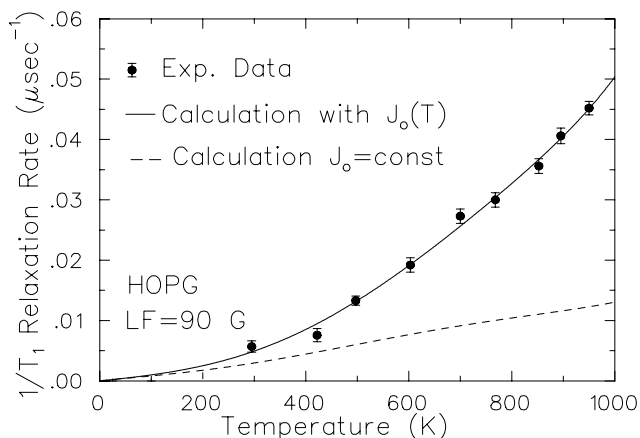


Fig. 60. Temperature dependence of the longitudinal relaxation rate  $1/T_1$  in pure graphite measured above RT. The solid and dashed lines represent our estimates.

This is attributed in part to a strong energy dependence in the density of states coupled with a small Fermi energy. A phenomenological model based on the specific graphite density of states and the temperature dependent coupling constant  $J(T)$  describes the  $1/T_1$  data rather well (see solid line in Fig. 60). The large extracted value of the Kondo temperature,  $T_K = 1852(40)$  K, is consistent with the strong-coupling limit picture. It is also worth noting that the conventional Kondo problem has only been extensively studied for normal metals where  $k_B T$  is much less than  $E_F$ , i.e. the degenerate electron gas. The situation in graphite is quite different: there,  $E_F$  is comparable to  $k_B T$ .

### CPC

Recent theoretical work by Affleck, Eggert and Takashi (AET) indicates interesting behaviour in an  $s=1/2$  Heisenberg anti-ferromagnetic spin chain with a non-magnetic single impurity [Eggert and Affleck, Phys. Rev. **B46**, 10866 (1992); Affleck *et al.*, J. Phys. **A22**, 511 (1989); Eggert and Affleck, Phys. Rev. Lett. **75**, 934 (1995)]. This behaviour is attributed to the gapless spectrum of magnetic excitations and may be considered the magnetic equivalent of the Kondo effect in normal metals. Weakening a single link in the chain as shown in Fig. 61 is a relevant perturbation; the system behaves at low  $T$  as if the chain was severed. In contrast, there is considerable experimental evidence that in most two and three dimensional magnetic compounds the muon impurity has a negligible effect, i.e. the local magnetic susceptibility tracks the bulk susceptibility.

As expected from the theory, any generic perturbation (which is not site-parity symmetric) is relevant and should result in a renormalization to a completely broken chain.

To test the theory, we conducted the  $\mu$ SR measurements on the quasi one dimensional  $s=1/2$  anti-ferromagnetic insulating chain – dichlorobis (pyridine)

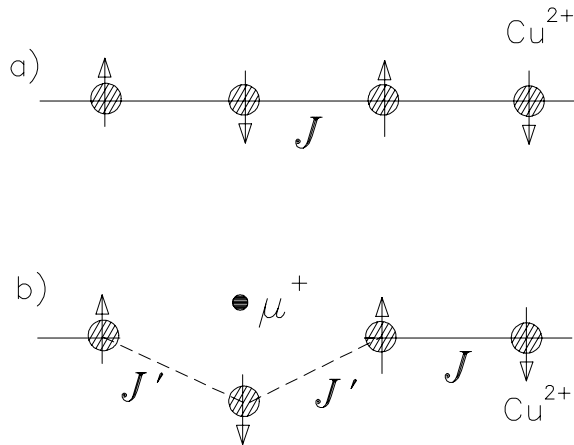


Fig. 61. A quantum spin chain with one altered link. A possible position of the muon is indicated by the arrow.

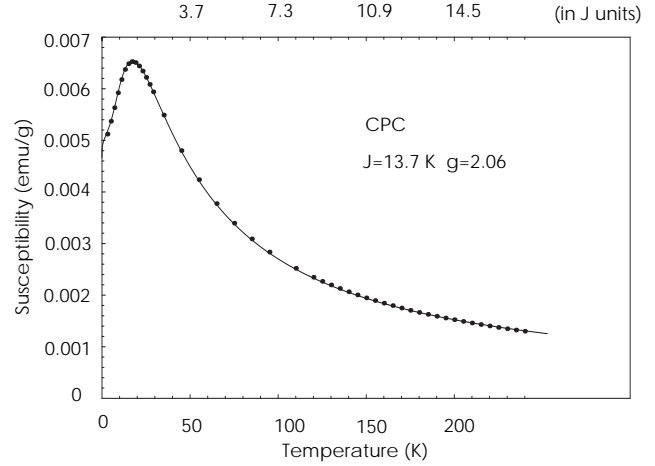


Fig. 62. Theoretical quantum Monte Carlo fit to the SQUID CPC data: The data were taken in an applied magnetic field of 1.45 T. The fit is provided courtesy of S. Eggert.

copper(II) (CPC). The AET theory predicts that the local magnetic susceptibility near an impurity in a spin  $1/2$  chain is dramatically different compared to the bulk magnetic susceptibility. To verify the AET theory, we compared the local spin susceptibility as measured by the muon spin precession frequency with the bulk magnetic susceptibility measured in a SQUID magnetometer. The theoretical fit to the experimental unperturbed susceptibility data is excellent over the entire temperature range (see Fig. 62).

The best fit yields a value of the intrachain coupling constant of  $J = 13.7(1)$  K and a  $g$ -factor of  $2.06(1)$ . This estimate of  $J$  is about 2% larger than previously reported [Takeda *et al.*, J. Phys. Soc. Japan **30**, 1330 (1971)].

In CPC the measured muon frequency shift shows a dramatic difference between the local and bulk magnetic response. The fast Fourier transforms display complex multiple frequency spectra present at low temperatures below 30 K (see Fig. 63).

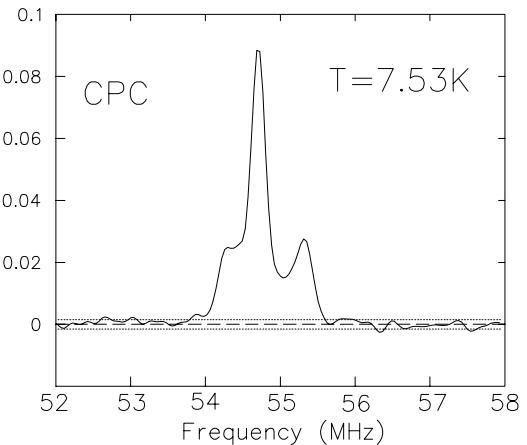


Fig. 63. FFT transform of the  $\mu$ SR signal at 7.53 K.

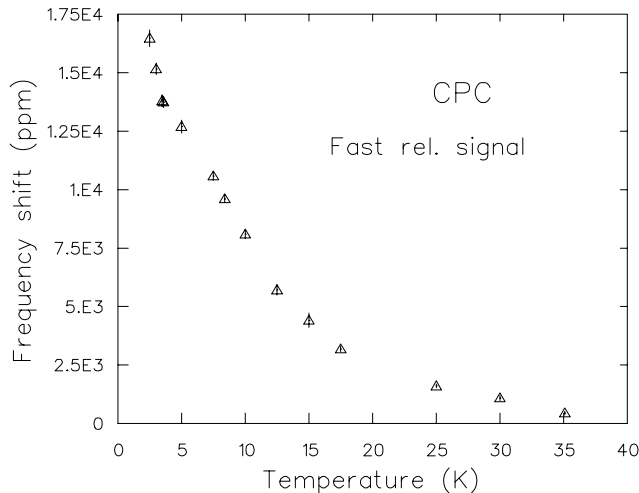


Fig. 64. Frequency shift of one of the fast relaxing  $\mu$ SR signals in CPC.

This probably represents localization of the muon at magnetically inequivalent sites. The characteristic maximum around 18 K seen in the unperturbed d.c. susceptibility is completely washed out in the frequency shift of the fast relaxing signals (see Fig. 64), which is clear evidence for a strong perturbation and thus supports the validity of the AET theory.

#### Experiment 775

##### Electron transport in insulators, semiconductors and magnetic materials

(J.H. Brewer, UBC; G.M. Luke, Columbia; V. Storchak, Kurchatov)

##### Influence of impurities on short range electron transport in GaAs

The electronic structure and dynamics of isolated atomic hydrogen (H) in semiconductors is of fundamental interest since it is the simplest and the lightest interstitial impurity. Unfortunately, direct information on isolated hydrogen is extremely limited due to its high mobility and reactivity. Most of the experimental information on the interstitial hydrogen atom comes indirectly from studies of the muonium ( $\text{Mu} = \mu^+e^-$ ) atom. However, one should always keep in mind that hydrogen and muonium are incorporated into a semiconductor in two very different ways. Hydrogen is introduced during the process of sample preparation and reaches thermal and chemical equilibrium before measurements start, while muonium is observed starting a few nanoseconds after the injection of energetic (about 4 MeV) muons into the sample [Schenck, *Muon Spin Rotation: Principles and Applications in Solid State Physics* (Adam Hilger, Bristol, 1986); Cox, *J. Phys.* **C20**, 3187 (1987); Brewer, *Muon spin rotation-relaxation-resonance* in *Encyclopedia of Applied Physics* (VCH Publishers, New York, 1994)

**11**, 23]. As the energetic  $\mu^+$  slows to an energy of a few tens of keV, in insulators and semiconductors the positive muon undergoes many cycles of electron capture and subsequent electron loss. If the last such collision leaves atomic Mu in its neutral charge state, muonium is said to have been formed promptly. If the  $\mu^+$  thermalizes as a positive ion, in many materials some of the excess electrons generated in its ionization track can reach the stopped muon and form muonium. This process of “delayed” muonium formation (DMF) is crucially dependent on the electron’s interaction with its environment or the electron mobility. Note that the characteristic length-scale of DMF is essentially microscopic – less than  $10^{-4}$  cm [Storchak *et al.*, *Appl. Mag. Reson.* **13**, 15 (1997)]. This fact offers a unique opportunity for study of electron transport to positive centres on a microscopic scale.

An essential feature of DMF is that the electrons start out spatially separated from the muon; this property is the key to distinguishing experimentally between delayed and prompt Mu formation by applying external electric fields [Storchak *et al.*, *Phys. Rev. Lett.* **75**, 2384 (1995); Eshchenko, Ph.D. thesis (Kurchatov Institute, Moscow, 1996) (in Russian)]. Relatively weak external electric fields ( $\sim 10^4$  V/cm) can sometimes overcome the muon-electron Coulomb attraction and thus reduce the probability of DMF, whereas electric fields of atomic strength ( $\sim 10^8 - 10^9$  V/cm) would be required to affect prompt (epithermal) Mu formation.

In most semiconductors two quite different types of muonium centres coexist with the diamagnetic state (or states) of the muon [Patterson, *Rev. Mod. Phys.* **60**, 69 (1988); Estle and Lichti, *Hyp. Int.* **97-98**, 171 (1996); Kiefl *et al.*, *Phys. Rev. Lett.* **58**, 1780 (1987)]. So-called “normal” muonium has an isotropic hyperfine interaction with a hyperfine constant of about half the free muonium value and is located at the tetrahedral interstitial site (and is thus denoted as  $\text{Mu}_T^0$ ). “Anomalous” or “bond-centred” muonium, with a small anisotropic hyperfine interaction, is located near the centre of the relaxed crystal bond (and is thus denoted as  $\text{Mu}_{BC}^0$ ).

Recent experiments with semi-insulating GaAs [Eshchenko *et al.*, *Phys. Lett.* **A264**, 226 (1999)] have shown complete suppression of the  $\text{Mu}_{BC}^0$  signal with electric field. This fact is illustrated in Fig. 65. One can see a large multi-frequency muonium signal for  $E = 0$ ; this beating is absent completely at high electric fields.

There are two possible explanations for the suppression of the  $\text{Mu}_{BC}^0$  signal by the external electric field. The first possibility is ionization of an initially bound muonium centre by the applied field. Alternatively, the track electrons and the muon may be

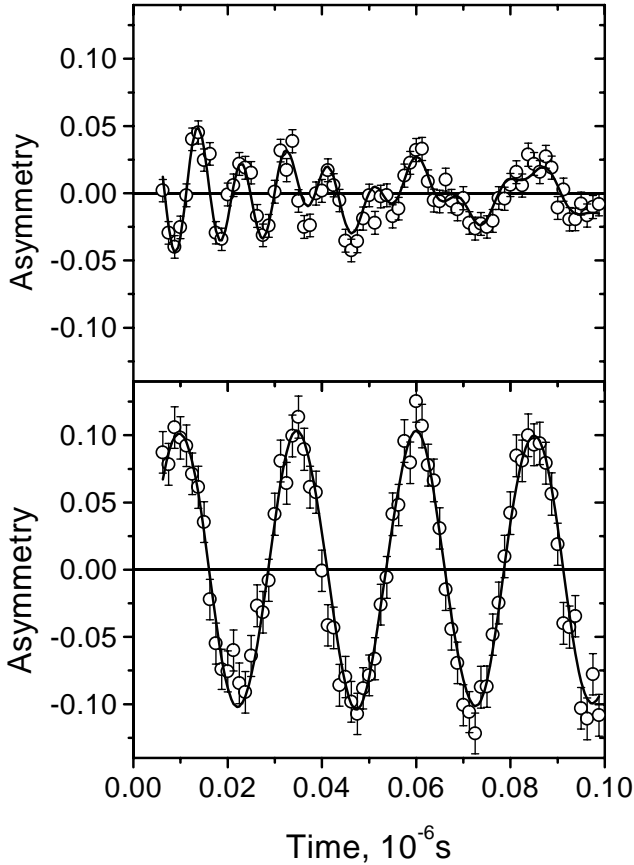


Fig. 65. Experimental  $\mu$ SR spectra in intrinsic GaAs at  $T = 10$  K in transverse magnetic field  $B = 3000$  G. Top: zero electric field. The theoretical curve is the sum of several muonium frequencies plus a small diamagnetic signal. Bottom: high external electric field (20 kV/cm). Only the diamagnetic signal is present.

initially separated, in which case the external electric field prevents electron transport to the muon.

The characteristic electric field ( $E_{\text{char}}$ ) required to change the diamagnetic/muonium fraction significantly is measured to be about 5 kV/cm in semi-insulating GaAs [Eshchenko *et al.*, *op. cit.*]. To ionize ground-state  $\text{Mu}_{BC}^0$  muonium, much higher electric fields (atomic scale) would be required. On the other hand, in GaAs a positive ion and a light electron in the  $\Gamma$ -valley ( $m^* \sim 0.07m_e$ ) can form a weakly bound ( $U = -7 \times 10^{-3}$  eV) macroscopic-sized ( $a_0 = 8.3 \times 10^{-7}$  cm) shallow donor state [Animalu, Intermediate Quantum Theory of Crystalline Solids (Prentice-Hall, Englewood Cliffs, N.J., 1977)]. The electric field  $E_i$  required to ionize this state can be estimated by equating the bias across the orbit,  $2eE_i a_0$ , to the binding energy [Knox, Theory of Excitons (Academic Press, New York, 1963)]. This rough estimate gives  $E_i \sim 5$  kV/cm in good agreement with the  $E_{\text{char}}$  observed experimentally. Thus the model of electric field induced ionization suggests ionization from the shallow

state, which in this picture is a metastable precursor for the observed Mu states.

In the alternative model one should consider initially separated free electrons moving (under the influence of the combined Coulomb and external electric fields) to the muon and/or to parent positive ions. At low temperature, where the electron mobility is very high, this motion is ballistic rather than the “classical” viscous flow behaviour. Assuming a Coulomb potential between the electron and the muon, from the characteristic field one can estimate the typical length scale of the interaction:  $R_{\text{char}} \sim \sqrt{e/(\epsilon E_{\text{char}})} \sim 10^{-6}$  cm, where  $\epsilon = 11.6$  is the dielectric constant of GaAs. On the other hand, the mean free path of a band electron in GaAs at 50 K is estimated to be  $\ell = (b/e)\sqrt{3kTm^*} \sim 6 \times 10^{-6}$  cm (where  $b \sim 1-2 \times 10^4$  cm<sup>2</sup>/V·s is the electron mobility), i.e. greater than  $R_{\text{char}}$ . From this estimate it is clear that even if an electron starts far from the muon, in the process of recombination it will eventually form (or at least pass through) the macroscopic size shallow quantum state mentioned above. An external electric field will bias the potential shape. In a weak external electric field, the electron falls to the muon through the shallow state. If the external electric field is higher than  $E_i$  the precursor shallow bound state never forms, the electron escapes capture and is lost. Thus, in this model an electric field of about  $E_i$  will prevent muonium formation with an initially separated track electron.

We report the direct evidence that the formation of the  $\text{Mu}_{BC}^0$  muonium centre in GaAs proceeds via transport of initially separated (to distances of more than  $3 \times 10^{-6}$  cm) excess electrons to the muon. To prove this we carried out experiments in GaAs samples with Cr impurities. The idea of the experiment was to place an impurity between the electron and the muon and thus influence electron transport to the muon.

Time-differential  $\mu$ SR experiments were performed on the M20 surface muon channel at TRIUMF. We tested two samples: a clean “intrinsic” GaAs sample with  $n_{\text{Cr}} < 5 \times 10^{15}$  cm<sup>-3</sup> and a sample with  $n_{\text{Cr}} = 3 \times 10^{16}$  cm<sup>-3</sup> and a defect density of  $n_d < 5 \times 10^4$  cm<sup>-3</sup>. Experimental data were obtained using a newly developed technique of  $\mu$ SR measurements in frequently switched external electric fields [Eshchenko *et al.*, *op. cit.*].

From the experiments in high transverse magnetic field [[Eshchenko *et al.*, *op. cit.*], it is known that the decrease with electric field of the  $\text{Mu}_{BC}^0$  signal is accompanied by a corresponding increase of the diamagnetic amplitude. This fact is illustrated at the top of Fig. 66. New experiments were performed in a weak transverse magnetic field of 100 G. At that field the  $\text{Mu}_{BC}^0$  signal relaxes too fast to be observed and the

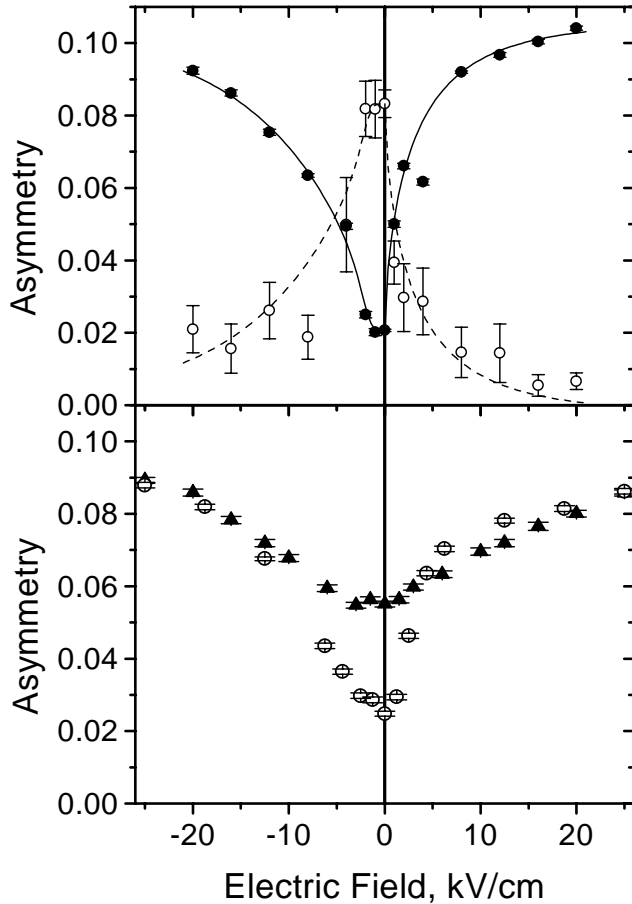


Fig. 66. Top: electric field dependence of the diamagnetic asymmetry (filled circles) and the sum of  $\text{Mu}_{BC}^0$  asymmetries (open circles) in GaAs at  $T = 10$  K. Positive electric field is in the direction of the initial muon beam momentum. The half-period of the alternating electric field is 0.005 s. The lines are to guide the eye. Bottom: electric field dependence of the diamagnetic asymmetry at  $T = 50$  K in GaAs with  $n_{Cr} < 5 \times 10^{15} \text{ cm}^{-3}$  (circles) and  $n_{Cr} = 3 \times 10^{16} \text{ cm}^{-3}$  (triangles). The half-period of the alternating field is 5 s. In both experiments the temperature was lower than the ionization temperature of shallow states ( $U \sim 80$  K).

$\text{Mu}_T^0$  frequencies are too high for the finite timing resolution of the spectrometer; thus the only observable signal is the diamagnetic one. Bearing in mind the results in high magnetic field (see top of Fig. 66), experiments in weak magnetic field give complete information about  $\text{Mu}_{BC}^0$  formation.

The electric field dependence of the diamagnetic amplitudes in GaAs samples with Cr impurities at  $T = 50$  K is shown at the bottom of Fig. 66. One can notice a remarkable difference between these dependences at low fields  $|E| < 10$  kV/cm, while at high fields the data practically coincide. A possible explanation of the different behaviour of the electric field dependence in the dirty sample in low fields could be the following. The characteristic distance between Cr centres in the dirty sample is  $R_{Cr} = n_{Cr}^{-1/3} \sim 3 \times 10^{-6}$  cm.

This value is higher than the radius  $a_0 = 8.3 \times 10^{-7}$  cm of the shallow donor state which we suggest is a precursor state for the ground state of  $\text{Mu}_{BC}^0$  in GaAs. Then in the dirty sample, Cr impurities can scatter or even capture track electrons which were initially located at a distance greater than  $R_{Cr}$  from the stopped muon, and the probability of muonium formation will be less than that in the “pure” crystal.

On the other hand, electric fields stronger than  $E_i \sim 5$  kV/cm will prevent the muon and electron from coming together regardless of the presence of impurities and the probability of muonium formation in any sample of GaAs will be almost the same.

The electric field dependence in the “pure” sample is almost the same as that measured in the semi-insulating sample (see Fig. 66). This fact implies that up to some level of impurity concentration (about  $10^{15} \text{ cm}^{-3}$ ) the process of muonium formation is independent of the small amount of impurities.

In conclusion, we have used the new  $\mu\text{SR}$  technique of measurements in alternating electric fields to study the influence of Cr impurities on short range transport of excess electrons to  $\mu^+$  centres in GaAs. Our results suggest that  $\text{Mu}_{BC}^0$  formation proceeds via electron transport to the stopped muon. Just after muon implantation into the sample, the muon and its track electrons are separated by distances greater than  $R_{Char} \sim 3 \times 10^{-6}$  cm. Under the influence of Coulomb attraction, track electrons approach the muon and/or their parent positive ions. For Cr concentrations greater than about  $n_{Cr} \sim 10^{16} \text{ cm}^{-3}$ , an electron can be captured/scattered by Cr impurities on its way to the muon. Those electrons which avoid scattering by Cr impurities may form a short lived shallow state with radius  $a_0 \sim 10^{-6}$  cm – the precursor of the ground state of  $\text{Mu}_{BC}^0$ . External electric fields higher than  $E_i \sim 5$  kV/cm prevent formation of this shallow state, thus diminishing the probability of  $\text{Mu}_{BC}^0$  formation.

## Experiment 776

### Rare-earth materials with disordered spin structures

(D.R. Noakes, Virginia State)

This experiment was a muon spin relaxation ( $\mu\text{SR}$ ) study of RE-Mg-Zn (RE=rare earth) quasicrystals and  $\text{PrP}_x$  induced moment “spin glasses”, as described in several previous Annual Reports. A paper on Monte Carlo simulations of the singlet-ground “crystalline electric field” (CEF) level fluctuation model for the observed  $\mu\text{SR}$  in  $\text{PrP}_x$ , described in previous Annual Reports, has been submitted to the Journal of Physics: Condensed Matter.

In the paramagnetic state (above the freezing temperature) of the Tb-Mg-Zn quasicrystal, monotonic

but non-exponential ZF- $\mu$ SR was observed. This was of form and temperature dependence observed in a number of disordered dense-moment magnetic materials. In the past, this form had been described in terms of phenomenological “power-exponential” relaxation

$$G_z(t) = \exp[-(rt)^p]$$

where  $r$  is a relaxation rate and the power  $p$  is near 1.0 (exponential relaxation) far above the magnetic freezing temperature, but falls as temperature is lowered, to values of 0.5 or less as the freezing temperature is approached [see, for example, Campbell *et al.*, Phys. Rev. Lett. **72**, 1291 (1994)]. ZF- $\mu$ SR in the paramagnetic Gd-Mg-Zn quasicrystal was exponential, however, except perhaps just above the freezing [both quasicrystal measurements were reported in Noakes *et al.*, Phys. Lett. **A238**, 197 (1998)]. There is no direct physical interpretation of power-exponential relaxation unless  $p$  is exactly 1.0 or 0.5 (the latter occurs for dilute spin glasses in the fast-fluctuation limit). It had been suggested that varying-power exponential relaxation is caused by a wide variety of moment fluctuation rates in the material [Heffner *et al.*, Phys. Rev. Lett. **77**, 1869 (1996)], but without detailed justification, until now. In a manuscript accepted for publication in Phys. Rev. B, we begin with a simple, broad, “double-square” distribution of exponential relaxation rates, representing a large number of muon sites in a material, each muon site experiencing a different local-field fluctuation rate. We integrate over the distribution to find a new analytic ZF muon spin relaxation function

$$G_{dsq}(t) = \frac{(w+1)e^{-\lambda_0 t/(w+1)} - we^{-\lambda_0 t} - e^{-(w+1)\lambda_0 t}}{2w\lambda_0 t},$$

where  $\lambda_0$  is the average relaxation rate in the distribution and  $w$  is a dimensionless width (the maximum relaxation rate in the distribution divided by the average). This relaxation function fits the ZF- $\mu$ SR data from the paramagnetic Tb-Mg-Zn quasicrystal, and corresponding data from paramagnetic amorphous DyAg [TRIUMF Expt. 347, originally reported in Hyp. Int. **31**, 303 (1986)], at least as well as the power-exponential relaxation function does, and the deduced parameters can be interpreted physically. We show that for the Tb-Mg-Zn quasicrystal and for *am*-DyAg, the wide distribution of moment fluctuation rates can be attributed to widely, randomly-varying rare earth CEF coupling strengths (not just randomly-varying CEF easy-axis directions), caused by the disorder in the materials. That then automatically explains why only exponential ZF relaxation was observed in the Gd-Mg-Zn quasicrystal: gadolinium is an *s*-state, spherical ion, unaffected by the CEF.

## Experiment 782

### Non-fermi-liquid behaviour and other novel phenomena in heavy-fermion alloys

(D.E. MacLaughlin, California, Riverside)

#### Non-Fermi liquids and heavy-fermion superconductors

The observed breakdown of Landau’s Fermi liquid paradigm in a number of metallic systems, among them certain *f*-electron heavy-fermion materials, has led to an explosion of effort to understand this non-Fermi liquid (NFL) behaviour. From the outset a number of mechanisms have been proposed to explain NFL phenomena; most work has concentrated on effects of a quantum critical point (QCP) separating magnetically ordered and paramagnetic phases at zero temperature. Early theories ignored the fact that most heavy-fermion alloys exhibiting such phenomena ( $Y_{1-x}U_xPd_3$ ,  $UCu_{5-x}Pd_x$ , ...) were disordered by chemical substitution.

After our NMR linewidth measurements in  $UCu_4Pd$  and  $UCu_{3.5}Pd_{1.5}$  demonstrated that the magnetic susceptibility in these materials was strongly inhomogeneous, two broad classes of theories began to address the role of disorder in NFL behaviour. In the “Kondo-disorder” approach, interactions between *f* moments are ignored and structural disorder gives rise to a broad distribution of Kondo temperatures  $T_K$ ; NFL behaviour arises from low- $T_K$  spins which are not in the Fermi-liquid state. In the “Griffiths-phase” picture, spin-spin interactions freeze low- $T_K$  *f* moments into clusters with a wide distribution of sizes; the larger clusters dominate the susceptibility and lead to divergent behaviour as the temperature is lowered. Both Kondo-disorder and Griffiths-phase scenarios seem to be compatible with observed  $\mu$ SR and NMR linewidths.

Recent  $\mu$ SR spin-lattice relaxation experiments in  $UCu_{5-x}Pd_x$  indicated, however, that the U-ion spin dynamics are better described by a cooperative picture in which critical slowing down occurs throughout the sample, rather than at (rare) low- $T_K$  spins or large clusters. The  $\mu$ SR relaxation rates are nevertheless widely distributed, and the dynamic behaviour closely resembles that of spin glasses. Thus an important question is whether the appropriate model is one in which disorder in the interactions dominates the dynamics, as in a spin glass above the glass temperature, or if, instead, the critical slowing down is still controlled by a QCP. Theoretical treatments exist which combine elements of both these viewpoints and describe a “quantum spin glass” with a suppressed or possibly zero glass temperature.

We have begun preliminary  $\mu$ SR measurements

on a novel praseodymium-based heavy-fermion superconductor, the “filled skudderudite” compound  $\text{PrOs}_4\text{Sb}_{12}$ . This material has a relatively high transition temperature,  $T_c = 1.85$  K, and a large effective mass,  $m^* \approx 50m_e$ . The intriguing aspect of this particular compound is that the  $\text{Pr}^{3+}$  ion may possess a nonmagnetic doublet  $\Gamma_3$  crystal-field ground state, in which case the usual spin-based Kondo model is not applicable and the system is expected to be a “quadrupolar Kondo” non-Fermi liquid.

The goals of our  $\mu\text{SR}$  studies of novel heavy-fermion materials are (a) to clarify the nature of the mechanism or mechanisms responsible for NFL behaviour under a variety of circumstances, and (b) to determine whether novel nonmagnetic heavy-fermion states are involved in praseodymium-based systems, particularly heavy-fermion superconductors.

### Progress to date

#### $\text{UCu}_4\text{Pd}$

In previous work we have studied local  $f$ -electron spin dynamics in the non-Fermi-liquid heavy-fermion alloys  $\text{UCu}_{5-x}\text{Pd}_x$ ,  $x = 1.0$  and  $1.5$ , using muon spin-lattice relaxation. The sample-averaged asymmetry function  $\overline{G}(t)$  indicates strongly inhomogeneous spin fluctuations, and exhibits the scaling  $\overline{G}(t, H) = \overline{G}(t/H^\gamma)$  expected from glassy dynamics. At  $0.05$  K  $\gamma(x=1.0) = 0.35 \pm 0.1$ , but  $\gamma(x=1.5) = 0.7 \pm 0.1$ . There is no sign of static magnetism  $\gtrsim 10^{-3} \mu_B/\text{U}$  ion in either material above  $0.05$  K. Our results strongly suggest that both alloys are quantum spin glasses. In  $\text{UCu}_4\text{Pd}$  the scaling exponent  $\gamma$  is small and temperature independent. In  $\text{UCu}_{3.5}\text{Pd}_{1.5}$ ,  $\gamma$  varies with temperature, increasing with decreasing temperature similar to spin-glass  $\text{AgMn}$ . This suggests that the spin-glass state found for  $x \gtrsim 2$  in  $\text{UCu}_{5-x}\text{Pd}_x$  modifies the low-frequency spin dynamics in  $\text{UCu}_{3.5}\text{Pd}_{1.5}$ . In both alloys,  $\gamma$  extrapolates to high temperatures in agreement with neutron scattering experiments.

Our collaborators at the University of Augsburg have reported specific heat  $C(T)$  and resistivity  $\rho(T)$  data from annealed and unannealed samples of  $\text{UCu}_4\text{Pd}$ . They found that a thorough annealing treatment modifies both  $C(T)$  and  $\rho(T)$ , the latter drastically; the residual resistivity is reduced considerably and, more surprisingly, the  $T$ -linear behaviour of  $\rho(T)$  at low temperatures is lost. The authors suggest that NFL behaviour in the annealed material is not driven by disorder and, by extension, that disorder is not involved in the unannealed materials either.

We therefore carried out relaxation measurements at low temperatures in annealed and unannealed samples of  $\text{UCu}_4\text{Pd}$  supplied by E. W. Scheidt, University of Augsburg. The data showed disorder in the spin dy-

namics of both samples; with similar values of the exponent  $\gamma$ . The measured relaxation rates were, however, about a factor of seven slower in the unannealed sample. No trace of magnetic ordering was found in either sample. This study has not been published to date, since our German collaborators have indicated that their annealing treatment was not successful in arriving at a sample with properties as previously reported. We are awaiting development of appropriate annealing techniques for the considerably larger specimens required for  $\mu\text{SR}$  experiments.

#### $\text{Ce}(\text{Ru}_{0.5}\text{Rh}_{0.5})_2\text{Si}_2$

This NFL alloy had previously been identified as possessing a disorder-driven NFL mechanism from thermodynamic measurements and a  $^{29}\text{Si}$  NMR study. But these NMR experiments were carried out in powder samples. The possibility has been raised that disorder introduced in the powdering process, or possibly in the original fabrication of the sample, was responsible for the NMR results, and that the mechanism for NFL behaviour in this system is not driven by disorder. We therefore obtained an extremely well-characterized single-crystal sample of  $\text{Ce}(\text{Ru}_{0.5}\text{Rh}_{0.5})_2\text{Si}_2$  from the group of Y. Myako at Osaka University. NMR on single crystals is difficult due to the small skin depth for radio frequency signals, but no such problem exists for  $\mu\text{SR}$ . Furthermore, the NMR experiment used field-aligned, epoxy-potted samples, which would not be suitable for  $\mu\text{SR}$  because a large fraction of the muons would stop in the epoxy. The single crystal  $\text{Ce}(\text{Ru}_{0.5}\text{Rh}_{0.5})_2\text{Si}_2$  sample was therefore ideal for a  $\mu\text{SR}$  study.

Analysis of the bulk susceptibility of such a crystal in the framework of disorder-driven Griffiths-phase and Kondo-disorder models for NFL behaviour yields relatively narrow distributions of characteristic spin fluctuation energies, in agreement with  $\mu\text{SR}$  linewidths that give the inhomogeneous spread in susceptibility.  $\mu\text{SR}$  and NMR data both indicate that disorder explains the “nearly NFL” behaviour observed above  $\sim 2$  K, but does not dominate the NFL physics found at low temperatures and low magnetic fields. A paper on these results has been published.

#### $\text{PrOs}_4\text{Sb}_{12}$

Heavy-fermion behaviour has been reported in a small number of praseodymium-based alloys and compounds.  $\text{Pr}^{3+}$  is a non-Kramers ion; if the crystal-field ground state is nonmagnetic and degenerate, a charge-scattering analogue of Kondo spin scattering can take place and give rise to the so-called “quadrupolar Kondo effect.” This can occur for a doublet  $\Gamma_3$  CEF ground state, although the degeneracy could be lifted by a cooperative Jahn-Teller effect. It seems possible, though,

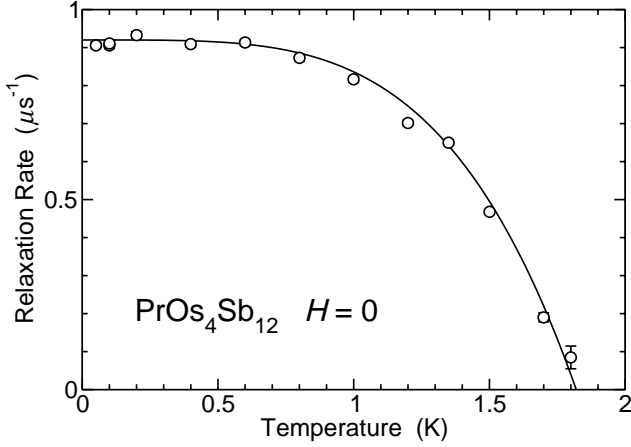


Fig. 67. Temperature dependence of vortex-state  $\mu^+$  relaxation rate  $\sigma_s(T)$  in the superconducting state of  $\text{PrOs}_4\text{Sb}_{12}$ . Curve: fit to  $\sigma_s(T) = \sigma_s(0)[1 - (T/T_c)^4]$ ;  $\sigma_s(0) = 0.92 \mu\text{s}^{-1}$ ,  $T_c = 1.83 \text{ K}$ .

that the observed heavy-fermion behaviour and superconductivity in  $\text{PrOs}_4\text{Sb}_{12}$  is associated with an unconventional “nonmagnetic” heavy-fermion state.

Initial results for the superconducting vortex-state relaxation rate  $\sigma_s(T)$  are given in Fig. 67. The zero-temperature value  $\sigma_s(0) \approx 0.9 \mu\text{s}^{-1}$  yields an estimated London penetration depth  $\lambda(0) \approx 3500 \text{ \AA}$ , which is quite short for a heavy-fermion superconductor. The data are consistent with the “two-fluid” temperature dependence  $\sigma_s(T) = \sigma_s(0)[1 - (T/T_c)^4]$ . The lack of temperature dependence of  $\sigma_s(T)$  at low temperatures suggests that we are dealing with an  $s$ -wave (or possibly  $p$ -wave) superconductor, but the data are very preliminary.

### Experiment 783

#### Knight shifts in unconventional superconductors: (U,Th)Be<sub>13</sub>

(G.D. Morris, LANL)

#### Introduction

Experiment 783 is investigating unconventional superconductivity in the  $\text{U}_{1-\delta}\text{Th}_\delta\text{Be}_{13}$  heavy-fermion materials. Muons in these cubic materials occupy a single crystallographic site midway between U atoms. However, the application of an external magnetic field generates *magnetically* inequivalent sites due to the presence of field-induced  $5f$  moments. With a magnetic field along the  $c$  axis, the two sites in the  $a - b$  plane are equivalent and situated such that the dipolar fields from the nearest  $5f$  U moments subtract from the applied field. These are termed the perpendicular sites with negative Knight shift  $K_\perp$ . For the site between U moments arranged along the field, the shift  $K_\parallel$  is positive. Overall, the resulting characteristic spectrum has one line shifted down from the silver reference line, and a line with twice as much intensity shifted up in

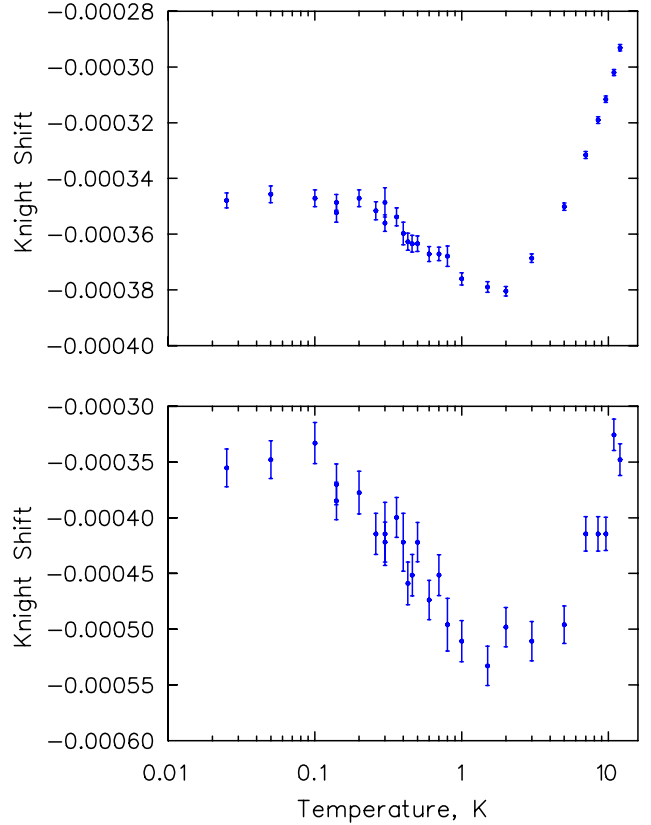


Fig. 68. Knight shifts at two magnetically inequivalent muon sites in  $\text{U}_{0.965}\text{Th}_{0.035}\text{Be}_{13}$ , with the sample oriented with (011) at  $45^\circ$  to the 1 T magnetic field.

frequency. Given the crystal structure, the magnitude and sign of the shifts and signal amplitudes unambiguously determine the muon sites.

In addition to the dipolar term, there is an RKKY interaction coupling the induced moment on the U atoms to the muon spin. Since the frequency shifts for the different sites are related, it is possible to unravel these various contributions to the Knight shift, yielding the pair spin susceptibility  $\chi_s(T)$  and hyperfine contributions to the Knight shift.

Substitution of a small amount of Th for U in  $\text{UBe}_{13}$  is known to produce a second peak in the specific heat at  $T_{c2} < T_{c1}$ , which is consistent with the onset of a second superconducting order parameter. Previous experiments performed under Expt. 783 measured the muon Knight shifts in  $\text{U}_{0.965}\text{Th}_{0.035}\text{Be}_{13}$  with the magnetic field applied along crystal axes. The principal finding of those experiments was the observation that the spin susceptibility probed by the muon drops with T between  $T_{c1}$  and  $T_{c2}$ , below which it remains constant [Sonier *et al.*, Phys. Rev. Lett. **85**, 2821 (2000)]. This is in contrast to the situation in pure  $\text{UBe}_{13}$  where the spin susceptibility continues to drop with temperature toward T = 0. It was also found



that in the normal state the hyperfine coupling between muon spin and  $5f$  electrons is anisotropic in both Th-doped and pure  $\text{UBe}_{13}$ .

#### Status of Expt. 783

In 2001 we began experiments to study the anisotropy of the Knight shift in  $\text{U}_{0.965}\text{Th}_{0.035}\text{Be}_{13}$ . Low temperature data ( $0.025 \text{ K} < T < 12 \text{ K}$ ) were collected with the external magnetic field oriented along the (110) direction in the cubic lattice. We plan to take additional data over a range of higher temperatures to complete the data set necessary for the analysis of the Knight shift in the superconducting state.

#### Experiment 784

##### Spin dynamics in the two dimensional spin system $\text{SrCu}_2(\text{BO}_3)_2$

(A. Fukaya, Y.J. Uemura, Columbia)

The spin arrangement of  $\text{SrCu}_2(\text{BO}_3)_2$  is topologically identical to the Shastry-Sutherland model, in which the ground state is an exact dimer state. The magnetic susceptibility decreases at low temperatures indicative of the spin gap ( $\Delta=34 \text{ K}$ ) associated with a singlet pair formation of dimers.

We have performed muon spin relaxation measurements in the pure and diluted  $\text{SrCu}_2(\text{BO}_3)_2$ . Figure 69 shows the temperature dependence of the zero-field  $\mu\text{SR}$  time spectra. As the temperature decreases, the relaxation rate increases below  $T=10 \text{ K}$ , and shows a saturation below  $T=3 \text{ K}$ . The line shape at low temperatures is nearly Gaussian, yet it cannot be easily decoupled by an application of longitudinal field, as shown in Fig. 70. These results indicate the existence of magnetically active spins which show slowing down of fluctuations with decreasing temperatures, yet remaining dynamic even at

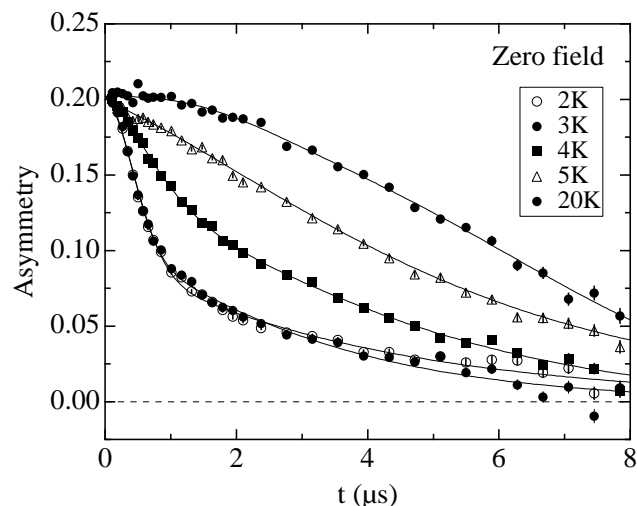


Fig. 69. Temperature dependence of the time spectra in zero-field.

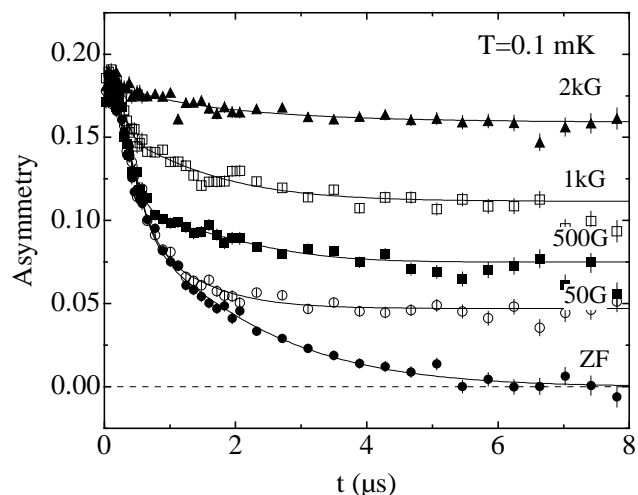


Fig. 70. Longitudinal field dependence of the time spectra at  $T=0.1 \text{ K}$ .

$0.1 \text{ K}$ . The present results are similar to the observation of muon spin relaxation in widely-believed spin gap systems, such as  $\text{NaV}_2\text{O}_5$  and  $\text{CaV}_4\text{O}_9$ . The “undecouplable-Gaussian” line shape is common to  $\mu\text{SR}$  results in the kagomé lattice and other geometrically frustrated spin systems. In a diluted system where 1% of Cu is substituted by non-magnetic Zn, we observed  $\mu\text{SR}$  results essentially identical to those in pure  $\text{SrCu}_2(\text{BO}_3)_2$ . This indicates that the observed spin relaxation is not due to impurity spins.

#### Experiment 791

##### Electronic structure and dynamics of charged muonium centres in semiconductors

(K.H. Chow, Alberta; B. Hitti, TRIUMF; R.F. Kiefl, UBC)

Results of experiments on muonium are generally considered to be the main source of information on isolated hydrogen in semiconductors. Hydrogen is an important impurity which can dramatically affect the electrical and optical properties of these technologically relevant materials. Recently, we published our observation of the reaction between  $\text{Mu}^+$  and the substitutional Zn dopant in heavily doped  $\text{GaAs:Zn}$  [Chow *et al.*, Phys. Rev. Lett. **87**, 216403 (2001)]. This was the first atomic scale study of the formation of a hydrogen or hydrogen-like complex, as it happens, with an intentional impurity in a semiconductor. An important extension of these studies is the sub-nanosopic characterization of the electronic structure of the isolated precursor state that is seen at low temperature. Such information is interesting for several reasons. First, it enables comparisons with the many theoretical calculations on the subject, which generally place the positively charged muon or proton at or near a distorted bond-centre position. Thus far, there has been no experimental evidence on the structure of  $\text{H}^+$  or  $\text{Mu}^+$  in a

semiconductor. Second, structural information on the isolated state will help us understand how the muon or hydrogen makes a transition from its precursor configuration to being part of a complex.

Information on the structure of a diamagnetic centre such as  $\text{Mu}^+$  is obtained by studying the dipole and muon-induced quadrupole interactions with the host Ga and As nuclei, all of which have spin  $3/2$ . The most powerful technique for this purpose is avoided level crossing (ALC), often called  $\mu\text{LCR}$ . In this method, a dip (also called a resonance) in the integrated muon polarization appears at values of  $\mathbf{B}$  where resonant cross-relaxation between the muon and neighbouring nuclear spins occurs due to avoided level-crossings in the combined energy levels. The positions of the resonances associated with a particular nucleus are determined primarily by  $Q$  and to a smaller extent by  $\theta$ , often giving a distinct fingerprint that identifies the neighbouring nucleus and its symmetry. Recall that  $Q$  is the strength of the quadrupole interaction and  $\theta$  is the angle between the applied magnetic field and the muon-nucleus direction.

We have recently completed our investigations of the structure and location of the precursor isolated  $\text{Mu}^+$  state mentioned above. Figure 71a summarizes the relevant results of our  $\mu\text{LCR}$  experiments in a heavily doped  $p$ -type GaAs:Zn sample at 50 K with  $\mathbf{B} \parallel \langle 100 \rangle$ . At this temperature, the isolated  $\text{Mu}^+$  centre is static. Only the regions where resonances are observable are shown. (These experiments are performed with field modulation, hence the derivative-like signals.) The two lower field resonances, located at  $\approx 1.9$  and  $\approx 3.0$  kG, can be unambiguously assigned to a nearest neighbour Ga atom. This is because the ratio of their positions is identical to the ratio of the  $^{69}\text{Ga}$  and  $^{71}\text{Ga}$  quadrupole moments ( $0.168 \times 10^{-24}$  e.cm<sup>2</sup> and  $0.106 \times 10^{-24}$  e.cm<sup>2</sup>). This is further confirmed by Fig. 71b, which shows theoretically the expected resonances. A single value of the electrical field gradient was used to produce this figure. (Note that for each Ga isotope, the signal-to-noise is too low to experimentally resolve the weaker of the pair.) On the other hand, the higher field resonances ( $\approx 6.4$  and  $\approx 7.35$  kG) are certainly due to an As atom ( $^{75}\text{As}$ , 100% abundant,  $I=3/2$ ), the only other atom in the host species in the lattice that can produce  $\mu\text{LCR}$  resonances. The unambiguous identification of Ga and As as nearest neighbors of  $\text{Mu}^+$  is certainly a very important breakthrough. However, a crucial piece of information is still lacking, namely how these atoms are oriented with respect to the muon. This information is obtained by performing  $\mu\text{LCR}$  experiments (not shown) at other major crystalline orientations, namely with  $\mathbf{B} \parallel \langle 110 \rangle$  and  $\mathbf{B} \parallel \langle 111 \rangle$ . The positions and strengths of the lines

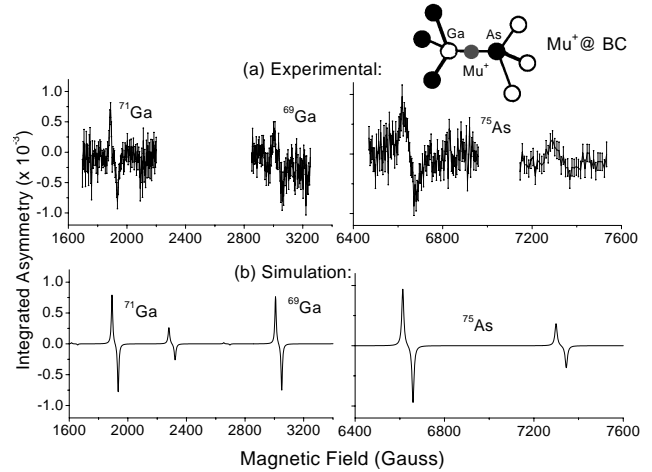


Fig. 71. (a)  $\mu\text{LCR}$  at 50 K in heavily doped  $p$ -type GaAs:Zn with  $\mathbf{B} \parallel \langle 100 \rangle$ . (b) Theoretical simulation as described in the text.

in Fig. 71a change in a manner that unambiguously confirms that the muon, the Ga, and the As atoms all lie on the same  $\langle 111 \rangle$  axis (i.e.  $\theta = 54.7^\circ$ ).

Thus, our results provide strong evidence that  $\text{Mu}^+$  is located near the centre of a Ga-As bond, as indicated in Fig. 71. Finally, we note that contained in our  $\mu\text{LCR}$  data is another piece of important information, namely the distances between  $\text{Mu}^+$  and the neighbouring Ga and As nuclei. We are currently in the process of extracting this information.

#### Experiment 804 Muonium in III-V nitrides (*R.L. Lichti, Texas Tech*)

The goal of TRIUMF Expt. 804 is to investigate the muonium analogue of hydrogen defect states in GaN and other group-III nitrides. During the past year we obtained the full temperature dependence of the QLCR resonances for several samples of AlN. These data represent diamagnetic  $\text{Mu}^+$  centres and show features related to their sites and dynamics. The likely stable  $\text{Mu}^+$  sites are nitrogen anti-bonding locations oriented into the channels formed by the 2H Wurtzite stacking order, commonly noted as  $\text{AB}_\perp[\text{N}]$ . The other likely site is a second anti-bonding location with  $\text{Mu}^+$  inside the most tightly confined cage region of the structure. The strong QLCR line in Fig. 72 is assigned to this metastable  $\text{AB}_\parallel[\text{N}]$  cage site. This signal is strongest in AlN samples with smallest grain sizes or otherwise highly defective.

The QLCR spectra from fine-grained polycrystalline AlN look very similar to that for the CVD film in Fig. 72, but with broader lines due to small anisotropies and splittings. Preliminary results from zero-field relaxation signatures assigned to the static  $\text{AB}_\parallel[\text{N}]$  cage sites and the more mobile  $\text{AB}_\perp[\text{N}]$  sites

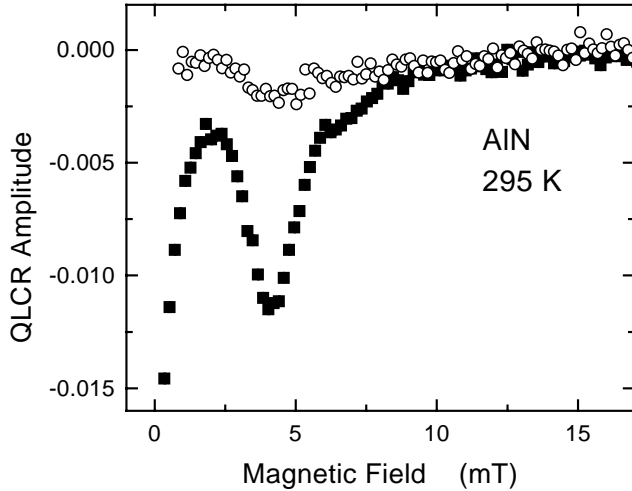


Fig. 72. Comparison of QLCR spectra from two AlN samples: a *c*-axis oriented CVD film (filled symbols) and a single crystal sample (open symbols). Differences imply that the metastable  $AB_{\parallel}$  state is less likely in better material.

had already suggested that the trapped cage state is preferentially formed in more defective material. The single crystal QLCR spectra verify this conclusion.

We will need relaxation data and QLCR spectra at other temperatures for good single crystal AlN to draw any firm conclusions regarding  $Mu^{+}$  dynamics in the best material. The following discussion provides a brief update on our present understanding of  $Mu^{+}$  dynamics in AlN from data on polycrystalline bulk samples and oriented films produced by a variety of techniques. The cage sites are populated in all of these samples, but the fractions vary widely and appear correlated with visual sample quality.

The results shown in Fig. 73 are from bulk polycrystalline AlN. The oriented films give very similar dynamics for the cage site, but show large variations in features assigned to  $Mu^{+}$  channel states. At the highest temperatures the main 4.1 mT resonance broadens and decreases in amplitude characteristic of either motion or disappearance of the metastable cage site. We associate this broadening with motion of  $Mu^{+}$  out of the  $AB_{\parallel}$  site into the mobile channel  $AB_{\perp}$  states. The barrier for this transition appears to be approximately 1.0 eV from both the QLCR results (Fig. 73) and from zero-field depolarization data. A Kubo-Toyabe zero-field component was earlier correlated with the strong QLCR line, and gave a  $Mu^{+}$  site change barrier ranging from about 0.9 to 1.1 eV depending on the precise value chosen for the static KT width [Lichti *et al.*, Physica B, in press].

An interesting outcome from these fits is that the linewidths associated with both the zero-field non-resonant component and the 6 mT resonant feature decrease as the amplitudes decrease at high temperature. At the moment this narrowing is not fully

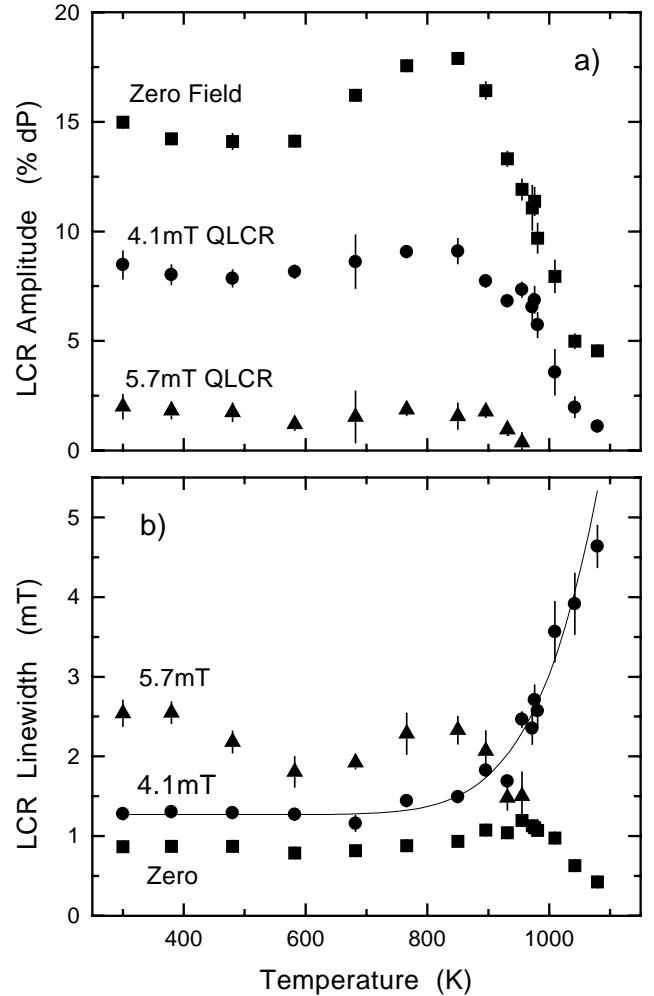


Fig. 73. Parameters from fits to QLCR spectra for polycrystalline AlN, including the non-resonant depolarization near zero field. The high- $T$  increase in width of the 4.1 mT line yields a  $0.99 \pm 0.12$  eV barrier for the  $Mu^{+}$  site change from  $AB_{\parallel}[N]$  to  $AB_{\perp}[N]$ .

understood, but may be related to a change in diffusion and associated averaging of electric field gradients related to the mobile  $Mu^{+}$  channel states. The change in width near 600 K for the weaker higher field line is correlated with a decrease in relaxation rate for the depolarization component tentatively assigned to the mobile  $Mu^{+}$  centres, suggesting that this line and the weakly relaxing zero-field component are in fact from the same states.

Late in the year with time shared between Expt. 804 and Expt. 865, several *n*-type GaN samples were examined in Belle at 3 T to search for a  $Mu^0$  precursor to one of the observed diamagnetic states. Such a precursor was implied below 50 K by earlier relaxation measurements. A small crystal film, *n*-type at  $10^{16} \text{cm}^{-3}$  obtained from NEC [Expt. 865 sample], showed beats implying a small hyperfine splitting along with a fast exponentially relaxing diamagnetic signal.

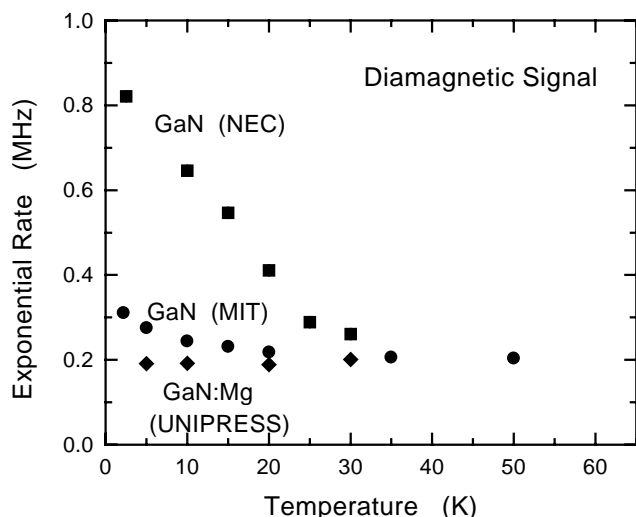


Fig. 74. The temperature dependent exponential relaxation rates for the NEC GaN sample (squares), HVPE thick film MIT GaN sample (circles), and Mg doped GaN single crystal from UNIPRESS (diamonds). The latter relaxation is actually Gaussian, even at the lowest temperatures.

The splitting is characteristic of a shallow donor  $\text{Mu}^0$  state as observed in several II-VI compounds and predicted for InN. Two of the Expt. 804 samples were similarly examined. A *c*-axis oriented film, grown by HVPE methods at MIT and having the same *n*-type concentration, showed similar characteristics although a slower diamagnetic relaxation rate obscured visibility of the beats. However, a small single crystal, obtained from UNIPRESS, doped with Mg to compensate the natural *n*-type character of GaN showed no sign of either the  $\text{Mu}^0$  state or the exponentially decaying diamagnetic signal. Figure 74 shows the low-*T* diamagnetic relaxation rates for these three samples.

One possible scenario consistent with this set of measurements is that a shallow donor  $\text{Mu}^0$  can be formed from one of the diamagnetic states in sufficiently *n*-type GaN. This  $\text{Mu}^0$  then ionizes at roughly 30 K, based on limited data on the two samples which showed the shallow  $\text{Mu}^0$  signature. We suggest that the exponential diamagnetic relaxation might represent  $e^-$  capture by a  $\text{Mu}^+$ , but existing data do not actually identify the original state. We conclude that there is a  $\text{Mu}^0$  state at low temperatures in *n*-type GaN, most likely by delayed formation. Whether the original diamagnetic state and the final state, presumably a  $\text{Mu}^+$ , following the  $\text{Mu}^0$  ionization are the same is yet to be determined.

### Experiments 815, 816 and 817: $\beta$ -NMR (*W.A. MacFarlane, R.F. Kiefl, TRIUMF/UBC*)

In the past year we have made significant advances in developing the  $\beta$ -NMR technique at ISAC. A major part of this progress is the successful development of the  $^8\text{Li}$  optical polarizer, which is described elsewhere in this Annual Report. The main result of this is that we now have available a high spin polarization (50% routinely and up to 70%) in the  $^8\text{Li}$  beam. In addition we have demonstrated that in a high magnetic field (3 T) we can maintain a well-focused beam while decelerating from 30 keV to at least 1 keV. This was shown by imaging the beam spot with a CCD camera viewing a scintillator target. Advances were also made in understanding the beam transport through the  $\beta$ -NMR optics. The Einzel lenses are now operated in a focus-to-parallel mode minimizing beam “snaking” through the optics and simplifying the field and energy dependence of the beam transport. In addition specific advances in understanding the  $^8\text{Li}$   $\beta$ -NMR probe are summarized in the following sections.

#### Deceleration and range straggling

To demonstrate that we can stop the  $^8\text{Li}$  beam in a thin structure, we undertook a study of thin noble metal films with the objective of comparing the range straggling to state of the art Monte Carlo calculations embodied in the SRIM2000 program. Noble metals were selected because their simple structure (face-centred cubic) yields simple resonances as we have already found in thick metal foils.

The dramatic contrast in the resonance signals between the metals which have a single narrow resonance near the Larmor frequency and the film substrates

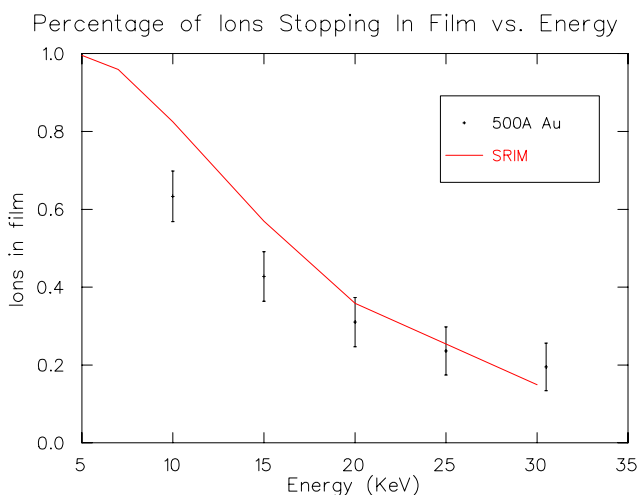


Fig. 75. A comparison of the relative  $^8\text{Li}$   $\beta$ -NMR resonance amplitude to the stopping fraction predicted by the SRIM program as a function of the Li beam energy for a 500 Å film of Au.

allowed us to clearly distinguish the signal coming from the thin film. The resonances were observed for several platform voltages, i.e. varying the beam energy from 30 keV down to 1 keV.

Range straggling was performed on a 500 Å Au film on SrTiO<sub>3</sub> substrate, using <sup>8</sup>Li<sup>+</sup>. The resulting spectra were appropriately scaled and fit to Gaussians. Amplitudes of these fits were then normalized against spectra at similar energies in an Au foil (which is thick compared to the implantation depth of the <sup>8</sup>Li<sup>+</sup>), and compared to SRIM2000 predictions. It should be noted that this process of normalization against Au foil provides only a lower bound on percentage of ions stopped in the film. One reason for this is that the resonance is broader in the thin film, possibly a consequence of disorder or a finite-size effect. Future work will involve obtaining spectra in thick Au films (>2000 Å), and normalizing against these spectra instead of the foil spectra.

### Thin metallic films

Aside from the demonstration of range straggling presented above, the results in thin metallic films are of interest in their own right. One motivation for this is that thin noble metal films are components of interesting heterostructures such as giant magnetoresistive multilayers. However, we also plan to use them as an integral part of the β-NMR probe in some circumstances. When we are investigating magnetism at the surface of a complex material, our idea is to use the simple <sup>8</sup>Li resonance in a thin noble metal overlayer to probe the magnetic field near but outside the sample. One clear reason for this is that the <sup>8</sup>Li resonance in a complex material may be complicated, for example, Fig. 76 shows the resonance in a 1000 Å film of the

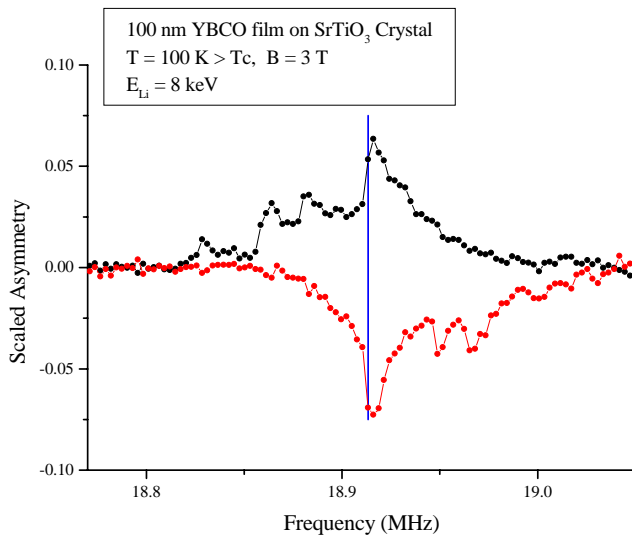


Fig. 76. The <sup>8</sup>Li β-NMR resonance in a 1000 Å film of YBCO in the two polarization channels. The line indicates the resonance frequency in MgO.

orthorhombic high temperature superconductor YBCO. In such a circumstance it may be easier to extract the interesting information from the simpler overlayer resonance.

Initial room temperature measurements of the <sup>8</sup>Li β-NMR resonance in the cubic noble metals Ag and Au showed a single narrow line, indicating a single site of cubic symmetry for Li. Surprisingly, as we cooled films of these metals, a second resonance appeared, and grew in amplitude at the expense of amplitude of the high T line. An example of this is shown in Fig. 77. Both lines appear at frequencies higher than the Larmor frequency in an insulator. Specifically in Ag, the two resonances are at +144 ppm and +242 ppm from the resonance frequency in MgO.

These data suggest that there are two distinct sites for Li in the FCC structure of Ag. In this scenario, we ascribe the small positive shifts to a Knight shift, i.e. to a direct coupling of the <sup>8</sup>Li nucleus to the Pauli spin susceptibility of the conduction band. This is a common effect in the NMR of metals, yielding significant temperature independent shifts. There are two cubic symmetry interstitial sites in the face-centred cubic lattice, the large octahedral (O) site and the smaller tetrahedral (T) site. Additionally there is the cubic

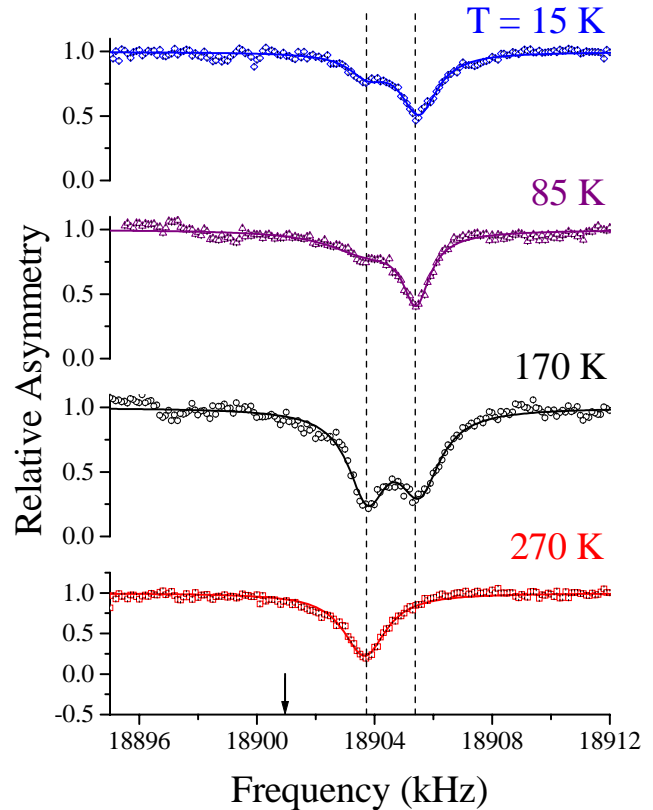


Fig. 77. The temperature dependence of the <sup>8</sup>Li β-NMR resonance in a thin film of silver. The two lines correspond to distinct crystallographic sites for Li in Ag. The arrow indicates the resonance position in the insulator MgO.

substitutional (S) site. It is likely that the two observed lines correspond to the O and S sites as the T site is probably too small to accommodate Li. We plan experiments to confirm this scenario in the near future.

In fact this is the first time that the Knight shift has been used to resolve two sites for an implanted  $\beta$ -NMR probe. The reason we are able to accomplish this is the high magnetic field (3 T) used in this measurement. Lower field studies in Cu did not observe such an effect [Ohsumi *et al.*, Hyp. Int. **120-121**, 419 (1999)].

### Insulators

Strontium titanate ( $\text{SrTiO}_3$ ) is an important substrate material for films of oxide materials such as high temperature superconductors. It is a transparent insulator with the cubic perovskite structure and exhibits a structural phase transition at  $\sim 100$  K to a low temperature tetragonal phase. This phase transition has been studied extensively and is considered a prototype of soft-mode structural phase transitions. Interestingly, neutron and synchrotron X-ray diffraction measurements indicate that there is distinct critical behaviour associated with this transition in a region near the surface of the crystal [Hirota *et al.*, Phys. Rev. **B52**, 13195 (1995)].

We have studied  $^8\text{Li}$   $\beta$ -NMR in  $\text{SrTiO}_3$ , and find that although it is cubic there is a significant quadrupolar splitting of the lines indicating that the local symmetry of the Li site is non-cubic. Figure 78 shows an example of the resonance in  $\text{SrTiO}_3$ . The electric quadrupole moment of the  $^8\text{Li}$  nucleus couples the nuclear spin to the electric field gradient (EFG) at the Li site causing the Larmor resonance to be split into a quartet of lines for the spin 2 nucleus. However, the high degree of polarization implies that only the

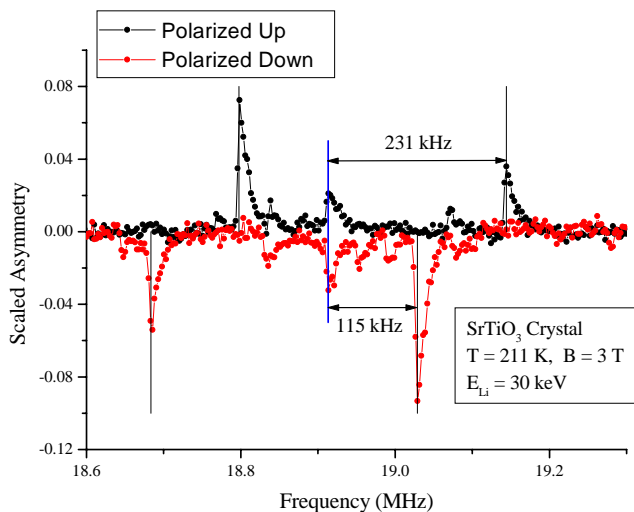


Fig. 78. The  $^8\text{Li}$   $\beta$ -NMR resonance in  $\text{SrTiO}_3$ . The central line indicates the Larmor frequency. The resonance is split by the quadrupolar interaction, with a characteristic frequency of  $\nu_Q \sim 115$  kHz.

$m = \pm 2$  states are populated appreciably. The applied rf magnetic field can then induce  $\Delta m = 1$  transitions, and we will observe only two lines of the quartet. However, instead, we find four lines – two distinct ones in each polarization channel, the inner two having higher intensity.

The likely explanation for this effect is that the Li site has a  $[100]$  symmetry axis, thus there are in fact three sites with  $[100]$ ,  $[010]$  and  $[001]$  principal axes in the cubic structure. The field applied along  $[001]$  distinguishes the  $[001]$  site from the other two. In fact the first order quadrupolar splitting for an axially symmetric EFG depends on the angle of the magnetic field relative to the EFG axis ( $\theta$ ) as

$$\delta\nu \propto 3 \cos^2(\theta) - 1.$$

So the two large resonances correspond to the  $[100]$  and  $[010]$  sites with  $\theta = 90^\circ$  and the outer lines to the  $[001]$  site with  $\theta = 0^\circ$ .

The results in  $\text{SrTiO}_3$  indicate that not only can  $^8\text{Li}$   $\beta$ -NMR be used as a local magnetic probe, but in some cases it is also sensitive locally to electrostatic fields in solids.

### Spin lattice relaxation

In addition to measuring the  $^8\text{Li}$  resonance, we have measured the spin lattice relaxation. The relaxation is due to coupling of the  $^8\text{Li}$  to the conduction electrons of the metal (Korringa relaxation) and demonstrates our ability to measure magnetic dynamics.

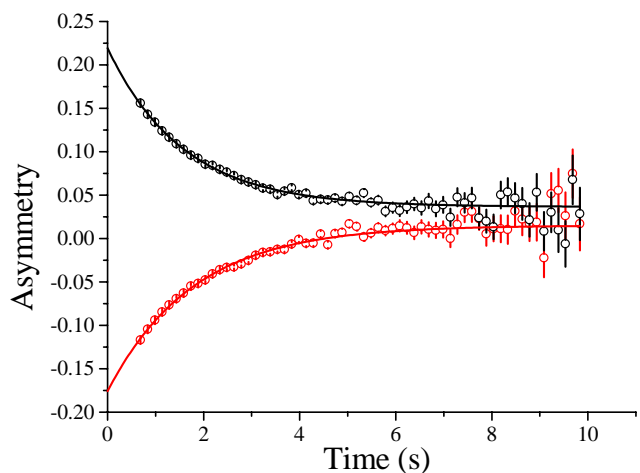


Fig. 79. The spin lattice relaxation of  $^8\text{Li}$  in Pd. In the experiment the beam was on for the first 0.5 s, then the decay of the asymmetry was monitored.

### Experiment 833

#### Muon spin relaxation studies on MnSi under applied pressure

(I.M. Gat, Columbia)

MnSi is one of the most investigated magnetic systems with itinerant electrons. The compound orders at  $T_c = 29.5$  K in a helical magnetic structure with a long period (180 Å). We present  $\mu$ SR studies on a single crystal of MnSi under applied magnetic field and

Relaxation rate of muon spins in MnSi under applied field

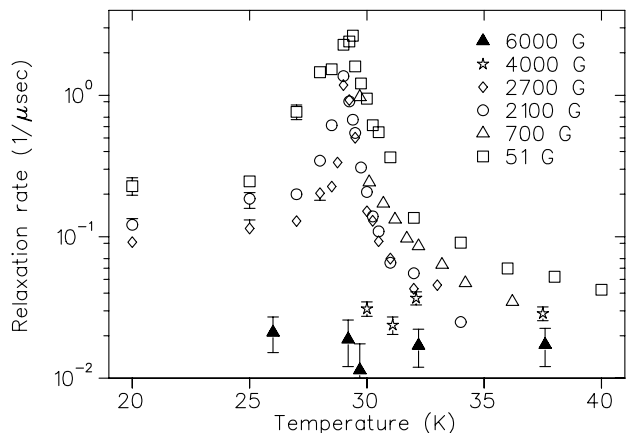


Fig. 80. Temperature dependence of the muon spin relaxation rate  $\lambda = 1/T_1$  in MnSi under zero field and applied magnetic fields of 51.5 G, 2115 G, 2700 G, 4000 G and 6000 G. Data under 700 G taken by Dr. Hayano's group [Hayano, *et al.*, J. Phys. Soc. Japan **49**, 1773 (1980)] are plotted for comparison.

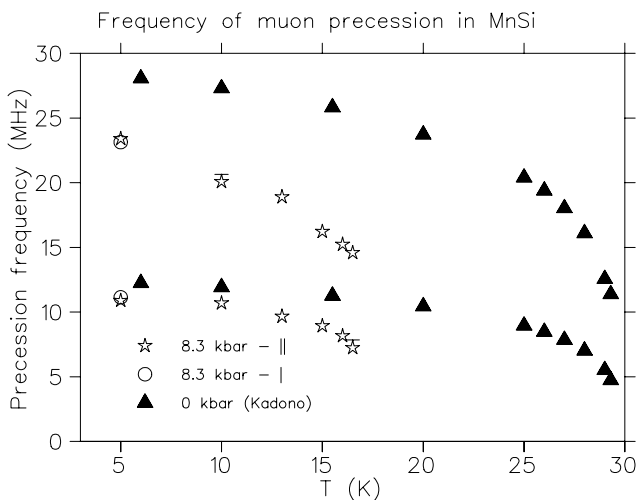


Fig. 81. The muon spin precession frequency in MnSi under an applied pressure of 8.3 kbar. The open circles represent the precession frequencies measured at a previous time. The agreement shows that the pressure didn't change between the times of the measurements. The data are compared with data taken by Dr. Kadono and his collaborators [Kadono, *et al.*, Phys. Rev. **B42**, 6515 (1990)] on MnSi at ambient pressure.

at zero magnetic field under an applied pressure of 8.3 kbar. The measurements confirm the predictions of the self consistent renormalization theory [Moriya, *Spin fluctuations in itinerant electron magnetism*]: close to  $T_c$  the relaxation time of muon spins,  $T_1$ , is proportional to  $T(1 - T_c/T)^2$ , while at higher temperature  $T_1$  is proportional to  $(1 - T_c/T)$ .

The relaxation time  $T_1$  shows an unexpected field dependence in the paramagnetic phase, for magnetic fields smaller than 3000 G. We propose an explanation for the field dependence of  $T_1$  based on the helical nature of the magnetic structure. A magnetic field of 4000 G completely suppresses the critical spin fluctuations. These findings are in agreement with the magnetic phase diagram of MnSi at ambient pressure (see Figs. 80 and 81).

### Experiment 834

#### $\mu$ SR study of transverse spin freezing in bond-frustrated magnets

(D.H. Ryan, McGill)

The random addition of antiferromagnetic (AF) exchange interactions to an otherwise ferromagnetic (FM) system leads to a loss of FM order through exchange frustration. In extreme cases, a spin glass (SG) is formed with random isotropic spin freezing and neither net magnetization nor long range order. At lower levels of frustration the system exhibits characteristics of both extremes as long-ranged FM order co-exists with SG order in the plane perpendicular to the FM order. On warming such a system from  $T = 0$  K, the SG order first melts at  $T_{xy}$  followed by the loss of FM order at  $T_c$ . This picture has emerged from mean field calculations, numerical simulations and experimental measurements.

The aim of Expt. 834 is to investigate the magnetic behaviour in the region of  $T_{xy}$  in some partially frustrated alloys. Specifically, numerical simulations predict that although the freezing of transverse spin components does not represent a phase transition, it should be accompanied by significant, but non-critical, magnetic fluctuations. Our initial work confirmed the expected signatures of transverse spin freezing could be observed using  $\mu$ SR, however, there was a clear disagreement between the values for  $T_{xy}$  determined by  $\mu$ SR and those obtained earlier by applied field Mössbauer spectroscopy. The latter values were systematically lower, by as much as a factor of two in the most extreme case.

Further measurements through 2000 were aimed at understanding this discrepancy. Using  $a\text{-Fe}_{90-x}\text{Ru}_x\text{Zr}_{10}$  we were able to observe the FM $\rightarrow$ SG cross-over and also make a direct comparison with  $T_{xy}$  values derived from zero-field Mössbauer spectroscopy. A more detailed series of measurements in

the a-Fe<sub>x</sub>Zr<sub>100-x</sub> system around  $x = 93$  confirmed that the deviation from the applied field Mössbauer values for  $T_{xy}$  was a systematic effect. These observations led us to suspect that the  $\sim 3$  T field used in the Mössbauer measurements greatly affects both the value of  $T_{xy}$  in any given sample, and also changes the critical concentration for the loss of ferromagnetic order.

We have now made two series of runs using Helios to apply fields of up to 5.5 T and measure the effects of an applied field on  $T_{xy}$ . The results of our first run using a-Fe<sub>92</sub>Zr<sub>8</sub> are shown in Fig. 82. We were able to observe the fluctuation peak at all fields used and thus followed  $T_{xy}$  as the field suppressed it by over a factor of four. This immediately confirms that the applied field is at the origin of the  $\mu$ SR – Mössbauer discrepancy. Theoretical predictions for the functional form of this suppression are limited to mean-field models which predict a dependence of the form:

$$T_{xy}(B) \propto T_{xy}^0 \left(1 - \frac{B^p}{A}\right)$$

where  $A$  is a constant, and predictions for  $p$  range from 2 [Gabay and Toulouse, 1981], 2/3 [Almeida and Thouless, 1978], or 1 [Fischer and Hertz, 1991]. Unfortunately, none of the three predicted forms describes the observed field dependence of  $T_{xy}$ . Visual inspection of the trend suggested a  $1/B$  dependence (i.e.  $p = -1$ ), in severe disagreement with the predicted forms. The simplest function that reproduced the data, allowed for a scaling of the suppression rate, and gave

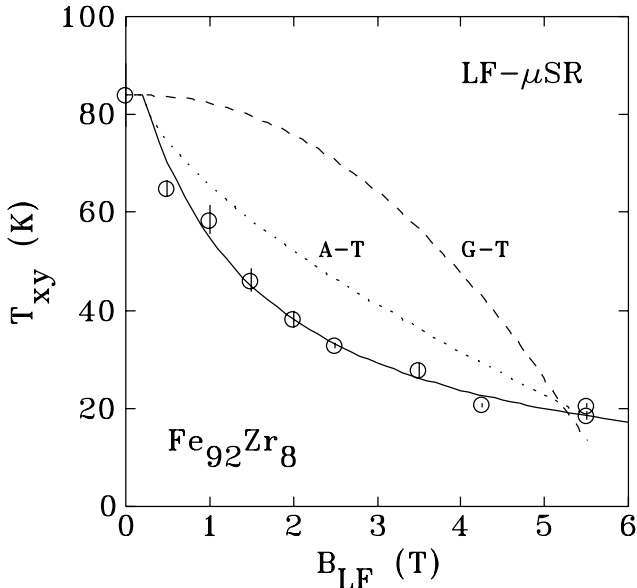


Fig. 82. Field dependence of  $T_{xy}$  measured by LF- $\mu$ SR in a-Fe<sub>92</sub>Zr<sub>8</sub>. The solid line is a phenomenological fit described in the text. Dashed (G-T) and dotted (A-T) lines show the mean-field predictions discussed in the text scaled to agree at 0 T and 5 T.

an asymptotic value of  $T_{xy}(\infty) = 0$  was found to be:

$$T_{xy}(B) = T_{xy}^0 \left(1 - \frac{B}{(J_s + B)}\right)$$

where the scale factor  $J_s$  took a value of  $1.5 \pm 0.3$  T, which is consistent with the 1.36 T saturation polarization of this alloy.

A more extensive series of measurements on four more a-Fe<sub>x</sub>Zr<sub>100-x</sub> samples has confirmed that the same functional form for the suppression is observed from the almost ferromagnetic  $x = 90$  right through to the spin-glass  $x = 93$ . Analysis is continuing on this data set.

In a parallel effort, we have developed selective excitation double Mössbauer (SEDM) spectroscopy as a viable probe of dynamics in magnetic materials. We have applied it to the study of the fluctuations at  $T_{xy}$  in a-Fe<sub>92</sub>Zr<sub>8</sub> and shown that two independent techniques yield the same fluctuation rates around  $T_{xy}$  (see Fig. 83). This agreement, coupled with the nature of the relaxation process detected by SEDM allows us to conclude that moment reversals are the dominant fluctuation in this material around  $T_{xy}$ .

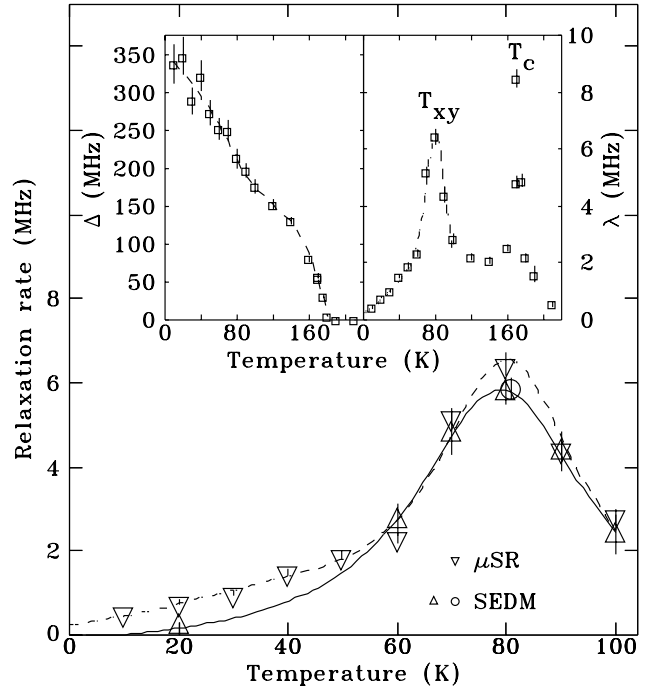


Fig. 83. Inset: Temperature dependence of the static ( $\Delta$ ) and dynamic ( $\lambda$ ) relaxation rates in a-Fe<sub>92</sub>Zr<sub>8</sub>. Dashed lines are guides to the eye. Body: Relaxation rates from ZF- $\mu$ SR fits ( $\nabla$ ) and SEDM fits ( $\Delta, \circ$ ) around  $T_{xy}$ . Lines are guides to the eye.



## Present status of Expt. 834

We will be continuing this work along two distinct lines.

The first involves tidying up the field shift problem. We have to complete the analysis of the July, 2001 runs so as to determine how the level of frustration affects the rate at which a field suppresses  $T_{xy}$ . In parallel with this analysis, we are also extending our Monte Carlo simulation work that led to the prediction of the fluctuation peak at  $T_{xy}$ , to include the effects of an external field. In this way we hope to provide some insight into the detailed origins of the field suppression.

The second issue involves addressing a claimed difference between our work on bond frustrated systems, where two, and only two transitions are observed, and a report for a site frustrated material where three distinct transitions have been claimed. Our numerical work shows only evidence for two transitions, as in the bond frustrated case. We expect to clear this up in summer, 2002.

## Experiment 835

### $\mu$ SR in doped HfNCl superconductors (*T. Ito, Columbia and CERC*)

The layered compounds intercalated ZrNCl and HfNCl (see the inset of Fig. 84) are superconductors with a maximum  $T_c$  of  $\sim 15$  K and  $\sim 25$  K. By the intercalation of alkali metal atoms and organic molecules, carriers are introduced and interlayer distance can be changed. We have performed transverse-field  $\mu$ SR studies on these compounds with magnetic field perpendicular to their layers. The samples were well aligned polycrystals pressed under uniaxial stress. The temperature dependence of the relaxation rate  $\sigma(T)$  is shown in Fig. 84.  $\sigma(T)$  in the field-cooling process shows a tendency of saturation at low temperatures, characteristic of  $s$ -wave superconductors.  $T_c$  is not affected by the interlayer distance.  $T_c$  as a function of  $\sigma(T \rightarrow 0)$  is plotted in Fig. 85.  $\sigma(T \rightarrow 0)$  of superconducting Hf(Zr)NCl is much smaller than that of conventional superconductors such as Nb. With overdoping, in spite of the increase of chemical doping level, superconducting carrier density and  $T_c$  decrease, as is observed in the overdoped high- $T_c$  superconductors. We see different tendencies between samples with and without organic molecules, where simple linear correlation is observed for each. We show that  $T_c$  is well correlated with  $n_{2d,s}/m^*$ , where  $n_{2d,s}$  is superconducting sheet carrier density. This correlation is common to high- $T_c$  superconductors and quasi-two-dimensional organic superconductors (BEDT-TTF) $_2$ Cu(NCS) $_2$ , which suggests universal superconducting condensation mechanism among these exotic superconductors.

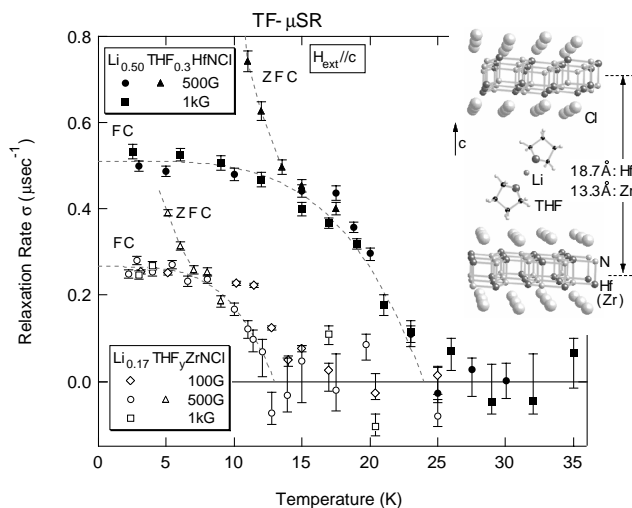


Fig. 84. The temperature dependence of the relaxation rate  $\sigma(T)$  in intercalated Hf(Zr)NCl.

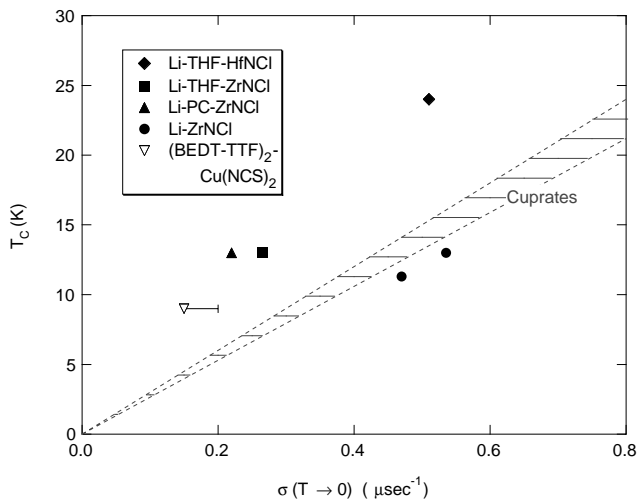


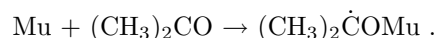
Fig. 85. The correlation between  $T_c$  and  $\sigma(T \rightarrow 0)$  of intercalated Hf(Zr)NCl.

## Experiment 842

### Mu-substituted free radicals in sub- and supercritical water (*P.W. Percival, SFU*)

The beam time used by Expt. 842 during 2001 was split between two projects: formation of muoniated radicals in aqueous solutions of acetone; and kinetics of the reaction between muonium and the formate ion in aqueous solution. In both cases, measurements were made over a wide range of temperature and pressure, from standard to supercritical conditions. Last year's report highlighted muonium kinetics, so the current report is devoted to free radical studies.

It is well established that muonium reacts with acetone as a pure liquid or in solution at "normal" temperatures by addition to the carbonyl oxygen:



However, in a preliminary investigation of muoniated radicals in supercritical aqueous solutions we found evidence that seemed to contradict this mechanism. Accordingly we carried out the systematic study summarized here.

At temperatures below 250°C the expected radical was detected by transverse field muon spin rotation ( $\mu$ SR). It has a rather low muon hyperfine constant which increases with temperature. At higher temperatures, however, a radical with a much higher hyperfine constant was detected. Examples of the  $\mu$ SR spectra are given in Fig. 86. Hyperfine constants were calculated from the radical precession frequency labelled  $R_1$  and the muon Larmor frequency, corresponding to the large truncated peak in the two spectra of Fig. 86. The results are summarized in Fig. 87.

It is obvious that two different radicals are formed. At low and intermediate temperatures our results are consistent with literature data, denoted by the open symbols in Fig. 87. The small shifts between data sets are consistent with changes in solvent properties for different concentrations of acetone. The question is: What is the identity of the “new” radical found above 250°C?

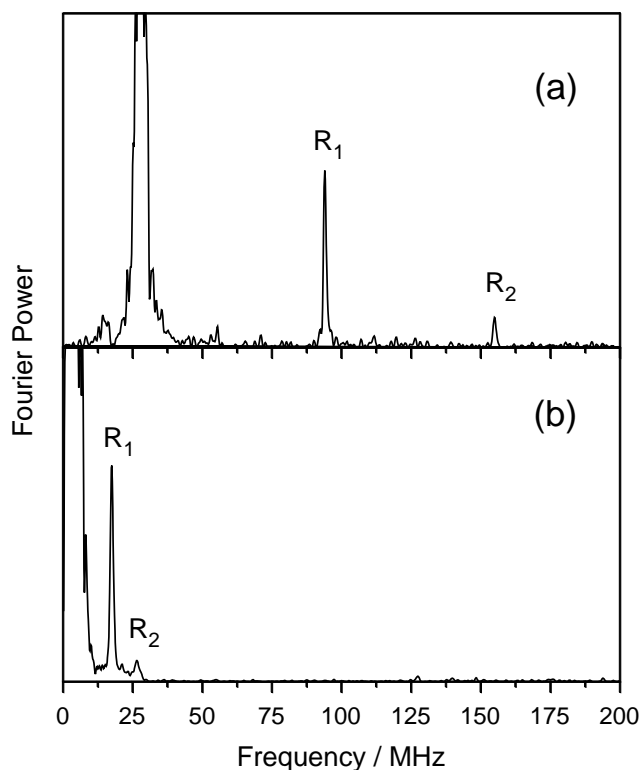


Fig. 86. Muon precession signals from aqueous solutions of acetone at (a) 370°C, 250 bar, 2 kG; (b) 170°C, 190 bar, 320 G. In each case the pair of peaks, denoted  $R_1$  and  $R_2$ , is characteristic of a muoniated free radical.

The key to this riddle is the known keto-enol tautomerism of acetone:



At low temperature the equilibrium is far to the left, i.e. there is very little of the enol formed. Unlike the usual keto form, the enol has a carbon-carbon double bond instead of the carbon-oxygen double bond. Apparently the equilibrium favours more enol at higher temperatures, since the new radical we have detected is consistent with the 1-muono-2-hydroxypropyl radical,  $\text{CH}_3\dot{\text{C}}(\text{OH})\text{CH}_2\text{Mu}$ , which would be formed by Mu addition to the C=C bond.

Full characterization of this radical is not yet possible, since it requires development of apparatus to perform muon avoided level crossing experiments on samples under the extreme conditions of supercritical water. Nevertheless this work serves to demonstrate the novel chemistry that can be discovered by means of muon studies of such systems.

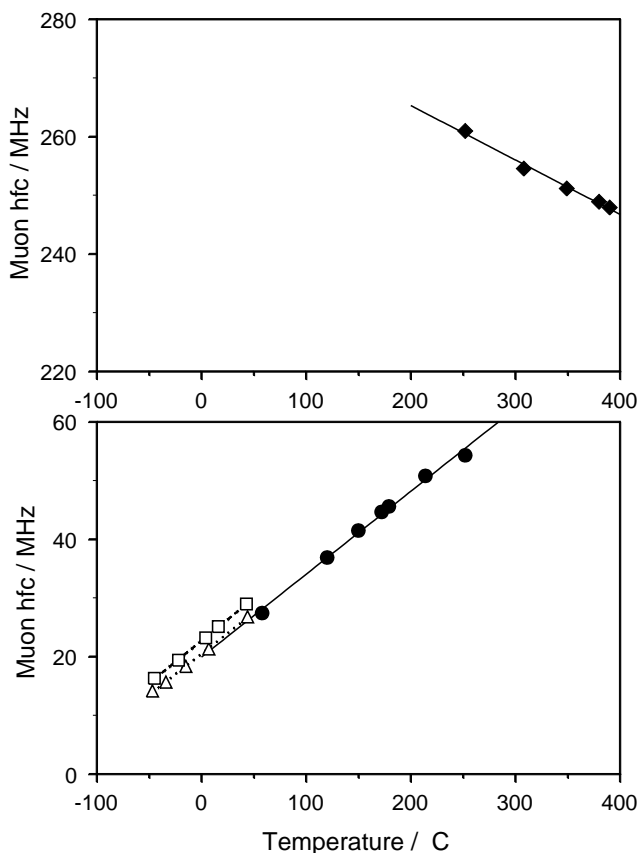


Fig. 87. Muon hyperfine constants for the two radicals detected in aqueous solutions of acetone (filled symbols) compared with literature data (open symbols).

## Experiment 846

### Complex order parameter symmetry in $\text{YBa}_2\text{Cu}_3\text{O}_{7-\delta}$ at low $T$ and high magnetic field (*J.H. Brewer, UBC; J.E. Sonier, SFU*)

Since the spring, 2000 beam period, we have been focused on  $\mu\text{SR}$  measurements of UBC grown  $\text{YBa}_2\text{Cu}_3\text{O}_{6+x}$  crystals in zero external magnetic field. At the December, 2000 EEC meeting we reported our observation of anomalous weak static magnetism in underdoped ortho-III ( $x = 0.67$ ) and optimally-doped ( $x = 0.95$ ) single crystals. Such weak magnetism had not been observed in early ZF- $\mu\text{SR}$  measurements of the  $\text{YBa}_2\text{Cu}_3\text{O}_{6+x}$  system. This was most likely due to a significant background signal in the older measurements. The anomalous weak magnetism we reported seemed to be correlated with the pseudogap crossover  $T^*$ . Consequently, we suggested that the result may be consistent with theories predicting the occurrence of spontaneous magnetic fields at temperatures below  $T^*$  [Sonier *et al.*, *Science* **292**, 1692 (2001)]. However, in the past year we have carried out additional measurements on underdoped ( $x = 0.80$ ) and slightly overdoped ( $x = 0.985$ ) crystals. These latest measurements were carried out using the LAMPF spectrometer, but with a side-axis (rather than axial) low-background insert. This experimental modification resulted in a marked improvement in the quality of the ZF- $\mu\text{SR}$  spectra, leading us to identify additional features in the temperature dependence of the muon spin relaxation rate. The results of our most recent study strongly suggest that the weak magnetism we have been observing is in fact associated with spatial inhomogeneity.

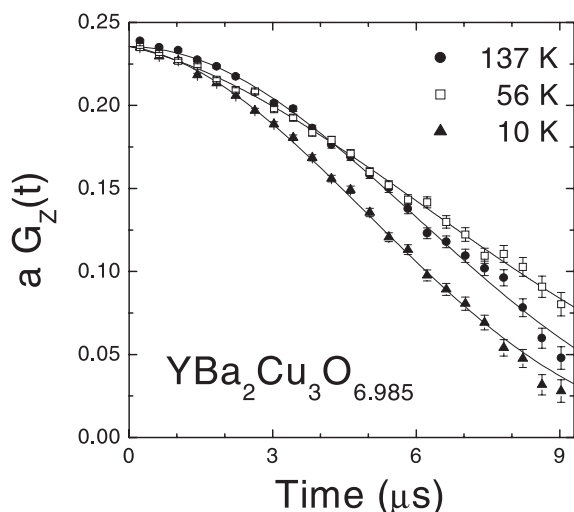


Fig. 88. The time evolution of the muon spin polarization in  $\text{YBa}_2\text{Cu}_3\text{O}_{6.985}$  in zero external field at  $T = 10, 56$  and  $137$  K. The signal at  $10$  K relaxes faster than at  $137$  K. At  $56$  K the signal at early times relaxes faster than at  $137$  K, but exhibits a slower relaxation beyond  $5 \mu\text{s}$ . This latter behaviour indicates a change in the relaxation rate  $\Delta$ .

In our studies we have found that the ZF- $\mu\text{SR}$  time spectra are well described by a relaxation function that is the product of a static Gaussian Kubo-Toyabe (KT) function and an exponential relaxation function

$$G_Z(t) = \left[\frac{1}{3} + \frac{2}{3}(1 - \Delta^2 t^2 \exp(-\frac{1}{2}\Delta^2 t^2))\right] \exp(-\lambda t).$$

The KT function describes the relaxation of the muon spin by the weak nuclear dipole fields. Generally speaking, the relaxation rate,  $\Delta$ , is not expected to depend on temperature. However, in the overdoped ( $x = 0.985$ ) sample, we find that this assumption leads to poor fits of the time spectra measured near  $55$  K. Near this temperature we observe a clear change in the ZF- $\mu\text{SR}$  signal (see Fig. 88) that can be accounted for by allowing  $\Delta$  to vary freely with temperature.

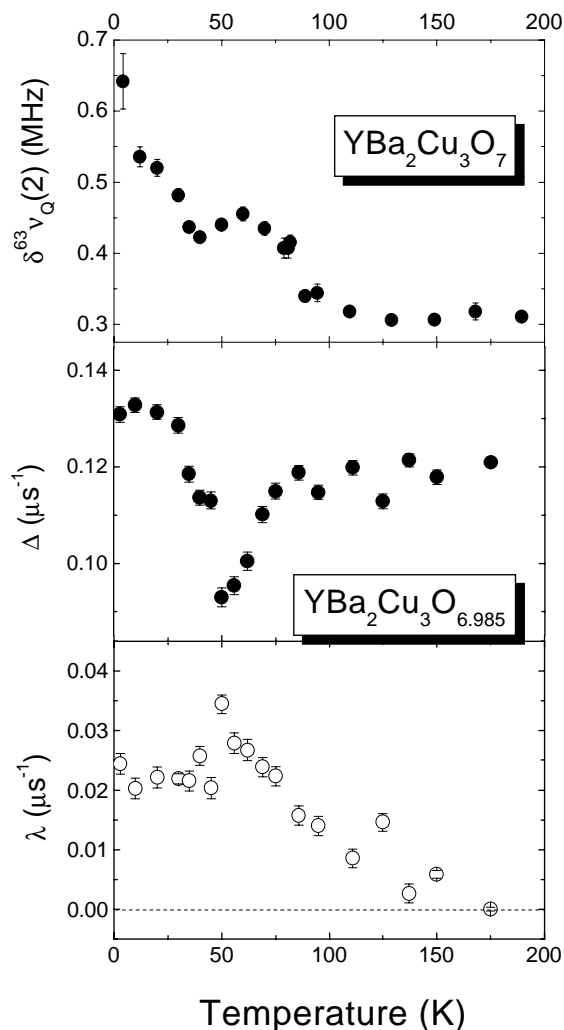


Fig. 89. Top panel: full width at half maximum of the  $^{63}\text{Cu}(2)$  NQR line in slightly overdoped  $\text{YBa}_2\text{Cu}_3\text{O}_{7-\delta}$  [from Grévin *et al.*, *Phys. Rev. Lett.* **84**, 1636 (2000)]. Middle and bottom panels: temperature dependence of the Gaussian relaxation rate  $\Delta$  and the exponential relaxation rate  $\lambda$  in  $\text{YBa}_2\text{Cu}_3\text{O}_{6.985}$  from ZF measurements taken with the initial muon spin polarization  $P_\mu(0)$  perpendicular to the  $c$ -axis of the crystal.

The resulting temperature dependence of  $\Delta$  shows several features, most notably a large dip near 55 K and a subsequent increase with decreasing temperature below 35 K (see Fig. 89). The latter behaviour was previously observed in the  $x = 0.95$  sample, but mistakenly attributed to a change in the exponential relaxation rate  $\lambda$ . As seen in Fig. 89,  $\lambda$  which arises from the weak magnetism of unknown origin, begins to increase below  $\approx 130$  K. What is most interesting is that all of these features occur at temperatures where NQR measurements have observed changes in the spatial distribution of charge in the  $\text{CuO}_2$  layers of  $x \approx 1.0$  samples [Grévin *et al.*, Phys. Rev. Lett. **85**, 1310 (2000)]. Furthermore, several groups have reported local structural changes occurring in  $\text{YBa}_2\text{Cu}_3\text{O}_{6+x}$  samples near  $T \approx 35$  K, 60 K and 120 K. In our most recent paper submitted for publication, we hypothesize that the weak magnetism associated with  $\lambda$  originates from hole depleted regions of the sample, and the noted features arise from a strong coupling of the charge, spin and lattice degrees of freedom. Given the very different nature of the experiments and the different samples investigated, we have concluded that these effects are an intrinsic property of  $\text{YBa}_2\text{Cu}_3\text{O}_{6+x}$ , and local structural changes likely occur near  $T \approx 35$  K, 60 K and 120 K for a wide range of hole concentrations.

Results of ZF- $\mu$ SR measurements on underdoped samples performed over the past year show that the local minimum in  $\Delta$  near  $T \approx 55$  K and the increase of  $\Delta$  at temperatures below 35 K become less pronounced with decreasing  $x$ . While the reduction in the size of these features may be related to changes in the  $\mu^+$  site(s) and/or increase in mass anisotropy, the  $\text{CuO}$  chain layers are a more likely cause. It has been suggested that the charge inhomogeneity observed in the  $\text{CuO}_2$  planes with NQR is induced by charge ordering in the  $\text{CuO}$  chain layers. Consequently, the  $T \approx 35$  K and  $T \approx 55$  K features are strongest for  $x = 1.0$ , where the chains are completely full.

### Experiment 847 Electron-doped high- $T_c$ superconductors (*J.E. Sonier, SFU; G.M. Luke, McMaster*)

We have been studying the temperature dependence of the magnetic penetration depth  $\lambda_{ab}$  in the vortex state of the electron-doped high temperature superconductor  $\text{Pr}_{2-x}\text{Ce}_x\text{CuO}_4$ . These measurements are unique in that they probe the superfluid density in the bulk of the sample. Although the family of electron-doped copper oxide superconductor was discovered in 1989, single crystals of  $\text{Pr}_{2-x}\text{Ce}_x\text{CuO}_4$  have only recently become available for  $\mu$ SR studies. The  $\text{Pr}_{2-x}\text{Ce}_x\text{CuO}_4$  system is of particular experimental interest because there is no large paramagnetic contribution from the rare earth ion (unlike the more

widely studied  $\text{Nd}_{2-x}\text{Ce}_x\text{CuO}_4$  system) to influence measurements of  $\lambda_{ab}$ . Besides studying the behaviour of  $\lambda_{ab}$ , we have also been investigating the magnetism in the  $\text{Pr}_{2-x}\text{Ce}_x\text{CuO}_4$  system. Such studies are aimed at determining the role of magnetism in electron-doped high- $T_c$  superconductivity and developing a complete generic phase diagram for these systems. Thus far, our studies in Expt. 847 have produced two important findings.

First, we have successfully extracted the in-plane magnetic penetration depth  $\lambda_{ab}$  from measurements of the internal magnetic field distribution in the vortex state of a  $\text{Pr}_{2-x}\text{Ce}_x\text{CuO}_4$  single crystal. This is a major achievement given the small size of the samples available to us, and the added complication of magnetism in the material. At low magnetic field ( $H = 90$  G) we observed the asymmetric  $\mu$ SR line shape characteristic of a vortex lattice. The magnetic penetration depth  $\lambda_{ab}$  and the additional broadening of the internal field distribution (due primarily to the presence of magnetic moments) were easily determined from fits of the spectra in the time domain. The results (Fig. 90) show that the temperature dependence of  $\lambda_{ab}$  found in the bulk of  $\text{Pr}_{2-x}\text{Ce}_x\text{CuO}_4$  single crystals is consistent with conventional  $s$ -wave superconductivity. This behaviour is qualitatively similar to that observed in the Meissner state by some of the other groups using surface-sensitive techniques. Thus the failure to observe a clear signature of  $d$ -wave pairing symmetry in these other magnetic penetration depth experiments on electron-doped high- $T_c$  superconductors cannot be ascribed to problems with the surfaces of these materials.

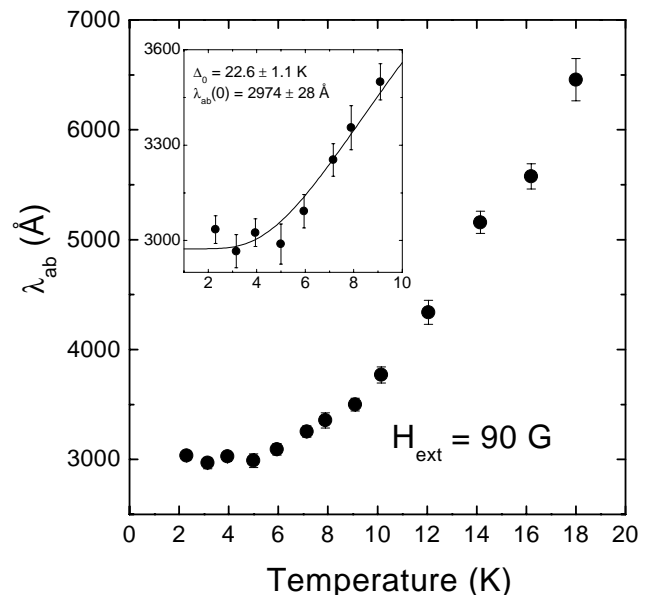


Fig. 90. Temperature dependence of  $\lambda_{ab}$  in the vortex state of a  $\text{Pr}_{2-x}\text{Ce}_x\text{CuO}_4$  ( $x \approx 0.15$ ) single crystal. The inset shows a fit for  $T \leq 9$  K to the BCS relation (solid curve).

Second, we have established that the superconducting phase of  $\text{Pr}_{2-x}\text{Ce}_x\text{CuO}_4$  contains sizeable magnetic moments that are inhomogeneously distributed in the sample. Figure 91 shows fits of the zero-field  $\mu\text{SR}$  time spectra to a stretched exponential relaxation function  $G_z(t) = \exp[-(\Lambda t)^\beta]$ , where  $\Lambda$  is the relaxation rate and  $\beta$  is the power. Measurements in a longitudinal field confirm that the internal magnetic fields are static. At the lowest and highest temperatures we find that  $\beta \approx 1$ , which is characteristic of dilute static magnetism. We associate the maximum that occurs near 50 K with a reorientation of the Cu spins, which has been previously observed in the parent compound  $\text{Pr}_2\text{CuO}_4$  by neutrons at high pressure. While we observe no long-range magnetic order (i.e. no coherent precession signal) in zero-external magnetic field, the sensitivity to the Cu-spin reorientation implies that there is some sort of short-ranged magnetic order. We are planning further studies of  $\text{Pr}_{2-x}\text{Ce}_x\text{CuO}_4$  to determine the precise origin of the internal magnetism that we have detected.

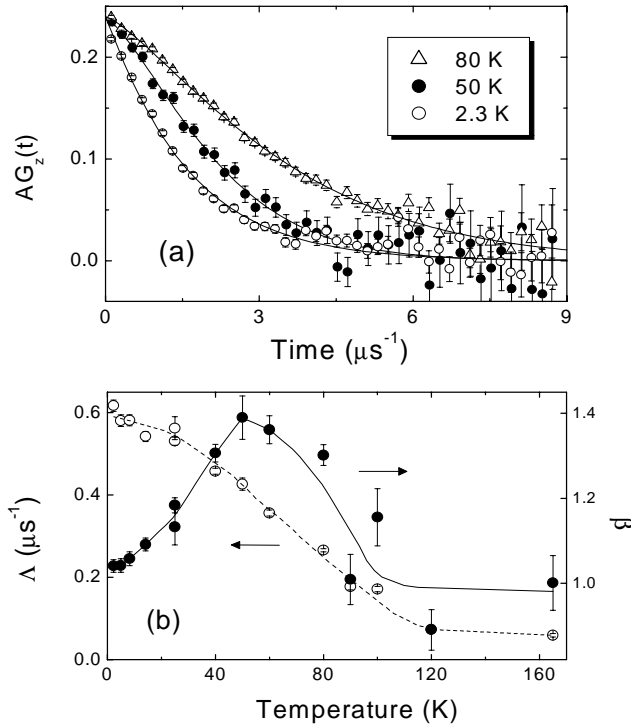


Fig. 91. Top panel: time evolution of the muon spin polarization in a superconducting  $\text{Pr}_{2-x}\text{Ce}_x\text{CuO}_4$  crystal for zero-external magnetic field. Bottom panel: results from fits of the zero-field  $\mu\text{SR}$  time spectra to a stretched exponential relaxation function  $G_z(t) = \exp[-(\Lambda t)^\beta]$ .

## Experiment 848

### Vortex state of $d$ -wave superconductors investigated by muon spin rotation

(*R. Kiefl, R. Müller, UBC/TRIUMF*)

#### Static fields in vortex cores of $\text{YBCO}_{6.50}$

Evidence for static fields induced in the vortex cores of ortho-II  $\text{YBCO}$  have been reported in previous Expt. 848 reports. The results are in press [Miller *et al.*, Phys. Rev. Lett. **88**].

#### Single transition to AF and SC groundstate in $\text{YBCO}_{6.35}$

Transverse field and zero field  $\mu\text{SR}$  relaxation/rotation measurements in ortho-II  $\text{YBCO}_{6.35}$  have revealed a single transition at  $T = 13.8$  K to a superconducting (SC) and antiferromagnetic (AF) state. Figure 92(a) shows the magnetization in  $\text{YBCO}_{6.35}$  measured in a small field. The sharp transition at  $T = 13.8$  K is good evidence for a bulk superconductor. Figure 92(b) shows the temperature dependence of the main frequency measured in zero field

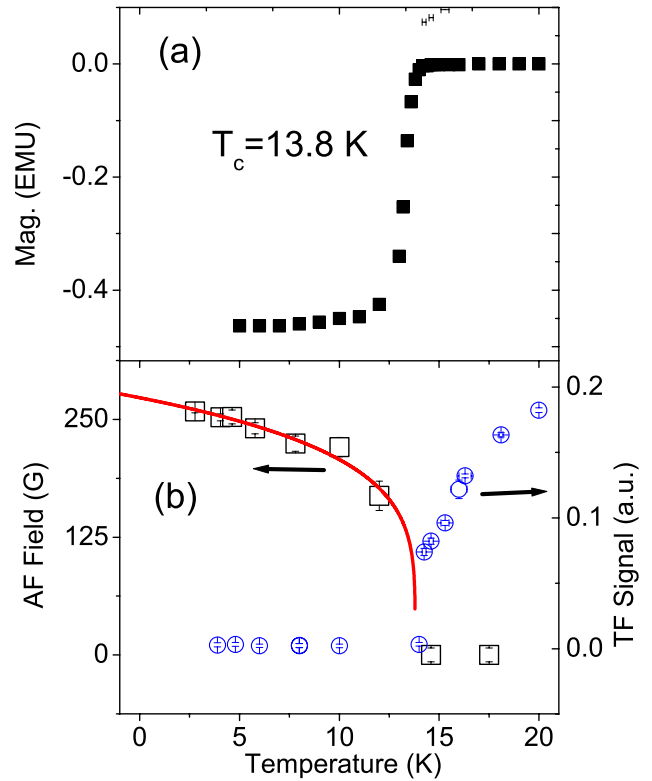


Fig. 92. Panel (a) temperature dependence of the magnetization in  $\text{YBCO}_{6.35}$  in a small field. A sharp superconducting transition is seen at  $T = 13.8$  K. Panel (b) (Left-hand scale) Magnetic field at a muon site below  $T_N$ . The low temperature value is approximately 90% of the field found in the parent  $\text{YBCO}$  compound. (Right-hand scale) Long-time asymmetry of the transverse field muon polarization signal, showing a transition near  $T_N$  to a 100% antiferromagnetic state.

(left-hand scale). The zero temperature frequency is approximately 90% of the frequency seen in the parent compound YBCO<sub>6.0</sub>. The right-hand scale seen in Fig. 92(b) shows the temperature dependence of the long-time  $\mu$ SR polarization asymmetry. The decrease in the asymmetry at  $T_N$  shows that the entire sample undergoes the transition to an AF state.

This finding is unusual in that previous reports of coexistent  $T_N$  and  $T_c$ , found in the LSCO family of superconductors, have pockets of antiferromagnetism surrounded by superconductivity, e.g. the AF nature of the low temperature ground state is not homogeneous. In YBCO<sub>6.35</sub>, it appears that all muons stop near large internal fields. The rapid damping of the zero field signal, however, seems to indicate that field distribution around the muon site(s) is large. The antiferromagnetism is quite disordered.

This work is currently under preparation for publication. The data are discussed in terms of stripes and cluster spin glasses.

#### Future plans

We plan to run a large single crystal of YBCO<sub>6.50</sub> in Belle in August to see if we can reproduce the signals from vortex core fields. This sample was used in a neutron scattering study that revealed no sharp peak at the AF wave vector after the application of a field, indicating that any vortex core antiferromagnetism must be spatially disordered in these crystals. Further, we intend to use OMNI to measure a slightly higher doped YBCO than in YBCO<sub>6.35</sub>, and see if we can measure the SC transition at higher temperatures and see the AF transition at lower temperatures.

#### Experiment 849

##### Spin structure and magnetic volume fraction of La<sub>2</sub>14 systems

(*Y.J. Uemura, Columbia; K.M. Kojima, Tokyo*)

Last year we reported that we found incommensurate spin density wave ordering in La<sub>2</sub>CuO<sub>4.11</sub> and La<sub>1.88</sub>Sr<sub>0.12</sub>CuO<sub>4</sub>. The amplitude of oscillations was less than expected from weak transverse field measurements, so we concluded that only a fraction of the sample is magnetically ordered.

More data and a careful analysis of the experimental results allowed us to extract some useful information.

We found unusual behaviour for the magnetic order parameter. To illustrate this, Fig. 93 shows the spectra for La<sub>2</sub>CuO<sub>4.11</sub> (LCO:4.11) and antiferromagnetic La<sub>2</sub>CuO<sub>4</sub> (AF-LCO). For conventional systems like AF-LCO, the amplitude of oscillations is nearly temperature independent, but frequency increases with decreasing temperature. In contrast, LCO:4.11 shows

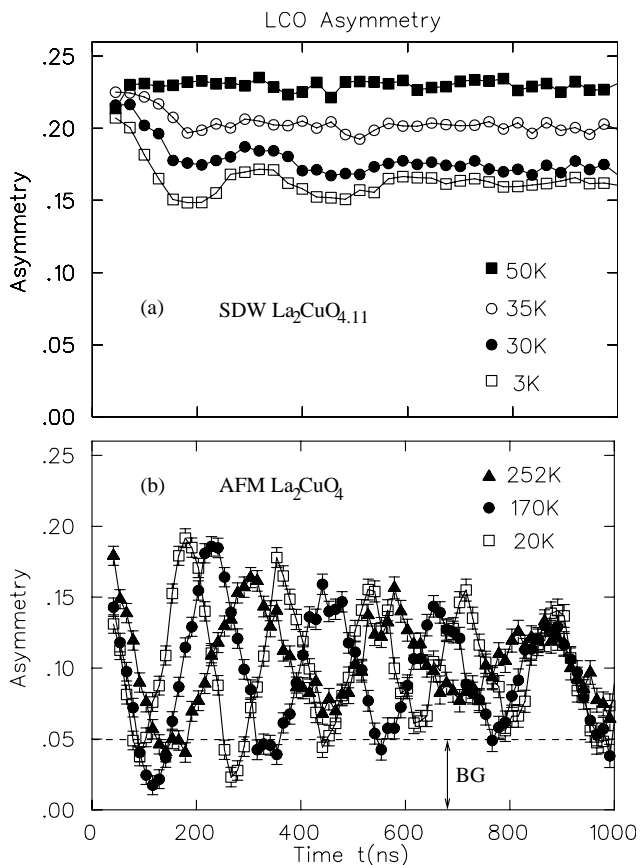


Fig. 93. Comparison between ZF- $\mu$ SR spectra of La<sub>2</sub>CuO<sub>4.11</sub> and antiferromagnetic La<sub>2</sub>CuO<sub>4</sub>.

an increased amplitude of oscillations as we lower the temperature, but frequency remains almost constant.

In order to elucidate this behaviour, a simple model was proposed. Magnetic ordering exists only in a certain fraction of the crystal. Computer simulations were performed for different configurations of regions with static magnetism. These can be seen in the inset of Fig. 94.

In order to decide which model best describes the experimental results, we looked at the fraction of muon sites that have a non-zero magnetic field and at the signal that one gets for this distribution.

The “sandwich model” contains completely ordered Cu planes. The resulting signal has a long lived Bessel-like oscillation, with little decay of non-relaxing signal, which does not fit experimental results well.

The “island model” contains circular regions with magnetic ordering. A density of 30% of the spins showing static magnetism gives a fraction of 40% of muon sites with non-zero magnetic field (as in the measured data for LCO:4.11). The relaxation of the oscillating signal is also a measure of the size of the “island”, which we estimate to be 15–30 Å.

A correlation of spin orientation in overlapping magnetic regions in neighbouring planes is a possible

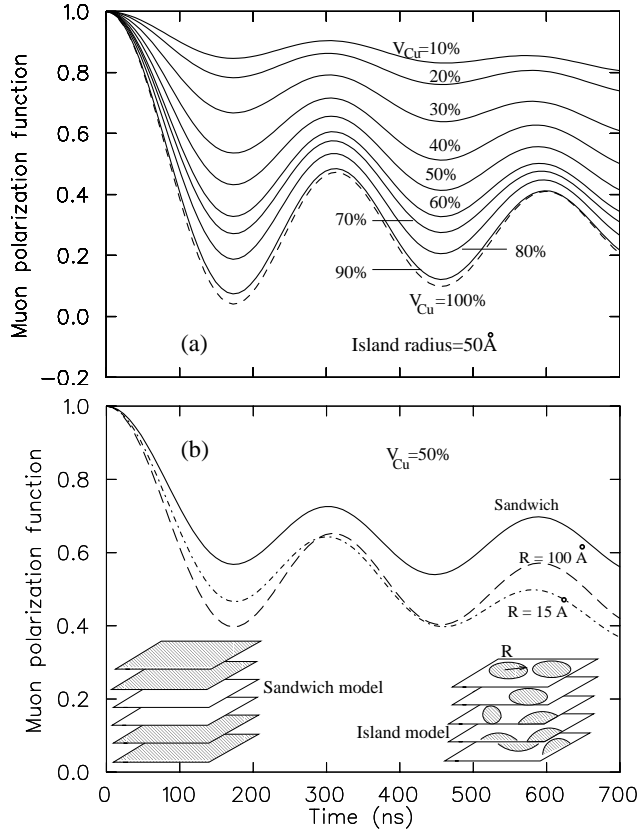


Fig. 94. Computer simulation results for different magnetic configurations.

explanation for the long range order, observed by neutron scattering.

In transverse magnetic field  $\mu$ SR measurements, sensitive to the in-plane magnetic field penetration depth  $\lambda_{ab}$ , the results for LCO:4.11 and LSCO:0.12 follow correlations found for underdoped, overdoped and Zn-doped HTSC systems in a plot of  $T_c$  versus the superconducting relaxation rate  $\sigma(T \rightarrow 0)$ . This indicates that the volume-integrated value of  $n_s/m^*$  (superconducting carrier density/effective mass) is a determining factor for  $T_c$ , not only in HTSC systems without static magnetism, but also in the present systems where superconductivity co-exists with static SDW spin order.

We have performed zero-field and transverse-field  $\mu$ SR of  $\text{La}_{1.85-y}\text{Eu}_y\text{Sr}_{0.15}\text{CuO}_4$ , where Eu doping stabilizes the “stripe” structures in the spin and charge degrees of freedom. In Fig. 95a, zero-field  $\mu$ SR spectra are shown for Eu concentrations  $y = 0.05, 0.1$  and  $0.2$ . The magnetic volume fraction, which is indicated by the amplitude of the precession in the  $t < 0.3 \mu\text{s}$  time range, increases as the Eu doping proceeds. The size of the ordered moments, as shown by precession frequencies, is independent to the Eu concentration, and is common to the frequency in the  $1/8$  carrier doping, where stripes are fully stabilized. These results

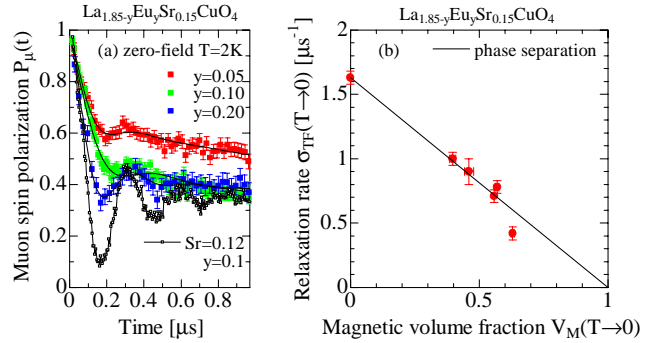


Fig. 95. (a) zero-field  $\mu$ SR of  $\text{La}_{1.85-y}\text{Eu}_y\text{Sr}_{0.15}\text{CuO}_4$ . (b) Superfluid density vs. magnetic volume fraction.

indicate that the static magnetism exhibits a *partial volume fraction*, with area covered by islands of ordered moments increasing as Eu doping proceeds, without changing the size of the ordered moments.

From transverse-field  $\mu$ SR, the superfluid density was estimated, and shown in Fig. 95b, as a function of the static magnetic volume fraction. There is a trade-off between the magnetic volume fraction ( $V_M$ ) and the superfluid density  $n_s/m^* \propto \sigma_{\text{TF}}$ . This suggests a phase separation between the magnetism and superconductivity. The solid line in Fig. 95b indicates a model where superfluidity originates only from the non-magnetic volumes. The results are interpreted in the context of the recent discoveries of microscopic phase separations between the superconducting phase and other phases.

### Experiment 852

#### Magnetic phases in geometrically frustrated rare earth pyrochlores

(S. Dunsiger, LANL; J. Gardner, NRC; R. Kiefl, UBC)

In systems where magnetic ions occupy the vertices of edge or corner sharing triangular units, the combination of the strength and sign of the interactions and local anisotropy may give rise to situations where there is no spin configuration which simultaneously satisfies all the magnetic couplings. Stacked triangular, kagomé, fcc, and pyrochlore lattices are all examples of such *geometric* frustration. The purpose of Expt. 852 is to apply  $\mu$ SR to further our understanding of the effect of this frustration on the ground state and low lying magnetic excitations in the pyrochlores  $\text{A}_2\text{B}_2\text{O}_7$ , where magnetic ions form a network of corner sharing tetrahedra. Unlike many other systems having geometric frustration, pyrochlores are noted for their high degree of chemical order, which is important for minimizing effects due to disorder.

Geometric frustration leads to the formation of a wide range of exotic ground states. A vast body of work has been carried out on  $3d$  and  $4d$  transition metal pyrochlores. These are generally insulators where novel

properties such as cooperative paramagnetism [Gardner *et al.*, Phys. Rev. Lett. **82**, 1012 (1999)] partial, non-collinear antiferromagnetic ordering [Raju *et al.*, Phys. Rev. **B59**, 14489 (1999); Champion *et al.*, Phys. Rev. **B64**, 140407(R) (2001)], spin-freezing [see, for instance Raju *et al.*, Phys. Rev. **B46**, 5405 (1992); Gingras *et al.*, Phys. Rev. Lett. **78**, 947, (1997)], and dipolar “spin-ice” behaviour [Harris *et al.*, Phys. Rev. Lett. **79**, 2554 (1997); Harris *et al.*, Phys. Rev. Lett. **81**, 4496 (1998); Bramwell and Harris, J. Phys. Cond. Matter **10**, L215 (1998); Ramirez *et al.*, Nature **399**, 333 (1999); Siddharthan *et al.*, Phys. Rev. Lett. **83**, 1854 (1999)] have been observed. There has, however, been growing interest in the interplay between itinerant and local moments in geometrically frustrated systems. The  $5d$  transition metal pyrochlores are mainly metallic, resulting from the extended nature of the  $5d$  orbitals. Despite the large number of transition metal compounds which crystallize in the pyrochlore structure and the wide range of physical phenomena observed in these materials, superconductivity had not been observed until the recent discovery of bulk superconductivity in the  $5d$  pyrochlore,  $\text{Cd}_2\text{Re}_2\text{O}_7$  [Sakai *et al.*, J. Phys. Cond. Matter **13**, L785 (2001); Hanawa *et al.*, Phys. Rev. Lett. **87**, 187001 (2001)].

Recent investigations [Sakai *et al.*, *op. cit.*; Hanawa *et al.*, *op. cit.*; Jin *et al.*, Phys. Rev. **B64**, 180503(R) (2001); Jin *et al.*, cond-mat/0108402 (2001); Hanawa *et al.*, cond-mat/0109050 (2001)] have demonstrated the existence of two phase transitions in this compound. The first, occurring at a temperature of about 200 K, is a continuous structural transition which is accompanied by drastic changes in resistivity and magnetic susceptibility. On further lowering the temperature,  $\text{Cd}_2\text{Re}_2\text{O}_7$  has been shown to exhibit bulk superconductivity below a sample dependent transition temperature of about 1 K [Sakai *et al.*, *op. cit.*; Hanawa *et al.*, Phys. Rev. Lett. **87**, 187001 (2001); Jin *et al.*, Phys. Rev. **B64**, 180503(R) (2001)]. Preliminary measurements in the superconducting state indicate that  $\text{Cd}_2\text{Re}_2\text{O}_7$  is a type-II superconductor with  $H_{c1}$  less than 0.002 T and estimates of the upper critical field,  $H_{c2}$ , ranging from 0.2 T to 1 T. None of the measurements reported to date extend below 0.3 K ( $T/T_c \sim 0.3$ ). We report the first measurements on  $\text{Cd}_2\text{Re}_2\text{O}_7$  below 300 mK, temperatures which are necessary (for  $T_c \sim 1$  K) to extract information about the superconducting order parameter symmetry. In July, 2000 we performed transverse field (TF) and zero field (ZF) muon spin rotation ( $\mu\text{SR}$ ) measurements on single crystal samples of  $\text{Cd}_2\text{Re}_2\text{O}_7$  in an Oxford Instruments dilution refrigerator on the M15 beam line at TRIUMF. The crystals were mounted such that the cubic (100) direction would be parallel to the applied

magnetic field direction. The ZF- $\mu\text{SR}$  measurements reveal very small internal magnetic fields which are characteristic of nuclear dipoles, indicating no significant electronic magnetism either above or below  $T_c$ . The TF- $\mu\text{SR}$  results provide the first measurement of the internal field distribution in the vortex state in this material. In particular, temperature dependent studies from 20 mK to 4 K indicate a penetration depth which levels off as  $T \rightarrow 0$ , suggestive of a fully gapped Fermi surface with a rather large zero temperature value of the penetration depth,  $\lambda(0) \sim 7500$  Å.

Figures 96(a) and (b) show typical  $\mu\text{SR}$  spectra in a transverse field of 0.007 T, for temperatures above and below  $T_c$  respectively. Examination of these data clearly shows an enhanced depolarization rate on entering the superconducting state resulting from the inhomogeneous field distribution associated with the flux line lattice. This represents the first experimental observation of the vortex lattice in  $\text{Cd}_2\text{Re}_2\text{O}_7$  and

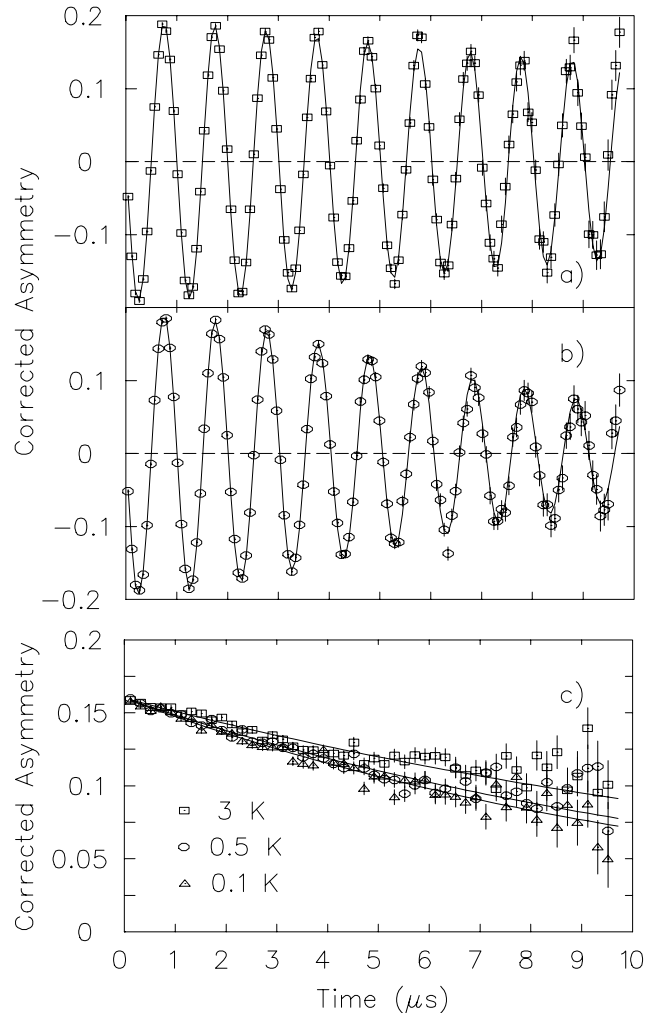


Fig. 96. Typical  $\mu\text{SR}$  spectra in  $\text{Cd}_2\text{Re}_2\text{O}_7$  obtained in a transverse magnetic field of 0.007 T at temperatures of (a)  $T=1.5$  K (above  $T_c$ ) and (b)  $T=100$  mK (below  $T_c$ ). (c) Zero field spectra in  $\text{Cd}_2\text{Re}_2\text{O}_7$  at various temperatures.



provides clear evidence that this material is a type-II superconductor. The observed increase in the TF line broadening below  $T_c$  can be attributed entirely to the vortex lattice since the ZF muon spin relaxation rate was small and roughly temperature independent below 2 K. Zero field measurements indicate no significant electronic magnetism in this superconductor, suggesting that magnetic frustration does not play a direct role in the superconductivity.

Following the work of Sonier *et al.* [Rev. Mod. Phys. **72**, 769 (2000) and references therein], a Ginzburg-Landau (GL) model has been applied to the magnetic field distribution for the single crystal. In GL theory, the size of the vortex core is determined by the applied magnetic field,  $H$ , and the GL coherence length normal to the applied field,  $\xi_{GL}$ , while the penetration depth provides the length scale of the decay of magnetic field away from the vortex core. The field distribution is calculated from the spatial distribution of magnetic field [Yaouanc *et al.*, Phys. Rev. **B55**, 11107 (1997)],

$$B(\mathbf{r}) = \frac{\Phi_0}{S}(1 - b^4) \sum_{\mathbf{G}} e^{-i\mathbf{G}\cdot\mathbf{r}} \frac{uK_1(u)}{1 + \lambda^2 G^2}, \quad (1)$$

where  $u^2 = 2\xi_{GL}^2 G^2(1 + b^4)[1 - 2b(1 - b^2)]$ ,  $K_1(u)$  is a modified Bessel function,  $\mathbf{G}$  is a reciprocal lattice vector of the vortex lattice,  $b = H/H_{c2}$  is the reduced field,  $\Phi_0$  is the flux quantum and  $S$  is the area of the reduced unit cell for a hexagonal vortex lattice.

As can be seen from Eq. 1, the field distribution depends on both the penetration depth and GL coherence length. The GL coherence length can be obtained from the known value of the upper critical field using the expression  $\xi_{GL} = (\Phi_0/2\pi H_{c2})^{1/2}$  where  $\Phi_0$  is the flux quantum. A range of values for  $H_{c2}$  has been reported and consequently, to provide a self-consistent measurement of  $\lambda$ , the field dependence of the linewidth was measured. To account for any possible instrumental field dependence in the linewidth, measurements were made above the transition temperature (2 K) at each field value after which the sample was field-cooled to 100 mK. The measured linewidth in the normal state was subtracted in quadrature from that observed at 100 mK and the results are plotted in Fig. 98 as a function of applied magnetic field. As can be clearly seen, the linewidth decreases almost linearly with applied field. This is attributed to the linear increase in the volume taken up by the vortices. The linewidth parameter,  $\sigma_{FC}$ , approaches zero at a field of 0.5 T which is our estimate of  $H_{c2}(T \rightarrow 0)$  and is consistent with measurements on other samples. This estimate of the critical field corresponds to  $\xi_{GL} \sim 260$  Å. Using this value, we obtain the penetration depth using the field distribution shown in Eq. 1. The resulting temperature dependent penetration depth is shown in Fig. 99.

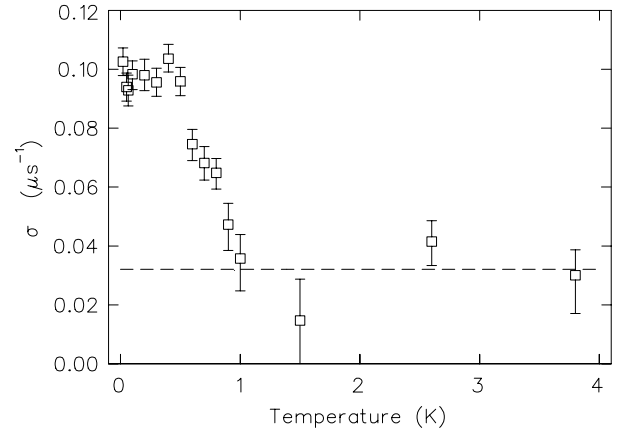


Fig. 97. Linewidth parameter  $\sigma$  as a function of temperature in a transverse magnetic field of 0.007 T applied along the (100) direction.

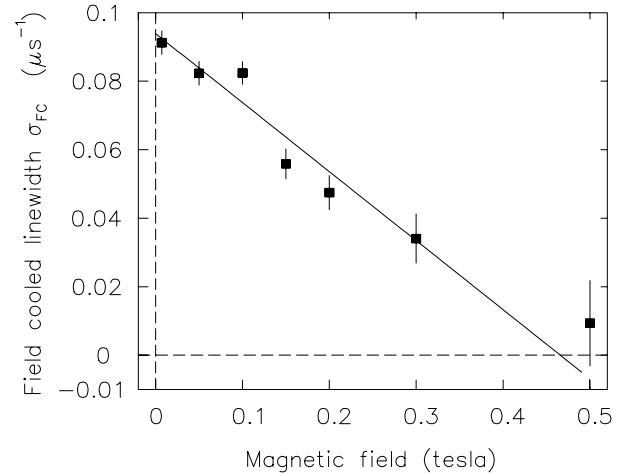


Fig. 98. Linewidth parameter  $\sigma_{FC}$  as a function of magnetic field applied along the (100) direction. The normal state contribution has been subtracted as described in the text. Measurements were taken at a temperature of 100 mK.

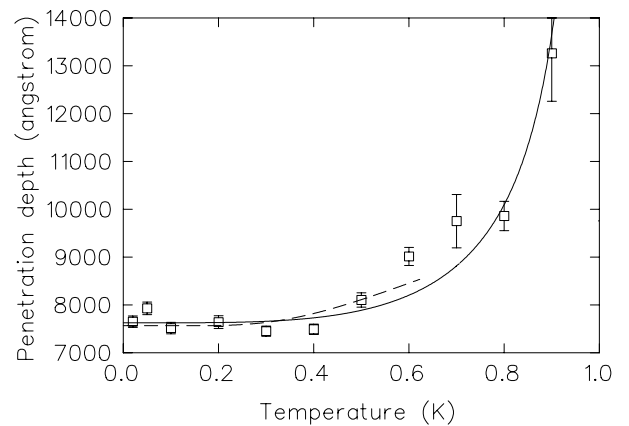


Fig. 99. Penetration depth as a function of temperature in a magnetic field of 0.007 T applied parallel to the (100) direction. The solid and dashed lines are fits to Eqs. 2 and 3 respectively.

As expected from the small values of linewidth, at the base temperature we observe a rather large value of the penetration depth,  $\lambda(0) \sim 7500 \text{ \AA}$ . We note that this value of penetration depth is significantly larger than most oxide superconductors where values ranging from 1000–2000  $\text{\AA}$  are typical [Uemura *et al.*, Phys. Rev. Lett. **66**, 2665 (1991); Aegerter *et al.*, J. Phys. Cond. Matt. **10**, 7445 (1998)].

As the penetration depth is related to the concentration of superconducting carriers, its temperature dependence is a measure of the low-lying electronic excitations. As such, the presence of a nodeless superconducting energy gap is indicated by a leveling off of the penetration depth as the temperature decreases below  $T_c$ . As is clearly seen in Figs. 97 and 99, the linewidth and penetration depth respectively become temperature independent as the temperature decreases below about 0.4 K, consistent with a fully gapped Fermi surface. Consequently, we conclude that the superconducting order parameter in  $\text{Cd}_2\text{Re}_2\text{O}_7$  is consistent with a nodeless energy gap suggesting either *s*-wave symmetry or exotic pairing symmetries, such as *p*-wave, which can also exhibit a fully gapped Fermi surface. For comparison, the solid line in Fig. 99 represents fits to the two fluid approximation

$$\frac{\lambda^2(0)}{\lambda^2(T)} = [1 - (T/T_c)^4], \quad (2)$$

while the dashed line is a fit to the BCS temperature dependence

$$\lambda(T) = \lambda(0) \left[ 1 + \sqrt{\frac{\pi\Delta_0}{2T}} \exp\left(\frac{-\Delta_0}{T}\right) \right] \quad (3)$$

where  $\Delta_0 = 1.74(11) \text{ K}$ .

The London penetration depth,  $\lambda$ , provides a direct measure of the ratio of superconducting carrier concentration to effective mass,  $n_s/m^*$ ,

$$\frac{1}{\lambda^2} = \frac{4\pi n_s e^2}{m^* c^2} \left( 1 + \frac{\xi_0}{l} \right)^{-1}, \quad (4)$$

where  $\xi_0$  is the Pippard coherence length, and  $l$  is the mean-free path. There is considerable uncertainty in estimates of the mean-free path with reported values ranging from 200–700  $\text{\AA}$  [Jin *et al.*, Phys. Rev. **B64**, 180503(R) (2001); Hiroi and Hanawa, cond-mat/0111126 (2001)] and it is unclear whether  $\text{Cd}_2\text{Re}_2\text{O}_7$  is a superconductor in the clean or dirty limit. Under the assumption of a clean superconductor, such that  $\xi_0/l \ll 1$ , a value of  $n_s m_e/m^*$  of  $5.0 \times 10^{25} \text{ m}^{-3}$  can be obtained using Eq. 4 and the measured penetration depth. It is important to note that this quantity depends strongly on the clean-limit assumption and a value of  $l \sim 200 \text{ \AA}$  leads to a dirty limit

superconductor with  $\xi_0 \sim 470 \text{ \AA}$  and  $n_s m_e/m^* \sim 1.4 \times 10^{26} \text{ m}^{-3}$ . Clearly, precise determination of the mean free path for  $\text{Cd}_2\text{Re}_2\text{O}_7$  is needed to allow accurate quantitative information to be extracted. If the material is in the clean limit, the present results provide strong evidence for a fully gapped Fermi surface.

## Experiment 876

### Disordered magnetism near magnetic instabilities in *f*-electron materials

(D.R. Noakes, Virginia State)

The discussion of this experiment in last year's Annual Report described ZF- and LF- $\mu$ SR measurements of UPdSn and members of the  $\text{PrAu}_2(\text{Si}_{1-x}\text{Ge}_x)_2$  alloy series. A short paper comparing the data from UPdSn to earlier data from CeCuSn was presented at the 2001 Strongly Correlated Electron Systems Conference in Ann Arbor, MI, in August, and will appear in the proceedings [Physica B, in press]. This year, additional measurements were made on  $\text{U}_{0.94}\text{Y}_{0.06}\text{CoAl}$  and at dilution refrigerator temperatures in  $\text{PrAu}_2\text{Si}_2$ .

#### $\text{U}_{0.94}\text{Y}_{0.06}\text{CoAl}$

Pure UCoAl has no spontaneous magnetic ordering to low temperatures, but a metamagnetic transition in a relatively low applied field of 0.8 T. Andreev *et al.* [J. Magn. & Magn. Mater. **196-197**, 658 (1999)] discovered that alloying small amounts of non-magnetic yttrium on the uranium site causes ferromagnetic ordering to occur. From about 1% Y to 6% Y, the Curie temperature is roughly constant near 15 K, but the 4.2 K bulk ordered moment rises from very small values to near  $0.1 \mu_B$  per formula unit (much less than the uranium free-ion moment of  $3.2 \mu_B$ ). Beyond 6% Y, both  $T_C$  and the ordered moment fall back toward zero. Other researchers had already established that there is very little muon spin relaxation in pure UCoAl. In August, we measured  $\mu$ SR in  $\text{U}_{0.94}\text{Y}_{0.06}\text{CoAl}$ , the composition of strongest ferromagnetism, at M20.

The polycrystalline sample was small, and, mounted on a silver backing, generated a relaxing asymmetry of only 0.055 when the full asymmetry measured in transverse field was 0.23 (the difference is generated by muons that missed the sample and stopped in silver, in which they do not relax in zero or longitudinal field). ZF relaxation was consistent with fields generated by the nuclear moments in the sample, with little, if any, indication of electronic moments, down to 20 K. A fast-relaxing signal consistent with the freezing of dilute electronic moments in the sample begins to appear near 16 K and increases in amplitude until it saturates at  $\simeq 0.034$  (representing about 60% of the sample volume) at 12 K and below. Figure 100 shows the ZF asymmetry spectrum at 3 K, with the solid line

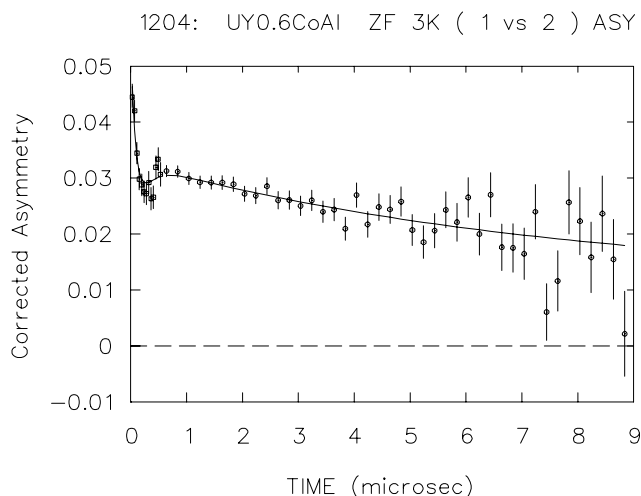


Fig. 100. ZF asymmetry spectrum of  $U_{0.94}Y_{0.06}CoAl$  at 3.0 K, with solid line showing the fit of the inhomogeneous-freezing model described in the text.

showing the fit of static Lorentzian Kubo-Toyabe relaxation (the frozen-state signal) plus a slowly-relaxing signal caused primarily by nuclear moments in the portion of the sample that remains paramagnetic. Measurements in longitudinal field support this model.

While static Lorentzian Kubo-Toyabe relaxation is normally associated with the frozen state of dilute-moment spin glasses, this relaxation function is primarily caused by a positionally-disordered distribution of dilute moments, and does not necessarily mean that the moment pointing directions are disordered. I have shown, using numerical simulations published in the *Journal of Magnetism and Magnetic Materials*, that long-range ferromagnetic order in a polycrystalline, dilute, magnetic alloy produces a ZF muon spin relaxation function that is difficult to distinguish from the standard Lorentzian Kubo-Toyabe. Independently, there are indications of ferromagnetism in our experimental data. When tens of Gauss transverse field are applied below 12 K, sufficient bulk magnetization develops in the sample to cause relaxation of muons that miss the sample, and when that field is removed, the sample has remnant magnetization that continues to affect the polarization of muons that miss the sample.

Our interpretation is that  $U_{0.94}Y_{0.06}CoAl$  is a dilute-moment ferromagnet. When yttrium is alloyed onto the uranium site, instead of all the remaining uranium ions each gaining a small moment, no more than one uranium per yttrium ion gains a moment, but each moment created is roughly of Bohr-magneton size. Further, only about 60% of the volume of our sample enters the ferromagnetic state. The other 40% appears to remain paramagnetic.

## $PrAu_2Si_2$

Measurements in 2000 on the  $PrAu_2(Si_{1-x}Ge_x)_2$  series described in last year's Annual Report were performed in a cryostat with a base temperature near 1.9 K. This was sufficient to allow us to detect ZF coherent oscillations in the antiferromagnetic states of  $PrAu_2Ge_2$  and  $PrAu_2(Si_{0.8}Ge_{0.2})_2$ . In  $PrAu_2Si_2$ , which is nominally a spin glass with  $T_g \approx 3$  K, however, we saw no clear freezing effect down to 1.9 K, and felt that data at dilution-refrigerator temperatures was needed. In 2001, we took advantage of an opportunity to collect a small amount of such data during an unrelated experiment, and found that there is only smooth variation of ZF behaviour with no clear indication of magnetic freezing down to 0.04 K. Thus, in spite of bulk-probe signatures of spin-glass freezing, in  $\mu SR$ ,  $PrAu_2Si_2$  looks more like a frustrated magnetic system with electronic fluctuations that slow down a bit as temperature is lowered, but never actually freeze. This is an unusual discrepancy with the bulk probe results that we are still trying to understand.

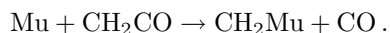
## Experiment 883

### Muoniated methyl and associated free radicals (*P. W. Percival, SFU*)

This is the first progress report on this project, which was first approved in June, 2000. It is a successor to Expt. 749, which applied the muon spin probe to investigate topical and/or fundamental questions in free radical chemistry. The general method for these projects involves addition of muonium (Mu) to an unsaturated molecule such as an alkene or arene, resulting in a free radical incorporating the muon in place of a proton. Such a radical is termed a muoniated radical, to emphasize the formal replacement of a hydrogen atom by muonium in what is otherwise a recognized chemical structure (cf. a deuterated molecule, which contains D instead of H). In terms of electronic structure there is no difference between the H and Mu analogues (at least, to the level of the Born-Oppenheimer approximation). In most respects the muoniated radical behaves like its H analogue and the muon can be viewed as a passive spin probe. However, the low mass of Mu compared to H can result in significant isotope effects, particularly to intramolecular motion.

The specific aim of Expt. 883 is to detect the muoniated methyl radical,  $\cdot CH_2Mu$ , and study its vibrational motion via measurements of electron-nuclear hyperfine constants as a function of temperature. A previous attempt (TRIUMF Expt. 546) failed to detect  $\cdot CH_2Mu$  due to the instability of the precursor, diazomethane ( $CH_2N_2$ ). However, we did manage to detect and study the trimethylsilyl derivative [Addison-Jones *et al.*, *Hyp. Int.* **106**, 143 (1997)]. Experiment

883 is based on an alternative strategy, using ketene as the radical precursor:



There are considerable practical difficulties involved in using ketene, which tends to polymerize in addition to posing significant safety hazards. Accordingly, we started with the relatively benign ketene dimer, which is a liquid at room temperature. Also, since any ketene sample will slowly evolve into an equilibrium mixture with its dimer, it was important to characterize the product of the reaction between Mu and diketene.

There are several potential sites for Mu addition in diketene (see structure 1 in Fig. 101). However, the transverse field  $\mu\text{SR}$  spectrum shows that only one product is formed. This is evident from the example in Fig. 102. The difference between the two radical precession frequencies (marked  $R_1$  and  $R_2$ ) is a direct measure of the muon hyperfine coupling constant (hfc). A different technique, muon avoided level-crossing spectroscopy, is used to determine proton hfc. An example of such a  $\mu\text{ALCR}$  spectrum is given in Fig. 103. The existence of two distinct resonances implies that the muoniated radical contains two sets of chemically inequivalent protons. A structure that satisfies these criteria is shown as 2 in Fig. 101. This assignment was supported by density functional calculations.

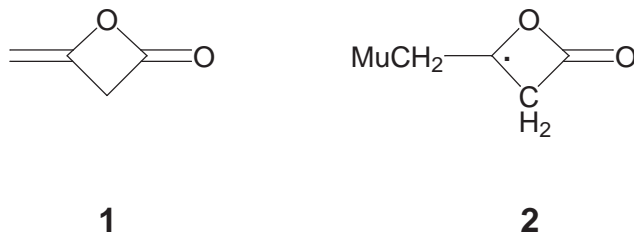


Fig. 101. The structure of (1) diketene; (2) the free radical formed by Mu addition to diketene.

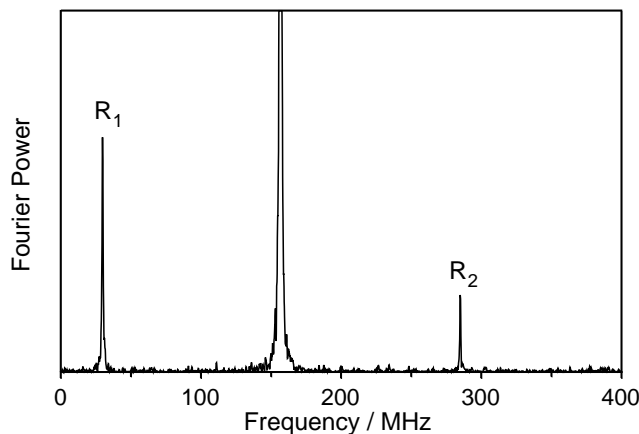


Fig. 102. Fourier transform  $\mu\text{SR}$  spectrum of the Mu adduct of diketene at 298 K and 11.6 kG.

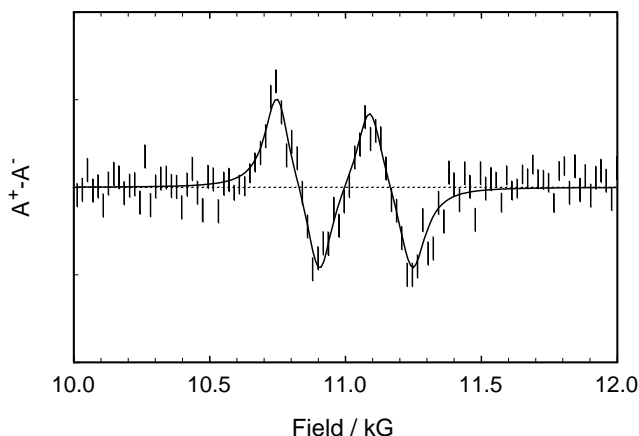


Fig. 103.  $\mu\text{ALCR}$  spectrum of the Mu adduct of diketene at 298 K.

Muon and proton hfc were determined at several temperatures between 280 and 363 K. The results are summarized in Table IX. The temperature dependence was modelled by taking into account the relative energies of the minimum energy conformations for rotation of the  $\text{CH}_2\text{Mu}$  group. Further details can be found in our publication [McKenzie *et al.*, Phys. Chem. Comm. **27**, 1 (2001)].

Table IX. Analysis of  $\mu\text{ALCR}$  spectra.

T/K	$A_\mu/\text{MHz}$	$A_{p1}/\text{MHz}$	$A_{p2}/\text{MHz}$
281.8	258.61	52.40(8)	46.62(8)
297.0	255.19	52.88(6)	46.56(5)
320.9	250.65	52.95(6)	46.21(5)
343.5	246.98	53.70(5)	46.56(6)
362.5	244.11	53.85(7)	46.60(7)

The next stage in the project was to use pure ketene as a sample. It was necessary to prepare fresh samples (by the pyrolysis of acetone) just prior to beam time, and store them in dry ice prior to mounting in a pre-cooled cryostat. Our success is evident from the spectra shown in Figs. 104 and 105. The muon and proton hfc

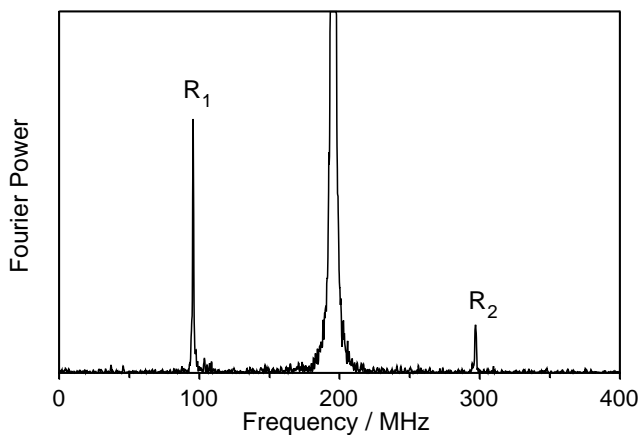


Fig. 104. Fourier transform  $\mu\text{SR}$  spectrum of the muoniated methyl radical at 184 K and 14.5 kG.

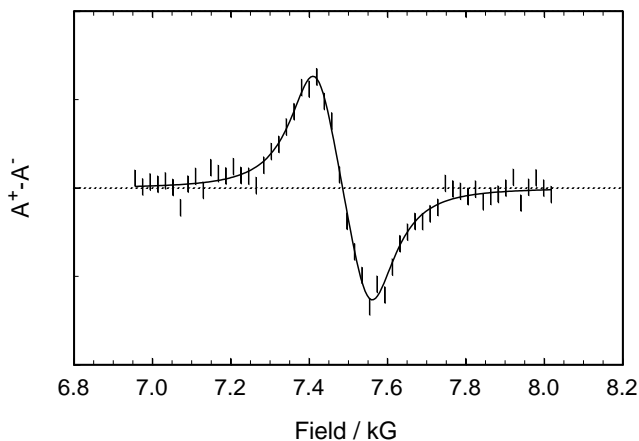


Fig. 105.  $\mu$ ALCR spectrum of the muoniated methyl radical at 184 K.

were determined to be  $-201.5$  MHz and  $-61.4$  MHz, respectively. Since the ratio of these numbers differs by only a few per cent from that of the muon and proton magnetic moments, we can deduce that the Mu and H are chemically equivalent (with a small isotope effect of about 3%). There is little doubt that the radical is indeed the sought-after methyl,  $\cdot\text{CH}_2\text{Mu}$ .

#### Experiment 884

**$\mu$ SR studies on magnetic ground state of  $S=1/2$  kagomé spin system  $\text{Cu}_3\text{V}_2\text{O}_7(\text{OH})_2 \cdot 2\text{H}_2\text{O}$**   
(A. Fukaya and Y.J. Uemura, Columbia)

A copper volborthite  $\text{Cu}_3\text{V}_2\text{O}_7(\text{OH})_2 \cdot 2\text{H}_2\text{O}$  is a system which has  $S=1/2$  Cu moments on a nearly kagomé lattice configuration [Hiroi *et al.*, J. Phys. Soc. Jpn. **70**, 3377 (2001)]. Antiferromagnetic coupling is inferred from the Weiss temperature  $\Theta = -115$  K of the susceptibility at high temperatures. The spin dynamics of this system is of much interest in view of the interplay between the geometrical frustration and the enhanced quantum effect due to  $S = 1/2$ , as well as of the comparison with theories available for the  $S = 1/2$  kagomé lattice antiferromagnet.

We performed ZF- and LF- $\mu$ SR studies in the pure  $x=1.0$  and diluted ( $x \geq 0.6$ ) compounds. Figure 106 shows the temperature dependence of the time spectra at LF = 100 G in the pure system. The relaxation rate increased with decreasing temperature, indicating slowing down of Cu spin fluctuations, and then showed saturation below  $T = 1.5$  K, as shown in Fig. 107. The LF dependence of the spectra at 50 mK was much smaller than that expected for static internal fields. These results, similar to the  $\mu$ SR results in  $S = 3/2$   $\text{SrGa}_{12-x}\text{Cr}_x\text{O}_{19}$  kagomé magnets [Uemura *et al.*, Phys. Rev. Lett. **73**, 3306 (1994)], indicate slow dynamic spin fluctuations persisting to  $T \rightarrow 0$ .

The magnetic dilution resulted in a dramatic reduction of the relaxation rate, as shown in Fig. 107.

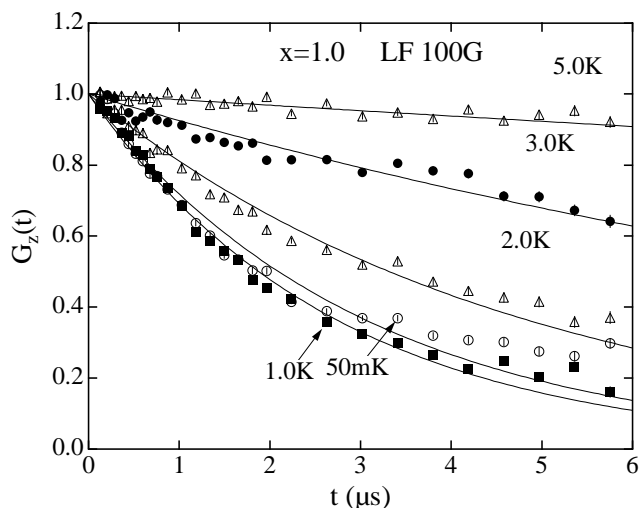


Fig. 106. Temperature dependence of the time spectra at LF = 100 G in the pure  $x = 1.0$  sample.

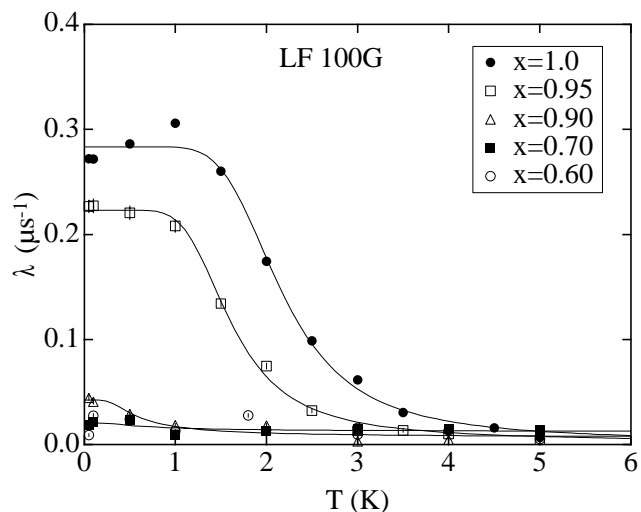


Fig. 107. Temperature dependence of the relaxation rate,  $\lambda$ , at LF = 100 G in various  $x$  samples.

This suggests that the observed relaxation in the pure system is not due to impurity spins. Instead, with increasing dilution (decreasing  $x$ ), the spin fluctuation becomes faster.

#### Experiment 890

**Anisotropic Kondo effect in  $\text{Ce}_{0.8}\text{La}_{0.2}\text{Al}_3$ ?**  
(D.E. MacLaughlin, California, Riverside)

The theory of the anisotropic Kondo model (AKM) has been studied extensively in recent years. In spite of this interest there have been few experimental studies of physical realizations of the AKM in systems of local d or f moments in metals, which were the earliest manifestations of the “ordinary” Kondo effect.

The heavy-fermion compound  $\text{CeAl}_3$  was long thought to exhibit a nonmagnetic “Kondo-lattice”

ground state.  $\mu$ SR and NMR studies showed, however, that inhomogeneous weak-moment magnetic order sets in below  $\sim 1$  K. Moreover, as lanthanum is doped onto cerium sites the specific heat coefficient  $\gamma(T) = C(T)/T$  is drastically modified, and a maximum in  $\gamma(T)$  at a characteristic temperature  $T^*$  ( $\approx 0.4$  K in  $\text{CeAl}_3$ ) moves up in temperature and grows into a large peak;  $T^* = 2.2$  K for  $x = 0.2$ . This behaviour was initially taken as evidence for development of a weak-moment magnetically ordered phase of  $\text{CeAl}_3$ , and attributed to reduction of the hybridization between Ce f electrons and ligand-derived conduction electrons.

This interpretation has been called into question on the basis of inelastic neutron scattering experiments on  $\text{Ce}_{0.8}\text{La}_{0.2}\text{Al}_3$ , which found a broad inelastic peak below  $T^*$ . This peak was taken as evidence for applicability of the AKM to the  $\text{Ce}_{1-x}\text{La}_x\text{Al}_3$  system. Zero-field  $\mu^+$  spin relaxation (ZF- $\mu$ SR) experiments at the ISIS pulsed muon facility indicated magnetic freezing at  $T = T^*$ , but the frozen moment was claimed to be weak ( $\sim 0.05 \mu_B/\text{Ce}$  ion), principally because no neutron diffraction peak was observed. Recent ZF- $\mu$ SR studies, also carried out at ISIS, conclude that for  $x = 0.05$  the magnetic freezing persists to temperatures well above  $T^*$ . This is taken as further evidence that the specific peak at  $T^*$  reflects the anisotropic Kondo effect and is unrelated to spin freezing.

Specific heat measurements in  $\text{Ce}_{0.8}\text{La}_{0.2}\text{Al}_3$  at applied fields of up to 14 T disagree with the theoretical behaviour of the AKM, however. Furthermore, the argument for applicability of the AKM depends strongly on evidence that the frozen moments are small, viz., the absence of neutron Bragg peaks. Neutron diffraction would not necessarily be sensitive to spin freezing of a glassy nature or short-range order, however, whereas the ZF- $\mu$ SR relaxation rate reflects spin freezing independently of the degree of long-range order.

We have carried out ZF- $\mu$ SR experiments in  $\text{Ce}_{1-x}\text{La}_x\text{Al}_3$ ,  $x = 0$  and  $0.2$ , at TRIUMF and PSI. For  $x = 0.2$  we observe a strongly damped but resolved oscillation in the muon asymmetry data at low temperatures, as shown in Fig. 108. For both La concentrations the precession frequency disappears at  $T^*$ , in disagreement with earlier results for  $x = 0.05$ , and in agreement with the expected result if  $T^*$  were a magnetic ordering transition temperature. The strong damping indicates a distribution of static local fields at muon sites, as might be expected in a strongly disordered substitutional alloy, but the oscillation reflects a fairly well-defined average local field. Asymmetry data for both La concentrations were fit assuming magnetic and nonmagnetic volume fractions; a ‘‘damped cosine’’ form was used for the precessing signal. The form of the relaxation function is

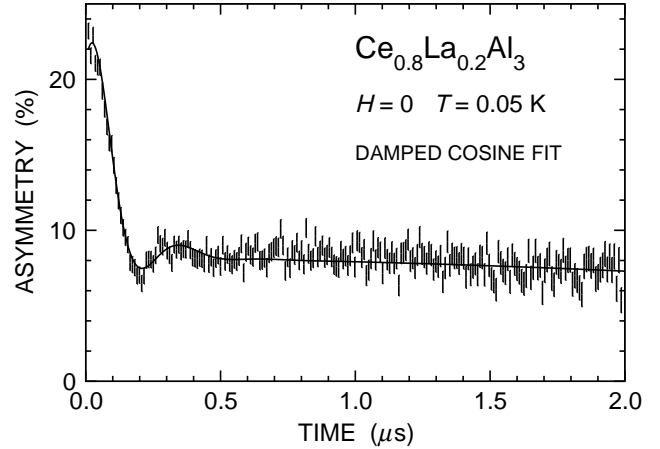


Fig. 108.  $\text{Ce}_{0.8}\text{La}_{0.2}\text{Al}_3$  asymmetry relaxation function.

$$G(t) = A_m \left[ \frac{2}{3} \exp(-\lambda_T t) \cos(2\pi\nu t + \phi) + \frac{1}{3} \exp(-\lambda_L t) \right] + A_n G_{\text{KT}}(t).$$

Here the relaxation from the magnetic volume fraction  $f_{\text{mag}}$  is modelled by the component with asymmetry amplitude  $A_m$ . The static field at the muon site is assumed to be randomly oriented. Relaxation of muons in the remaining nonmagnetic fraction is due to nuclear dipolar fields and is described by a static Kubo-Toyabe function  $G_{\text{KT}}(t)$ ; thus  $f_{\text{mag}} = A_m/(A_m + A_n)$ . The relaxation rates  $\lambda_T$  and  $\lambda_L$  characterize the transverse and longitudinal relaxation, respectively; the former is expected to be dominated by static disorder whereas  $\lambda_L$  reflects dynamic spin-lattice relaxation.

The temperature dependence of the fit parameters is given in Fig. 109. It can be seen that  $\nu(T)$  (a) is independent of  $x$  at low temperatures, (b) decreases markedly as  $T^*$  is approached from below, and (c) is suppressed to zero at  $T = T^*$  for  $x = 0.02$ . Unfortunately the muon stopping site in  $\text{CeAl}_3$  is not known, otherwise the ordered moment  $\mu_{\text{ord}}$  could be estimated accurately. Estimates of  $\mu_{\text{ord}}$  range from  $0.11$  to  $0.5 \mu_B/\text{Ce}$  ion in  $\text{CeAl}_3$ , which is 2–10 times larger than the neutron-diffraction upper limit reported previously, and the muon frequencies in  $\text{CeAl}_3$  and  $\text{Ce}_{0.8}\text{La}_{0.2}\text{Al}_3$  are the same. The entropy release at  $T^*$  implies  $\mu_{\text{ord}} \approx 0.3 \mu_B/\text{Ce}$  ion, comparable to values obtained from NMR and other measurements.

In  $\text{CeAl}_3$ ,  $\nu(T)$  is not completely suppressed to zero and  $\lambda_T(T)$  increases rapidly at  $T^*$ ; this can be understood as an effect of inhomogeneity in the transition temperature, as observed in  $\text{La}_2\text{CuO}_4$ . No such increase in broadening is observed in  $\text{Ce}_{0.8}\text{La}_{0.2}\text{Al}_3$ .  $\text{CeAl}_3$  also exhibits a decrease of  $f_{\text{mag}}$  as  $T^*$  is approached from below; this is also not seen in  $\text{Ce}_{0.8}\text{La}_{0.2}\text{Al}_3$ .

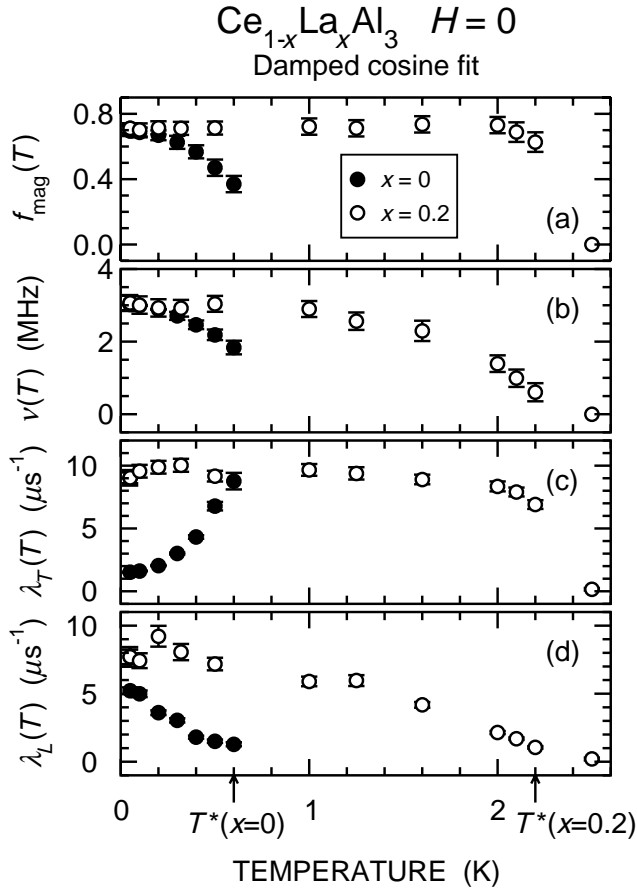


Fig. 109. Temperature dependence of (a) magnetic volume fraction  $f_{\text{mag}}(T)$ , (b) precession frequency  $\nu(T)$ , (c) transverse relaxation rate  $\lambda_T(T)$ , and (d) longitudinal relaxation rate  $\lambda_L(T)$  from ZF- $\mu$ SR in  $\text{Ce}_{1-x}\text{La}_x\text{Al}_3$ ,  $x = 0$  and  $0.2$ .

In conclusion, our ZF- $\mu$ SR data are consistent with a scenario in which the specific heat anomaly in  $\text{Ce}_{1-x}\text{La}_x\text{Al}_3$  is associated with the onset of static magnetism below  $T^*$ , with or without long-range order. In particular, there is no sign of such static magnetism above this temperature in  $\text{Ce}_{0.8}\text{La}_{0.2}\text{Al}_3$ .

### Experiment 891 Superconductivity and magnetism in $\text{Ce}_n\text{T}_m\text{In}_{3n+2m}$ (G.D. Morris, LANL)

#### Introduction

Experiment 891 is investigating superconductivity and magnetism in the family of Ce-based heavy-fermion superconductors  $\text{Ce}_n\text{T}_m\text{In}_{3n+2m}$ ,  $\text{T}=\text{Rh}, \text{Ir}, \text{Co}$ . These materials share a common crystal structure made up of layers of  $\text{CeIn}_3$  and  $\text{TIn}_2$  stacked along the  $c$  axis. Their superconducting and magnetic properties vary widely with composition, so the set of materials provides a rich phase diagram (Fig. 110) for a systematic study. Of particular interest is the region of the

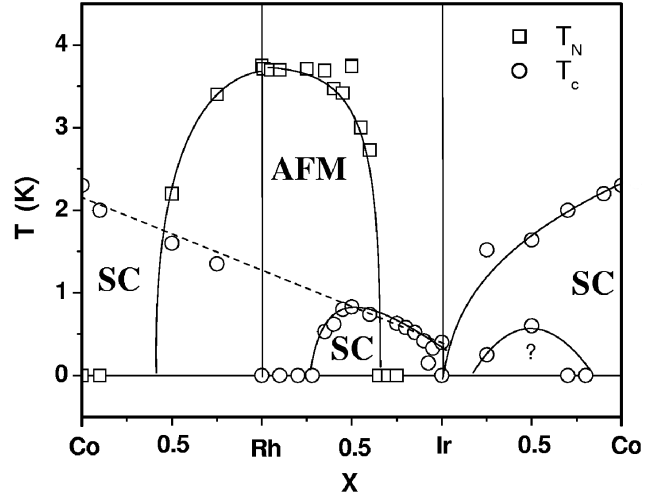


Fig. 110. A composition-temperature diagram of  $\text{CeTIn}_5$  materials showing the superconducting (SC) and antiferromagnetic (AFM) phases [Pagliuso *et al.*, condmat/0107266].

phase diagram where superconductivity and AFM order coexist.

Muon spin relaxation experiments can provide unique information in several ways. The relative shift in muon precession frequency (Knight shift) probes the local spin susceptibility of electrons responsible for superconductivity. Linewidths reflect the magnetic field distribution, in principle enabling a determination of magnetic penetration depth in the superconducting state. In zero applied field the muon is a sensitive probe of internal fields generated by spontaneous magnetism.

#### $\text{CeIrIn}_5$

We performed a zero field experiment to search for spontaneous magnetism in a single crystal of  $\text{CeIrIn}_5$ . The experiment was carried out after quenching the superconducting solenoid of the dilution refrigerator and accurately zeroing the residual magnetic field to less than 20 mG. (Field zeroing was accomplished using the Mu signal in Si as a magnetometer because Mu has a gyromagnetic ratio 103 times larger than the muon.) The ZF muon spin relaxation (Fig. 111) was found to be well characterized by a static Gaussian Kubo-Toyabe function with a temperature-independent relaxation rate  $\sigma_{\text{KT}}=0.239(4) \mu\text{s}^{-1}$  across  $T_c$ . No evidence for spontaneous magnetism in superconducting  $\text{CeIrIn}_5$  was found.

#### $\text{CeIr}_{0.75}\text{Rh}_{0.25}\text{In}_5$

Substituting Ir with Rh in  $\text{CeIr}_x\text{Rh}_{1-x}\text{In}_5$  at first suppresses  $T_c$ , with a minimum at about  $x = 0.93$ , followed by a steady rise in  $T_c$  with the Rh fraction.  $\text{CeRhIr}_5$  at ambient pressure is known from neutron scattering experiments to be an antiferromagnet with  $T_N = 3.8$  K. This material has an incommensurate

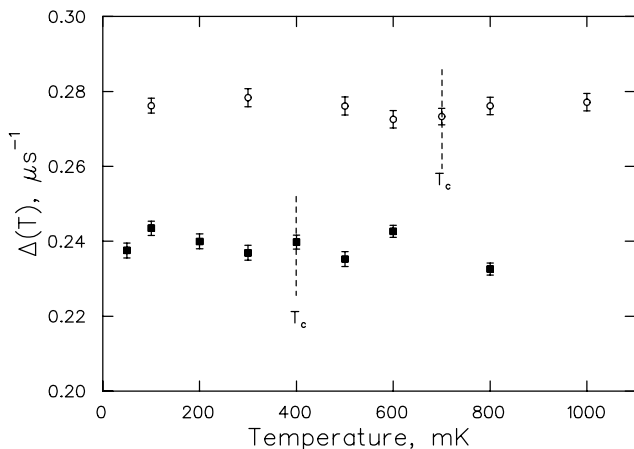


Fig. 111. Kubo-Toyabe relaxation rates  $\Delta(T)$  in  $\text{CeIr}_{0.75}\text{Rh}_{0.25}\text{In}_5$  (circles) and  $\text{CeIrIn}_5$  (squares) show no significant change across their respective superconducting transition temperatures  $T_c$ .

magnetic order in which n-n Ce moments are antiferromagnetically aligned within the  $a - b$  plane, but twist  $107^\circ$  per unit cell along the  $c$  axis. Muon spin relaxation experiments can probe the magnetism on a microscopic scale, and preliminary results indicate that the superconductivity and magnetic order coexist locally. This past summer we performed zero field measurements on the  $x = 0.75$  composition, over a range of temperatures from 0.1 to 1 K to search for the development of local magnetic moments near  $T_c$ . The spin relaxation rate was found to be temperature-independent at  $\sigma_{KT} = 0.276(2) \mu\text{s}^{-1}$  across  $T_c$ .

#### Status of Expt. 891

We plan to continue to survey a variety of the Ce-based HF materials, including n=2, m=2 materials, to study the relation between magnetism and superconductivity in this family of heavy fermion superconductors.

#### Experiment 894

##### Muonium kinetics and free radical formation in solutions of fullerenes

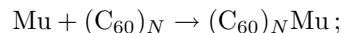
(B. Addison-Jones, UCC Kamloops)

The objective of this experiment is to obtain information on muonium substituted fullereryl radicals in aqueous solution. This project evolved from previous results (Expts. 749 and 654) on such radicals in organic solvents. Experiment 894 was initiated in December, 2000 and approved for further beam time in June, 2001.

Aqueous solutions of fullerenes have long been sought for their application in biological systems. For example, it has been reported that substituted fullerenes inhibit HIV-1 protease activity. Due to the inherent hydrophobicity of fullerenes, these solutions

were of low concentration or involved derivatizing the fullerene with a hydrophilic substituent. Recently, two new methods of producing aqueous fullerene solutions have been published, one involving the use of ultrasound and the other using redox reactions. Our group has tested both methods with the aim of producing solution concentrations high enough for detection of free radical signals and muonium decay rates. To date, concentrations of up to  $100 \mu\text{M}$  have been prepared. These were characterized using UV absorption and dynamic light scattering, the latter with the cooperation of the SFU Physics Department. Aqueous fullerenes are thought to be colloidal in nature, with a range of cluster sizes. Dynamic light scattering provides the hydrodynamic radius of these particles in solution. Kinetics results from time-differential  $\mu\text{SR}$  measurements of muonium decay rates, together with application of diffusion controlled reaction theory, then allows us to determine the number of  $\text{C}_{60}$  molecules per cluster.

The original proposal aimed to study the kinetics of muonium addition to  $\text{C}_{60}$  by two methods, from muonium decay and from radical signal amplitudes in low magnetic field. If thermalized, Mu adds to a colloidal  $\text{C}_{60}$  particle consisting of  $N$   $\text{C}_{60}$  molecules according to



the first-order decay rate of muonium is given by  $\lambda = k_{\text{Mu}}[(\text{C}_{60})_N]$  where  $k_{\text{Mu}}$  is the second-order rate constant for the reaction. Experimentally, the decay rate in pure solvent ( $\lambda_0$ ) must be taken into account, to give

$$\lambda_{\text{exp}} = \lambda_0 + k_{\text{Mu}}[(\text{C}_{60})_N].$$

Note that since  $N$  was originally unknown, only  $k'[\text{C}_{60}]$  could be determined, where  $k' = k_{\text{Mu}}/N$ . Muonium decay rates have been measured in 7–10 G with varying  $[\text{C}_{60}]$ , yielding a rate constant of the order of  $10^{10} \text{M}^{-1}\text{s}^{-1}$ . The high value of the rate constant places this reaction in the diffusion controlled, as opposed to activation controlled, regime.

If the conventional Smoluchowski and Stokes-Einstein equations for diffusion controlled reactions apply to this reaction, the experimental rate constant should depend on the diffusion constants ( $D$ ), radii ( $R$ ), the Avogadro number ( $N_{\text{Av}}$ ) and solvent viscosity ( $\eta$ ) according to:

$$k = 4000\pi N_{\text{Av}}(R_1 + R_2)(D_1 + D_2)$$

where

$$D = k_{\text{B}}T/6\pi R\eta.$$



In this case,  $R(C_{60N}) \gg R_{\text{Mu}}$  and  $D_{\text{Mu}} \gg D(C_{60N})$ , hence:

$$k = 4000\pi N_{\text{Av}} R(C_{60N}) D(\text{Mu}).$$

$R(C_{60N})$  was measured by dynamic light scattering for a  $3.67 \mu\text{M}$  colloidal sample, yielding a mean value of  $100 \pm 46 \text{ nm}$  with no significant temperature dependence. The large variation in  $R$  is expected as  $C_{60}$  clusters, like many colloids, exist over a range of  $N$  values. Applying the above equations together with kinetics results then gave a mean cluster number of  $N = 98 \pm 46$ . This is in good agreement with published theoretical predictions based on molecular dynamics simulations.

To date, observations of radical signals from these colloidal  $C_{60}$  samples have been inconclusive. This may be due to product instability or additional mechanisms dephasing the Mu signal in the radical. Agreement of kinetic data based on the product,  $(C_{60})_N\text{Mu}$ , with that based on muonium decay is desirable as it provides direct evidence that the rate determining step in the reaction is indeed  $\text{Mu} + (C_{60})_N$ . However, new results for  $^{12}\text{C}_{60}$  in an organic solvent, decalin, have been obtained. The use of an isotopically pure sample has eliminated extra splitting of the radical signals due to the presence of  $^{13}\text{C}_{60}$ . During reaction, loss of phase

coherence between the precessing muonium spin and the muon spin in the radical reduces the signal intensity. The resulting radical polarization is given by:

$$P(\nu_{ij}) = \lambda^2 / (\lambda^2 + \Delta_{ij}^2)$$

where  $\Delta_{ij}$  depends upon the difference in precession frequency between muonium and the radical product. Selected  $\mu\text{SR}$  spectra for two representative fields are shown in Fig. 112. Results based on this method give a decay rate  $\lambda = 2 \times 10^8 \text{ s}^{-1}$ , which is in accord with muonium decay results. However, the activation energy appears to be considerably higher than that obtained from muonium decay measurements. We continue to investigate whether it is indeed our mechanism or the application of conventional diffusion controlled reaction theory which needs modification in this case.

### Experiment 912

#### Formation, structure, and dynamics of muonium in GaAs studied by EF-ALC-RF- $\mu\text{SR}$

(S.R. Kreitzman, TRIUMF; V.G. Storchak, Kurchatov; K.H. Chow, Alberta)

The goal of Expt. 912 is to improve the understanding of muonium formation, structure, and dynamics in certain bulk semiconductors by developing several new techniques to study such phenomena. These new methods are based on combining three, well-proven, powerful techniques: electric field EF- $\mu\text{SR}$ , radio frequency RF- $\mu\text{SR}$ , and avoided-level crossing (often called  $\mu\text{LCR}$ ). Our plan was to initiate the experimental program by applying our new approaches to the technologically important semiconductor GaAs. On the one hand, these studies provide a “proof-of-principle” test of our new methods. At the same time, the results of these experiments dramatically enhance our understanding of the formation processes of light impurities in semiconductors. In this report, we briefly outline our preliminary progress in the development and application of these techniques.

The first of the two new techniques that we will describe combines EF with ALC. In semi-insulating GaAs at low temperatures, virtually no diamagnetic muonium is formed upon muon implantation. However, primarily from conventional transverse field measurements [Eshchenko *et al.*, Phys. Lett. **A264**, 226 (1999)], it is well established that by applying an electric field either along or in opposition to the incoming muon, one can increase the formation probability of diamagnetic muonium (with a concomitant decrease in the likelihood of forming to  $\text{Mu}_{BC}^0$ , the paramagnetic muonium state located near the centre of a Ga-As bond). However, no spectroscopic evidence exists regarding the site or the charge of the diamagnetic state,

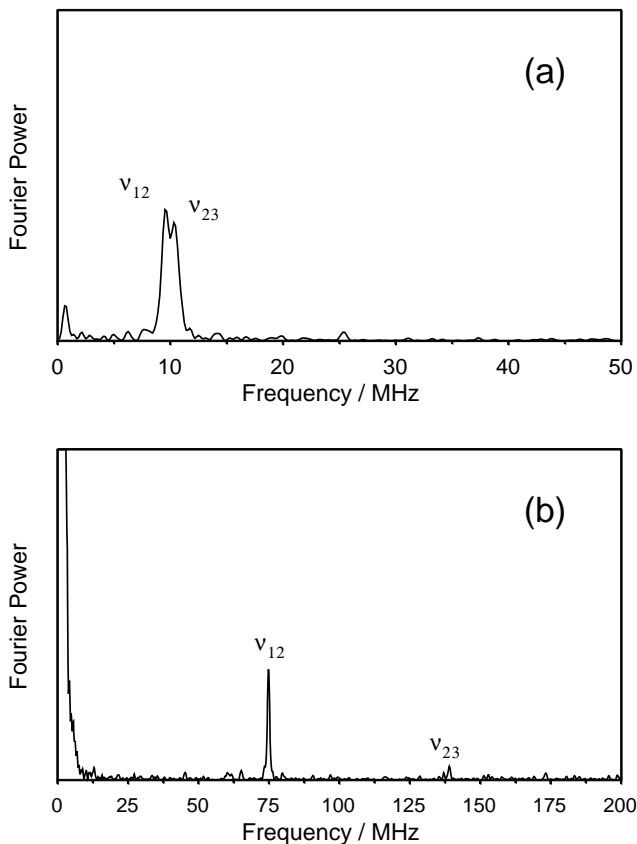


Fig. 112. Precession signals due to  $\nu_{12}$  and  $\nu_{23}$  in the radical  $^{12}\text{C}_{60}\text{Mu}$  at (a) 7 G; (b) 77 G.

although the most likely candidates are either isolated  $\text{Mu}^+$  or  $\text{Mu}^-$ . Our goal with the EF-ALC technique was to obtain direct spectroscopic evidence which will allow us to elucidate the nature of this centre. Our plan was to enhance the diamagnetic signal by applying an electric field, and then compare it with the experimentally identified ALC signatures of isolated  $\text{Mu}^+$  and  $\text{Mu}^-$  in heavily doped GaAs. As described in Expt. 791 in this Annual Report, for example, these two isolated states are easily distinguished since they give rise to ALC resonances that occur at very different magnetic fields. Our preliminary EF-ALC results are shown in Fig. 113. The existing data suggest the intriguing result that a resonance associated with  $\text{Mu}^+$  (due to the nearest neighbour  $^{71}\text{Ga}$  isotope) is seen in the direction of the electric field that we have labelled E+, while no such resonance is observed with the electric field in the opposite direction (E-). (The electric field is applied either parallel or anti-parallel to the incoming muon direction.) In other words, the data indicate that different charged states of muonium are formed depending on the direction of the electric field. In the upcoming beam period, our intention is to test if this conclusion is indeed correct by improving the signal-to-noise ratio of the signal, and to search for the signature resonances of  $\text{Mu}^-$  that exist at lower fields.

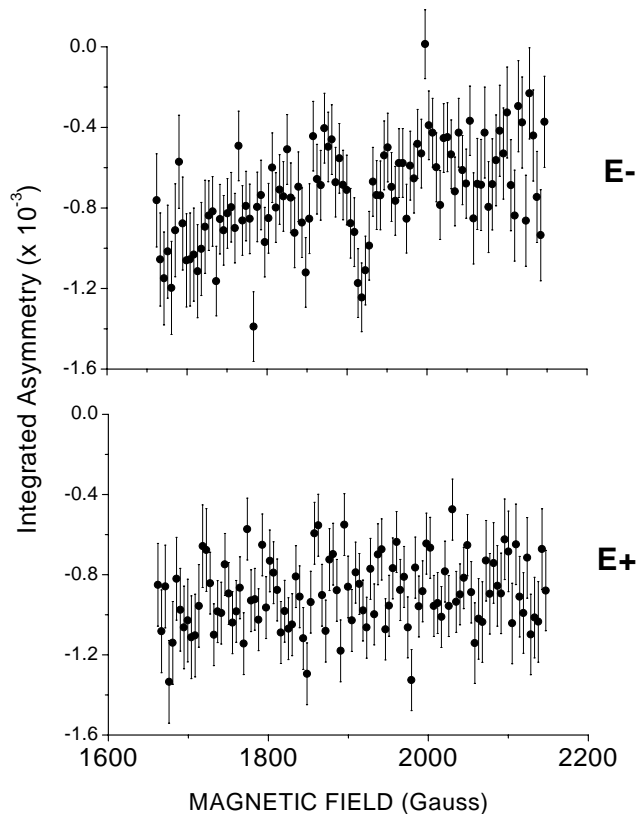


Fig. 113. EF-ALC spectra at 10 K in semi-insulating GaAs with  $\mathbf{B} \parallel \langle 100 \rangle$ .

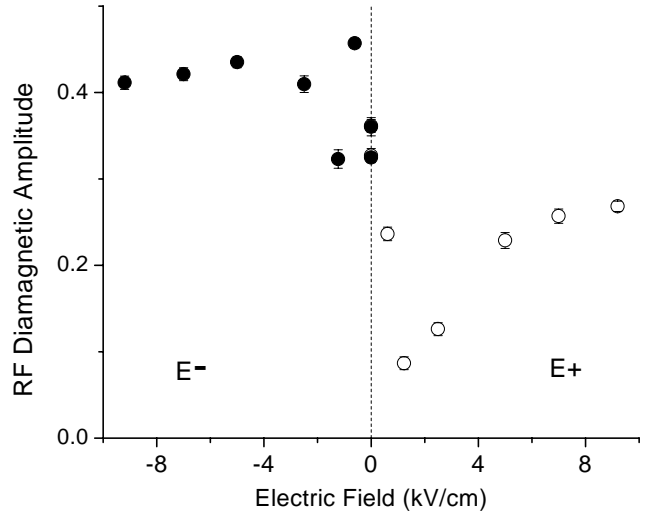


Fig. 114. EF-RF spectra at  $\approx 50$  K in semi-insulating GaAs with  $\mathbf{B} \parallel \langle 100 \rangle$ .

The second of the two new techniques is based on combining EF- $\mu$ SR with RF- $\mu$ SR. The electric field is used to modify the concentration of electrons around the muon and change initial muon/muonium fractions (as alluded to above), and RF- $\mu$ SR is used to directly detect and study the dynamics of the final muonium/muon states that are formed. An example of the EF-RF data is shown in Fig. 114, which plots the electric field dependence of the diamagnetic amplitude in the E+ and E- directions. It is clear that we can detect an enhancement in the rf diamagnetic signal when the electric field is applied. At the same time, there appears to be a dramatic difference between the results in the electric field directions, especially at small values of E. This behaviour is unexpected and was not observed in the conventional TF- $\mu$ SR studies. Further studies are clearly needed to understand the underlying mechanism responsible for formation of the final diamagnetic state(s).

In conclusion, our results, although preliminary, strongly suggest that the two new techniques will play an important role in future studies of muonium in semiconductors. Already, we have obtained fascinating science results using both new methods which we intend to pursue during the next beam period.

#### Experiment 915 Muonium in semiconductor alloys (*R.L. Lichti, Texas Tech*)

Semiconductor alloys are being developed for specific applications, especially for heterojunction based devices, or for situations where a specific band gap is desired. Hydrogen is an important impurity in many semiconductors because of its chemical activity, especially its capacity to bond with other impurities to modify their electrical or optical activity. Experiment

915 continues our efforts to obtain detailed information on the behaviour of isolated H impurities by studying its light pseudo-isotope, muonium, which is far more accessible, experimentally. We chose to concentrate on the  $\text{Si}_{1-x}\text{Ge}_x$  alloys during the initial week of beam time for this experiment, taken in mid-November. Our main goal was to determine how hyperfine constants for the two neutral muonium states,  $\text{Mu}_{BC}^0$  and  $\text{Mu}_T^0$ , vary across the alloy range. For instance, is there a single alloy-averaged hyperfine value or does the local mix of nearest neighbours yield distinct spectra? Based on motional properties this could be the case for  $\text{Mu}_{BC}^0$  but would not be expected for the mobile T-site species.

We examined three samples with  $x = 0.2, 0.5,$  and  $0.77$  to broadly span the full range. All spectra were with  $\mathbf{B} \parallel [100]$ ; the four BC orientations are equivalent. Figure 115 shows hyperfine spectra at 3 T and roughly 70 K for the three samples. The displayed region includes the diamagnetic frequency,  $\text{Mu}_{BC}^0$  spectra, and the lower field  $\text{Mu}_T^0$  line. There are small shifts for the BC peaks and all lines are broader for the two higher Ge content samples compared with  $x = 0.20$ . The very broad  $\text{Mu}_T^0$  feature for the  $x = 0.77$  sample, as well as the much sharper line for  $x = 0.2$ , are reproduced near 1400 MHz, confirming that these lines are from the isotropic  $\text{Mu}_T^0$  centre with a hyperfine value near 2000 MHz. No clear  $\text{Mu}_T^0$  spectra were observed for the 50/50 alloy.

In addition to the differences seen in the spectra at any particular temperature, the temperature dependences were significantly different for each sample, and apparently do not vary linearly between those of the elemental parent materials. We will need to perform a more careful time-domain analysis before the temperature variations seen in the Fourier spectra can be made quantitative. For the  $x = 0.2$  sample we see low temperature growth of both neutrals at the expense of the diamagnetic signal up to above 50 K. The  $\text{Mu}_T^0$  signal amplitude peaks around 70 K followed by transfer from the T site into the BC site at least up to the BC ionization region between 160 and 200 K. For Si, the T to BC transfer occurs well above the BC ionization region which is around 140 K, while for Ge bi-directional site transfers occur below 100 K, while the onset of  $\text{Mu}^0$  ionization is near 160 K; thus in many respects the  $x = 0.2$  sample shows dynamics closer to those for the minority Ge component, while the hyperfine spectra are much more like those in Si.

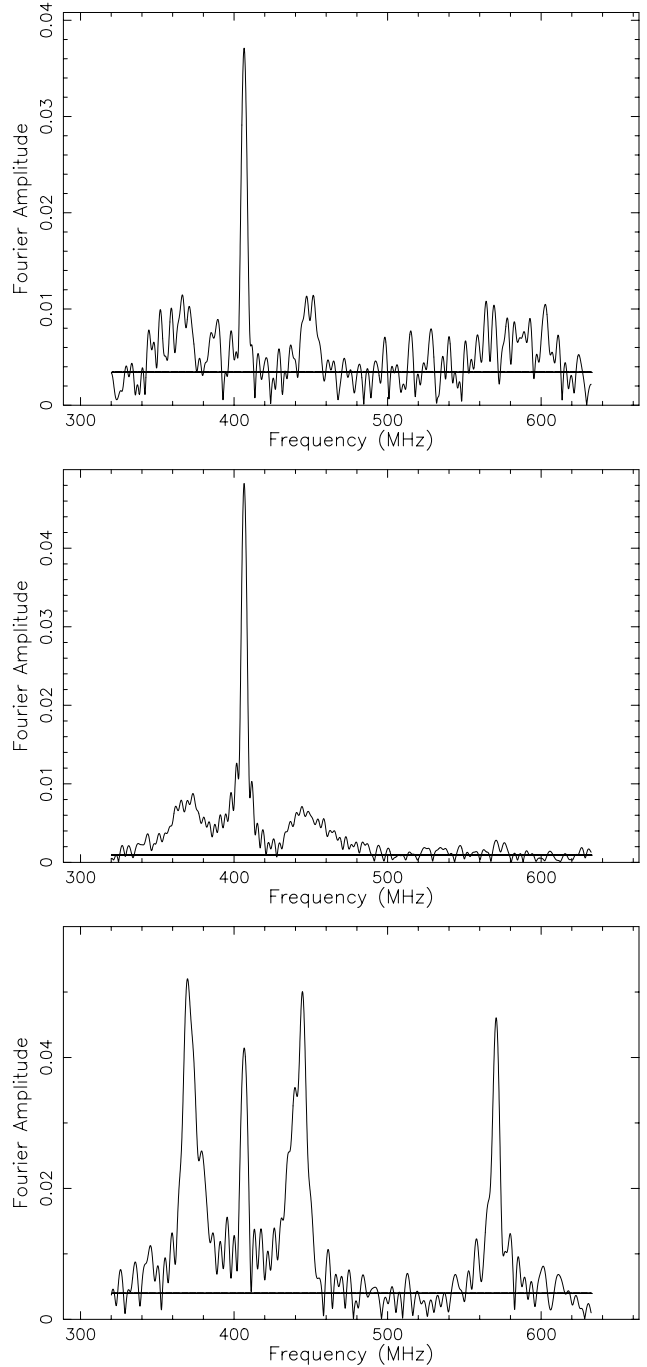


Fig. 115. Hyperfine spectra for three  $\text{Si}_{1-x}\text{Ge}_x$  alloy samples: from bottom to top,  $x = 0.20, x = 0.50,$  and  $x = 0.77$ . Crystals were provided by I. Yonenaga, Tohoku University.

### Experiment 916

**QLCR of diamagnetic muonium states in GaP**  
(*R.L. Lichti, Texas Tech*)

Zero-field depolarization functions imply that there are several different diamagnetic muonium states present in doped GaP. TRIUMF Expt. 916 has as its main goal the identification of these different states us-

ing quadrupolar level-crossing resonances (QLCR) as our primary technique. The Ga isotopes produce two sets of nearly identical resonances at a field ratio of 1.59 giving a clear signature of Ga near neighbours to the muon location. Since P has no quadrupolar nuclei, any line not having such a partner must be related to an impurity atom. We started our investigation by examining an  $n$ -type sample near room temperature where the expected state is an isolated  $\text{Mu}^-$ . This state should be in the  $T_{\text{Ga}}$  interstitial location, based on theory and earlier results from GaAs [Chow *et al.*, Phys. Rev. **B51**, 14762 (1995)]. The spectra for a  $p$ -type GaP:Zn sample were also obtained at 670 K where the state should be a  $\text{Mu-Zn}$  pair based on zero-field results and analogy to results for GaAs:Zn.

Figure 116 displays part of the room temperature spectra for the  $n$ -type sample. Due to time constraints, we concentrated on a high statistics run to verify lines seen between 20 and 36 mT in an initial scan. Both data sets are shown in the figure; the line just below 30 mT is confirmed by the high statistics results but the two smaller lines within this region remain suspect. Additional data over a broader field region will be required to get structural data for the expected  $\text{Mu}_T^-$  state. Based on the single strong line seen thus far the field gradient is somewhat larger than for the same state in GaAs. The line at low field is probably from a  $\text{Mu}^+$  state locally tunneling around a central P atom, since we expect a mix of  $\text{Mu}^+$  and  $\text{Mu}^-$  in this  $10^{16}\text{cm}^{-3}$   $n$ -type sample. Any additional work on  $\text{Mu}^-$  will use more heavily doped material.

Figure 117 is the high temperature result for the  $\text{Mu-Zn}$  complex in heavily Zn-doped  $p$ -type GaP. These spectra are very similar to what we observed for this pair state in GaAs [Chow *et al.*, Phys. Rev. Lett. **87**, 216403 (2001)]. We speculated that this low field

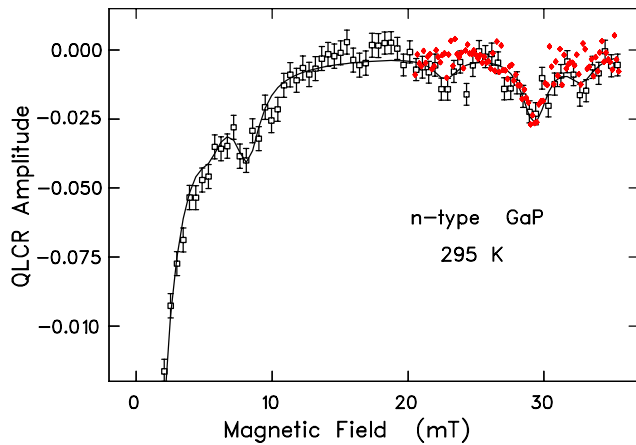


Fig. 116. Partial QLCR spectra for  $n$ -type GaP at room temperature. The filled points (red) are for a high statistics run, verifying a strong resonance at 29.5 mT: this should be part of a four line  $\text{Mu}_T^-$  spectra similar to GaAs results.

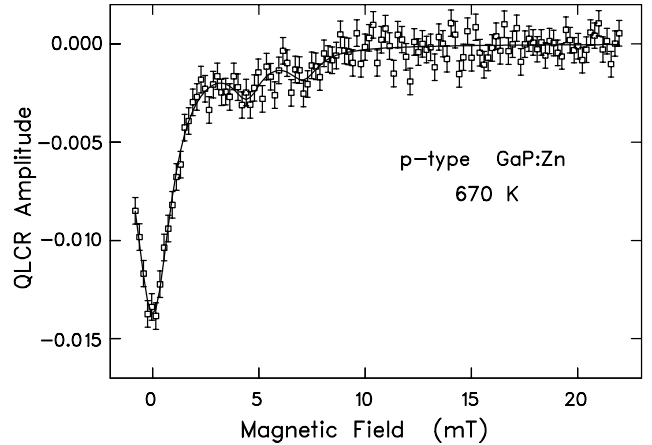


Fig. 117. The QLCR spectra for the  $\text{Mu-Zn}$  complex in  $p$ -type GaP:Zn shown here are nearly identical to the spectra for this complex at 530 K in GaAs, and imply a dynamic excited-state structural configuration.

feature is produced by  $\text{Mu}^+$  local motion around the P (or As) near neighbour to the Zn impurity. This would be an excited state structure for the  $\text{Mu-Zn}$  pair rather than the  $\text{Zn-Mu-P}$  bond-centred ground-state configuration as expected for an acceptor-H complex. We note the similarity between the 670 K QLCR and the low field features in Fig. 116. If our state and structural assignments are correct, both of these cases (excited state structures of an isolated  $\text{Mu}^+$  and of the  $\text{Mu-Zn}$  complex) involve local  $\text{Mu}^+$  motion among the BC locations around a central P atom; thus they ought to yield very similar QLCR spectra, as observed.

### Experiment 917

#### Correlation between magnetism and transport properties of thermoelectric oxides

(*J. Sugiyama, Toyota Central R&D Labs; J.H. Brewer, UBC/TRIUMF*)

Two cobalt oxides,  $\text{Ca}_3\text{Co}_4\text{O}_9$  and  $\text{Na}_x\text{CoO}_2$ , were recently reported to exhibit metallic conductivities and extraordinary, large thermoelectric power coefficients (above  $+100 \mu\text{V/K}$  at 300 K), for reasons currently unknown. In order to investigate the role of magnetism on transport properties of such “good” thermoelectric oxides, muon spin rotation and relaxation ( $\mu\text{SR}$ ) spectroscopy has been used for polycrystalline  $\text{Ca}_3\text{Co}_4\text{O}_9$  and  $\text{Na}_{0.7}\text{CoO}_2$  samples in the temperature range between 290 and 2.5 K. It was found that  $\text{Ca}_3\text{Co}_4\text{O}_9$  exhibits a magnetic transition below  $T_c^{\text{onset}} \approx 100$  K with a transition width of  $\Delta T_c = 70$  K. At temperatures below 100 K, two types of relaxation were observed using a weak transverse field  $\mu\text{SR}$  technique with  $H = 104$  Oe; one exhibits a fast relaxation rate on the order of  $10 \mu\text{s}^{-1}$  and the other a slow one of about  $0.1 \mu\text{s}^{-1}$  (see Fig. 118). Furthermore, zero field  $\mu\text{SR}$  measurements suggested the existence of an

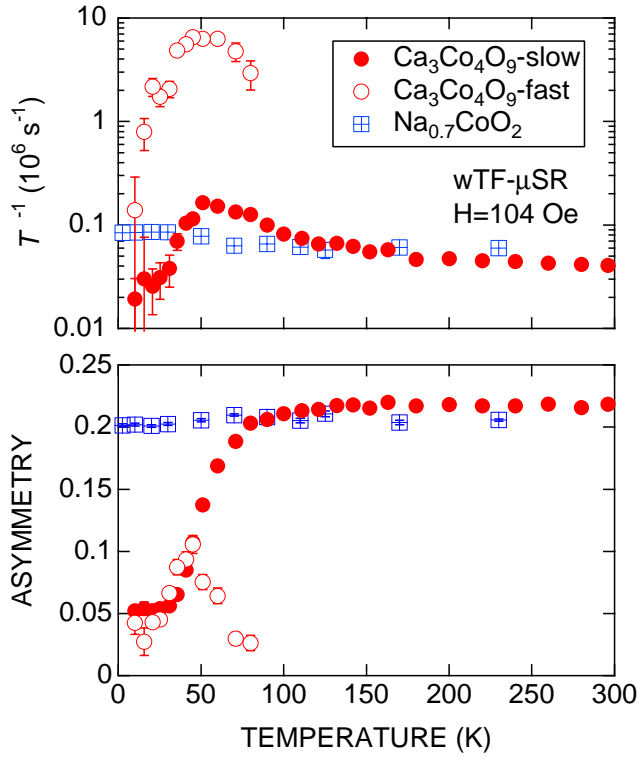


Fig. 118. Temperature dependence of relaxation rate and asymmetry of  $\text{Ca}_3\text{Co}_4\text{O}_9$  and  $\text{Na}_{0.7}\text{CoO}_2$ .

incommensurate spin density wave state below  $T_c^{\text{onset}}$  (i.e.  $T_c^{\text{onset}} = T_{SDW}$ ).

This SDW transition was not detected by a dc susceptibility measurement, though a ferromagnetic transition was observed at 19 K in the  $\chi$  vs.  $T$  curve. On the other hand, the resistivity vs.  $T$  curve exhibited a broad minimum around 80 K; in other words,  $\text{Ca}_3\text{Co}_4\text{O}_9$  showed metallic behaviour above 80 K while semiconducting below 80 K. Therefore, the SDW transition was found to be associated with the change in the transport properties of  $\text{Ca}_3\text{Co}_4\text{O}_9$ .

The  $\mu$ SR studies on  $\text{Na}_{0.7}\text{CoO}_2$  indicated no magnetic transitions around 100 K. Considering the difference of crystal structures between  $\text{Ca}_3\text{Co}_4\text{O}_9$  and  $\text{Na}_{0.7}\text{CoO}_2$ , the Co ions in the rock salt-type layers of  $\text{Ca}_3\text{Co}_4\text{O}_9$  were likely to play a dominant role to induce the SDW transition around 100 K.

## LIFE SCIENCES

### Introduction

This year represented the penultimate effort in establishing PET as a tool for clinical research in the local hospitals that now possess hybrid PET/SPECT cameras (Lion's Gate and St. Paul's) or have a request into government for a full body PET system (VGH) by establishing a mechanism whereby the FDG will be supplied by VGH in the coming year(s) through co-operation between the local hospitals, TRIUMF and MDS Nordion. In keeping with the TRIUMF effort to provide the resources for the affiliated universities to establish their own PET programs, we have supplied the University of Alberta with  $^{18}\text{F}$ -fluoride with which they prepare their own FDG. This approach will continue until the installation of their cyclotron, scheduled for the summer of 2002. Thus TRIUMF has served the community well in making PET available at a relatively early stage in the Canadian context.

Strong collaborations with several departments at UBC continued to rely upon the unique radioisotope production capabilities of TRIUMF. The anticipated arrival of the new high-resolution research tomograph will herald a new era in PET imaging with resolution and sensitivity unsurpassed anywhere in the world.

### Experiment LS0

#### PET facilities

(*K.R. Buckley, TRIUMF*)

The PET facilities comprise the TR13 13 MeV  $\text{H}^-$  cyclotron, the ECAT 953B/31 tomograph, and ancillary equipment such as counting and data acquisition systems.

#### Personnel

Dr. Dirk Becker, a postdoctoral fellow in targetry, left us in the spring to take up a position closer to home in Europe. Carolyn English returned from maternity leave at the end of the summer giving us two full time nuclear medicine technologists for scanner operations.

Dr. John Wilson of the Cross Cancer Centre came to TRIUMF in mid-November to learn cyclotron operation and carry out the irradiations for the production of  $^{18}\text{F}$  for shipment to Edmonton. Dr. Wilson will stay until their cyclotron facility is ready in Edmonton in the spring of 2002. We are currently sending  $^{18}\text{F}$  to the Cross Cancer Centre in Edmonton three times per week.

#### TR13 cyclotron

Usage of the TR13 cyclotron dropped this year in delivered beam due to a decreased demand for irradiation of lithium targets for the production of  $^7\text{Be}$  (LS8). The total number of runs increased to 848 vs. 808 last

year. The production of  $^{18}\text{F}$  for shipment to Edmonton began in earnest this year with 91,240  $\mu\text{A min}$  of beam being delivered to target.

Downtime this year was much less significant than last year and was caused by a variety of faults. The only repair of major significance was the need to replace the rf amplifier controller with a TRIUMF built unit. This controller looks after the startup and shutdown of the rf tube and its interlocks. The unit that came with the amplifier is obsolete and no parts are available for repairs. Other amplifiers on site and at other installations of the TR series of cyclotrons have small PLC units in place of this controller. Our controller has failed and at present the amplifier is manually started and shut down while this new controller is being assembled.

Ten extraction foil changes were required through the year and all targets were rebuilt at least once. The new niobium target for the production of  $^{18}\text{F}$  continues to perform well. Some difficulties attributed to this target in mid-summer were eventually traced to contaminated  $^{18}\text{O}$ -water. The target exhibited very high beam-on pressure and residual pressure in the target at beam-off. The target was disassembled and cleaned twice with no change in performance until new  $^{18}\text{O}$ -water was tried. Fortunately only 4-5 ml of water were left in the suspect vial. Four ion source filament changes have been performed this year.

A target to allow scattered protons (from a beam of a few nanoamperes) to be extracted to atmosphere was constructed and operated in the spring and summer for a few sessions of several hours each. This target was in support of the HERMES collaboration to allow testing of a wire chamber detector. The target consisted of a carbon foil and beam stop mounted in vacuum and a thin kapton foil over a side port at  $45^\circ$  for the scattered protons. Interlocks of beam current and radiation fields were instituted to allow operation of the cyclotron with one shield open. The open shield space was used to install the detector to be tested. Tests were conducted in the evening to prevent disruption of the normal production runs.

Presently there are six target locations occupied of the available eight. These consist of:

- one  $^{18}\text{O}$ - $\text{O}_2$  gas target;
- one  $^{18}\text{O}$ -water target;
- one  $^{16}\text{O}$ -water target;
- one  $\text{N}_2/\text{H}_2$  gas target;
- one experimental gas target;
- one lithium metal target.

The lithium target (LS8) has a reserved location and is installed and removed for each production. This

target runs routinely for 15 hours at 50  $\mu\text{A}$ . The target was only run once this year. At least one run of approximately 40 hours duration is needed in the near future for the production of a high activity  $^7\text{Be}$  target. It is anticipated that this will be the last run required.

### ECAT tomograph

Block detector failures continue to be the dominant mode of failure for the camera. We are routinely repairing blocks in-house and have replaced 7 blocks this year; all were component failures in the voltage dividers. We have still not assembled the necessary components to properly calibrate the blocks prior to returning them to the scanner. At present only a simple visual balance of PMT outputs is performed on the bench and the block set-up routine in the scanner performs the fine tuning.

Programmable logic chips in the position/energy processors continue to fail occasionally and several chips in 3 different buckets have been replaced this year. TRIUMF electronics is able to program new chips for us.

An intermittent problem with 2D reconstructions in the front end encountered late in 2000 was found to be due to the array processor, which was replaced in February.

An instability problem with the camera calibration has arisen and this is presently attributed to one high voltage power supply. A spare has been obtained to allow off-line servicing of this supply. The current required by the ECAT gantry exceeds the capability of any of the high voltage supplies available at TRIUMF.

### Statistics

Table X. TR13 run data.

Total runs conducted	848	
Total runs lost	8	
Integrated charge delivered	631,357	$\mu\text{A}\cdot\text{min}$
Delivered to – LS2	160	
– LS3	262,573	
– LS4	55,327	
– LS8	144,199	
– LS13	33,611	
– LS24	33,172	
– LS32	91,240	
– LS33	477	
– LS39	4,580	
– LS47	300	
– LS49	3,282	
– LS52	2,436	

Table XI. ECAT scan data.

Total scans conducted	379
Total scans lost	52
Lost to – patient	10
– scanner	13
– chemistry	6
– cyclotron	8
– staffing	15

### Experiment LS2

#### Synthesis of radiohalogenated carbohydrates for use as imaging agents in PET and SPECT (*M.J. Adam, TRIUMF*)

This project was divided into two parts. Part 1 was on the synthesis and evaluation of 2,2-dihalo-sugars for use as imaging agents. Part 2 was on the synthesis and evaluation of glycosidase inhibitors as imaging agents for lysosomal diseases.

#### Part 1. 2,2-dihalo-sugars

The use of 2-deoxy-2- $^{18}\text{F}$ fluoro-D-glucose (FDG) to study glucose metabolism has seen extensive clinical applications, especially in cardiology and oncology. Because of the growing importance of FDG/PET for clinical use, we decided to study close analogues of FDG, 2,2-dihalo sugars, to see how they compared. To this end we synthesized 2-deoxy-2,2- $^{18}\text{F}$ difluoro-glucose and 2-deoxy-2- $^{123}\text{I}$ iodo-2-fluoro-mannose (FIM). The latter compound was synthesized as a possible SPECT version of FDG. Previous studies indicated that the fluoro substituent stabilized the iodine in position 2, as compared with 2-iodo-glucose. Unfortunately, the stability of FIM *in vitro* does not extend *in vivo*. Following injection, the product is rapidly de-iodinated. Therefore, based on this finding, we have decided to put this part of the project on hold indefinitely.

#### Part 2. Glycosidase inhibitors

We have previously synthesized 2-deoxy-2- $^{18}\text{F}$ -fluoro- $\beta$ -mannosyl  $^{18}\text{F}$ -fluoride and shown that it behaves as a mechanism-based inhibitor of *Agrobacterium* sp.  $\beta$ -glucosidase. *In vivo* experiments indicate that this compound undergoes partial hydrolysis to produce 2-deoxy-2-fluoro-mannose, which can become phosphorylated and trapped within the cell. We then turned our attention to  $^{18}\text{F}$ -labelling at the 6 position so that the label cannot be lost during such glycoside hydrolysis, and cannot be phosphorylated. The mechanism-based glycosidase inhibitor 2,6-dideoxy-2-fluoro-6- $^{18}\text{F}$ -fluoro- $\beta$ -D-glucopyranosyl fluoride (2,6FGF) was synthesized in 69% overall chemical yield, and in 9% radiochemical yield (decay corrected), as a potential imaging probe for glycosidase. Unfortunately, binding studies with

glucocerebrosidase were unsuccessful after many attempts. Due to a possible fatal flaw in the experimental design, coupled with the lack of funding, we have decided to bring this project to an end. The PI will focus attention on radio-metallated carbohydrates as described in LS53.

This project has produced seven publications and two Ph.D. theses (J. McCarter and A. Wong) over its lifetime.

### **Experiment LS3**

#### **Synthesis of radiopharmaceuticals for positron emission tomography**

*(M.J. Adam, TRIUMF)*

Daily routine production of up to 10 radiopharmaceuticals is currently performed with 3–4 radiopharmaceuticals synthesized on any given day. FDG is sent once per week to each of Vancouver, Lions Gate and St. Paul's Hospitals for research in cardiology and oncology. Out of these 10 radiopharmaceuticals, five (FDOPA, Raclopride, TBZ-OH, SCH23390 and MP) are used most heavily. There has been a decline in the number of Raclopride preparations from last year, but Raclopride remains the most heavily used radiopharmaceutical. Most of the Raclopride preparations this year are for the "Scatchard Analysis" experiment that Doris Doudet is performing on monkeys. These experiments require 3–4 Raclopride preparations each day where one is at a high specific activity (SA) of 5–10 Ci/ $\mu$ mol, and the others have carrier added to give a range of SAs of 2–35 Ci/mmol at time of injection. All preparations for these experiments are assayed by HPLC prior to injection to confirm the specific activity. There was a total of 523 production runs in 2001 for CIHR/PET and external users, with 369 radiopharmaceutical syntheses carried out just for the TRIUMF/UBC PET Program.

The demand for FDG from our group remains low. However, most of our FDG production is being used by Lions Gate, St. Paul's and Vancouver Hospitals for studies in oncology and cardiology (details in LS13, 24, 40, 48 and 49 proposals). We currently send FDG to these hospitals one day per week in amounts sufficient for imaging approximately 3–4 patients. Vancouver Hospital is setting up an FDG synthesis system and the plan is to send only  $^{18}\text{F}$ -fluoride to Vancouver Hospital in future and they will make the FDG for themselves and for all other local hospitals.

We have also started shipping  $^{18}\text{F}$ -fluoride to Edmonton on a regular basis for clinical cancer imaging (see LS32 proposal). We began shipping approximately 1 Ci once per week and are now shipping three days per week. The Cross Cancer Centre in Edmonton has sent a chemist/trainee (Dr. John Wilson) to TRIUMF for a few months to carry out these runs and to learn

cyclotron operations and PET chemistry. Nordion is handling the airline transport and Edmonton is paying all the transportation costs and the cost of the  $^{18}\text{O}$ -water used in the target. The Cross Cancer Centre is able to carry out 5–6 patient scans with each shipment of radiofluorine from TRIUMF.

The synthesis of  $^{11}\text{C}$ -PMP was brought into the routine category this year. PMP is an acetylcholinesterase inhibitor that will be used by Dr. Chong Lee to study dementia in Parkinson's disease (PD) and diffuse Lewy body disease. Previous studies in post-mortem brains have shown that choline acetyltransferase activity, but not muscarinic cholinergic receptors, was markedly reduced in PD, diffuse Lewy body disease and Alzheimer's disease, and that neocortical cholinergic deficits correlate with severity of dementia in PD, diffuse Lewy body disease and Alzheimer's disease. As reduced cholinergic activity in the neocortex correlates with marked neuronal loss in the nucleus basalis of Meynert, these observations suggest that loss of cholinergic neurons in the basal forebrain may play a significant role in the pathogenesis of dementia in PD and diffuse Lewy body disease as well as in Alzheimer's disease.

Recently, tracers for cholinergic neurons have become available for PET studies in human subjects. By using PET to explore cholinergic factors that contribute to the development of dementia in both PD and diffuse Lewy body disease, we will cultivate a better understanding of the pathogenetic mechanisms underlying dementia in PD and diffuse Lewy body disease. This should ultimately lead to better strategies for the pharmacological management of PD and diffuse Lewy body disease. This year we have carried out 18 preparations averaging over 30 mCi per run. A grant application to fund further research with this agent has been submitted by Dr. Lee and an abstract has been submitted to the American Academy of Neurology meeting.

One of the new projects started this year is the synthesis of  $^{11}\text{C}$ -Carfentanil for Dr. de la Fuente's research on Parkinson's disease. Dr. de la Fuente demonstrated, for the first time, that there was a measurable increase in the amount of dopamine released into the synapse when a placebo was administered, thus showing a chemical basis for the placebo effect. He now wants to extend this research to look at other receptor systems that might be involved, such as the opioid system. As with most new radiopharmaceutical projects, the synthesis of the precursor is the most labour intensive part. The synthesis of the precursor will take approximately six steps starting from a commercially available intermediate. Fortunately, we have had significant help and advice from Drs. Danals (Johns Hopkins U.) and Jewett (U. Michigan) on the synthesis of the



precursor and labelled product.

The synthesis of  $^{18}\text{F}$ -labelled oligonucleotides has also been started this year to complement the Anti-sense research that has been ongoing in Dr. Stoessl's lab. To start, we are repeating the procedure of the INSERM French group and are attempting to attach a fluorinated aromatic group to the phosphorothioate end of the above oligo. So far we have demonstrated that we can attach the non-radioactive label to the oligo and purify it on HPLC. Attempts to synthesize the  $^{18}\text{F}$ -labelled version have proven to be somewhat problematic. Unfortunately, it requires a multistep synthesis where the  $^{18}\text{F}$  is introduced in the first step, making the procedure very difficult to carry out. We are attempting to find alternative, simpler methods for the  $^{18}\text{F}$ -labelling of these oligos.

We continue to use TBAF in most of the  $^{11}\text{C}$  methyl iodide reactions to enhance and stabilize the yields. We are fortunate to still obtain the nitro precursor of Setoperone as a gift from Janssen Pharmaceuticals. We are also grateful to ASTRAZENECA AB for the gift of Raclopride Tartrate, used as carrier for the Scatchard experiments, and dihydroxy-Raclopride as the precursor for labelling. This year we have implemented the "loop" method for  $^{11}\text{C}$ -methylations. In this method the gas phase methyl iodide is passed through the HPLC loop which contains the precursor such as dihydroxy-Raclopride. However, in order to use this method, we must first convert the dihydroxy-raclopride precursor to the free base since it is originally in the HBr salt form. All other precursors are synthesized in-house, which requires a major time commitment from Dr. Lu.

The new hot cell has been installed in the PET chemistry lab and is being used for all of the  $^{11}\text{C}$ -chemistry. All of the older FDG and FDOPA chemistry systems were installed in the old hot cell and they are now slowly being rebuilt. These systems are about 15 years old and also need to be redesigned.

#### **Experiment LS4**

##### **TR13 targets for PET radioisotope production** (*T. Ruth, TRIUMF*)

The highlights for this past year were to characterize the  $^{18}\text{F}$ -fluoride gas target and successfully operate the target at 50  $\mu\text{A}$ . More recently, in collaboration with researchers from the University of Wisconsin, we have developed a flow-through target for the production of  $^{11}\text{CH}_4$ . This target enabled us to produce over 1.5 Ci of  $^{11}\text{CH}_4$ , about double our production rate using a static target. Preliminary results in measuring the specific activity (SA) indicate that there is more carrier present than in the static runs. The SA will have to be improved if this new approach is to become routine.

#### **Experiment LS8**

##### **Radiotracers for the physical and biosciences** (*T. Ruth, TRIUMF*)

Researchers in the Botany Department at UBC continue to undertake a wide range of experiments, bringing together physiological and biochemical studies using  $^{13}\text{N}$  and molecular studies at the gene level, to further our understanding of nitrogen absorption and transport within plants.

##### **Rice research: (Australian National University, Canberra)**

In continuance of our basic work on  $\text{NH}_4^+$  absorption by rice plants, we have cloned one gene (AMT1.1) that encodes a high-affinity  $\text{NH}_4^+$  transporter and are currently examining its expression. It appears not to respond to the N status of the plant, rather it may respond to plant carbohydrate status. The Australian National University has already developed new strains of rice over-expressing this gene and has requested our assistance to measure  $^{13}\text{NH}_4^+$  uptake by these over-expressers. We have successfully demonstrated that one line of the rice variety, JARRAH (line 75-4), absorbs  $\sim 40\%$  more  $^{13}\text{NH}_4^+$  than the parental line which expresses the normal level of the gene. This 40% increase is sustained in plants grown at low N or high N, and is therefore a promising transgenic line. We will next determine patterns of  $^{13}\text{NH}_4^+$  efflux in this line. Clearly, if it is effluxing  $^{13}\text{NH}_4^+$  at higher levels than parental lines, we have made little progress.

##### **Nitrogen uptake in trees: a collaboration with CELLFOR**

This project is funded by NSERC and BCRI for 3 years. The goal is to over-express the high-affinity  $\text{NO}_3^-$  transporter gene, (AtNrt2.1), that we cloned from *Arabidopsis thaliana* [Zhuo *et al.* (1999)], in hybrid spruce and in poplar seedlings. Since spruce is notoriously inefficient at absorbing  $\text{NO}_3^-$  [Kronzucker *et al.* (1997)], our goal is to increase the seedling vigour of these plants for reforestation programs. We used tobacco as a model system to evaluate the methodology, and have successfully produced transgenic tobacco plants and obtained a limited number of lines that over-express the high-affinity transporter gene. Unfortunately, none of these shows increased  $^{13}\text{NO}_3^-$  uptake. We have also generated poplar plants over-expressing this gene and will soon have results regarding rates of  $^{13}\text{NO}_3^-$  uptake in these transgenic plants. Based on some work on an algal model plant conducted in Spain, it may be that two genes must be expressed in order to achieve  $\text{NO}_3^-$  uptake. Mamoru Okamoto (Ph.D. candidate) has recently cloned the second gene and we are now generating the gene constructs necessary to over-express

both genes in our tree species. Assays of  $\text{NO}_3^-$  uptake will be conducted in standard fashion using  $^{13}\text{NO}_3^-$ .

A preliminary report on this work was presented by Dr. Simon at Bonn, September, 2000.

**$^{13}\text{NO}_3^-$  influx in the fungus *Aspergillus nidulans*; a structure function study of gene sequence and  $\text{NO}_3^-$  uptake: a collaboration with St. Andrews, Scotland**

Together with our Scottish collaborators, we have cloned and sequenced the two  $\text{NO}_3^-$  transporters of this fungus. They have similar (but not identical) gene sequences, but have very different affinities for  $\text{NO}_3^-$  and different maximum velocities. Having the gene sequences and the physiological characterization, it will be possible to generate chimeric proteins and switch the genes' function from high to low affinity, etc. We will test the resultant strains using  $^{13}\text{NO}_3^-$ . This will make it possible to place  $\text{NO}_3^-$  transport kinetics on a sound structural basis and to manipulate transport within existing genes.

**$^{13}\text{NH}_4^+$  uptake by roots of *Arabidopsis***

We have isolated insertional mutants in which the gene encoding the high-affinity  $\text{NH}_4^+$  transporter (AMT1.1) in *A. thaliana* is disrupted. The point of this methodology is to critically test the hypothesis that the gene in question is actually crucial for  $\text{NH}_4^+$  transport. Since this gene was cloned in 1994, four related high-affinity genes have been identified from this species. To what extent do these other genes participate in  $\text{NH}_4^+$  transport? By rendering the AMT1.1 inactive it is possible to evaluate the potential role of the other genes. Dr. Brent Kaiser has continued this work and has fully characterized the molecular biology aspects of this mutant. In our last report Dr. Kaiser had begun to characterize  $\text{NH}_4^+$  transport in these mutants. He has demonstrated that despite complete disruption of this gene, the plant shows only a 30% reduction of  $\text{NH}_4^+$  uptake. Using molecular methods, Dr. Kaiser has shown that the loss of the AMT1.1 function is compensated by over-expression of other members of this family of genes. We have isolated another gene-disrupted strain and we will soon begin to measure  $\text{NH}_4^+$  influx in this strain using  $^{13}\text{NH}_4^+$ . Our ultimate goal is to be able to assign functions to all of these genes.

**Nuclear orientation experiments**

Researchers in the Physics Department need a long-lived isotope of silver for the nuclear orientation experiments. In April, the PET group provided a sample of  $^{110\text{m}}\text{Ag}$  produced by proton irradiation of a Pd foil. This procedure also produces other silver isotopes, in particular  $^{105}\text{Ag}$ . Measurements in our laboratory at UBC in May indicated that the activity of  $^{110\text{m}}\text{Ag}$  was 280  $\mu\text{Ci}$ , while that of  $^{105}\text{Ag}$  was 3.5 mCi. However, the

half-lives of the two isotopes are 255 d and 40 d, respectively. Therefore, by waiting a few months, the  $^{105}\text{Ag}$  activity would decay by an amount sufficient that a low temperature nuclear orientation (LTNO) experiment on  $^{110\text{m}}\text{Ag}$  could be performed.

The motivation for the experiment is that there have been relatively few studies of impurities in insulating, ordered magnets, and we decided to study oriented Ag nuclei in a suitable antiferromagnet to determine the hyperfine field which reflects the atomic magnetization. A previous experiment at Louvain-la-Neuve by a UBC-Leuven collaboration had indicated a small anisotropy for  $\gamma$ -rays in the decay of  $^{104}\text{Ag}$  that had been implanted into  $\text{MnCl}_2 \cdot 4\text{H}_2\text{O}$ . However, the sample temperature in this experiment was relatively high ( $\sim 90$  mK) and, subsequently, thorough analysis showed that this effect could not be distinguished from zero within experimental error. Therefore, the original intent of the present experiment was to dope  $^{110\text{m}}\text{Ag}$  into the same crystal and perform an LTNO experiment at a much lower temperature ( $\sim 35$  mK).

In May and June, attempts were made to grow a crystal of  $\text{MnCl}_2 \cdot 4\text{H}_2\text{O}$  from a saturated solution of  $\text{MnCl}_2$  containing both  $^{54}\text{Mn}$  and  $^{110\text{m}}\text{Ag}$  (and  $^{105}\text{Ag}$ ). The former grew into the crystal as expected, but very little of the monovalent silver isotopes went in. A literature search was then made for insulating magnets with a composition that included a monovalent, metallic ion. The candidate that emerged was  $\text{Rb}_2\text{MnCl}_4 \cdot 2\text{H}_2\text{O}$ . This is an antiferromagnet with a Néel temperature  $T_N = 2.2$  K. We have grown some crystals of this salt, but we have to refine the technique to produce some plate-like samples, incorporating  $^{54}\text{Mn}$  and  $^{110\text{m}}\text{Ag}$ , on which to perform the LTNO measurements. This research is on-going.

In the LTNO technique, one measures the directional distribution of radiation from an oriented ensemble of nuclei. For the axially symmetric case, the normalized intensity of  $\gamma$ -radiation in direction  $\theta$  to the orientation axis, normalized to the "warm" count at 1 K, is given by

$$W(\theta) = \sum_{k_{\text{even}}} B_k A_k Q_k P_k(\cos \theta).$$

Here the  $B_k$  describe the orientation of the nuclei and contain the solid state information, the  $A_k$  depend on the observed and preceding transitions in the nuclear decay, the  $Q_k$  are detector solid angle corrections, and the  $P_k$  are the ordinary Legendre polynomials. Significant values of  $B_k$  are obtained when the nuclei experience a sizeable hyperfine interaction and are cooled to millikelvin temperatures in a dilution refrigerator.

## **PET attenuation source**

The Montreal Neurological Group, headed by Dr. Thompson, has developed a new technique for attenuation correction measurements using a positron-emitting isotope embedded in a plastic scintillator. This group wishes to explore the possibility of implanting  $^{22}\text{Na}$  from the ISAC facility into a plastic scintillator.

## **Experiment LS10**

### **Aptamer imaging agents**

*(H. Dougan, TRIUMF)*

Work was completed and a manuscript submitted on the evaluation of DNA aptamers directed towards thrombin as potential thrombus imaging agents. The paper examines the biochemistry of aptamer binding to clot bound thrombin. Exosite 1 aptamer (directed to the fibrinogen binding site on thrombin) showed strong binding to free thrombin, and strongly inhibited coagulation, but had undetectable interaction with thrombin in clots. Exosite 2 aptamer (directed to the heparin binding site on thrombin) also binds strongly to free thrombin, but has little anticoagulant potency. However, exosite 2 aptamer readily bound to thrombin in clot models, demonstrating potential as an imaging agent. The difference between the two aptamers arises from the exosites' involvement in clot architecture, where exosite 1 on thrombin is masked by binding at specific sites on the fibrin matrix, while exosite 2 on thrombin is not masked in this way. However, in clots in living rabbits, exosite 2 aptamers did not diffuse sufficiently in the short time available to establish detectable binding compared to a non-binding control (ovalbumin). More stable nucleic acid analogues may permit imaging in the future by extending the time available for interaction between aptamer and clot. Workers in the United Kingdom have reported that the thrombin concentration is roughly 40 nM in natural human thrombi, surprisingly high for an enzyme catalyst. The central role played by thrombin in thrombosis, coupled with the reasonable thrombin concentration reported in human clots, should stimulate further efforts to master the practical problems impeding thrombin-based imaging.

## **Experiment LS29**

### **Production and distribution of FDG (and other tracers) for clinical studies**

*(T. Ruth, TRIUMF)*

Following the workshop on the distribution of FDG held at the LSPEC Review of 1996/1997, discussions ensued as to how best to provide FDG to the local community for clinical utility. There is no mechanism established for real-cost reimbursement. In addition, TRIUMF management does not wish to engage

in a commercial venture dealing with radioactive substances. However, there continues to be interest in access to FDG and other tracers, both for research purposes and for clinical applications. While the research uses for these tracers can continue to be supplied under existing protocols, there is still a growing need for access to large quantities of either the radiopharmaceuticals such as FDG or  $^{18}\text{F}$ -fluoride as precursor.

Since this project's first submission in 1998, a number of new and continuing developments warrant mentioning. First, a local company, IPET, has established a fee-for-service clinical PET centre at the B.C. Research facility adjacent to TRIUMF. IPET tried negotiating with MDS Nordion for the supply of FDG. As indicated above, TRIUMF has chosen not to be involved as a supplier for non-research purposes.

Over the last year, IPET has completed a Health Canada Investigative New Drug (IND) trial for the safety of  $^{18}\text{F}$ -FDG prepared on the IPET site. That trial was to have been completed in December, 2001. Concurrently, IPET is in the process of preparing an IND application for the efficacy of FDG in monitoring metabolic status in cancer patients. In addition, MDS Nordion has expressed interest in supplying  $^{18}\text{F}$ -fluoride once their new TR30 cyclotron has been installed and commissioned.

## **Results from this past year**

Vancouver Hospital and Health Sciences Centre (Oak Street site): A total of 24 FDG shipments were made in 1999, a further 30 shipments in 2000 and 24 in 2001.

Lions Gate Hospital: A total of 15 FDG shipments were made in 1999, a further 27 shipments in 2000, and 35 in 2001.

St. Paul's Hospital has received 6 shipments of  $^{18}\text{F}$ -fluoride and 5 shipments of FDG this year.

## **Experiment LS33**

### **Evaluation and improvement of a dual head coincidence camera**

*(V. Sossi, UBC)*

The ADAC molecular coincidence dual head camera was installed at Lions Gate Hospital in North Vancouver in August/September, 1997. The attenuation correction hardware and software were implemented in September, 1999.

The Siemens E.Cam Duet PET/SPECT camera was installed at St. Paul's Hospital in May, 2001.

## **Studies accomplished**

1. Development of random event estimate from simulated single event distributions. Development of software tools for data analysis and simulations.

2. Acquisition of all the data relative to the NEMA NU-2-2001 test on the Siemens E.Cam Duet PET/SPECT camera.

#### Current studies

1. Implementation of a model based scatter correction method.
2. Testing of the Fourier rebinning (FORE) provided by the manufacturer.
3. Repeat of a subset of the NEMA NU-2 measurements after FORE implementation.
4. Analysis and partial analysis of the performance test done on the Siemens E.Cam Duet PET/SPECT camera.

#### Future studies

The software will be used to develop and implement a model based scatter correction and obtain an estimate of the random event distribution for a dual head camera. A new method to correct for random events will also be investigated.

#### Experiment LS35

##### Development of $^{18}\text{F}$ labelled nitroimidazole PET imaging agents for tissue hypoxia

(*M.J. Adam, TRIUMF*)

Hypoxia in cells and tissues is an important component of various pathological states (e.g. ischemia and stroke). Hypoxic tumour cells are extremely important within cancer treatment because they are more likely to survive radiation and chemotherapy, leading to an increase in tumour resistance to treatment. More recent evidence suggests that hypoxia is related to the aggressiveness of disease. Such studies employed a microelectrode, used in many centres, but were limited because of invasiveness and the requirement for an accessible tumour.

Derivatives of 2-nitroimidazole are used extensively as hypoxia markers. The 2-nitroimidazoles are not metabolized in oxygenated tissues, but bind to macromolecular proteins after reduction in hypoxic cells. This permits detection by a variety of techniques. For example, the products of such binding for the (pentafluoropropyl)acetamide (EF5) and (trifluoropropyl)acetamide (EF3) derivatives of 2-nitroimidazole can be detected by specific fluorescent antibodies.

The synthesis of  $^{18}\text{F}$ -EF5 has now been developed and was achieved by preparing the allyl precursor and fluorinating it with  $^{18}\text{F}$  elemental fluorine in trifluoroacetic acid. The radiochemical yield is 17% after HPLC purification.

Several syntheses have been performed for cell and animal studies. Initially we carried out cell studies to determine the effects of hypoxic and aerobic conditions

on the uptake of EF5. This experiment indicates that about 10-fold more hot EF5 is concentrated in cells under hypoxic conditions as compared to aerobic conditions, and that the addition of cold EF5 has little effect. The gamma counting results were basically the same as those obtained by using cold EF5 and flow cytometry. These cell experiments were followed by rat experiments; rats with 9L tumours were injected with  $^{18}\text{F}$ -EF5 and imaged on our PET tomograph, followed by dissection to determine biodistribution. An image of the brain tumour in the rat was obtained. The next stage of the research is to proceed to human studies. Two proposals have been submitted for funding. One study will focus on the use of EF5 in lung cancer, and the other on breast cancer.

Progress this year has been slow due to a lack of funds. The grant application by Stephen Chia was rejected. The budget in this application contained funds for the chemistry and automated system that is required for the routine production of EF5. A British Columbia Lung grant to Skov and Gelman will allow for an initial screening test of cold EF5 in 12 patients along with 6 hot EF5 experiments in humans. Ethics approval for these experiments is still required. During the year, Cameron Koch and Syd Evans from the University of Pennsylvania visited TRIUMF and discussed their latest research on EF5. They were very impressed with our facilities at TRIUMF and they would like to work closely with us on future collaborative experiments. At BCCA they are carrying out research on prostate cancer and its connection to hypoxia. They have determined that there are different levels of hypoxia at the 3 stages of progression of the disease. These findings suggest that PET imaging with EF5 might be useful in determining the progression of the disease.

#### Experiment LS38

##### Modelling of the $^{18}\text{F}$ -fluorodopa tracer

(*V. Sossi, UBC*)

Two areas were investigated: the role of dopamine turnover in early Parkinson's disease, and the ability of the tissue input graphical model to accurately quantify changes in dopamine synthesis and storage.

##### Increase in dopamine turnover occurs early in Parkinson's disease: evidence from a new modelling approach to PET $^{18}\text{F}$ -fluorodopa data

An increase in dopamine turnover has been hypothesized to occur early in Parkinson's disease as a compensatory mechanism for dopaminergic neuronal loss. A new approach to the determination of dopamine turnover was developed using four hour  $^{18}\text{F}$ -fluorodopa (FD) PET data. An effective dopamine turnover, which is an estimate of dopamine turnover, has been

measured using its inverse, the effective dopamine distribution volume (EDV). This new method is based on a reversible tracer approach and determines the EDV using a graphical method.

Six normal (N) subjects and ten very early Parkinson's disease (PD) subjects underwent a four hour FD scan. EDV and the plasma uptake rate constant  $K_i$ , a marker of dopamine synthesis and storage, were compared according to their ability to separate the PD from the N group. EDV was the better discriminator (93.8% correct classification versus 81.3% for  $K_i$ ). EDV decreased by 65% in the PD relative to the N group, while the decrease in  $K_i$  was 39%.

These results show that changes in EDV are measurable with PET earlier than changes in the dopamine synthesis and storage rate, indicating that EDV is a sensitive marker for early PD and that a dopamine turnover increase likely serves as an early compensatory mechanism.

**The presence of 3-O-methyl-[ $^{18}\text{F}$ ]fluoro-DOPA (3OMFD) influences the evaluation of the  $^{18}\text{F}$ -fluorodopa tissue input uptake rate constant in a disease dependent way: a study in Parkinson's disease**

## Introduction

Parkinson's disease (PD) is characterized by the loss of dopaminergic neurons, thus decreasing the system's ability to produce and store dopamine (DA). Such ability is often investigated using  $^{18}\text{F}$ -fluorodopa (FD) positron emission tomography (PET) and quantified with a variety of different models. A commonly used model is the modified Patlak graphical approach [Patlak *et al.*, *J. Cereb. Blood Flow Metab.* **3**, 1 (1983); Patlak and Blasberg, *J. Cereb. Blood Flow Metab.* **5**, 584 (1985); Martin *et al.*, *Ann. Neurol.* **26**, 535 (1989)]. This approach allows for a plasma and a tissue input function yielding the respective uptake rate constants  $K_i$  and  $K_{\text{occ}}$ . This method requires the presence of an irreversible compartment and the absence of any non-trapped tracer metabolite. This last assumption is violated by the presence of the FD metabolite 3OMFD. For the plasma input function, this violation can be overcome [Martin *et al.*, *op. cit.*]. The tissue input function, however, includes an indistinguishable component due to the 3OMFD, thus making the evaluation of  $K_{\text{occ}}$  susceptible to a downward bias. Nevertheless,  $K_{\text{occ}}$  has been used extensively to quantify DA synthesis and storage. The disease discriminating and quantifying ability of  $K_i$  and  $K_{\text{occ}}$  have already been widely investigated with discrepant results [Hoshi *et al.*, *J. Cereb. Blood Flow Metab.* **13**, 57 (1993); Takikawa *et al.*, *J. Nucl. Med.* **35**, 955 (1994); Dhawan *et al.*, Quantification of brain function (Academic Press, 1996) p.219]. In this study we show that contrary to the value of  $K_i$ ,

the value of  $K_{\text{occ}}$  depends on the time interval used for its evaluation and that the magnitude of the 3OMFD derived bias is disease dependent. Consequently,  $K_{\text{occ}}$  is likely a better disease discriminator, but less accurate in quantifying changes in DA synthesis and storage.

## Methods

Six normal subjects (N) and fifteen mild PD patients (motor component of the Modified Columbia Scale score  $14.3 \pm 5.7$ ) underwent a four hour FD scan ( $9 \times 10$  min, 30 min interval,  $12 \times 10$  min). 23 blood samples were taken and selected ones analyzed for metabolites. The first 90 min of data were considered for this study.  $K_i$  and  $K_{\text{occ}}$  were evaluated from data points acquired between 20 and 70 min ( $K_{i70}$ ,  $K_{\text{occ}70}$ ) and 20 and 90 min ( $K_{i90}$  and  $K_{\text{occ}90}$ ) for the caudate and putamen separately. The ratio  $K_i/K_{\text{occ}}$  was calculated in each case. The comparisons between  $K_{i70}$  and  $K_{i90}$  and between  $K_{\text{occ}70}$  and  $K_{\text{occ}90}$  were used to estimate the bias as a function of the time interval. The comparison of  $K_i/K_{\text{occ}}$  between the N and the PD group was used to estimate the bias disease dependence. The ratio  $K_i/K_{\text{occ}}$  is mathematically predicted to be equal to  $K_1/k_2$  (the clearance rates from plasma into tissue and from tissue into plasma). Since  $K_1/k_2$  would not be expected to vary appreciably between normals and PD patients [Dhawan *et al.*, *op. cit.*], any difference in the  $K_i/K_{\text{occ}}$  ratio between the N and the PD group can be attributed to the bias introduced by the presence of the 3OMFD in the tissue input function.

## Results

Results are presented in Table XII.

## Observations

1. The value of  $K_i$  does not change as a function of time interval for either group. It exhibits the typical rostrocaudal gradient for the PD group. The value for  $K_{\text{occ}70}$  is larger than  $K_{\text{occ}90}$  for both groups. This is indicative of the downward bias introduced by 3OMFD. The bias is present even for the normal group even for evaluation times  $< 90$  min.
2. The  $K_i/K_{\text{occ}}$  values are appreciably higher compared to  $K_1/k_2$  [Dhawan *et al.*, *op. cit.*], which is indicative of the bias due to 3OMFD.
3.  $K_i/K_{\text{occ}}$  changes with time interval for both groups as expected from the  $K_{\text{occ}}$  results, but while it is the same between the two groups for the caudate (the less affected part of the striatum), it increases significantly in the PD group compared to the N group ( $p < 0.05$ ) for the putamen, thus demonstrating a progressive underestimate of  $K_{\text{occ}}$  for increased disease severity.

Table XII. Results of plasma and tissue uptake rate constant measurements.

	Caudate	Putamen	Caudate	Putamen
	$K_{i90}^*$		$K_{i70}^*$	
Normal	$1.89 \pm 0.26$	$1.81 \pm 0.19$	$1.89 \pm 0.24$	$1.81 \pm 0.17$
PD	$1.44 \pm 0.33$	$1.00 \pm 0.36$	$1.41 \pm 0.36$	$1.03 \pm 0.37$
	$K_{occ90}^*$		$K_{occ70}^*$	
Normal	$1.19 \pm 0.11$	$1.07 \pm 0.09$	$1.38 \pm 0.11$	$1.22 \pm 0.09$
PD	$0.91 \pm 0.12$	$0.51 \pm 0.18$	$1.02 \pm 0.16$	$0.59 \pm 0.20$
	$K_{i90}/K_{occ90}$		$K_{i70}/K_{occ70}$	
Normal	$1.58 \pm 0.17$	$1.70 \pm 0.19$	$1.37 \pm 0.143$	$1.41 \pm 0.16$
PD	$1.59 \pm 0.33$	$2.05 \pm 0.59$	$1.38 \pm 0.265$	$1.83 \pm 0.52$

\*values expressed in  $10^{-2}$

## Conclusion

These results show that the presence of 3OMFD in the tissue input function causes a downward bias in the  $K_{occ}$  estimate and the magnitude of the bias is disease dependent.  $K_{occ}$  may therefore be a good disease discriminator, but may not accurately quantify changes in DA synthesis and storage capability.

## Experiment LS39

### Positron emission profiling (PEP) for pulp and paper fluid dynamic studies

(*T. Ruth, TRIUMF*)

Multiphase flows are very common in industrial applications. One such example is in the pulp and paper industry where a suspension of wood pulp fibres is filtered and consolidated, at very high speeds, to form a sheet of paper. Papermaking suspensions are composed typically of a mixture of fibres with a wide distribution in both length and diameter. Each class of fibre behaves differently during the filtration process depending upon the hydrodynamic force applied and its degree of mobility in the formed network. Ascertaining these effects is difficult as these suspensions are opaque and difficult to visualize at reasonable penetration depths. Clearly, there is a need to visualize the motion of the individual classes of components in a fibre suspension in order to better understand the development of the physical properties of paper.

Recently, we have conducted a gravity-settling experiment at TRIUMF to test the feasibility of using PET as a novel visualization method. In this work, a selected class of "long-fibres" was radioactively labelled and allowed to settle in an untreated fibre suspension (with a distribution of fibre lengths). The suspension was agitated and allowed to settle under the action of gravity in a cylindrical jar. A similar study was conducted in March, and the data are now being used to develop a mathematical description of the motion of fibres in a network.

From these studies it is clear that this visualization technique has potential to help clarify the behaviour of mixtures of fibres with differing lengths. We propose that this technique be used to visualize the motion of fibres in a swirling flow; this is relevant to an apparatus called a hydrocyclone. A hydrocyclone employs centrifugal forces to separate solid particles from the suspending fluid. Hydrocyclones are used primarily to remove dirt particles, but have recently been used to separate the fibre suspension into different length classes.

During this past year, we explored the transient settling process of papermaking fibres with positron emission tomography (PET). Approximately 4 days of camera time were used for this. Here, the motion of fluorine-18 labelled papermaking fibres were visualized settling in the midst of a suspension of non-radioactive fibres. The experimental conditions were such that the particle Reynolds number was always low and the consistency of the suspension was set at the levels found industrially. From this we identified two distinct regimes of settling depending upon the initial consistency of the suspension. At low consistency, the sedimentation rates of the individual fibre fractions within the suspension were found to be somewhat similar. At higher consistencies, fibres began to flocculate and differences in mobility between the individual fractions that make up the suspension were observed. In a separate study, these differences in mobility could be linked to the final paper properties.

## Experiment LS42

### Configuration modelling and image reconstruction studies on a depth encoding research tomograph

(*V. Sossi, UBC*)

## Summary

The high resolution research tomograph (HRRT) has been purchased and is expected to be delivered by CTI in April/May, 2002. The final detector design

consists of two 10 mm deep layers of LSO and LYSO (LSO doped with yttrium) respectively. Novel reconstruction methods and quantification algorithms will be explored for this tomograph.

#### **Accomplished**

Crystal position decoding algorithms were investigated. Spatial resolution estimates as a function of  $\gamma$  incidence angle were obtained by simulating two detectors placed opposite to each other at varying angles.

#### **Current work**

Spatial resolution estimates for a specific source location in the tomograph are under way. Data sets from the HRRT located in Cologne have been obtained and existing reconstruction and normalization source code was obtained from CTI. Patient motion correction issues are being investigated.

#### **Future plans**

The following issues are going to be addressed:

1. Data reconstruction techniques.
2. Design of a point source to map the tomograph point spread function.
3. Detector normalization algorithms.
4. Data transfer and storage schemes.
5. Patient motion correction.

#### **Experiment LS44**

##### **Development of a “formation” (areal density) measurement device for pulp and paper studies** (*T. Ruth, TRIUMF*)

This research aims at developing an experimental device to measure areal density (areal density has units of mass/surface area and is traditionally called basis weight in the pulp and paper industry) or “formation” of paper directly using a linear  $\beta$ -radiation source. In this work we propose to measure formation by pulling a paper sample through a collimated beam of electrons from a source embedded in a long linear rod. The source will be perpendicular to the motion of the paper. The emergent radiation intensity will be sampled by a linear detector and used to analyze mass-density variation. The key advantage of the proposed apparatus is that areal density variations can be measured over large areas continuously. This will aid in understanding the development of paper properties and enable optimization of the forming section of paper machines.

#### **Background**

The term “formation” is traditionally used by papermakers to describe the uniformity or cloudiness of the paper sheet. For about two thousand years, formation has been traditionally evaluated by a “look

through” in which the paper sheet is held in front of a bright light. As light transmission is affected by many factors, such as surface roughness and the degree of bonding, true measurements of formation are currently conducted by the attenuation of  $\gamma$ -radiation.

The simplest method to characterize formation is to define its contrast, that is the standard deviation of the areal density distribution. The most commonly employed laboratory instrument is a point-to-point measuring device using a  $^{147}\text{Pr}$  point source having a circular inspection zone of 1 mm in diameter. The measuring head traverses the paper sample and records a large number of local basis weights. From this the standard deviation is calculated. In another method, the paper is sandwiched between a  $^{14}\text{C}$  sheet and an X-ray film. The paper is exposed for a period of time and the film is developed. The intensity of the image on the film is proportional to the areal density of the paper. This image is then digitized and the formation analyzed in the same fashion as the optical formation analyzer. Both of these techniques are inherently slow. A fast, automated, 2-dimensional method of measuring the areal density variation over a piece of paper is required before formation is accepted as a quality control parameter.

#### **Project description**

The proposed instrument would resemble a desktop scanner that uses a  $\beta$ -radiation source and detector instead of a visible light source and detector. The instrument consists of several sub-systems that need to be developed and integrated. These systems include (1) a uniform linear radiation source, (2) linear  $\beta$ -ray detector, (3) mechanical scanning system, and (4) image construction and analysis software.

#### **Work accomplished this year**

- Sub-systems (1) and (2) have been purchased and have been delivered.
- The mechanical scanning system has been designed and is currently being fabricated.
- Image construction and analysis software has been designed and programmed.

#### **Experiment LS46**

##### **Modelling of the dopaminergic system in more severely affected PD patients**

(*V. Sossi, UBC*)

Parkinson’s disease is characterized by a progressive loss of dopaminergic terminals and by a reduced neurotransmitter dopamine level in the striatum. The radiotracer  $^{18}\text{F}$ -fluorodopa (FD) is often used to quantify the uptake rate constant of the neurotransmitter dopamine (DA) into the pre-synaptic vesicles. Traditionally the FD kinetics are described by an irre-

versible model approach reflecting the DA trapping in the vesicles. The plasma input or the tissue input Patlak graphical approach is applied to the tracer time activity distribution to obtain the uptake rate constant  $K_i$  or  $K_{occ}$ , respectively. In patients with advanced PD the ability to retain dopamine can be so decreased that the irreversibility assumption is no longer valid, leading to a model dependent bias in the parameter estimate.

We have found that in this situation a quantitative assessment of disease progression becomes analysis model dependent. Care therefore needs to be taken when assessing effects of therapy or when investigating compensatory mechanisms that compare changes in different dopaminergic sub-processes involved in Parkinson's disease.

### **Experiment LS50**

#### **Antisense imaging nucleic acids for Parkinson's disease**

*(H. Dougan, TRIUMF)*

Parkinson's disease is a debilitating movement disorder which afflicts nearly 100,000 Canadians. It arises from progressive loss of dopamine-producing cells in the midbrain. Parkinson's disease is a principal research interest for the TRIUMF PET group and the Neurodegenerative Disorders Centre at UBC. The current imaging technology is based on labelled neurotransmitter and receptor antagonists. Important aspects of the loss of dopamine-producing cells are thought to depend on processes downstream from the receptors. There is an interest in measuring expression of the relevant genes through imaging of the mRNA of known genes of interest. In their past work, the UBC collaborators introduced antisense DNA directed to the D2 receptor mRNA and to dopamine transporter mRNA into rat brains. Delivery by capillary tubes assisted crossing the blood-brain-barrier and targeting the midbrain. The rats developed behavioural disorders and biochemical changes consistent with depletion of the "sense" mRNA by the "antisense" DNA probe. Ideally one could image and quantify such mRNA using radiolabelled DNA probes, as suggested by the experiments with rats. Working towards this goal, we have been successful in the radioiodination of the specialized sulfurized DNA used in the experiments with rats. The intention is to detect the mRNA by autoradiography based on  $^{125}\text{I}$ , and then go on to imaging the mRNA using positron emitters.

### **Experiment LS51**

#### **Auger therapy for prostate cancer**

*(H. Dougan, TRIUMF)*

Prostate cancer is the most prevalent cancer in men and the second leading cause of cancer death in

Canada. Prostate cancer is the principal research interest of the Prostate Centre in Vancouver. Early treatment is effective when the tumour is confined to the gland. When the cancer has spread outside the gland, androgen ablation therapy leads to the death of 99% of the malignant cells by an apoptosis-dependent mechanism. Normal prostate cells are also lost. The surviving 1% of tumour cells have altered phenotype, namely androgen independence (AI). Ideally, the killing of the small AI tumour cells could be improved, leading to improved therapy. The present proposal exploits the Auger electrons released following the decay of  $^{123}\text{I}$  and  $^{125}\text{I}$ . The aim is to test the hypothesis that the interaction of an iodoandrogen steroid (EMIVNT) with the androgen receptor will deliver the iodoandrogen in close enough proximity to the DNA that the ensuing DNA damage will cause cell death. To date we have been successful in preparing two suitable steroids (EMIVNT and ZMIVNT) with potential for Auger therapy. Both have been labelled to high specific activity using  $^{125}\text{I}$ . Biochemical assay of receptor binding has begun and is encouraging. The intention is to complete the biochemical characterization. Then the  $^{123}\text{I}$  compound will be prepared and assayed with cancer cells to determine whether killing due to Auger electrons is observed.

### **Experiment LS52**

#### **Comparison of commercial FDG synthesis systems**

*(T. Ruth, TRIUMF)*

A comparison will be made between two commercial FDG synthesis units to ascertain their reliability and the purity of the FDG product and the efficiency of production. These results will enable the local community to choose the most appropriate route for preparing FDG for the Lower Mainland. The studies will involve 10–20 syntheses using each unit, and monitoring yields and purity of FDG.

The results for the case where the synthesis box at the IPET scan centre was used involved two sources of  $^{18}\text{F}$ -fluoride, the TRIUMF niobium water target and the silver target from PETNet in Seattle. For the  $^{18}\text{F}$ -fluoride produced from the Nb target the decay corrected FDG yield was 61% ( $n = 16$ ) and for the Ag-target the yield was 51% ( $n = 15$ ).

In a separate study, we sent  $^{18}\text{F}$ -fluoride to the University of Alberta PET Centre, located at the Cross Cancer Centre, where they produced FDG using a different synthesis unit and slightly different chemical process. The decay corrected yield for this unit was 64% ( $n = 34$ ).

From these results it appears that the two synthesis units are comparable with respect to decay corrected



yields and that the niobium target provides higher radiochemical yields.

Future experiments will make use of a third synthesis unit located at Vancouver General Hospital.

### Experiment LS53

#### Synthesis of $^{99m}\text{Tc}$ and $^{186,188}\text{Re}$ sugar derivatives

(*M.J. Adam, TRIUMF*)

An NSERC strategic grant has recently (October, 2001) been awarded (M.J. Adam, PI, \$78,200/year for 3 years) to carry out research on the synthesis of technetium and rhenium labelled carbohydrates for use in nuclear medicine imaging and therapy. Dr. Adam will be collaborating with Dr. Orvig in the UBC Chemistry Dept. and AnorMED (M. Abrams, CEO). A post doctoral fellow (Dr. Simon Bayly) and a graduate student (Cara Fisher) have been hired to complete the group.

Radiolabelled carbohydrates have been of significant interest to nuclear medicine due to the success of 2- $^{18}\text{F}$ -fluoro-2-deoxy-glucose (FDG) as an imaging agent in positron emission tomography (PET). This success has naturally raised the question of whether a single-photon emitting glucose analogue with similar properties to FDG can be developed for use with single-photon emission computed tomography (SPECT). Be-

cause of the relatively short half-life of  $^{18}\text{F}$  (110 min) its use is limited to facilities that have an accelerator in close proximity to chemistry laboratories and medical facilities. This fact makes it impractical for the FDG method to be widely used in medicine.  $^{99m}\text{Tc}$  is the most widely used isotope in SPECT due to the fact that it is a generator produced, commercial isotope which makes it convenient to use and relatively inexpensive. It also has ideal physical properties for imaging. The drawback to this isotope is that it must be attached to the molecule via a chelate or organometal conjugate, which may perturb the system being studied. A SPECT analogue based on a widely available isotope such as  $^{99m}\text{Tc}$  would make these agents available to the broader medical community. Among elements of the same series as Tc, the isotopes  $^{186}\text{Re}$  and  $^{188}\text{Re}$  show promise in the development of therapeutic strategies. For a  $\beta^-$  emitting radioelement to be therapeutically useful, a half-life of between 12 h and 5 days is preferred; moreover, for a 1 MeV  $\beta^-$  particle, the depth of penetration into tissue is approximately 5 mm. Furthermore, if some of the disintegrations are accompanied by a 100–300 keV photon, the behaviour of the radioelement can be conveniently followed by using a gamma camera. The nuclear properties of  $^{186}\text{Re}$  and  $^{188}\text{Re}$  are optimal for these purposes.

## THEORETICAL PROGRAM

### Introduction

Theoretical research at TRIUMF is centred on the TRIUMF Theory group, a group consisting of four permanent members, six to seven research associates, about six graduate students, and many visitors. Its main research interests are physics beyond the standard model, lattice QCD, intermediate energy nuclear physics, and low energy nuclear reactions. In addition to carrying out its own independent research, it provides support for the TRIUMF experimental program and acts as a resource for the experimentalists.

The four permanent members of the Theory group are: Harold W. Fearing (group leader), Byron K. Jennings, John N. Ng and Richard M. Woloshyn. Erich W. Vogt (professor emeritus, UBC) is an associate member. We have had two sabbatical visitors this year, Helmy S. Sherif and Chaoqiang Geng. Our research associates are: W. Chang (since September), A.K. Dutt-Mazumder (since September), J. Escher, S.K. Gosh (until September), C.P. Liu (since September), S. Kondratyuk, X. Kong (until September), A.D. Lahiff, G. Rupak, and W. Schadow (until September). The graduate students associated with the group are: C. Bird, T. Ebertshauser, F. Okiharu, C.C. Liu, E. Ho, I.L. Ho, and T.H. Wu.

The visitors to the Theory group this year include:

K. Abazajian	F. Khanna	S. Reddy
K. Amos	R. Lewis	A. Rinat
A. Arbuzov	H. Lipkin	A.E. Santana
S. Beane	M. Locher	T. Schaefer
B. Campbell	G. McLaughlin	E. Swanson
D. Chang	A. Mekjian	I. Towner
A. Czarnecki	D.-P. Min	W. Wilcox
A. Gal	M. Patel	D. Wilkinson
N. Hambli	D. Phillips	C.E. Wolfe
J. Jose	I. Popescu	S. Wong
C.S. Lam	M. Ramsey-Musolf	L. Zamick
S. Karataglidis		

### The Theory Research Program

#### Neutrinos in extra dimensions

(*J.N. Ng; C.S. Lam, McGill*)

We investigate the possibility that the large mixing of neutrinos is induced by their large coupling to a five-dimensional bulk neutrino. In the strong coupling limit the model is exactly soluble. It gives rise to an oscillation amplitude whose squared-mass difference is independent of the channel, thus making it impossible to explain both the solar and the atmospheric neutrino oscillations simultaneously.

#### Neutrino mass in the Zee model and muon $g-2$

(*J.N. Ng; H.J. He, D. Dicus, Texas*)

Existing neutrino oscillation data strongly point to new physics beyond the standard model (SM). We study a minimal modification of the Zee-mechanism with an additional singlet Zee-scalar  $K^{++}$  (but the same SM fermion spectrum), which radiatively generates the neutrino Majorana masses from the two-loop. With this scheme, we construct a class of models with minimal U(1) family symmetry (à la Froggatt-Nielsen) to naturally explain the neutrino oscillations and lepton mass spectrum, as well as the BNL muon  $g-2$  anomaly. The  $3 \times 3$  radiative neutrino mass-matrix is found to exhibit nearly bi-maximal mixing, while the  $K^{++}$  scalar is shown to be generically light, with essentially flavour non-diagonal Yukawa couplings. Implications for lepton flavour-violation processes are further analyzed.

#### Testing discrete symmetries with $\eta$ decays

(*C.Q. Geng, Tsing Hua, Taiwan*)

The radiative decay  $\eta \rightarrow \pi\pi\gamma$  can be a probe of new physics that violates charge conjugation ( $C$ ) and time reversal ( $T$ ) symmetries. We discuss the measurements required to facilitate such observations. We also show how these studies complement the searches for new physics such as neutron electric dipole moment experiments.

#### Strangeness current in the nucleon

(*R. Lewis, Regina; W. Wilcox, Baylor; R.M. Woloshyn*)

The contribution of the strange-quark current to the electromagnetic form factors of the nucleon is being studied using lattice QCD. The strange current matrix elements from our lattice calculation are analyzed in two different ways: the differential method used in an earlier work by Wilcox, and a cumulative method which sums over all current insertion times. The preliminary results of the simulation indicate the importance of high statistics, and that consistent results between the varying analysis methods can be achieved. Several criteria useful in assessing the robustness of a signal extracted from a noisy background have been developed. No signal satisfying these criteria has yet been seen.

#### Charmed baryons in lattice QCD

(*R. Lewis, Regina; N. Mathur, R.M. Woloshyn*)

Masses of singly and doubly charmed baryons were calculated in quenched lattice QCD using an improved action of the D234 type on an anisotropic lattice. The mass differences between spin  $3/2$  and spin  $1/2$

baryon states were calculated and compared to mass differences between vector and pseudoscalar mesons. The suppression of spin splittings in mesons containing heavy quarks, characteristic of quenched QCD simulations, was not observed in the baryon sector. The mass dependence of colour hyperfine effects is discussed within the context of the quark model and heavy quark effective theory.

### Quark interactions on baryons

(*F. Okiharu, Nihon; R.M. Woloshyn*)

A project to study quark-quark interactions using the methods of lattice QCD and to compare them to quark-antiquark interactions has been started. This work is motivated in part by empirical evidence which shows a seemingly simple relationship between spin splittings of mesons and baryons. It is also aimed at addressing a recent controversy concerning the nature of gluonic flux distributions within baryons. Initially we will calculate the three-quark potential from baryonic Wilson loops to try to understand the flux distribution. Then the plan is to extend the calculation to the spin dependent parts of the potential and to make a detailed comparison with the quark-antiquark interaction.

### Baryon resonance extraction from pion-nucleon data in a covariant approach

(*A.D. Lahiff; C. Bennhold, George Washington Univ.*)

There are a large number of baryon resonances observed experimentally in meson-baryon scattering processes. It is important to be able to extract the properties of these resonances from the experimental data in a reliable way. We are developing a relativistic model of pion-nucleon scattering based on the 4-dimensional Bethe-Salpeter equation which, at present, includes the  $\pi N$ ,  $\eta N$ , and an effective  $\pi\pi N$  channel. This covariant model will be used to extract resonance masses and partial decay widths from experimental data on the reactions  $\pi N \rightarrow \pi N$ ,  $\pi N \rightarrow \pi\pi N$ , and  $\pi N \rightarrow \eta N$ .

### Covariant model of anti-kaon nucleon scattering

(*A.D. Lahiff*)

A covariant meson-exchange model of the  $\bar{K}N$  interaction is constructed using the multi-channel Bethe-Salpeter equation, which is solved by means of a Wick rotation. The  $K^-p$ ,  $\bar{K}^0n$ ,  $\pi^0\Lambda$ ,  $\pi^+\Sigma^-$ ,  $\pi^0\Sigma^0$ ,  $\pi^-\Sigma^+$ ,  $\eta\Lambda$ ,  $\eta\Sigma^0$ ,  $K^+\Xi^-$ , and  $K^0\Xi^0$  channels are taken into account. The interaction kernels are constructed from the  $s$ - and  $u$ -channel baryon poles and  $t$ -channel vector meson pole diagrams obtained from the usual SU(3)-symmetric  $BBP$ ,  $BBV$ , and  $PPV$  interaction Lagrangians (here  $B$ ,  $P$ , and  $V$  represent the  $J^P =$

$1/2^+$  baryons, the pseudoscalar mesons, and the vector mesons, respectively). All propagators are multiplied by dipole form factors, with the same cutoff mass used everywhere. The basic coupling constants are fixed from other sources, such as decay widths and vector-meson dominance. With just one free parameter (the cutoff mass), a good description of the available  $\bar{K}N$  data is obtained from below threshold to 300 MeV laboratory momentum. The  $\Lambda(1405)$  and  $\Lambda(1670)$  resonances are generated dynamically as  $\bar{K}N$  and  $K\Xi$  quasi-bound states, respectively.

### Unitarity and the Bethe-Salpeter equation

(*A.D. Lahiff; I.R. Afnan, Flinders*)

We investigate the relationship between different three-dimensional reductions of the Bethe-Salpeter equation and the analytic structure of the resultant amplitudes in the energy plane. This correlation is studied for both the  $\phi^2\sigma$  Lagrangian and the  $\pi N$  system with  $s$ -,  $u$ -, and  $t$ -channel pole diagrams as driving terms. We observe that the equal-time (or Klein) equation, which includes some of the three-body unitarity cuts, gives the best agreement with the Bethe-Salpeter result. This is followed by other 3-D approximations that have less of the analytic structure.

### Effects of meson loops on the interaction of the $\Delta$ resonance

(*S. Kondratyuk*)

The dressed  $\Delta$  propagator and  $\pi N\Delta$  vertex are calculated including meson loop corrections up to infinite order. Thus a self-consistent procedure is developed in which the nucleon and  $\Delta$  propagators and vertices are treated on the same footing. The dressing procedure is part of a  $K$ -matrix approach to the pion-nucleon scattering, pion photoproduction and Compton scattering. The central ingredient of the method is a system of coupled integral equations which is solved by iteration, including the loop corrections with the  $\pi$ ,  $\rho$  and  $\sigma$  mesons. The obtained propagators and vertices are consistent with the important constraints of unitarity, analyticity and crossing symmetry for the scattering amplitude. The effects of the meson loop corrections on the  $\pi NN$  and  $\pi N\Delta$  form factors are qualitatively similar. A good description of the pion-nucleon phase shifts is obtained even though the few input parameters are tightly constrained due to the nonperturbative nature of the procedure. The description of the P33 phase shift is improved by the dressing of the  $\Delta$  resonance.

### The equivalence theorem and the Bethe-Salpeter equation

(*S. Kondratyuk, A.D. Lahiff, H.W. Fearing*)

The independence of the scattering matrix on the choice of interpolating fields is known as the

equivalence theorem. To examine the validity of the equivalence theorem in typical non-perturbative approaches to hadronic processes, we solve the Bethe-Salpeter equation for two-particle scattering in a field-theoretical model using two Lagrangians related by a field transformation. The kernel of the equation consists of the sum of all tree-level diagrams for each Lagrangian. The solutions differ even if all four external particles are put on the mass shell, which implies that observables calculated by solving the Bethe-Salpeter equation depend on the representation of the theory. We argue that the principal origin of this representation-dependence is the well-known fact that certain classes of loop graphs are not generated by the equation with a tree-level kernel. An important implication of our result is that the choice of a convenient representation is an additional model assumption in traditional dynamical approaches based on the Bethe-Salpeter equation.

### Irreducible pionic effects in nucleon-deuteron scattering below 20 MeV

(*L. Canton, INFN, Padova; W. Schadow; J. Haidenbauer, IKP-Jülich*)

The consequences of a recently introduced irreducible pionic effect in low energy nucleon-deuteron scattering are analyzed. Differential cross sections, nucleon (vector) and deuteron (vector and tensor) analyzing powers, and four different polarization transfer coefficients have been considered. This  $3NF$ -like effect is generated by the pion-exchange diagram in the presence of a two-nucleon correlation, and is partially cancelled by meson-retardation contributions. Indications are provided that such types of effects are capable of selectively increasing the vector (nucleon and deuteron) analyzing powers, while in the considered energy range they are almost negligible on the differential cross sections. These indications, observed with different realistic nucleon-nucleon interactions, provide additional evidence that such  $3NF$ -like effects indeed have the potential to solve the puzzle of the vector analyzing powers. Smaller but non-negligible effects are observed for the other spin observables. In some cases, we find that the modifications introduced by such pionic effects on these spin observables (other than the vector analyzing powers) are significant and interesting and could be observed by experiments.

### The one-pion-exchange three-nucleon force and the $A_y$ puzzle

(*L. Canton, INFN, Padova; W. Schadow*)

We consider a new three-nucleon force generated by the exchange of one pion in the presence of a  $2N$  correlation. The underlying irreducible diagram has been recently suggested by the authors as a possible candidate

to explain the puzzle of the vector analyzing powers  $A_y$  and  $iT_{11}$  for nucleon-deuteron scattering. Herein, we have calculated the elastic neutron-deuteron differential cross section,  $A_y$ ,  $iT_{11}$ ,  $T_{20}$ ,  $T_{21}$ , and  $T_{22}$  below break-up threshold by accurately solving the Alt-Grassberger-Sandhas equations with realistic interactions. The results indicate that this new  $3NF$  diagram provides the possible additional contribution, with the correct spin-isospin structure, for the explanation of the origin of this puzzle.

### Photonuclear reactions of three-nucleon systems

(*W. Schadow; O. Nohadani, W. Sandhas, Bonn*)

We discuss the available data for the differential and the total cross sections for the photodisintegration of  $^3\text{He}$  and  $^3\text{H}$ , and the corresponding inverse reactions below  $E_\gamma = 100$  MeV, by comparing with our calculations using realistic  $NN$  interactions. The theoretical results agree within the error bars with the data for the total cross sections. Excellent agreement is achieved for the angular distribution in the case of  $^3\text{He}$ , whereas for  $^3\text{H}$  a discrepancy between theory and experiment is found.

### Few-body states in Fermi systems and condensation phenomena

(*P. Schuck, ISN Grenoble; M. Beyer, G. Röpke, Rosstock; W. Schadow; A. Schnell, Washington*)

Residual interactions in many particle systems lead to strong correlations. A multitude of spectacular phenomena in many particle systems are connected to correlation effects in such systems, e.g. pairing, superconductivity, superfluidity, Bose-Einstein condensation, etc. Here we focus on few-body bound states in a many-body surrounding.

### Three-nucleon portrait with pion

(*L. Canton, G. Pisent, INFN, Padova; W. Schadow; T. Melde, J.P. Svenne, Manitoba*)

We report on recent results obtained by the above collaboration on the collision processes involving three nucleons, where we pay particular attention to the dynamical role of the pion. After discussing the case at intermediate energies, where real pions can be produced and detected, we have considered the case at lower energies where the pions being exchanged are virtual. The study has revealed the presence of some new pion-exchange mechanisms, which leads to a new three-nucleon force of tensor structure. Recently, the effect of this tensor three-nucleon force on the spin observables for neutron-deuteron scattering at low energy has been analyzed, and will be briefly reviewed.

## Spin observables for pion production from $pd$ collisions

(L. Canton, G. Pisent, INFN, Padova; W. Schadow; J.P. Svenne, Manitoba)

We have calculated the proton analyzing power  $A_{y0}$  of the pion-production reaction from  $pd$  collisions for one energy close to threshold, and for another in the region of the  $\Delta$ -resonance. A fair reproduction of the experimental data could be obtained in both cases with a model which includes isoscalar and isovector  $\pi N$  rescatterings in  $s$  waves, as well as the  $p$ -wave rescattering mechanisms mediated by the  $\pi NN$  and  $\pi N\Delta$  vertices. For the analyzing power at threshold we found that the initial-state interaction (ISI) is also quite important.

## Sigma-term and pion-nucleon amplitude near threshold: beyond few pion-loop corrections

(S. Kondratyuk)

The nucleon sigma-term describes how the nucleon mass changes with varying quark mass and as such is an important link between fundamental degrees of freedom of QCD and properties of hadrons. In particular, it serves as a measure of the explicit chiral symmetry breaking. The sigma-term can be calculated from the pion-nucleon scattering amplitude in the sub-threshold region, where it is constrained by chiral low-energy theorems. In this work the nucleon sigma-term is computed using a dynamical relativistic-invariant, unitary and crossing symmetric model in which certain analyticity constraints are also implemented. The most important hadronic degrees of freedom are included in the model: the nucleon, the  $\Delta$  resonance, the  $\pi$ ,  $\rho$  and  $\sigma$  mesons. The interactions of the nucleon and the  $\Delta$  with the pion are calculated in a self-consistent dressing procedure through solving a system of coupled integral equations for the corresponding Green's functions. Compared to existing effective perturbative approaches, the present calculation allows one to study effects of multiple meson loops on the sub- and near-threshold amplitude. In particular, we find that these effects are rather important for the sigma-term. The calculated amplitude at the sub-threshold Cheng-Dashen point threshold is compatible with the values extracted from dispersion data analysis. The calculated pion-nucleon scattering lengths are also consistent with experiment, as well as the phase shifts up to pion energies of 800 MeV. The good description of the amplitude both below and above the threshold region is achieved because the essential analyticity and unitarity structure of the calculated Green's functions is correctly reproduced. This in turn is effected by utilizing dispersion techniques in solving the dressing equations.

## Vector mesons in the nuclear medium

(A.K. Dutt-Mazumder)

One of the contemporary issues of high energy nuclear physics has been to study the in-medium properties of hadrons. In particular, the behaviour of vector mesons in a thermal bath has become a cardinal focus for quite some time. This is because of two reasons. Firstly, they can decay into a photon and dileptons and provide a penetrating probe to the hot and dense nuclear system temporarily produced in high energy heavy ion collisions. Secondly, there has been a prediction that in hot and/or dense matter their masses might undergo a reduction indicating partial restoration of chiral symmetry.

We have studied the properties of light vector mesons, viz.  $\rho$ ,  $\omega$  and  $\phi$  in various phenomenological models including QCD sum rule. We have shown that the  $\rho$  meson spectral function undergoes dramatic changes in the nuclear medium and could hardly be interpreted as quasiparticle excitation anymore. Furthermore, we also have discussed various symmetry breaking effects viz. the Lorentz symmetry breaking and the violation of charge conjugation symmetry in hot and dense nuclear matter, which, unlike vacuum, might lead to a mixing of different quantum states resulting in a different dilepton spectra than what one expects without taking these additional effects into account. Presently we are focusing on the possibilities of delineating such signals in the experiments to be performed at GSI, CERN and RHIC.

## Consistency between the low-energy nucleon Compton scattering and sum rules

(S. Kondratyuk; O. Scholten, Groningen)

The purpose of this work is to focus attention on the general question of agreement between the polarizabilities extracted from the low-energy expansion of the amplitude and those obtained from the sum rules. The Gerasimov-Drell-Hearn and Baldin-Lapidus sum rules are evaluated in the dressed  $K$ -matrix model for photon-induced reactions on the nucleon. For the first time the sum  $\alpha + \beta$  of the electric and magnetic polarizabilities and the forward spin polarizability  $\gamma_0$  are explicitly calculated in two alternative ways – from the sum rules and from the low-energy expansion of the real Compton scattering amplitude – within the *same* framework. We find agreement between the two methods in the leading order terms related to the anomalous magnetic moment (the Gerasimov-Drell-Hearn sum rule) and  $\alpha + \beta$  (the Baldin-Lapidus sum rule), but some violation in the next order related to  $\gamma_0$ . This discrepancy at third order can be understood on the basis of model approximations in the treatment

of the self-energy and vertex corrections of the  $\Delta$  resonance. Consistency between the two ways of determining the polarizabilities is a measure of the extent to which basic symmetries of the model are obeyed. In particular, the agreement found at the leading orders shows that the model obeys the essential causality constraints.

### **Polarized photons in radiative muon capture**

(*S.-I. Ando, South Carolina; D.-P. Min, Seoul; H.W. Fearing*)

We discuss the measurement of polarized photons arising from radiative muon capture. The spectrum of left circularly polarized photons, or equivalently the circular polarization of the photons emitted in radiative muon capture on hydrogen, is quite sensitive to the strength of the induced pseudoscalar coupling constant  $g_P$ . A measurement of either of these quantities, although very difficult, might be sufficient to resolve the present puzzle resulting from the disagreement between the theoretical prediction for  $g_P$  and the results of a recent experiment. This sensitivity results from the absence of left-handed radiation from the muon line and from the fact that the leading parts of the radiation from the hadronic lines, as determined from the chiral power counting rules of heavy-baryon chiral perturbation theory, all contain pion poles.

### **The anomalous chiral perturbation theory meson Lagrangian to order $p^6$ revisited**

(*T. Ebertshäuser, S. Scherer, Mainz; H.W. Fearing*)

We present a revised and extended construction of the mesonic Lagrangian density in chiral perturbation theory (ChPT) at order  $p^6$  in the anomalous (or epsilon) sector,  $\mathcal{L}_{6,\epsilon}$ . After improving several aspects of the strategy we used originally, i.e., a more efficient application of partial integration, the implementation of so-called Bianchi identities, and additional trace relations, we find the new monomial sets to include 24  $SU(N_f)$ , 23  $SU(3)$ , and 5  $SU(2)$  elements. Furthermore, we introduce 8 supplementary terms due to the extension of the chiral group to  $SU(N_f)_L \times SU(N_f)_R \times U(1)_V$ .

### **Radiative muon capture by $^3\text{He}$**

(*E.C.Y. Ho, H.W. Fearing*)

The rate of the nuclear reaction  $^3\text{He} + \mu^- \rightarrow ^3\text{H} + \gamma + \nu_\mu$  has been calculated using both the elementary particle model (EPM) approach and the impulse approximation (IA) approach. Using the EPM approach, the exclusive statistical radiative muon capture (RMC) rate for photon energy greater than 57 MeV is found to be  $0.245 \text{ s}^{-1}$  and the ordinary muon capture (OMC) rate to be  $1503 \text{ s}^{-1}$ . The IA calculation exhibits a slight dependence on the type of trinucleon

wave function used. The difference between the IA and EPM calculation is larger for RMC than for OMC. To resolve the difference between the two approaches a more detailed investigation including meson exchange corrections will be required.

### **Infrared regularization in relativistic chiral perturbation theory**

(*C. Bird, H.W. Fearing*)

Chiral perturbation theory is a useful tool in the study of low energy reactions involving light particles. However, the inclusion of heavy particles in chiral perturbation theory results in large contributions from loop diagrams which violate the standard power counting scheme. We review two methods, referred to as heavy baryon chiral perturbation theory and infrared regularization, which remove the high energy effects of the heavy particles and which therefore do not violate the power counting scheme. We then use these two methods to calculate the amplitude for pion photoproduction to fourth order and prove that the two amplitudes are equivalent.

### **Double radiative pion capture in heavy baryon chiral perturbation theory**

(*H.W. Fearing; C. Unkmeir, S. Scherer, Mainz*)

The process  $\pi + p \rightarrow n + \gamma + \gamma$ , or equivalently  $\gamma + p \rightarrow n + \pi + \gamma$ , is of interest because one of the contributing sub-diagrams contains the pion Compton scattering reaction and the question arises whether or not a measurement of these processes would give somewhat the same information as could be obtained from pion Compton scattering, were it possible to do that experiment directly. Experiments are under way both at TRIUMF and Mainz to investigate these processes. We have calculated the amplitude for the doubly radiative capture process in heavy baryon chiral perturbation theory to one loop order, that is, to  $\mathcal{O}(p^3)$ . The low energy constants involved are the same as those we evaluated earlier in calculations of muon capture and singly radiative pion capture. The amplitude is, however, extremely complicated and efforts are under way to simplify our result enough to make it possible to easily compare with experiment.

### **The induced pseudoscalar coupling of the proton weak interaction**

(*T. Gorringer, Kentucky; H.W. Fearing*)

Of the fundamental couplings which contribute to the weak interaction of nucleons, the induced pseudoscalar  $g_P$  is least well known. There is a well known theoretical prediction, the Goldberger-Treiman relation, coming from PCAC, which can be strengthened using the techniques of chiral perturbation theory. Empirical information comes primarily from both ordinary

and radiative muon capture. We are preparing a review summarizing what is known theoretically about  $g_P$  and what can be extracted from data on muon capture in nuclei and on the proton.

**The asymmetry in quasielastic electron-deuteron scattering due to the parity-nonconserving nucleon-nucleon interaction**

*(C.P. Liu, W. Haxton, INT/Washington; M. Ramsey-Musolf, Connecticut; G. Prézeau, Caltech)*

By measuring the asymmetry factors in elastic electron-proton and quasielastic electron-deuteron scattering, one can determine the strange magnetic form factor,  $G_M^s$ , and the isovector axial form factor (seen by the electron),  $G_A^e(T = 1)$ , at a certain  $Q^2$  set up by the experiment. The former provides a way to explore the strangeness content of a nucleon, which is a result anticipated by QCD, while the latter could be used to constrain the anapole form factor of a nucleon, which could be understood as a radiative correction in the unified electroweak theory. According to the results published by the SAMPLE collaboration, the experimental value for  $G_A^e(T = 1)$  is much larger than the theoretical prediction, and this puzzle has already caught a lot of attention. One key assumption made when interpreting the measured asymmetry is the static approximation, which pictures proton and neutron as independent particles. Although it seems reasonable at the quasielastic limit, however, it needs to be further confirmed given such a big theory-vs.-experiment discrepancy. As the parity-nonconserving nucleon-nucleon interaction also contributes to the asymmetry in the deuteron case, we would like to clarify the role it plays in the SAMPLE experiment and see if it helps to resolve the puzzle.

**Radiative corrections in the superallowed Fermi  $\beta$  decay**

*(C.P. Liu, W. Haxton, INT/Washington; M. Ramsey-Musolf, Connecticut)*

The unitarity of the Cabibbo-Kobayashi-Maskawa matrix is extremely important for the test of the standard model and the constraint of physics beyond. In the unitarity relation of the first row, i.e.  $\sum_i |V_{ui}|^2 = 1$ , the element  $V_{ud}$  is the dominant one. Currently the most precise value for  $V_{ud}$  comes from the superallowed Fermi  $\beta$  decay (the precision is about two times better than what is achieved in free neutron decay), which gives  $|V_{ud}| = 0.9740 \pm 0.0005$ . Combined with the values of  $V_{us}$  and  $V_{ub}$ , the unitarity has failed by  $2\sigma$ . One uncertainty in the extraction of  $V_{ud}$  comes from the estimation of the radiative corrections. Since the nuclei are many-body systems, how the radiative corrections are modified by the nuclear correlation, and how the

nuclear Green's function is different from the free particle propagator are what we are trying to figure out and we hope to improve previous work on this subject.

**Nuclear structure effects in nucleon capture reactions**

*(J. Escher, B.K. Jennings, H.S. Sherif)*

Nucleon capture reactions play an important role in our understanding of astrophysical phenomena. For example, exact knowledge of the  ${}^7\text{Be}(p, \gamma){}^8\text{B}$  cross section is necessary for calculating the neutrino flux generated in the sun, the  ${}^{13}\text{N}(p, \gamma){}^{14}\text{O}$  process plays an important role in the hot CNO cycle, and the  ${}^7\text{Li}(n, \gamma){}^8\text{Li}$  reaction is a key element of primordial nucleosynthesis in inhomogeneous big bang scenarios. We have been studying spectroscopic amplitudes, spectroscopic factors, and their significance for the description of single-particle transfer reactions such as nucleon capture. We demonstrated that spectroscopic amplitudes (overlap functions) contain both single-particle and many-nucleon aspects of the nuclear many-body problem. In principle, the amplitudes can be obtained from a fully microscopic model. We presented two alternative approaches, each based on a set of exact coupled-channels equations, from which we derived several well-known approximation schemes, such as Hartree, Hartree-Fock and two distinct single-particle models. We considered the implications of our results for the calculation of reaction cross sections in potential-model approaches and illustrated how microscopic structure effects arise naturally in the relevant transition matrix elements and can be (in part) accounted for via spectroscopic factors.

**Spectroscopic amplitudes from shell model and cluster model approaches**

*(J. Escher, B.K. Jennings)*

A reliable calculation of nuclear reaction cross sections must include both one-body and many-body effects. For single-particle transfer reactions this can be accomplished through the use of spectroscopic amplitudes (overlap functions). Obtaining these amplitudes, however, requires solving a set of complicated coupled differential equations or a fully microscopic model. Recent advances in nuclear many-body theory have resulted in highly accurate microscopic treatments for very light nuclei. For heavier systems one has more traditional approaches available such as the shell model or the cluster model, both of which include some many-nucleon correlations and provide reasonable approximations to the full problem. Currently, we are exploring possibilities for obtaining realistic spectroscopic amplitudes from shell model and cluster model approaches.

## Nuclear structure and solar neutrinos

(*B.K. Jennings, J. Escher*)

The  ${}^7\text{Be}(p, \gamma){}^8\text{B}$  reaction at solar energies ( $E_{cm} \leq 20$  keV) is relevant to neutrino physics since the neutrino event rate in the existing chlorine and water Čerenkov detectors is dominated by the high-energy neutrinos produced in the subsequent  $\beta$  decay of  ${}^8\text{B}$ . Precise knowledge of the neutrino flux generated in the sun will help to place constraints on possible “new physics” scenarios such as neutrino flavour oscillations. Direct measurements of the  ${}^7\text{Be}(p, \gamma){}^8\text{B}$  reaction at energies corresponding to astrophysically relevant temperatures are very difficult, since the cross section diminishes exponentially at low energies. The reaction rate has to be deduced by extrapolating the measured absolute (laboratory) cross section from energies above 100 keV to the astrophysically relevant regime. While theoretical considerations have established the energy dependence of the cross section for energies below about 400 keV, the overall normalization of the cross section is more difficult to obtain. We are currently exploring several options for improving the theoretical predictions for this quantity. The goal of this project is to provide a better determination of the reaction rate and thus to contribute to a clearer understanding of this rare, but crucial, solar fusion process, as well as to achieve more accurate estimates of the neutrino flux from our sun.

## Partial dynamical symmetry in an interacting fermion system

(*J. Escher; A. Leviatan, Hebrew Univ.*)

Symmetries play an important role in dynamical systems. They provide labels for the classification of states, determine selection rules, and simplify the relevant Hamiltonian matrices. Algebraic, symmetry-based models offer significant simplifications when the Hamiltonian under consideration commutes with all the generators of a particular group (“exact symmetry”) or when it is written in terms of the Casimir operators of a chain of nested groups (“dynamical symmetry”). However, the application of exact or dynamical symmetries to realistic Hamiltonian systems has its limitations: usually the assumed symmetry is only approximately fulfilled, and imposing certain symmetry requirements on the Hamiltonian might result in constraints which are too severe and are incompatible with experimentally observed features of the system. Alternatively, one can consider breaking the symmetry of a system in a specific way which might result in mixing of representations (i.e. quantum labels) for some of the states, while retaining good symmetry for a subset of eigenstates. This intermediate symmetry structure is referred to as a “partial dynamical symmetry” (PDS).

Partial symmetries have been investigated in both bosonic and fermionic descriptions of nuclei, in the context of supersymmetry, as well as in molecular physics. We have studied PDS in fermionic models of the nucleus, introduced a family of Hamiltonians with partial SU(3) symmetry, and shown that these Hamiltonians are closely related to the quadrupole-quadrupole interaction, an important ingredient in models that aim at reproducing quadrupole collective properties of nuclei. The new scheme was employed to describe spectra and electromagnetic transition rates of prolate, oblate, and triaxially deformed nuclei, and to study the structure of the associated eigenstates.

## Symplectic shell model and multi- $\hbar\omega$ correlations in electron scattering observables

(*J. Escher*)

A microscopic theory for deformed nuclei, which takes proper account of the Exclusion Principle and of inter-shell couplings, is given by the Symplectic Shell Model. The model uses symmetries of the nuclear many-body system to classify and truncate the enormous shell model space while retaining the multi-shell quadrupole correlations which lead to deformation. It is able to reproduce intra-band and inter-band E2 transition strengths between low-lying, as well as giant, resonance states without introducing proton and neutron effective charges, and its observables are expressible in microscopic shell-model terms. We apply the symplectic model to light ( $p$ -shell and  $sd$ -shell) nuclei and investigate the influence of multi-shell correlations on nuclear charge and current densities. Such studies are important since they allow one to place quantitative limits on the contributions to the nuclear current from meson exchange. Furthermore, since electron scattering observables provide a direct probe of the nuclear current, this study is able to shed light on the dynamical character of nuclear rotational motion and thus it addresses one of the unsolved fundamental questions of nuclear structure physics.

## Shell closures in nuclei far off stability

(*J. Escher, B.K. Jennings*)

Whereas the magic numbers are very well established for stable nuclear species, little is known about the shell structure of nuclei far off the line of stability. This information, however, is very valuable, not only for achieving simplifications in the descriptions of these nuclei, but also in the context of astrophysics. Nuclear abundances from the astrophysical  $r$ -process, for example, depend on the shell closures in neutron-rich nuclei beyond the iron region. Traditional experimental signatures for magic numbers involve primarily systematic features, such as the energies and electromagnetic



transition strengths of the first excited states in even-even nuclei or nucleon separation energies of odd-A chains. Our recent work suggests that a new measure for shell closures in a given even-even nucleus can be found in the adjacent  $A\pm 1$  nucleon systems. Since the proposed new signature involves spectroscopic information on very specific excited states of the immediate neighbours only, it is different from and comple-

mentary to traditional approaches. Furthermore, the new signature provides some quantitative measure for the goodness of shell closures in the region considered. We have been testing this new signature for stable nuclei, for which there is much spectroscopic information available, and are now working on applications to the oxygen isotopes near the neutron drip line.

## EXPERIMENTAL FACILITIES

### Proton Irradiation Facility

(*E.W. Blackmore, TRIUMF*)

There was an increased demand for beam time on the TRIUMF proton irradiation facility (PIF), with several new groups of users requesting testing time. There were five scheduled beam periods, three with only the low energy beam BL2C available and two with both beams available. The September 13–18 beam period was not fully used as the unfortunate events of that week prevented travel for some of the users. Some of this work was rescheduled later in September and then during the December 12–18 run, when once again both beams were available.

Table XIII lists the laboratories and companies that have used beam since PIF was developed in 1996, and the types of devices that were tested. Typically many of these users are repeat customers, with seven of these groups using beam during this past year.

Table XIII. TRIUMF PIF users (1996–2001).

Organization/company	Typical testing programs
<u>Canadian</u>	
DREO, T&N, CAL Corp. EMS Passat, Crestech, SFU	SEE in SRAM, DRAM; DD in GaAs & QW LEDs; neutron and proton dosimetry; TID in MEMs
DREO/Health Canada	Biological samples
MD Robotics (SPAR)	SEE, TID in Pentium computers, monitors, cameras
Bubble Technology, RMC	Bubble detectors for neutron and proton dosimetry
ABB Bomem	DD in laser diodes
Dynacon Enterprises Ltd.	SEE, TID in micro- satellite components, attitude control
Canadian Space Agency	SEE, TID in microgravity experiment components
ATLAS (UofA)	SEE, TID in calorimeter readout electronics
<u>Foreign</u>	
NASA/GSFC	SEE, TID, SET, DD in optocouplers, spacecraft electronics
DERA (UK)	SEE in SRAM, DRAM
Vanderbilt University	DD in GaN devices

The flexibility in the beam delivery system was again demonstrated with DREO carrying out single event upset (SEU) studies at energies increasing from 20 to 500 MeV, BTI/RMC requiring proton fluences of  $10^3/s$  over a 10 cm diameter to test the response of bubble detectors to 100 MeV protons, and several other users requiring dose exposures to  $10^{13}$  protons/cm<sup>2</sup> for total dose and displacement damage studies.

Vancouver was the host city in July for the Nuclear and Space Radiation Effects Conference, the IEEE sponsored conference for this field in North America. About 500 delegates attended, mostly from the United States and Europe. On the last day of the conference a tour of the proton irradiation facility at TRIUMF was provided, with a lot of interest generated. Several papers at the conference were presented on data taken at TRIUMF.

A Faraday cup for measuring the proton beam current at the test position was designed and commissioned during the year. The thickness of the copper absorber in the Faraday cup was made compatible with energies up to 225 MeV to allow calibrations to be carried out on both beam lines. With careful design of the insulator arrangement, the biased electron suppressor, and good vacuum, the Faraday cup had a dark current of less than 1 pA at a bias voltage of 300 V. Figure 119 shows the current calibration on the low energy beam line, comparing the three methods of fluence calibration: the Exradin T1 ion chamber, the Faraday cup, and direct proton counting at low intensity.

A number of users have indicated an interest in having calibrated neutron beams. Previously, the neutron flux and energy spectrum were measured downstream of a beam stop which was just thick enough to stop the incident proton beam. The measurements were made using Bonner Spheres, supplemented with carbon activation for higher energies. With the help of a visitor from Australia, a more careful measurement was

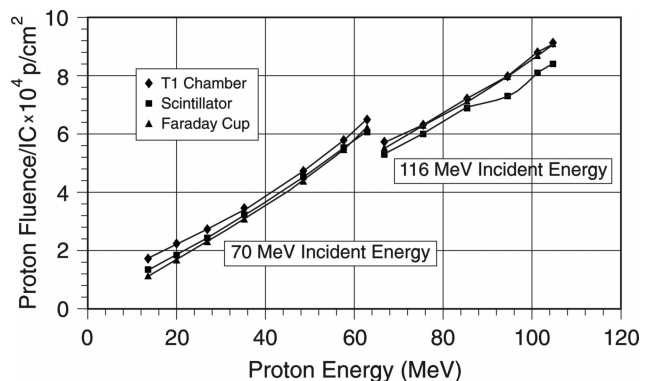


Fig. 119. Calibration of proton fluence.

carried out in May for incident 110 MeV protons on a 20 mm thick lead stop. The neutron dose equivalent rate is limited to about 0.1 to 0.2 kRad/hr using this technique due to the proton beam current limits in the PIF area. This is useful for neutron dosimetry work and possibly some SEU studies. For total dose and displacement damage studies, an absorbed dose of 10–100 kRad (1 MeV neutron equivalent) is required, which is not feasible at PIF. However, some initial neutron activation studies on the most easily accessible neutron beam at the TNF high intensity beam dump at TRIUMF have given some encouragement that neutron damage studies could be carried out in this location.

### Proton Therapy Facility

(*E. W. Blackmore, TRIUMF*)

During the year, 8 patients were treated for ocular melanoma with protons, bringing the total number of patients treated at TRIUMF to 68. Figure 120 shows the patient numbers per year since the facility started. This year there was one patient from Oregon, the first U.S. patient, with the remaining patients from western Canada. There is some hope of attracting patients from eastern Canada once the results of the treatments to date are published.

Control and monitoring of proton therapy equipment and dose delivery is carried out using a dedicated computer, PTCS0, which is part of the TRIUMF cyclotron control system. The dedicated computer which previously was a VAX 4100 running VMS was replaced with an ALPHA Station Model 600, also running VMS. The controls software was transferred to this new computer and, after extensive quality assurance testing, was used for patient treatments in December.

Since 1995 the treatment planning program EYEPLAN has run on the VAX computers ERICH/REG which are part of the TRIUMF cluster running VMS. A decision has been made to retire these computers by the summer of 2002. Work has begun to transfer the planning software to the dedicated PTCS0 computer. This may require a change to the graphics packages or to the method of digitizing the X-ray positioning films.

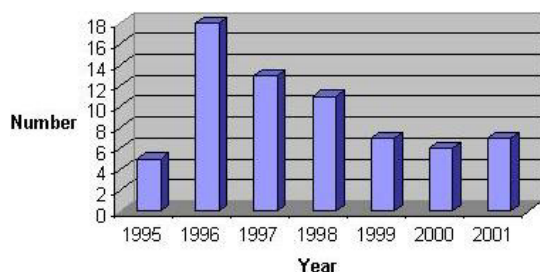


Fig. 120. Number of patients treated per year with protons at TRIUMF.

### $\mu$ SR User Facility

(*S. Kreitzman, TRIUMF*)

$\mu$ SR user facility supported operations ran very smoothly during 2001. This, coupled with an almost undisturbed proton beam production schedule, resulted in the delivery of over 70 weeks of beam to 46 experiments carried out by approximately 20 groups. The major spectrometer usage (in weeks) was LAMPF (22), DR (15), Belle (now HiTime) (12) and Helios (8). Of note is that the DR (dilution refrigerator; 12 mK base temperature) ran for 11 weeks continuously without any significant problems. The technical aspects of the  $\beta$ -NMR experiment were also in good shape with the commissioning of rf technology allowing for frequency selective adiabatic polarization inversion.

On the political side, NSERC, the funding agency that is responsible for the  $\mu$ SR user facility MFA (major facility access) grant, unilaterally extended that grant (at the previous 1999 funding level) for two additional years. Since this grant exclusively supports the salary component of the facility's operation, and we were expecting to reapply (to cover, in part, the costs of salary inflation), we were forced to request an extraordinary supplement to this funding level in order to re-establish a financial environment which would allow staff retention. The results of this submission will be known in 2002.

Major facility developments which highlighted the year were:

- Delivery and commissioning of new American Magnetics 7 T high field magnet, HiTime.
- Fabrication of the new Helios spectrometer stand.
- Testing and finalization of the prototype uLB (ultra low background) insert.
- Installation (as yet uncommissioned) of new Linux data acquisition computers in all beam lines.
- Commissioning of  $\beta$ -NMR rf hardware that allows for adiabatic frequency selective excitation pulses.
- Reconstruction of the Miss Piggy 1.6 K cryostat to make it much more responsive.

The following material outlines these and related developments more fully.

### Spectrometers

#### HiTime

The major functional spectrometer upgrade was that of the delivery and installation of a new American Magnetics designed 7 T magnet for the HF (high field/frequency) spectrometer. This magnet and spectrometer, now christened HiTime, shows significant

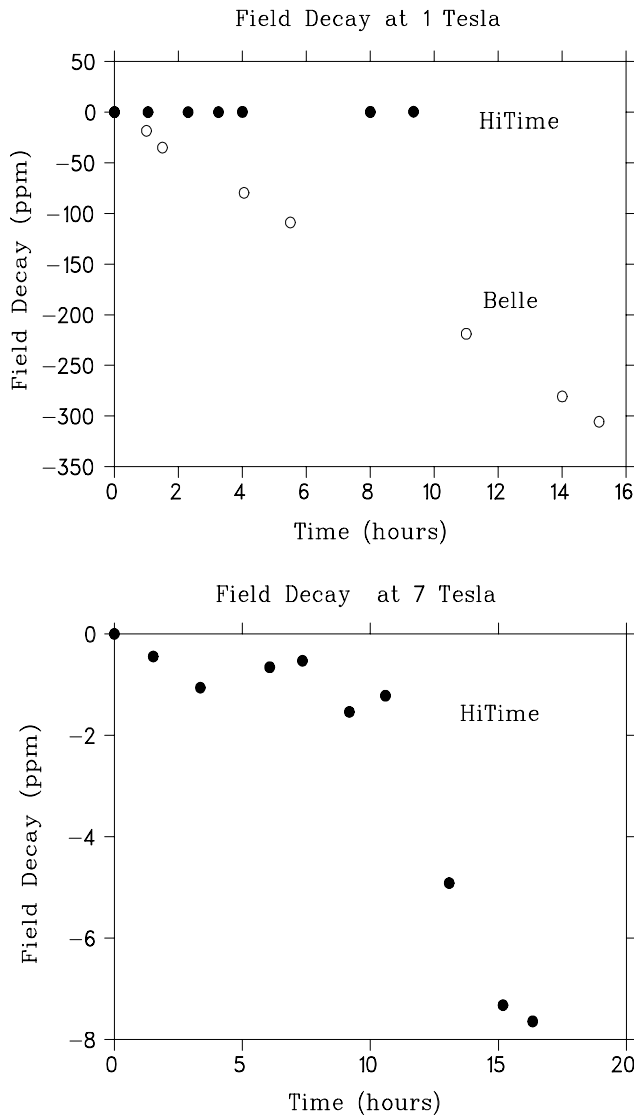


Fig. 121. Drift of the new HiTime magnet as compared with the original Belle magnet. The improvement is about a factor of 300.

improvements (see Figs. 121 and 122) in the two magnetic field parameters that count in high field  $\mu$ SR, namely field stability and homogeneity. The vastly improved stability will allow very long runs (lasting over a day if required) in which the field drift will still be well within the static distribution imposed by the magnet's (smaller) inhomogeneity.

### Helios

From an operational point of view, the fabrication of a new Helios stand will allow much more rapid and reliable set up of this spectrometer. All counter sets have full skeletal support mounted on a heavy duty platform and rail system. Cryostat mounts have been redesigned with the goal of simple reliable and reproducible user adjustment. In addition, a design implementation with safety concerns taken into account

### Field Inhomogeneity Comparison @ 7T, 8x8mm

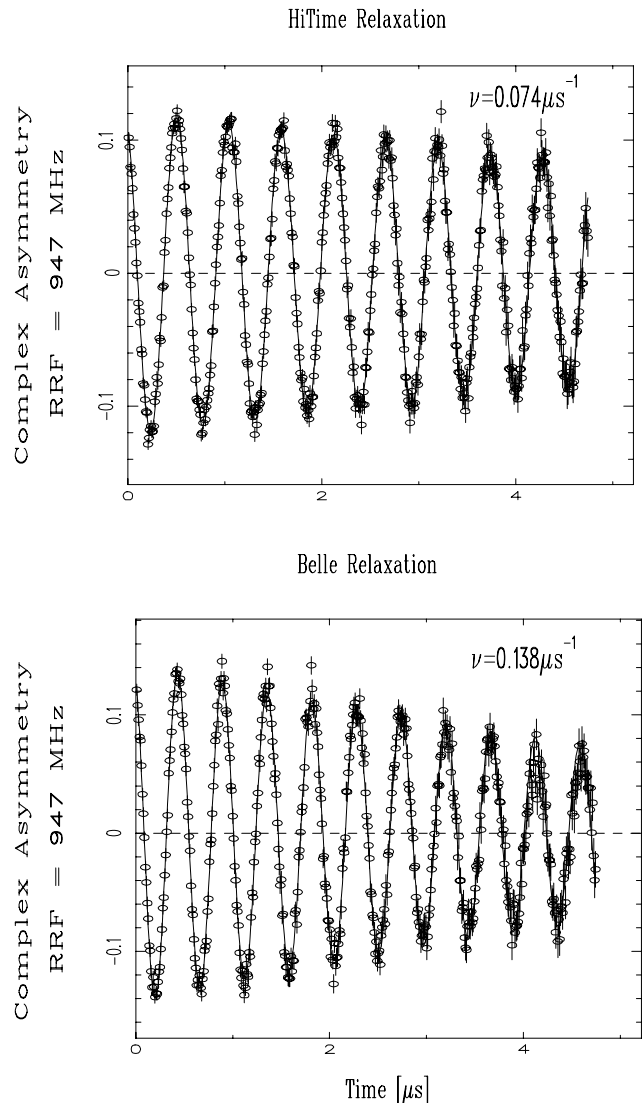


Fig. 122. Relaxation rate of the new HiTime magnet as compared with the original Belle magnet. The sample is an  $8 \times 8$  mm pure Ag, which has an undetectable intrinsic relaxation rate. The decay of these spectra is then a measure of the external field's inhomogeneity. Even though the positioning in the HiTime magnet was not optimized, its decay time and hence homogeneity is at least twice that found in the old Belle.

from the outset now makes Helios very accessible regarding cryogenic management procedures.

### Inserts

The capability to carry out experiments on samples (historically) considered too small for  $\mu$ SR has been addressed by the commissioning of our newest generation low-background insert. The distinguishing feature of this in-cryostat device is that it contains a muon

aperture and active muon collimator in very close proximity to the sample, thereby keeping stray muons to a minimum. Coupled with a veto for muons which miss the sample, and position selective positron coincidence for the up, down and backward counters, this results in raw background rates that are about 1/1000 of the incoming muon rate. This low background rate allows small samples to be measured without the spurious background signals overly obscuring the physics being probed.

### **Cryogenics**

#### **Miss Piggy**

A major redesign of the internals of the cryostat originally provided by Quantum Technologies had resulted in greatly improved cycle and stabilization times. Although a complete 290 K cool down from warm takes about 2.5 hours, once the outer shields have been cooled (often needs to be done only once) 200 K temperature traversals take less than 30 minutes.

#### **New horizontal gas flow**

A new HGF cryostat had been added to the cryogenic arsenal. It is almost an identical copy of our venerable existing HGF but with the additional feature of having a side access beam window. This increased versatility has already been put to good use in a series of experiments that required beam injection perpendicular to the cylindrical axis of cryogenic high pressure cells.

### **$\beta$ -NMR**

Further technical progress in the  $\beta$ -NMR program has been logged with the installation and testing of rf excitation capabilities (quadrature modulation), that allow for the application of frequency selective adiabatic pulses. These are the pulsed equivalent of an CW (continuous wave) polarization inversion in a limited frequency range. The pulsed equivalent of such capability greatly increases the experimental flexibility of the  $\beta$ -NMR experiment to map out line shapes accurately. The interested reader can refer to the recent article in the Journal of Magnetic Resonance, **153**, 155-177 (2001) or online at <http://www.idealibrary.com/links/toc/jmre/153/2/0>.

#### **Facility information and documentation**

Please refer to our Web site <http://musr.triumf.ca> for full access to a broad range of facility resources and information.

### **Beam Lines**

*(C. Ballard, TRIUMF)*

The Experimental Support group, which includes the Beam Lines group, is part of the Science Division and is responsible for the installation, alignment

and maintenance of the experimental facilities at TRIUMF as well as the primary beam lines. As in 2000, the group supplied technical assistance to the existing experiments, primary and secondary channels in the meson hall as well as technical support to ISAC and CERN. The group also supported two co-op students and two summer students during the year.

In ISAC, the end of 2000 saw the completion of the MEFT and HEBT installations resulting in beam through DTL. In the year 2001, the group assisted on the LEBT installation including the polarimeter leading to the Osaka experiment and the  $\beta$ -NMR high voltage platform. The  $8\pi$ , DRAGON and TUDA experiments were installed and were taking data by the end of 2001. The success in ISAC was, in part, achieved through the coordinated efforts of Science Division, Cyclotron Division and ISAC Division. The planning of ISAC-II took place in the latter half of 2001.

In the vault, January's efforts were focused on the upgrade of beam line 1A. After 25 years of service, elements on the beam plane at the head end of 1A required an overhaul. The maintenance involved electrical and water header reconstruction. The upgrade went remarkably well.

In the meson hall, the group was also involved in completing the installation of the TWIST experiment in M13, which involved an area reconfiguration, the assembly of a 70 ton steel yoke for a large (1 m bore) superconducting solenoid, analogue and digital cable booms and a rolling platform for electronics racks.

Other projects in the meson hall included the continuation of the overhaul of the M9 separator, repairs to the M15 separator, M13 beamblocker, M9 beam blocker, upgrades to the M11 area and the TNF. The group also performed preventative maintenance on the water packages, vacuum systems and magnet power leads as well as the ongoing technical assistance to the proton irradiation facility, proton therapy, PET, ATLAS,  $\mu$ SR, and experimental support in the proton hall.

The CERN collaboration involved two technicians and a summer student on the assembly of nine PFN (pulse forming network) tanks. The tanks will be used in the LHC collider at CERN. Each tank weighs over 2 tons and consists of a bank of capacitors and resistors bathed in a silicon-based oil. The assembled tanks will be tested at TRIUMF and sent to Geneva.

The Beam Lines group continued to provide alignment assistance to ISAC, TWIST, Remote Handling and the RF group.

## Cryogenic Targets

(C. Marshall, TRIUMF)

A major construction project was the design, construction and testing of a new target for Expt. 744. The liquid hydrogen target was required to have low-mass walls in order to keep to a minimum the interaction with the electrons emitted by the nuclear reaction under study. In addition, the target and its supports had to fit into a small volume in the middle of a large magnet while allowing free entry and exit of the beam.

After extensive testing, a Divinycell and Kapton composite was utilized for the low-mass outer windows of the cryostat. A horizontal “wicking” heat pipe was designed to cool the tightly constrained target cell. However, its performance proved more development time was required, and it had to be abandoned. The work of design, fabrication, testing and installation was completed in time for a run with beam in early December, with the target operating successfully.

The second new target project was a liquid hydrogen cell for Expt. 875, a study of muon scattering. A dual length target cell (rotatable) with cooling system was designed and built to be mounted in a vacuum chamber supplied by the experimental group. The experiment did not run in 2001 due to delays in assembling other parts of the experiment.

Work was begun on reviving the polarized proton target for use in the CHAOS spectrometer (Expt. 862). The work involved upgrades to the control system, electrical services, and piping. Many of the components of the dilution refrigerator and its gas handling systems, having been out of service for years, required servicing and repairs. A new target angle will require modification of the cryostat and target cell.

## Computing Services

(C. Kost, TRIUMF)

### Overview

The new gigabit backbone has been extremely stable in supporting the over 800 networked devices connected to it. The FDDI ring has been removed. The increase in PC-based Linux systems continues unabated. Security concerns, hardware maintenance/upgrades, software management, etc. are largely mitigated by requiring adherence to site standards – although there is still a strong desire to reduce the number of flavours of Redhat Linux. Some local experience with configuring small clusters, along with acquiring information on mass tape and disk storage systems, has taken place in anticipation of a positive response to a Canadian Foundation for Innovation (CFI) application to fund a major (1500 cpu, 7Tb disk, 70Tb tape) farm to be located at UBC and used by several UBC departments (including TRIUMF). The phase-out of legacy hardware continued.

## Modular approach

TRIUMF has taken a modular approach to provide an integrated computing environment. Enhancements to several modules took place this year:

- Linux backup facility is now based on a Super DLT tape system – with one drive and seven slots for an uncompressed capacity of about 770 Gbytes.
- Addition of a dual-cpu (1.0 GHz) PC running Windows-2000, to provide 20 more X sessions (mostly NCD terminals and Linux boxes) with the ability to run Windows applications.
- Windows print/file server/master domain controller upgraded from NT-4 to dual 1 GHz P3 Win2000.
- Replaced name and SNMP server with a faster PC.
- Replaced some colour X Window (NCD) terminals with PCs running Linux.
- Added 2 more colour laser printers to provide improved support for production of presentation transparencies.
- Added more memory and disk space to our central mail facility (which will see a complete upgrade next year).
- Wireless access (with minimal 56-bit encryption requirements) has been put in place in several key site locations.

## Linux

Redhat Linux 6.2 and 7.2, the recommended standard at TRIUMF, continues to increase its dominance at the lab. Automatic nightly updates (mostly security related) are now regularly performed for more than 70 machines (representing the majority of Linux machines).

## Hardware

TRIUMF collaborated as part of the UBC proposal for a 1500 CPU Linux farm, with 7 Tbytes of disk storage and 70 Tbytes of tape storage – which was part of a Canadian Foundation for Innovation (CFI) application put forth by a WestGrid consortium of several universities and other institutions located in BC and Alberta. TRIUMF would use about 25% of the UBC resources. It would prototype the much larger resources required to do future collaborative analysis of the ATLAS (CERN) experiment. A positive response is anticipated early in 2002.

Figure 123 shows the continued expansion (to a total of 32) of the use of Nortel Networks Baystack 450-24T switches strategically located around the site.

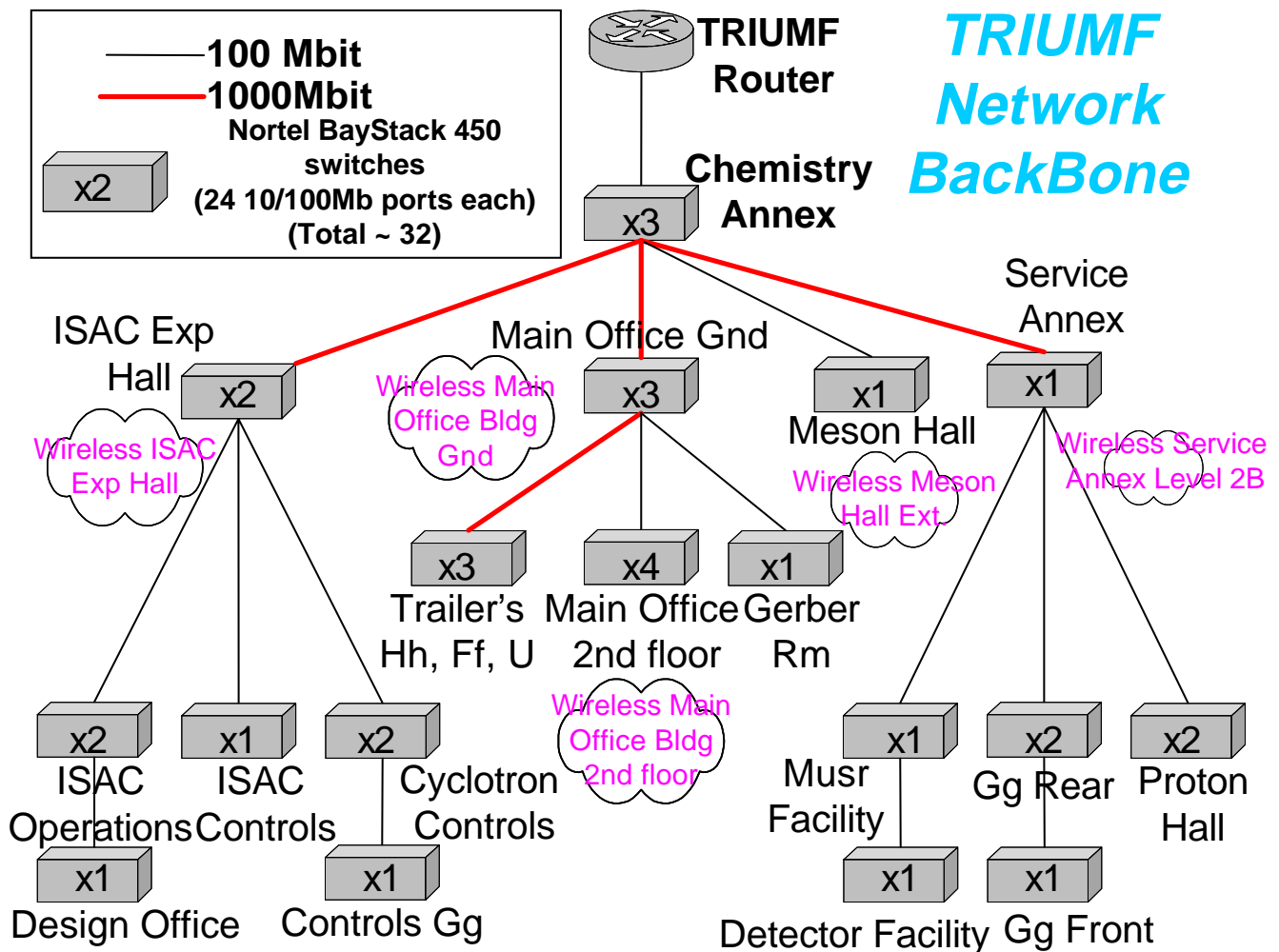


Fig. 123. TRIUMF network backbone.

### Computer security

This was a significant year in that the entire Internet was hit by the Code Red and Nimda worms, which generated an unprecedented amount of network traffic and have still not been eradicated. TRIUMF was fortunate in having few Microsoft Web servers, but of those we have, half were infected (and found fairly quickly). We continue to run an automated scan reporter which contacts ISPs and machine owners about significant network scanning events. The reporter receives automated replies and occasional “thank you” notes. Subsequent to the Code Red worm, we started another reporter designed to alert owners of infected Windows PCs directly via a popup box. Some visualization tools were written for tracking worm progress and looked at the theoretical limits of worm propagation.

2001 also saw a large increase in the number of e-mail-borne viruses. Of note were the SirCam virus which targetted addresses found in Web pages as well as in address books, and the Magistr virus which con-

tinues to be found on a regular basis. The antivirus software reports to the sender where possible and again we receive occasional “thank you” notes and questions.

There has also been a significant rise in the amount of unsolicited (spam) mail arriving at TRIUMF, some having content beyond publicly accepted standards. The greater use of e-mail by staff has meant that more people are exposed via deliberate or inadvertent publishing of their address. A filter system, based on a number of on-line “blacklists”, allows users to filter mail from tagged domains.

In response to the increase in socially unacceptable material spams, we have created an experimental keyword-based filter to augment the domain-based one. We have also moved to a pro-active anti-spam measure – all sites sending us mail are tested for open relay and immediately added to an on-line blacklist. The process also tries to contact machine owners or ISPs. The process also detects some open “contact forms” which have been used to send pornographic spam in particular. A

“desktop security” committee was set up which meets regularly to discuss security concerns on different computing platforms with a view to formalising a security policy for TRIUMF and getting formal authority to control Internet access to devices at TRIUMF.

### Video conferencing

A new computer was installed, dedicated to Internet based VRVS conferencing. An ISDN-based computer is regularly used for a number of conferences. A VRVS reflector was set up for use by the HEP community. A new computer, using RealVideo, and dedicated to Web casting, was used successfully to broadcast the annual meeting of the TRIUMF Users Group.

### Network measurements

We continue to participate in the SLAC Pinger and the Oxford Tracing projects for WAN monitoring, as well as participating in the Bandwidth Challenge for SC2001. We also monitor the internal TRIUMF network for device availability and location using arpwatch, and extended this to gather data from the Baystack switches.

### Software developments

#### Physica

This internationally popular, general purpose data analysis/display program continues to improve as reported bugs were fixed and requested enhancements were added – such as removing practical limits to the number of lines, DO loops, IF statements, and labels in a macro script.

- Increased flexibility of logarithmic axes.
- Enhanced unformatted file reading.
- Newfile qualifier on Write allows for unique file names in UNIX.
- Contour plots without axes can now have legends.
- Support for writing, reading, digitizing, and overlaying PNG bit-maps.

Much progress has been made for porting Physica to Windows, with about 30 new functions, 5 new operators, and about 20 new commands in place. The on-line help feature was completely redone, replacing the traditional Windows help structure with the newer and more flexible compiled html structure. Every new feature in the program has been documented in the on-line help.

A proof of principle Web based version of an on-line form of Physica was successfully implemented. It uses a modified Physica for Linux executable, together with a cgi script, and perl scripts to interpret the output of the

Web based forms, allowing the browser user to interactively create Physica scripts and produce PNG graphics which are then displayed in the browser. PostScript hardcopy of the graphics is available.

An external user, Dr. Edward Sternin of Brock University, has already utilized the Web based version for “Physica-based data acquisition and analysis” for use by the undergraduate physics labs. For details refer to <http://ohm.labs.brocku.ca/physica/>.

### GEANT4

An overview and survey paper on the GEANT4 project and software is expected to be published in a peer-reviewed journal in 2002. A member of our group edited chapter 3, “Software Process”, composed of contributions from six section authors, as well as writing a new Introduction to the paper and participating in numerous teleconferences and author consultations.

Continuing last year’s introduction of Tinderbox, an automated distributed Web based system testing framework, a series of cookbook recipes, detailing non-invasive changes to test scripts allowing Tinderbox monitoring and archiving of GEANT4 test jobs, were developed in collaboration with people at CERN. This work is scheduled for completion in 2002.

### GEANT4 hadronic physics

Two new physics process classes, G4LEpp and G4LEnp, implementing  $p-p$  and  $n-p$  elastic scattering in the energy range 10 MeV to 1.2 GeV were written in consultation with L.G. Greeniaus and P. Wellisch. The classes are self-contained and incorporate differential cross section data obtained from the SAID database. These classes were then included in the GEANT4 4.0 release.

### TRIUMF-CERN LHC collaboration

As part of our collaboration with CERN, we successfully applied the TRIUMF developed hybrid fast-multipole technique to the computation on beam-beam forces in the LHC. New results obtained for head-on and parasitic collisions were reported in a Phys. Rev. ST-AB paper.

In conjunction with a visit to CERN work was begun on extending the simulation code to include longitudinal effects, which had not previously been included in such studies. Presentations were given at CERN and TRIUMF group meetings to explain the physical and computational aspects of the problem and to get comments on it. This new study requires extensive (multi-processor) computing resources and can act as one of the seed applications for developing and testing parallel commodity cluster facilities at TRIUMF.



## Beam dynamics

The multiparticle simulation code ACCSIM continues to be used in a wide variety of accelerator applications including, most recently, proton driver studies for neutrino factories and internal cooling simulations for muons in FFAG's.

This year's goal was to make ACCSIM a stand-alone program, free of the need to use Dimad as a pre-processor for calculating lattice parameters and matrices. There were many good reasons for doing this, not least of which was the difficulty of working with transverse space charge, where the Dimad lattice elements had to be laboriously split into small pieces to allow ACCSIM to do space charge calculations within the elements.

Careful consideration of the various ways to proceed with this project, taking account of the present code and the ACCSIM user community, many of whom are not familiar with C++ and F90, led us to the solution of adapting Fortran code from MAD and Dimad, which had the bonus of being field-proven through many years of use.

With the permission of the Dimad and MAD authors, we incorporated the necessary routines for (1) parsing lattice input and generating data structures, (2) calculating lattice optical functions, and (3) computing element transfer matrices. To keep a maintainable architecture for ACCSIM, modifications to the new routines were kept to a bare minimum, and data were transferred cleanly from MAD to Dimad to ACCSIM data structures for the successive stages of input, run preparation, and simulation.

The expanded program has performed well in all tests so far, and in particular the automation of intracolumn space charge was found to agree closely with previous results for various rings. Pending further refinements and new documentation, it is now in "beta testing" and is available to users by request.

The new ACCSIM was promptly put to work to study coherent space-charge resonances. We set up a simulation framework for the Fermilab Booster using ACCSIM, TRANSOPTR, and Matlab, to demonstrate that coherent (envelope) resonances present practical intensity limitations in such rings. A paper on this work was presented at PAC 2001.

## Miscellaneous

- A Windows C++ version of the two-body kinematic program, Kin2Body, is now available.
- TRMAIL now facilitates Web browsing, filtering, vacation default/forwarding, and disk space usage analysis.
- VMS mail on the DAC VMS cluster was shut down. Plans are to de-activate this cluster in

2002.

- Most Linux systems are now reasonably secure.
- A complete TRIUMF Web pages redesign is scheduled for 2002.
- Plans were completed to move our central computing support hardware and personnel to the new ISAC-II building scheduled for occupancy in early 2003.

## Data Acquisition Systems

(*R. Poutissou, TRIUMF*)

### Overview

The TRIUMF data acquisition system MIDAS is now deployed over 20 stations around the laboratory. These machines also provide significant off-line analysis resources and disk storage.

Table XIV. Computer systems with MIDAS software managed by the DAQ group.

Name	Location	Type
isdaq01	ISAC-LE, $\beta$ -NMR, TRINAT	2xPII/450
isdaq02	ISAC-LE, GPS, LTNO	PIII/500
isdaq03	ISAC-HE, TUDA	2xPIII/550
isdaq04	ISAC-HE, DRAGON	2xPIII/550
isdaq05	ISAC-LE, Osaka	PIII/1000-256
isdaq06	ISAC-HE	PIII/1000
isdaq08	ISAC-HE, $8\pi$	2xPIII/1000
midtis01	TRINAT DAQ	2xPIII/550
midtis02	Detector Facility	PPro/200
midtis03	LTNO platform DAQ	PII/350
midtis04	GPS DAQ	2xPIII/550
midtis05	DRAGON floor DAQ	PII/350
midmes01	Detector Facility	PIII/500
midmes03	RMC DAQ	2xPIII/550
midmes04	Meson hall tests	PII/350
midmes05	Detector Facility	PII/350
midmes06	$8\pi$ Slow Control	PII/166
e614slow	TWIST Slow Control	PII/400
midtwist	TWIST DAQ	2xPIII/1000
midm9b	M9B $\mu$ SR DAQ	2xPIII/600
midm15	M15 $\mu$ SR DAQ	2xPIII/600
midm20	M20 $\mu$ SR DAQ	2xPIII/600
dasdevpc	DAQ development and Web server	PIV/1700

### MIDAS software

The software development effort for MIDAS this year has been focused towards: a) support for newer hardware modules such as Hytech PCI/CAMAC, Wiener PCI/VME interfaces and other VME modules, b) improved user interface for experiment control through the Web browser, c) Web documentation, d) driver portability across different operating systems.

The DAQ group has also contributed to the 12<sup>th</sup> IEEE Real Time Congress on Nuclear and Plasma Sciences, Valencia, June, 2001, with a paper entitled *Real time control/monitoring and data acquisition system for nuclear polarization experiments with implanted radioactive ions*.

There was a significant effort on documentation (see <http://midas.triumf.ca/docmidas/index.html>).

### **NOVA software**

Version 2.2 of the NOVA analysis system was released during 2001. Several experiments at TRIUMF (and elsewhere) are using NOVA both for real-time monitoring of their experiment and subsequent data analysis. An interface/data unpacker was developed for the DRAGON experiment, and the TRINAT analysis code was modified to allow them to upgrade to the newest version of the software.

### **ISAC systems**

Support for new experimental zones has been provided, in particular for TUDA, where specific software code has been written to accommodate the private event analyzer running on Solaris computers. DRAGON, TOJA and Osaka are other experiments where the DAQ group has been involved in set-up and running support.

The six DAQ machines in the two counting rooms are organized in a NIS cluster to allow each group access to all CPUs, data disks and logging facilities transparently. We presently offer a CDrom RW drive, Exabyte 8500 drives and a DLT 4000 drive.

### **$\beta$ -NMR at ISAC**

Further modifications and improvements were made to the  $\beta$ -NMR data acquisition system. In particular, problems with stepping the voltage of the sodium cell (via EPICS) were investigated and solved. Several new features required by experimenters were added. The process of changing between different experimental modes was simplified, and extensive documentation was written.

### **TWIST**

The full TWIST DAQ with two front end FASTBUS crates was commissioned. A special MIDAS task called the Event Builder was developed to combine a portion of events from each of the FASTBUS crates. Sustained data rates of 2500 events/sec and 5 Mbytes/sec were obtained. Logging is done to a DLT8000 drive.

A completely functional implementation of the slow controls system for the TWIST experiment was completed during 2001. The system includes multiple front

ends, interfacing several programmable digital voltmeters, a CAMAC branch and a custom serial interface responsible for control and monitoring of the 260 post-amplifier boards required for the experiment. High voltage control and monitoring is carried out via CAMAC. In addition, several parameters of the proton beam are provided by the TRIUMF Controls group via a CAMAC memory unit.

All slow controls data are maintained in the MIDAS on-line database (ODB), where they are immediately available (via a Tcl interface) to the experimenter. Parameters are continually monitored and checked against user-selectable limits. When a parameter goes outside these limits, an alarm is immediately raised, informing the shift crew of the problem. The system worked well during engineering runs in 2001, and is being upgraded in preparation for physics runs in 2002.

A preliminary version of a similar system was implemented for DRAGON, providing them with access to many of their beam line elements.

### **$\mu$ SR systems**

For  $\mu$ SR, work continued on the new MIDAS-based system. A prototype MIDAS front end was written to replace the present front end (running on a PowerPC under VxWorks). Our student returned and incorporated support for a SIS3803 scaler into the new front end, and added the histogram readout. He also modified the Tcl/Tk user interface.

### **Other experimental stations**

In the meson hall, both the RMC and the CHAOS DAQ were in use during 2001 and required support from the DAQ group. JLAB Hall D detector studies by the Regina group and aerogel tests by the Manitoba/CalTech  $G\theta$  group used the meson DAQ facilities.

Three DAQ stations are provided in the detector facility. They were used in turn for detector developments by the BNL E949 group, the KOPIO group, the DRAGON group, the TWIST group and the HERMES group.

### **Detector Facility**

(*R. Henderson, TRIUMF*)

This year has been a very active and successful year for the Detector Facility. The facility has been almost fully occupied with the Expt. 614 project (TWIST).

The TWIST project is a sophisticated experiment which hopes to measure the Michel parameters to ten times the precision they are now known. TRIUMF members are playing a central role in this collaboration. Robert Henderson has designed the various detector modules and was largely responsible for the de-

sign of the complex “cradle” that holds, aligns and services the nineteen modules in the experiment. Robert Openshaw designed and commissioned the complex gas system. Wayne Faszler designed and built the high precision wire surveyor, and oversees module assembly, testing and QC. In December, the TWIST project finished a highly successful commissioning run of the full detector stack (19 modules) in the solenoid at full field (20 kG). The cradle and detectors were then returned to the Detector Facility for module cleaning, minor repairs and axial compression tests. The cradle will return to M13 in April, 2002 for further commissioning and the start of data-taking.

The TWIST detector module used so far is not the final design. It will be used for the first year of commissioning and data-taking. A final target module with a 6-position wheel is being designed. A low pressure TEC (time expansion chamber) is also being designed. This detector will be placed upstream of the solenoid yoke, to measure incoming muon polarization. All 19 TWIST modules are in operation, spare modules are being completed. This has been a major effort of the Detector Facility and an extremely successful one. The new target module and TEC will be fabricated and tested in the facility, but the group’s contribution to TWIST will taper off in the next six months.

In the scintillator shop, the large NC machining effort for TWIST is nearing completion. In addition, a variety of scintillators have been built, the biggest customer being the  $\mu$ SR group. E929 at BNL also required several scintillator jobs. Two of these were small, but highly complex assemblies. This year fewer scintillators were required at TRIUMF and the shop committed to making a large number of scintillators for the  $G\theta$  experiment at CEBAF, this involves about 0.9 man-years of shop time over an 18 month period. After significant delays, the  $G\theta$  group finalized the design and these scintillators are now in production.

The construction of the ATLAS modules is expected to be finished by June, 2002, concluding a highly successful production and testing program at TRIUMF. The ATLAS project has been using most of the Detector Facility’s large clean room (originally called the HERMES and then BABAR clean room). The Detector Facility did a great deal to set up ATLAS for production. Since then we have only needed to contribute 100% of Rich Maharaj’s time and 30% of Peter Vincent’s time. Production and shipping of ATLAS modules to CERN has been steady. The end of module production completion will free up two clean rooms and their shared use of the “semi-clean” room near RMC.

Our other major activity has been design and prototyping work for the KOPIO experiment. This is a

very large project planned for BNL and has enthusiastic support from DOE. Doug Bryman is head of the TRIUMF/KOPIO group and Robert Henderson has joined the collaboration. It is expected that TRIUMF will be responsible for design, fabrication and testing of the large pre-radiator modules required. The experiment will require 32 modules, plus two spares. Each module has an area of  $2.5 \times 2.5$  m and consists of 8 wire-planes sandwiched between 9 scintillator layers. The wire-planes have anode and cathode-strip readouts and the scintillator layers use wave-shifting-fibre readout. Each module weighs approximately 2 tons.

This project (if NSERC approved) will be of comparable size to the ATLAS calorimeter work at TRIUMF and will be the major project in the Detector Facility for the next four years. At present it represents a significant design and prototyping effort with a goal of first pre-production module by mid-2003.

## GEANT4

(*P. Gumplinger, TRIUMF*)

Modern high energy physics experiments pose enormous challenges in software engineering. Of particular importance is the ever-increasing demand for large-scale, accurate and comprehensive simulations of the particle detectors used in these experiments. The demand is, in part, driven by the escalating size, complexity, and sensitivity of the detectors and, in part, by the availability of moderate-cost, high-capacity computer systems on which larger and more complex simulations become possible. Similar considerations arise in other disciplines, such as: radiation physics, space science, nuclear medicine and, in fact, any area where particle interactions in matter play a role.

In response to this, a new object-oriented simulation toolkit, GEANT4, has been developed. The toolkit provides a diverse, wide-ranging, yet cohesive set of software components which can be employed in a variety of settings. These range from simple one-off studies of basic phenomena and geometries, to full-scale detector simulations for experiments at the Large Hadron Collider and other facilities.

In defining and implementing the software components, all aspects of the simulation process have been included: the geometry of the system, the materials involved, the fundamental particles of interest, the generation of primary events, the tracking of particles through materials and electromagnetic fields, the physics processes governing particle interactions, the response of sensitive detector components, the generation of event data, the storage of events and tracks, the visualization of the detector and particle trajectories, and the capture and analysis of simulation data at different levels of detail and refinement.

Early in the design phase of the project, it was recognized that while many users would incorporate the GEANT4 tools within their own computational framework, others would want the capability of easily constructing stand-alone applications which carry them from the initial problem definition right through to the production of results and graphics for publication. To this end, the toolkit includes built-in steering routines and command interpreters which operate at the problem set-up, run, event, particle transportation, visualization, and analysis levels, allowing all parts of the toolkit to work in concert.

At the heart of this rather diverse collection of code is an abundant set of physics models to handle the interactions of particles with matter across a very wide energy range. Data and expertise have been drawn from many sources around the world and in this respect GEANT4 acts as a repository that incorporates a large part of all that is known about particle interactions; moreover it continues to be refined, expanded and developed. A serious problem with previous simulation codes was the difficulty of adding new or variant physics models; development was difficult due to the increasing size, complexity and interdependency of the procedure-based code. In contrast, object-oriented methods have allowed us effectively to manage complexity and limit dependencies by defining a uniform interface and common organizational principles for all physics models. Within this framework, the functionality of models can be more easily seen and understood, and the creation and addition of new models is a well-defined procedure that entails little or no modification to the existing code.

GEANT4 was designed and developed by an international collaboration, formed by individuals from a number of cooperating institutes and universities, including from Canada: TRIUMF, UBC, University of Alberta and the University of Montreal. It builds on the accumulated experience of many contributors to the field of Monte Carlo simulation of physics detectors and physical processes. While geographically-distributed software development and large-scale object-oriented systems are no longer a novelty, we consider that the GEANT4 Collaboration, in terms of the size and scope of the code and the number of contributors, represents one of the largest and most ambitious projects of this kind. It has demonstrated that rigorous software engineering practices and object-oriented methods can be profitably applied to the production of a coherent and maintainable software product, even with the fast-changing and open-ended requirements presented by physics research.

For example, GEANT4 is an ideal framework for modelling the optics of scintillation and Čerenkov

detectors and their associated light guides. This is founded in GEANT4's unique capacity of commencing the simulation with the propagation of a charged particle and completing it with the detection of the ensuing optical photons on photo sensitive areas, all within the same event loop. This functionality of GEANT4 was developed exclusively at TRIUMF and is now employed world-wide in experimental simulations as diverse as ANTARES, AMANDA, LHCb and HARP.

In GEANT4 the concept of *optical photons* is a class of particles detached from their higher energy *gamma* cousins. This implementation allows processes to be associated to them arising from the wave like property of electromagnetic radiation. Optical photons are produced in the simulation as a result of Čerenkov radiation, scintillation, or transition radiation, and the GEANT4 catalogue of processes at optical wavelengths includes refraction and reflection at medium boundaries, bulk absorption and Rayleigh scattering.

The collaboration provides user support and documentation for the toolkit. The documentation includes installation, user and reference guides, and a range of training kits. User support covers help with problems relating to the code and assistance with using the program. We welcome and respond to enhancement requests, and of course, a user may expect assistance in investigating anomalous results. To facilitate the communication, a Web-based reporting system and a list of frequently asked questions (FAQs) are available on the public GEANT4 Web page.

GEANT4 employs the concurrent versions system (CVS) which maintains a central repository for all documents and source code and provides all the necessary functionality for change management. When new or modified code is tagged for testing, CVS automatically sends the relevant information to an extended version of Bonsai, a Web-based CVS query and database system. Bonsai has been modified to support tags-based processing and to provide an on-line form where developers can submit new tags for system testing. Another Web-based tool, Tinderbox, is being expanded and adapted to GEANT4 and will provide automated monitoring, logging, and problem detection and reporting (including hyperlinks to suspect source code) for all system tests, both completed and in progress. To aid with both development and testing, we maintain an indexed and cross-referenced source code browsing facility based on LXR. The bug reporting system is a customized version of the open source reporting tool Bugzilla. Besides routing the problem to specialists, it tracks and documents the responses until the problem is resolved. The Collaboration also maintains a Web-based user forum, G4Hypernews, with sub-forums according to areas of different interest.

TRIUMF collaborators have been active in almost all areas of user support, documentation, testing and quality assurance, and in particular the development of associated tools. We continue to make upgrades to the most venerable hadronic physics package provided with GEANT4. In 2001, we added classes describing  $p - p$  and  $n - p$  elastic scattering in the energy range of 10 MeV to 1.2 GeV. The classes are self-contained and incorporate differential cross section data from the SAID database.

We have assisted Rachid Mazini, from the University of Montreal, in the comparison of GEANT4 with ATLAS test beam data for the Hadronic End-cap Calorimeter and Forward Calorimeter. One of us traveled for this purpose to Montreal in January, 2001. In the first quarter of last year, we supervised a co-op student, Yong Liang Zhao, who developed a GEANT4 based simulation program for the TWIST experiment. This work produced remarkable results for the prediction of how surface muons range out in the detector and come to rest in the stopping target. We have also assisted over a period of four months, and mostly by e-mail, an undergraduate student at the University of Montreal, David Cote-Ahern, to develop and test the correctness of spin tracking in GEANT4.

TRIUMF collaborators have been responsible for obtaining and editing contributions from section authors of two chapters in the GEANT4 General Paper. We have also authored several sections. The paper is now in semi-final draft and is expected to be submitted for publication in early 2002. We have contributed to the general review of the structure and content of GEANT4 documentation on the Web. For these and Technical Steering Board matters, we participated in numerous video- and teleconferences throughout the year and two of us attended the annual GEANT4 workshop in Genoa, Italy, in July.

Collaboration development highlights in 2001 include two incremental releases in April and June, and a major new release, 4.0, in December. The program now supports secondary particle production cuts per material, random number generator seeding per event, and magnetic fields assigned to volumes. The TRIUMF team helped prepare the requirement for some of these improvements. Finally, the full migration of GEANT4 to CLHEP 1.7 has been achieved.

The GEANT collaborators are: J. Chuma, P. Gumplinger, F.W. Jones, C.J. Kost, M. Losty, TRIUMF; L.G. Greeniaus, University of Alberta.

### Scientific Services

(*M. Comyn, TRIUMF*)

The Scientific Services group encompasses the Publications Office, Library, Information Office, and Conferences. Its activities during 2001 included: producing

the 2000 Annual Report, the TRIUMF preprints, and the KOPIO draft technical design report; refining the new database system for the Library; updating the display material in the front lobby; and supporting eleven past, present and future conferences and workshops.

### Publications Office

The TRIUMF Annual Report Scientific Activities has been truly electronic since 1998. Electronic files have been used throughout, from initial contributor submission, through editing, transmission via ZIP disk to the printer, and subsequent direct printing on a Xerox Docutech system. The same files are used for the WWW versions of the report which are available at <http://www.triumf.ca/annrep> in both Portable Document Format and PostScript file formats. Unlike the monochrome paper version, the electronic versions allow those figures which were submitted in colour to be both viewed and printed in colour. The WWW version of the 2000 report was available to readers five weeks before the printed version. During the last two months of 2001, over 300 people accessed the 2000 Annual Report via the WWW. The Annual Report mailing list has been reduced and the trend is expected to continue as people become more accustomed to accessing the information over the WWW. This will result in less copies having to be printed, with subsequent cost savings.

In an attempt to aid and encourage authors to submit Annual Report contributions in the correct format, the instructions available on the WWW were refined. The  $\LaTeX 2_{\epsilon}$  skeleton file was upgraded to introduce new features, and the instructions document which all authors should consult was expanded to include details of these new features, plus additional information on the correct production of Encapsulated PostScript files for the figures.

Illegal code embedded in Encapsulated PostScript files continues to be a major problem in electronic publishing. Some software packages, such as the TRIUMF graphics routines, fully conform to the Encapsulated PostScript specifications, whereas many do not. In order to alert authors to problems encountered with files they submitted the previous year, and in an attempt to prevent similar problems recurring, a post-mortem of the 182 figures in the 2000 Annual Report was produced and included on the Web site to supplement those for the 1998 and 1999 Annual Reports. This analysis and explanation of solutions is viewed as an ongoing project which will evolve as new procedures are devised and software packages become available for editing bad PostScript code. Superior TRIUMF scientific publications should result. See <http://www.triumf.ca/annrep/figures.html> for details.

TRIUMF preprints are now only produced electronically, and immediately posted on the WWW at <http://www.triumf.ca/publications/home.html> to allow rapid dissemination of the publications. This has replaced the traditional distribution of paper copies by mail, resulting in significant savings of both cost and labour.

Considerable effort was expended producing the KOPIO draft technical design report for review by the U.S. National Science Foundation.

A L<sup>A</sup>T<sub>E</sub>X 2<sub>ε</sub> skeleton file was produced, based on modifications to the book document class and other style files, to allow future volumes of *Advances in Nuclear Physics* to be published with almost exactly the same format as previous editions which were produced using proprietary and extremely complex T<sub>E</sub>X code. Superior automated features were also introduced.

Work for the Joint Accelerator Conference Website (JACoW) committee included refining the L<sup>A</sup>T<sub>E</sub>X 2<sub>ε</sub> templates for use initially at the Particle Accelerator Conference (PAC2001), which was held in Chicago in June, and later at future conferences in the JACoW series. An invited review talk on trends in electronic publishing over the last five years and predictions for the future was given at the JACoW Workshop held in Frascati in March.

## Library

The Library budget was increased in 2001 to compensate for rising journal subscription costs and unfavourable exchange rates for 2002 renewals, thereby maintaining the list of journals which have been acquired since the last cutbacks in 1998. However, the journal subscription budget and electronic access alternatives are constantly under review.

The Library made very few book purchases in 2001 and continues to rely on donations for most of its acquisitions.

The Oracle database system implemented in 2000 was refined to facilitate efficient Library operations. It allows accurate tracking of the journal subscription acquisitions and hence aids subsequent timely requests to publishers for any missing volumes. It also identifies any volumes which have been illegally removed from the Library prior to the annual spring bookbinding exercise. All books loaned from the TRIUMF Library are entered in the database and automatic e-mails are sent to borrowers who fail to return a book after a month, followed by weekly reminders. This system has proved to be extremely successful at ensuring the prompt return of books, with the added advantage that several borrowers have also returned books which have been out for extended periods. Records for books acquired before 1970 have to be entered manually whenever they

are first loaned, and all new acquisitions have to be entered. Outstanding loan reports can be generated easily.

The Library operates on a self-serve basis and manages with minimal support for day-to-day operations.

## Information Office

Following a resignation early in the year, the Information Office and Conference functions were combined.

The Information Office coordinated tours for over 1,900 people during 2001. The general public tours were conducted by a summer student during the June to August period when tours were offered twice a day. Compared to recent years, a record number of people (290) took a record number of tours (68) during the three month period. Throughout the remainder of the year for the twice weekly general public tours, and for the many pre-arranged tours given to high school students and others, a small, dedicated group of TRIUMF staff acted as tour guides.

During the year new display panels for PET were produced as part of an effort to gradually redesign the layout of the lobby. The ISAC model was also upgraded to show new low and high energy beam lines and facilities.

The TRIUMF Welcome Page, which is accessible directly at <http://www.triumf.ca/welcome> or via the TRIUMF WWW Home Page, continues to receive over 5,000 visits each year. The series of WWW pages were developed by two co-op students. They are intended to provide an overview of TRIUMF in a format understandable to the general public. The virtual tour of TRIUMF allows people to “visit” from anywhere in the world via the WWW, or to gain a good introduction before coming to TRIUMF for a real tour. The latter is particularly intended for students using TRIUMF and its science as part of school projects. The Information Office responds to any questions posed by visitors to the site. Some of the pages were updated during the year. At year end efforts began to use outside resources to totally overhaul those parts of the TRIUMF Web site directed at the general public.

Various TRIUMF images found on the WWW pages continue to be in demand for use in text books and on other Web pages.

Use of the Sony VPL-PX20 LCD data projector purchased in 2000 increased rapidly as more speakers gave seminars and presentations using MS PowerPoint, Star Office, and other applications.

Support was provided to the TRIUMF Users’ Group throughout the year by the TUEC Liaison Officer.

## Conferences

During 2001 support was provided for the following conferences and workshops.

- 38<sup>th</sup> Western Regional Nuclear and Particle Physics Conference (WRNPPC'01) and Workshop on Experimental Facilities for ISAC-II, Lake Louise, AB, February 15–18 (58 delegates).
- Summer Nuclear Institute at TRIUMF (SNIT 2001), TRIUMF, July 9–20 (24 delegates).
- Low Temperature Nuclear Orientation Workshop, TRIUMF, August 9–10 (25 delegates).
- Future Opportunities for Neutrino Physics Workshop, Dunsmuir Lodge, Sydney, Vancouver Island, BC, November 8–11 (75 delegates).
- TRIUMF Users' Group Annual General Meeting, TRIUMF, December 12 (49 delegates).

In addition, preparations were made for the following future conferences and workshops.

- Joint Belle-BaBar Workshop on Detector Issues, TRIUMF, February 14–16, 2002.
- Workshop on Low Energy Precision Electroweak Measurements (LEPEM2002), TRIUMF, April 4–6, 2002.
- TITAN Workshop, TRIUMF, April 11–13, 2002.
- Alpha Therapy Workshop, TRIUMF, April 29, 2002.
- 14<sup>th</sup> International Conference on Electromagnetic Isotope Separators and Techniques Related to Their Applications (EMIS XIV), Victoria, May 6–10, 2002.
- Summer Nuclear Institute at TRIUMF (SNIT 2002), TRIUMF, June 10–21, 2002.
- Big DRAGON Workshop, TRIUMF, July 18–19, 2002.

## Sudbury Neutrino Observatory

(*R. Helmer, TRIUMF*)

The first physics results from the SNO experiment were published this year, including the fluxes measured with the charged current (CC) reaction with deuterium and the elastic scattering (ES) reaction with electrons. SNO measured

$$\phi_{\text{SNO}}^{\text{CC}}(\nu_e) = 1.75 \pm 0.07(\text{stat})_{-0.011}^{+0.012}(\text{syst}) \\ \pm 0.05(\text{theor}) \times 10^6 \text{ cm}^{-2}\text{s}^{-1}$$

and, assuming no flavour transformations,

$$\phi_{\text{SNO}}^{\text{ES}}(\nu_x) = 2.39 \pm 0.34(\text{stat})_{-0.14}^{+0.16}(\text{syst}) \\ \times 10^6 \text{ cm}^{-2}\text{s}^{-1}.$$

The difference between the <sup>8</sup>B flux measured with the ES and CC reactions is  $0.64 \pm 0.40 \times 10^6 \text{ cm}^{-2}\text{s}^{-1}$ , or  $1.6 \sigma$ .

The rate of ES reactions has been measured to much higher statistical and systematic precision by the Super-Kamiokande collaboration [Fukuda *et al.*, Phys. Rev. Lett. **86**, 5651 (2001)], and, again assuming no flavour transformations, leads to

$$\phi_{\text{SK}}^{\text{ES}}(\nu_x) = 2.32 \pm 0.03(\text{stat})_{-0.07}^{+0.08}(\text{syst}) \\ \times 10^6 \text{ cm}^{-2}\text{s}^{-1}.$$

The SNO result is consistent with this flux measurement. The difference between the Super-Kamiokande ES measurement of the  $\nu_x$  flux and the SNO CC measurement of the  $\nu_e$  flux is  $0.57 \pm 0.17 \times 10^6 \text{ cm}^{-2}\text{s}^{-1}$ , or  $3.3 \sigma$ . This result provides strong evidence that part of the flux measured by Super-Kamiokande consists of another active flavour distinct from  $\nu_e$ .

The total flux of solar neutrinos can be determined from the combined ES and CC measurements, assuming transitions to active neutrino flavours. Comparison with the ES results from Super-Kamiokande yields

$$\phi(\nu_{\mu\tau}) = 3.69 \pm 1.13 \times 10^6 \text{ cm}^{-2}\text{s}^{-1}$$

and

$$\phi(\nu_x) = 5.44 \pm 0.99 \times 10^6 \text{ cm}^{-2}\text{s}^{-1}.$$

This total is consistent with theoretical expectations ( $5.05 \pm 1.00 \times 10^6 \text{ cm}^{-2}\text{s}^{-1}$ ) [Bahcall *et al.*, Astrophys. J. **555**, 990 (2001)].

SNO is now firmly into the data-taking phase of the experiment, and the need for infrastructure support from TRIUMF is greatly diminished. During the past year only some small parts required for the deployment of one of the calibration sources were fabricated here.

## DRAGON Facility

(*D. Hutcheon, TRIUMF*)

DRAGON (**D**etector of **R**ecoils **A**nd **G**ammas **O**f **N**uclear **R**eactions) is a facility for the study of radiative capture reactions with unstable beams, of interest in nuclear astrophysics. Its principal components are: a windowless gas target; an array of scintillation counters to detect the capture  $\gamma$ -rays; an electromagnetic mass separator to transport the heavy product of the reaction and separate it from the beam; and a detector of the heavy recoil particles.

During 2001 the major components of the separator and gamma array were installed, commissioning measurements carried out using stable beams, and a first experiment run with unstable beam (Expt. 824). The facility demonstrated an ability to detect reactions as rare as one per  $10^{12}$  incident particles in a <sup>21</sup>Na beam. When combined with the intense beams available from ISAC, DRAGON provides capabilities unmatched anywhere else in the world.

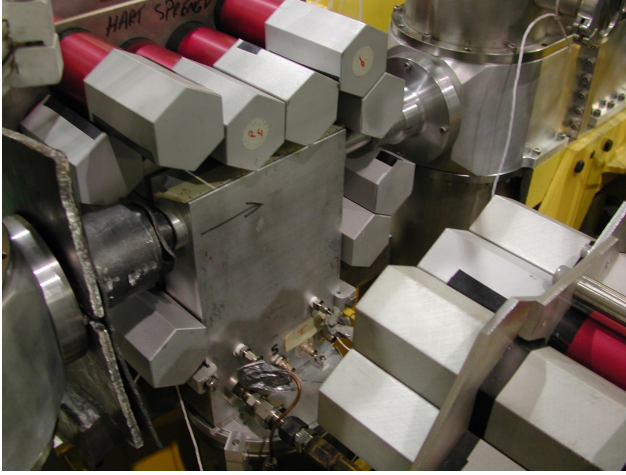


Fig. 124. The DRAGON array of BGO detectors with one half of the array pulled back to show the vacuum box of the gas target.

### Installation

The gamma array consists of 30 hexagonal BGO scintillators, close-packed around the vacuum box of the gas target. The solid angle coverage is  $\approx 80\%$  and the efficiency for detecting a  $\gamma$ -ray in the full-energy peak is calculated to be 45–55%. The 30-fold segmentation was chosen because of the expected background of 511 keV annihilation quanta due to beam-spill at the target – most beams of interest decay by positron emission. The BGO scintillators are mounted horizontally on two frames, each frame mounted on a trolley which can be rolled aside to provide access to the gas target.

The electromagnetic separator, 20 m long, consists of 2 large magnetic dipoles, 2 electrostatic dipoles, 10 quadrupoles, 4 sextupoles and 4 pairs of steering magnets. Faraday cups and X-Y slits are located in diagnostics boxes at 3 focus locations, and beam-centring monitors at 6 additional places. Installation of electromagnetic components was completed and the assembly of the vacuum/diagnostics system took place in stages during the first 8 months of the year. The only significant problem was the inability of a supplier to produce all of the required ceramic insulation tubes for the high-voltage supplies of the electrostatic dipoles, which are intended to run at up to 200 kV; substitute tubes made of nylon were installed on one of the two EDs, and have proven adequate for experiments to date (up to 155 kV). Further details about the installation of diagnostics and the ED units appear in the Engineering section of the Accelerator Technology Division chapter of this Annual Report.

The DRAGON control system is based on EPICS, the ISAC site standard. Through a graphical interface the user has an integrated view of the separator magnets and diagnostic devices (Faraday cups, slits,

beam-centring monitors), and of the pumps, valves and gauges of the gas target and separator vacuum systems.

The recoil ions from the capture reaction were detected at the end of the separator in a double-sided silicon strip detector (DSSSD) located 0.5 m beyond the slits at the final focus. Position resolution of 3 mm was set by the width of the front and back strips. The total area covered by the DSSSD was 48 mm  $\times$  48 mm.

### Gas target profile

The profile of target gas density along the beam direction was measured using the  $\gamma$ -rays from de-excitation of the 4.43 MeV state of  $^{12}\text{C}$ , produced by the  $^{15}\text{N}(p,\alpha)^{12}\text{C}$  reaction. Two arrangements of gamma detection were used. In the first, a partial BGO array, on only one side of the target, measured a resonance yield and calculated its position centroid for different beam energies. In the second method, a single detector was collimated so as to view a short section of the target, at  $90^\circ$  to the beam direction. The beam energy was set to an off-resonance region and yields measured as the collimated detector was scanned parallel to the beam direction.

The measurements showed that most of the gas seen by the beam lay within the central gas cell, but significant amounts of gas were in the target vacuum box and the nearest differential pumping tubes. This does not affect capture experiments with narrow resonances, but complicates the analysis of experiments looking at direct capture or at broad resonances.

### System performance

Strong resonances at 270 keV/u and 762 keV/u in the  $^{21}\text{Ne}(p,\gamma)^{22}\text{Na}$  reaction were a useful tool for studying the performance of DRAGON. The spectrum of  $\gamma$ -rays measured in coincidence with  $^{22}\text{Mg}$  ions from the 762 keV/u resonance is shown in Fig. 125.

Beam suppression by the separator depended strongly on the energy of the beam and on the opening of slits. The beam background came predominantly in a peak at nearly the full beam energy, clearly resolved from the recoil product at higher beam energies. Figures 126 and 127 show the heavy-ion energy spectra in the DSSSD for singles events and in coincidence with a  $\gamma$ -ray, for the 762 keV/u and 260 keV/u resonances. The separator suppression factors were  $4 \times 10^{-10}$  and  $3 \times 10^{-12}$  at 270 and 762 keV/u, respectively. Further suppression can be achieved by cuts on energy, position and timing in the DSSSD, the cuts being most effective at higher beam energies. No beam background was seen in the DSSSD energy spectrum for events with a coincident  $\gamma$ -ray.

The performance of DRAGON with unstable beam reactions is reported in the section on Expt. 824 in this Annual Report.



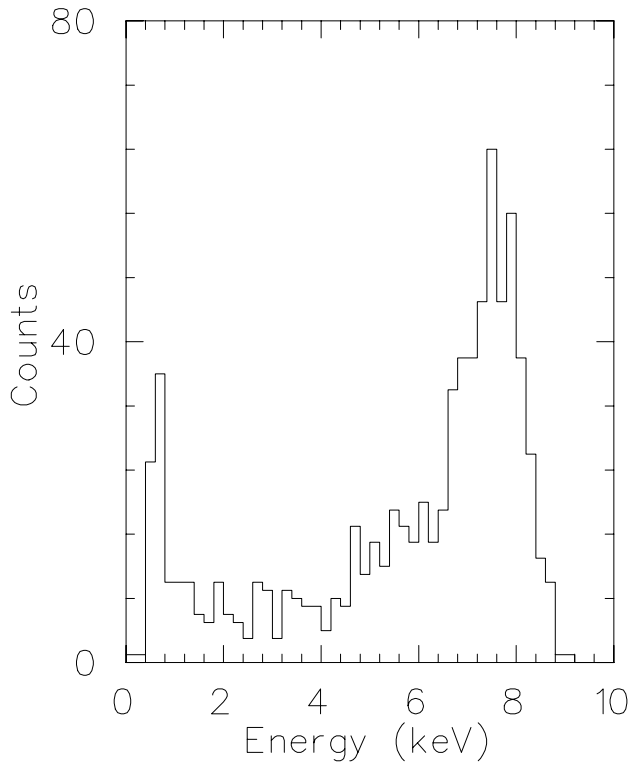


Fig. 125. Response of the BGO array to  $\gamma$ -rays from decay of the state at 7.47 MeV excited by the  $^{21}\text{Ne}(p, \gamma)^{22}\text{Na}$  reaction.

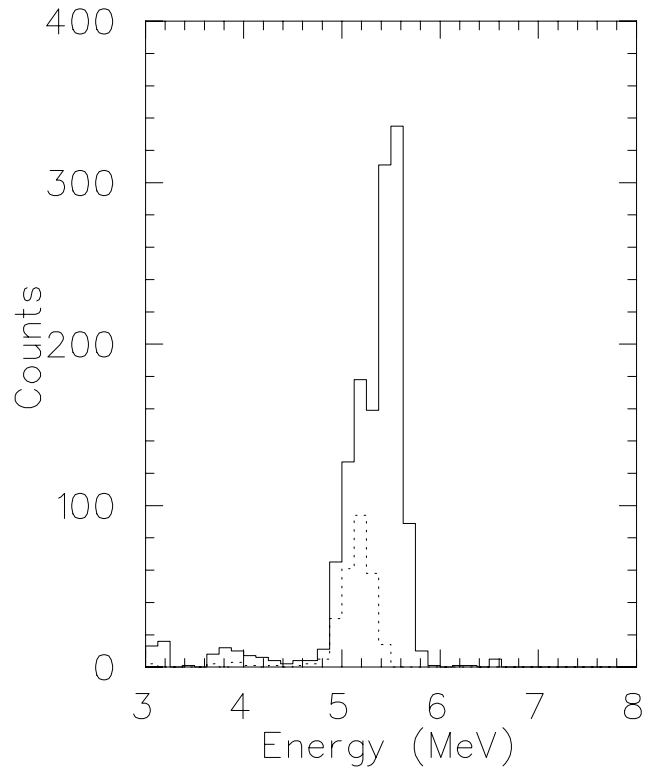


Fig. 127.  $^{22}\text{Na}$  recoils (5.2 MeV peak) and beam background (5.5 MeV) produced by a 265 keV/u  $^{21}\text{Ne}$  beam. The dotted histogram shows recoils in coincidence with capture  $\gamma$ -rays.

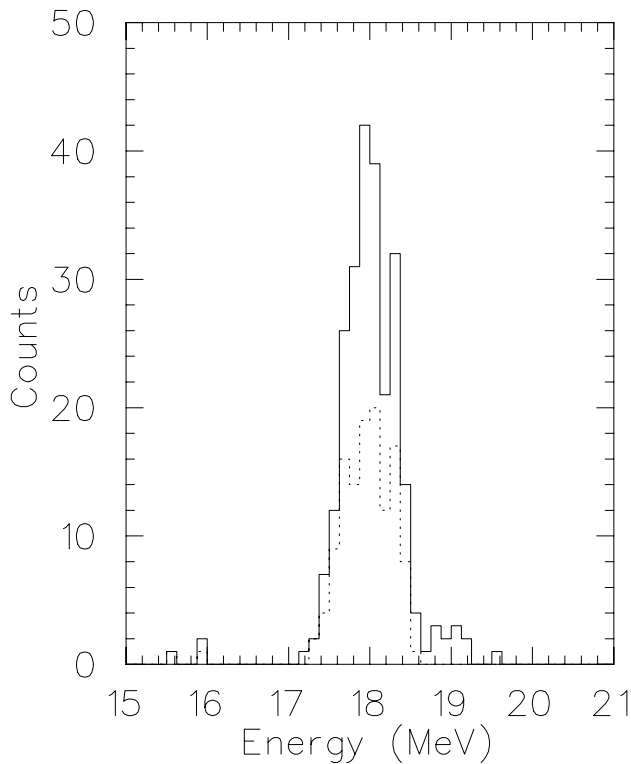


Fig. 126.  $^{22}\text{Na}$  recoils (peak at 18 MeV) and beam background (19 MeV) produced by a 767 keV/u  $^{21}\text{Ne}$  beam. The dotted histogram shows recoils in coincidence with capture  $\gamma$ -rays.

### $8\pi$ Spectrometer

(G. Hackman, TRIUMF)

The 2000 Annual Report reviewed the  $8\pi$  spectrometer, its installation at TRIUMF, and the physics program to be carried out with it. In the year 2001, new mechanical support flanges and hevimet collimators were fabricated, and now all 20 Compton suppression shields and 17 HPGc detectors are installed in the close-packed configuration needed for the beta-decay program (see Figs. 128 and 129). The original signal-processing and acquisition system is now functional. The liquid nitrogen computer-control codes were ported to Linux on a Pentium-based PC, however, hardware conflicts within the PC have delayed final migration to that platform. The beam line was constructed and stable beam was delivered to the target location. For the large solid-angle inner beta array, several prototype fast-plastic scintillator detectors were tested leading to a new barrel-shaped geometry with light pipes.

There are currently three approved experiments using the  $8\pi$  spectrometer: “Isospin symmetry breaking in superallowed Fermi beta decays” (Expt. 909, C.E. Svensson), “High-K isomers in neutron-rich  $A = 170$  to 190 nuclei” (Expt. 921, P.M. Walker, spokesperson),

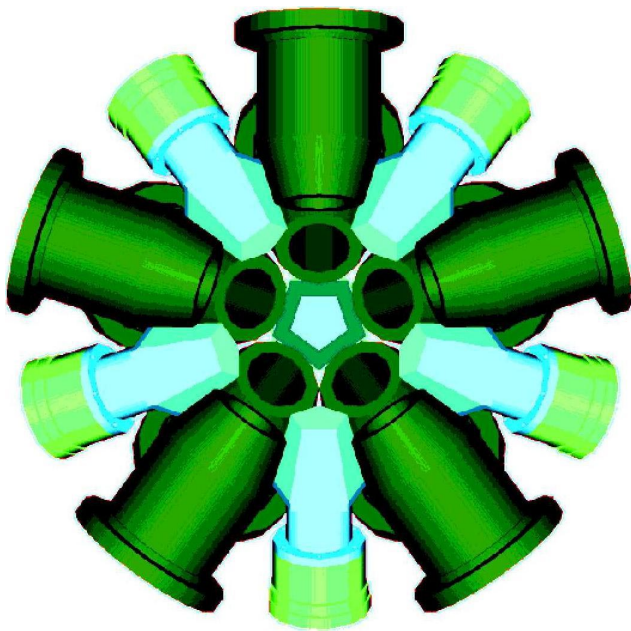


Fig. 128. Model of the close-packed  $8\pi$  configuration.

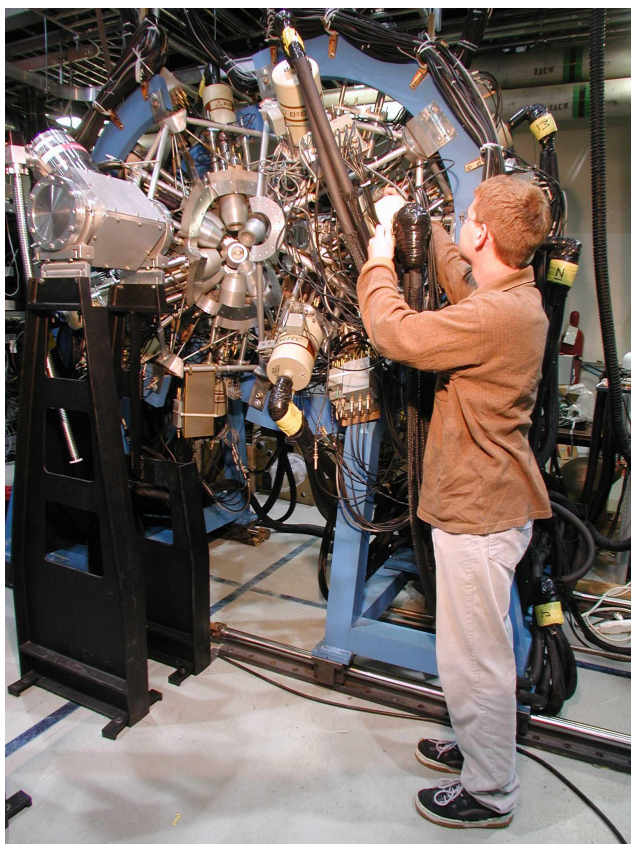


Fig. 129. Photograph of the  $8\pi$  as of August, 2001.

“Octupole deformation and spin-exchange polarization of odd- $A$  radon isotopes: toward radon electric dipole moment measurements” (Expt. 929, C.E. Svensson and T.E. Chupp). The latter two were approved at the

December, 2001 EEC meeting, where a letter of intent on the spectroscopy of neutron-rich  $A \sim 90$  nuclei (G. Hackman) was also considered. To handle the event rates and obtain the precision needed for these experiments, the data acquisition system will be upgraded with FERA ADCs and bit registers and a high-precision 10 MHz clock.

Of the 19 collaborators who actively participated in reassembling the  $8\pi$  spectrometer and designing the inner beta-detector array in 2001, eight were students and seven were from six foreign institutions: G.C. Ball, G. Hackman, P. Bricault, J. McDonald (TRIUMF), C.E. Svensson, A. Phillips, E. Vandervoort (U. Guelph), J.C. Waddington, R.A.E. Austin, G. Grinyer, P. Klages (McMaster U.), L. Stern (U. Victoria), J.L. Wood, D. Kulp (Georgia Tech. U.), E. Zganjar (Louisiana State U.), D. Hodgson (U. Surrey), P.E. Garrett (LLNL), D. Ward (LBNL), D.C. Radford (ORNL).

In addition to preparing the  $8\pi$  for ISAC-I experiments, members of this collaboration prepared an NSERC major equipment grant request for a large “clover” detector as a prototype for TIGRESS, which will be a multi-detector Compton-suppressed HPGe array optimized ultimately for ISAC-II.

#### Low Temperature Nuclear Orientation at ISAC (P. Delheij, TRIUMF)

The LTNO set-up is a facility to orient nuclei from the radioactive ion beam source TRIUMF-ISAC. In the past year considerable effort was devoted to arrive at NMRON measurements: the resonant change of the polarization as the frequency of the applied rf field is scanned through the Larmor frequency. Off-line sources of  $^{60}\text{CoFe}$  and  $^{54}\text{MnNi}$  were fabricated in a reducing atmosphere of an argon/hydrogen mixture with a composition of 98/2. To check for possible (magnetic) contamination, some Fe foils were examined at SFU Physics by B. Heinrich and K. Myrtle in their auger electron spectrometer. This device provides the option to clean the surface by sputtering with an Ar beam. It was found that the foils were covered by a layer of carbon and oxygen with a thickness of approximately 5 nm. After removing this layer with the Ar ion beam an exposure of 3 minutes to ambient atmosphere restored this layer with a thickness that was very close to the original value.

In Fig. 130 the NMRON results are shown for  $^{60}\text{CoFe}$ . The off-resonance intensity in the direction parallel to the orientation axis is reduced by 44% due to the polarization of the  $^{60}\text{Co}$  at a temperature of 11 mK. Therefore, an intensity increase is observed when (partial) destruction of the polarization takes place if the frequency of the applied rf field equals the Larmor frequency. External magnetic fields of 2 kG and

### NMRON Pol. destruction for $^{60}\text{Co}$ in Fe

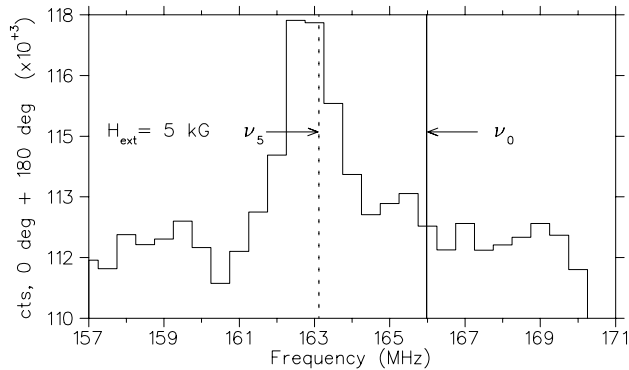
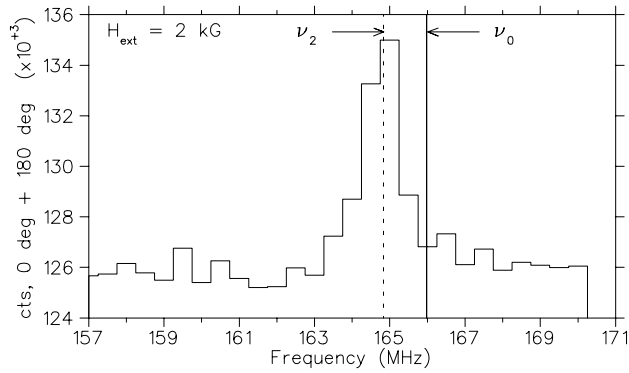


Fig. 130. Shown are two rf scans in an external magnetic field of 2 kG and 5 kG. The experimental data are in good agreement with the expected resonance frequencies  $\nu_2$  and  $\nu_5$ .

5 kG cause shifts  $\nu_2$  and  $\nu_5$  respectively away from  $\nu_0$  [165.957(5) MHz, Hagn and Eska in Proc. III Int. Conf. on Hyperfine Interactions, Karlsson and Wappling, eds. (Uppsala, 1974) p. 148], the Larmor frequency in zero external field. It should be noted that the resonance frequency is lowered because the hyperfine field is negative.

Approval for Expt. 893 was obtained, an experiment to resolve the discrepancy between the experimental result [ $+54 \pm 10$  kG, Allsop *et al.*, Hyp. Int. **15/16**, 313 (1983)] and the theoretical value [ $-261$  kG, Cottenier and Haas, Phys. Rev. **B62**, 461 (2000)] for the hyperfine field of Rb in Fe. The data that are shown in Fig. 131 demonstrate that substantial anisotropies can be obtained for the gamma emission in the decay of  $^{79}\text{Rb}$ . By a judicious choice of gamma line intensity ratios (i.e. 688 keV/622 keV and 161 keV/155 keV), polarization effects up to 0.2 have been measured. Taking these ratios provides an internal normalization for beam intensity fluctuations. Furthermore, they are insensitive to beam motion effects. Part of the  $\gamma$ -rays

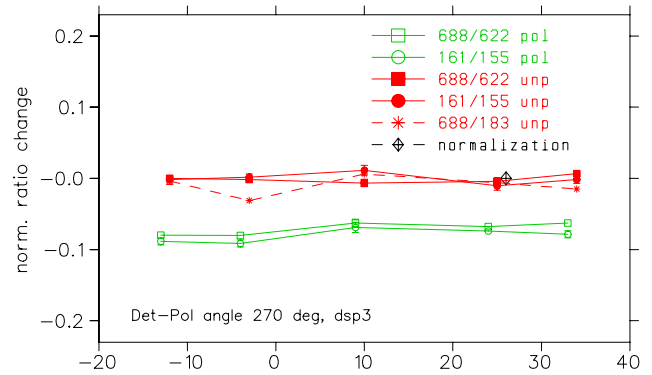
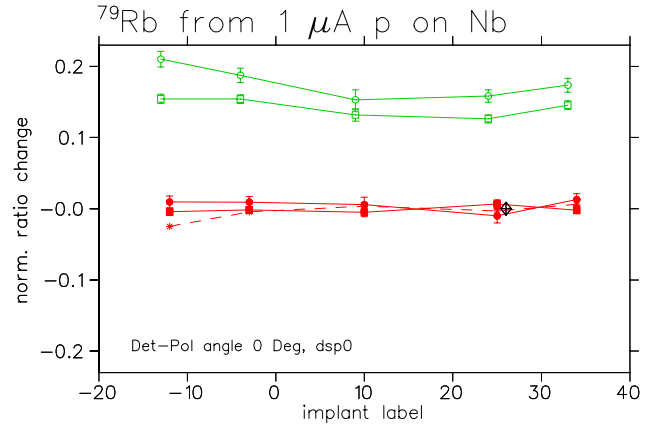


Fig. 131. The polarization effects in the gamma transitions following the decay of  $^{79}\text{Rb}$  are plotted versus time.

that reach the detectors are transmitted through the copper cold finger. The transmission varies with  $\gamma$ -ray energy. Selection of gamma transitions that are close in energy, 688–622 and 161–150, minimizes this possible error source. Conversely, selecting a large energy difference, 688–183, provides a check on the stability of the beam position over time. The last intensity ratio changes by 60% if the transmission length through the copper changes by 5 mm. Only about half the  $\gamma$ -rays are filtered in this way. Therefore, a maximum deviation in the ratio of 4% indicates that the beam spot movement is less than 0.7 mm.

The polarization results for  $^{75}\text{Ga}$  at LTNO are described by P. Mantica under Expt. 863 in this Annual Report.

Collaborators on the LTNO are: P.P.J. Delheij, C.A. Davis, TRIUMF; B. Turrell, J. Pond, R. Kiefl, Univ. of British Columbia; K.S. Krane, P. Schmelzenbach, J. Loats, C. Stapels, Oregon State University; J. Wood, D. Kulp, Georgia Institute of Technology; P. Mantica, A.C. Morton, A.D. Davies, D. Groh, Michigan State University; H. Haas, Hahn Meitner Inst.; S. Cottenier, K.U. Leuven.

## CYCLOTRON OPERATIONS DIVISION

### INTRODUCTION

The good performance achieved during year 2000 in terms of cyclotron availability and beam production was maintained during 2001, with 92.4% availability for scheduled cyclotron hours and 95% for scheduled BL1A beam charge. The recently installed beam line 2A and 2A extraction probe were very reliable, and did not cause significant downtime for ISAC. While the 2A maximum operating proton beam current was gradually increased to 40  $\mu\text{A}$ , attention had to be paid toward reducing the occurrence of 2A beam spill monitor trips caused by occasional beam deviations, related to sudden beam energy variations at extraction, produced by beam instabilities at cyclotron injection. Extracting the 2A beam in the shadow of the 1A stripping foil helped reduce the amplitude of these transverse beam perturbations. In addition, increasing the horizontal aperture of two protect monitors down 2A increased the energy acceptance of the beam line, making its protection systems less sensitive to small energy instabilities. The facility which experienced most problems was beam line 2C4, for the production of  $^{82}\text{Sr}$ . Most problems originated from the fact that after the winter 2001 shutdown maintenance, the solid target facility (STF) could not be properly realigned. The entrance channel defining the beam acceptance was found rotated horizontally by 20 mrad. To avoid the lengthy realignment work of the STF in the cyclotron vault and the corresponding high dose exposure, it was decided to redirect the incident proton beam with the help of a newly installed powerful steering magnet, so it would match the rotated target channel acceptance. Installation and adjustment of the new magnet could be performed during shutdown or maintenance periods.

Toward year-end, high intensity beam delivery was hampered by water leaks and became very unpredictable to say the least. A small water leak in the quadrupole triplet downstream of T2 increased gradually during the fall. The rather complex intervention on this leak could have taken place only during a major shutdown. It was therefore decided to operate with the increased leak rate up to the point where reduced water cooling could have jeopardized the integrity of quadrupole coils. The danger limit for thermal damage was reached right at the end of the high intensity schedule, not causing, therefore, interruptions to the high intensity beam production. The triplet water leak triggered a shift in site priorities. Part of the planned T2 area refurbishing was actually scheduled for the 2002 winter shutdown. In addition to the triplet repair, it became necessary to proceed with the removal of the

obsolete M8 secondary beam line and with the installation of the new shielding configuration around M8 and triplet to prepare for the future triplet replacement. The design work for the reconfiguration of the area had actually been brought ahead during 2001, so that most of the new shielding blocks (concrete and iron) could actually be manufactured and procured before year-end.

No cyclotron developments had been budgeted for during the 1995–2000 five year plan and all cyclotron accelerator resources not immediately required for operations or maintenance were assigned to ISAC projects. One important exception, however, came as a byproduct of work on ISAC rf cavities and could go ahead since it did not require significant funding or manpower resources. This is a reliably operating 4th harmonic rf booster cavity. The booster had been conceived and prototyped during KAON studies, but had never been operated reliably because of an inadequate rf coupler. The coupler problem was solved and reliable operation of the booster could start. The cavity would provide two important features: (1) it would allow the reduction by about a factor of two of the time length of a single rf beam pulse, to about 2 ns (as requested by the CHAOS experiment); (2) it would also allow the reduction of the  $\text{H}^-$  beam electromagnetic stripping losses by about 30% because of the two-fold increase in energy gain per turn at high cyclotron beam energies. This would allow the total extracted current to be increased in future from  $\sim 200 \mu\text{A}$  to  $300 \mu\text{A}$  without increasing total beam losses or cyclotron activation beyond levels previously reached at  $200 \mu\text{A}$  without booster operation.

With the new five year plan, which started in April, 2000, the drastic policy of not allowing developments and improvements to the cyclotron was modified. Developments in the direction of an increase of the total intensity of the cyclotron beam were authorized. Development beam shifts were scheduled again and a beam physicist was assigned to cyclotron beam studies. The  $300 \mu\text{A}$  goal, which will allow us to satisfy ISAC beam requirements without reducing the beam intensity delivered to present users, was given priority. A  $250 \mu\text{A}$  intermediate step was given higher priority in order to satisfy immediate ISAC requirements. By year-end a tune of  $250 \mu\text{A}$  peak had been achieved in a  $\sim 50\%$  duty cyclotron mode with  $>60\%$  cyclotron acceptance. A  $300 \mu\text{A}$  peak had also been achieved at 50% duty cycle, but only with 50% acceptance. An analysis of beam losses through the cyclotron showed that, for the  $300 \mu\text{A}$  beam, a significant loss of intensity occurred in the cyclotron centre region around the

second or third turn. Electrode overheating was also localized to the first quarter turn after injection. The insertion of a water cooled beam scraper to protect the overheating electrodes, together with a close inspection of the centre region at the second or third turn radius, were planned for the coming winter shutdown.

A cyclotron refurbishing program, started in April, 2000, continued in 2001 as planned in the current five year plan. A major accomplishment was the overhaul of the vault section of BL1A and the radiation hardening, or rearrangement to locations not directly exposed to cyclotron radiation, of electric cables, water hoses, and other non-radiation-hard components. Another major undertaking was the replacement, before year-end, of three large distribution power transformers (1250 kVA, 1250 kVA, and 750 kVA) after it was determined that the quality of the insulation had diminished below acceptable standards. The Ascarel insulating oil (PCB) was an environmental risk in case of failures, earthquake, or fire damage. The replacement of the transformers with new environment-friendly units was flawless and occurred during the Christmas break week, causing minimum disruption to the laboratory.

Another completed refurbishing initiative was the procurement and installation of eight new regenerators in the two 20 K B20 cryosystems serving the cyclotron tank cryopanel. New compressors were also installed in several injection line cryopumps. Modifications were introduced in the cyclotron high energy probes and in beam line monitors for reliable operation. In the central control system, obsolete or inefficient components were replaced with recent upgraded technology. A new waster load and refurbished combiners were produced for the main rf amplifier system. New reliable polarity switches were installed for some of the beam line power supplies.

Refurbishing work will continue over the remaining three years of the five year plan. High priority items include: (1) completion of the work in BL1A extension between T2 and TNF with the installation of the new replacement triplet; (2) refurbishing of the BL2C4 isotope production station; (3) replacement of the vacuum control system; and (4) replacement of the control system for resonator tip tuning and completion of the rf amplifier refurbishing. High priority should also be given to the area around the T1 target including the replacement of the M11 septum magnet.

The first two years of the plan have been addressing very urgent requirements. In a few cases they were very timely indeed. It is essential that the priority for cyclotron refurbishing be enhanced and maintained at a high level.

## BEAM PRODUCTION

Beam delivery for 2001 was quite successful with production very similar to the previous year. Cyclotron performance continued to be enhanced by the use of the rf booster which was on during most of the high current running, partly to satisfy the occasional demand for 2 ns pulse-width beam but also to improve the cyclotron transmission (typically between 60% and 65%) and reduce the tank beam spill. Eighteen weeks of shutdown left 5075 hours scheduled for beam operation. The cyclotron was actually available for 4680 hours, with an above average availability of 92.4%. Totals include 230 hours for development and tuning and, as shown in Fig. 132, were split roughly 10:1 between high current beam production and low intensity operation, namely the proton irradiation facility (PIF) production in 1B/2C1. As Fig. 133 shows, the total beam charge delivered to meson hall experiments along BL1A was 481 mA h or 95% of that scheduled, one of the better results for the past ten years, although the total charge was lower than some years because of current limitations while using graphite targets at 1AT1. In addition to the BL1A charge, there were 84 mA h delivered at 85 MeV to the solid target facility (STF) in beam line 2C4 for the production of radiopharmaceutical generators, as well as 37 mA h, triple the previous year's charge, to the west target station in BL2A2 for the production of radioactive ion beams (RIB) in ISAC. A maximum total of 210  $\mu$ A was extracted down the three operating proton lines. Seven patients were treated for ocular melanoma during four proton therapy (PT) sessions in beam line 2C1 operated at 74 MeV. The annual downtime of 372 hours (Fig. 134) was well below average with the rf, as usual, responsible for the greatest share of this time (48%) followed by power failures (14%) and power supply problems (9%). The operational record and beam to experiments for the year 2001 are given in Tables XV and XVI.

### Winter Shutdown

Cyclotron shutdown activities began early in January. The extent and complexity of some of the tasks, especially those in high radiation fields, as well as competing demands for key personnel in other areas, contributed to a revision of the original shutdown schedule, extending it about two weeks in order to achieve the desired goals.

In the cyclotron vault a long-anticipated electrical and cooling services upgrade to the front end of BL1 took place with modifications to the combination magnet (CM1), the first three quadrupole magnets (1VQ1, Q2 and Q3) and the dipole magnet (1VB1). In order to minimize dose exposure from residual activation, work

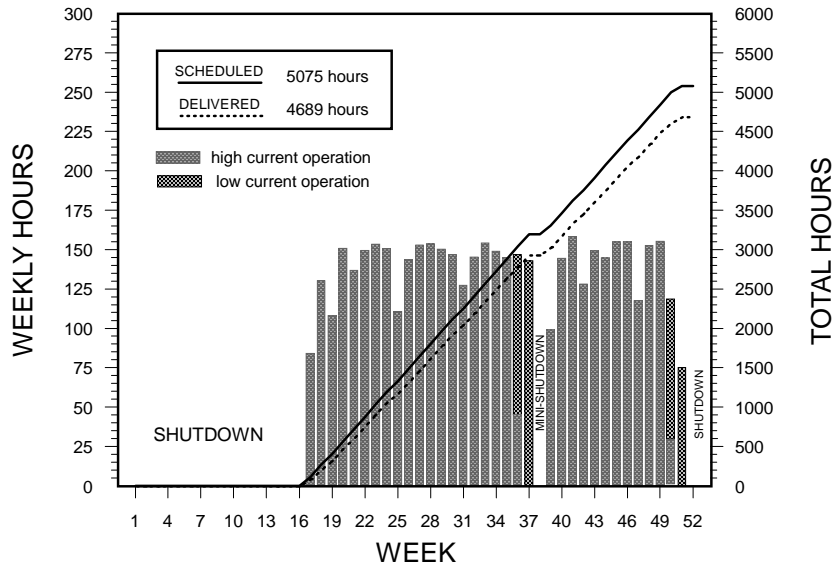


Fig. 132. Operational hours for 2001.

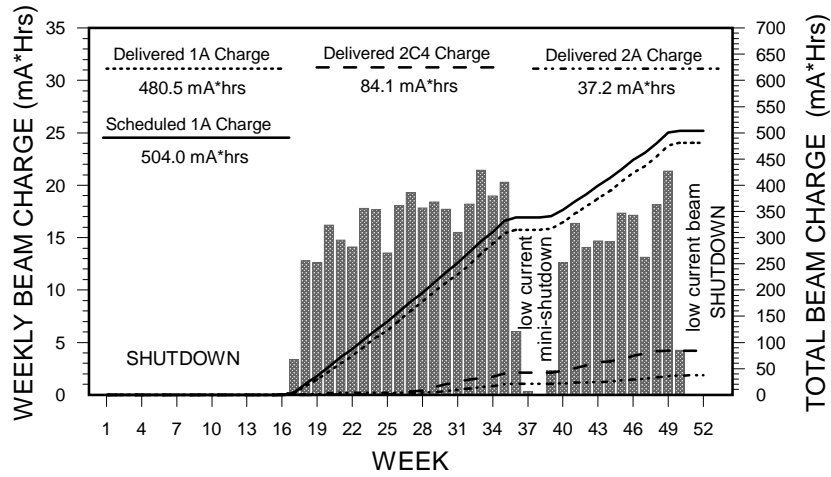


Fig. 133. Beam delivery for 2001.

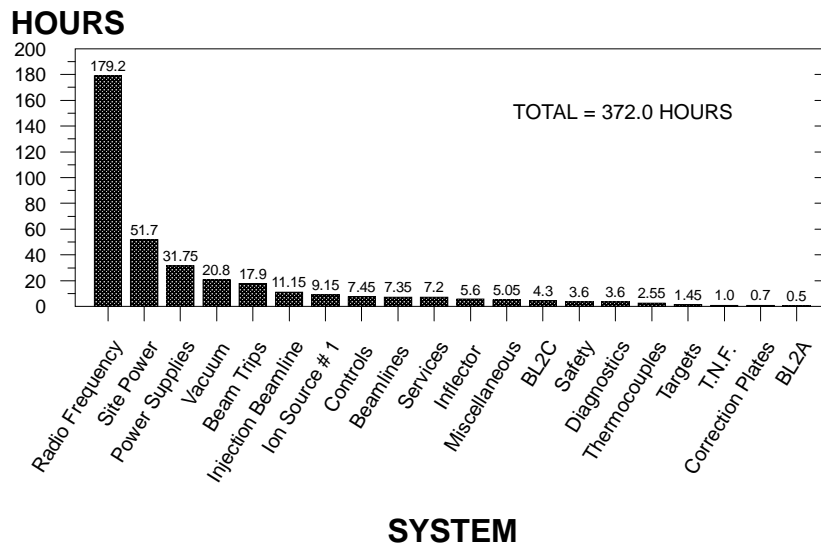


Fig. 134. Cyclotron downtime for 2001.

Table XV. Operational record for 2001.

	Scheduled hours			Actual hours		
<u>Cyclotron off:</u>						
Maintenance	391.0			414.80		
Startup	221.0			172.40		
Shutdown	3028.5			3027.00		
Other	0.0			6.50		
Cyclotron downtime	0.0			372.00		
Overhead	20.5			54.35		
Totals	3661.0			4047.05		
<u>Cyclotron on:</u>						
Development	146.0	+	0.0 P*	136.45	+	0.00 P
Cyclotron tuning	278.5	+	0.0 P	94.05	+	0.00 P
Beam to experiments	4650.5	+	0.0 P	4458.45	+	0.00 P
Totals	5075.0	+	0.0 P	4688.95	+	0.00 P
Actual/Scheduled = 4688.95/5075.0 = 92.4% availability						
<u>Beam to experiments:</u>						
1A Production	4245.5	+	0.0 P	4052.35	+	0.00 P
1A Development/tuning	4.0	+	0.0 P	7.65	+	0.00 P
1A Down/open/no user	147.0	+	0.0 P	178.85	+	0.00 P
1B Production	242.0	+	0.0 P	36.00	+	0.00 P
1B Development/tuning	0.0	+	0.0 P	4.40	+	0.00 P
1B Down/open/no user	12.0	+	0.0 P	179.20	+	0.00 P
Total 1A+1B production	4487.5	+	0.0 P	4088.35	+	0.00 P
2A2 Production	3356.5	+	0.0 P	2706.20	+	0.00 P
2A2 Development/tuning	0.0	+	0.0 P	14.70	+	0.00 P
2A2 Down/open/no user	1294.0	+	0.0 P	1737.55	+	0.00 P
2C1 Production/tests	648.0	+	0.0 P	148.45	+	0.00 P
2C1 Development/tuning	0.0	+	0.0 P	2.15	+	0.00 P
2C1 Down/open/no user	783.0	+	0.0 P	1146.90	+	0.00 P
2C4 Production+tests	3215.5	+	0.0 P	1947.55	+	0.00 P
2C4 Development/tuning	0.0	+	0.0 P	128.75	+	0.00 P
2C4 Down/open/no user	4.0	+	0.0 P	1084.65	+	0.00 P
1A Beam charge	503,957		$\mu\text{A h}$	480,546		$\mu\text{A h}$
2A Beam charge	45,111		$\mu\text{A h}$	37,172		$\mu\text{A h}$
2C4 Beam charge	153,750		$\mu\text{A h}$	84,117		$\mu\text{A h}$

P = Polarized source on-line (although not necessarily polarized beam)

\*There was no BL4 production this year; nor was the POL (I4) source used.

Table XVI. Beam to experiments for 2001.

Experiment *	Channel	Schedule#	Scheduled		Delivered	
			h	$\mu\text{A h}$	h	$\mu\text{A h}$
334	M9B	99	208.0	27040	204.60	24978
614	M13	99	746.0	104210	718.70	100351
614	M13	100	1547.0	165847	1485.70	164545
677	M20B	100	123.0	17220	124.80	17702
744	M9A	100	700.0	79775	693.95	78483
746	M15	100	150.0	19550	154.20	19950
751	M15	99	150.0	21230	144.50	18513
768	M15	99	277.0	24920	244.65	21916
775	M20B	99	150.0	8640	119.15	6653
775	M20B	100	146.0	16790	136.55	15603
777	M15	99	92.0	11040	89.45	9912
777	M20B	99	150.0	19500	153.10	19349
782	M15	99	150.0	19500	153.10	19349
783	M15	99	150.0	19500	124.15	15602
784	M20B	99	150.0	21000	150.20	22300
791	M15	99	119.0	14930	102.50	11768
791	M20B	99	127.0	15240	129.45	14958
791	M15	100	128.0	14195	136.25	15028
804	M20B	99	150.0	18000	147.45	16250
804	M15	100	69.0	7935	69.55	7805
822	M15	100	150.0	16500	135.60	14893
833	M9B	99	273.0	38220	257.75	36652
833	M9B	100	150.0	19550	154.20	19950
834	M20B	99	300.0	39000	299.25	36915
842	M9B	99	173.0	23990	167.60	21334
842	M9B	100	146.0	16790	136.55	15603
846	M20B	99	300.0	36000	298.20	34671
846	M20B	100	127.0	14605	122.85	14412
847	M20B	99	300.0	42230	287.65	38578
848	M20B	99	127.0	16510	129.90	16330
848	M20B	100	150.0	15230	156.10	16176
851	M20B	99	127.0	16280	125.50	15263
852	M15	99	150.0	19500	149.80	18553
852	M15	100	277.0	17717	219.80	17262
860	M20B	99	119.0	14930	102.50	11768
862	M11	99	1122.0	125870	1039.15	111848
865	M15	100	81.0	9315	84.55	9555
868	M15	99	150.0	21000	133.95	18573
868	M20B	99	150.0	21000	133.95	18573
869	M9A	99	694.5	74630	611.50	62219
876	M20B	99	123.0	17220	123.80	18079
877	M9B	99	150.0	21000	150.20	22300
878	M9B	99	150.0	21000	143.15	20065
881	M15	99	150.0	18000	145.40	16821
881	M15	100	150.0	15230	156.10	16176
883	M20B	99	150.0	19500	124.15	15602



Table XVI (cont'd.)

Experiment *	Channel	Schedule#	Scheduled		Delivered	
			h	$\mu\text{A h}$	h	$\mu\text{A h}$
883	M15	100	146.0	16790	145.45	16159
884	M15	99	127.0	15240	113.75	12684
885	M15	99	150.0	21000	143.15	20065
889	M15	99	150.0	19500	149.45	18362
890	M15	99	127.0	16510	129.90	16330
891	M15	99	277.0	33240	282.25	32808
894	M20B	99	148.5	17820	128.65	14864
894	M20B	100	277.0	17717	219.80	17262
895	M15	99	273.0	38220	274.00	40379
896	M15	99	148.5	17820	128.65	14864
896	M20B	99	127.0	15240	113.75	12684
898	M20B	100	150.0	16500	135.60	14893
911	M11	100	135.0	18900	136.50	19339
912	M20B	100	150.0	19550	154.20	19550
915	M15	100	127.0	14605	122.85	14412
916	M20B	100	128.0	14195	136.25	15028
917	M20B	100	296.0	34040	299.55	33519
918	M15	100	146.0	16790	136.55	15603
DEV	M15	99	58.0	6960	58.00	6338
HallD	M11	99	300.0	42230	278.45	37086
HiTime	M15	100	123.0	17220	124.80	17702
ISAC RIB†	2A2	99,100	3356.5	45111	2706.20	37172
ISOPROD	2C4	99,100	3215.5	153750	1947.55	84117
M11test	M11	100	127.0	14605	115.55	13122
PIF	2C1	99,100	569.0	0	128.95	0
PIF	1B	99,100	242.0	0	36.00	0
P.THERAPY	2C1	99,100	79.0	0	19.50	0

\* See Appendix D for experiment title and spokesman.

† Total proton beam on target for all ISAC RIB experiments and tests.

started with the cyclotron lid down and began with the removal of the BL1V shielding to more freely access and remove beam line components for refurbishing. Shielding blocks were used to construct a bunker in the vault basement to provide a workplace for individual quadrupole upgrades. This work was done and the quads were reinstalled after the tricky CM1 upgrade was completed *in situ*. Buckling up the beam pipe's vacuum joints was delayed when measurements indicated a 2 mm horizontal displacement of the quads with respect to their initially measured positions. This may have resulted from a relatively strong earthquake on February 28. Alignment was brought back to tolerance by pushing the beam line platform slightly with the help of a bracing structure and jack.

Another vault job was the removal of the STF in BL2C4 to attempt repairing the target position limit switches. This was attempted at the end of the shutdown and resulted in some dose exposure because of the fiddly nature of the work.

Shutdown lid-up work was scheduled in two batches to fit in with BL1V upgrade work requirements. The Probes-Diagnostics group serviced the BL2C, BL1 and BL2A extraction probes (the latter equipped with a modified L-arm to hold nine disposable foils); upgraded the HE1 probe trolley and replaced the vertical drive ferrofluidic feedthroughs on both HE1 (because it failed) and HE2 (preventative). The group worked with the Alignment group to measure probe positions to verify proper indexing. The Engineering Physics group

removed the inflector for servicing and found some noticeable play in and misalignment of the deflector electrodes as well as a smaller but measurable misalignment of the inflector electrodes that was thought to account for the tuning anomalies of the previous running period. Further centre region work included correction plate inspections and continuity checks as well as rf surface cleaning in a small area roughened by sparking.

The third main area of activity was in the meson hall where shielding blocks were shuffled to complete a number of MRO tasks including 1AT1 and 1AT2 water package servicing; M9 T2 beam blocker rebuild; monitor work (1AM9's leaking gas package repaired and 1AM8 rebuilt); O-ring and active system water filter changes as well as work on the M11 and M13 beam blockers. The 1AQ11 vacuum leak at its downstream indium seal was repaired. Its platform was realigned after being discovered out of position a few mm high and south. Leak checking was done in M11 to find a large leak near M11B2 that was subsequently repaired. After a lengthy battle with water leaks, a rebuilt M9A rf separator was installed.

There was much more work done by many other groups; listed above are mostly jobs undertaken in high dose exposure areas. Because of the long shutdown and the number of such jobs, a few workers had to get permission to exceed their 30-day and/or quarterly sliding dose guidelines. No one exceeded any regulatory limits. The final total shutdown dose was 130 mSv distributed among 102 workers.

### Beam Schedule 99

Startup was delayed a few days to repair the HE1 ferrofluidic feedthrough which failed (air leak) after the main magnet was turned on. Once tuning started it was confirmed that the realignment of the BL1 vault quads and of the 1AQ10-11 doublet was adequate. Although the first two weeks of production saw quite a lot of rf downtime with a variety of IPA problems, beam delivery improved considerably after this was sorted out and the performance for schedule 99 was quite good with a cyclotron availability of 92% and a BL1A charge delivery of 315 mA h or just over 93% of that scheduled. As mentioned above, the BL1A currents were lower than usual due to the use of graphite targets at 1AT1 as requested by Expt. 614 (TWIST) in M13. The second such target held up very well, being removed after 170 mA h and 11 weeks with currents ranging up to 130  $\mu$ A, whereas the first one lasted only nine days and 25 mA h at currents below 120  $\mu$ A before falling apart. BL1A currents were raised as high as 150  $\mu$ A for the remaining month of the high intensity portion of the schedule with a Be target at 1AT1. After one development shift's further exploration of some earlier probe

position measurements, the 1A energy was reduced by about 7 MeV to correspond to 500 MeV. BL1A had little downtime itself although it was home to a couple of steadily increasing water leaks. One of these was located at the M11 header in the 1A tunnel and it was temporarily patched until proper repairs could be made during the September mini-shutdown. Another leak that grew quickly during August was identified as originating somewhere in the 1AQ14-15-16 (triplet) cooling circuit.

In addition to BL1A's charge, BL2C4 received 43 mA h, less than half of its scheduled charge, primarily due to problems arising from a misaligned STF when it was reinstalled. The resulting kink in the line made tuning impossible until a corrective steering magnet was added and commissioned towards the end of June. After this intervention the line received about 75% of the remaining scheduled (55 mA h) charge. A few trips resulted from running the new steering magnet too close to its thermal limit and plans were made to replace it with a water-cooled one during the September mini-shutdown.

BL2A2 fared somewhat better, receiving 80% of its total scheduled 26 mA h at currents of up to 40  $\mu$ A. Startup with the niobium target was plagued by excessive sparking in the ISAC west target station and only 60% of the charge scheduled for that target was delivered before production ended in late May to switch to a tantalum target. With the new target, BL2A received 87% of its scheduled 20 mA h charge before stopping in week 36 for the next target change (to SiC). For a while there was a bothersome number of spurious 2A tunnel radiation trips until, during a beam development shift, it was shown that the frequency of these trips could be substantially reduced by extracting in the shadow of the extraction 1 stripper which would reduce stray high energy beam bursts.

BL2C1 was used at 74 MeV for three separate proton therapy (PT) sessions during which a total of six patients were treated. This line was also used at energies of 70 and 116 MeV and currents of a few nanoamps to irradiate objects in the proton irradiation facility (PIF). Two weeks of low current (BL2C1 and BL1B) operation were scheduled at the end of the high intensity period to allow the cyclotron fields to decay prior to the September mini-shutdown. PT went well but subsequent production was pretty spotty as many of the scheduled PIF users cancelled because of travel problems in the wake of September 11.

Scheduled development shifts focused primarily on higher current in order to achieve the higher total extracted currents required when ISAC runs full steam, with particular attention to both tune reproducibility and centre region effects. In these shifts, 300  $\mu$ A equiv-

alent was attained with up to 170  $\mu\text{A}$  run down BL1A albeit with machine acceptance seemingly limited to 50% instead of the normal 60%. Some time was also allotted for OPS training during which shift operators had time to practice machine and beam line tuning and calibrations or assist with development work.

### Fall Mini-Shutdown

This week of extended maintenance started two days early after the PIF run finished prematurely. There was no plan or need to raise the cyclotron lid; the main jobs included routine diagnostic, beam line, vacuum, targets and plant MRO. As well, the 2C4 corrective steering magnet was replaced with a water-cooled one and the failure-prone M13 beam blocker was repaired again. Individual doses received ranged up to 0.77 mSv and totalled around 3 mSv for these jobs. Measurements of copper active low conductivity water (Cu ALCW) system loss rates confirmed increases in the leaks at the 1A downstream triplet and M20Q1. After a careful evaluation of the problem, upcoming repair was deferred to the winter shutdown. Cyclotron systems were started up on time to meet the demands of the following beam schedule.

### Beam Schedule 100

Cyclotron performance was somewhat better for these 13 weeks with an availability of 93% and a delivered 1A charge of 166 mA h or 100% of that scheduled, typically at currents of 120  $\mu\text{A}$  (with carbon targets at 1AT1) but including a couple of weeks at 140  $\mu\text{A}$  when Be targets were requested. Cyclotron downtime was just under 10 hours per week, quite reasonable considering it included 30 hours of power outage and recovery resulting from a wind storm during a PIF run at the end of the beam schedule. The rf booster was off for a few weeks in the middle of the high intensity period because of PA problems; otherwise it was on to help the cyclotron run more efficiently.

By far the most troublesome aspect of the 1A operation was the growing Cu ALCW system leak, presumably due to a worsening of the 1A triplet leak. This approached critical levels with respect to possible overheating of the quadrupole coils, causing some anxiety as well as localized flooding and ground fault trips on the associated power supplies before the water was finally able to be turned off at the beginning of the low current portion of the schedule. Tests at that time confirmed that the triplet leak had grown to 45 or 50 litres per hour while leaks at M20B1 (new, 20 l/h) and M20Q1 (5 l/h) accounted for most of the remaining measured losses from the Cu ALCW system. Because of these leaks the triplet repair, the removal of the M8 front end elements and the replacement of some of that

area's metal and concrete shielding were given higher priority for the winter shutdown.

In addition to the BL1A charge, there were 41.5 mA h delivered (82%) to the STF in BL2C4 which ran reasonably well with the water-cooled corrective steering magnet. Towards the end of the schedule, there were tuning problems which were ultimately attributed to a worn stripping foil and although this reduced the beam intensity, it did not significantly compromise the total charge required for the two rubidium targets irradiated for processing at MDS Nordion.

The completion of the final 2A2 target change (to SiC) lasted a few days longer than anticipated. The beam line ran quite successfully at currents ranging from 5 to 15  $\mu\text{A}$  to provide various ISAC experiments with nearly 16 mA h of incident beam or 85% of that scheduled. BL2A2 beam delivery continued during the last two weeks of the schedule in parallel with PT and PIF.

BL2C1 (at 74 MeV) was used for a proton therapy session with one patient treated. As for all of the other PT sessions this year, the high intensity source was on-line, so the ISIS pepperpot was required to limit the injected beam current during patient treatment; BL2C1 was also used as a lower energy complement to PIF operation at 200, 350 and 500 MeV in BL1B. Samples were irradiated with currents of 1 nA or less. Because of heavy user demand and a significant loss of time due to power failures, 2C1 operation (at 70 and 116 MeV) and 1B operation ran simultaneously in the common experimental area, creating, at times, a rather hectic pace; but everything was completed on time.

A couple of development shifts during this period again involved centre region studies for injection at higher current. Scans were done with low energy probes to analyze differences between a 250  $\mu\text{A}$  equivalent tune with 62% cyclotron beam acceptance (obtained by empirically extrapolating normal 200  $\mu\text{A}$  conditions) and the 50% tune resulting from the 300  $\mu\text{A}$  development shifts. Centre region studies were also dedicated to identify electrodes subject to excessive heating for the higher injected currents. There was also a BL1A tuning shift to confirm a theoretical tune for BL1A with the T2 target out and the last triplet off should the necessity arise.

Cyclotron systems were turned off before the Christmas weekend just as holidays and winter shutdown were beginning. One final major operation was undertaken before year-end, namely the replacement of the three main service annex (pcb-oil) transformers. This was well-planned and executed, and completed in a couple of long days so that power was available upon people's return to work in 2002.

## BEAM DEVELOPMENT

The high current beam development work, aimed at increasing TRIUMF's extracted current from 200  $\mu\text{A}$  to 300  $\mu\text{A}$  so that 100  $\mu\text{A}$  can be supplied to ISAC without limiting the current to other users, continued during 2001.

The maximum output of TRIUMF's cusp ion source was increased from 470  $\mu\text{A}$  to 700  $\mu\text{A}$  by increasing the radius of the source's extraction aperture and by installing permanent magnets at the exit of the source to compensate for the steering produced by the stray cyclotron magnetic field. We were then able to accelerate 300  $\mu\text{A}$  at 50% duty cycle to 500 MeV with an ISIS transmission of over 90% and a cyclotron transmission of 50%.

Although the ISIS transmission obtained with 300  $\mu\text{A}$  was similar to that obtained with lower currents, the 50% cyclotron transmission was lower than the 63% obtained during 180  $\mu\text{A}$  production tunes and the 62% obtained with a 250  $\mu\text{A}$  development tune. Radial scans with the low energy probe LE2 indicate that the difference in transmission is largely due to additional vertical losses on the second or third turn ( $\sim R \approx 17$  in.) when running 300  $\mu\text{A}$ . This is probably the result of the increased space charge. Although the lower transmission shouldn't prevent TRIUMF from running 300  $\mu\text{A}$  at 100% duty cycle, one of our goals is to better understand the loss mechanism and to determine the best injection optics for this current.

A major obstacle to high current operation was the centre region heating resulting from these beam losses. This can damage components and is thought to contribute to the centre region rf sparking which commonly occurs during high current operation. During the first few turns the negative phase ions are defocused and may be lost on the beam scrapers. However, these scrapers are water cooled, therefore these losses should not cause any problems. Radial losses occur when far off phase ions don't gain enough energy crossing the injection gap to keep them from spiralling into the vertical walls of the rf resonator quadrants surrounding the centre post. Although the quadrant walls are water cooled, they are reinforced with vertical stainless steel ribs which extend radially outward and intercept a portion of the lost beam. Since stainless steel is a poor conductor of heat, these ribs can overheat. Thermocouple measurements and calculations indicated that ribs #2 and #3, located 55° and 75° after the injection gap are most prone to overheating. A water cooled beam stopper was designed to shield these ribs from the lost beam. The stopper will be installed during the January, 2002 shutdown and will be tested when cyclotron operation resumes.

Since excessive spills are one of the major problems

associated with high current production, understanding and controlling the injected emittance is important. Future plans call for the installation of a dedicated emittance measuring rig and emittance limiting slits in ISIS. In addition, work should go forward on an improved low emittance cusp source.

Considerable effort was devoted to developing a 300  $\mu\text{A}$  equivalent tune with ISIS and tank spills low enough to allow operation at 100% duty cycle. We are close to achieving this goal, however, some additional tuning will be required to find a fully optimized solution. By the end of 2002, we hope to be able to satisfy the immediate users' demand of a total internal 250  $\mu\text{A}$  production beam to be partially extracted to the three high intensity beam lines (1A, 2A and 2C4).

## RADIO FREQUENCY SYSTEMS

### RF Operations

The total rf downtime for the year was 180 hours. The combination of sparking, crowbars and out of driven accounted for 85 hours. The next major downtime component of 55 hours was caused by an instability in the gain of the IPA (intermediate power amplifier) driver stage. After changing out tubes and various components, the problem was traced to a poor filament connection on the tube socket fingerstock ring. The evidence indicates that this situation was there for a long time and was the cause of many problems with the IPA. The next downtime cause (17 hours) was the repair of a water leak in a transmission line capacitor station.

The 150 kW tube in the rf booster amplifier developed a grid to cathode short and was replaced by a spare one. Along with the tube replacement, all the amplifier circuits were serviced and tested. A kapton bypass capacitor was found severely damaged by a water leak in the amplifier cooling circuit. This could explain many of the rf booster instabilities experienced in the past.

### RF Refurbishing

A substantial effort was dedicated to rf refurbishing.

The IPA amplifier can now be switched to a resistive load for troubleshooting. The load, as incorporated in the present amplifier design, is shown in Fig. 135.

Fabrication and assembly of three powerful (up to 1 MW output power) combiners are now complete (see Fig. 136). Signal level measurements have been performed on two combiners. The new combiners will replace the original ones, which are very difficult to maintain and adjust. Moreover, the new combiners will enable cyclotron operation with two PAs instead of four during repairs to one or both other units.



Fig. 135. IPA resistive load.

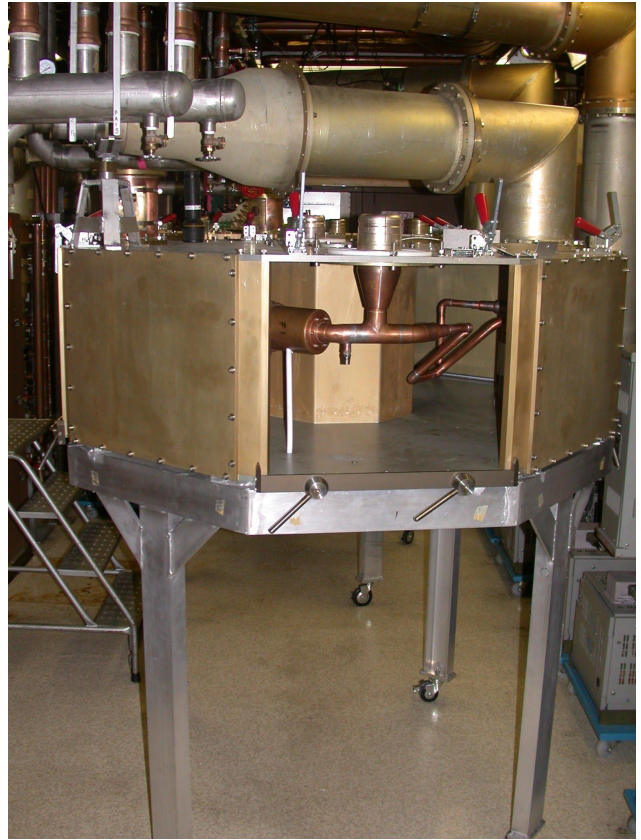


Fig. 136. New 1 MW rf combiner.

The 500 kW resistive load has been developed at TRIUMF and is close to being fully assembled (see Fig. 137). Its design has incorporated some parts from the old “Continental” resistive load: 9 in. transmission line matching taper, water pump and valves. The load is meant for power testing the combiners and PAs.

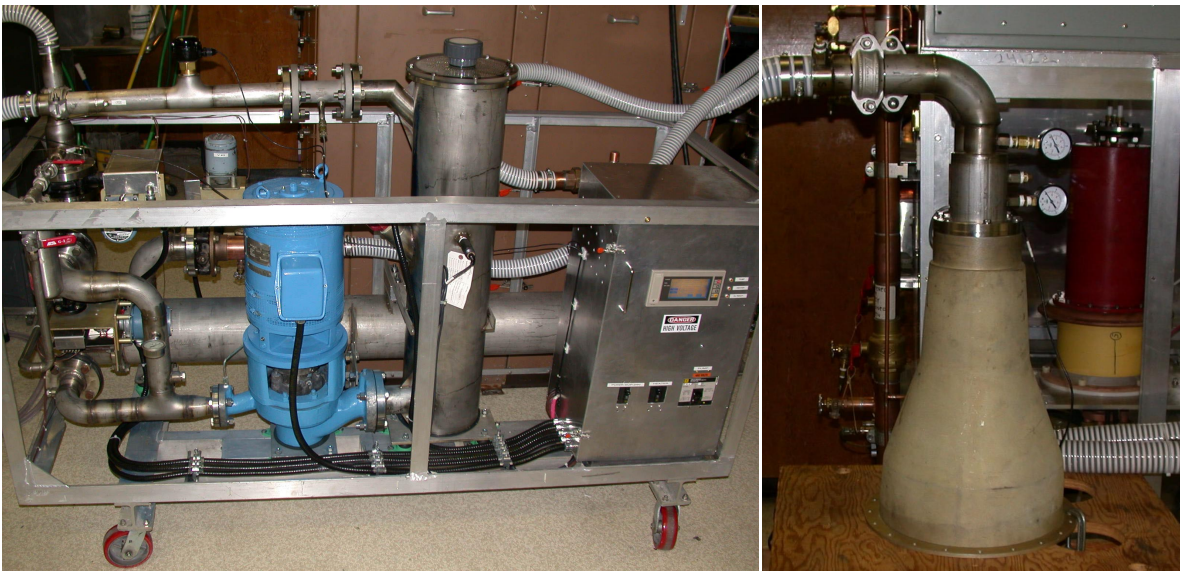


Fig. 137. 500 kW resistive load.

## RF Support

### RF separator

The rf separator for the M9 muon beam line experienced many water leaks in the plates and centre conductors. New plates were fabricated but they also developed water leaks. During the last rf tests some material from nearby solder joints was deposited on the coupling loop and surrounding area causing damage to the surfaces. The damaged surfaces were cleaned up and the assembly was sent out for copper plating to shield the solder joints from rf fields. Water leaks have now been repaired and the whole separator assembly has been vacuum leak checked and is being re-installed in the beam line.

### ISAC

The RF group was also responsible for the following projects in ISAC-I, as reported in the ISAC section of this Annual Report.

- Testing, installation and commissioning of the high-beta buncher and low-beta buncher in the HEBT line.
- Testing, installation and commissioning of the bunch rotator and dual frequency chopper in the MEBT line.
- Study of the rf quality of copper plated surfaces.
- Partial installation of a phase measuring system for the DTL rf systems.

## RADIO FREQUENCY CONTROLS

### Cyclotron

An upgraded rf control system was built and ready for use with either the separator or the third harmonic buncher.

### ISAC

The entire ISAC rf system was commissioned successfully. This includes a prebuncher, 1 RFQ, 5 DTLs, 6 bunchers, 1 chopper and 1 bunch rotator. They range in power from 100 W to 25 kW. Four different frequencies of 11 MHz, 23 MHz, 35 MHz and 106 MHz are necessary to drive these 15 cavities, which are then individually amplitude and phase regulated.

### ISAC-II

The rf control system for the superconducting prototype cavity was designed and built. Due to the extremely high Q anticipated, the design is based upon a self-excited loop. Frequency and phase control are achieved by modulating the phase of the drive signal.

## CYCLOTRON PROBES AND DIAGNOSTICS

In addition to normal MRO activities and ISAC work, there were a number of major repair jobs completed this year. A large inventory of aging diagnostics is in need of attention, so a refurbishment program is attempting to remedy the chronic problems. The most severe of these are high duty-cycle devices such as key cyclotron probes and monitors. Of particular concern are those with bearings and ferro-fluidic feedthroughs that have been in service since the first years of operation. This year, non-routine repairs were done on the following devices: 1AM8, HE1, 2C4 wire scanner, and 2C4 protect monitor.

For more details, the Diagnostics group biweekly meeting notes are available electronically via the Operations CYCINFO information service on the site computer cluster (accessible also through the TRIUMF home page on the WWW). The cyclotron shutdown activities, including the report on the ISAC DB0 installation, are summarized in detail in the Diagnostics group meeting notes of April 27, 2001.

### Probes MRO

In order to permit higher proton beam currents to the ISAC production targets, the 2A extraction probe commissioning foil mechanism consisting of a rotating cartridge of reusable foils which had a beam current limitation of about 15  $\mu$ A was changed to a standard disposable foil pack similar to that in use on beam line 1.

The 2C extraction probe was cleaned, inspected and relubricated. No heat or mechanical damage was found. New foils were installed. The standard load of 2C foils lasts about six months.

Extraction probe Ex1 was removed for routine service. A minor realignment was done on the L-arm to remedy a fault with the L-arm latch pin actuation. An improved latch pin design will be installed at the next service.

The high energy probe HE1 was removed and the recirculating bearing was replaced with a brass roller as was done with HE2 in the previous shutdown. Design concepts for a new high energy probe were advanced this year, and some detailing has been done. The radial drive ferro-fluid feedthrough (f/t) failed at the end of December, 2000, and was replaced during the winter shutdown. The replacement f/t failed at startup, necessitating an emergency repair. There is a concern about the other ferro-fluid f/ts. In particular, the slits and flags f/ts will be inspected during the winter shutdown in 2002.

## Monitor MRO

All vault and standard beam line monitors were serviced during the shutdowns. The refurbishment program described in the last Annual Report was begun and, through the efforts of a co-op student, the monitor replacement assemblies have been advanced almost to completion. Some parts are required from monitors in service, and the gas pack heads await windows being manufactured by the shop electron beam welder. The work should be completed in the coming year.

The apertures for halo beam line 2A monitors 2AVM7 and 2AM8 were opened to 60 mm to reduce the number of spurious radiation trips caused by proton beam instabilities.

An unplanned service of the 2C4 protect monitor was done which included the replacement of radiation damaged cabling. New scanning wire monitors have been built for beam line 2C and will be installed during the winter shutdown in 2002.

## VACUUM AND ENGINEERING PHYSICS

### Vacuum

The cyclotron vacuum system operated normally for the most part. There was a failure in the B20 cryogenerator that required extensive repairs, but the impact on beam production was minimal. As part of the cyclotron refurbishment program, the four 20 degree regenerators in each of two cryogenerators were replaced at a cost of \$80 k. This restored the refrigeration capacity to the design level and the used units are useful spares. Towards the end of the operating period it was noticed that the tank pressure was higher than normal on the south side of the dee gap. Residual gas analysis indicates a small air leak which will be addressed in the spring, 2002 shutdown.

A large part of the Vacuum group effort was directed to the various ISAC vacuum systems. The group experienced some change during the year with the retirement of one member and the transfer of another within TRIUMF.

### Engineering Physics

The inflector, correction plates, and thermocouple system operated normally during the year. During routine maintenance of the inflector, some misalignment of both the inflector and deflector plates was noticed and corrected. The deflector plates were actually found to be loose, and this was also corrected. There are some minor issues with the correction plates and thermocouples that will be addressed in the winter, 2002 shutdown.

Most of the engineering physics effort was directed to various ISAC hardware issues.

## ISIS

The CUSP ion source and injection line continued to operate well for the past year with only minor down time due to spurious interlock faults caused by aging equipment. As for the past few years, there were no major activities undertaken as ISIS personnel were involved in the completion of ISAC projects. These include the low energy polarimeter, the Osaka beam line, GPS1,  $8\pi$ , and the target conditioning box.

ISIS had requested refurbishing funds (\$75 k) for the replacement of fifteen aging cryopump compressors over a three year period. The existing compressors were installed as part of a major upgrade from diffusion pumps to cryopumps many years ago. The intent is to stagger the installation of the new compressors over a three to five year period such that future replacement costs would not fall into one year. This year, five compressors were installed and funds became available to purchase an additional five compressors that will be installed later in 2002. The remaining five compressors will be installed in 2003–2004.

The successful operation of the new ISAC facility will require the development of higher current targets. In order to be able to provide sufficient proton beam to ISAC without curtailing other users, an ion source low emittance beam current of 500 to 600  $\mu\text{A}$  will be required to increase the current capability of our cyclotron to 300  $\mu\text{A}$  at 500 MeV. An examination of the ion source optics led to a revised design of the extraction system. The extraction lens was modified and, with compensation for the stray cyclotron magnetic field in the source region, an  $\text{H}^-$  current of 700  $\mu\text{A}$  was achieved at the 12 keV Faraday cup (arc power: 120 V/10 A). This beam, although with slightly larger emittance, was successfully transported to the cyclotron and used for 300  $\mu\text{A}$ , 500 MeV 50% duty cycle development tests.

An upgrade of the optically pumped polarized ion source was undertaken to replace the aging ECR rf system and to increase beam current such that this source could be used, in a non-polarized mode, as an emergency backup for the CUSP source in case of failure. Once upgraded, the source could provide, in a polarized mode, useful beam intensities ( $\sim 10 \mu\text{A}$ ) for ISAC, combining ISAC modest intensity beam requirements in pre-shutdown periods with the requirements of polarized beam users, therefore maintaining access to the polarized beam facility during periods of time before shutdowns. In collaboration with BNL, a new HV power supply was specified and procured to meet the warranty requirements of the klystron tube. Work on the power supply continues at BNL with delivery to TRIUMF expected in early 2002.

In order to increase the source output current, a

new biased sodium vapour jet ionizer cell and solenoid magnet were designed. This combination increases the acceptance of the ionizer cell while reducing the emittance of the beam for better transport efficiencies. The new components have been bench tested and will be installed in 2002. The recommissioning of the ion source is expected to take place in the first quarter of 2002.

## PRIMARY BEAM LINES

### BL1A Vault Section

With the exception of the combination magnet, elements of the vault section of beam line 1 were installed in the early 1970s using components that were not radiation hard. Further, the routing of many cables repeatedly crossed the median plane close to the beam line resulting in radiation damage to insulation. Although the system has operated reasonably well through the intervening years, radiation damage to power and water circuits and wiring for monitors, valves, and other components has required frequent repairs. Because of the compact construction and proximity of shielding, repairs have been both dose intensive and difficult. Consequently, it was decided to refurbish this section of the beam line as a high priority for the refurbishing program.

This major upgrade began in January of this year. Refurbishment of the combination magnet (1VCM1), the first three quadrupoles (1VQ1/2/3), and the 19.8° dipole (1VB1) was of primary concern. To improve the servicing layout, a decision was made to move all services to the south side of the beam line and to replace existing rubber cooling hoses with flexible stainless steel ones. An estimated three months of activity was foreseen.

The work began with a detailed radiation survey of the area. This showed radiation levels somewhat higher than anticipated; thus additional shielding was required for work done locally. The exact location of each element was measured, cabling was labelled, and photographs of the existing installation were taken as reference.

Work on the combination magnet involved a reconfiguration of the cooling water services to eliminate as many soft-solder connections as possible. These were replaced with individual runs of swaged connections from new supply and return headers located at some distance from the beam line. This work was done *in situ* because of the complexity involved in disassembly of the magnet and because of dose considerations.

The work was further complicated because of limited access due to the presence of a cyclotron support post that also had a hot spot (4.5 R/h on contact) at beam height on its southwest face. Local shielding was provided with lead blankets for the post as well as lead

sheets that provided shielding from the magnet itself. Lead chevrons were placed in the magnet gap.

Disassembly of the cross connections proved to be easy. However, the stub lengths of the bottom coil sub-header were too short for the required compression fittings and it was necessary to remove them and replace them with longer stubs. This proved to be difficult and the lower headers were taken to the Machine Shop where the extensions were brazed on.

The time required for, and dose obtained by, personnel during this operation were effectively doubled because of the problems encountered with the lower section of the coil.

To service the remaining three quadrupoles and monitors, a bunker was constructed in the lower vault using shielding blocks removed from beam line 1A and smaller blocks from the cyclotron shielding. A shielding wall with removable plugs (borrowed from the Remote Handling group) was installed. The resulting much-reduced radiation field facilitated working on the magnets.

Inspection of the quadrupoles showed that coils had withstood the radiation. These were left in place. Inter-coil connections were replaced with circular 0.75 in. solid copper bus material, custom formed for each connection. They were also modified to eliminate any beam-plane transition and to permit connections to quadrupole 1VQ3 from the bottom. Those for quadrupoles 1VQ1/2 cross the median plane but the power cabling was routed behind new shielding that was installed by the combination magnet; their power connections are now accessible from the top. All power cabling is on the south side of the beam line in a tray that also has terminations for sacrificial wiring to the buss bars. The former can be replaced in sections from the upper vault.

Because quadrupoles 1VQ1 and 1VQ2 had a common beam tube and were mounted on a common stand and quadrupole 1VQ3 was on its own stand, the latter was used to test the above improvement strategy. Work proceeded well and a test of the refurbished magnet indicated that the methodology of repair was satisfactory.

Following the successful refurbishment of 1VQ3, the remaining two quadrupoles were stripped of their services and their captive beam tube was cut with a large tubing cutter. Quadrupole 1VQ2 was then removed to the bunker and refurbished in a similar manner to quadrupole 1VQ3.

Quadrupole 1VQ1 does not have direct crane access and it was necessary to construct a cantilever beam to lift the quadrupole to the 1VQ2 location where direct crane access was available. This quadrupole was then refurbished in the bunker.



All three quadrupoles were then meggered and tested at 300 A to establish that there were no hot spots and that their magnetic fields were the same as before the refurbishment. They were reinstalled and their alignment was checked. Comparison of before and after alignment data showed that all three quadrupoles were approximately 2.5 mm further south than had been the case before the quadrupoles were removed. Because all three quadrupoles showed the same displacement, and quadrupoles 1VQ1/2 shared a common support whereas quadrupole 1VQ3 had its own support, it was concluded that the beam line platform had moved during a moderate earthquake that had occurred in the interim. Repeated measurements using a Leica Total Station and optical measurements confirmed that the support platform appeared to have a southward rotation, the rotation being centred on the 19.8° dipole that lies downstream of quadrupole 1VQ3. Consequently, the west end of the platform was moved north 2.5 mm using a hydraulic jack bolted to the floor on the southwest corner. This was done in small steps while watching the alignment points. Using this method, the quadrupoles were realigned to their initial positions.

Buss bars for the combination magnet were relocated under the beam floor in the vault basement. A short length of cabling that can be easily replaced connects the magnet to its buss bars.

Cabling for controls, monitors, and valves was installed in an elevated cable tray to the north of the beam line. Beam plane crossings were eliminated. Interlock cables for these elements were replaced and the termination box was made larger to ease servicing.

### **BL1A West-East Section**

A troublesome vacuum leak had been detected downstream of the 1AT1 target of beam line 1A. Its location, however, had been difficult to pinpoint. This leak was finally traced to an indium seal at the downstream exit of the 1AQ10/11 doublet. It was found that quadrupole 1AQ11 was slightly tilted; one edge of its support stand was sitting on a lifting lug. This was corrected and the vacuum joint replaced. No further problems have been encountered with this connection.

It had been known for some time that there was a water leak in the quadrupole triplet 1AQ14/15/16 that lies downstream of the 1AT2 target. In October, 1999 a total system loss of 10 l/h had been noted. Of this, 6 l/h were ascribed to the triplet. The total leak rate began to increase quickly in August of this year. By the end of September it reached 26 l/h (of which 13 l/h were attributed to the triplet) and by the end of October the total leak rate had increased to approximately 40 l/h. However, because the radiation level in the area in which these elements are located was

extremely high, a decision was made to keep a close watch on the leak rate and try to continue to operate until year-end. It had already been planned to enter the area and fix any leaks in the upcoming January, 2002 shutdown. By the end of the year the total leak rate had increased to 70 l/h, a rate that was at the limit of what could be sustained. When beam was shut off in December, water losses of 45 l/h were attributed to the triplet, 20 l/h to M20B1, and 5 l/h to M20Q1. These are to be attended to during the January, 2002 shutdown.

In addition to the above shutdown activities, a diverse number of MRO projects were undertaken in the meson hall and in ISAC. The former involved normal filter changes, servicing the M11 and M13 beam blockers, and ongoing support of the secondary channel separators. ISAC work was centred on DRAGON, HEBT, and DBO.

The vault upgrade work at the beginning of the year was nominally a project of the Beam Lines group. Ultimately, however, the services of 43 persons were required to accomplish the tasks. Without the excellent cooperation of all those involved, the work could not have been accomplished on time. The Beam Lines group would like to thank those who assisted throughout the shutdown. In particular, J. Tanguay and K. Trithart, by devising the 1AVQ1/2/3 service details, made a significant contribution to the success of the project.

### **Beam Line 2C Production**

The production of the radioisotope  $^{82}\text{Sr}$  in the solid target facility (STF) on 2C4 continued to be the major use of 2C beam time. The solid target facility was removed in the spring shutdown for servicing but it was reinstalled misaligned with respect to the proton beam. Isotope production was delayed by five weeks while efforts were made to compensate for the misalignment by tuning. A steering magnet was added approximately 2 m upstream of the target and various software protections were added to allow for routine isotope production in this configuration. There was less operating time this year, 107 days compared with 135 days last year because of the tuning difficulties but there was a production of 81.15 mA h and a yield of 31.12 Ci at the end of bombardment, compared with last year's production of 95.50 mA h and a yield of 31.87 Ci. This improved make-rate is a result of optimizing the production schedule with shorter target irradiations with consistently high beam currents. Five targets were irradiated this year compared with seven targets last year.

The beam extraction foil that is used for isotope production is a 0.20 in. wide curtain of 0.001 in. diameter pyrolytic graphite fibres. There were only two production foils on the 2C extraction probe; 75.77 mA h

were run on one foil because the other foil with 8.38 mA h created a larger beam halo. The foil with higher dose appeared to be failing at the end of the run. Nominally the dose would be shared between the two foils so the highest dose that had been previously run on a 0.20 in. foil was 50 mA h. Three 0.20 in. wide foils will be installed in the next operating period because the foils can only be changed when the cyclotron lid is raised. An increased operating period with only one lid up each year is now preferred.

There were 36 days scheduled for proton therapy and 23 days scheduled for the proton irradiation facility on 2C1.

## CONTROLS

The Central Control System (CCS) performed well during 2001 and was responsible for only 7.45 hours of downtime. Most of the downtime was due to hardware failures such as power supply faults. The level of failures can be expected to rise as the existing control system ages unless new equipment is substituted for old. In addition, repairing existing hardware is becoming more difficult as replacement parts are not always available. Cyclotron control refurbishing is meant to alleviate this.

The goals set out for the year were largely accomplished. These included starting to replace the existing secondary beam line controls, replacing the last VAX that has a production role with another Alpha, completing the phase out of the FDDI network infrastructure for switched Ethernet, and starting the replacement of the existing disk systems. Typically, the new replacements offer much better performance and improved functionality but there are some tradeoffs because the new equipment is often less expensive and not as well engineered, particularly for long term maintenance.

## CCS Facilities

There were numerous software changes in applications and infrastructure. The requests for enhancements and other modifications are almost continuous on the heavily used applications such as the display pages (XTpages), the logged data playback/live update (Xstrip), and the event scans and interlock trips (Scans). The work on these applications is important and consumes a significant amount of the available resources.

Infrastructural changes occurred in a variety of areas such as security, network statistics, printing, and the low level acquisition software. Security issues have been addressed on a number of fronts, with network access and functionality being reviewed and tightened. Secure connections are now the common login. Improvements in the statistics on network usage have

been pursued. Better data have been helpful but the new switched Ethernet needs more diagnostic capabilities (to be explored in the next year). There was also an issue when printing from Windows/PCs. It is common for control system users to display their X Window output on a Windows/PC. Printing the displays seen in this environment was improved nicely when a freeware print product (Xwpick) was enhanced on site.

CCS hardware also changed in numerous ways. The changes came in the form of improvements to existing equipment, replacements of old equipment by new, and the installation of additional new items. An example of an enhancement is the upgrading of the memory on the database computer. Replacements came in several areas. Examples are, the fibre channel disk storage taking over from the DSSI storage, the network where the FDDI has been phased out and switched Ethernet has completely replaced it, and in computer upgrades such as an Alphastation 600 which was replaced by an Alphastation DS10 and a VAX that was replaced by the Alphastation 600. An example of supplemental equipment is the addition of a colour laser printer. Along with these changes is the removal of numerous pieces of equipment such as the FDDI hardware, battery charger systems, and VAXes.

Time and effort was spent on monitoring the system, and on diagnosing and correcting problems. This year was not without its hardware faults but these are felt to be reasonable given the size of the CCS and the age of many of the components. The X Window terminals have problems about once per month but there are 50 terminals and the older ones are more than 10 years old. It is remarkable that these X terminals function so well given their age; consider working on a 10+ year old PC. Power supplies continue to reinforce their image of being a weak link, with 2 CAMAC crates and an Alpha server suffering power supply failures. A variety of other components also had problems, for example printers, DACs, ADCs, crate controllers, the old DSSI disk systems hungup, the 3 way valve controller, switches, etc. A problem that had a larger impact was when the UPS system failed to perform on one occasion. The UPS has in general been a tremendous and reliable asset.

The refurbishing goals have been met in part. Old DSSI disk storage systems, one in the Development Cluster and one in the Production Cluster, are being replaced. The new fibre channel storage is operational in the Development Cluster and providing significantly improved performance, functionality, and reliability. The fibre channel hardware for the Production Cluster has been purchased and will be installed next year. A newly designed ADC module has been slow in coming to fruition. The basic design and prototyping

have been largely completed but the final debugging and production boards have suffered from lack of sufficient site priority.

### **Secondary Beam Lines**

Work on replacing the existing secondary beam lines controls was started and has progressed very well. M13 (TWIST) was designated as the first beam line to be converted. The existing CAMAC hardware with some changes has been integrated into a serial CAMAC branch from a VME crate. A pair of Sun Sunblade 100s has been configured for development and production running. Using EPICS software this set-up has been used to replace the existing functionality and provide new features. The initial requirements for TWIST have been met but requests for enhancements are anticipated when TWIST starts intensive data-taking next year. Other beam line controls, starting with M20, will be converted to this configuration. Additional support will be needed in the area of diagnostics and a tape drive will be added to provide the required backup.

### **Other Systems**

Support for other systems has been provided as needed. Beam line 2C controls have run smoothly and have received only minor attention. One exception was when the beam line was changed to provide extra beam steering using 2CSM4. At that time, machine protection scans were added to constrain operational parameters.

The proton therapy operator interface software was moved from a VAX to an Alpha. This configuration was tested and the first treatment has been completed. As a further upgrade, we hope to have UPS provided for various proton therapy components in the next year.

Help was given for the TWIST experiment. Additional data gathering has been provided. In one case, a data transfer of cyclotron parameters was set up on an ongoing basis. In another case, target scans were done while monitoring the protect plates and other readbacks. This and other support will likely continue during TWIST's duration.

### **Miscellaneous**

With the VMS support being phased out in the Data Analysis Centre computing, a number of programs are now being supported by the Controls group. One example is the Dose program used by the Safety and Operations groups for keeping track of pencil dosimeter use. Help has been given on the porting of Dose and the program should be moved over and operational by the end of the spring shutdown, 2002. Another example is the Eyeplan program used by the B.C. Cancer Agency for treatment planning. Support for porting of Eyeplan will be given in the next year. In

other areas, work has already started and will continue on a variety of security issues and in hardware and software readout of a VME based current-to-voltage and digitizer board used with multiwire chambers.

## **OPERATIONAL SERVICES**

### **Remote Handling**

#### **ISAC**

Support work for ISAC development was the predominant activity for Remote Handling for the year, expending over two-thirds of the Group manpower, with completion of the east target station vacuum tank, construction of new target, exit, entrance and dump modules, and assembly of ion beam optics elements.

Remote Handling activities for the year included design and installation of a new remotely accessible spent target storage vault, refinement of the remote crane system and hot cell facilities. A catastrophic electrical failure in the ISAC target module #1 required replacement in the hot cell of the entire target/extraction column assembly.

#### **Cyclotron servicing**

The spring shutdown required routine Cu-blocker removal, shadow shield installation, video survey, and radiation surveys. The 2C extraction probe was removed again this year for work by Diagnostics, along with HE1 and HE2.

During the year, the remote cyclotron servicing system controls and trolleys were reworked and maintained. Heavy workloads postponed cyclotron elevating system maintenance for yet another year.

#### **Beam lines servicing**

The principal spring shutdown activity was in support of the beam line #1 front end refurbishment. Assistance was given with magnet services upgrade for 1VCM1, 1VQ1,2,3 and 1VB1, and new indium vacuum seals installed in the section after completion of the work.

A recurrence of a vacuum leak at 1AQ11 required replacement of the indium seal and realignment of the flange and joint support assembly.

Work began on the scheduled decommissioning of beam line M8. A current area shielding layout perspective drawing was completed, a proposed shielding revision approved, and new shielding designed and specified. Over 32 tons of concrete shielding and 100 tons of steel shielding blocks were completed by year-end.

## Hot cells and targets

Servicing for the T1 and T2 cooling packages required filter changes, demineralizer pressure transducer replacement, resin can exchange, water release, and a change of the water flow nozzles in an attempt to recalibrate control rack signals.

The T1-Mk1 target was removed from the beam line for replacement of a leaking Pb-coated “C”-seal in the hot cell. This leak released over 17 l of water into the target vacuum vessel. New 10 mm pyrolytic graphite targets were installed at positions #2 and 5, and the T1-Mk2 target had a new 10 mm graphite target installed at position #2. One of the two target beam blocker air pressure amplifiers was rebuilt. The T1 profile monitor had air flow control valves installed.

The M9 beam blocker was moved into the hot cell for replacement of the actuators with revised design, larger bore air cylinders. Assistance was given to 2C beam line for resin can change/disposal, and with a target holder latching problem. Similar assistance was provided to TNF for resin can servicing.

Hot cell housekeeping required a change of the ventilation roughing and pre-filters, as well as disposal shipping of hot cell garbage, and redistribution of active component storage.

## Magnet Power Supplies

2001 saw the final commissioning of power supplies related to ISAC-I for the experimental areas. Difficulties were encountered with the old M8 supplies which suffered multiple water leaks, specifically on MD1 and MD2, Q10 supplies.

During the spring shutdown, M13 polarity switches were replaced as well as the cabling to these switches.

Precision DCCT current monitoring equipment was installed for the remaining power supplies for M13 to achieve the desired stability and reproducibility of that channel required for Expt. 614.

A new steering element was introduced for BL2C to compensate for target misalignment. This involved the pulling of new power cables from a trim coil junction box as well as running new interlock cables.

As part of the BL1A upgrade, new interlock terminations for the front end magnets were done.

A satisfactory heat sink has been generated to replace the original Wakefield and this will be used to retrofit the supplies in future.

The balance of the group’s activities was providing experimental support as well as MRO for the power supply system.

Coordination was provided for the BL1A front end refurbishing as well as the PCB transformer replacement project.

## Electrical Engineering Services

### Electrical Systems

ISAC-I continued to be the focus of the engineering efforts. About 50 engineering and large installation work orders in support of accelerator and experimental programs were carried to completion.

Major refurbishing projects included:

- The rewiring of the dc feeder at the front end of BL1A in the cyclotron vault with new terminations, cabling, buss bars, and cable tray installation;
- The replacement of three Askarel (PCB coolant) transformers during the Christmas shutdown.

The transformer procurement and replacement was carried out over a period of 12 months under the overall project coordination of TRIUMF. Five firms worked alongside TRIUMF staff. Beaver Electrical Machinery Ltd. performed the initial testing and feasibility study, VECO Canada Ltd. provided the engineering services, Partner Technologies Ltd. of Regina manufactured the replacement transformers, PVK provided the electrical installation, and Trans-Cycle Industries of Kirkland, Ontario carried out the removal and disposal of the PCB liquid and the transformer carcasses.

The three Askarel transformers had been in service for 30 years. Dielectric property tests and dissolved gas analyses revealed significant deterioration of the winding insulation and clearly indicated the need for their urgent replacement. The reliability and continuity of service of these transformers are too important for cyclotron operation to risk keeping them in service in those conditions. The removal of these units from the site also eliminates a significant risk and liability associated with the operation of PCB chemicals.

The electrical department responded to about 250 trouble calls and was involved in about 130 minor installation requests. Typical maintenance activities included servicing lighting systems, motors, air conditioning controls, panel boards and transformers, HV switchgear, breakers, and capacitor banks. About 10 motors were replaced, including four in the cooling tower complex. Lighting maintenance took a good share of the electrical crew time with the replacement of about 400 ballasts and a large number of fluorescent tubes. Continuing engineering support was provided to TRIUMF users and MDS Nordion. Completed major tasks included electrical services for TWIST, the M9 He polarized targets, and the CP42 power supply upgrade. Improved dc cabling was also installed for CP42. M13 polarity switch wiring was replaced as part of the polarity switch replacement program. Engineering support was also provided to the new MDS Nordion project, TR30-2.

Electrical maintenance requirements have increased significantly since the addition of the ISAC-I facility and will increase even further with the ISAC-II buildings. It is vital to the service continuity and reliability that we add to the staffing level to cope with the increased workload.

A number of system components have aged. The regular replacement program of obsolete equipment was sidelined during the construction of ISAC-I. It is important to restart it to continue to deliver the continuity of service and reliability we are accustomed to.

### Power Delivery

A severe windstorm that swept the UBC campus on December 15 caused extensive power outages and operational disruptions. Some equipment damage resulted and the electrical crew was busy around the clock to clean up and repair the damage.

Power management continued as a routine activity. The monthly averaged peak power demand increased a mere 1.8% to 6857 kVA from 6736 kVA a year earlier (Fig. 138). The maximum peak power demand was reached in August with 8871 kVA, a good 5% higher than last year. After steady increases over the last three years, the electricity consumption bucked the trend. It decreased 2.3% to 51.99 GWh in 2001 from 53.21 GWh in 2000 (Fig. 139). The largest consumption also occurred in August (6.0 GWh). The power factor (PF), averaged over the calendar year remained unchanged at 96.1% (Fig. 140).

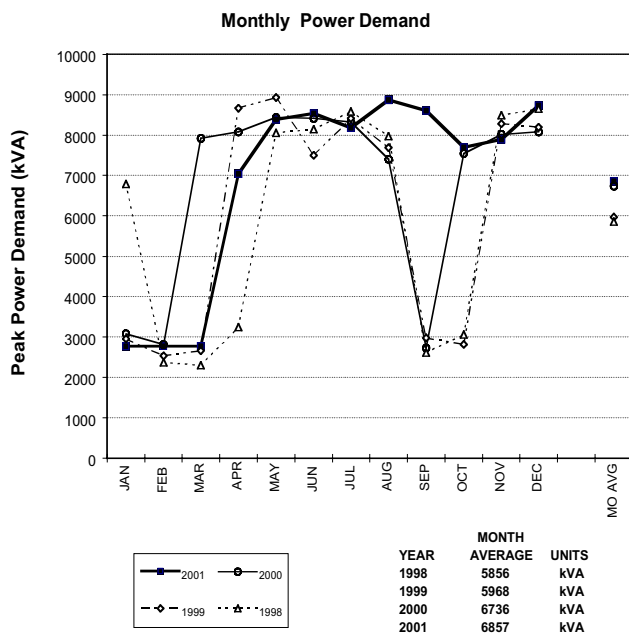


Fig. 138. Electrical system power demand – four year comparison.

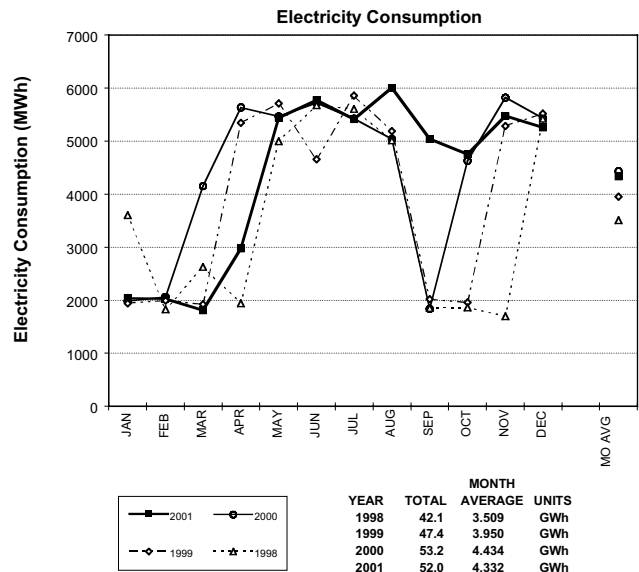


Fig. 139. Electrical system energy consumption – four year comparison.

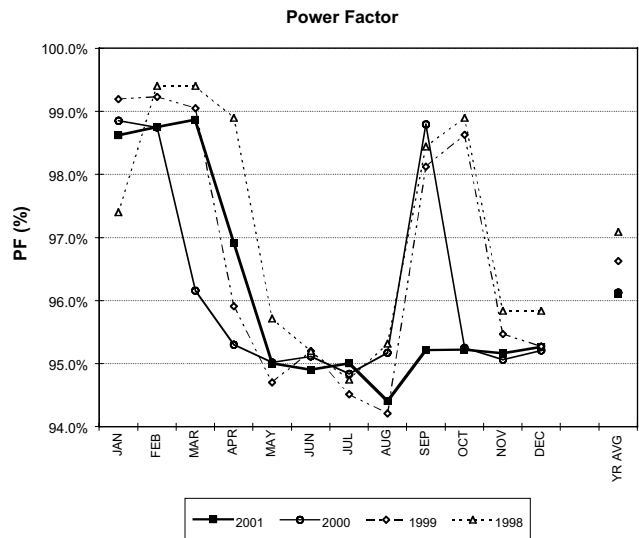


Fig. 140. Electrical system power factor – four year comparison.

### Mechanical Services

#### ISAC

The 2001 effort was concentrated on ISAC. The experimental hall completion included a wide range of work, including cooling water, compressed air, and vacuum lines to HEBT and experimental areas, completion and commissioning of the DRAGON hydrogen exhaust system, gas tubing and alarms. Other ISAC jobs included a third controlled temperature water loop for TRINAT, a mechanical hoist in the penthouse hay loft, the connection and the commissioning of alarms for six fume hoods, spent target vault ventilation and exhaust, high level alarms for the three filling points

for the decontamination sump, and vacuum roughing lines to the CDS room. One ISAC development job was the modification of the experimental hall roof top heating units to act as exhaust fans for summer operation, and the installation of a test area of open floor grating on the mezzanine. This is intended to reduce the air temperature on the mezzanine in summer, by moving more outdoor air through the building, and allowing it free convection access to the mezzanine. Other development jobs included modification to chilled water supply lines to the electrical room to allow more efficient operation of chiller 2 in winter, venting the decontamination and sanitary sumps for odour control, and DDC operational improvements. A list of MRO work was carried out.

Engineering assistance was provided for the ISAC-II building project, and the Superconducting RF Laboratory at B.C. Research.

### **Main site interventions**

The single largest project was the abandonment of the underground diesel storage tank. This job was required by the University of B.C. for environmental protection, and included test drillings in the nearby area to search for possible pre-existing diesel oil leakage into the ground water (there was none), pumping out and disposal of the nearly 5000 gallons of oil (more difficult than imagined because of high sulfur content of the old

oil, and some water contamination inside the tank), excavation of the top of the tank, cutting a manhole in the top, power washing the inside, filling the tank with low strength (excavator ready) concrete, and finally backfilling and repaving the area. Other significant jobs were the transformers T1, T2, T3 replacement, the combination magnet CM1 resericing in the vault, the refurbishment and re-commissioning of the M8 building HVAC, and new upgraded HVAC for the auditorium. Other MRO work included the board room HVAC, the el. 264 electrical room Buffalo AC unit replacement, a new boiler water feed line, new laminar flow diffusers for the main office building clean room and lab, M13 gas lines, RH control room AC, tricky temporary and, later, permanent repair of a water leak in a beam line 1A copper pipe, the startup of Expt. 614 power supply AC, and new exhaust ductwork for M11. A fire suppression system was installed in the kitchen and a new pressure gauge and flow switch installed in the remote handling building sprinkler system. A maintenance software package was purchased and installed to systematize procedures and record keeping for Plant group. The application and startup of this system will carry on into 2002.

Engineering assistance was given to MDS Nordion and ATG for various jobs, including the new expansion project. This work included site water shutdowns because of related intervention on the mains.

# ISAC PROJECT

## INTRODUCTION

This has been the first full year of ISAC-I operation. Accelerated radioactive ion beams were successfully transported to both the TUDA and DRAGON stations allowing the nuclear astrophysics experimental program to commence. The year has also been a beneficial learning experience for operations and maintenance personnel, experimenters, accelerator personnel and beam schedulers. The initial investment in engineering has paid off. The proton beam on target has been gradually increased as maintenance experience was gained and now 20 kW driver beam powers are operational. Long target lifetimes are being observed. Target exchanges and module repairs can be accomplished with very little personnel exposure. Contamination has been successfully contained as planned. A second target station had been envisioned to reduce the servicing impact on beam scheduling. In response to user demand for more beam time, a major initiative this year has been the fabrication of the east target station. The second target station will increase the number of scheduled hours each year, provide a quick backup for early target failures, reduce the risk when developing new targets, and provide additional isotopes by accommodating an ECR ion source. New target materials, beams and ion sources are being developed.

ISAC-II is rapidly becoming a reality. Immediately following provincial government funding approval for ISAC-II civil construction, an aggressive schedule was adopted. A team was put into place that transformed a concept based on requirements into a cost-effective facility design. By year-end the design was nearly ready to be sent out for tender. Significant progress also occurred on the technical front. The collaboration with ISN (Grenoble) has successfully characterized an ECR charge state booster to a point where a purchasing decision could be made and many components of the ECR have now been ordered. Beam dynamics studies of the linac have refined the superconducting accelerator layout. A prototype superconducting cavity was built in collaboration with INFN-LNL (Legnaro) and successfully tested. A cryostat has been built at TRIUMF and characterization of the cavity will continue in a newly refurbished laboratory.

## ISAC OPERATIONS

This year was the first complete year of operation of the ISAC-I low energy facility. The first quarter was devoted to shutdown activities. Beam schedule 99 began in the second quarter and carried on through the summer and, in parallel, the accelerator team com-

missioned the high energy systems using beam from the off-line ion source (OLIS). Beam schedule 100 began in the fourth quarter and continued until year-end. There was less reliance on beam physicists during routine beam operation of LEBT although their assistance was always welcomed. The MEBT and HEBT beam operation required extensive support from the beam dynamics experts. A typical change of energy through the accelerators required three or more hours of procedures – including documenting the existing parameters, switching to a stable pilot beam, adjustment of the energy and retuning of matching elements, documentation, then switching to RIB. Most operators have been able to proceed on their own after a few assisted energy changes, but there are still occasions that challenge even the experts. The members of the ISAC Operations group take great pride in their contributions to the successes of the experiments and major ISAC milestones that have been highlighted elsewhere in this Annual Report.

Operational performance statistics are provided for the ISAC beam production of RIB from ITW and stable beam from OLIS. These are summarized separately for each beam schedule in Tables XVII–XXVIII. In some instances OLIS was used by an on-line experiment as part of procedures to change mass or energy. Other times it was used for commissioning or when the RIB was unavailable, such as during a maintenance period. As a single user facility of RIB, there is an incentive to minimize activation when the beam is not required. This is done by stopping the RIB on a Faraday cup in the target station and, for longer periods, turning off the proton beam. For Operations purposes, these appear as “off” time for each experiment. Some of this time may be due to a cool down period during an acquisition cycle, or overhead for the experiment such as changing of samples or collection tapes. Therefore care must be taken in using these statistics for analyzing the efficiency of the scheduled experiment beam time usage. The off time is included in the hours recorded as available for RIB. For most systems, the downtime is a sum of many various problems, e.g. for controls, related to the programmable logic controller hardware and EPICS program. “Beam line 2A unavailable” indicates times when the proton beam is off for a variety of reasons including scheduled cyclotron maintenance. “ISAC idle” includes time when the proton beam may have been available but, in the absence of system failures, ISAC RIB was not delivered, e.g. when trained operators were not available or experiments were unable to take beam, etc. In schedule 99, the major faults were the failure of a

target high current connector which resulted in a HV problem; a thermal relay problem in IMS:MB1; and a failure of the OLIS waveguide Y-bend. In schedule 100, the major problems were related to the weather – high winds causing a lengthy site power outage, and heavy rains resulting in perimeter drains backing up into the building, eventually causing water damage on LEBT HV feedthrough. Over the year, RIB was available for 2,390.2 hours out of 3505 hours scheduled, for a combined cyclotron/ISAC system performance of 68.2%.

Training for the accelerated beam operation was provided by way of 22 formal lectures, and by informal on-the-job training by the beam dynamics experts during operation. As with the LEBT systems, the lectures were videotaped for future use in the training of new operators. Setting up of a systematic approach to training (SAT) program and completion of an ISAC Operations Manual have been high priority tasks falling into the capable hands of Mike Hauser, the training and documentation coordinator. These activities are

complementary to each other and progress on one is helpful to the other. The Documentation Manual was given a higher priority and was very near to completion at year-end. Development of the training program will resume in 2002. Another development was the implementation of a Web-based work permit system. This was provided by coop student Wendy Wiggins under the supervision of Chris Payne.

In the control room, a new console desk was installed. It has permitted the addition of a second layer of monitors to display the many controls and graphics that are required for the operators to be effective in beam delivery. It will also permit more operations in parallel, which has been a severe limitation and source of frustration in these early days. In the coming year, in addition to providing beam for the scheduled experiments and performing systems maintenance, the major effort will be to establish and complete the SAT training program for ISAC operators.

Table XVII. ISAC beam schedule 99: April 25 – September 5 (weeks 17–36). ITW beam to ISAC experiments (hours).

Experiment number	Scheduled	Actual	Tune	Off
$\beta$ -NMR commissioning	264.00	10.75	13.70	65.15
E815 ( $\beta$ -NMR)	312.00	237.25	7.85	15.10
E823 (GPS2)	300.00	149.05	16.05	3.65
E826/828 (LTNO)	192.00	43.45	40.40	60.35
E863 (LTNO)	156.00	89.25	22.45	0.00
Yield	120.00	57.15	26.30	2.40
Mass separator development	48.00	12.00	0.00	0.00
E812 (TOJA)	336.00	159.25	29.90	98.90
Total	1,728.00	758.15	156.65	245.55

RIB available  $758.15 + 156.65 + 245.55 = 1,160.35$  hours.  
 Combined cyclotron/ISAC performance  $1,160.35/1,728.00 = 67.1\%$ .



Table XVIII. ISAC beam schedule 99: April 25 – September 5 (weeks 17–36). Breakdown of ITW radioactive beams to ISAC experiments (hours).

Isotope	$\beta$ -NMR comm.	E815 $\beta$ -NMR	E823 GPS2	E826/828 LTNO	E863 LTNO	Yield	Mass separator development	E812 TOJA	Total
$^7\text{Li}^*$	7.75	4.75				1.00		12.50	26.00
$^8\text{Li}$	3.00	232.50				0.20		140.00	375.70
$^{16}\text{O}^*$								+6.75	6.75
$^{23}\text{Na}$						0.75			0.75
$^{39}\text{K}$						13.60	12.00		25.60
$^{74}\text{Rb}$			118.75			0.25			119.00
$^{75}\text{Ga}$					88.05	0.50			88.55
$^{75}\text{Rb}$						0.50			0.50
$^{79}\text{Rb}$				0.65					0.65
$^{80}\text{Rb}$			30.30		0.90				31.20
$^{84}\text{Rb}$					0.30				0.30
$^{85}\text{Rb}^*$				6.50					6.50
$^{91}\text{Rb}$				36.30					36.30
Other						40.35			40.35
Total	10.75	237.25	149.05	43.45	89.25	57.15	12.00	159.25	758.15

\* stable beam

+ from OLIS

Table XIX. ISAC beam schedule 99: April 25 – September 5 (weeks 17–36). ITW systems downtime and overhead.

ISAC system	Hours
Controls	15.65
Magnet power supplies	9.70
MEBT rf	0.50
OOPS	2.00
Polarizer	2.25
RFQ	1.35
Site power	2.00
Target station (HV breakdown)	182.30
OTHER	
Beam line 2A unavailable	148.10
Cyclotron maintenance	181.35
Cyclotron development/training	23.90
ISAC idle	41.25
ISAC startup	4.60
ISAC cooldown	92.00
Target changes	73.50
Target/ion source conditioning	46.00
Procedures	19.40
ITW/LEBT tuning	121.15
HEBT tuning	8.65
Shutdown	48.00
Total	1,023.65

Table XX. OLIS operation June 4 – September 5 (weeks 23–36). Beam to ISAC experiments (hours).

Experiment number	Scheduled	Actual	Tune	Off
DRAGON commissioning	468.00	159.80	45.15	180.80
E812 (TOJA)	360.00	126.40	52.90	182.60
E879 (TUDA)	360.00	159.60	16.30	98.60
Test (LTNO)	0.00	1.25	8.00	5.00
Total	1,188.00	447.05	122.35	467.00

Beam available  $447.05 + 122.35 + 467.00 = 1,036.40$  hours  
 OLIS performance  $1,036.40/1,188.00 = 87.2\%$

Table XXI. OLIS operation June 4 – September 5 (weeks 23–36). Breakdown of OLIS beams to ISAC experiments (hours).

Isotope	DRAGON commissioning	E812 TOJA	E879 TUDA	Test LTNO	Total
<sup>12</sup> C				0.50	0.50
<sup>13</sup> C		119.65			119.65
<sup>14</sup> N				0.75	0.75
<sup>15</sup> N	65.90				65.90
<sup>16</sup> O	93.90	6.75			100.65
<sup>21</sup> Ne			159.60		159.60
Total	159.80	126.40	159.60	1.25	447.05

Table XXII. OLIS operation June 4 – September 5 (weeks 23–36). OLIS systems downtime and overhead.

ISAC system	Hours
Controls	5.75
DTL rf	24.40
HEBT rf	2.15
Charge-exchange stripper	3.50
MEBT rf	1.45
Pre-buncher	1.00
RF controls	5.50
RFQ	6.00
Safety	1.40
Site power	1.50
Ion source	44.75
OTHER	
ISAC maintenance	330.90
Development	2.20
ISAC idle/no user	531.60
ISAC startup	2.00
Procedures	171.10
MEBT tuning	0.40
HEBT tuning	12.00
Total	1,147.60

Table XXIII. ISAC beam schedule 100: September 26 – December 3 (weeks 39–51). ITW beam to ISAC experiments (hours).

Experiment number	Scheduled	Actual	Tune	Off
E815 ( $\beta$ -NMR)	372.00	265.40	3.10	26.60
E824 (DRAGON)	660.00	382.10	30.65	18.70
E879 (TUDA)	541.00	396.40	12.80	3.85
E903 (Osaka)	48.00	57.20	0.00	0.00
Yield	84.00	32.05	1.00	0.00
Mass separator development	72.00	0.00	0.00	0.00
<b>Total</b>	<b>1,777.00</b>	<b>1,133.15</b>	<b>47.55</b>	<b>49.15</b>

RIB available  $1,133.15 + 47.55 + 49.15 = 1,229.85$  hours

Combined cyclotron/ISAC performance  $1,229.85/1,777.00 = 69.2\%$

Table XXIV. ISAC beam schedule 100: September 26 – December 3 (weeks 39–51). Breakdown of ITW radioactive beams to ISAC experiments (hours).

Isotope	E815 $\beta$ -NMR	E824 DRAGON	E879 TUDA	E903 Osaka	Yield	Total
$^7\text{Li}^*$	30.75					30.75
$^8\text{Li}$	234.65			3.00		237.65
$^9\text{Li}$				54.20		54.20
$^{21}\text{Na}$		382.10	396.40		0.55	779.05
Other					31.50	31.50
<b>Total</b>	<b>265.40</b>	<b>382.10</b>	<b>396.40</b>	<b>57.20</b>	<b>32.05</b>	<b>1,133.15</b>

\* stable beam

Table XXV. ISAC beam schedule 100: September 26 – December 3 (weeks 39–51). ITW systems downtime and overhead.

ISAC system	Hours	ISAC system	Hours
		OTHER	
Controls	17.90	Heavy rainfall	8.00
DTL rf	1.45	Beam line 2A unavailable	146.70
Electrostatic power supplies	2.35	Cyclotron & ISAC maintenance	170.70
Magnet power supplies	7.90	Cyclotron development/training	70.45
MEBT rf	2.15	ISAC idle	25.30
OOPS	2.55	ISAC startup	12.00
Polarizer	6.15	Target changes	38.50
RF controls	0.50	Shutdown	72.00
RFQ	1.90	Target/ion source conditioning	65.75
Safety	0.25	Procedures	129.50
Services	5.00	ITW/LEBT tuning	83.55
Site power	38.65	RFQ tuning	0.75
Target station	34.75	MEBT tuning	0.30
Vacuum	7.95	DTL tuning	0.70
	cont'd.	HEBT tuning	1.50
	<b>Total</b>		<b>955.15</b>

Table XXVI. ISAC beam schedule 100: September 26 – December 3 (weeks 37–51). OLIS beam to ISAC experiments (hours).

Experiment number	Scheduled	Actual	Tune	Off
DRAGON commissioning	216.00	112.70	13.55	6.30
E824 (DRAGON)	204.00	157.35	20.60	37.85
E879 (TUDA)	48.00	*81.30	7.80	1.50
8 $\pi$ commissioning	0.00	3.50	0.00	0.00
Total	468.0	354.85	41.95	45.65

\*was to have received ITW beam ( $^{21}\text{Na}$ ), but ITW was not ready

Beam available  $354.85 + 41.95 + 45.65 = 442.45$  hours

OLIS performance  $442.45/468.00 = 94.5\%$

Table XXVII. ISAC beam schedule 100: September 26 – December 3 (weeks 37–51). Breakdown of OLIS beams to ISAC experiments (hours).

Isotope	DRAGON commissioning	E824 DRAGON	E879 TUDA	8 $\pi$ commissioning	Total
$^{14}\text{N}$				3.50	3.50
$^{21}\text{Ne}$	112.70	157.35	81.30		351.35
Total	112.70	157.35	81.30	3.50	354.85

Table XXVIII. ISAC beam schedule 100: September 26 – December 3 (weeks 37–51). OLIS systems downtime and overhead.

ISAC system	Hours
Controls	8.70
Diagnostics	0.25
DTL rf	11.65
Electrostatic power supplies	0.60
HEBT rf	3.35
Magnet power supplies	8.70
MEBT rf	3.00
Charge-exchange stripper	0.40
RF controls	2.00
RFQ	1.00
Site power	42.50
Ion source	93.30
Vacuum	0.65
OTHER	
ISAC maintenance	363.75
Development	4.20
ISAC idle/no user	1,238.30
Startup	12.50
Shutdown	108.00
Procedures	133.15
OLIS/LEBT tuning	11.70
RFQ tuning	3.30
MEBT tuning	4.20
DTL tuning	4.90
HEBT tuning	18.45
Total	2,078.55

The history of operation of ISAC production targets is given in Table XXIX. Several target changes were performed this year. Schedule 99 started with a target of niobium foils. Shortly after startup, it began to spark and consequently operation was compromised, resulting in delivery of beam at a reduced energy. On inspection at a rescheduled early target change, it was discovered that a high current connection had failed due to a design flaw, and the insulators on the target service tray were coated with vaporized metal. The tray was exchanged remotely in the south hot cell. These activities are discussed in the remote handling report. The service took about 7 weeks, beam off to beam on. The next target was one of tantalum foils and was in operation for a total of 17,279  $\mu\text{A h}$  at a proton current of about 20  $\mu\text{A}$ . Finally, a target of SiC pellets was used for delivery of Li beams to the high energy area. It received 16,010  $\mu\text{A h}$  with most operation at beam currents up to 15  $\mu\text{A}$ . Until the east target station is commissioned, the turn around for a target change is about ten days. This includes a two day cool down period, five days to effect the change and three days for conditioning of the new target.

Table XXIX. ISAC target history.

Target ID	In date	Out date	Charge $\mu\text{A h}$	Thickness $\text{g}/\text{cm}^2$	Power $\mu\text{A h} \times$ $\text{g}/\text{cm}^2$	Comments
CaO #1	25-Nov-98	15-Dec-98	70	36.00	2,520.0	Failure due to EE short
CaO #2	20-Dec-98	15-May-99	363	31.10	11,289.3	Failure due to EE short
Nb foils #1	14-Jul-99	20-Oct-99	3,242	11.10	35,986.2	Failure due to TBHT-t/c problem
Nb foils #2: R1	01-Nov-99	09-Dec-99	3,149	11.50	36,213.5	Removed for 100 $\mu\text{A}$ tests
Dump only	10-Dec-99	10-Dec-99	43	0.00	0.0	100 $\mu\text{A}$ test
Talbert	17-Dec-99	12-Jan-00	197	10.00	1,970.0	100 $\mu\text{A}$ test
Nb foils #2: R2	17-Mar-00	04-Jun-00	5,913.8	11.50	68,008.7	Total: Nb foils #2 R1 + R2
Ta foils #1	10-Jun-00	19-Jul-00	3,515.83	21.25	74,711.4	Removed for $\text{CaZrO}_3$
$\text{CaZrO}_3$ #1 R1	24-Jul-00	21-Aug-00	518.7	42.27	21,925.4	9.45 g $\text{Ca}/\text{cm}^2$ , 21.51 g $\text{Zr}/\text{cm}^2$
$\text{CaZrO}_3$ #1 R2	02-Oct-00	18-Nov-00	838.0	42.27	35,422.3	9.45 g $\text{Ca}/\text{cm}^2$ , 21.51 g $\text{Zr}/\text{cm}^2$
SiC #1 R1	18-Nov-00	10-Apr-01	2,155.0	7.43	16,011.6	7.43 g $\text{SiC}/\text{cm}^2$ : 5.05 g $\text{Si}/\text{cm}^2$ , 2.38 g $\text{C}/\text{cm}^2$
Nb foils #3:R1	13-Apr-01	31-May-01	3,766.0	22.00	82,852.0	1026 foils – 40 $\mu\text{A}$ rating
Ta foils #2	08-Jul-01	13-Sep-01	17,279.0	43.60	753,364.4	1026 foils – 40 $\mu\text{A}$ rating
SiC #2 R1	18-Sep-01	16-Jan-02	16,010.0	29.90	478,699.0	29.9 g $\text{SiC}/\text{cm}^2$

## SAFETY AND RADIATION CONTROL

### Licensing

An application to construct the ISAC-II facility was prepared and sent to the Canadian Nuclear Safety Commission (CNSC) late in 2001. The application was accompanied by a safety analysis report that described the hazards associated with the proposed operation of ISAC-II and the design features that will mitigate these hazards. It is expected that the licence will be issued early in 2002.

### Access Control and Radiation Monitoring

The ion beam radiation monitoring system (IBRMS) was expanded to accommodate the operation of the ion beam accelerator system and the high-energy experiments as well as a number of changes to the layout of the low energy beam lines. A users manual was also published for this system. The target storage facility in the target maintenance hall was included in the target hall access control interlock system so as to allow access only when the target storage facility shielding door is closed. Design was started on incorporating the interlocks for the east target station. Considerable effort went into standardizing the interlock requirements for high-voltage systems. All new systems will be expected to conform to these standards and some systems may need to be retrofitted.

### Commissioning

Radiation surveys were performed during the commissioning of the DTL section of the ISAC accelerator system. The primary source of radiation is the X-rays generated by the parasitic acceleration of electrons. RF

power levels were established that limit the X-ray production to acceptable levels during access to the DTL shielding enclosure. The access control system for the accelerator enclosure will be interlocked so that access is allowed only when the rf power is below these levels.

## REMOTE HANDLING GROUP

### Target Modules

Following design revisions for the second generation ISAC east target station modules, work began on assembly of new target, exit, entrance and dump modules by Remote Handling personnel. Although these modules are similar to the west station in design, changes to the containment box and services duct require new assembly procedures.

### Target Hall

The target hall is being prepared for a more demanding, two-station, higher current beam schedule by the end of 2002. Provision for improved safety and contamination control included additional cleaning and radiation sampling stations set up within the hall, and an intermediate monitor check established adjacent to the target station access area. Contamination control blanket tarpaulins have been provided throughout the hall, and lock-up safety procedures have been reviewed to better suit routine hall work activities.

The largest new target hall project for the year was the shielded spent targets storage vault that was designed, assembled and commissioned in the spring. This unit is remotely accessible by the target hall crane and allows interim storage of up to twenty-four individual spent targets and two larger bins for component trays, all for later re-use or eventual disposal.

## Hot Cell Facility/Targets

Installation of the access shielding doors, and double chain drive modifications to the turntable have now completed the major hot cell construction. Refinement of operations has included new tooling for connecting gas-line equipped targets, and the fitting of a breathable air system into the hot cell service anteroom.

A catastrophic failure in target module #1 required the full month of June for hot cell repair. Poor electrical conduction of a target oven heater connection, inside the lower containment box, vaporized material plating many of the high voltage insulators. This required entire replacement of the target/extraction column assembly to be performed remotely. The containment box was opened, additional holes drilled/tapped, all services disconnected, the extraction column support tray removed, a new assembly installed and services re-connected and tested by manipulator operation. This was a first-time hot cell endeavour for this magnitude of work.

Commissioning of the target hall spent target storage vault was completed and four previously irradiated targets (CaZrO<sub>3</sub> #1, SiC #1, Nb #3, Ta #2), as well as the damaged TM #1 extraction column, are now stored in the vault for future re-use or disposal.

During the year there were three remote target changes performed on target module #1 (Nb #3, Ta #2, SiC #2). The Ta #2 target heat shield was removed in the hot cell to examine physical characteristics of the high power (40  $\mu$ A) run. The target oven tube was found to be distorted by heat expansion and the method of mounting.

Two surface source extraction columns were assembled this year; the replacement for the damaged TM #1 column, and one intended for the conditioning box. Assembly of a third extraction column for TM #2 has begun.

Design of a test apparatus for decontaminating materials has been completed and assembly is under way. Design work began on a manipulator support/installation cart for easier replacement and servicing of the hot cell master-slave manipulators.

## Remote Crane System

The control console for the remote crane was improved with additional closed circuit video monitors, switching and console racks. A laser ranging system was installed on the crane down-hall travel motion, providing more accurate feedback for remote crane operations.

## ISAC TARGETS AND BEAMS

In 2001 the ISAC operating licence was upgraded to allow unlimited 100  $\mu$ A  $p^+$  beam current operation

for all target materials with the exception of actinide targets. Two targets (Nb #3 and Ta #2) have now operated with proton currents up to 40  $\mu$ A. This is calculated to be the limit of the target design originally intended for beam currents in the range of 1–3  $\mu$ A. Additionally, a ceramic pellet target (SiC #2) was operated for an extended period with a proton current of 15  $\mu$ A to deliver <sup>21</sup>Na beams to the ISAC accelerators and the TUDA and DRAGON experimental stations.

At the beginning of the 2001 ISAC run schedule, the Nb #3 foil target was installed to provide <sup>74</sup>Rb beams for Expt. 823, and <sup>79</sup>Rb beams for Expt. 828/LTNO. The Nb #3 target consisted of 1026 Nb foils (0.025 mm thickness) with a total target thickness of 22 g Nb/cm<sup>2</sup>. The target thickness, volume and foil surface area were approximately double that of the previous Nb foil targets. Throughout the Nb #3 target running period, there were problems with breakdowns of the target high voltage system. The inability of the target module to maintain a 30 kV beam energy precluded <sup>8</sup>Li beam delivery to the polarizer and  $\beta$ -NMR experimental station. In spite of the voltage problems, the target run lasted from April 17 to May 24. The Nb #3 target received 3766  $\mu$ A h of beam and was operated at proton currents up to 40  $\mu$ A. Yields of Li, Rb and Ga radionuclides were measured as a function of proton current.

At the end of the Nb #3 running period, inspection of the target revealed that a steel washer had overheated and evaporated metal onto the high voltage insulators. The target support structure and extraction electrode system were removed from the target module and replaced with a new unit. Removal and replacement operations were performed inside the ISAC hot cell using remote handling techniques. The replacement procedure was successfully completed during June and the target module was ready for installation of a new target in early July.

The Ta #2 target consisted of 1050 Ta foils (0.025 mm thickness) with a total target thickness of 43.6 g Ta/cm<sup>2</sup>. As with the Nb #3 target, the Ta #2 target had approximately twice the total thickness, volume and foil surface area of the previous Ta #1 target. The yields of Li isotopes were measured as a function of proton current up to a maximum of 40  $\mu$ A. A <sup>11</sup>Li ( $t_{1/2} = 8.5$  ms) yield of  $2.2 \times 10^4$ /s was achieved at 40  $\mu$ A. Ta #2 operated from July 16 to September 5 and received a total of 17,279  $\mu$ A h of proton beam, the equivalent of  $3.9 \times 10^{20}$  protons. For most of the running period, it operated with a 20  $\mu$ A proton beam delivering <sup>8</sup>Li beams of  $2 \times 10^8$ /s to the ISAC accelerators. The <sup>8</sup>Li was the first accelerated radioactive beam at ISAC. Ta #2 currently holds the record for being the longest operational ISAC target.

To date, the second longest-lived ISAC target is SiC #2. This target was in operation from October 3 to December 18 supplying accelerated  $^{21}\text{Na}$  beams to Expts. 824 and 879 at the DRAGON and TUDA experimental stations, polarized  $^8\text{Li}$  to Expt. 815 at the  $\beta$ -NMR station and the first polarized  $^9\text{Li}$  beam for initial calibrations for Expt. 903 and the polarimeter station. The SiC #2 target consisted of 163 pressed pellets of SiC + 10% molar excess graphite powder. The average pellet thickness was 1.2 mm with an average pellet density of  $1.73\text{ g/cm}^3$ . The  $29.9\text{ g SiC/cm}^2$  thickness was approximately 4 times the thickness of the previous SiC #1 target. Initial target operation started on October 3 with a proton current of  $3\text{ }\mu\text{A}$  for Expt. 879, followed by  $15\text{ }\mu\text{A}$  operation in November for the other experiments. The initial  $^{21}\text{Na}$  yield at  $15\text{ }\mu\text{A}$  was  $2.5 \times 10^9/\text{s}$  while that of  $^{22}\text{Na}$  was  $2 \times 10^{11}/\text{s}$ . Both yields were observed to slowly decrease with time, finishing with  $5 \times 10^8/\text{s}$  and  $5 \times 10^{10}/\text{s}$ , respectively, towards the end of the run on December 6. Total proton beam charge was  $16,010\text{ }\mu\text{A h}$ , corresponding to  $3.6 \times 10^{20}$  protons on target.

## ION SOURCES FOR ISAC

### Electron Cyclotron Resonance (ECR) Source

The design of a radiation hard ECR source for the ISAC radioactive beam facility has been completed.

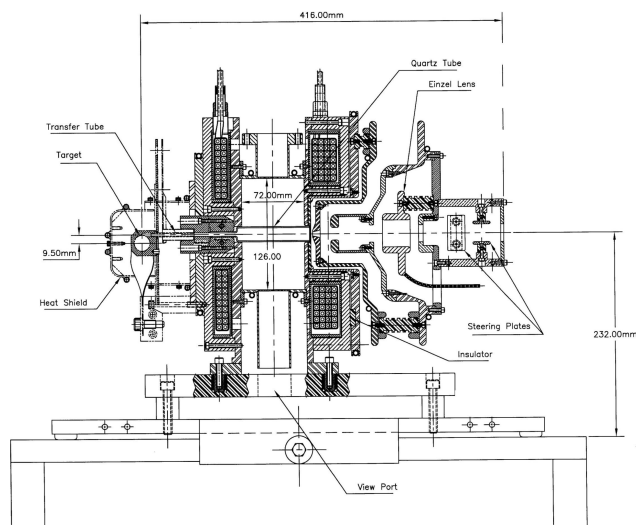


Fig. 141. The radioactive isotopes produced at the target drift toward a quartz tube located inside the cavity of a 2.45 GHz electron cyclotron resonance (ECR) ion source. A unique feature of this source is that the quartz plasma chamber is considerably smaller ( $\sim 80$  times) than the resonant cavity in order to increase the efficiency for the extraction of short half-life isotopes. This ion source has a high efficiency for ionizing gaseous species in a single charge state. This source will be used to produce ion beams of nitrogen, oxygen, and neon from zeolite targets, as well as that of Xe, Kr, Ar, and Cl isotopes using Ta, Nb, and CaO targets, respectively.

The ion source with its 0–60 kV extraction system is coupled to the radioactive isotope production target via a small transfer tube (Fig. 141). For a typical ISAC target, the copper coils of the ECR source will be exposed to a dose rate of about  $10^5\text{ Gy/h}$  for a  $100\text{ }\mu\text{A}$  – 500 MeV incident proton beam. The whole assembly will be located beneath a 2 m thick steel shielding structure.

The fabrication of the source is nearing completion. It will be tested in the ion source test stand (ISTS) during the first half of 2002. A new vacuum chamber has been built to accommodate the ECR source in the ISTS. Figure 142 shows the source under assembly. This source will be installed in the east target module during the second half of 2002.

### Off-Line Ion Source (OLIS)

The source operated satisfactorily throughout 2001 delivering more than 5200 hrs of a variety of beams. It continued to provide helium, nitrogen and neon beams to the RFQ, DTL, MEBT, and HEBT for accelerator studies. It also supplied  $^{21}\text{Ne}$ ,  $^{15}\text{N}$ ,  $^{24}\text{Mg}$ , and  $^{13}\text{C}$  beams for the DRAGON and TUDA experiments. Although the microwave source, installed at the OLIS terminal, was designed to produce beams only from gaseous elements, it could also supply the Mg beam, however, at a cost: damage due to sputtering shortens the lifetime of the source. For the low energy area, OLIS delivered  $^{14}\text{N}^{2+}$  beam to tune the Osaka and  $\beta$ -NMR beam lines.

Since beams of alkaline and metallic elements are being requested by several experimental groups on a regular basis, a new concept for the off-line ion source was proposed. The new OLIS terminal will house three sources: the present microwave source for gaseous

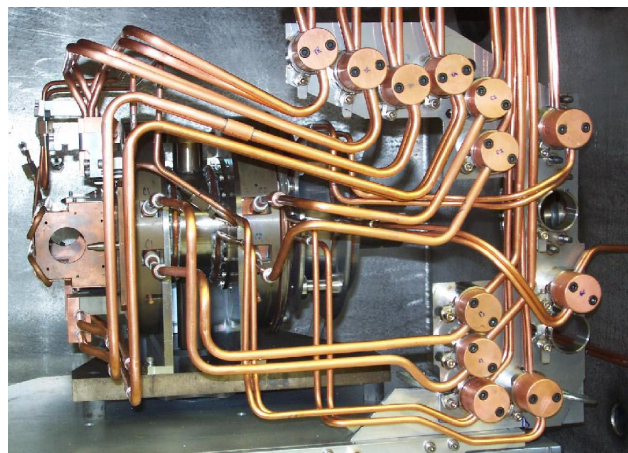


Fig. 142. The target ion source extraction assembly on a self-aligning tray. This picture shows the combined current, voltage and cooling quick disconnect feeder lines. The target-ion source is serviceable via remote handling.

beams, a surface ion source for alkaline beams, and a source to produce metallic beams. In spring, 2002 the new terminal with initially two sources will be assembled. The installation of the source for metallic beams is foreseen in 2003. The future OLIS terminal will be capable of producing almost all ions requested by the experimental groups.

### Charge State Booster (CSB)

The research collaboration program set up between the Institut des Sciences Nucleaires (ISN-Grenoble) and TRIUMF to study the properties of the ISN-PHOENIX-ECR source as a charge breeder device was brought to completion in November, 2001. The result of these measurements indicates that this system can fulfill TRIUMF requirements in terms of breeding efficiency and breeding time of the  $1^+/n^+$  process. A sample of some gaseous, metallic and alkaline elements relevant to the ISAC experimental programs (such as Ar, In, Ag, Zn, Sn, Sr, Ga, Co, Rb, K and Na) was studied. The results are listed in Table XXX. Based on these results, an order will be placed in January, 2002 to acquire the PHOENIX source from PANTECHNIK (France). This firm has been licensed by ISN to manufacture the source based on the ISN design.

This source will be incorporated as an extension to the TRIUMF  $1^+$  ion source test stand in 2002–03 for further tests and in preparation for its future installation in the ISAC-I hall.

Table XXX. The breeding efficiency,  $\eta$ , and time,  $\tau$ , for various isotopes.

	$\eta(\%)$	$\tau(\text{ms})$
$^{40}\text{Ar}^{1+}/6^+$	5	100
$^{115}\text{In}^{1+}/18^+$	4.6	120
$^{109}\text{Ag}^{1+}/17^+$	3	75
$^{64}\text{Zn}^{1+}/10^+$	2.8	50
$^{120}\text{Sn}^{1+}/19^+$	4.1	150
$^{88}\text{Sr}^{1+}/14^+$	3.6	125
$^{69}\text{Ga}^{1+}/11^+$	2	80
$^{59}\text{Co}^{1+}/9^+$	2	100
$^{85}\text{Rb}^{1+}/13^+$	5	100
$^{39}\text{K}^{1+}/9^+$	7.9	70
$^{23}\text{Na}^{1+}/8^+$	1.8	–

### ISAC POLARIZER

At the beginning of the year, the following laser system changes were made to increase the  $^8\text{Li}$  polarization:

a) The mode spacing of the Ti:sapphire dual-frequency laser was accurately measured by observing the beat frequency between the two modes, and was corrected to precisely match the 382 MHz  $^8\text{Li}$  ground state hyperfine splitting.

b) The laser frequency was locked to a frequency-stabilized He-Ne laser, thus reducing laser drift to approximately 3 MHz/hour. This obviated the previous need to vary the Na cell bias to compensate for laser drift.

c) Acoustically-generated noise on the laser frequency was reduced from approximately 40 to 20 MHz RMS by placing a vibration damping layer between the water-cooled argon-ion pump laser and the laser table. Water cooling to the Ti:sapphire laser remains the largest contributor to frequency noise.

d) Smaller apertures were placed on the Na vapour target (reduced to 12 mm from 16 mm) and the He gas target (reduced to 8 mm from 10 mm), to maximize overlap between the ion and laser beams. The smaller apertures reduced the overall transmission efficiency by a factor of 0.82.

e) A 19 MHz electro-optic phase modulator (EOM) was ordered to artificially increase the instantaneous laser frequency bandwidth of  $\sim 1$  MHz. Such an EOM placed in the laser beam produces cw laser frequency sidebands at 19 MHz intervals. The purpose was to ensure that  $^8\text{Li}$  atoms are always near resonance with the laser or the sidebands during their  $2 \mu\text{s}$  transit time in the polarizer. Without the sidebands, many atoms would not see the laser due to the acoustically-generated noise on the laser frequency. It was also thought that the likely Doppler-broadened absorption width of the beam was  $\sim 40$  MHz.

The first polarized  $^8\text{Li}$  run, scheduled for May, was almost completely lost due to target ion source problems. However, very important information was obtained over three shifts about the energy spread in the beam. Laser induced fluorescence from a 20 keV  $^7\text{Li}$  beam showed that multiple collisions in the Na vapour created a low energy tail in the beam that could be eliminated by reducing the Na vapour density (unfortunately reducing the neutralization yield at the same time). The energy width at typical Na densities was approximately 5 eV or, equivalently, over 100 MHz absorption bandwidth in a 30 keV  $^8\text{Li}$  beam. The energy spread in the incident beam was less than 2 eV (FWHM).

In light of the above knowledge, as well as polarization calculations that showed it was advantageous to optically pump at more closely spaced frequency intervals, another 28 MHz EOM was obtained in time for the next polarized  $^8\text{Li}$  run in August. Combining the two EOMs in series easily permitted broadening of the laser to cover 100 MHz, as well as providing finely spaced frequencies at about 10 MHz intervals. That was a big success, and transverse  $^8\text{Li}$  polarizations of up to 70%, saturated with laser power, were measured at the polarimeter. (The original longitudinal polariza-



tion is converted into transverse polarization by a  $90^\circ$  electrostatic bend just before the polarimeter. The polarimeter is described in the LEBT section.) However, calculations showed that the polarization under our experimental conditions should have been nearly 100%. The apparent loss of polarization will require further investigation. The August run marked the commissioning of the ISAC polarizer as an experimental facility.

The final run in November/December was used to continue the  $\beta$ -NMR data-taking begun in August, and to polarize  $^9\text{Li}$  for the first time at ISAC. Experiment 903 requires highly polarized  $^{11}\text{Li}$ , but sufficient beam was not available using the SiC ISAC target. The more easily produced isotope,  $^9\text{Li}$ , was used to check neutron detectors and other apparatus. Since the ground state hyperfine splitting is different in  $^8\text{Li}$  and  $^9\text{Li}$ , only one of the dual laser frequencies could be used for optical pumping. Both ground state levels were optically pumped, however, using a tunable EOM to create laser sidebands 852 MHz either side of the main laser frequencies, thus matching the  $^9\text{Li}$  hyperfine splitting. The combination of the dual-frequency laser and EOM reduced the effective laser power by a factor of one-third, which may explain the low polarization that was achieved. The polarization was thought to be 30–40%, although the latest information on  $^9\text{Li}$   $\beta$ -decay branching ratios implies that the polarization was half that. The final run was also used to test Cs vapour as the neutralizer target. It was hoped that its smaller excitation energy than Na and greater mass would produce less energy broadening in the beam. Not unexpectedly, the neutralization yield was lower, since Cs also yields  $\text{Li}^-$  ions, but unfortunately the energy broadening was also worse than with Na.

In future, a high power, single frequency ring laser and EOM combination must be used to achieve high polarization of any isotope other than  $^8\text{Li}$ . Our experience with the old Spectra-Physics ring laser mentioned in last year's report has been disappointing. It is no longer supported by the manufacturer, which has in fact abandoned the field, and despite a significant effort, it is still not functioning properly. At year-end, the decision was made to buy a new ring dye laser from Coherent Inc. in time for the next polarized run.

## BEAM DYNAMICS

### Theory

Canonical transformations have been found which eliminate the derivatives of strength functions in dipole benders. Previously, this has been achieved for quadrupoles. This allows simple calculation of lowest-order aberrations without any detailed knowledge of fringe field shapes.

### Software

The beam transport code TRANSOPTR has been ported to Linux. Aberration calculations have been added for both magnetic and electrostatic dipole benders. As well, a Wien filter has been added.

A general electrostatic bender has been written for COSY- $\infty$ .

### Hardware Designed

The new 3-way bender design has been used to re-design OLIS (off-line ion source). This will allow 3 different sources to be attached, to broaden the selection of stable ions.

A new section of beam line has been designed and built, and commissioning has started. This is for the  $8\pi$  experiment. It is located in place of GPS1, which has in turn been relocated to the ILE section.

Additional commissioning of the  $\beta$ -NMR platform has been done. In this post-polarizer section of beam line, two additional branches have been designed and installed: a polarimeter, and a beam line section for the Osaka experiment.

### ISAC CONTROLS

Detailed design and implementation of additional sections for the ISAC control system proceeded smoothly and the following major milestones were achieved:

- Vacuum, optics and diagnostics control for the HEBT beam line beyond the Prague magnet.
- Vacuum, optics and diagnostics control for the TUDA and DRAGON beam lines as well as the TUDA experiment.
- Upgrades to the laser control and stabilization for the ILE2 beam polarizer.
- Vacuum, optics and diagnostics control for the ILE2A1 polarimeter.
- Vacuum control for the Osaka (ILE2A3) beam line.
- Vacuum, optics and diagnostics control for the  $8\pi$  experiment (ILE1A) beam line.

During the year, control for approximately 500 new devices was added to the ISAC control system, bringing the total to 1850 controlled devices.

### Hardware

Two new VME crates were added to the control system, one to separate the control of the ILE1 and ILE2 beam lines and a second to back up the overloaded HEBT IOC.

An additional PLC breakout cabinet was built, pre-wired, and installed for the vacuum systems of the DRAGON beam line. All vacuum devices for the

HEBT, HEBT2, and HEBT3 beam lines, as well as for the DRAGON experiment, were connected and commissioned. The vacuum controls for the  $8\pi$  beam line and the Osaka experiment beam line were commissioned.

160 new CAN-bus controllers were installed for the supplies of the HEBT and TUDA, DRAGON and  $8\pi$  beam lines.

Development was started on a separate EPICS control system for a target conditioning station, consisting of a vacuum box with ion source, and a beam line with analyzing magnet. A PLC breakout panel was installed and hookup to the vacuum devices is complete.

The control system wiring documentation was made available on the Controls group's Web server. For easy access, screen dumps of the EPICS synoptic screens are incorporated in HTML pages. The Web buttons, which in the control system call up device control panels, call up the wiring diagrams for the respective devices. For semi-automatic maintenance of this documentation, an auto-print program was written to generate PDF files from the documentation drawings. Perl scripts connect these PDF files automatically to the Web page buttons.

## Software

The PLC ladder logic programs for the vacuum systems of HEBT, TUDA, DRAGON,  $8\pi$  and Osaka beam lines were tested and commissioned.

ISAC standard EPICS display pages and supporting scripts were created for all new subsystems. Device control panels for all new optics and diagnostics devices were created using the edd display editor.

This year saw a continuation of efforts to enhance the ISAC relational device database (IRDB) and automate the production of new controls subsystems.

The process for automatic generation of vacuum device control panels was refined and the first generation of panels was put into production. These panels improve the interlock visualization and contain hyperlinks to control panels for devices, which are involved in interlocks [Keitel, ICALEPCS 2001, San Jose, November 27–30 (in press)].

The automatic generation of CAPFAST subsystem schematics based on reports from the IRDB is now the standard process for generating EPICS runtime databases. Missing information from subsystems, which had been installed during the previous years, was added to the IRDB. Now all subsystem schematics are generated and updated automatically [Keitel and Nussbaumer, *ibid.*]. Force and bypass summary screen generation was reworked, to achieve a consistent look and feel with other panels.

Laser control of the ILE2 beam polarizer [Nussbaumer *et al.*, *ibid.*] had performance and reliability of

the closed loop stabilization system improved. The system is now capable of maintaining laser stabilization for periods of many hours without operator intervention. A control strategy has been developed using custom software, and will be the basis for planned future performance upgrades. Areas for additional reliability upgrades have been identified.

Control support was added for the MEBT bunch rotator, MEBT chopper, and HEBT buncher rf systems, as well as for the new OLIS beam attenuators.

For the Prague magnet and the MEBT dipole magnets, closed-loop current stabilization was implemented based on feedback from the hall probes.

Beam line scaling algorithms were developed for DRAGON and for the accelerator physicists.

For the target commissioning station, the PLC program and all EPICS software for the vacuum system controls were developed and commissioned; work on the optics and diagnostics systems is in progress.

## System and Development Support

Two more SUN workstations were added in order to remove some software development bottlenecks. A considerable amount of time had to be spent on system maintenance for the development and production machines in order to catch up on operating system upgrades, rationalizing of configurations, and enhancing security.

A Linux-based firewall was installed, which separates the ISAC control system IOCS, PLCs, SUN application servers and Linux consoles from the rest of the TRIUMF site.

More documentation, tutorial material and troubleshooting information was added to the ISAC controls Web site.

During the mini-shutdown in September, the EPICS software was upgraded to the latest stable release 3.13.5 without any significant problems.

An attempt was also made to upgrade the IOC operating system to vxWorks release 5.4, in order to make use of the Tornado II tools. This upgrade led to networking and performance problems, which could not be resolved in the time available. The upgrade was rolled back to vxWorks 5.3 without problems.

Toward the end of the year, preparations for the installation of the second ISAC target station were under way. The conceptual design calls for independent operation of the east and west stations. This will require the installation of two more PLCs and significant modifications to the existing ladder software.

## Commissioning and Operation

During this year, we saw a transition from commissioning of large subsystems to commissioning of

smaller systems in parallel with regular beam delivery. The simultaneous operation of radioactive and stable beams was successfully supported. This mode, however, made it increasingly difficult to schedule enough time for enhancements, reliability improvements and regular maintenance. The conversion of the operations console PCs from Windows to Linux was completed and resulted in considerably reduced frustration levels of the operations crew. During the shutdown periods, Chris Payne from ISAC operations was again a valuable addition to the Controls group.

## RF SYSTEMS

### RFQ

The RFQ operated reliably for the various settings of this year's beam commissioning and production. The only troubles experienced for a few weeks in spring were the spontaneous trips caused by ac power ripples or transients. The problem was tackled with filtering and delaying signals in the amplifier interlock circuits. High power pulsing has been performed once to reduce the buildup of dark currents.

### MEBT

#### Bunch rotator

The triple gap split ring 106 MHz buncher devoted to bunch rotation in the MEBT was commissioned this year and operated very reliably. The tank, originally fabricated for the prototype DTL buncher, was modified to accept a new bunch rotator structure. Development and fabrication were done at INR RAS, Russia. Tuning and tests were accomplished at TRIUMF. The buncher is specified for rather moderate effective voltage of 80 kV and consumes about 5 kW at full power. This device at start up requires an rf conditioning for up to half an hour. The bunch rotator at assembly phase is shown in Fig. 143.

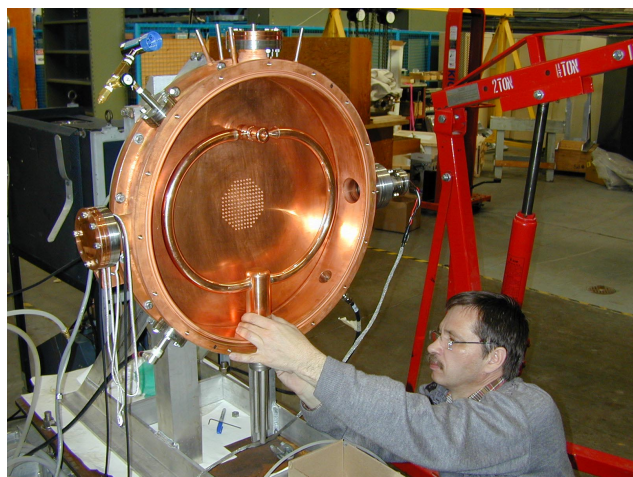


Fig. 143. Bunch rotator assembly.

### Choppers

The dual frequency chopper was commissioned this year and operated very reliably. Structurally, it consists of two independent rf systems of 5.9 MHz and 11.8 MHz but is combined in a common housing box. In addition to rf voltage, a dc bias is applied to the chopper plates. The chopper requires relatively low voltages, maximum of about 7 kV, and didn't show any problem in operation. Figure 144 shows the dual frequency chopper with open covers. The bunch rotator and chopper installed in the MEBT line are shown in Fig. 145.

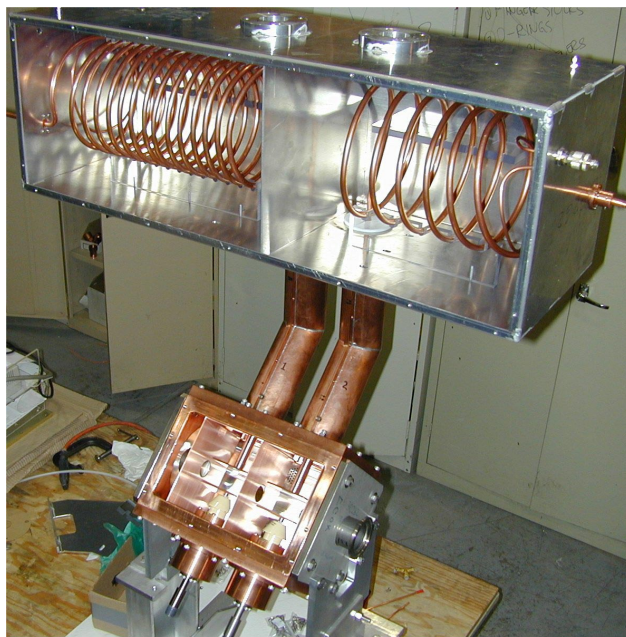


Fig. 144. Dual frequency chopper assembly.

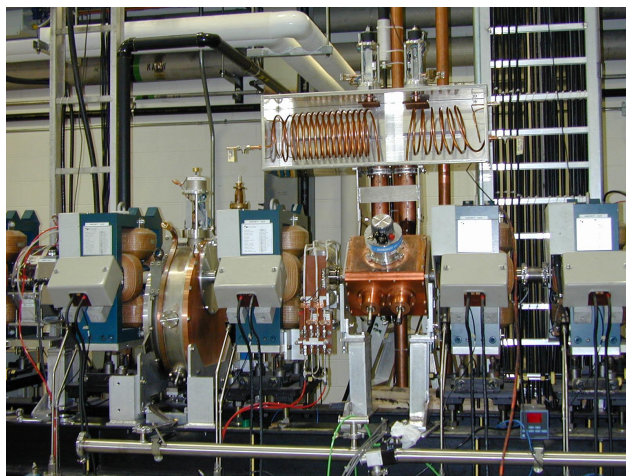


Fig. 145. Bunch rotator and chopper installed in the MEBT.

## Rebuncher

The MEBT 35 MHz rebuncher in general showed sufficiently good performance during beam production this year, though there were a few problems, which gave us some downtime with this device:

- Accelerating voltage instabilities were caused by rf interference from 106 MHz devices located in the same VXI crate. This was overcome with a proper module screening and input signal filtering.
- A capacitive tuner (operating in the frequency automatic feedback loop) failed to move three times (during two months' time). The problem was fixed with a stepper motor control unit replacement.
- Three out of four power modules in the rf amplifier were found to be burnt right before the winter shutdown. The remaining module was just sufficient to provide required rf power for reduced mode of the linac operation ( $A/q = 4$ ).

All troubles most probably were triggered by the unstable operation of the commercial rf amplifier, which could easily fall into parasitic oscillations when loaded with an unmatched high-Q resonant load. In the shutdown, the amplifier will be modified to meet operational conditions.

## DTL

The variable energy DTL is based on five independent, interdigital H-type (IH) structures and three triple gap split ring bunchers, all operating at 106 MHz. All eight DTL resonators are powered by identical 25 kW rf amplifiers developed and assembled at TRIUMF. All systems have been tested up to maximum specified power (see Table XXXI) required for  $A/q = 6$ , but routinely operated mostly at about 4/9 of full power ( $A/q = 4$ ) according to scheduled experiments. The DTL general view is presented in Fig. 146.

### IH tanks

DTL IH rf systems showed very reliable operation during beam commissioning and production this year. The only problem we faced in March, when the system was first commissioned, was that DTL #3 was multipactoring and sparking at high rf levels. The reason was found to be soldering flux trapped in the vacuum pocket behind the downstream hose cone during fabrication (see Fig. 147). Evaporation

of flux in the vacuum volume contaminated tank surfaces and a ceramic window in the coupler. After surface cleaning and nose cone screening with an additional copper electrode, the sparking and multipactoring were suppressed and the tank could stand a maximum specified voltage. But shortly after the problem was resolved, the ceramic rf window broke due to excessive heat dissipated in the deposited layer on the inner surface of the ceramics (see Fig. 148). Another coupler (DTL #1) also came to a critical

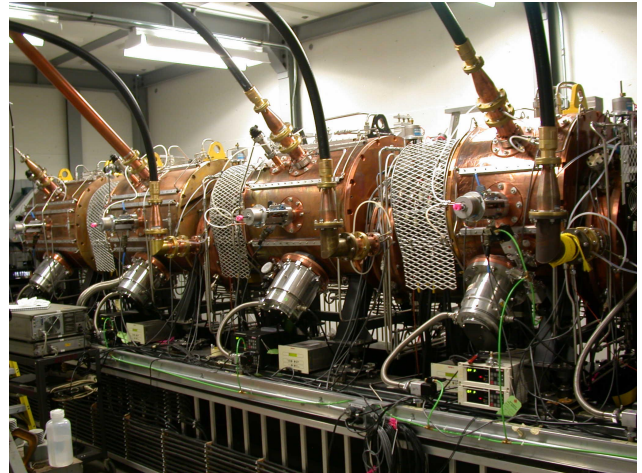


Fig. 146. DTL tanks and bunchers enclosed in the lead shielded bunker.



Fig. 147. DTL #3 nose cone spoiled with a soldering flux.

Table XXXI. Maximum required rf power for DTL systems.

DTL1	BUN1	DTL2	BUN2	DTL3	BUN3	DTL4	DTL5
4 kW	8 kW	10 kW	9 kW	16 kW	12 kW	19 kW	24 kW

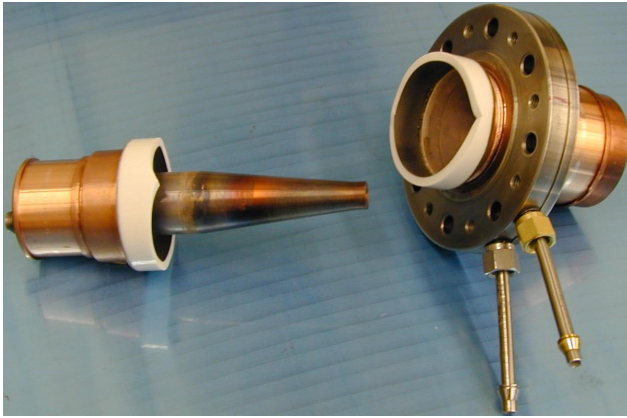


Fig. 148. DTL #3 coupler broken window.

condition. Detailed inspection showed a copper layer spattered all the way around on the coupler inner surfaces. The coupler had been replaced.

During the first year of operation, two powerful rf tubes (4CW25, 000-B) failed, showing grid to cathode short circuit.

### Triple gap bunchers

All DTL bunchers operated reliably during commissioning and beam production phases. The only problem we faced was the failure of buncher #1 power coupler. Detailed inspection showed an aluminum deposition on all inner surfaces of the coupler. Aluminum spattering was very surprising because no aluminum was used in the entire rf structure. The only source for this metal was found to be the  $\text{Al}_2\text{O}_3$  ceramic window, which was indeed eroded due to sparking.

To prevent rf windows from damage in future, two precautionary measures were implemented:

- All the couplers were equipped with infrared temperature sensors.
- High standing wave (VSWR) protection was introduced into the rf interlock.

## HEBT

### Low-beta buncher

The 11.9 MHz low-beta (2.2%) buncher was completed and installed in the HEBT (see Fig. 149) during the September shutdown. It contains two long drift tubes supported with ceramic feedthroughs and two inductive coils located outside the vacuum vessel. The device was successfully tested at full specified voltage of 30 kV requiring only 2 kW of rf power.

### High-beta buncher

The 35 MHz high-beta (3.2%) buncher was commissioned last spring and showed reliable operation in a full range of specified voltages ( $U_{\text{eff}} = 30\text{--}270$  kV).

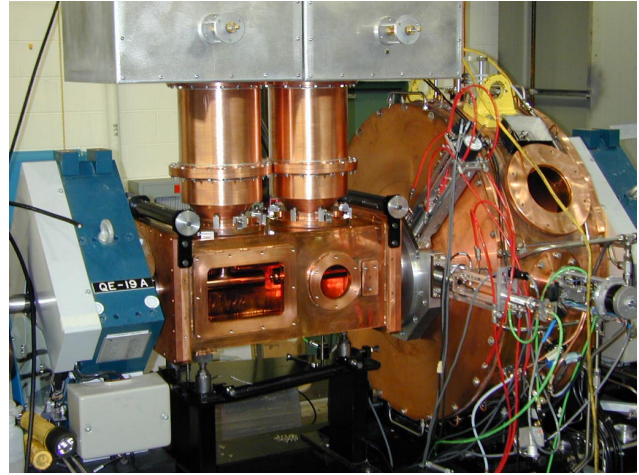


Fig. 149. Low- and high-beta bunchers installed in the HEBT.

Maximum required power is 12 kW. The buncher installed in the HEBT line is shown in Fig. 149.

## ISAC DIAGNOSTICS

### Target Diagnostics

The preseparator diagnostics box DB0 was replaced with one in which the service requirements are more practical. The redesigned DB0 has all mechanics mounted external to the vacuum with independently operated drives for the following devices: slit jaws (left and right) shown in Fig. 150, Faraday cup and scanning wire shown in Fig. 151. For simplicity of the mechanics, the new design utilizes stepping motor drives mounted externally for each of the devices so coupled motions must be done through software. All limit switches are mounted externally. There are no position encoders, the positions are derived by software tracking of the step pulses sent to the motors.

The diagnostics for the east target station (ITE) were designed, and much of the work completed, by year-end. The east target station is to be operational by the spring of 2002 so installation work will be done during the winter shutdown. Three new proton beam monitors will be installed – two for ITE and an additional one for ITW. The diagnostics in the ITE entrance module are identical to those in ITW; they were completed and mounted on the module in December. The mechanics for the ITE exit modules devices required redesign. Most of the parts were ready by year-end; assembly and installation is to be done early in the winter shutdown. ITE:harp5B was built and ready for installation early in the new year.

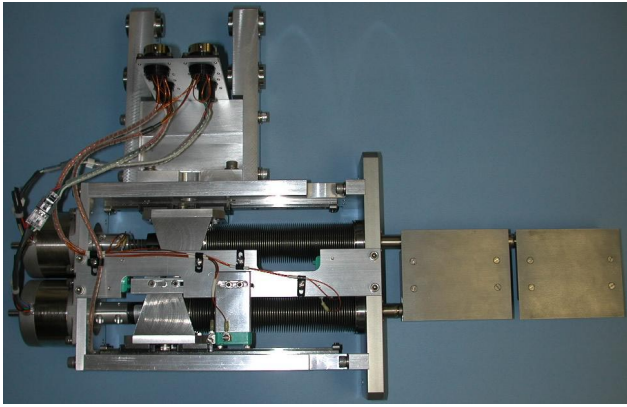


Fig. 150. DB0 slit assembly.

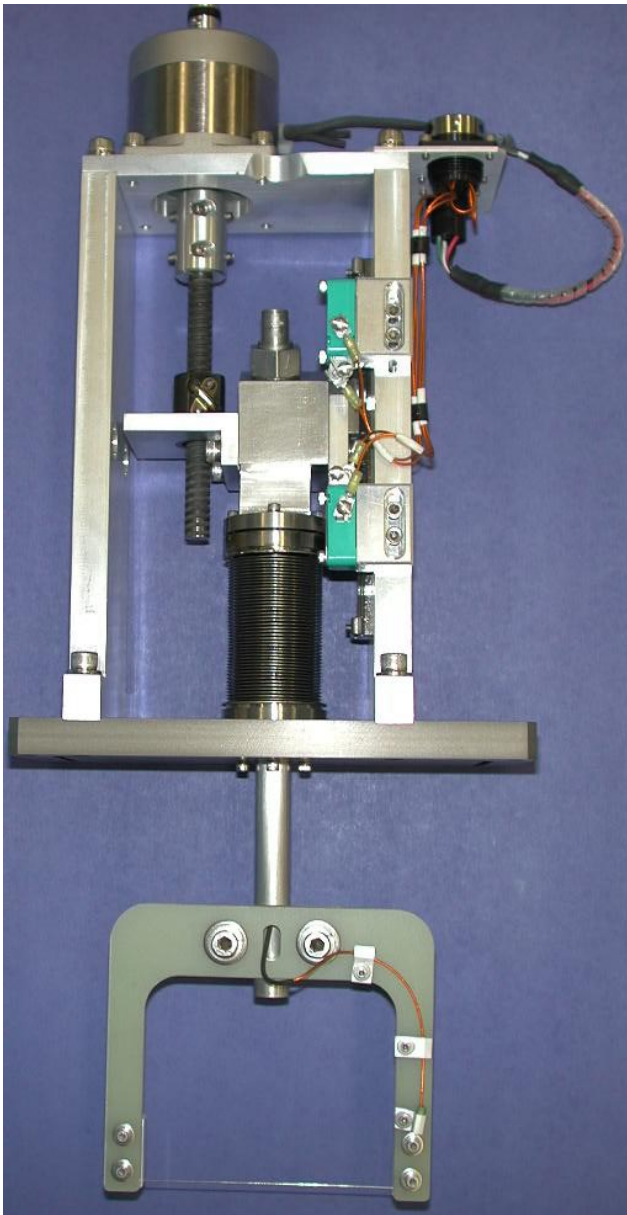


Fig. 151. DB0 wire scanner assembly.

## MRO

Mounting techniques were developed for a variety of foil types procured for the MEBT stripping foils. A working space was equipped in the ISAC cold chemistry lab and a significant effort was devoted to providing foils as needed for commissioning and operation. The diagnostics electronics support provided electronics modules, cabling and system integration for the diagnostics of the new ISAC installations of HEBT and TUDA. ISAC development projects included the installation of a multi-position beam attenuator, a channeltron, and other devices such as fast Faraday cups and wire scanners.

## Waste beam monitor

A system has been developed to continuously monitor the flux of radioactive ions. It consists of a 2.25 in.<sup>3</sup> BC412 plastic scintillator placed below the vacuum chamber in MEBT that contains the charge selection slits. It responds to the  $\gamma$ - and energetic X-rays produced when the unwanted charge states decay to more stable isotopes. The states neighbouring the desired mass are dispersed by the MEBT bending magnet and hit the slits or the beam pipe between the two. The flux of neighbouring masses should mimic the flux of the mass selected when the ion source, accelerator or stripping foil parameters change. The PMT output is discriminated, level converted and passed to a VME scalar. The rate is displayed via the EPICS system.

## Cables

A variety of different cables have been laid to the five diagnostics stations in the HEBT, DRAGON and TUDA lines. These should assist with the timely provision of special monitors and the development of diagnostics.

## Silicon detectors

Silicon detectors have been used in conjunction with scattering foils in two different applications. The first provided an extra calibration of a momentum spectrometer, the Prague magnet, using known resonances in the  $^{12}\text{C}-\alpha$  elastic scattering excitation function. The geometry is shown in Fig. 152. The target consisted of a  $20 \mu\text{g}/\text{cm}^2$  layer of gold evaporated on the upstream side of a  $20 \mu\text{g}/\text{cm}^2$  layer of carbon and was placed at  $45^\circ$  to the beam. The scattering angle of  $98^\circ$  is close to the optimum of  $105^\circ$ . The amplifiers and MCA were calibrated using a three-component  $\alpha$  source. The energy measured from elastic scattering of  $\alpha$ s from gold agreed with the nominal 1 MeV/u after corrections for kinematics and energy loss in the target. The lower energy elastic peak from carbon was quite clean when the beam was well tuned. The total

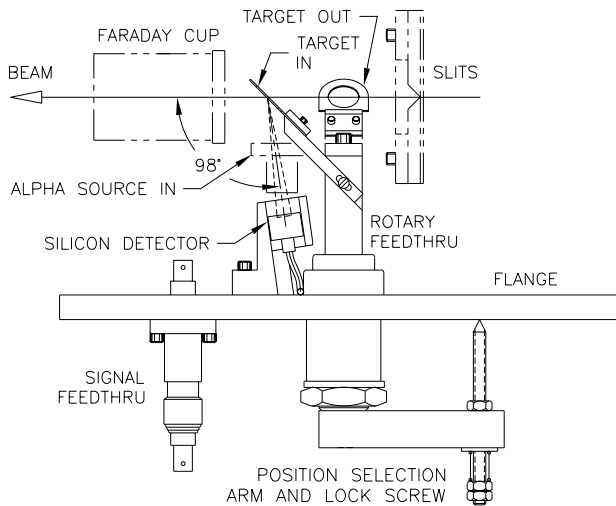


Fig. 152. The target holder can be rotated to one of three positions. One position places the foil in the beam path, the second places an alpha source in front of the detector, and the last is blank.

number of counts in the peak at 3.82 MeV, from the 4.256 resonance, was recorded as the nominal helium beam energy was varied between 4.05 and 4.5 MeV. The results were normalized using the counts in the gold peak since we did not have a digitized Faraday cup signal synchronized with the data acquisition. The resonance edge could be seen clearly and implied, after correction for small losses in the target, a beam energy  $\sim 20$  keV higher than that inferred from the magnet setting.

The second application measured the distribution in time of the ion beam and was used to optimize the setting of the rf bunchers. Particles were scattered into a 50 mm<sup>2</sup> Canberra PIPS detector from a gold target supported on a thin carbon foil. A 2003BT Canberra pre-amplifier was used most of the time and the E and T signals sent to linear and timing filter amplifiers (TFA) respectively. The TFA output passed through a CFD to provide the start signal for a time-to-pulse-height converter. The stop signal was obtained using a discriminator to transform the fundamental 11.67 sine wave from the accelerator rf synthesizer into a train of NIM pulses and then halving that frequency. The data could be displayed in correlated E-T (i.e. E- $\phi$ ) form or as a 1-D time distribution. Bunch widths as low as 0.95 ns FWHM were measured and the energy resolution was  $\sim 22$  keV. The 2-dimensional display showed tightly bunched distributions in the buckets expected for various chopper and buncher modes. Particles only fell outside the buckets when devices were grossly mistuned. This meant that the easier to set up 1-D display could be used for optimization of stable beams. The decay products of radioactive ions scattered into the detector will be registered along with the primary ion. The former will not be correlated with the rf clock and

could form a continuous background. Silicon detectors, as opposed to secondary electron based detectors such as MCPs, do not give a large response to electrons and photons but do record  $\alpha$  and other ion emission. An E-T display from a <sup>8</sup>Li beam showed the scatter of decay products but the narrow primary beam peaks stood out sufficiently from the background that 1-D displays could be used for tuning. The latter will be displayed via EPICS using a VME TDC.

An associated benefit is the use of the ion count rate and the known Rutherford cross sections to estimate beam current at levels below the response of a Faraday cup.

The resolution is sufficient for tuning purposes. Better resolution was obtained for 1-D distributions by using a ZKL-2R5 Mini-Circuits pre-amp. Further improvements could be achieved, at the cost of an increased background, by using an MCP. Both the count rate per pA and the time resolution would be improved by scattering at more forward angles. This requires optimizing the layout of this apparatus with other diagnostic equipment.

#### Beam attenuator

A compact arrangement of meshes, or sieves, has been placed in box IOS DB7 in order to attenuate the stable beam current from levels suitable for tuning the accelerators and beam lines to levels tolerable to particle detectors. There are 5 rods 1.5 in. apart operated by air cylinders with speed reducers. Each rod carries one screen. Most laboratories place two sets of attenuators sufficiently far apart that the beam emerging from each hole in the first set expands to cover the mesh structure of the second. Having all meshes in one box means that the aperture size and spacing of the rear-most grids must be scaled down by the drift ratio of, say, 1 m to 75 mm. We use drilled copper plate or commercial wire sieves on the front pistons both to supply small changes in beam flux and to absorb any high wattage. Commercial nickel sieve material with 5  $\mu$ m holes spaced 50  $\mu$ m and polycarbonate filters with a random distribution of 5, 8 or 12  $\mu$ m holes are used for the rear rods. Several filters with random distributions may be stacked to give high degrees of attenuation. Reduction factors of 10 to 4000 have been measured for single screens and higher factors have been obtained with combinations. The reduction factor varied by less than 6% as an <sup>16</sup>O<sup>+</sup> beam was steered over the surfaces and the expected ratio agreed with the measured ratio to a similar precision.

The recalibration will be repeated periodically to check that the finer screens are not deteriorating due to beam exposure, either radiation damage or holes being covered by fragments of oil or dirt drifting up or down the beam pipe.

## Danfysik emittance rig upgrade

The Danfysik emittance rig consists of a profile monitor placed about 0.5 m downstream of a slit. The two move stepwise across the beam together. The rig had been moved downstream of the DTL, just ahead of the Prague magnet. At the same time, the electronics were upgraded from a dc amplifier-per-channel system to a scanning charge integrator system using a VICA 96 VME module. The Danfysik profile monitor is an array of metal lines etched on a solid insulating substrate, however, and beam deposition had led to electrical conduction between adjacent lines. The effect of this leakage had been reduced in the dc amplifiers by using very low offset op amps to reduce the line-to-line voltages. With the new system it was found that the voltages produced across the input capacitors as the charges accumulated led to excessive leakage through the deposition. The substrate was replaced with a new harp consisting of fifteen 0.005 in. diameter Au plated Mo wires spaced 0.8 mm apart supported in vacuum by a G10 frame. This eliminated the leakage and with the charge integrator system it was possible to obtain an emittance measurement using a 1 nA  $O^{+4}$  beam using a dwell time of 800 ms. The dwell time is the time during which the motion of the slit pauses for each complete profile measurement. The new system permits long integration times of the current collected by the harp wires and the dwell time may be increased proportionately. It was possible to obtain a very clean emittance scan for a 25 epA beam using a dwell time of 4 s and background subtraction

## RF multiplexer

A solid state rf multiplexer has been developed. It has a wide bandwidth from 4 MHz to 5 GHz and can be controlled by GPIB or through Ethernet via an adapter. It will be used with oscilloscopes and phase meters to increase the number of inputs.

## Phase probe

A non-intercepting pickup was installed in the diagnostics box in front of the high-beta buncher. It is a narrow band device, resonant at the fourth harmonic of the bunch frequency, 47.5 MHz, with a loaded Q of 200. The sensitivity was measured using a 50 nA beam of  $^{16}O^{+4}$  and was found to be  $0.9 \mu V_{RMS}/nA$ . The phase jitter of the beam with respect to the rf system synthesizer was measured using an HP8508A vector voltmeter. The result was  $\pm 2^\circ$  at 47.5 MHz. A jitter of  $\pm 1^\circ$  can be achieved with 10 nA of beam by adding a pre-amp.

## Stripline FFC

The 50  $\Omega$  cone type fast Faraday cups in use in the MEBT and HEBT lines are too long in the beam di-

rection for use in the diagnostic boxes of the DTL. An assembly drawing of a short stripline type cup for use there has been made.

## BEAM COMMISSIONING

### MEBT

The MEBT optics and rf devices have been fully commissioned with beam. A bunch rotator and chopper are installed upstream of the stripping foil. The 106 MHz split ring bunch rotator is the slightly modified prototype buncher for the DTL. It provides a time-focus of the beam on the stripping foil to reduce the emittance growth due to energy straggling. The device results in improved capture by the DTL and reduced longitudinal emittance at the experiment.

The chopper has two modes of operation, one giving a bunch spacing of 85 ns removing 5% of the beam, and the other a bunch spacing of 170 ns that removes 53% of the beam. The chopper consists of a series of two sets of plates located where horizontal divergence has been minimized followed by selecting slits near the stripping foil  $\sim 90^\circ$  phase advance downstream. Each plate pair has one plate driven at rf voltage (11.8 MHz and 5.9 MHz respectively) and the other compensating plate is dc biased to produce zero deflecting field at the base of the rf waveform to reduce transverse emittance growth. In the first mode the two 35.4 MHz side-bands in the pulse structure (Fig. 153(d)) are deflected at 11.8 MHz (Fig. 153(a)) yielding the time structure shown in Fig. 153(e). In the second mode the side-bands plus every second main pulse are deflected by adding the 5.9 MHz deflection (Fig. 153(b)) from the second set of plates to yield the combined deflecting field shown in Fig. 153(c) giving the time structure measured in Fig. 153(f).

Beam simulations show that such a chopper should not increase either the transverse or longitudinal emittance. Two lumped circuits drive the rf voltage on the plates up to  $\sim 7$  kV each. The chopper is now operational and proves very reliable and easy to tune. A profile monitor at the chopper slit is used to record beam deflection and to optimize the chopper phase and then the dc bias is set to optimize transmission through the chopper slit.

### Full DTL Beam Tests

The full DTL was installed in the latter half of 2000 (Fig. 154) with the first beam accelerated to full ISAC energy of 1.53 MeV/u on December 21, 2000.

Beam commissioning in January, 2001 with the complete DTL using  $^4He^{1+}$  beams established the DTL rf parameters and beam optics settings for over twenty different energy set-points covering the full specified operation range. Initial phase and amplitude set points



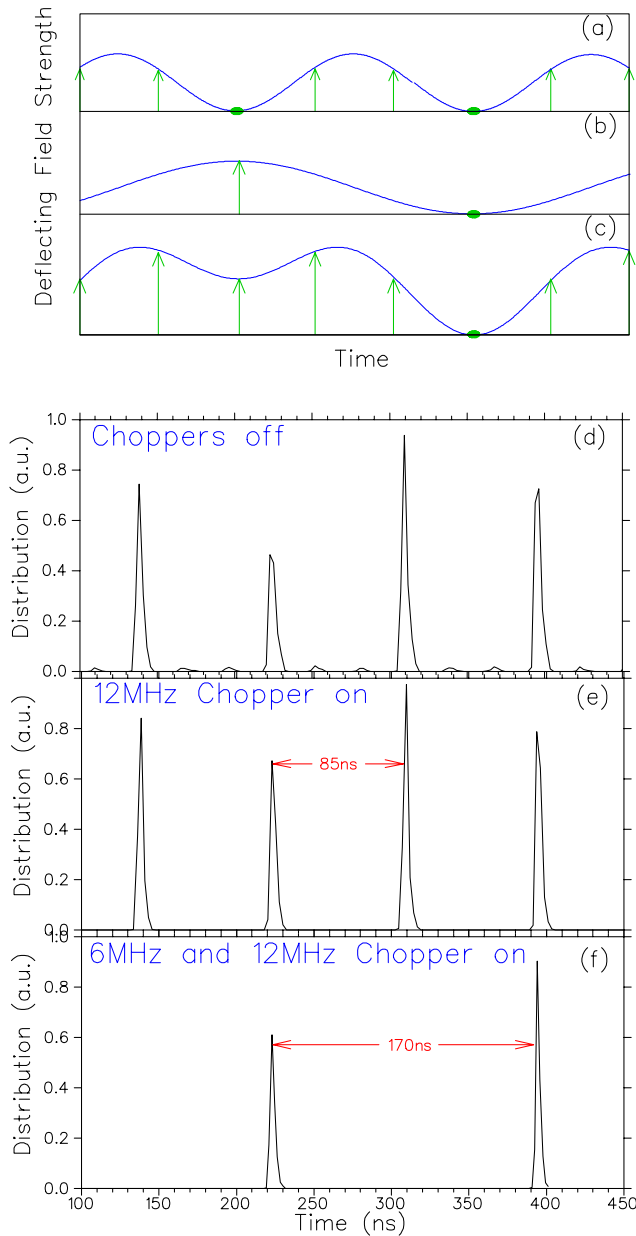


Fig. 153. Output time structure from the RFQ is shown in (d). The field produced by the 11.8 MHz chopper plate (a) produces an 85 ns time structure shown in (e). The field produced by the 5.9 MHz plate in (b) is combined with the 11.8 MHz deflection to produce the combined deflection shown in (c) and generates the time structure given in (f).

are determined empirically by beam energy measurement; each accelerator component is turned on and optimized sequentially before advancing to the next device. The DTL triplets are adjusted to optimize transmission with each large energy step.

The transmission through the DTL was over 95% for all cases. A summary plot of the accelerated beams is given in Fig. 155.

Longitudinal beam quality for all beams is as predicted. Sample spectra and associated pulse width 5 m

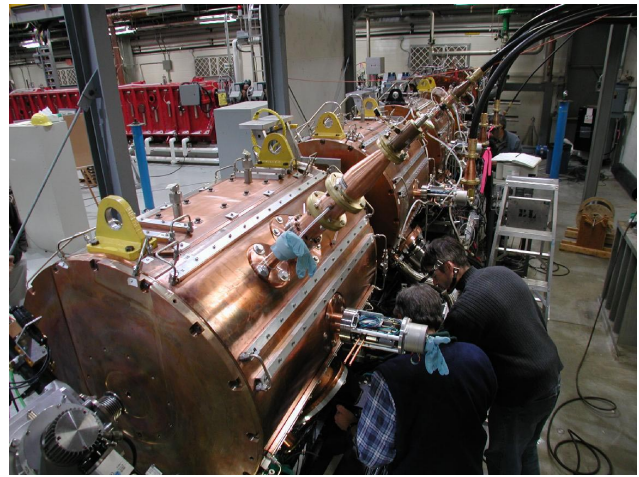


Fig. 154. The ISAC 106 MHz DTL.

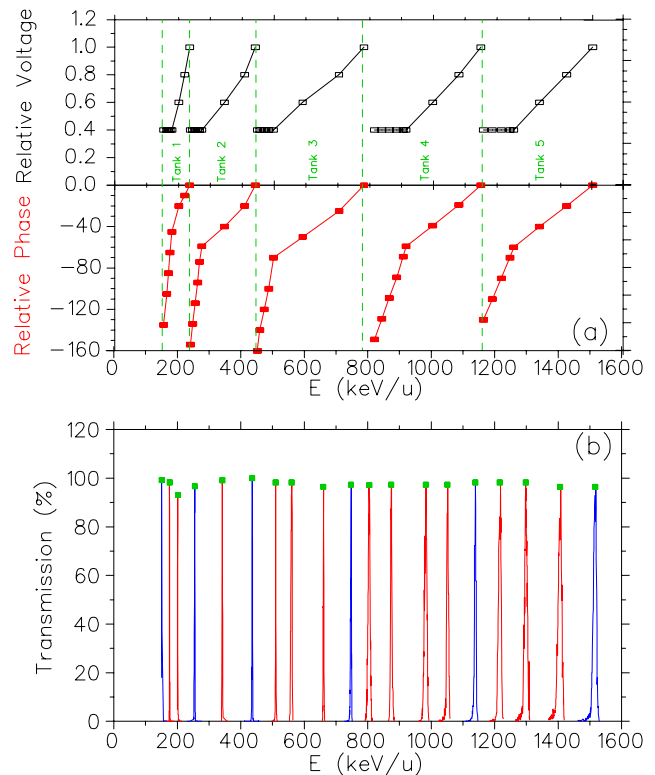


Fig. 155. Shown in (a) are the DTL rf set-points established through beam simulation. In (b) we plot the measured transmission for the various beams that have been accelerated through the DTL during commissioning studies with  $^4\text{He}$ .

downstream of the DTL are recorded for a wide range of energies corresponding to both conditions where the last operating tank is operating at the design voltage, Fig. 156, and conditions where the last operating tank is at a detuned voltage, Fig. 157.

#### Final energy

The ISAC DTL is designed for a maximum energy of 1.53 MeV/u and for a maximum  $A/q = 6$ . The

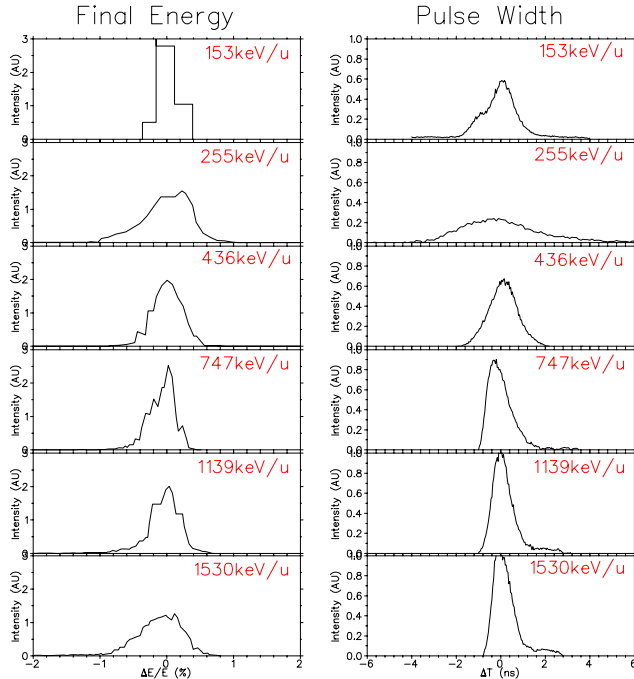


Fig. 156. A sample of energy spectra and associated pulse width measured 5 m from the DTL for tanks operating at design voltage.

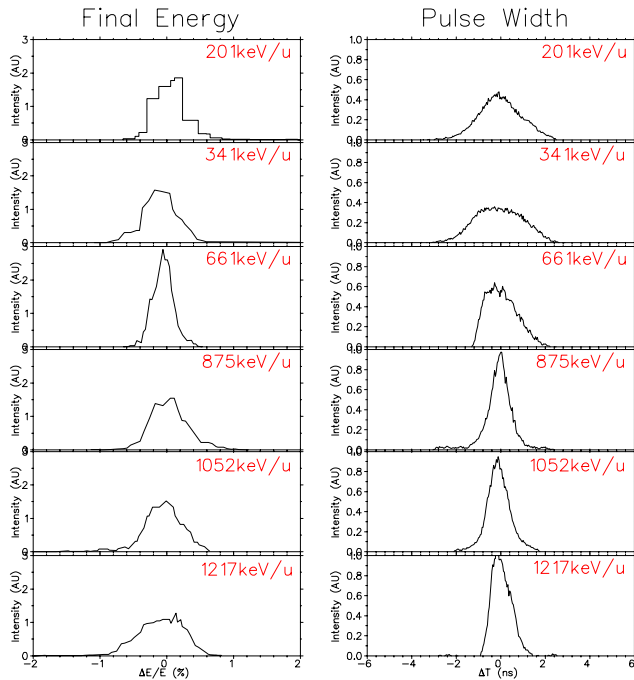


Fig. 157. A sample of energy spectra and associated pulse width measured 5 m from the DTL for the last tank operating at a detuned voltage.

DTL essentially operates as a fixed velocity accelerator with voltage and phase detuning in the last operating tank to accelerate to a reduced energy. The full energy range from 0.153–1.53 MeV/u can be spanned by this method. Conversely it is possible to reach a higher

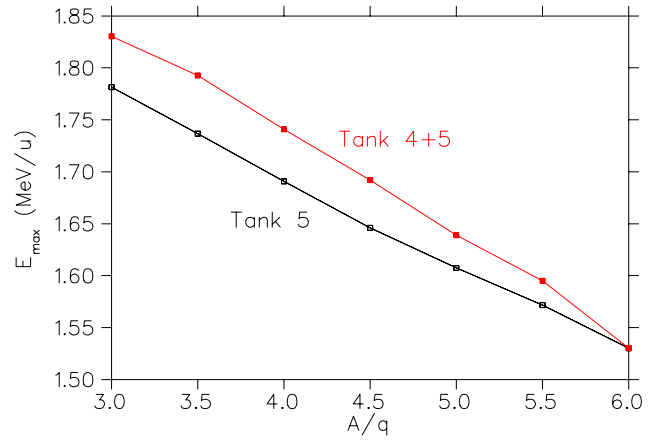


Fig. 158. Final beam energy simulated for two cases. In the first case Tank 5 voltage is operated at maximum and the phase is altered to maximize the acceleration. In the second case both Tank 4 and Tank 5 are maintained at maximum voltage.

final energy than specified by increasing the voltage in the last operating tank and optimizing the phase for maximum acceleration. Assuming that the maximum voltage in a tank occurs for  $A/q = 6$ , then these higher energies are only possible for  $A/q < 6$  values. Since the higher voltage increases the particle velocity above the design value, phase slippage during the tank crossing occurs. Therefore as the relative voltage increases, the incident particles must be pushed to more and more positive phases to achieve maximum acceleration. Some additional energy can be achieved by increasing the relative voltage on the second to last tank to maximize the energy entering the last tank. The gain cannot be duplicated by increasing the voltage in all tanks since the large phase slip caused by accelerating particles with a velocity higher than designed does degrade longitudinal beam quality. Simulated final energies for two cases, one where Tank 5 alone is increased in voltage, or the second where both Tank 4 and Tank 5 are used, are given in Fig. 158.

## HEBT

The high energy beam transport (HEBT) feeds two target stations 23 m and 30 m downstream of the DTL: the DRAGON windowless gas target and recoil mass spectrometer, and the TUDA multi-purpose detector array. The HEBT is composed of four basic sections: a section to match the beam from the DTL to the HEBT, a diagnostic section and bunching section, achromatic bend sections to deliver beams to the experiments and matching sections to focus the beam to the experimental targets.

The diagnostic section is used by accelerator personnel for beam commissioning and pre-tuning before experiments. Included in the section are a high dispersion  $90^\circ$  analyzing magnet for beam energy and en-

energy spread analysis and a transverse emittance rig. A low- $\beta$  ( $\beta_0 = 0.022$ ) 11.8 MHz rebuncher and a high- $\beta$  ( $\beta_0 = 0.032$ ) 35.4 MHz rebuncher are positioned on either side of a double focus positioned 12 m downstream of the DTL. The 11.8 MHz rebuncher is a three-gap structure driven by two lumped element circuits with up to 30 kV required on each drift tube. The 35.4 MHz buncher is a two-gap spiral device similar to the MEBT rebuncher with up to 170 kV required on the drift tube.

The HEBT line including the high- $\beta$  buncher has been commissioned in April, 2001. Figure 159 shows the beam time distribution close to the DRAGON target for the buncher off and on. The low- $\beta$  buncher has been commissioned in September, 2001. Both bunchers perform as specified giving the flexibility to adequately bunch the beam over the whole energy range of the DTL.

## Beam Delivery

### Stable beams

Stable beams of  ${}^4\text{He}^{1+}$ ,  ${}^6\text{Li}^{2+}$ ,  ${}^{13}\text{C}^{3+}$ ,  ${}^{14,15}\text{N}^{4+}$ ,  ${}^{16}\text{O}^{4+}$ ,  ${}^{21}\text{Ne}^{5+}$ , and  ${}^{24}\text{Mg}^{6+}$  have been delivered to the two experimental facilities at various beam energies. The early stable beam delivery periods proved essential both in training the operators and in determining hardware improvements and required developments prior to first scheduled radioactive beam delivery of  ${}^8\text{Li}$  in mid July. Although the ISAC DTL is a variable energy device, it still essentially operates as a fixed velocity linac (except for the last operating tank) so that phase relationships between cavities are fixed regardless of particle mass and charge and only the voltage need be scaled, shortening beam tuning time. Small energy steps down to 0.1% are easily realized by linear voltage or phase steps in the last operating DTL tank. New beam tunes are established by a beam physicist with round the clock delivery by ISAC operations staff. The ISAC operators have quickly adjusted to the new

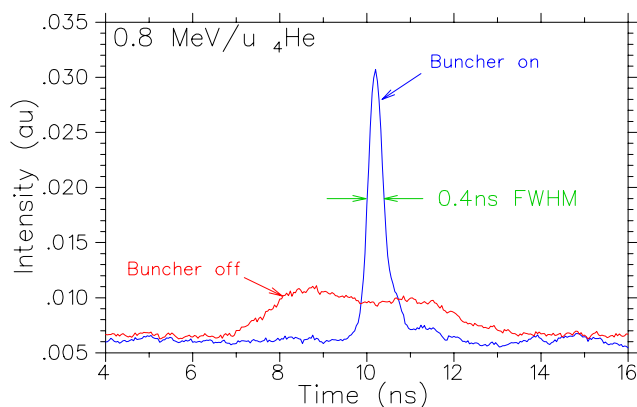


Fig. 159. Beam time distributions measured on a fast Faraday cup near the DRAGON target for high- $\beta$  buncher off and on.

accelerators and now handle routine procedures such as foil changes, energy changes and recovering beam delivery after hardware trips.

Several early improvements have been added that greatly reduce linac tuning time. Foil changes are facilitated by a global phase shifter between the pre-stripper and post-stripper accelerator sections to account for slight differences in foil thickness. A cold trap surrounding the stripper foil has now minimized foil thickness changes and lifetime issues due to carbon build-up.

### Radioactive beams

The first radioactive beam to be accelerated at ISAC was  ${}^8\text{Li}^{2+}$  delivered to the TOJA facility that occupied the target location on the TUDA line. This first run was instrumental in establishing operational procedures to deliver radioactive beams to target. The beam delivery starts first by choosing a stable pilot beam from OLIS with the same  $A/q$  as the radioactive beam for both the pre-stripper and post-stripper lines. In the case of  ${}^8\text{Li}^{2+}$ , we used  ${}^{16}\text{O}^{2+}$  from the source and  ${}^{16}\text{O}^{4+}$  in the post-stripper section as the pilot beam. The beam tune is established and optimized to the correct energy and delivered to the experiment. In parallel, the radioactive beam is optimized through the mass separator and low energy optics transport. Once both beams are established it is straightforward to switch from stable to radioactive beams. The low energy bend electrode in the switchyard is switched to change the beam path from OLIS to the mass-separated beam. Next the optics and steering in the switchyard section are optimized to match the radioactive beam to the accelerator. This is done by maximizing the beam to a Faraday cup just upstream of the RFQ. Since the stable beam and the active beam come from different platforms there is a small energy difference between beams so a phase shifter is used to optimize the phase of the beam entering the RFQ by maximizing the accelerated beam to the stripper foil box. Lastly the beam is sent through the DTL to experiment. The global phase shifter between RFQ and DTL can be used to cancel any differences between the interaction of the pilot beam and the radioactive beam in the stripping foil.

At present the radioactive beams are mostly tuned by standard high intensity diagnostics including Faraday cups and scanning wire profile monitors. A low intensity timing diagnostic consisting of a gold foil and silicon detector was added upstream of the TUDA facility to help tune the buncher for low-intensity beams. A multi-head pepperpot device was added after OLIS that can change the intensity of the stable beam by several orders of magnitude. This is very useful to aid

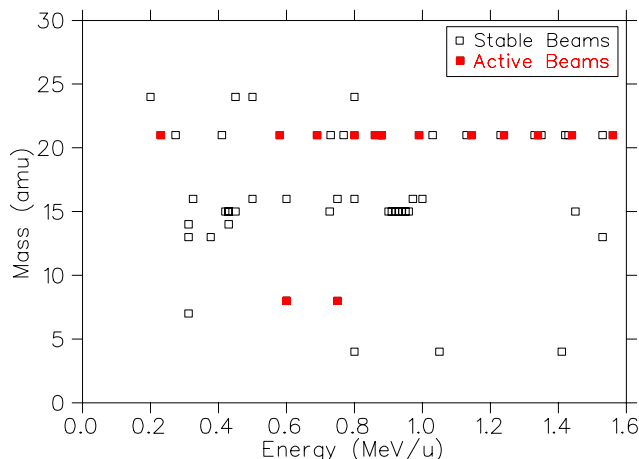


Fig. 160. A summary of stable and radioactive accelerated beams delivered to experiment in 2000.

in tuning through experimental target chambers where damage to detectors is a concern.

A summary of the stable and radioactive beams delivered to experiment in 2000 is shown in Fig. 160.

## LEBT

Four new beam lines have been constructed this year as extensions to the LEBT section of ISAC. They are: GPS1,  $8\pi$ , polarized beam lines polarimeter, and Osaka.

### GPS1

The general purpose station (GPS) has been relocated to the northwest corner of the LEBT area to facilitate the installation of  $8\pi$  in this location, and has been re-designated as GPS1. In order to accomplish this relocation, the beam line was extended 2 m to avoid interference with polarizer equipment. Four new electrostatic quadrupoles were added for beam transport purposes. The beam line will be commissioned in early 2002.

### $8\pi$

The  $8\pi$  beam line was designed to bring the beam to the  $8\pi$  spectrometer. This line is the longest extension added this year to the LEBT with one  $45^\circ$  electrostatic bend, twelve electrostatic quadrupoles, two pairs of  $x$  and  $y$  slits, four emittance scanners, and three Faraday cups. The vacuum system consists of two independent sections pumped by turbo molecular pumps with fore pumps for each section.

The beam line was installed and commissioned in November, 2001 with stable beam from the off-line ion source (OLIS).

### Polarimeter

The polarimeter system was designed for nuclear polarization measurements of an ion beam emanat-

ing from the polarizer. The design incorporates an ultra high vacuum system for future experiments using low-magnetic-field  $\beta$ -NMR at cryogenic temperatures on the target. The UHV system operates at  $1.2 \times 10^{-10}$  torr and consists of three vacuum chambers pumped by two 500 l/s turbo molecular pumps, and one 1000 l/s cryopump. The ion beam is focused onto a stopper foil (target) placed in the centre of the last chamber, where the nuclear polarization is measured by observing the beta-decay asymmetry with plastic scintillator telescopes placed outside the chamber. Helmholtz coils provide a magnetic field of up to 0.02 T to maintain nuclear polarization. The polarimeter system also can be used for other experiments with minor modifications or extensions. The polarimeter was commissioned in August, 2001, and has successfully measured the polarization of  $^8\text{Li}$  and  $^9\text{Li}$  beams.

### Osaka

The Osaka beam line is another extension of the polarized section of LEBT and is designated as a general purpose facility for polarized beams. The line has been designed and named for the first experiment on it – Expt. 903: Professor Shimoda’s group from Osaka University. Their run is planned in 2002 with polarized  $^{11}\text{Li}$  beam.

The line includes one  $45^\circ$  electrostatic bend, nine electrostatic quadrupoles, two emittance scanners, and a Faraday cup. The Osaka beam line vacuum system is an extension of a section between the polarizer and  $\beta$ -NMR. It is pumped by a turbo molecular pump installed on the bend box in addition to the existing turbo molecular pump with the roughing-backing collector extended from the existing fore pump.

The Osaka beam line should be commissioned in early 2002.

## MASS SEPARATOR

During 2001 the ISAC facility delivered several radioactive ion beams. Even though the commissioning of the mass separator was never completed due to lack of time, we were able to tune the beam with sufficient reliability over the year. The highlight is the complete separation of  $^{75}\text{Ga}$  and  $^{75}\text{Rb}$ . The mass difference is only  $1.61 \times 10^{-4}$ , which corresponds to a resolving power larger than 6000.

During the year several users reported beam intensity instabilities that look like a rapid decrease and a slow recovery. We monitor the beam intensity on a Faraday cup just after the mass separator over several hours without seeing any instability except for high voltage sparks which show a fast decrease and rapid recovery. The investigation will continue during this shutdown period.

During the 2001 winter shutdown period we worked on the high voltage Faraday cage around the mass separator and proceeded to the installation of the insulation transformer and high voltage power supply.

During the 2002 winter shutdown period we will finish the installation of the services and the safety equipment for operation under high voltage conditions and in March we have three weeks scheduled for commissioning of the mass separator and the high voltage platform.

## EAST TARGET STATION

In January, a decision was made to complete the east target station to be operational by the spring of 2002 as a top priority for ISAC. Previous to this, the main effort was directed towards supporting the operation of the west target station, completing many unfinished tasks in the target hall, remote handling, building spare target modules (TM2) in case of problems with TM1 in service, and TM3 to house the ECR source that was in development, to be completed later in 2001. In order to achieve completion of the east target station, the project was broken down into work packages and schedules. The major work packages with a brief description are as follows:

### Modules

It was realized at this time that removal of the TM1 containment box tray (supporting the surface source extraction column) remotely in the hot cell was not possible due to interference between the extraction column and the services from the service duct (i.e. H<sub>2</sub>O lines and conductors). TM1 at that time had not accumulated much radioactivity and this deficiency was corrected with a hands-on modification outside of the hot cell. It was also realized that providing services (down the service duct) for an ECR source (TM3) could not be dealt with in the same way due to the greater number of conductors and increased complexity of the extraction column.

In order to ensure that the containment box tray supporting the extraction column and/or the service tray can be removed from the target module in the hot cell, the entire service philosophy was revisited. This resulted in an intensive design study which introduced the use of 14 water block/current connectors allowing all services from the containment box tray to be disconnected from those coming down the service tray, allowing for both tray removals. Special tooling and fixtures were designed to allow this complex procedure to be accomplished in the hot cell by manipulators. The simpler surface source uses only those water blocks necessary, hence the target module now caters to either source. This redesign work was timely since progress on the design of the ECR had been delayed and now

a more coordinated approach could be employed. This was particularly true regarding the ECR waveguide, details of which proved to be an engineering challenge in order to accommodate it through the shield plug and interface with the HV ECR cavity through a choke.

When TM1 was redesigned to produce TM2 (etc.) the reason was to improve accessibility to the service duct as well as simplify many aspects of the design and also improve manufacturability. It was also the intention to utilize the same design for the EXIT modules for the east target station. This, coupled with a new optics design for both EXIT modules, required considerable redesign of the service cap, service duct contents, containment box and contents, as well as the optics themselves and all linkages and actuators for the diagnostics.

The entrance and dump modules required no fundamental changes other than the fact that they are mirror images of the west station due to the proton beam offset relative to the centre of the module. Hence a new set of drawings was required and there is no interchangeability with the west station.

### 2A beam line

Work had commenced on the design of the 2A switching magnet (2AB3) early in 2000. The schedule for manufacture, delivery, mapping, etc., allowed for a timely installation to meet the east target station schedule. The remainder of the beam line 2A3 to the east target station mimicked that of the west station and therefore required the ordering and manufacture of components ready for installation, which could only commence during the shutdown (i.e. 2002).

### East module access area (EMAA)

(Note: This area is actually the volume below the shield plugs and above the vacuum tank.)

At the beginning of this report period the east target tank had been installed and aligned and no further action had taken place. In February, this work package was planned and a schedule was drawn up to complete all work necessary to render the east station operational in May, 2002.

The EMMA work package included:

- EMMA preparation. This work involved completion of the diaphragm air sealing system which is part of the overall nuclear ventilation system, completion of the 5b shielding package between the east tank and the preseparator magnet, installation of the east tank top plate and seal (and check for leaks), installation of the upstream proton beam window and window shield plug, etc., and installation of the inter modular connector (IMC). This is a pneumatically actuated capsule

that is installed in the tank at 3 locations and connects the target/EX1/EX2 modules together and then to the RIB exit beam line to separate primary from secondary vacuum to minimize potential contamination.

- EMEA layout. In order to maximize accessibility (and minimize dose), installation of all services such as cabling, air lines, vacuum lines, H<sub>2</sub>O lines, cable trays, etc., is controlled by an installation layout which is supervised by the target hall coordinator. An ECR source (TM3) requires installation of a 2.45 GHz waveguide to connect to the module waveguide flange at the top of the service cap. It was decided that the best arrangement would be to install the power supply and generator in the electrical room, and then the magnatron, isolator, and autotuner would be located in the EMEA. These items required attention to provide the location and support necessary, and designed such that a piece of waveguide could be detached quickly for module removal.

## Services

At the time of installation of the west target station, none of the services were extended to the east target station. However, the H<sub>2</sub>O and vacuum systems are sized to handle both. Due to operational requirements, both systems required modifications to allow the non-operational station to condition targets (i.e. H<sub>2</sub>O and vacuum required). These systems were designed and installation commenced in the fall. High voltage services from the electrical room Faraday cage would mimic those of the west station, but installation could not commence until the shutdown (January, 2002). The HV containment chase had been prepared previously. There were two grounding circuits required to be installed from the electrical room through the HV chase and EMEA, to the preseparator area and to the mass separator. One is a heavy cable for building ground, and the other rf type ground to deal with the eventuality of a HV spark over. These will be dealt with as construction and installation progress.

## Faraday Cage and Electrical Room

As mentioned, nothing had been done to provide high voltage services to the east target station prior to 2001, and construction work in the electrical room was only allowed when the west station was not operating. During the year, construction was scheduled to take advantage of maintenance days, and target change shutdowns to conduct the Faraday cage, necessary services, cable trays and electronics racks. All required power supplies, transformers, controllers, etc., were ordered early in the year.

## Other Systems

Information regarding the control system related to proton beam, radioactive ion beam, and target protect, are found elsewhere in this Annual Report under Controls. Safety systems related to the east target station can be found in this Annual Report under Operational Safety. This describes the philosophy of the safety interlock system. Operation of the west target station has shown that radiation emanating from the H<sub>2</sub>O package and transport piping is too high and requires shielding (as was expected initially). The H<sub>2</sub>O package currently has shielding but there are too many shine paths. This was inspected and a proposal approved by the Safety group. Installation will commence in 2002.

## ISAC PLANNING

This year the Planning group was involved in planning, scheduling, coordinating and expediting several sub-projects for ISAC.

Various plans and PERTs were prepared and updated regularly with manpower estimates and analysis to identify critical areas and resolve any problems. ISAC priorities were evaluated and higher priority was assigned to: the east target station with an aim to install in the winter, 2002 shutdown and optimize RIB operation for the ISAC experimental program; expedite the low energy experimental program that included a first data run at  $\beta$ -NMR; move GPS1; Osaka beam line; and commission TUDA and DRAGON with stable beams and RIB.

On the accelerator side, major milestones (after beam to 1.5 MeV/u in December, 2000) included installing and commissioning the 11 MHz buncher by September to facilitate commissioning of high energy experiments (TOJA, TUDA and DRAGON) by November. Manpower planning was done, activities were coordinated and expedited, and the above goals were achieved on schedule.

Technical details and progress on PERTed activities are described elsewhere in this report under the respective principal group. However, following is a summary of the main projects along with the major milestones achieved.

## East Target Station

This project received high priority and had to be fast-tracked for installation in the January, 2002 shutdown. The project was broken down into 9 work packages that included: 2A beam line, IMC, MAA, Faraday cage, target hall, services, controls, safety, and 5 target modules (entrance, dump, exit 1 and 2, and target module). Major highlights of these work packages included: 2A beam line (switching dipole received in September, monitors and associated beam line hardware received in December), Faraday cage (constructed

by July and isolation transformer, high voltage and other power supplies procured by October), target hall (including modification and commissioning of south hot cell and storage silos in July, alignment components and water packing shielding in November), controls (including 2A controls, target protect interlocks and RIB controls for vacuum system, beam optics and beam diagnostic systems). Work on modules was a major work package that required extensive Design Office and Machine Shop effort. Several design modifications were made for better manufacturability and handleability. Shield plugs were ordered in April, with a staged delivery for most modules in July. Below is a summary of the modules work packages:

- Dump module included shield plug dump and pipes which were designed by the University of Victoria engineering group and fabricated in October. Entrance module included shield plugs, diagnostics (2A 3M19, M20, collimator) and associated electronics.
- Exit modules 1 and 2 included shield plugs, containment boxes, service and pumping ducts, service caps, optics (water-cooled), diagnostics (collimator 3 and harp 3 for exit 1, and collimator 5, harps 5A, 5B and Faraday cup).
- Target module required extensive design changes compared to that for the west target station to also accommodate ECR source. It included shield plug, service cap, containment box and ion source. Although diagnostic components were very similar in design, the fabrication and assembly took longer due to a manpower shortage in the Diagnostics group.

### Target Conditioning Box

An alternative conditioning system was designed and fabricated by December to expedite the process of changing and conditioning ISAC targets. Assembly was delayed to January, 2002, due to lack of manpower.

### HEBT

After completing HEBT1 (up to upstream of benders to DRAGON and TUDA beam line), and delivering beam to 1.5 MeV/u in December, 2000, resources were focused to complete chopper and bunch rotator (July), and 11 MHz buncher (September).

### Low Energy Experiments

These included moving GPS1 to a new location, modifications to LTNO and yield station, and  $\beta$ -NMR (new polarimeter, modifications to laser system, HV platform, and Oxford magnet). Extensive work was done on planning, coordinating and expediting activities and critical components from the Machine Shop

and outside suppliers for  $\beta$ -NMR, laser polarization systems, spectrometer, and associated LEBT components. The first data run on  $\beta$ -NMR was completed in the summer with polarization >65%, platform operation at 24 kV, and new polarimeter. Among other low energy experiments, the Osaka beam line was installed and tested in October/November with new chamber and associated services. The  $8\pi$  beam line with a simple chamber was installed and commissioned with a test beam in December.

### High Energy Experiments

These involved DRAGON and TUDA. Installation of HEBT components up to the TUDA experimental station, with associated services, was finished in March. A special room was designed and constructed for the TUDA detector system electronics, with all services and a special grounding system. The first stable beam to TUDA was delivered in March. First RIB was delivered to TOJA in June, and to TUDA in September, after commissioning the 11 MHz buncher.

### DRAGON

After completing installation of most components up to MD2 in December, 2000, the overall progress on DRAGON installation was relatively slow due to lack of technical resources. Several initial tests were done to commission the gas targets with its control system. Alpha tests up to the charge slits were done in January, and continued down the line as services were completed. DRAGON was commissioned with stable beam in October, followed by RIB in November.

### ISAC-II

PERTs were prepared that included work on specifications and design of a superconducting rf test facility and dummy cavity. A construction contract was awarded in October, and a test facility at B.C. Research was constructed at the end of November. Plastic roof and doors for the clean area, and hoist delivery was delayed to January, 2002. A Nb cavity was received from Legnaro in early summer. A dummy cavity was tested in a cryostat (without rf) in October, and (with rf) in December, with a plan to repeat these tests at B.C. Research in early February, 2002, followed by cold tests on the Nb cavity with rf controls in March, 2002. Milestones were established for the ACOT meeting in November, with an aim to be ready for 5.8 MeV/u at  $A < 60$  by April, 2005. Detailed schedules of ISAC-II projects were prepared that included: medium-beta cavities (with cryostats, refrigeration system and solenoid, with an aim to test first cryo module by summer, 2003); high-beta cavities system; charge state booster system which included tests on test stand with an aim to order CSB by December,

and test the whole system in the test stand by October, 2003; HEBT transfer system and H<sup>-</sup> HEBT to experimental stations.

### CONTRACT ADMINISTRATION

In the past year four contracts were awarded: Brandt Industries Ltd. of Saskatchewan manufactured the east target module and the east exit #1 and exit #2 modules. Brandt also manufactured the east dump and east entrance modules under a second contract.

Sunrise Engineering Ltd. of British Columbia manufactured the poles for the beam line 2A 15° switching dipole magnet. Sunrise also assembled the magnet, with Sigmaphi of France supplying the coils.

### Personnel Resources

In 2001 the average monthly personnel effort for ISAC decreased by approximately 7.6 people to an average of 76.15 FTE people per month (see Fig. 161). In 2000 the FTE effort per month was 83.75 people. The decrease was mainly due to a change in the monitoring system of personnel effort. Effective September 1, 2001, the recording of effort for the science facilities ended as the science construction phase was considered complete.

The average monthly personnel effort per system in 2001 (see Fig. 162) is described in Table XXXII.

Table XXXII. Personnel effort per system.

System	Monthly FTE
Project management & administration	3.90
Beam line 2A	1.35
Target station	9.33
LEBT	6.49
Accelerator	11.77
Science facilities (TRIUMF personnel)	13.40
Science facilities (non-TRIUMF personnel)	1.42
Infrastructure	8.91
Integration	16.89
ISAC-II	2.69
<b>Total average FTE monthly personnel</b>	<b>76.15</b>

Figure 163 shows the average monthly FTE personnel working on ISAC for the year 2001 based on the type of personnel.

The average monthly FTE personnel effort per system spent on ISAC science for the year 2001 is shown in Fig. 164. Note that the monitoring of personnel effort for ISAC science was discontinued August 31 as construction was considered complete.

The total personnel effort for ISAC since the start of the project January 1, 1996 to December 31, 2001 has been 422.77 years of work, based on a FTE work-month of 150 hours per person.

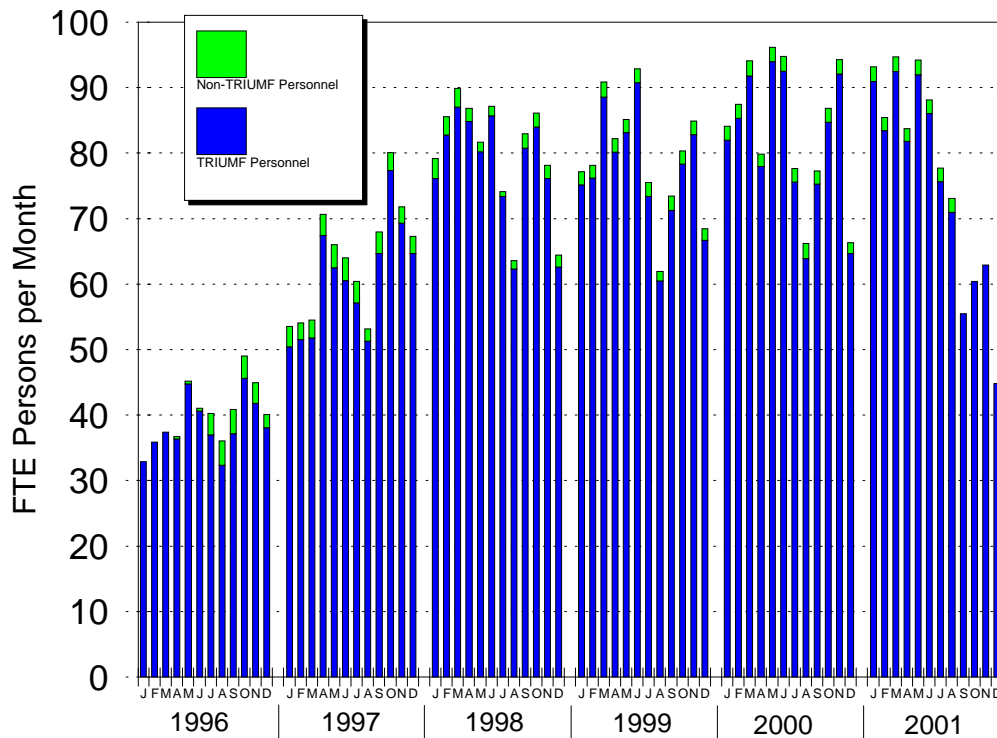


Fig. 161. ISAC monthly personnel effort, January 1, 1996 to December 31, 2001.



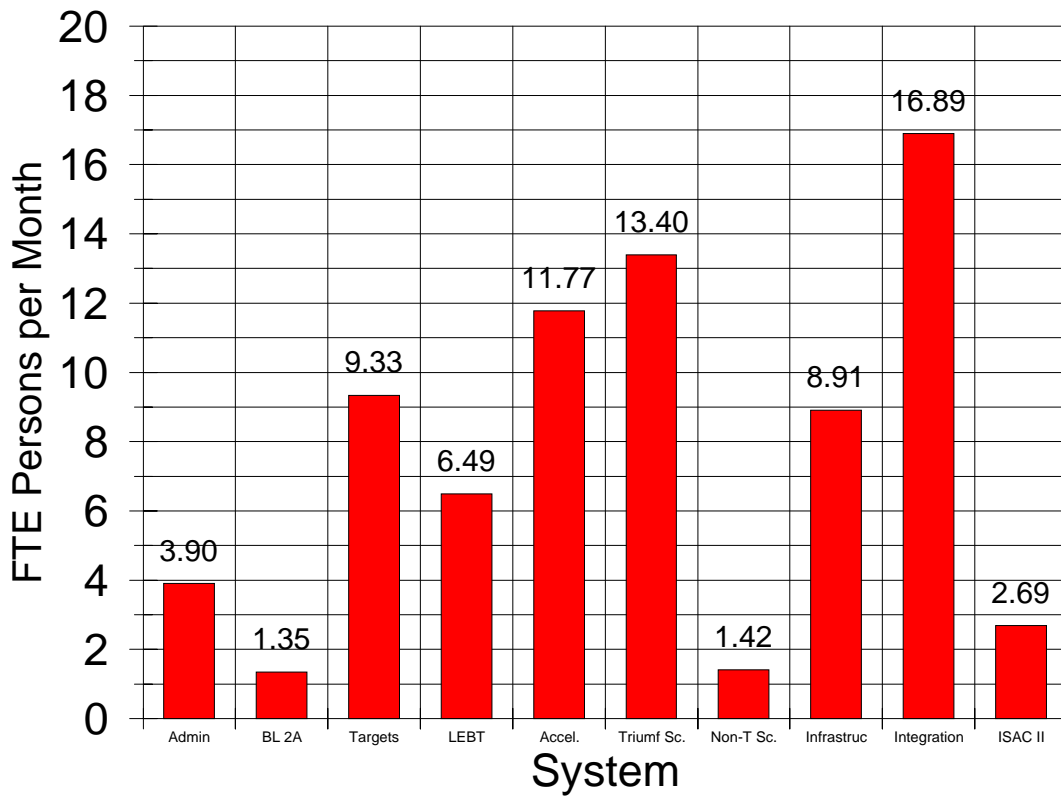


Fig. 162. ISAC average monthly personnel effort, shown by system for 2001.

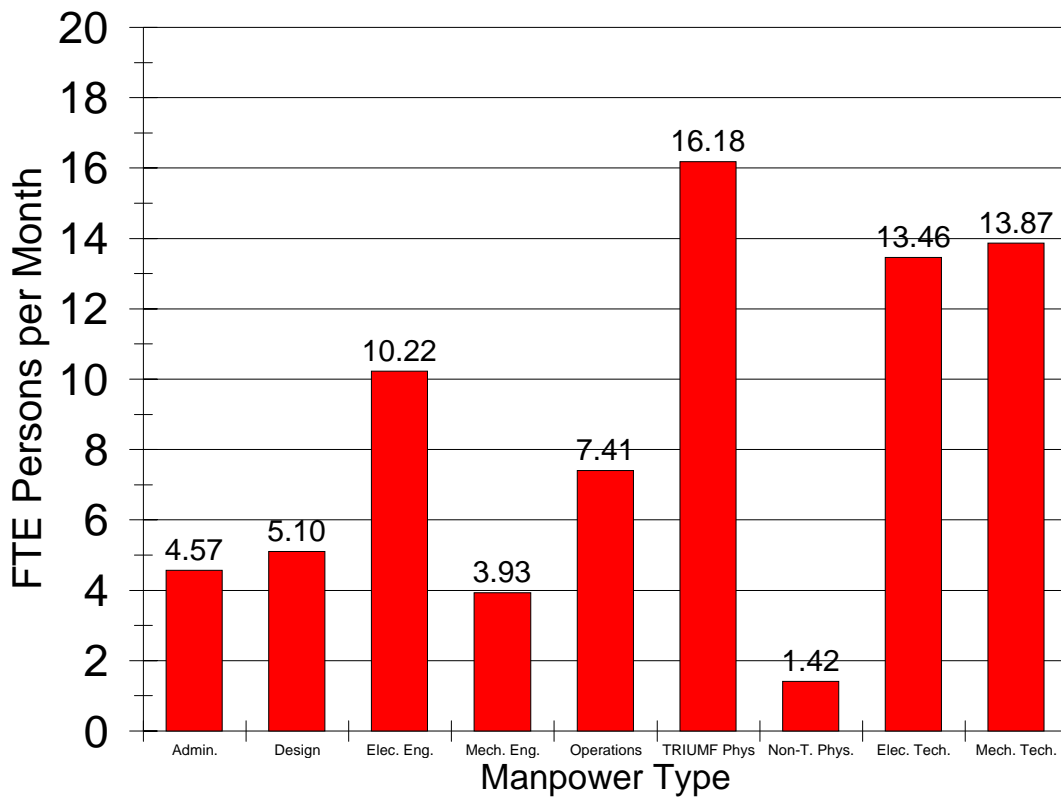


Fig. 163. ISAC average monthly personnel effort, shown by personnel type for 2001.

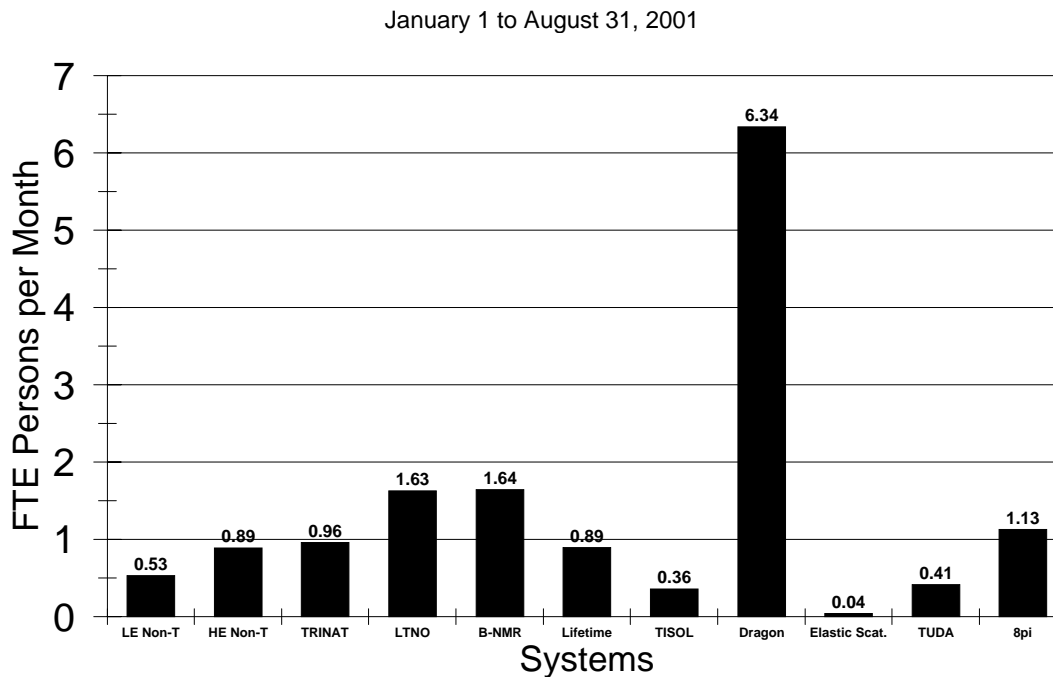


Fig. 164. ISAC average monthly personnel effort, science facilities, for January 1 to August 31, 2001.

## CONVENTIONAL FACILITIES AND INFRASTRUCTURES

ISAC continued to be the focus of the engineering and installation efforts. The ISAC-II expansion project received funding approval in April and was kick-started in earnest in May. Close coordination work continued with the Accelerator groups, the Engineering group and the Science Division for the installation and commissioning of the experimental facilities. This included attendance at regular and engineering meetings and participation in the engineering design review.

### Mechanical Services

ISAC consumed a majority of the 2001 effort. ISAC experimental hall completion comprised a wide range of work including cooling water, compressed air, and vacuum lines to HEBT and experimental areas, completion and commissioning of the DRAGON hydrogen exhaust system, gas tubing and alarms. Other ISAC completion jobs included a third controlled temperature water loop for TRINAT, mechanical penthouse hay loft hoist, connection and commissioning alarms for 6 fume hoods, spent target vault ventilation and exhaust, high level alarms for the three filling points for the decontamination sump, and vacuum roughing lines to the CDS room. One ISAC development job was the modification of experimental hall roof top heating units to act as exhaust fans for summer operation, and the installation of a test area of open floor grating on the mezzanine. This action is intended to reduce the air temperature on the mezzanine in summer, by moving

more outdoor air through the building, and allowing it free convection access to the mezzanine. Other development jobs included modification to chilled water supply lines to the electrical room to allow more efficient operation of chiller 2 in winter, venting the decontamination and sanitary sumps for odour control, and DDC operational improvements. A list of MRO work was carried out.

Engineering assistance was provided for the ISAC-II building project, and the SCRF room at B.C. Research.

### Electrical Services

Engineering efforts focused on the experimental facilities, the target conditioning facility and the east target. Completed tasks included services for experiments like DRAGON, TUDA,  $8\pi$ , the polarimeter, Osaka, and the power distribution for the 60 kV bias target conditioning system. The 60 kV bias distribution for the mass separator was also completed. For the MEBT a new supply and wiring were provided to accommodate a new Stinson steerer, which replaced an AECL steering magnet. About 40 installation orders were processed for ISAC alone. The largest single task was the design of the grounding and the ac power distribution for the east target ion source terminal. The initial target grounding concept was revised and expanded to include the east target. The experience gained with the operation of the west target ion source led to changes to the initial grounding scheme

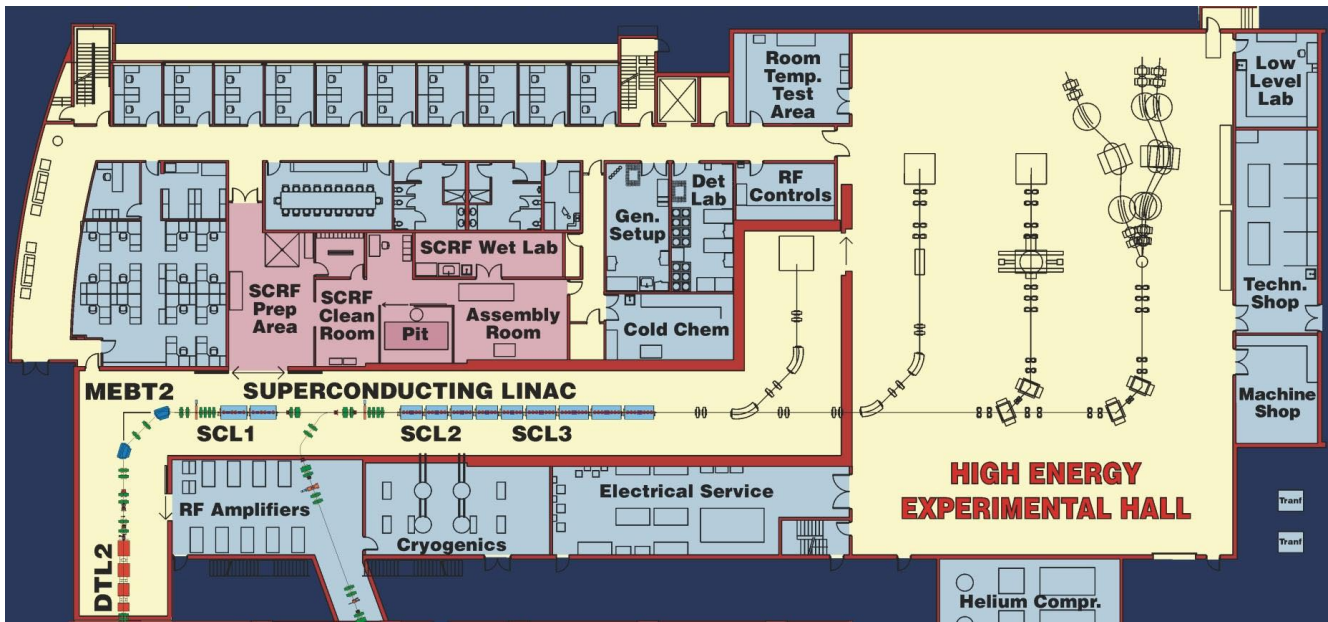


Fig. 165. ISAC-II expansion: ground floor.

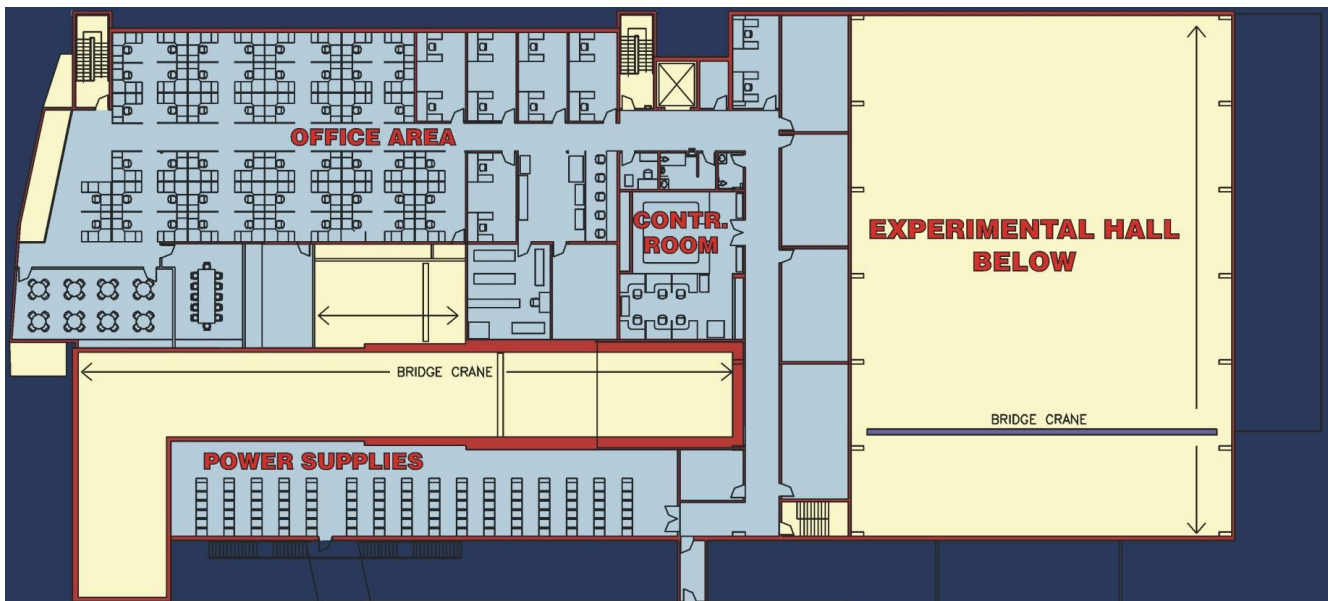


Fig. 166. ISAC-II expansion: upper floor.

proposed. The new concept is based on the idea of a “STAR” grounding referenced to the mass separator. This is used as the common signal reference ground point (SRG) for both target systems. Apart from this common point, the east target SRG is completely separated from the west target SRG. This evolution came about to eliminate problems associated with potential ground loops – and associated operational disruptions – between the two target systems. Installation of the services for the east target station is still in progress with commissioning scheduled for winter, 2002.

The conduit installation for the various radiation systems and the HV interlock systems was extensive.

On the maintenance front we had a couple of serious problems to address. The RFQ main contactor relay started malfunctioning during the fall. The over-current protection function was not working properly. It will be replaced during the winter shutdown. On December 15, a severe wind storm hit the Lower Mainland causing a series of successive power outages of the 60 kV transmission line to the UBC campus. One of the ISAC power distribution centres feeding the mechan-

ical services, MCC-X, suffered a partial short circuit and caught fire. The electrical crew had to work around the clock to restore service and minimize disruption to the experimental program.

### ISAC-II Conventional Construction

The buildings portion of the ISAC-II expansion project started in earnest upon receiving funding approval from the provincial government in April. The Province funded the base request of \$8.7 M through the B.C. Knowledge Development Fund, in support of the experimental program. \$1.0 M was added by TRIUMF to build much needed office space for research and technical staff that has been housed in temporary trailers for a long while. UMA Management Services Ltd. was appointed as project manager in early June, followed shortly thereafter by the appointment of PBK Architects Ltd. and Cochrane Engineering Ltd. for the architectural and the engineering design.

The new expansion will be built to the north of ISAC-I. It includes office space for about 90 research and technical staff, laboratory and technical support space, the accelerator and support functions, building services and a high-energy experimental hall (see Figs. 165 and 166). The total finished floor space is approximately 55,000 sq ft. The construction site will be very busy throughout 2002 due to space limitations and the concurrent construction of the MDS Nordion TR30-2 project.

The project went through a very involved approval process with the University of British Columbia and the Province of British Columbia. The process included planning committees, advisory design committees, design review committees, public hearings and four board meetings. The development permit was issued in November.

The conceptual design was fully developed by the end of the summer. The detailed design was near completion by year-end.

Preparatory work, including the office trailer relocation and the relocation of the 69 kVA power line from the ISAC-II building footprint, was completed during the fall.

The construction was broken down into two main packages: the site preparation package to allow for the advancement of the work, and the main building package to take the building to completion. The site preparation package was tendered and awarded in December with construction scheduled for completion in February, 2002. The tendering of the main building package is slated for late January, 2002 with substantial completion scheduled for December, 2002 and beneficial occupancy in January, 2003.

### ISAC-II ACCELERATOR

In the past year the ISAC-II accelerator design and prototyping was advanced on a number of fronts:

- In an effort to finalize the building layout, realistic designs for transport lines and accelerators were developed and simulated. This set the position for the SC-DTL in the new hall at  $(x, y) = (15.66, 19.0)$  m with respect to the ISAC accelerator N-S, E-W intersection point as reference.
- An optimized cryomodule concept was developed to maintain a more consistent beam envelope throughout the linac.
- Multi-charge particle dynamics were simulated in the code LANA, complete with transfer lines, isopath bend sections and realistic cryomodule dimensions.
- A two stage installation scenario was advanced. In a first stage, the full energy 1.5 MeV/u beam from the ISAC DTL-I will be transported via the HEBT transfer line from the ISAC-I E-W beam line to the ISAC-II E-W beam line and injected into the medium- $\beta$  section of the ISAC-II superconducting linac. Up to seven cryomodules may be installed in the original installation with all five medium-beta modules (twenty cavities) and up to two high-beta modules (twelve cavities) giving  $E = 5.8$  MeV/u for  $A/q = 6$ . In the final stage, the low-beta cryomodule (eight cavities) and last high-beta cryomodule (eight cavities) would be added for  $E = 6.5$  MeV/u for  $A/q = 7$ . Beam transport was designed assuming that the future installation would be compatible with the existence of the initial installation.
- A medium- $\beta$  cavity prototype designed and built in collaboration with INFN-LNL was successfully tested in Legnaro. Specifications for the order of twenty medium- $\beta$  cavities were prepared.
- A SCRF test lab was established at B.C. Research and a test cryostat was designed, built and tested.

Figure 167 shows a schematic for the ISAC-II linac with stage 1 and stage 2 installations complete. The work is summarized below.

#### Linac Lattice

Beam dynamics simulations have been done to maintain the possibility of utilizing multi-charge acceleration in the ISAC-II superconducting linac to preserve beam intensity and/or allow the possibility of a second optional stripping stage to boost the final ion energy. In initial lattice studies, Legnaro/JAERI-style four cavity cryomodules were assumed, separated by

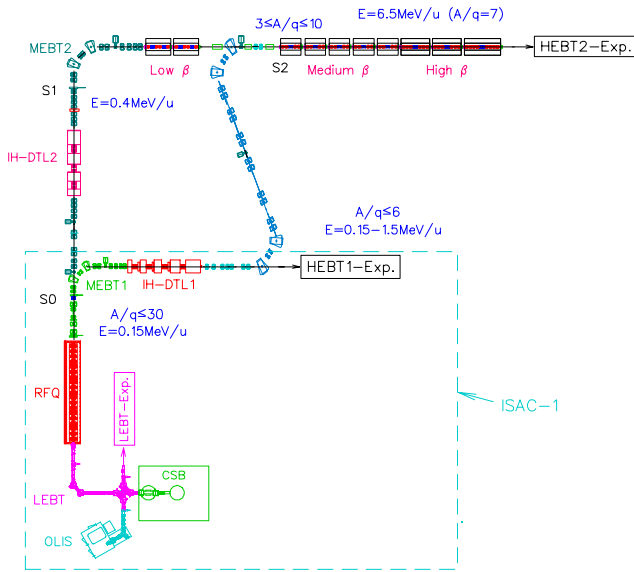


Fig. 167. A schematic for the ISAC-II linac with stage 1 and stage 2 installations complete.

focusing magnets at room temperature. The studies show that superconducting solenoids are the optimum focusing element for transporting beams with multiple-charge states.

The choice for superconducting solenoids allowed us to re-think the cryomodule specification with a goal to rationalize the transverse optics. Four different cryomodule layouts are now specified, one for each of the low- and medium-beta sections and two for the high-beta section (see Fig. 168). The number of focusing elements is varied along the accelerator length for a reduced transverse envelope and the diagnostic boxes are positioned at waists in the transverse envelopes. Beam dynamics studies in the low-beta cryomodule showed that we can reduce longitudinal emittance growth by using one long module of eight cavities and four solenoids. The last solenoid at the exit

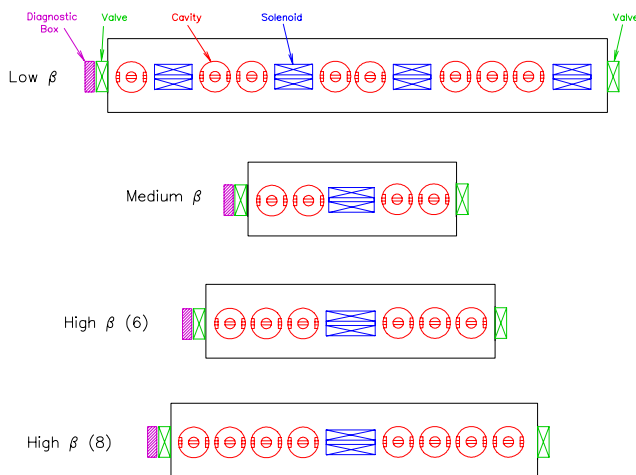


Fig. 168. Proposed cryomodule layout for the three sections of the ISAC-II SC linac.

of the cryomodule is used to help match the beam to the medium-beta section. The module has a length of 4.28 m from cell centre to cell centre. A cryomodule cell consists of the cavities, the solenoid(s), isolation valves and a diagnostics box. The cryomodule cell length for the four cavity medium-beta cryomodules is 2.09 m. In order to incorporate twenty high-beta cavities, it is considered to use two, six cavity cryomodules with a length of 2.76 m each and one, eight cavity cryomodule of 3.32 m. The new cryomodule concept also allows the possibility of optimizing the transverse dimensions of each cavity type. This will receive further study.

## Stage 1 Installation

### HEBT transfer

The HEBT transfer section transports the 1.5 MeV/u,  $B\rho \leq 1.22$  Tm beam from after DTL-I to the medium- $\beta$  section of the superconducting linac. The transfer section, shown in Fig. 169, is configured as an S-bend system composed of two symmetric doubly achromatic  $\sim 118^\circ$  bend systems with two, four quadrupole periodic transport sections joining the two bend sections. A 35 MHz buncher in between the two 4Q systems provides a longitudinal match to the medium- $\beta$  section of the SC linac. The second 4Q system matches the beam in the transverse planes to the medium- $\beta$  section of the SC linac.

Each achromatic bend is configured as a QQDQQDQQ system and transports the beam from double focus to double focus. The second achromatic bend has the extra condition of  $R_{12} = R_{34} = 0$  to allow transverse matching to the SCDTL by the upstream 4Q system. All dipoles are identical with rectangular poles.

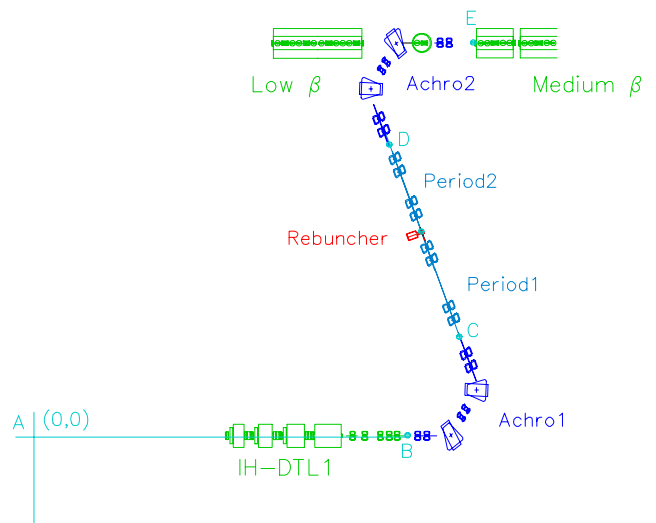


Fig. 169. The HEBT transfer line for ISAC-II stage 1.

## Linac optics for stage 1 installation

The transport and accelerator dynamics for stage 1 were simulated using LANA. The simulation includes all transport from the output of the ISAC DTL to the end of the 7-module ISAC-II SC linac. Thus far we have only considered cavity fields using a “square-wave” approximation. Realistic cavity fields will be added to the LANA model in the future. This means that no transverse components to the cavity fields have been added so far. Likewise no cavity or solenoid misalignments have been considered.

The complete transfer line plus the full seven cryomodules were simulated with LANA for two single charge cases corresponding to ions with  $A/q$  of 3 and 6. A summary of the the envelopes in the SC-DTL are shown in Fig. 170.

In both cases, matching and acceleration are straightforward. The lattice easily accommodates the rf defocusing from the high gradient cavities with only slight transverse emittance growth. Minor longitudinal emittance growth occurs due to the rather large debunching at the position of the 35 MHz rebuncher. We could also consider lowering the frequency of this buncher to avoid the growth.

Beam simulations were also done to study the multi-charge beam dynamics for the stage 1 installation. The reference ion for the multi-charge runs is  $^{132}\text{Sn}$  with an equilibrium charge state of  $Q_0 = 31$  when stripping at 1.5 MeV/u. For the simulations we assume a foil is inserted at the entrance of the medium-

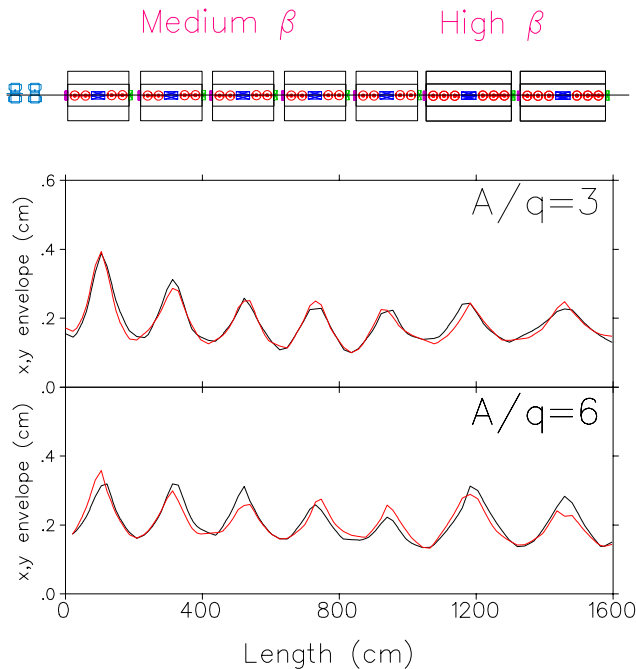


Fig. 170. Transverse beam envelopes are shown as a function of length for the SC-DTL (stage 1) for  $A/q$  of 3 and 6.

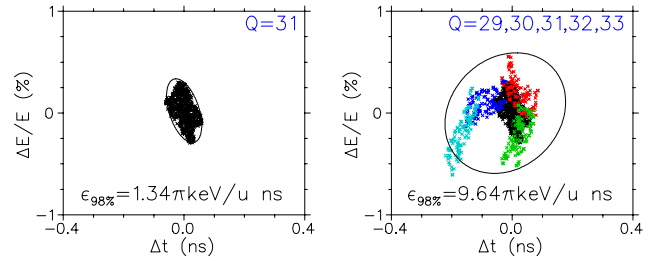


Fig. 171. Final longitudinal phase space ensembles for both a single charge state,  $^{132}\text{Sn}^{31+}$  (20% of the beam), and multiple charge states,  $^{132}\text{Sn}^{29+,30+,31+,32+,33+}$  (80% of the beam) after acceleration through the SC-DTL linac (stage 1).

beta section. Five charge states,  $Q = 29, \dots, 33$ , are accelerated through the SC linac. The transverse optics are very well behaved. The final phase ellipses are shown in Fig. 171. The longitudinal emittance is broadened since each charge ends up in a different region of phase space. The transverse emittance experiences relatively little increase.

## Stage 2 Installation

### Beam transport

The MEBT transfer section transports the beam from the ISAC-I MEBT to the IH-DTL-II in the N-S vault of the new ISAC-II building.

The beam is transported from the double focus at the MEBT-I stripping foil,  $(\beta_{x,y}) = 0.08$  mm/mrad, through two 4Q periodic transport cells to a double focus upstream of a matching section to the IH-DTL-II. A 35 MHz rebuncher at this double waist, plus a 4Q section, matches the beam to the new linac. The first section utilizes the first two quadrupoles of the charge selection section of MEBT-I with a central drift between doublets to accommodate the MEBT-I dipole. The optics from ISAC MEBT to IH-DTL-II are displayed in Fig. 172.

The second medium energy beam transport (MEBT-II) section is required to deliver the beam from IH-DTL-II to the low- $\beta$  section of the superconducting linac. As in the ISAC MEBT-I the transport is composed of three sections: a matching section to give a three dimensional focus on the stripping foil at 0.4 MeV/u, a 90° bend section for charge selection (or charge acceptance) and a matching section before the superconducting linac. The MEBT-II section is shown in Fig. 173. The design  $A/q$  is 30 before the stripping foil and 7 downstream of the stripping foil.

The first section is composed of six quadrupoles in a combination of two triplets to give a double waist near the centre of the section to allow the insertion of a buncher to give a time focus on the ISAC-II stripping foil.

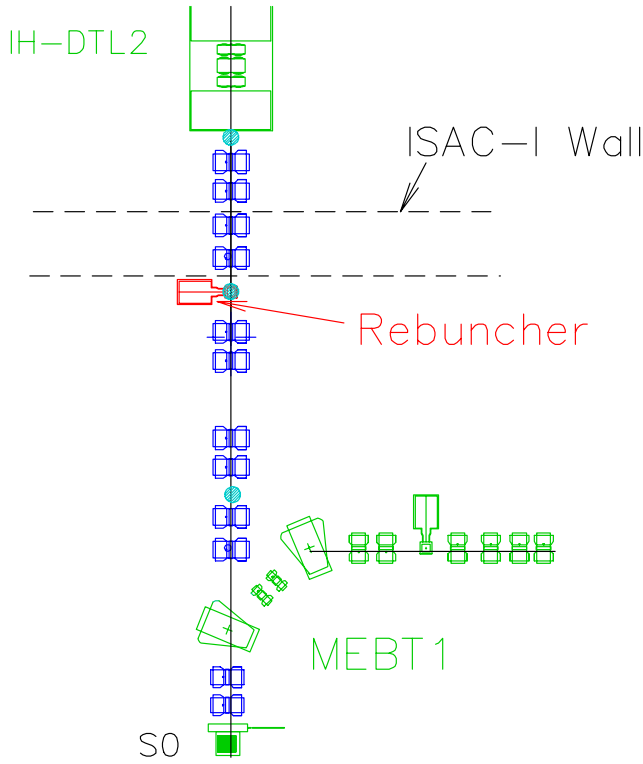


Fig. 172. The beam transport between ISAC MEBT and IH-DTL-II.

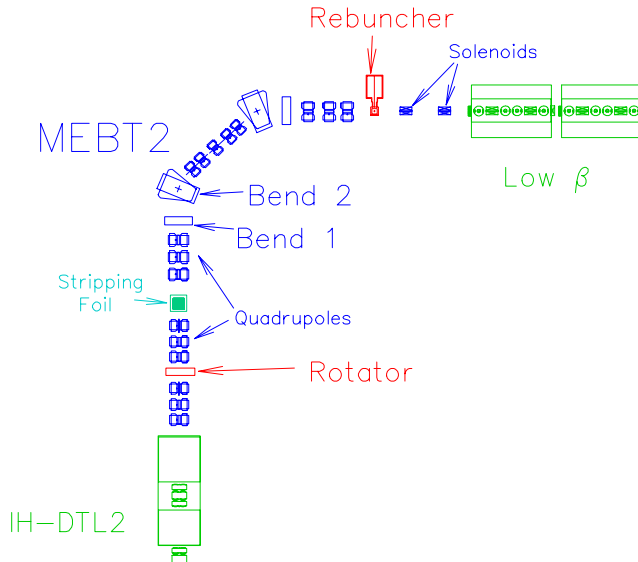


Fig. 173. The beam transport between IH-DTL-II and the low- $\beta$  section of the SC-DTL.

Since we want to maintain the possibility of multi-charge acceleration in ISAC-II, the charge selection section must be made not only achromatic but also isopath (same path length for each charge state) so that we maintain the proper phasing of the various charge states. A small reverse bend dipole is employed to provide a negative path difference dispersion that is cancelled by the path difference in the main dipole.

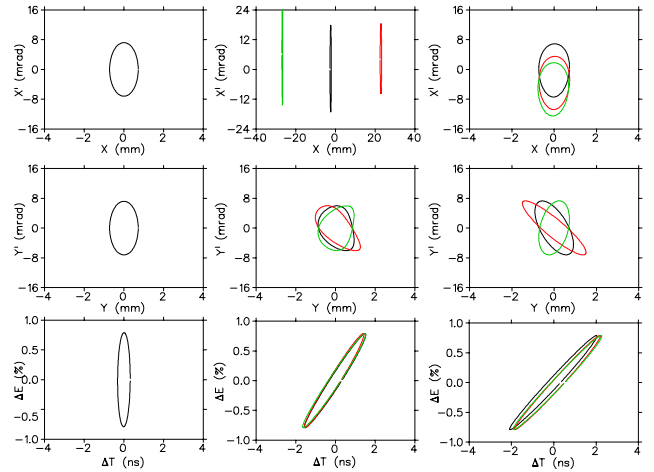


Fig. 174. Beam ellipses for horizontal (top), vertical (middle) and longitudinal (bottom) planes for three charge states,  $\Delta Q/Q = 0, +5\%, -5\%$  (black, red, green), at the stripping foil (left), mid-point (middle) and end (right) of the charge selection isopath section.

The quadrupoles between dipoles achieve the double achromaticity. Symmetric quadrupoles before and after the benders produce a unitary matrix in  $x$  and  $y$ . Higher order multipoles are added to provide correction due to the large perturbation caused by the relatively large differences in charge state,  $\Delta Q/Q = \pm 5\%$ . Beam simulation results showing beam emittances for three charge states,  $\Delta Q/Q = 0, +5\%, -5\%$ , are summarized in Fig. 174.

In order to provide a reasonable match for all ions with  $3 \leq A/q \leq 7$ , we chose a buncher position optimized for the lighter ions where the longitudinal acceptance is smaller due to the relatively strong accelerating gradient. A 35 MHz buncher is centred at the double focus provided by the isopath section. In order to optimize the acceptance of multi-charge beams, a system of two superconducting solenoids has been chosen over a four quadrupole system.

The beam transport section in between the low- $\beta$  and medium- $\beta$  sections of the SC-DTL will be installed to coexist with the HEBT transfer line components so that beams could be switched from one line to the other to allow flexibility in the operation.

The transport section in question takes the beam from the output of the low- $\beta$  accelerator with beam energy varying from 1.2 MeV/u to 2.3 MeV/u for ions ranging from  $A/q = 7$  to 3 respectively, and rebunches with a superconducting 70 MHz buncher followed by a solenoid to match the beam to the medium- $\beta$  section (Fig. 175).

### Linac simulations for stage 2

Beam simulations for the stage 2 installation include the complete beam transport from ISAC-II stripping foil, the low-beta SC-DTL section, the matching

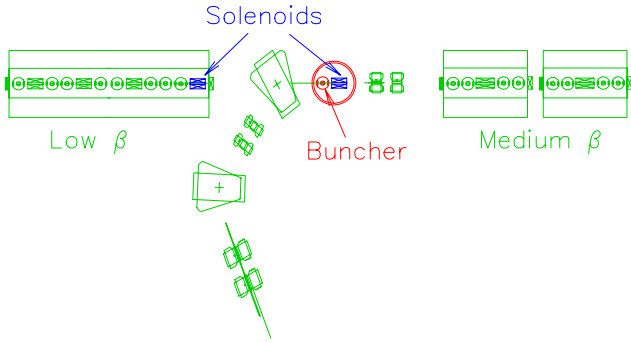


Fig. 175. The beam transport between the low- $\beta$  and medium- $\beta$  section of the SC-DTL.

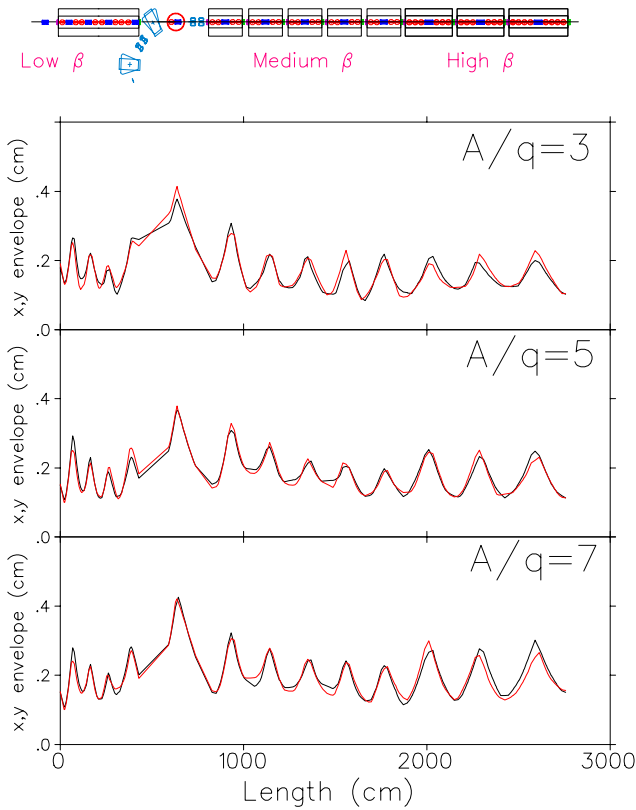


Fig. 176. Transverse beam envelopes are shown as a function of length for the SC-DTL (stage 2) for  $A/q$  of 3, 5 and 7.

between low- and medium-beta sections and the five medium and three high-beta cryomodules, for singly-charged ions with  $A/q = 3, 5, 7$ .

In all three cases, matching and acceleration deliver good quality beams. The ion dependent matching at the entrance to the low-beta section and between the low- and medium-beta sections does generate some small longitudinal emittance growth. A detailed plot of the beam envelopes for the acceleration only for the three cases is given in Fig. 176.

For multi-charge simulations, three possible stripping foil positions are considered: foil 1 at the ISAC-II

foil location before the isopath section, foil 2 at a position just upstream of the low-beta cryomodule and foil 3 at a position just upstream of the first medium-beta cryomodule. In the study, foil 1 and foil 2 positions are used interchangeably to show the effect of the imperfect isopath optics on the multi-charge beam dynamics. Foil 3 was added to simulate cases where the accelerator is configured in energy boost mode. In multi-charge runs, three charge states ( $^{132}\text{Sn}^{20+,21+,22+}$ ) are accelerated after foil 1 or foil 2, encompassing 57% of the beam, and five charge states ( $^{132}\text{Sn}^{30+,31+,32+,33+,34+}$ ) are accelerated after foil 3, encompassing 80% of the beam. By comparison, a single charge state ( $^{132}\text{Sn}^{21+}$ ) from foil 1 or foil 2 would encompass 21% of the beam, while a single charge state ( $^{132}\text{Sn}^{31+}$ ) from foil 3 would encompass 20%.

Simulations show that any combination of foil 2 and 3 produce beam envelopes with almost no discernable difference between the single-charge and multi-charge runs. This shows the inherent stability of the transverse lattice and inter-linac matching section. The final longitudinal phase ellipses comparing single-charge and multi-charge particle ensembles for different combinations of foil 2 and foil 3 cases for the stage 2 installation are shown in Fig. 177.

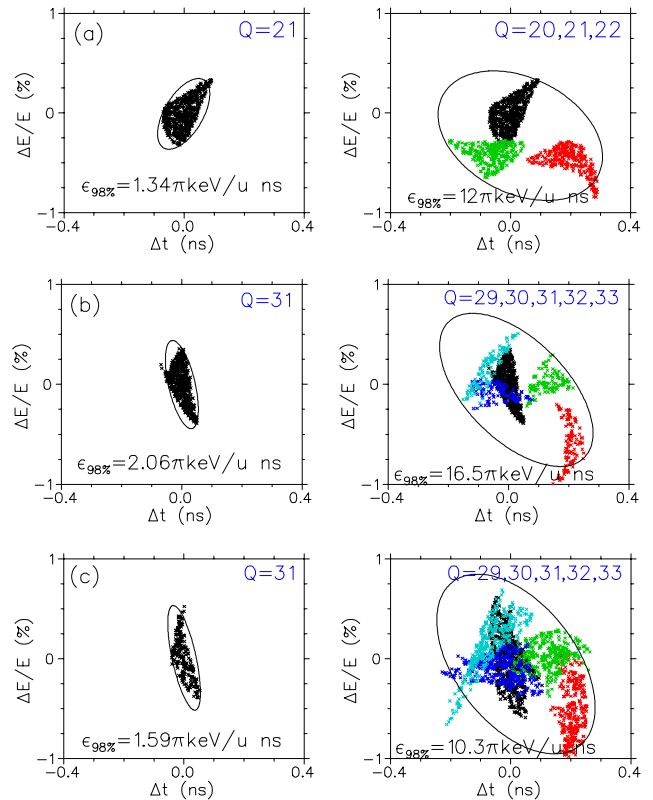


Fig. 177. Final longitudinal phase space ensembles for single- and multi-charge simulations of  $^{132}\text{Sn}$  for (a) foil 2 only (7.4 MeV/u), (b) foil 3 only (10.3 MeV/u) and (c) foil 2,3 (10.3 MeV/u) simultaneously.



In the case of foil 1 the three charges are somewhat mismatched, transversely, after the isopath section and have slightly different arrival times, leading to large envelope perturbations in the low-beta section. Some improvement is found by optimizing the accelerator to transport  $Q_0 = 20.4$  so that the accelerated charges will have relative errors of  $\Delta Q/Q = -2\%$ ,  $3\%$  and  $8\%$  from the linac tune. In this case the acceptance for the lowest charge is sufficient to contain the mismatched beam. One further problem is that at  $\Delta Q/Q = 8\%$  the transverse focusing strength of the linac lattice is near the stability limit and so transverse emittance growth, especially in light of the initial mismatch from the isopath, is increased. Nevertheless transmission is near 100% for the foil 1 multi-charge case.

### SCRF Developments

Although the program at TRIUMF is still in its infancy, a number of developments are under way including the fabrication and test of a medium-beta cavity prototype, the fabrication and cryogenic test of a test cryostat and the design of an SCRF laboratory.

#### Medium-beta cavity

A medium- $\beta$  quarter wave bulk niobium cavity has been designed in collaboration with INFN-Legnaro,

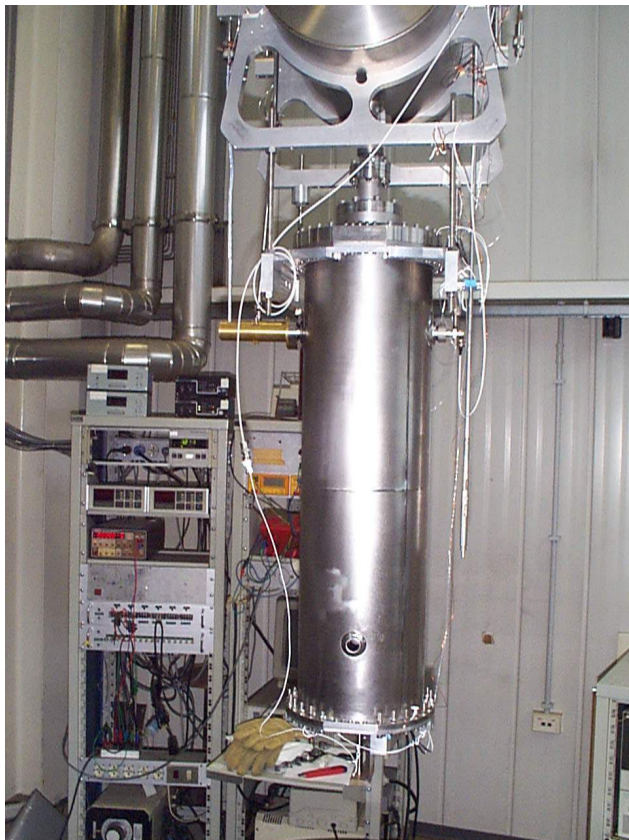


Fig. 178. TRIUMF medium-beta prototype cavity before cold test at INFN-LNL.

fabricated in Italy, received chemical polishing in CERN, and was rf tested in Legnaro. The cavity is shown in Fig. 178 prior to the first cold test. This cavity differs slightly from the Legnaro resonators in that the bottom tuning plate is now made from niobium sheet rather than sputtered niobium on a copper substrate, and additional rigidity has been added at the top plate to reduce the cavity detuning due to fluctuations in the pressure of the cryogenic system.

Multipactoring conditioning, started at room temperature, was completed during resonator pre-cooling with an elapsed time of about four hours. After cool-down to 4.2 K the cavity was pulse conditioned for 1 hour in  $3 \times 10^{-5}$  mbar helium. Results of the first rf test are shown in Fig. 179. The cavity performance exceeds the ISAC-II requirements with an accelerating gradient of 6.7 MV/m for 7 W dissipated at 4 K. A peak gradient of 11 MV/m was achieved. The cavity is now being prepared for further rf tests at TRIUMF.

Specifications for cavity fabrication are now being written. An order for twenty medium-beta cavities will be placed in industry early in the new year.

#### Test cryostat

A test cryostat has been designed and built in a collaboration between TRIUMF and Quantum Technologies of Whistler, B.C. The cryostat is shown in Fig. 180.

The cryostat vacuum vessel is 2.4 m high by 0.8 m in diameter. A LN<sub>2</sub> side shield holds a volume of 200 l and is directly connected to a copper bottom shield, baffled to allow adequate conductance for pumping. A top shield of copper is bolted to a copper flange at the top of the LN<sub>2</sub> vessel with bolt access available through six KF-50 flanges on the top plate. This copper flange is cooled by a copper cylinder inserted in the LN<sub>2</sub> vessel to a depth of 65 cm. The top plate assembly consists of two large flanges that allow separate removal of either the helium dewar/cavity assembly or the LN<sub>2</sub> vessel. The LHe vessel holds a volume of 48 l.

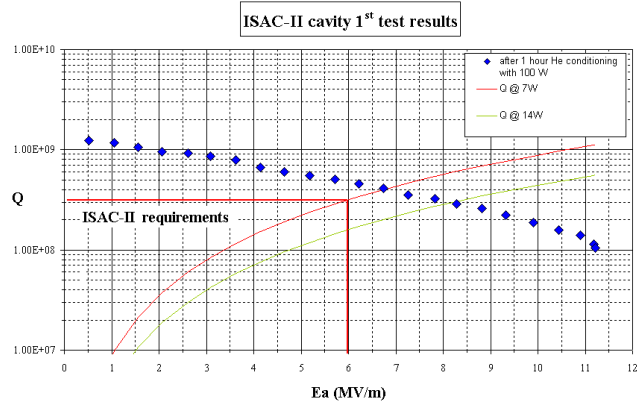


Fig. 179. Results of the first rf test on the medium-beta cavity at INFN-LNL.

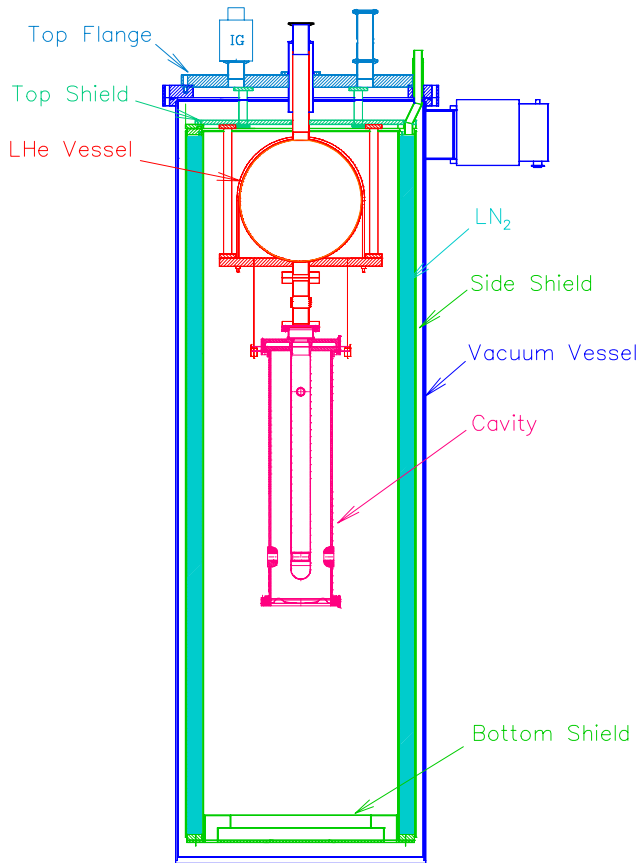


Fig. 180. ISAC-II test cryostat with cavity.

A “dummy”, full scale, medium-beta cavity has been fabricated in copper for cryostat tests and to establish test procedures. Initial cryostat tests have been completed. The top plate, top shield, LHe reservoir and dummy cavity are shown in Fig. 181 prior to assembly in the cryostat. The LHe boil off rate has been established by both measuring the flow of the escaping gas and by charting cavity temperature with time after a fill. A static heat load of 1.2 W was found corresponding to a boil off of 1.4 l/hr. The loss rate for LN<sub>2</sub> is 1.5 l/hr. The vacuum pressure in the cryostat was  $5 \times 10^{-7}$  while warm, and  $8 \times 10^{-10}$  torr while cold.

### SCRF test laboratory

A temporary superconducting rf test lab is now being installed in a space rented by TRIUMF at B.C. Research. It is intended that the space will be occupied for at least two years until the SCRF area in the new ISAC-II building is available for occupancy. We expect completion of the temporary lab space in two months. The laboratory includes a test area with a sunken cryostat pit for high field rf testing, and clean areas for cavity assembling and high pressure water rinsing (Fig. 182). The total space comes to  $\sim 100$  m<sup>2</sup>.



Fig. 181. ISAC-II test cryostat inner assembly with dummy copper cavity.

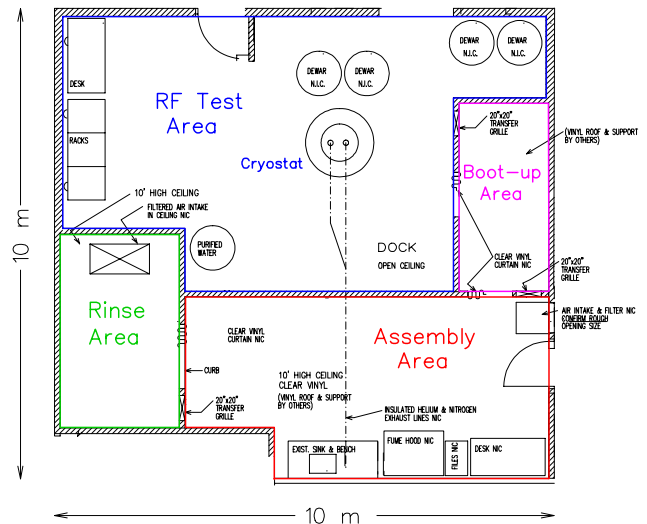


Fig. 182. The SCRF test facility being installed at B.C. Research.

## ACCELERATOR TECHNOLOGY DIVISION

### INTRODUCTION

This past year has seen a number of engineering and design projects come to fruition with successful commissioning and operation. One of these has been the DRAGON spectrometer where much of the installation was carried out in 2000, but commissioning of the electrostatic dipoles was delayed due to problems with ceramic feedthroughs. DRAGON was commissioned with stable beam in October and the first experiment with radioactive ion beams was carried out in November. Another significant milestone was reached with the commissioning of the 2 T solenoid magnet in its 60 ton iron return yoke for the TWIST experiment.

In terms of engineering and design effort, the largest project this past year has been the design of the east target station for ISAC. The switching magnet for beam line 2A, which permits the proton beam to be delivered to either of the two target stations, was completed and field mapped. Improved remote handling capability is being built into the target modules, as well as the services for running an ECR ion source. By the end of the year most of the modules were nearing completion and the entrance and dump modules were in fact installed before the Christmas break.

Some design work has started on the ISAC-II project related to the superconducting rf cavities. A 1200 sq ft test facility was constructed in the nearby BC Research complex for initial testing of the cavity and cryostat.

At Victoria the ATLAS engineering work is nearing completion. The large HEC assembly table was fabricated by a firm in Toronto and was nearing completion by the end of the year. The signal feedthrough project is in the final stages of manufacturing and testing. The engineering effort is now switching to supporting the design of the ISAC targets. At Carleton the TRIUMF engineer is involved in the tooling and assembly of the FCAL modules for ATLAS.

The Machine Shop was again heavily used for fabricating components for ISAC and supporting the experimental program. This year fabrication work valued at more than \$1.6 million was carried out in the TRIUMF shop and about \$0.5 million worth of work was sub-contracted to outside firms through the Machine Shop. In preparation for the ISAC-II and MDS Nordion building construction projects, a number of trailers were relocated and some were removed from the site. A contract for 29 new concrete shielding blocks was awarded and the blocks produced to replace some deteriorating blocks in the BL1A tunnel.

The Electronics Services group provided considerable support for the TWIST experiment this year, in-

cluding the production of amplifier and other modules and large numbers of cables. PC support was increased with another full-time technician and an improved service for regularly scheduled backups. The Electronics Development group continued to put most effort on the ISAC control system and has started to take responsibility for the design and installation of safety related systems.

### BEAM DYNAMICS

Three beam dynamics studies are reported this year, in addition to those for the CERN collaboration. The first is a continuation of the joint study with Brookhaven of the possibility of extracting very short proton bunches for the KOPIO experiment. The second, in support of a Fermilab study of muon acceleration in an FFAG ring, explored the best rf voltage and (fixed) frequency to use when the traversal time is too short to allow synchronization of the rf with the orbit frequency. The third investigated the effect of space-charge in destabilizing an intense circulating beam by moving it on to a betatron resonance.

#### Micro-Bunching at Brookhaven AGS

Particle beam simulations in support of the proposed rare kaon decay  $K_L \rightarrow \pi^0 \nu \bar{\nu}$  experiment have continued. The very short kaon bunches required are produced by extracting 0.15 ns rms long proton bunches with 40 ns separation with the aid of rf manipulations. Last year, the longitudinal dynamics of a variety of schemes were considered, resulting in the choice of fundamental and anti-phased fourth harmonic rf. This year, the simulations were elaborated to include the  $\frac{1}{3}$ -integer betatron resonance responsible for extraction in the horizontal plane. For this purpose, the SLEX computer program for the study of slow extraction schemes, written by Wienands for the KAON Factory proposed in the late 1980s, was simplified by eliminating the  $\frac{1}{2}$ -integer resonance dynamics and married with LONG1D which performs the longitudinal tracking. New graphical and analysis software was also written for displaying and processing the output.

Using the LONG1D-SLEX code a new effect was discovered that limits extraction efficiency. Because of the longitudinal motion, the betatron tune varies as particles are carried toward resonance. Figure 183 shows the circulating and extracted longitudinal phase spaces. The gap between neighbouring rf buckets acts as a venturi; and so the narrower the constriction in rf phase (i.e., the microbunch length), the faster is the motion in momentum. When it is fast enough, as occurs when the shortest bunches are demanded, some particles pass through the betatron resonance

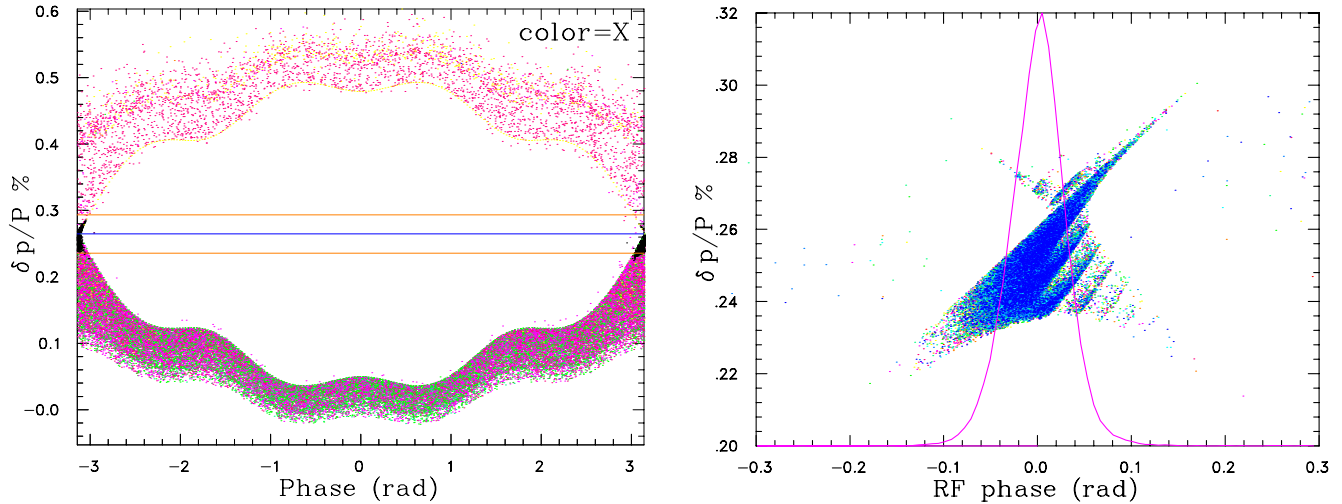


Fig. 183. Circulating longitudinal phase space and extracted microbunch shape.

without building up sufficient amplitude to be extracted. Parameters which promote this effect, in which some protons fail to be extracted, are increased machine chromaticity, slower magnetic field ramp, larger cavity voltages, etc. The presently favoured scheme uses a 3 s magnet cycle, the natural chromaticity, and 150 kV on each of the 25 and 100 MHz cavities. This yields 0.15 ns rms bunches, but leaves 7% of the beam circulating. Curative measures such as manipulation of the betatron tune will be studied.

### Muon Acceleration in an FFAG

Muon accelerators have proved difficult to design because of potentially heavy losses from decay. Another concern is the cost of expensive rf cavities. The current baseline approach is a recirculating linac; but these have proved costly and present an acceptance bottleneck. Collaborators at FNAL have promoted the concept of a non-scaling FFAG (fixed field alternating gradient) accelerator. Such machines have exceptionally large acceptance both transversely and longitudinally; and superconducting rf and magnet technology could advance their reach into the multi-GeV regime. The proposed FFAG has a 2 km circumference, injection and extraction energy of 6 and 20 GeV, respectively, 300 equal cells each with up to 6 rf stations, and a train of up to 400 bunches; acceleration is completed in a few turns. A major drawback is the large change in pathlength as a function of energy. Thus traversal time, which must be synchronized with the rf waveforms, changes significantly from cell to cell of the lattice; and the rf adjustments would be impractically large to achieve in the microseconds circulation time.

We have developed a strategy to optimize acceleration of a bunch train. Initially, the ideal phases and

gap-crossing times, cavity-by-cavity and turn-by-turn, are recorded for a single synchronous particle. To select the optimal frequency and actual phases, one guesses a frequency and then calculates the phases at the gap-crossing times of the ideal particle. The mean-square deviation of the fixed-phases from the ideal values is summed over all rf stations and turns. A search is then made to find the “best frequency” which minimizes this sum. As for other synchronous machines, it is found to be necessary to use a modest over-voltage and to run off the crest of the rf wave to accelerate a finite emittance. The voltage is optimized numerically so as to minimize the bunch-to-bunch variation of the extraction energy. Next, the longitudinal phase plane is flooded with trial particles; those which survive the complete acceleration to 20 GeV are recorded and used to map out both the input admittance and the output emittance. The main conclusion is that useful admittances ( $\approx 1$  eV s) can be achieved with acceleration at 200 MHz in 5 or 6 turns using best phases and voltage up to 14 MV/cell (over voltage  $\approx 30\%$ ). The transport is non-linear and the useful phase space is compromised. Acceleration over more turns may allow a reduction of costs associated with rf systems. If 100 MHz rf, with 6.5 MV/cell, is used the admittance rises to 2 eV s and acceleration can be extended to 10 turns. In all cases, addition of a second harmonic roughly doubles the admittance but the non-linear effect is augmented.

### Multi-Turn Simulation of Coherent Betatron Resonance with Space-Charge

The space-charge envelope code, TRANSOPTR, has been paired with the tracking and simulation code, ACCSIM, to study the half-integer betatron resonances in a high intensity proton ring and, in particular, the relationship of coherent-mode frequencies with

the incoherent (Laslett) tune as a function of beam intensity, and the existence of space-charge intensity limits due to detuning of the coherent modes on to a resonance.

The TRANSOPTR code was used to solve the envelope equations to establish a stable set of initial conditions in a given intensity range. The matched solutions for the beam have been used to generate initial distributions of macro-particles which were run through the modified ACCSIM multi-particle tracking code. This approach allowed us to validate the space-charge simulation and to provide a clear benchmark against which to measure resonant growth.

This technique has been used to investigate the  $\frac{1}{2}$ -integer stopband at  $\nu_x = 13/2$  in the FNAL booster lattice, when space-charge depresses the envelope eigentune to 13. We have demonstrated that the resonance occurs not when the incoherent tune is near  $13/2$ , but when half the envelope tune is (see Fig. 184). The two-tune shifts differ by a factor of 0.68.

An interesting finding of these studies was that, while matched solutions exist for intensities which are beyond the limit imposed by the envelope instability, these solutions cannot be accessed by increasing intensity slowly. Moreover, single-turn injection of a beam that is matched, but beyond the envelope instability, is only stationary for the artificial Kapchinsky-Vladimirsky (KV) distribution; when the distributions are different from KV, the rms beam sizes grow until the beam is large enough that the tune shift has fallen below threshold.

This has practical implications for multi-turn injection in storage rings. As well, for a bunched beam, where particles with large synchrotron amplitude

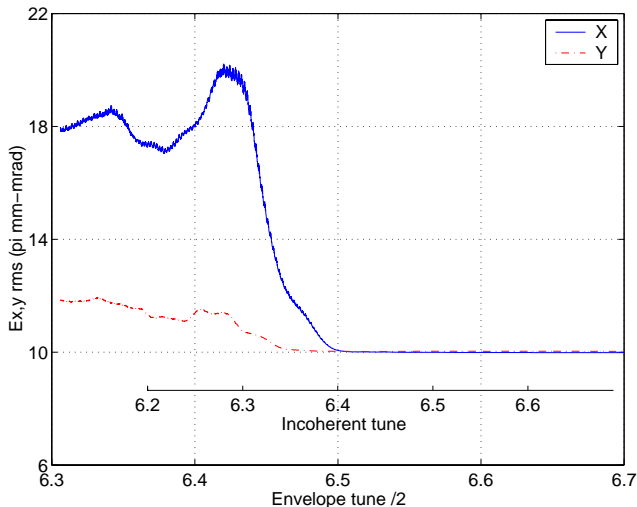


Fig. 184. Emittance growth as the intensity is swept from 0–2.5 A. This is plotted as a function of tune, so the curve proceeds from right to left. Resonance occurs at  $I = 1.3$  A, corresponding closely to when the envelope tune is 13. The simulation used  $10^4$  macro-particles.

circulate between regions of high and low local charge density, the space-charge limit is likely imposed by the envelope instability. Even if the  $\frac{1}{2}$ -integer stopband is very narrow, for intensity beyond the limit, there will be some part of the bunch always on the envelope resonance, and this will cause emittance growth.

## MAGNETS

In addition to contract supervision on the fabrication of the CERN twin aperture quadrupoles described in the CERN collaboration section, work was carried out on a number of other magnets during this year.

In order to permit the proton beam in beam line 2A to be switched between the west target station and the new east target station, a new dipole magnet with two output legs is required. The design of the 2A switching magnet was completed and the order for manufacture placed in March. Sunrise Engineering (Surrey, BC) delivered the magnet in October. The coils were fabricated by Sigma Phi (France). The magnet was field mapped and ready for installation by the end of the year (see Fig. 185).

The conceptual design of a Wien filter to spin precess radioactive ions (sodium, potassium, nitrogen, lithium, and fluorine) for the  $\beta$ -NMR experiment was completed. This was reported in “A Wien filter for TRIUMF’s  $\beta$ -NMR experiment” [TRI-DN-01-5].

A pair of Helmholtz coils was designed and fabricated at TRIUMF for the ISAC polarimeter station.



Fig. 185. The BL2A switching magnet in location.

This was reported in “Concept design of a Helmholtz coil pair for the ISAC polarimeter station” [TRI-DN-01-11].

Sicom Industries (BC) manufactured quadrupole steel assemblies for the spare DTL quadrupole triplet, and Danfysik (Denmark) fabricated coil assemblies.

The concept design of a 60 Hz steering magnet to paint the high intensity proton beam on to the ISAC targets is nearing completion.

### Experiment 614 – TWIST

In preparation for mapping of the TWIST solenoid at fields up to 2.2 T, an existing “Bonnie dipole” was modified to achieve a flux density of 2 T. This dipole was used to calibrate 14 Bell BHT-910 Hall probes from  $-2$  T to  $+2$  T. Calibration coefficients were calculated and entered into new software for collecting the field data. The Hall probes were mounted on the initial 6-way probe apparatus. Initial field profiling showed a gradient in the  $B_z$  field with  $Z$ . A detailed comparison of measurements and predictions at approximately half-current showed that the field asymmetry was probably due to coils that were shifted in  $Z$  by approximately 30 mm; the resulting coil forces at full field (2.2 T) would be well outside the manufacturer’s specified limit of 1 tonne.

The superconducting solenoid was removed from the yoke. An internal support strut was found not to be connected; this was rectified and the solenoid repositioned in the yoke. The TWIST solenoid was remapped at several currents. Measurements were carefully assessed, in light of the predictions, to determine the position of the coils and therefore the resultant forces on the coil assembly. The analysis showed that, at a current of 144 A, the coils are within 1.1 mm, 1.3 mm and 1.9 mm of the centre of the yoke in  $X$ ,  $Y$  and  $Z$ , respectively. Simulations at full current ( $\approx 245$  A) show that the resultant coil forces are well within the manufacturer’s specifications.

The predicted field at the centre of the solenoid has an absolute value of approximately 3% more than the measured field at a coil current of 228 A. Figure 186 shows the measured field at a current of 228 A and the predicted field at a current of 221 A (i.e., 228 A less 3%). There is excellent agreement between the shapes of the measurements and predictions. The measured field has a slope upon it, which is thought to be due to the coils being slightly (1.9 mm) off-centre of the yoke in the  $Z$ -direction. The magnitude of the field “lobes” decreases as the current is increased.

A talk detailing the first results and problems of the TWIST magnet mapping was presented at the 12<sup>th</sup> International Magnet Measurement Workshop, Grenoble, France, October 1–4.

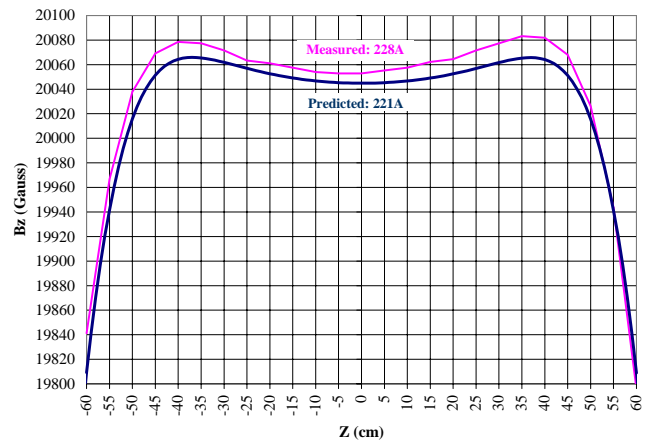


Fig. 186. Measured field at 228 A and predicted field at 221 A, along  $X=0$ ,  $Y=0$ .

### Magnet Measurements

Other magnets surveyed this year included a spectrometer magnet, a  $\beta$ -NMR superconducting solenoid, a water cooled 2C steering magnet, and a 2A switching dipole.

### Kickers

As mentioned in the 2000 Annual Report, the Kicker group designed a fast kicker (see Fig. 187) to study the characteristics of an existing charge booster designed by ISN (Grenoble, France), to assess the suitability of using this charge booster at TRIUMF. This

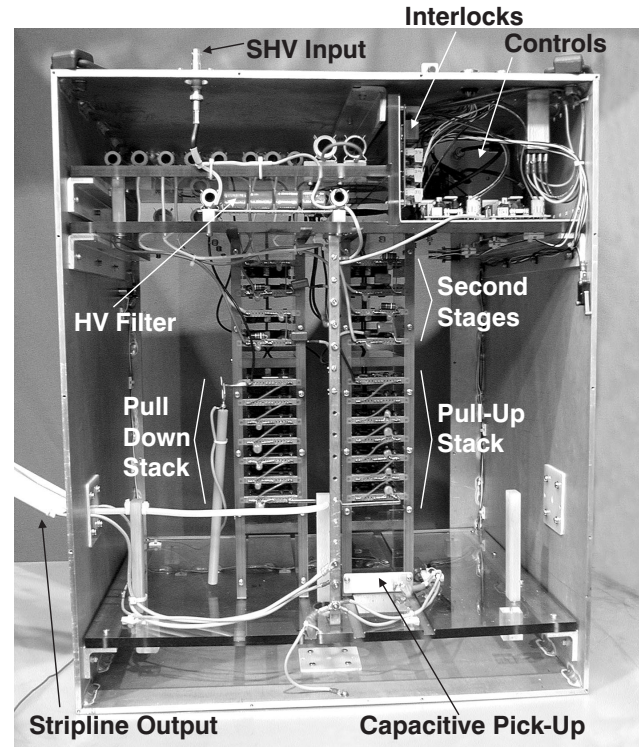


Fig. 187. Rear view of charge booster kicker.

fast kicker will subsequently be used in the TRIUMF-ISAC facility for time-of-flight separation of the chosen charge and to recycle the higher and lower charges back to the charge booster. This will increase the efficiency from 10–60%. ISAC is presently capable of accelerating only isotopes with atomic mass up to 30. The charge booster will allow ISAC to accelerate all masses in the periodic table. The kicker is unique because of its ability to produce variable output voltages up to  $-3.5$  kV, and variable pulse widths and repetition rates from dc to greater than 50 kHz, with rise and fall times of better than 65 ns. The kicker was successfully commissioned in Grenoble in February, 2000, and is now back at TRIUMF waiting to be installed in ISAC. The FET stack can produce  $-6$  kV pulses at repetition rates of up to 15 kHz.

A paper regarding design of the kicker was presented at the 13<sup>th</sup> IEEE International Pulsed Power Conference, Las Vegas, June 17–22.

## MECHANICAL ENGINEERING

Mechanical engineering work at TRIUMF is initiated by the submission of a Request for Engineering Assistance (REA) form which is assessed and assigned according to the size and schedule of the task. Large, complex projects may require a team approach guided by the assigned engineer. Many of the ISAC REAs fall into this category (i.e., east target station modules, and DRAGON). Some requests were submitted prior to this report period, the work being extensive enough to require several years for completion, i.e., DRAGON, Expt. 614.

There were 29 ISAC REAs submitted during the year. However there were, as well, about 8 REAs carried over from the previous year of which perhaps 3 are long term projects. In non-ISAC engineering, there were 19 REAs submitted plus about 4 carried over from the previous year.

As in the past, in this report period there was continuous participation of engineering personnel in performing engineering analyses, consideration of safety related issues, design reviews and other ad hoc engineering related small jobs.

### ISAC East Target Station

The major work load was again in support of ISAC. In January it was decided that completion of the east target station would be the first priority for the ISAC project. The goal was to have an operational east target station in early 2002, and the Engineering group was asked to coordinate the overall project.

In order to achieve this objective the project was broken down into 9 work packages and schedules, which are detailed packages supporting the following major activities as listed and briefly described below.

## Modules

Prior to this report period, 2 target modules had been built (TM2 and TM3), but were incomplete insofar as services ( $H_2O$ , high voltage, high current and signals) and service connections at the bottom of the service duct were concerned. The requirement is to be able to remove not only the containment box tray (i.e., ion source extraction column), but also the service tray in case of HV problems. This means disconnecting the services in such a way as to allow both trays to be removed in the hot cell when necessary. The problem is making a connection which allows the transmission of  $H_2O$ , in and out, as well as being able to transmit up to 1000 A across the interface. For a surface source the problem is simpler and the  $H_2O$  block connection could be avoided. An ECR source (TM3) does not allow this option due to the increased number of services. This problem was dealt with during this report period and has resulted in a solution requiring a set of fixtures such that all subsequent target modules are built to be identical (i.e., any tray will fit any target module). TM2 and TM3 will be completed with this new set-up early in 2002. The assembly fixtures are necessary to ensure that each half of the  $H_2O$  connection block is accurately placed so that they will mate with any tray combination.

At the same time, design commenced on the rest of the east station modules (i.e., entrance, dump and exit). The entrance and dump modules are identical to the west station modules except they are mirror images, and hence required a new drawing package for the east station.

The exit modules for the east station use the same module design as used for TM2 and TM3. However, the contents of the exit modules differ from that of the west station due to a new optics design and also improvements required in the service ducts. The new optics design also required considerable alteration to diagnostics (and actuation) in both exit modules.

All the above design work was accomplished, as well as manufacture of the major module components. Assembly of all modules was well under way by the fall of 2001, and entrance and dump modules were installed just prior to the Christmas break. Figure 188 shows a view of the module assembly area.

Components to be installed in the target and exit modules (i.e., extraction column, all services, optics and diagnostics) were released to the shop starting mid-year and all packages released for manufacture by the end of the year.

Installation of the target module TM2 and both exit modules is scheduled for completion by April 10, 2002.



Fig. 188. View of module assembly area.

### 2A3 beam line

This task mainly involved design and manufacture of the 2A switching magnet (2AB3). This work commenced early in 2000 and the magnet is ready for installation during the shutdown in early 2002 along with the rest of BL2A3.

### Electrical room and east Faraday cage

Nothing had been done up to this report period to provide HV services to the east station and work could only proceed during maintenance days and target change intervals. This was done and the Faraday cage constructed, services run, racks and cell trays installed, and power supplies, transformers and controllers were ordered. Work is progressing well and will be completed by April 10, 2002 when the west target station is next scheduled to operate and access to the electrical room will be limited to maintenance days.

### Target hall service systems

All service systems (i.e., H<sub>2</sub>O, vacuum, electrical, ventilation, compressed air, etc.) have been installed and are operational for the west target station but have not been completed for the east station. The H<sub>2</sub>O system distribution manifold and some pipe runs were completed in this report period. However, the bulk of the work on all systems could not commence until the shutdown in mid-December. The H<sub>2</sub>O and vacuum systems will require revision due to the requirement of running the off-line station as a conditioning station which requires all services simultaneously. HV chase work will mimic that of the west HV chase, except that 4 gas lines will be required to provide target gases from the Faraday cage.

### Controls and safety interlocks

This work requires that a control and interlock system be provided allowing operation of both stations

independently. Details of these systems can be found in the ISAC section of this report under Safety and Radiation Control.

### East station module access area (EMAA)

This is the volume below the shield plugs and above the top of the east vacuum tank. Apart from placing and aligning the east vacuum tank, nothing had been done at the start of this report period to complete this work package. Therefore the following work was necessary: completion of the 5b shielding package between the east tank and the preseparator magnet; installation of the east tank top plate, seal and leak checking; installation of the proton beam entrance window; installation of the 3 intermodular connectors in the east vacuum tank; completion of the nuclear ventilation system sealing; and layout of the EMMA for all services such that adequate access is assured.

### DRAGON

#### Electrostatic dipole vacuum tanks

Both the ED1 and ED2 stainless steel vacuum tanks were clad with  $\frac{1}{4}$  in. thick lead sheets all around them for X-ray shielding. All lead sheets were pre-cut: pie shaped for the top and bottom spherical heads, and straight panels for the tank's vertical sides. Most of the lead cutting was done off-site, but some trimming was done at TRIUMF for custom fitting. The top and side panels were glued to the tanks using 5 minute epoxy #1130K06 (made locally by Industrial Formulators, Burnaby, BC) and the bottom lead sheets were glued using 3M Scotch Grip #1357 contact cement. This type of lead work was done at TRIUMF for the first time. It was a very labour intensive task and was very well executed by the TRIUMF personnel involved.

Figure 189 shows lead sheets being installed on the bottom of the ED1 tank at TRIUMF.



Fig. 189. Lead sheets being installed on the bottom of the ED1 tank.



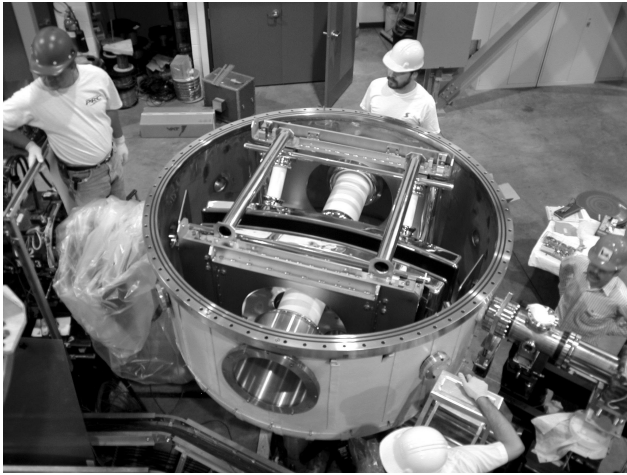


Fig. 190. ED2 installed in its vacuum tank.

### Electrostatic dipoles (ED1 and ED2)

The electrostatic dipole (ED1) was reinstalled in the lead clad ED1 vacuum tank and aligned to the beam line using alignment jigs. Field clamps were installed and aligned to ED2 electrodes using precision machined jigs. The ED2 assembly was then installed in the lead clad ED2 vacuum tank and aligned to the beam line using its alignment jigs and looking along the beam centre. After alignment, the position of the dipole assemblies was recorded using TRIUMF's new Leica Total Station system. If the dipole assemblies have to be removed for any reason, they can be reinstalled without using the beam port centres for alignment.

Figure 190 shows ED2 installed in its vacuum tank.

### High voltage power supplies for EDs

The manufacturer of the ceramic feedthroughs for the high voltage stack could only produce two feedthroughs successfully and submitted regrets for the remaining order. These two feedthroughs were used in the ED2 vacuum tank. A nylon feedthrough assembly was designed and manufactured as an alternative. Two of these assemblies were used in the ED1 vacuum tank. Both the ceramic and nylon feedthroughs were filled with two atmospheres (absolute) of  $\text{SF}_6$ . A residual gas analyzer (RGA) was installed on the ED1 vacuum tank. The ED1 and ED2 vacuum tanks were evacuated and the RGA scan revealed there was a large water content present in the ED1 tank. The tank was mildly baked to about  $60^\circ\text{C}$  using heating tapes. The nylon feedthroughs were also heated to about  $60^\circ\text{C}$  using heating guns. After pumping for a few weeks, vacuum in the ED1 tank was in the order of  $2.8 \times 10^{-8}$  torr, and  $1.8 \times 10^{-8}$  torr in ED2. The high voltage stacks were installed and the high voltage power supplies turned on. Conditioning of the electrodes began.

By year-end both electrostatic dipoles had been conditioned to 140 kV.

### Beam line components

In 2001 most of the installation of the DRAGON beam line was completed.

Highlights of DRAGON construction included:

- Design, fabrication and installation of a new gas target box and positioning tables complete with gamma array detectors.
- Installation and alignment of all diagnostic boxes, diagnostic devices, e.g. slits (vertical/horizontal, Fig. 191), Faraday cups and beam position monitors. Profile monitors are partially assembled.
- Completion of the vacuum system.

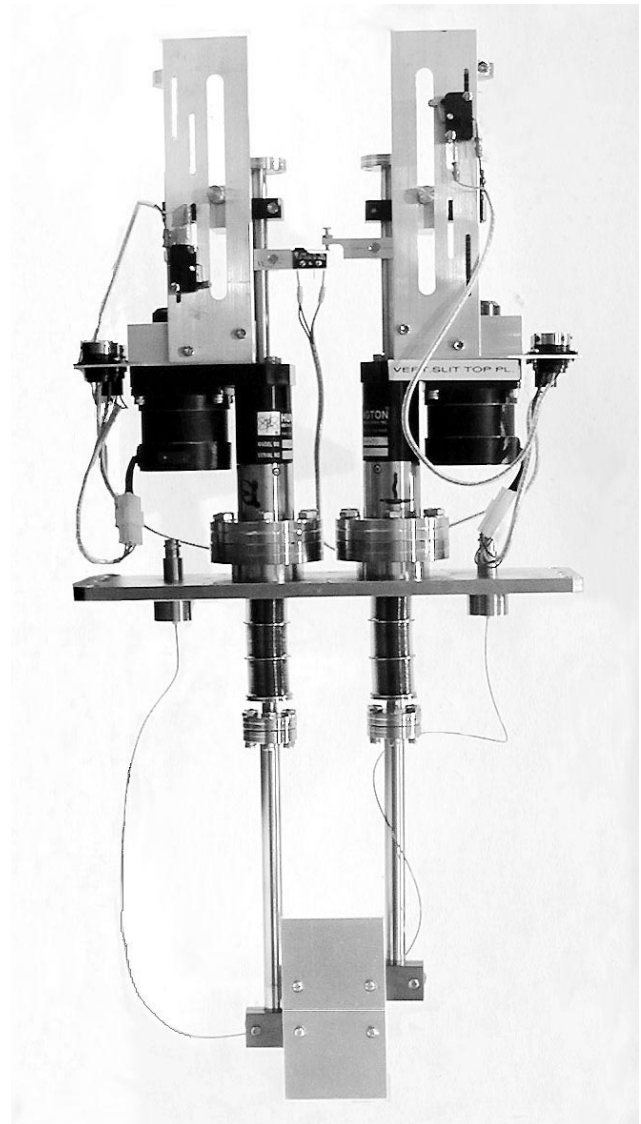


Fig. 191. Vertical/horizontal slits.

For alignment of the diagnostic boxes, special alignment jigs were used that mount to the ports of the diagnostic devices. Jigs (dummy devices) are also used to pre-align the diagnostic devices, therefore eliminating alignment of a device in the beam line after repair or when installing a new device.

Work is continuing on the lead shields and supports for the charge/mass slits boxes, the security fence, and the working platform on one side of the beam line. Most of the fabrication is complete and installation is planned for spring, 2002.

## Engineering – Other

### Experiment 614 (TWIST)

With the successful completion of the assembly of the Expt. 614 magnet steel yoke in the M13 experimental area at the end of 2000, continued engineering support was provided during installation, alignment and testing of the Oxford Instruments superconducting solenoid magnet in the steel yoke early in 2001. The solenoid magnet was cooled over several weeks from room temperature to liquid helium temperature and energized to a fraction of the rated maximum current. At this relatively low current the uniformity of the magnetic field in the bore of the magnet was measured. During field measurements it was discovered that the internal support structure of the solenoid magnet was not properly restraining solenoid coils from movement. The solenoid was accidentally quenched during a low-power ramp-down while this movement was being investigated. It was decided to warm the solenoid back to room temperature to allow for disassembly and inspection, and eventual repair of the solenoid support structure. When the solenoid was disassembled it was discovered that some of the components comprising the support structure were not properly fastened, and in one case was actually missing. Once the support components were eventually replaced, Engineering recommended that load cells be installed on the support structure to allow the forces experienced by the internal supports to be measured. The solenoid was re-assembled with load cells installed, the assembly leak checked, then cooled to liquid helium temperatures, and field uniformity tests resumed. Load cells proved useful in providing an indication of the correct centring of the solenoid magnet within the steel yoke, by minimizing the forces experienced by the solenoid support structure.

In the fall, a uniform field of 2 T was achieved in the bore of the Expt. 614 solenoid.

### Other support

Ongoing engineering support was also provided throughout the year for the operation and maintenance

of the M9B superconducting solenoid and helium refrigerator.

### $G\theta$ experiment

The  $G\theta$  superconducting magnet mapper project was completed with a final visit to the Nuclear Physics Laboratory (NPL) in Champaign, Illinois. Several laboratories in the US expressed interest in using this to map their own magnets because of its high accuracy and easy to program features implemented via the TRIUMF developed graphical user interface (GUI). It is also portable. For example, a group from Indiana University visited NPL to get a close look and demonstration of the gantry in action.

Numerous phases of the gantry system development have been reported and documented on the Web.

The gantry has been used successfully throughout the year at NPL with no electro/mechanical or software incidents. With special tuning and data averaging, the gantry's repeatability has been verified at  $\pm 25 \mu\text{m}$  using laser alignment techniques. Note that the 3D Hall probe head can cover a  $4 \text{ m} \times 4 \text{ m} \times 2 \text{ m}$  spatial volume. What makes this unit so useful is its portability and the GUI software. Very simple point-to-point position data text files need to be written and the machine takes care of the rest after a few simple mouse clicks.

### Other projects

Numerous analysis/design projects performed included the following:

- BL1 T2 target cassette development – Thermal analysis of the BL1 T2 target cassette, to investigate internal temperatures of the beryllium target rod. It was discovered that nucleate boil cooling is very likely occurring at the coolant surface given the incident beam currents presently used (and is necessary for the target to cool sufficiently).
- ISAC-II superconducting rf cavity development – A new design for the tuner diaphragm of the ISAC-II superconducting rf cavity was investigated via finite element analysis (FEA) software and a prototype built from niobium for development because it met the stiffness/stress requirements well.
- A proposal was written in the form of a design report for a new servo controlled electro/mechanical system to operate the tuner diaphragm of the ISAC-II superconducting rf cavity, with a high Q, to an accuracy of  $1 \mu\text{m}$  with a bandwidth of 100 Hz. It uses state-of-the-art direct drive linear motor motion technology.

- Finite element analysis of the ISAC-II superconducting rf cavity was performed to determine deflections, stresses, natural frequencies and mode shares. RF FEA will be done using deflection data to determine the frequency shift of the cavity due to liquid nitrogen pressure fluctuations.
- TPC detector – Analytical and FEA calculations were done of thin foil vacuum windows to investigate very thin foil support design technology for the solar axion search project (CAST) being built at CERN. Various combinations of sub-micron thickness foils backed by fine wire mesh and/or very thin honeycomb structures were investigated. Spherical and flat configurations were looked at. The latter proved simpler and cheaper to make, although the spherical shape is much stronger and can be made to provide higher radiation transmission values. However, it does not sufficiently offset the cost of producing it. A small 8 mm diameter kapton window (400 nm), which is supported by a Ti strongback, has been purchased and works well. The next step is to develop a 50 mm diameter self-supporting beryllium window.
- Other analysis – Many structural analyses were performed for various groups at TRIUMF, and fabrication approvals given.

### Engineering – Victoria

The organization and housekeeping practices for the TRIUMF labs and Machine Shop at the University of Victoria were reviewed to ensure the work and research being performed is carried out safely. A complete overhaul of the entire lab and storage space was performed, which involved disposing of and recycling many unused chemicals and obsolete equipment. Proper storage for flammable and hazardous materials has now been provided and all work is being performed in a safe and orderly manner.

### ISAC target stations

The targets designed for the ISAC target stations are being modified to handle the increased heat dissipation required when they are operated with the increasing proton beam currents. Annular fins along the length of the target have been considered with various mounting patterns, sizes and shapes. For each case, a thermal analysis is being studied to determine if sufficient heat dissipation will occur.

Contributions were made to the design and detail of the beam dump modules for the west target station. Similar contributions have been made for the east target station. Drawings of all the dump module components have been provided and the dump element for

the east target station was successfully produced, assembled and delivered to TRIUMF.

### Signal feedthrough project

There is continuing support for the ATLAS feedthrough project, which is entering the final stages of manufacturing and testing. To date, half of the required fifty feedthroughs have been made, and several have already been sent to CERN. Acceptance tests were successfully carried out at the CERN site on all the shipped feedthroughs. There are some thermal analyses which are ongoing to determine if sufficient heat is being provided by an external heater plate to avoid condensation developing on the feedthrough cables.

### Hadronic endcap (HEC)

Contributions to the design and manufacture of the HEC assembly table are ongoing. The critical components being constructed in Canada were closely supervised and the control actuators for the project were carefully researched.

### Engineering – Carleton

#### ATLAS forward calorimeters (FCAL)

This year the final assembly of FCAL module 3C began. This involved setting up and aligning two end plates on the assembly stand and then “stacking” the module. This was the process of inserting 8224 copper tubes and approximately 641,000 tungsten spacer slugs. Each slug is approximately 2.6 g in weight and 9.89 mm long. Once this was complete the tubes were “swaged” into place. This was accomplished with custom tooling, developed and built at Carleton, which expanded the tube ends into small grooves in the end-plates. The swaging gives the module its structural strength. The outer absorbers were then installed to protect the outermost tubes from damage. The last steps to be completed, before shipping the module to CERN in July, 2002, are the installation of approximately 14,300 ground pins and the inserting of the 8224 tungsten anode rods. Final assembly of FCAL 3A is to begin in February, 2002, for shipment in January, 2003.

A module cradle, to support the module’s final mass of 4000 kg, was also designed and built this year. The cradle will be used for shipping, for module handling at CERN, and for final assembly of the module into the liquid argon support tube. The design of the packing and container for shipment by aircraft was also started.

Figure 192 shows the completely stacked module awaiting ground pins and anode rods.



Fig. 192. Completely stacked FCAL module awaiting ground pins and anode rods.

## PLANNING

This year the Planning group was involved in planning, scheduling, coordinating and expediting several sub-projects for ISAC; planning and coordinating activities for two scheduled shutdowns (December 22, 2000 – April 25, 2001 and September 19–26); prototype chambers for KOPIO, M8 decommissioning, and 1A triplet repairs and replacement.

## ISAC

Various plans and PERTs were prepared and updated regularly with manpower estimates and analysis to identify critical areas and resolve any problems. ISAC priorities were evaluated and higher priority was assigned to: the east target station with an aim to install in the winter, 2002 shutdown; expedite the low energy experimental program that included the first data run at  $\beta$ -NMR, move GPS1, install the Osaka beam line; and commission TUDA and DRAGON with stable beams and RIB.

On the accelerator side, major milestones (after beam to 1.5 MeV/u in December 2000) included: install and commission the 11 MHz buncher by September to facilitate commissioning of high energy experiments (TOJA, TUDA and DRAGON) by November. Manpower planning was done, activities were coordinated and expedited, and the above goals were achieved on schedule.

Technical details and progress on PERTed activities are described elsewhere in this report under the respective principal group. However, following is a summary of the main projects along with the major milestones achieved.

### East target station

This project received high priority and had to be fast-tracked for installation in the January, 2002 shut-

down. This project was broken down into 9 work packages and the major highlights of these work packages included: 2A beam line (switching dipole received in September, monitors, and associated beam line hardware received in December), Faraday cage (constructed by July and isolation transformer, high voltage and other power supplies procured by October), target hall (included modification and commissioning of south hot cell and storage silos in July, alignment components and water package shielding in November), controls (included 2A controls, target protect interlocks and RIB controls for vacuum system, beam optics and beam diagnostic systems).

The work on the target modules required extensive Design Office and Machine Shop effort. Several design modifications were made for better manufacturability and handleability. Shield plugs were ordered in April, with a staged delivery for most modules in July.

### Target conditioning box

An alternative conditioning system was designed and fabricated by December to expedite the process of changing and conditioning ISAC targets. Assembly was delayed to January, 2002, due to lack of manpower.

## HEBT

After completing HEBT1 to the benders for the DRAGON and TUDA beam lines and delivering beam to 1.5 MeV/u in December, 2000, resources were focused to complete the chopper and bunch rotator (July), and 11 MHz buncher (September).

### Low energy experiments

This work included moving GPS1 to a new location, modifications to LTNO and yield station, and  $\beta$ -NMR. Extensive work was done on planning, coordinating and expediting activities and critical components from the Machine Shop and outside suppliers for  $\beta$ -NMR, laser polarization systems, spectrometer, and associated LEBT components. Among other low energy experiments, the Osaka beam line was installed and tested in October/November with a new chamber and associated services, and the  $8\pi$  beam line with a simple chamber was installed and commissioned with a test beam in December.

### High energy experiments

Installation of HEBT components up to the TUDA experimental station, with associated services, was finished in March. A special room was designed and constructed for the TUDA detector system electronics, with all services and a special grounding system. The first stable beam to TUDA was delivered in March. First RIB was delivered to TOJA in June, and to TUDA in September, after commissioning the 11 MHz buncher.

## DRAGON

After completing installation of most components up to MD2 in December, 2000, the overall progress on DRAGON installation was relatively slow due to lack of technical resources and ceramic feedthrough problems. Several initial tests were done to commission the gas target with its control system. Alpha particle tests up to the charge slits were done in January, and continued down the line as services were completed. DRAGON was commissioned with stable beam in October, followed by RIB in November.

## ISAC-II

PERTs were prepared that included work on specifications and design of a superconducting rf test facility and dummy cavity. A construction contract was awarded in October, and a test facility at BC Research was constructed at the end of November. A dummy cavity was tested in a cryostat (without rf) in October, and (with rf) in December, with a plan to repeat these tests at BC Research in early February, 2002 followed by cold tests on a niobium cavity with rf controls in March, 2002. Detailed schedules of ISAC-II projects were prepared that included: medium beta cavities (with cryostats, refrigeration system and solenoid, with an aim to test the first cryo module by summer, 2003); high beta cavities system; charge state booster system which included tests on the test stand with an aim to order the CSB by December; and test the whole system on the test stand by October, 2003; HEBT transfer system; and H<sup>-</sup> HEBT to experimental stations.

## Shutdown Activities

There were two shutdowns during the year: the winter shutdown (December 22, 2000 – April 25, 2001), and a short maintenance shutdown (September 16–26). Major jobs completed in the winter shutdown included: electrical and cooling services; upgrade to the front-end of BL1; and replace target position limit switches for the solid target facility in BL2C4. Most of the vault services upgrade work was done with the lid down to minimize dose levels, and service modifications for the quads were done one at a time in the bunker constructed in the vault basement. A 2 mm horizontal displacement of the quads with respect to their initially measured position was discovered and led to some delay in completing final beam pipe and vacuum connections. Lid up jobs included: probes MRO on 2C, EX1, EX2A; measure probe positions in the tank to verify proper indexing; remove and service inflector; rf surface cleaning; and inspection of correction plates. The lid had to be raised a second time on April 6 to upgrade the HE1 upright and replace vertical drive ferro

fluidic feedthroughs for HE1 and HE2, which delayed the beam operation by one week. Meson hall jobs included: MRO work on water packages for 1AT1, 1AT2; rebuild M9T2 beam blocker; rebuild 1AM8, MRO on 1AM9 (leaking gas package); repair vacuum leak on 1AQ11; repair M11B2 leak; and install rebuilt M9A rf separator.

## Fall mini shutdown

Premature finishing of the PIF run gave a head-start by two days. There was no plan to raise the lid in this shutdown. The only major jobs included the installation of the water-cooled steering magnet (2C4) and repair of the M13 beam blocker. Measurements of Cu ALCW system loss rates confirmed increased water leaks in the 1A triplet and M20Q1, which were deferred to the winter, 2002 shutdown.

## TWIST

The Planning group was actively involved in planning and monitoring TWIST activities. In spite of a few technical difficulties, half of the detector stack was powered up in the detector facility in July and moved and tested upstairs in November, along with the commissioning of the 2 T solenoid in the 60 ton iron return yoke. More commissioning continued in the November/December beam run.

## KOPIO Preradiator

A PERT was prepared for prototype chambers at level 2, 3A, 3B and 4 with associated electronics R&D, scintillators R&D, and simulations.

## DESIGN OFFICE

The ISAC project received 10,967 hours of Design Office time, which was 70.3% of available hours. The office prepared conceptual and detailed designs for many different aspects of the project. Specifically, and in order of magnitude, they were: (a) east target and exit modules, including ECR target; (b) LEBT beam diagnostics, polarimeter and  $8\pi$  beam line components, and upgrades for LTNO and OLIS; (c) DRAGON electrostatic dipoles and beam diagnostics; (d) HEBT1 and 2 beam line components for service to DRAGON and TUDA; (e) ISAC-II cavity development; and (f) components for the installation of the 2A3 beam line and upgrades to the mass separator.

The CERN contribution received 11.6% of Design Office time, with most effort concentrated on the pulse forming network and HV switches.

TRIUMF projects received 15.2% of Design Office time, for a magnetic field mapper and front-end diagnostics for Expt. 614 (TWIST),  $\mu$ SR solenoid support stand and sample mounting system, cyclotron HE probe redesign, and BL1A MRO.

Photographic and visual art services continue in support of seminars, conferences and publications.

## MACHINE SHOP

The TRIUMF Machine Shop, with 22 technicians, produced approximately \$139,000 worth of fabricated and machined components for various on-site groups each month. The shop charge out rate is \$66.50/hour. The distribution by TRIUMF divisions and other groups is shown in Table XXXIII. In addition, 277 separate work packages worth more than \$536,000 were sub-contracted through the Machine Shop to local industrial companies.

Table XXXIII. Machine Shop utilization.

ISAC Development	50.8%
Science	32.4%
Cyclotron	5.0%
Cyclotron Refurbishing	3.4%
ISAC Operations	2.4%
NSERC	1.5%
ISAC-II	1.5%
MDS Nordion	1.4%
CERN	1.1%
Affiliated Institutions	0.5%
Accelerator	0.1%
Administration	0.1%

## BUILDING PROGRAM

Funding approval for the new ISAC-II experimental hall set the year 2001 apart from other years. The Building department was called upon to assist outside consultants in the development of the conceptual and final design for this new facility.

Clearing and preparing the construction site for ISAC-II became a priority involving disposal of several office trailer units and trailer complex S, the former Design Office for 21 years. Other office trailer units A, Ll, Mm, P, Pp, Aa, and the two-storey MDS Nordion complex Ss, were moved to other locations on the TRIUMF site and reconnected to their respective services.

The Building department designed and contracted construction of a cryostat test facility for ISAC-II in rented space at the neighbouring BC Research complex. The approximate 1200 sq ft partitioned space comprises a test area, docking space, boot-up room, assembly area and rinse room, together with all required services including HEPA filters and exhausters.

Several smaller finishing projects had to be carried out in the ISAC-I complex:

- Design and construction of the DTL exclusion area, consisting of steel framework and plywood-lead-plywood removable shielding panels;

- Contracting construction of three additional 6 ft × 6 ft × 10 ft high reinforced concrete target storage vessels for the target hall;
- Design and construction of the 9 ft-6 in. × 9 ft-6 in. × 9 ft-0 in. high electrically shielded room for the high voltage source to the east target station.

The annual contract for maintenance and repair work to various TRIUMF buildings consumed \$34,000. A further \$13,500 was spent on interior repainting, much of it in the TRIUMF main office building.

The roof of the now 30-year-old accelerator building has deteriorated to a point where only a complete replacement of the same will offer a satisfactory remedy. A start was made in 2001 with replacement of the section over the proton area at a cost of \$92,000.

Decommissioning and removal of beam line M8 in the meson hall resulted in the need for reconfiguration of the shielding blocks in this area. The Building department designed and contracted construction for a total of 29 new reinforced concrete shielding blocks, mainly of the 2 ft × 3 ft × 6 ft category, to replace specially shaped and also deteriorated blocks in the beam line 1 tunnel.

Parallel in timing with the ISAC-II project, MDS Nordion began their northward extension of the radiochemistry annex and construction of a new TR30 cyclotron. The Building department liaised with MDS Nordion and its consultants on the conceptual building design, particularly concerning matters of underground services relocation, general access and spacial separation of ISAC-II and MDS Nordion interests.

## ELECTRONICS SERVICES

### Overview

TWIST was the operative word for a majority of the group this year. A concerted effort involving six members of Electronics Services ensured that all components and services requested by the TWIST group were delivered on time. Site communications managed to upgrade the majority of the remaining antiquated network cabling, as well as dealing with the major trailer move for ISAC-II. PC support saw a personnel change and instigated new procedures for tracking equipment. CERN support was another major component for the department.

### Technical Support

Support of the TWIST experiment was one of the top priority jobs for Technical Support this year. Jobs for TWIST included: coordinating final assembly and testing of 300 TWIST postamp/discriminator modules including a dozen control boards; PC layout and coordinating assembly of a new PACT module; design and

assembly of a number of low voltage power systems; a CAMAC based 64-channel HV control and monitoring system; as well as design of cables for the above systems. The prototyping and initial testing of a new 32-channel 16-bit ADC CAMAC board was started for the Controls group. Small jobs included a special serial interface built for the PET group, chamber PC boards for the DRAGON experiment, ISAC target protect thermocouple modifications, and modifications to a very complicated rf control box for  $\beta$ -NMR.

### PC Support

There have been several changes in this department throughout 2001. Keith Ng was hired as a full-time technician in May and our communications technician has been providing some part-time assistance. New helpdesk software was purchased to track hardware, log service calls, and organize tasks. It was implemented in early July, and has greatly assisted us in staying organized. We have developed an asset tracking system such that incoming hardware is tagged at receiving, and existing equipment is tagged when serviced, so that histories are now being created to aid with servicing. Due to the introduction of the helpdesk software in the middle of the year, the number of specific tasks performed, as shown in the last Annual Report, is not available. However, a general review of the year indicates that the volume of service calls is somewhat higher compared to 2000, with the exception of e-mail and network related support calls being noticeably higher. More time was dedicated to developing the department services such as licence management, Web site revisions, and improved access to data. The results of this effort will be seen in 2002.

The Novell server was upgraded to NetWare 5.1 on new hardware and about 15 new users have been added, for a total of 74 users. The PC backup service has been improved by standardizing the schedules and tape rotation periods. Several data recoveries were successfully completed. A 100-user site wide licence for Winzip was purchased to bring the site into compliance with licensing. A significant effort was put forth to identify AutoCAD usage on site by preparing a survey and tallying responses. The results were forwarded to Purchasing.

### Electronics Repair Shop – Nucleonics

As in recent years, much of the effort in the Electronics Repair Shop has gone into repairing increasingly ancient equipment, often requiring rebuilding of decrepit assemblies and re-engineering them to make modern components replace ones that are obsolete and unavailable. In total, 238 pieces of electronic equipment were repaired and/or recalibrated. This included: 13 terminals, 48 monitors, 7 SCSI devices, 73 power

supplies (which included 25 NIM devices, 21 CAMAC devices, 20 high voltage units, and 7 generic types), 46 nucleonics modules (of which 38 were NIM and 8 were CAMAC), 7 test equipment devices, and 44 miscellaneous electronic devices. Some of this specialized equipment included cryogenic controllers, turbo pump controllers, vacuum leak detectors, and milling machine readouts for the Machine Shop. This department successfully refurbished 14 CAMAC crates from the Chalk River surplus pool, saving the TWIST experiment tens of thousands of dollars.

### High Level Software Support

High level software support had a very diverse year. Work included the entire gambit from using new software applications and programming techniques to supporting systems that are 20 years old. Some of the new work included using a Java data acquisition system for charge booster studies at ISN (Grenoble, France),  $\beta$ -NMR solenoid measurements, as well as TWIST magnet measurements. For the LTNO slow control system (MIDAS), a new DVM and network analyzer were installed. For ISAC, there was assembly and installation of DRAGON and  $8\pi$  stepping motor drives as well as modifications of the ISAC DB0 diagnostics motor drives. For the main site, support was given to BL2C probe TRIMAC upgrades for activity logging, and completion of the new thermocouple measurement program (TRIMAC-C) for controls. For M15, there was the repair of M15 separator high voltage supplies as well as the slit controls. Dave Morris continues to be an active First Aid attendant as well as a TRIUMF tour guide. Dave made the Dean's list graduating from the PCST program at Langara College this year.

### Site Communications

It has been a rather busy year with the extra role in PC support, the re-location of trailers to make way for ISAC-II and MDS Nordion expansion, and major upgrades for both meson and proton hall buildings. There was an acceleration in the installation of the newer 100 base-T wiring to replace the older troublesome Thinet cables. Areas with new cabling included the meson extension service annex, proton hall extension and mezzanine, ISIS and level 264. New cables were installed for TUDA and DRAGON as well as ISAC and Stores. In total, over 200 cables were installed. The trailer move this year was another major job. This included preparation of the trailers to minimize downtime for communications. Five trailers were involved with over 60 communication drops. Other work included assisting in the estimate for a security camera system for the site, documentation for the Ethernet system, and assisting PC support one or two days each week.

## Electronics Shop

The Electronics Shop was very busy producing what seemed like “a million and one” cables for TWIST during the first nine months of the year. Many more cables were in production for ISAC, DRAGON diagnostics,  $8\pi$  spectrometer, DAQ, BCP07 experiment, detector facility, magnet, Osaka,  $\beta$ -NMR and TUDA, as well as many more delay cables for TRIUMF Stores. Again we had many orders for flow-switch interlock boxes, IGOR CAMAC modules, bias supplies, and QSX modules for BL2A and ISAC. Waltraud Dilling gives ongoing daily support to the TRIUMF library.

## Experimental and Target Support

The majority of work was supporting CERN projects, the TWIST experiment, as well as some ISAC work. For CERN, there was assembly and testing of pulse forming networks (PFNs) as well as bias supply PCBs for the switch tanks. Work was also done on the 3 kV and 66 kV switching supplies. Efforts for TWIST included assisting in setting up racks and cabling, along with testing and debugging various systems. In ISAC, work was started for the east target protect system due for installation in early February, 2002. Target support included maintenance for 1AT1 and 1AT2.

## ELECTRONICS DEVELOPMENT

This year again, a large fraction of the group’s effort went into support of the ISAC control system design and installation, and the CERN collaboration. Klara Pelzer joined the group as junior technician.

## ISAC Support

The group provides all hardware installation support for the ISAC control system. As part of this function, the production of 100 CAN-bus modules for power supply control, and 33 VME modules of various types was organized. The modules were tested after delivery.

Testing and calibration of the Gauss-meter module was completed and a resolution of better than 1 part in  $10^4$  was achieved. 18 modules were built and installed on the OLIS and HEBT dipole magnets and the DRAGON beam line quadrupoles.

The four high voltage power supplies for the DRAGON electrostatic dipoles were successfully commissioned.

Design and construction of a chopper for the charge state booster was completed and used successfully in tests at Grenoble.

A gas valve controller for the ISAC west target station was installed and integrated into the ISAC control system.

## CERN

Substantial changes to the digital acquisition board (DAB) functional specification Rev5 by CERN required a complete redesign of the DAB VME module. The horizontal and vertical wide-band time normalizer (WTBN) digitizers now connect directly to the DAB as mezzanine cards. These cards receive an analogue signal from the front-end WTBN via fibre optic cables. The DAB II supports two additional operating modes: (i) Global Orbit Histogramming – to obtain distribution of data during an acquisition; and (ii) Post-mortem – which is used to diagnose and understand beam loss or sudden beam dumps in the LHC. The calibration mode has changed so that beam position data can be acquired with no beam synchronous timing signals present. Two DAB II prototype modules were shipped to CERN in October for preliminary tests. Two members of the group went to Geneva in November to test the integration of the WTBN with the DAB II. The primary functions of the module were tested successfully, however, modifications and additional features will be required for the next beam test in June, 2002. A substantial amount of time was spent on the design of PLL and DSP circuits, which were later removed from the revised DAB specs.

Two members of the group spent a month each in Geneva to help with the testing and integration of the TRIUMF designed hardware and software into the CERN systems.

## Safety Systems

A first attempt was made at improving QA for the TRIUMF safety systems by dividing the responsibility between the TRIUMF Safety group and the Electronics Development group. Safety will be responsible for the requirements specification and testing. The Electronics Development group will be responsible for the design and installation of the systems. A Modicon Momentum series PLC system was designed and installed to enforce the DTL exclusion area. A similar system was designed for the mass separator HV lock-up area.

## Miscellaneous

A Web-based information system was developed using Perl cgi-scripts for use by both Electronics Development and ISAC Controls groups. It keeps track of Requests for Engineering Assistance (REA), Engineering Change Requests, and other project related information. Any group member can add comments via a Web browser. Group members on a project’s notification list are notified of any additions by e-mail.

Design work was completed on an NMR readout module, which can replace the existing NIM modules. Board layout for a prototype module has started.



The M9 vacuum system was fully supported with an EPICS system. This system will later be integrated with the new EPICS based secondary channel control system.

For the ISAC  $\beta$ -NMR experiment, two VME modules were developed on fairly short notice. They interface to a commercial rf synthesizer and allow fast steering of the  $\beta$ -NMR rf program. Another module was constructed for the Data Acquisition group.

A generic VME module tester was designed and constructed, and final application software is being written.

A new NIM fibre optic transceiver was designed and 6 modules built. NIM pulses less than 10 ns in width can be transmitted across the light link. Each card consists of two transmitters or receivers. Up to four cards

of mixed types are fitted into a standard NIM housing.

Four VME multipurpose I/O modules were constructed for the Data Acquisition group.

For the TRIUMF Diagnostics group, five VICA VME harp readout modules were produced.

A system for applying a bipolar voltage of 1 kV across a test sample was constructed and tested for the  $\mu$ SR group.

A four-channel remote integrator low current module was designed. The module communicates over the standard CAN-bus link. Initial results have demonstrated a resolution of better than 50 fA.

The VQSX beam current readout module underwent a redesign, and current ranges were adjusted to better match the requirements for ISAC.

# CERN COLLABORATION

## INTRODUCTION

This is the seventh year of the collaboration between TRIUMF and CERN which is producing accelerator components for the Large Hadron Collider (LHC) project. Three technical projects and two beam dynamics studies are presently being carried out. Twenty-four tasks have been successfully completed. The total funding for this work over the two Five-Year Plans (2000–2010) is \$40.5 million, of which \$11 million is for TRIUMF salaries and the remainder is for equipment and outside contract costs.

The largest contribution, in terms of dollars, is for the production of 52 special magnets for the two beam cleaning insertions in the LHC. These twin aperture quadrupoles are warm or copper coil magnets to permit operation with the anticipated beam losses in this region where the beam is carefully collimated to avoid beam losses in the superconducting magnets in the rest of the ring. In 1999, ALSTOM Canada (Tracy, Quebec) was awarded the contract for the production of the first 17 of the twin aperture quadrupole magnets. ALSTOM had previously built a prototype magnet which did not meet the magnetic field requirements, so changes to the lamination design and assembly tooling were required. The first series magnet was delivered to CERN in March of this year, after satisfying the required assembly tolerances at the factory. Magnetic field measurements on this magnet carried out at CERN proved the magnet to be acceptable. The contract was then extended to 52 magnets and further production started. By the end of the year, ALSTOM was producing magnets at the planned rate of two per month.

TRIUMF is also designing and building 6 resonant charging power supplies (RCPS), 9 pulse forming networks (PFN), and 20 thyatron switch tanks for the LHC injection kickers. This work is being carried out at TRIUMF in a specially built clean room with overhead crane coverage. The RCPS were completed in 2000 and one of them was tested at 66 kV operation this year. The 9 pulse forming network tanks were assembled and tested satisfactorily at low voltage. There was excellent agreement between the pulse measurements and the PSpice predictions used for the design. Orders have now been placed for all of the components for the 20 switch tanks, with assembly scheduled for 2002.

The remaining technical work is an instrumentation task which involves the design and fabrication of electronics for the readout of the LHC beam position monitors (BPM). A prototype of this VME based data acquisition board (DAB) was successfully tested in the SPS beam during the summer of 2000. However, a decision at CERN to remove these electronics modules

from the high radiation environment of the LHC tunnel required some redesign. Some additional features were also added. Laboratory tests were carried out at CERN in November on the revised design and satisfactory operation was demonstrated. Ten modules are now being produced for beam tests in 2002. TRIUMF has also arranged for the production of 2300 filter pairs for the analogue portion of the BPM readout.

The main beam dynamics involvement has been the design and optimization of the beam optics for the collimation insertions. The work this year was aimed at improving the robustness of the collimation system and making modifications to the design for cost savings. TRIUMF is also assisting with the study of beam-beam interactions at the LHC collision points using a simulation code developed at TRIUMF.

The LHC cost review carried out at CERN in the latter part of the year indicated that the cost-to-completion of the accelerator and experimental areas had increased by about 18% over the original estimate. The impact of this cost overrun on the completion schedule for the LHC is still not determined. In any case the components being provided by TRIUMF should be delivered as scheduled.

## BEAM DYNAMICS

The simulation study of beam instability induced by interactions between the two beams at the LHC collision points has been extended to include the effect of “parasitic collisions” between bunches approaching and leaving the crossover; a promising start has also been made to include longitudinal motion within the bunches in the simulation. For the LHC collimation system, the priority was updating the cleaning insertion optics to take account of economy-driven changes in the magnet lattice. Studies of the robustness of the LHC collimation system against alignment and magnetic field errors were thereby delayed, but have now restarted with fresh impetus from the new Collimation Task Force at CERN. The study of resonance-free optics in the LHC was completed by investigations confirming its insensitivity to octupole and skew sextupole errors.

## Coherent Beam-Beam Effects in the LHC

This year we continued to study coherent modes of beam-beam interactions using a simulation code based on a hybrid fast-multipole (HFM) field solver, originally developed at TRIUMF for space-charge calculations. Of particular concern are the so-called “parasitic collisions”, where counter-rotating bunches of protons pass each other in close proximity as they approach the actual collision point. Although these long-range

encounters involve weaker electric fields than the head-on collisions, there are many more of them and hence there is a greater potential to excite unstable modes.

We found that the HFM method, which easily accommodates varying distance scales, provides efficient and accurate field solutions for parasitic collisions, allowing a fully self-consistent multi-particle simulation. With traditional mesh-based field solvers, such simulations become prohibitively expensive due to the exponential scaling of computation time with the size of the solution region.

A number of different scenarios involving head-on collisions with different betatron tunes, beam intensities, and beam sizes, as well as early tests and results for long-range collisions, have now been studied [W. Herr *et al.*, Phys. Rev. ST Accel. Beams **4**, 054402 (2001)], with further long-range results to be reported in 2002. For both types of collision, the simulations revealed the expected coherent modes with frequencies in good agreement with analytical predictions.

For head-on collisions with equivalent beams, the potentially unstable  $\pi$  mode is isolated from the incoherent continuum of frequencies. On the other hand, sufficient differences of intensity, betatron tune, or beam size between the two beams will shift the  $\pi$  mode into the continuum, where it will be Landau-damped. Our simulation tool allows us to quantify these effects and hence predict what operational parameters are needed to avoid coherent beam-beam instabilities.

Later in the year, we began a new study of another issue relatively unexplored by simulation: the effect of longitudinal motion in coherent beam-beam interactions. Extending the model fully to three dimensions escalates the cpu requirements to the supercomputer realm. However, we have developed a longitudinal slicing algorithm that makes the problem tractable on a small computing cluster. The simulation code has been extended to support this model and has been tested on a single processor. In 2002 we plan to parallelize the code with MPI for use on a small Linux cluster being installed as a “seed” facility at TRIUMF.

### LHC Collimation

Lattice work included rematching the beam optics for the collimation insertions in LHC Version 6.3. As a result of an engineering proposal for standardization of the connection cryostat (to save 0.5 MSF), the quadrupole Q7 (left and right, IR3 and IR7) had to be moved by 3 m. This was done without a serious loss of performance.

Improving the robustness of the collimation system was the main subject during the second half of 2001. This was done as part of the work of the CERN Collimation Task Force (see <http://www.cern.ch/LHC-collimation>), whose final statement is to be issued in

November, 2002. Ongoing studies include: modification of the collimator set-up (probably longer collimators) to ensure protection against accidental impact on them by a large fraction of the LHC beam; modelling steady multi-turn losses with DIMAD; and a search for the most dangerous optical error that would affect momentum collimation.

### Resonance-Free LHC Optics

This study was completed in 2001. Resonance-free LHC optics make it possible to cancel the effect of non-linear resonances. However, the resonance-free condition itself can be destroyed by large gradient errors. For nominal and resonance-free lattices we computed:

- $Q1''$  and  $Q2''$ , the second derivatives of tunes with respect to momentum, associated with the skew sextupole field error  $a_3$ ;
- resonance driving terms and the reduction in long term dynamic aperture due to octupolar errors:  $b_4$  and  $a_4$ .

It was demonstrated that resonance-free optics make it possible to tolerate the nominal  $a_3$  error and 3–10 times the nominal  $b_4$ ,  $a_4$  errors, without taking advantage of their correction systems. Gradient errors three times larger than the nominal ones do not destroy these benefits (see Fig. 193).

## CONTROLS AND INSTRUMENTATION

### LHC Orbit System Components

The electronics intended to read out the LHC beam position monitors (BPM) comprise a calibrator, 70 MHz low-pass filter, wide-band time normalizer (WBTN), and 40 MHz digitization. As a result of radiation tests performed at CERN in 2000, it was decided to move much of the LHC BPM electronics out

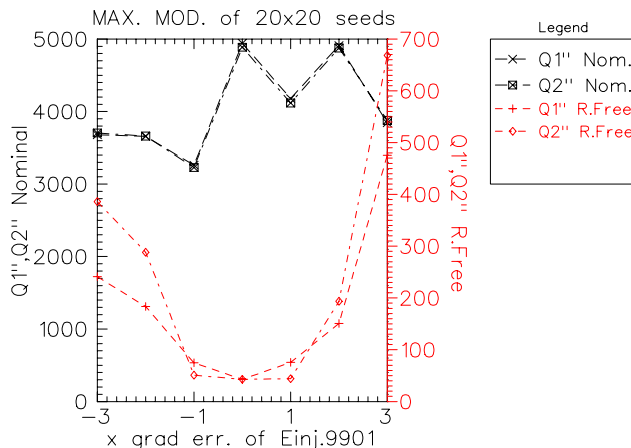


Fig. 193. Second order chromaticity (400 seeds) caused by skew-sextupole field error in main LHC bends. The resonance-free optics (right scale) have smaller parasitic chromaticity than the nominal, even for three times the nominal gradient errors.

of the radiation fields in the tunnel. This required re-design of the CERN normalizer and the TRIUMF digital acquisition board (DAB) which uses two complex programmable logic devices. The WBTN was repackaged as two modules: an analogue part remaining in the LHC tunnel, and a digital part moved to a mezzanine card on the DAB module. The WBTN analogue signal is transmitted through a 3 km fibre optic cable to the DAB II module which accepts two mezzanine cards, one for each plane of the BPM. After review of these changes, the specification document was revised in May and the following operation modes were defined:

- Orbit: continuous, real time closed orbit measurement.
- Capture: turn-by-turn measurement for selected/all bunches/batches and data averaging.
- Histogramming: record the distribution of data with one global orbit acquisition, and histogram for data validation.
- Post-Mortem: provide a history of the beam orbit and turn-by-turn position in order to diagnose and understand beam loss or sudden beam dumps.
- Calibration: asynchronous acquisition (not reliant on the 40 MHz bunch clock and the 11 kHz revolution frequency).

All three acquisition modes (orbit, capture and histogramming) can proceed in parallel. The post-mortem and histogramming additions resulted in considerable increase in design complexity, as did the decision to acquire horizontal and vertical signals without the beam synchronous timing. Unlike the first DAB prototype, the DAB II is not responsible for providing timing and control for WBTN calibration. Instead, so as not to rely on beam synchronous timing, calibration is done in the LHC tunnel using an oscillator on the WBTN front-end.

Three DAB II cards were assembled, including a “dummy” WBTN mezzanine card to simulate BPM data. After successful local tests of the redesigned hardware and application software, the cards were delivered in November to CERN where laboratory tests on the DAB/WBTN combination demonstrated their correct functioning. During this time the prototype LHC BPM system became operational in the SPS, and the bunch-by-bunch measurement capability was used extensively to understand the electron cloud instability which may limit LHC-beam intensity. Figure 194 shows the horizontal oscillation amplitude of each bunch in the LHC batch for 1000 turns. Marginal stability could be reasserted by changing the machine chromaticity.

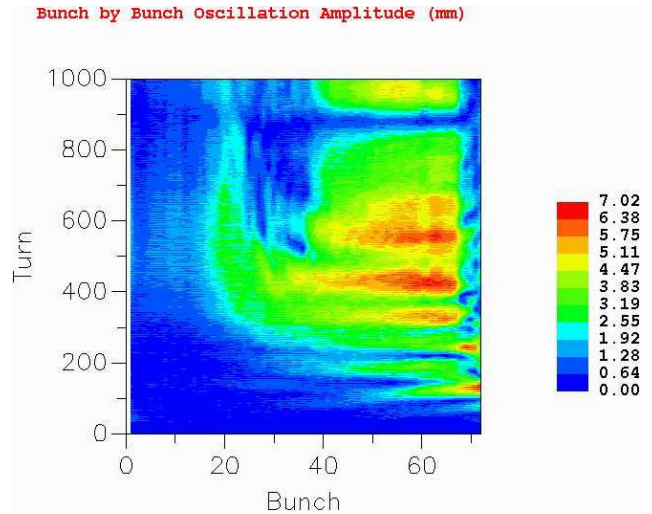


Fig. 194. Bunch-by-bunch oscillation amplitude (mm).

Although further hardware modifications will be required to correct minor problems with VME interrupt handling, and possibly to add further functionality, it is anticipated that ten DAB II modules will be delivered to CERN in June, 2002 for beam tests in the SPS and, depending on the outcome, 60 pre-production modules might be ordered in 2003.

#### Filter pairs

The matching criterion for the filter pairs now calls for the 3 dB corner frequencies to be within 1 MHz. The filter manufacturer, Lorch Microwave, promised that the time responses will match within 100 ps. The pre-production run of 150 pairs of 70 MHz low pass filters was received from Lorch in April. Ten pairs were retained at TRIUMF and 140 pairs were sent to CERN where testing of 26 pairs confirmed electrical measurements made by Lorch during the manufacture.

Testing of the radiation hardness of the filters was begun concurrently at CERN and TRIUMF in August. Three filters tested at TRIUMF, using a beam of 67.3 MeV protons with a dose rate of 7.3 Gy/min, were exposed to 200 Gy, which is the anticipated lifetime exposure at the LHC. Sensitive tests with a network analyzer found no change in electrical properties, and no corrosion was found when the irradiated filters were opened for inspection. The lengthy test at CERN, with an estimated dose rate of 20 Gy/week, accumulated an exposure of 900 Gy including the possibly more damaging effects of neutrons. CERN measurements confirmed no changes in the electrical properties and no corrosion. A mis-steered proton beam in the LHC could cause up to 2 W dissipation in the 50  $\Omega$  resistor inside a filter. At TRIUMF, a filter heated by 2 W rose 47°C in temperature and the time delay through it increased by 15 ps, which is considered acceptable. The other characteristics remained constant.

The production run of 2150 pairs arrived at TRIUMF in October, much ahead of the original delivery schedule. Lorch Microwave measured 13 electrical parameters of each filter and made this database available as an Excel spreadsheet. A LabVIEW program, interfaced to a network analyzer, will be used to test a 5% sample of the filter pairs, and shipment to CERN is anticipated in February, 2002.

## MAGNET DEVELOPMENT

TRIUMF has agreed to provide CERN with fifty-two twin aperture resistive quadrupole magnets for the LHC cleaning insertions. In 1999, TRIUMF awarded ALSTOM Canada Inc. (Tracy, Quebec), a contract to manufacture the first 17 quadrupoles. During 2000, ALSTOM prepared tooling and started working on the first production magnet. Some technical difficulties in welding the stacks of laminations to the required straightness tolerance, and a period of labour problems, delayed completion of this first magnet. Mechanical measurements of the assembly accuracy are carried out with a special pole distance measurement device (PDMD) at the factory. This device measures the distance between flat-parts of the poles at four gaps for each aperture. The acceptance criterion requires a tolerance of  $\pm 100 \mu\text{m}$  for 90% of the length of the magnet. Figure 195 shows the results for one of the apertures of the first magnet.

The first magnet satisfied these requirements and was air-freighted to France, arriving at CERN on March 5. CERN made preliminary mechanical and magnetic field measurements of the magnet, and on April 3, accepted the magnet. Measurements on the magnet were reported in a paper presented at MT17 [Clark, Proc. 17<sup>th</sup> Int. Conf. on Magnet Technology (MT17), Geneva, September 24–28, 2001 (IEEE Trans. Appl. Superconductivity, in press)].

After the first magnet was delivered, ALSTOM and TRIUMF negotiated the extension of the contract from

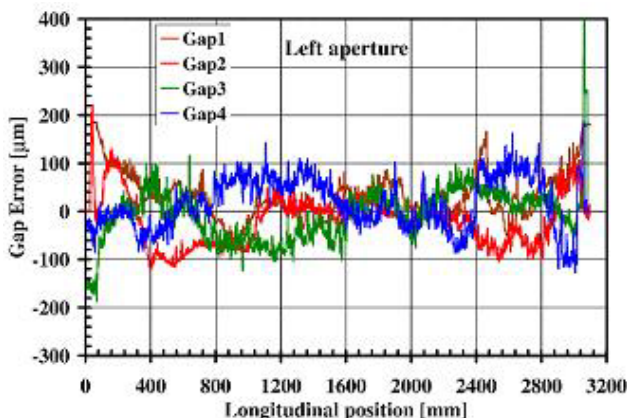


Fig. 195. Measured pole distance errors on MQW001 as a function of the longitudinal position in one of the apertures.



Fig. 196. Layout of the so-called TRIUMF shop at ALSTOM.

17 to 52 magnets. ALSTOM reorganized the project, bringing in a full-time project manager/engineer. The production shop was also reorganized and a second coil mold and stacking table fabricated to enable the magnets to be produced at a rate of two per month. DELSTAR Inc. (Montreal, Quebec), replaced SIGMA as the coil winder, with the coil insulation and impregnation continuing to be carried out at ALSTOM. Figure 196 shows the layout of the so-called TRIUMF shop at ALSTOM.

The year-end saw 3 production magnets at CERN and 3 magnets in transit to CERN. The production rate peaked at 3 magnets per month just before Christmas. ALSTOM expects to deliver at least 24 magnets in 2002.

The method of reviewing the quality of the two types of laminations punched for these magnets was also presented at MT17 [Clark, *op. cit.*].

## KICKER MAGNETS

In collaboration with CERN, TRIUMF has designed and is in the process of assembling and testing 4 CERN LHC injection kicker systems plus spares. Each LHC injection kicker system will consist of 1 resonant charging power supply (RCPS), two  $5 \Omega$  pulse forming networks (PFN), 4 thyatron switch tanks, and 2 kicker magnets. The LHC injection kicker magnet systems must produce a kick of 1.3 Tm each with a flat-top duration which is variable up to  $7.86 \mu\text{s}$ , a rise time of 900 ns, and a fall time of less than 3 ms. The combination of ripple and stability in the field from all kicker system components must be less than  $\pm 0.5\%$ . A prototype kicker magnet has been assembled at CERN and is ready for testing. Six RCPS, including the prototype, have been assembled at TRIUMF. The prototype has been extensively tested at CERN and one production model has undergone preliminary testing at 66 kV



Fig. 197. Four completed RCPS and 8 PFN in storage on the proton hall roof, prior to tests.

operation. Fully documented RCPS tests will be performed early in 2002. Nine PFN have been designed and assembled at TRIUMF and tested at low voltage. Figure 197 shows the completed PFN and RCPS in storage on the proton hall roof beams. Testing of prototype thyatron switch tanks has been completed at CERN, and design of the production models has been completed at TRIUMF. Orders have been placed for all of the components for 20 switch tanks that will operate at 66 kV.

### RCPS

An RCPS has two parallel outputs, to charge two  $5\ \Omega$  PFN to 66 kV. The RCPS has a 2.6 mF storage capacitor bank charged to 3 kV. A thyristor is used to switch the energy on the capacitor bank onto the primary of a 1:23 step-up transformer of low leakage inductance. The output of the secondary is transferred to two  $5\ \Omega$  PFN through two coaxial cables, two diode stacks and two  $70\ \Omega$  resistors. The RCPS is designed so that the PFN can be charged up to 66 kV in less than 1 ms at a repetition rate of 0.2 Hz.

The TRIUMF Kicker group has completed the series production of 5 RCPS, which incorporate several improvements over the prototype RCPS. The two dummy loads that were used for prototype PFN testing at CERN were returned to TRIUMF. New  $1.1\ \mu\text{F}$  dummy load capacitors rated at 66 kV, which were received from ZEZ Silko (Czech Republic), have been installed and tested. Each  $1.1\ \mu\text{F}$  dummy load represents a 28 cell PFN. A standard test procedure has been developed for RCPS to be tested at TRIUMF. The tests will proceed early in 2002.

### PFN

Each  $5\ \Omega$  PFN is composed of two parallel  $10\ \Omega$  lumped element delay lines (Fig. 198) consisting of 4.3 m long precision wound coils, high voltage and high

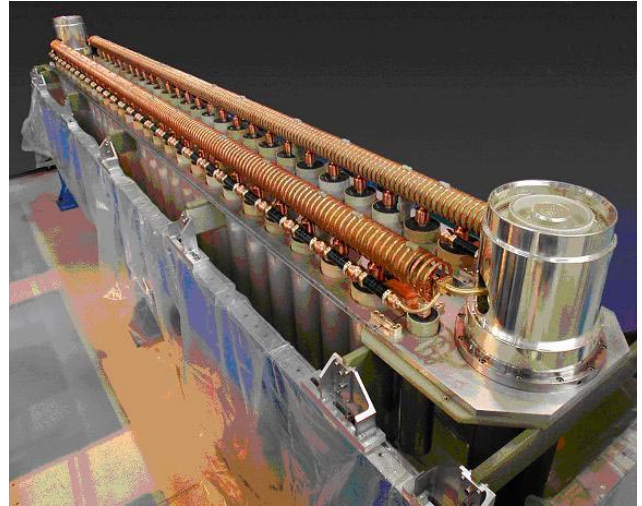


Fig. 198. One of 9 PFN under construction at TRIUMF.

current capacitors, and damping resistors. There is a thyatron switch tank at each end of the  $5\ \Omega$  PFN.

Nine PFN have been built and tested at low voltage at TRIUMF to ensure that performance is within specifications. High voltage tests will be carried out following the manufacture of high voltage switch tanks at TRIUMF. The PFN were charged to 10.0 V and discharged into a precision  $5\ \Omega$  load using a fast switching MOSFET with very low ( $11\ \text{m}\Omega$ ) on-state resistance. The low voltage charging and switch circuits were modelled with PSpice in order to understand and therefore compensate for the measurement system calibration errors. Measurements in which the PFN was replaced with a 5 mF capacitor bank with a low parasitic inductance and series resistance established the calibration. All of the PFN, with numbering from 2 through 10, were measured without damping resistors installed; PFN #2 was measured with and without damping resistors. The ripple without damping resistors was less than  $\pm 0.5\%$  on 8 of the 9 PFN, and  $\pm 1\%$  on PFN #4. Voltage ripple for PFN #2, with damping resistors, was better than  $\pm 0.3\%$ . The predicted kick rise time for PFN #2, from 0.2–99.8%, was 900 ns for a pulse with a flat-top of  $8.54\ \mu\text{s}$  duration and a ripple of less than  $\pm 0.2\%$ , which meets the required specifications. There was no attempt to set up a low voltage dump switch to measure the fall time at low voltage. The absolute average measured flat-tops (Fig. 199) of the 9 PFN were within  $\pm 0.1\%$  of each other, indicative of quality control during manufacture of the PFN. A procedure was developed for accurately measuring pulse performance of the PFN. The results of pulse measurements are compared with PSpice predictions in Fig. 200. There is a 0.25% discrepancy between the absolute value of the flat-top as measured and calculated by PSpice. However, the detailed shapes of the

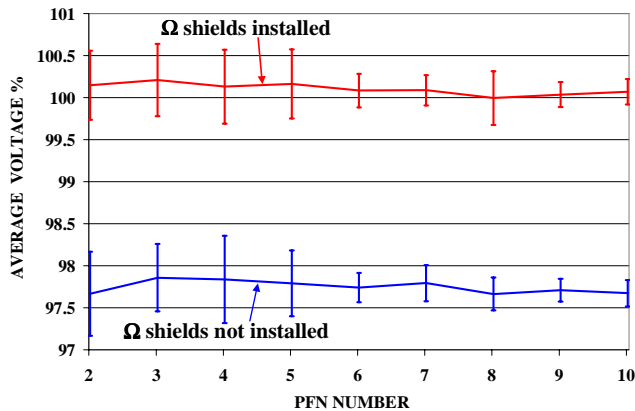


Fig. 199. Measured average flat-top voltage normalized to 200 V charging voltage (from 2  $\mu$ s to 9  $\mu$ s) with no damping resistors installed (error bars represent the maximum peak to peak ripple).

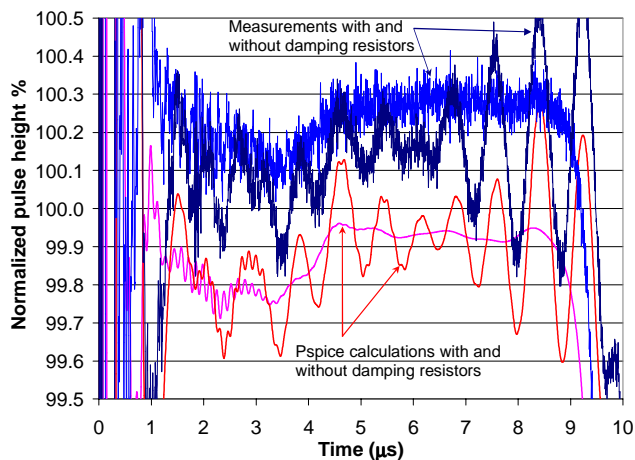


Fig. 200. PFN #2 measured and calculated pulse waveforms with and without damping resistors installed.

measured and calculated pulses are in excellent agreement.

## Thyratron Switch Tanks

The thyratron switch tanks will mount on the ends of the PFN tanks. The main switch (MS) thyratron will be connected to a 5  $\Omega$  transmission line kicker magnet via 10 parallel 50  $\Omega$  coaxial cables, and the kicker magnet output is connected to a 5  $\Omega$  resistive terminator. The dump switch (DS) thyratron will also be connected to a 5  $\Omega$  resistive terminator.

The TRIUMF Kicker group, in collaboration with CERN, has designed a prototype HV grid/heater/reservoir bias circuit for the thyratrons. Two prototype bias circuits were built and bench tested at TRIUMF, and sent to CERN in September, 2000. CERN installed a prototype bias circuit in a prototype thyratron switch tank and completed power tests. CERN requested several modifications and a new feature. Two new bias boxes were built and bench tested at TRIUMF, and shipped to CERN in November. However, CERN has requested, following successful completion of power tests early in 2002, that TRIUMF supply 34 bias boxes; 20 of these will be used in the LHC injection kickers and 14 are to be used in the MKE (SPS extraction) CERN kicker system.

Redesign of all 20 thyratron switch tanks was completed. 184 drawings have been reviewed, all components have been ordered, and contracts awarded to the following machine shops: Sicom Industries (BC), Talvan (BC), Sunrise Engineering (BC), PDE, Acrodyne and Carleton University. Components started to arrive at the end of 2001, and most should be received in January/February, 2002. We expect to complete the design and place orders for the dump switch terminating resistor assemblies, thyratron transport jigs and lifting frames for the switch tanks early in 2002.

## Specifications

Two specifications were issued.

# TECHNOLOGY TRANSFER DIVISION

## INTRODUCTION

Technology Transfer is the TRIUMF division responsible for applied and commercial interactions between the laboratory and outside companies and institutions. It is composed of a small group dedicated to the transfer of TRIUMF generated technologies to the commercial and medical world, together with the Applied Technology group. This latter group is responsible for the operations of the on-site commercial cyclotrons that are owned by MDS Nordion, and produce medical isotopes for use in Canada and around the world.

## TECHNOLOGY TRANSFER

Since its inception, the fundamental research at TRIUMF has generated innovative advances in science and technology that have been moved out into the economy to provide economic and social benefits for all Canadians. This has been achieved through the conventional approach of licensing to commercial companies as well as through donations to non-profit and medical institutions. In addition, technical knowledge has been transferred to numerous TRIUMF suppliers to assist in the provision of products to meet TRIUMF's unique requirements, which in turn has allowed those same companies to explore additional markets with their new skill sets. The experience of TRIUMF provides a real example of the benefits that can be obtained from fundamental research, even in the relatively short term.

The major commercial success in the application of TRIUMF's research has certainly been its association with MDS Nordion for the production of radioisotopes with far reaching medical applications. The relationship with TRIUMF has lasted for over 21 years and has allowed MDS Nordion to establish an enviable position in the world marketplace for cyclotron produced isotopes. The year 2001 saw a further milestone in the cooperative effort as MDS Nordion embarked on an ambitious \$20 million expansion program for their facility at the TRIUMF site. The centrepiece of this expansion will be a new TR30 cyclotron, based on the original TRIUMF design, that is projected to be in operation by the end of 2002, producing an array of radioisotopes for medical applications.

## APPLIED TECHNOLOGY GROUP

### 500 MeV Isotope Production Facility

During this year, the 500 MeV irradiation facility received 258 mA h. Ten targets were irradiated, six targets delivered to produce  $^{82}\text{Sr}/^{82}\text{Rb}$  for MDS Nordion.

### CP42 Facility

The total beam delivery for 2001 was 794 mA h. The weekly beam delivery graph is shown in Fig. 201 and the quarterly time evolution of the beam delivery is shown in Fig. 202. The downtime and maintenance statistics are analyzed in Fig. 203 and compared with the TR30.

Work is still proceeding on the CP42 control system upgrade and the multi output power supply.

### TR30 Facility

The total beam delivery for 2001 was 2906 mA h. The weekly beam delivery graph is shown in Fig. 204 and the quarterly time evolution of the beam delivery is displayed in Fig. 202. The downtime and maintenance statistics are analyzed in Fig. 203 and compared with the CP42.

A major upgrade of the rf system was completed, which reduced the downtime of the machine considerably. Two new types of target station have been developed and tested successfully (1C, 1A prototype). ATG is planning to replace the two high current target stations for palladium production (1B, 2B) within the next year.

### ATG Development Projects

ATG introduced new 3D design and thermal modelling software for enhanced engineering of cyclotron and target station components. Major improvements to the solid targets have been achieved.

ATG continues to be actively involved in the layout and technical planning for the MDS Nordion facility expansion project.

## RADIOISOTOPE PROCESSING (MDS NORDION)

During the year 2001, MDS Nordion shipped large quantities of short-lived medical radioisotopes produced using the TR30 and CP42 cyclotrons. The main radioisotopes produced and shipped were iodine-123 used for thyroid imaging and research, palladium-103 used in prostate brachytherapy, and indium-111 used for monoclonal antibody imaging.

The MDS Board of Directors approved a facility expansion and acquisition of a new cyclotron to be completed by January, 2003 to meet the increasing demand for cyclotron radioisotopes.

The TRIUMF 500 MeV cyclotron was used to produce large-scale batches of strontium-82 whose daughter product, rubidium-82, is used in PET studies for imaging blood flow.



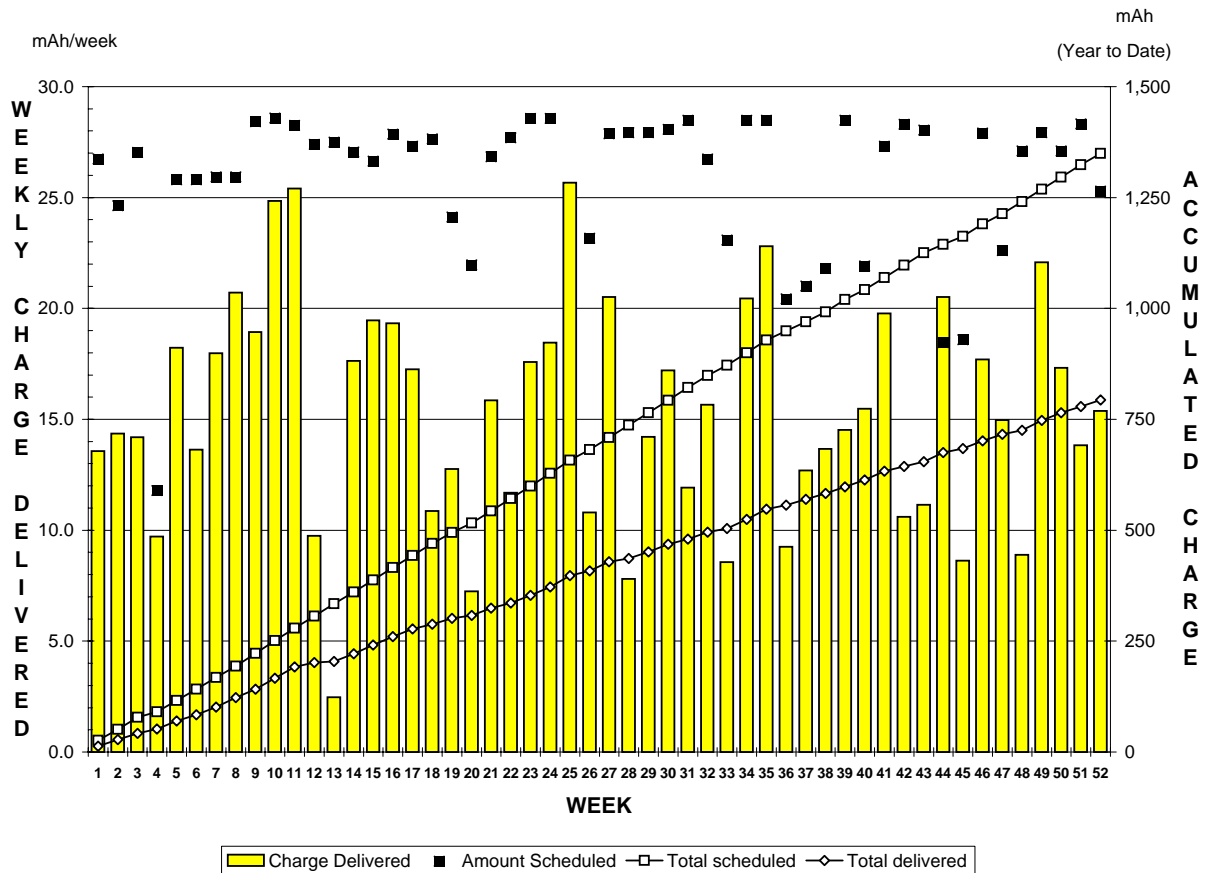


Fig. 201. Weekly beam delivery for the CP42.

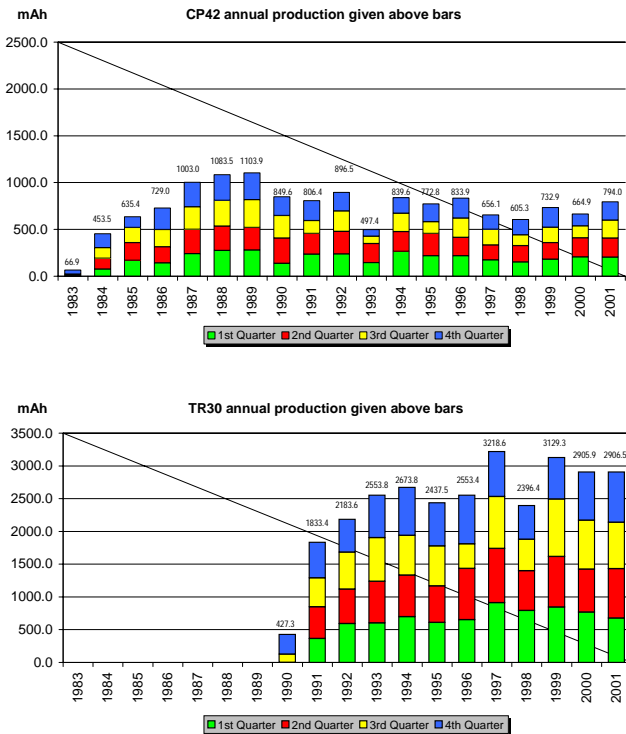


Fig. 202. Annual time evolution of the beam delivery for the CP42 (top) and the TR30 (bottom).

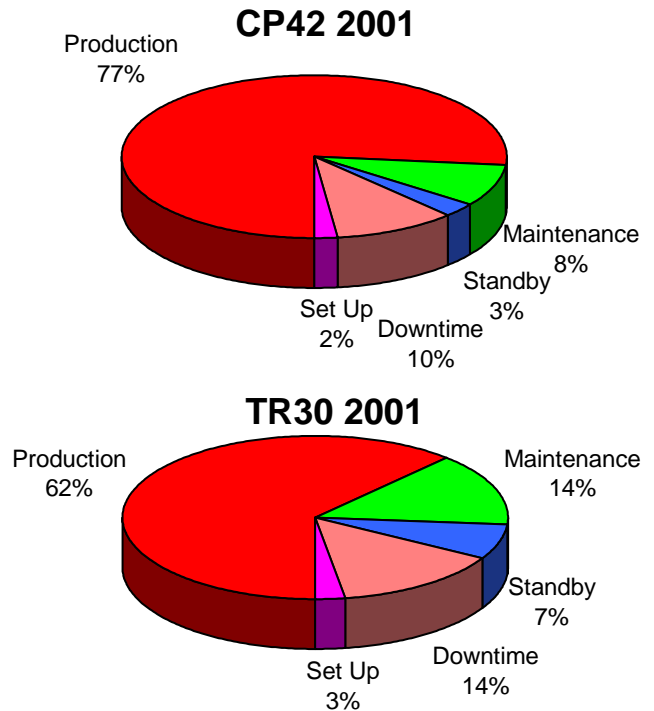


Fig. 203. Breakdown of downtime and maintenance for the CP42 (top) and the TR30 (bottom) during operational hours.

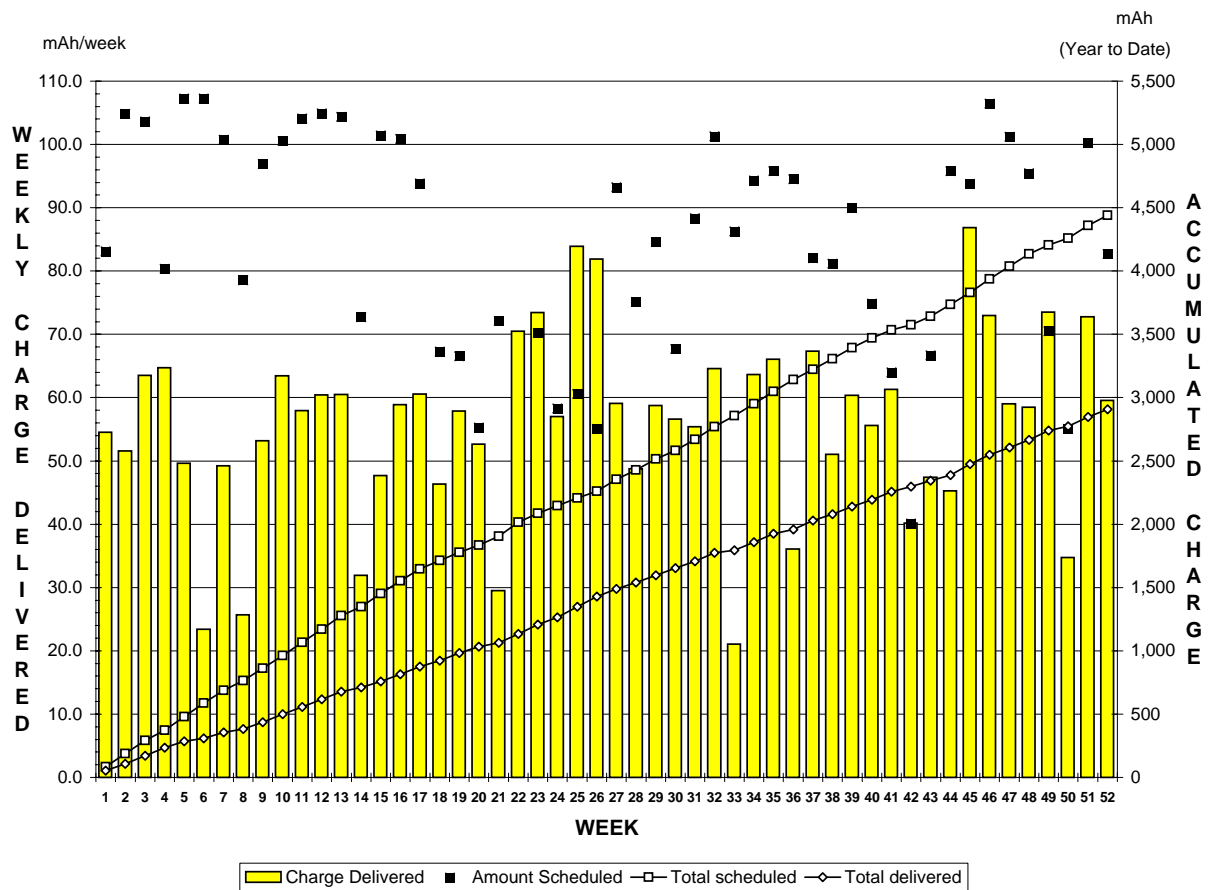


Fig. 204. Weekly beam delivery for the TR30.

## ADMINISTRATION DIVISION

### INTRODUCTION

The Administration Division is made up of Human Resources and Administration, Accounting and Materials Control, Administrative Computing, and Safety. The manager of each group reports to the Director. A summary of Division activities is included in this report.

### HUMAN RESOURCES AND ADMINISTRATION

All employees are reviewed for performance on an annual basis. The period covered for Performance Planning and Review was changed this year to coincide with the calendar year. Reviews will be completed in early 2002 and cover the 18 month period ending December 31, 2001. A number of Personnel Policies and Procedures, applicable to all employee groups, were approved by the TRIUMF Board of Management for implementation.

Work continues on a system to keep track of both short term and long term visitors. It is expected to be completed in 2002 and will enable TRIUMF management to be able to account for all visitors on site. All visitors will be recorded in a database, which will keep track of data such as their home institution, length of stay, contact person at TRIUMF, radiation badge, and keys issued.

The insurance program was renewed with a small increase in premium from the previous year and third party liability coverage remains at \$50 M. All buildings operated by TRIUMF are owned by the University of British Columbia and insurance coverage for these buildings and contents is provided by the Canadian Universities Reciprocal Insurance Exchange (CURIE).

Site security has been reviewed. A proposal is being prepared for management which will include the installation of motion detectors with cameras, as well as a card system for access behind the security fence. Security guard coverage has increased and all vehicles accessing the site behind the security fence are required to have a permit.

Negotiations with UBC for the construction of the ISAC-II building were successfully concluded. A contract for site preparation was awarded and construction is expected to start in March, 2002.

McMaster University became an Associate Member of the Joint Venture effective October 1, 2001. There are currently five full member and six associate member universities in the Joint Venture. Each full member university has two voting members on the Board of Management. Two additional voting members are appointed by the Board from the private sector. The

associate members each retain one non-voting member on the Board.

TRIUMF must now comply with Federal Treasury Board requirements under a Results-based Management and Accountability Framework. The purpose of this framework is to establish a mechanism to help the National Research Council and TRIUMF: i) collect performance information related to this initiative; ii) track delivery of commitments and reporting; iii) describe how the success of TRIUMF will be evaluated over time; and iv) provide direction for on-going and future planning.

### OPERATIONAL SAFETY

#### Licensing

The application for the new TRIUMF operating licence that was submitted to the Canadian Nuclear Safety Commission (CNSC) received its first hearing on December 13, 2001. The second hearing is scheduled for February 28, 2002. This licence will cover the operation of all cyclotrons at TRIUMF as well as that of ISAC-I. Applications were submitted for licences to construct the new TR30 cyclotron and ISAC-II. Each of these applications was accompanied by a safety analysis report that included an analysis of the hazards and the design features of each facility that would mitigate these hazards.

#### Training

A renewed emphasis has been put on the training of accelerator operators at TRIUMF. The safety training coordinator was assigned to assist in the development and documentation of the training program for the four groups of operators: the 500 MeV Cyclotron Operations, the Applied Technology Group, ISAC Operations, and the TR13 Operators. The goal is to develop these programs following the Systematic Approach to Training. The design will try to identify training modules that may be common to the training of all operators so as to avoid duplication of effort.

#### Occupational Health and Safety

All aspects of the occupational health and safety program continued to run smoothly. Regular inspections of the fire alarm and sprinkler systems were scheduled. The TRIUMF Accident Prevention Committee continued its program of regular site inspections. A new housekeeping task force was established with oversight responsibility for ensuring that all housekeeping issues receive prompt attention.

## Interlocks and Monitoring

The work to improve the reliability of the radiation monitoring systems for the 500 MeV cyclotron continued this year. A number of features that improved the frequency of testing of the various components of the system were implemented. The documentation of all stages of the specification and design of the systems was completed following the protocol that has been developed for quality assurance of safety systems.

The radiation monitoring system for ISAC was extended to include the accelerator system and the high-energy beam lines, as well as the changes implemented in the low energy lines. The DTL shielding enclosure was interlocked so as to prevent access when the accelerator is in a state that might generate X-ray fields. In the target maintenance hall the target storage facility was included in the access control interlock system. Design efforts were started to provide adequate interlocks for the operation of the east target station.

Specifications were written for the new TR30 cyclotron access control interlock system and radiation monitoring system. The decision was made to have the construction of these systems contracted out to off-site suppliers.

## Personnel Dosimetry

The program that tracks the readings entered by users of the direct reading dosimeters was moved from the VAX cluster to the Controls cluster after support for the VAX cluster was withdrawn. The program was also upgraded to allow multiple sign-out stations. This allowed ISAC to establish a dosimeter sign-out station in the ISAC experimental hall. The collective dose for

Table XXXIV. Collective dose for TRIUMF personnel by group.

Group	Dose (mSv)	Fraction of Total (%)	Median (mSv)
Applied Technology	96.2	30.9	4.6
Safety Group	26.8	8.3	0.6
Tech Support	25.1	7.8	1.8
500 MeV Operations	23.0	7.2	0.8
Life Sciences	22.3	6.9	1.2
Remote Handling	19.6	6.1	1.9
Vacuum Group	15.4	4.8	1.3
Beam Lines/Probes	13.2	4.1	3.0
Plant Group	12.2	3.8	0.4
Outside Contractors	11.2	3.5	0.1
ISAC Operations	10.9	3.4	0.5
RF Group	4.4	1.4	0.7
ISIS	2.4	0.7	0.3
Others	38.3	11.9	—
<b>Total</b>	<b>321.0</b>	<b>100.0</b>	<b>0.3</b>

TRIUMF personnel for the year 2001 was 321 mSv as measured by the direct reading dosimeter service. This dose is approximately 5% lower than the previous year. Table XXXIV shows the breakdown of the collective dose by various work groups.

## ADMINISTRATION COMPUTING AND COMMUNICATIONS

### Management Information Systems

MIS development continued in many areas in 2001; of particular note were changes relating to HR, the site directory, and the administration Web server.

In HR, a new database structure and set of applications were put into use to record organizational positions and appointments. This database should provide improved control of HR budgets, and also makes the organizational structure of TRIUMF available in a computerized form.

An LDAP (lightweight directory access protocol) directory has been set up that includes all TRIUMF employees. This directory can be used as a central e-mail and telephone directory for PC clients, and also includes some organizational information from the HR position, appointment, and employment databases. It is planned that this directory will be expanded to include visitors to TRIUMF.

Development has also continued on the administration Web server <http://admin.triumf.ca>. Of particular note are the implementation of a “personalized portal”, which provides access to data that is tailored to each user; improvements in the Purchasing area to enable generalized searching through the full PO database; Web database applications to publish the TRIUMF Calendar of Events, Room Bookings, Travellers and Visitors list, and TRIUMF’s management structure. The personalized portal was tested as a means for account holders to prepare budget submissions on-line for the 2001–02 budget year, and it is expected that this will become the preferred method for budget submissions in the future.

### Word Processing Systems

The major change in word processing systems in 2001 was that many PC users migrated to the Windows 2000 platform, which supports the most current versions of the various application suites in use at TRIUMF (from Microsoft, Corel, and IBM/Lotus). These Windows 2000 PCs are configured to use the administration AS/400 as a Windows file-and-print server. This server was also set up to provide file-and-print services to the site Citrix server and OS/2 clients, which allowed all administration users to be consolidated on a single server and share files, regardless of client platform (Windows 2000, OS/2 Warp, or Networkstation).

## Telephones

The site telephone system operated nearly flawlessly in the 2001 calendar year. The central switch, which had reached its full capacity at the end of 2000, was expanded to allow for expected growth. The switch software was also upgraded to the most recent release

level; the software previously installed was no longer supported by the software vendor.

The number of telephone lines used for incoming dial-up was reduced from 22 to 18, due to a reduction in usage that is due to users moving to high-speed Internet access at home. It is likely that this trend will continue over the next few years.

## CONFERENCES, WORKSHOPS AND MEETINGS

### 2001 WESTERN REGIONAL NUCLEAR AND PARTICLE PHYSICS CONFERENCE

The 38<sup>th</sup> annual Western Regional Nuclear and Particle Physics Conference was held February 16–18 at the Chateau Lake Louise. This marked the 18<sup>th</sup> consecutive year that the conference was held at the Chateau. This year the conference was organized by Simon Fraser University and TRIUMF. The organizing committee consisted of Gordon Ball (Chair), John D'Auria, Peter Jackson, Elly Driessen, Martin Comyn and Eileen Conning. Sponsors of this year's meeting were Simon Fraser University, TRIUMF, TUEC, The Canadian Association of Physicists and The University of Alberta (who provided carry-over funds from WRNPPC 2000). Attendance was high this year with 58 participants, 8 invited talks and 14 contributed talks (10 by students). The program covered a wide variety of topics of current interest in subatomic physics with invited talks given by:

- Hendrik Schatz, NSCL, Michigan State University, *Radioactive Beam Experiments for Nuclear Astrophysics*
- Mark Chen, Queen's University, *Neutrino Oscillation Update*
- John Carr, CPPM, IN2P3, *ANTARES: A Neutrino Telescope in the Mediterranean Sea*
- Nathalie Knitz, TRIUMF, *Open Questions in the Nuclear Structure of the Second Potential Well*
- Joe Mildener, TRIUMF, *Recent Results from E787*
- Michel Lefebvre, University of Victoria, *Status of Higgs Particle Searches*
- Marcello Pavan, University of Regina/TRIUMF, *CHAOS and QCD Chiral Dynamics*
- John Behr, TRIUMF, *Atom Traps for Beta Decay Studies*
- Peter Krieger, Carleton University, *And Now the End is Near: Physics Results from LEP2*

The calibre of the student talks was excellent with three prizes awarded to:

- Laura Stumpf, University of Victoria, *The  $\tau^- \rightarrow \mu^- \nu_\mu \nu_\tau$  Branching Ratio Measurements at OPAL*
- Shawn Bishop, Simon Fraser University, *Classical Novae and the Astrophysical  $^{21}\text{Na}(p, \gamma)^{22}\text{Mg}$  Nuclear Reaction Rate: A First Astrophysics Experiment at DRAGON*
- Jaret Heise, University of British Columbia, *Searching for Supernovae with the Sudbury Neutrino Observatory*

The format of the meeting was the same as in previous years with a short session on Friday evening followed by a reception, morning and evening sessions on Saturday with the afternoon free to enjoy skiing, skating, or hiking and the final session on Sunday morning. Thanks to all the participants for making WRNPPC 2001 a great success. Next year the meeting will be hosted by the University of British Columbia.

### WORKSHOP ON EXPERIMENTAL FACILITIES FOR ISAC-II

This year the WRNPPC was preceded by a workshop on Experimental Facilities for ISAC-II. The workshop began on Thursday evening (February 15) and continued on Friday (February 16). In April, 2000, TRIUMF received approval to upgrade the ISAC radioactive beam facility. This upgrade (called ISAC-II), scheduled for completion in 2006, will provide radioactive beams for all masses up to  $A = 150$  at energies up to 6.5 MeV/u. The aim of this workshop was to discuss the experimental facilities required to exploit the physics potential of ISAC-II. At the present time the Canadian nuclear structure/astrophysics community has identified the need for three new instruments: a high efficiency segmented HPGe detector array, a large acceptance magnetic spectrometer and a multi-segmented charged particle detector array. The workshop, sponsored by TRIUMF, was well attended with 38 participants, 7 invited talks, 3 contributed talks and lots of time for discussion. A summary of the workshop was presented at the start of the WRNPPC meeting on Friday evening. The invited speakers included:

- Pierre Bricault, TRIUMF, *ISAC-II: Accelerator Complex and Experimental Area*
- Alfredo Galindo-Uribarri, ORNL, *Research Tools of the HRIBF*
- Paul Nolan, University of Liverpool, *EXO GAM: a  $\gamma$ -Ray Detector for Exotic Nuclei* (this talk was given by Kai Vetter because Paul Nolan was unable to attend)
- Kai Vetter, LBNL, *Signal Processing in Segmented Ge Detectors*
- Carl Svensson, University of Guelph, *TIGRESS: Concepts for a Next Generation  $\gamma$ -Ray Spectrometer at ISAC*
- Philip Woods, University of Edinburgh, *Nuclear Structure and Astrophysical Reactions of Exotic Proton-Rich Nuclei Using ISAC-II*
- Wolfgang Mittig, GANIL, *A Variable Optical Mode Spectrometer for the Study of Reactions Induced by Secondary Beams*

In addition to identifying key areas for research and development at ISAC-II, the workshop provided an excellent venue for the Canadian community to seek international collaborators to join in this unique physics opportunity.

## SUMMER NUCLEAR INSTITUTE AT TRIUMF

The 2001 Summer Nuclear Institute at TRIUMF was held July 9–20. The topics were chosen to be of interest to a wide range of the graduate students involved in the experimental program at TRIUMF. The lecturers and their subjects are given below:

- Prof. L. Lyons, Oxford University, *Statistics for Experimenters*
- Dr. M. Dombisky, TRIUMF, *Isotope Production Methods at ISAC*
- Dr. J. Ng, TRIUMF, *Topics in Particle Physics at the Precision Frontier*
- Prof. J. Deutsch, Université Catholique de Louvain, *Weak Interaction Tests of the Standard Model*
- Prof. P. Depommier, Université de Montréal, *Spin and Polarization*
- Dr. J. Behr, TRIUMF, *Atomic Physics for Subatomic Physicists at ISAC*
- Prof. J. Kluge, GSI, *Atomic Physics (Techniques) at Accelerators*
- Dr. J. Escher, TRIUMF, *Nuclear Reaction Rates for Astrophysics*
- Prof. S. Kahana, Brookhaven National Lab, *Relativistic Heavy Ion Collisions: A Primer*

As in previous years, the general format involved three lectures each morning with an informal tutorial and discussion session in the afternoon. There were 24 registrants. The Institute was organized by J.-M. Poutissou, K.P. Jackson and G.C. Ball.

## INTERNATIONAL LOW TEMPERATURE NUCLEAR ORIENTATION WORKSHOP

Previous meetings on low temperature nuclear orientation (LTNO) have been held in Bad Honnef, Leuven, Oxford, and Oak Ridge. It was decided to host an international LTNO workshop in Vancouver at TRIUMF in 2001 because LTNO has been actively pursued at UBC for several decades, and, particularly, because of the installation of the new LTNO facility at ISAC. The meeting, which took place on August 9–10, was jointly organized by UBC (B. Turrell) and TRIUMF (P. Delheij) with valuable assistance from C. Davis, E. Driessen, and K. Elliott.

25 participants from groups in Asia, Australia, Europe, and North America attended. LTNO is used to

investigate problems in condensed matter, nuclear and fundamental physics, and talks and discussions covered recent work in all these fields. J.-M. Poutissou welcomed the participants and described the new ISAC facility. B. Turrell gave tribute to two colleagues, E. Hagn (Munich) and L. Vanneste (Leuven) who had died recently. They both had made outstanding contributions to LTNO, and this workshop was dedicated to their memory.

W. Brewer described the work of the Berlin group. A systematic and precise determination of nuclear spin-lattice relaxation rates for dilute *nd* impurities in Fe and other ferromagnetic hosts had been completed and analyzed. Results of studies on the multilayer systems  $[\text{Fe}/\text{Ag}]_x$  and  $[\text{Co}/\text{Ag}]_x$ , and the “exchange bias” trilayer Co/Au/CoO were also discussed.

N. Severijns gave an overview of work by the Leuven group. His group had studied problems in all the areas mentioned above. T. Phalet presented results obtained from an LTNO study of the multilayer system  $[\text{Fe}/\text{Ag}]$  that revealed an out-of-plane orientation of the Ag hyperfine field. S. Versyck described on-line experiments at ISOLDE-CERN and Louvain-la-Neuve in which beta asymmetry measurements were used to probe meson exchange currents in first-forbidden beta decay in the lead region. B. Delaure discussed a weak interaction trap for charged particles (WITCH) to be set up at CERN. It will be used for very high precision measurements of the energy spectrum of ions recoiling after beta decay, the motivation being to search for physics beyond the standard model.

C. Tramm from P. Herzog’s Bonn group reported on two investigations: the first was the measurement of hyperfine fields in the CoPd alloy system; the second was a study using the MAPON technique of quadrupole interactions after warm and cold implantation of  $^{82}\text{Br}$  into iron.

From Oxford, J. Rikovska Stone discussed on-line NMRON measurements of ground state magnetic moments of odd-*A* isotopes in the vicinity of doubly-closed shell nuclei and the interpretation of these results. N.J. Stone reported on a program of experiments involving direct proton emission and beta-delayed proton and neutron emission from oriented nuclei designed to study quantum barrier penetration.

S. Ohya detailed the “brute force” experiments of the Niigata group using a 12 T magnet to perform NMRON on Ce, Nd and Pm isotopes. He also discussed the possibility of on-line LTNO in Japan. T. Ohtsubo described NMRON measurements to determine the magnetic moments of Sc isotopes recoil-implanted into iron.

D. Chaplin, from Canberra, paid tribute to pioneering Canadian work using various LTNO techniques to study antiferromagnetic insulators, and presented

recent results on these systems and on rare earth-transition metal metamagnetic alloys. W. Hutchison described experiments utilizing MAPON combined with beta detection to measure electric field gradients in various crystallographic directions in iron. They also had studied  $^{54}\text{MnCo}$  (fcc), and detected NMR in iron via the Mössbauer effect.

From the Munich group, E. Zech described how cold rolling of polycrystalline iron or nickel foils could produce a nearly uniform orientation of the crystallographic axis. These foils could then be used as quasi-single crystals. G. Seewald made two contributions: the first was an improved tight binding model for the spin-orbit induced electric field gradient in cubic ferromagnets; the second concerned nuclear spin-lattice relaxation of iridium isotopes in iron.

P. Delheij described the installation of the LTNO facility at TRIUMF-ISAC and the experimental program planned for this new facility. He gave two examples: preliminary measurements on  $^{79}\text{Rb}$ , and a proposal for the measurement of parity violation in the mass 225 region.

B. Turrell reported on the UBC measurements of an anomalous frequency pulling effect in quasi-2-dimensional manganous acetate tetrahydrate, the successful experiments by the UBC-Leuven collaboration to implant  $^{56}\text{Mn}$  into antiferromagnetic insulators, and studies of the effect of the NMRON line in  $^{54}\text{MnMnCl}_2 \cdot 4\text{H}_2\text{O}$  due to cobalt impurities of various concentrations.

In a special invited talk, S. Cottenier described how one can make *ab initio* calculations of hyperfine fields and presented some case studies relevant to LTNO. The participants also enjoyed two talks about other experimental programs at TRIUMF-ISAC. J. Behr described the trapping of radioactive ions with lasers and how the study of their beta decay properties was being used to test weak interaction physics. R. Kiefl discussed the production of low energy spin-polarized nuclei, e.g.  $^8\text{Li}$ , and their use to probe ultrathin films and surfaces. There was also a tour of the ISAC experimental hall.

## MATERIALS SCIENCE WORKSHOP

In 2001 the TRIUMF Users' Executive Committee (TUEC) sponsored a series of workshops on topics relevant to TRIUMF science in anticipation of a Long Range Planning Committee (LRPC) meeting sometime in 2002. One of these topics was materials science, by which was meant mainly condensed matter physics and chemistry. The title of the workshop was New Opportunities for Accelerator-Based Materials Research in Canada.

Naturally we were most interested in areas of these fields where accelerators like TRIUMF can make important contributions, such as  $\mu\text{SR}$  and  $\beta\text{-NMR}$ , but

we also hoped to explore opportunities for coordinated development of other accelerator-based materials science probes like synchrotron radiation or spallation neutrons.

Based on initial User response and logistic necessity, the workshop was held at TRIUMF on the weekend of August 11–12, 2001. The format was extremely informal and adaptable in response to fresh ideas, a sort of “think tank with lectures”.

Informality notwithstanding, a few formal talks were important to “get the ball rolling”. For the final catchment, see the Program at <http://musr.triumf.ca/conf/ws2001/prog.html>.

To facilitate free discussion before the workshop, we set up an “electronic bulletin board” (BB) where people could post their thoughts and peruse those of others. This BB is still available at the Web site <http://musr.triumf.ca/conf/ws2001/bb.html> but its content has now been absorbed into the ongoing  $\mu\text{SR}$  Bulletin Board at <http://musr.triumf.ca/bb/MUG/> which provides a continuing forum for members of the TRIUMF  $\mu\text{SR}$  Users' Group (MUG) (see <http://musr.triumf.ca/users/>).

The workshop was attended “in person” by 23 participants; another 20 or so members of the TRIUMF materials science community participated electronically. Discussions focused mainly on the TRIUMF  $\mu\text{SR}$  User Facility, whose home page URL is probably obvious by now, so we were unsuccessful in our attempt to engage practitioners of related accelerator-based probes; but this is probably due to short notice and the fact that the workshop was, after all, at TRIUMF.

An extract of the program is as follows:  
 Friday, August 10, RECEPTION 4554 W. 11th Ave.  
 Saturday, August 11 – TRIUMF Auditorium  
 Morning Session: “SCIENCE SHOW & TELL” (new results/ideas as a warm up)

- J. Brewer, *Welcome*
- J. Brewer,  *$\mu^- \text{SR}$  on Nuclei with Spin*
- K. Ghandi, *Chemistry in Pressurized Water Nuclear Reactors Probed by  $\mu\text{SR}$*
- D. Fleming, *Molecular Motion in Zeolites: Static  $\text{MuC}_6\text{H}_6$  in  $\text{NaY}$*
- I. McKenzie, *Novel Alpha Muoniated Radicals*
- K. Matsuta, *Nuclear Moment of  $^{16}\text{N}$  Studied by  $\beta\text{-NMR}$*
- R. Kiefl, *Tour & Demonstration of  $\beta\text{-NMR}$  Experiment at ISAC*

Afternoon Session: “FRIENDLY FACILITIES” (management, accessibility, reliability, versatility)

- S. Kreitzman, *TRIUMF  $\mu\text{SR}$  User Facility*



- Open Discussion
- S. Cottrell, *RAL-ISIS  $\mu$ SR User Facility*
- Open Discussion
- (Panel) *Barriers to Participation – What Keeps People Away From  $\mu$ SR?*
- Open Discussion

Sunday, August 12 – TRIUMF Auditorium  
 Morning Session: “NEW CAPABILITIES” (hardware ideas from the fantastic to the pragmatic)

- J. Brewer, *Ultra-Slow Muons at TRIUMF?*
- K. Chow, *The MULTI Spectrometer*
- M. Larkin, *Spatially Resolved  $\mu$ SR*
- S. Cottrell, *Upgrade Plans at ISIS*
- J. Brewer, *Replacing M8 – a New Concept Surface Muon Channel*

Afternoon Session – “POLITICS” (strategies and tactics for design development, support of existing facilities, grant applications, etc.)

- J. Sonier, *Refurbishing M9A and MULTI Spectrometer*
- Open Discussion
- (Panel) *Major Facility Access Grant(s)*
- Open Discussion
- CLOSURE and Good-bye

## FUTURE OPPORTUNITIES IN NEUTRINO PHYSICS

Neutrino physics is currently commanding a great deal of interest world wide. Recently, attention has been focused on strong hints of neutrino oscillations in which one flavour of neutrino can metamorphose into another. These hints have come from studies of neutrinos produced both in the atmosphere [Fukuda *et al.*, Phys. Rev. Lett. **86**, 5656 (2001)] and in the sun [Abdurashitov *et al.*, Phys. Rev. **C60**, 055801 (1999); Hampel *et al.*, Phys. Lett. **B447**, 127 (1999); Altmann *et al.*, Phys. Lett. **B490**, 16 (2000); Fukuda *et al.*, Phys. Rev. Lett. **86**, 5651 (2001); Cleveland *et al.*, Astrophys. J. **496**, 505 (1998); Ahmad *et al.* (SNO collaboration), Phys. Rev. Lett. **87**, 071301 (2001)], with Canadian physicists making a significant contribution to the solar studies through construction and operation of the Sudbury Neutrino Observatory (SNO) [Ahmad *et al.*, *op. cit.*; Boger *et al.*, Nucl. Instrum. Methods **A449**, 172 (2000)]. The interest stems from the fact that oscillations imply neutrinos are massive particles and there is mixing among the generations, while in the standard model neutrinos are massless and do not mix. Hence, oscillations provide evidence of physics beyond the standard model. Many new experiments have been proposed and/or are under way to study further both the properties of neutrinos themselves and to use them

as a probe to study other phenomena. Participation by Canadian physicists in some of these experiments has received a high priority in the recent report of the Five Year Planning Committee for Subatomic Physics in Canada. In order to explore the avenues by which Canada could continue to make significant contributions to this effort and to identify a potential community which would be interested in the program, a workshop entitled *Future Opportunities in Neutrino Physics* was held by the Canadian neutrino physics community. The workshop was organized under the auspices of the TRIUMF Users’ Executive Committee, TRIUMF, the Sudbury Neutrino Observatory, and the Institute of Particle Physics. It was held from November 9–12 in the Dunsmuir Lodge, near Sydney, B.C.

Sessions were generally arranged to begin with an invited talk summarizing the status of a particular aspect of the field at the present time. These were followed by contributed talks aimed at discussions of future experiments which could address the questions to be answered, and finally by shorter, more specific proposals for some of these experiments. To begin the workshop, however, an overall view of the whole field was presented by John Ellis. Of prime interest to future neutrino measurements are the determination of  $\theta_{13}$ , the angle which in a sense connects the atmospheric and solar measurements, and  $\delta$ , a possible *CP* violating phase in the MNS matrix, the neutrino equivalent of the CKM matrix of the quark sector.

In the session on solar and atmospheric neutrinos, Yoji Totsuka brought us up to date on the status of currently operating experiments and outlined the contributions expected soon from Borexino and KamLAND. He pointed out that the currently operating experiments have been good for discovering surprises – the atmospheric neutrino anomaly, solar neutrino deficit, etc. – but also that they have insufficient resolving power for measuring the underlying parameters well. KamLAND can do this for solar neutrinos if the large mixing angle solution is the correct solution for the solar anomaly, while Borexino will see a large day-night difference if the *low* solution is correct. Unfortunately for Yoji Totsuka and the other Japanese who attended the workshop, the calamity at SuperKamiokande occurred while they were in flight returning to Japan. Everyone was devastated to hear about this disaster, and all hope that repairs will go speedily and satisfactorily so this wonderful detector will be back online as quickly as possible.

Later in the session, Hamish Robertson summarized the status of our understanding of the MNS matrix and presented a summary of future solar experiments, particularly those with low energy thresholds, which will further our knowledge of the pa-

rameters of this matrix. Chang Kee Jung discussed UNO as representative of a future versatile, megaton-scale, water Čerenkov detector useful for studies of nucleon decay, solar/atmospheric/supernova neutrinos, and accelerator-based neutrino oscillation experiments. Ideas for several other detectors were also presented in this session. Some are aimed at most or all of these same measurements (3M, AquaRICH), while others are aimed more specifically at supernova (LAND, OMNIS) or atmospheric (Monolith) neutrinos. A common thread among many of these proposals is that they all aim to take the next step in observation of oscillation phenomena. For example, UNO, 3M, AquaRICH and Monolith would all search for the first oscillation swing in the atmospheric neutrino anomaly. The status of the supernova early warning system (SNEWS) was also described in this session.

Viktor Zacek summarized the situation generally in particle astrophysics. There were more detailed presentations of double beta decay (Jean-Luc Vuillermier) and underwater neutrino telescopes (Paschal Coyle). In recognition of the growing interdependence between standard model type physics with astrophysics and cosmology, we also heard about the PICASSO dark matter experiment based at the Université de Montréal (Marie di Marco) and the STACEE  $\gamma$ -ray astronomy experiment (David Hanna). Both these experiments were of particular interest because of the Canadian involvement. David Sinclair discussed the plans for an upgrade to some of the facilities at SNO, particularly the excavation of a new hall for smaller scale experiments. Tony Noble brought us up to date on the much larger equivalent in the U.S. with a summary of the recent discussions at Homestake.

One session was devoted to a discussion of neutrino factories, in which muons in a storage ring decay in long, straight sections. There would be unprecedented fluxes of neutrinos and the beams would be well collimated. Construction of such facilities is beyond the present planning period, but R&D is being carried out now and it might prove fruitful to take part in that effort. Alain Blondel presented an overview and the R&D work going on in Europe, and Ken Peach and Yoshi Kuno summarized studies taking place in Britain and Japan, respectively. Debbie Harris summarized activities in the U.S., particularly with respect to the possible non-oscillation physics which could be done at a near detector.

The session on accelerator-based long baseline oscillation experiments began with a general overview by Ron Shrock. He presented an excellent theoretical outline of the ways in which neutrino masses and mixings can be generated, and how these in turn can lead to neutrino oscillations. He then reviewed the current ex-

perimental evidence for oscillations and the new information which might become available in the near- and mid-term as results from the currently, or soon to be, operating experiments come in. The information expected from these experiments includes measurement of the energy spectrum in muon neutrino disappearance experiments, looking for dips caused by oscillations, comparison of neutral current and charged current interaction rates to check for evidence of sterile neutrinos, and looking for tau appearance in  $\nu_\mu \rightarrow \nu_\tau$  oscillations. Combining all these purposes can be used to confirm atmospheric neutrino results and to further constrain the mixing parameters. Further down the road, with more intense (superbeam) facilities it will be possible to explore  $\nu_\mu \rightarrow \nu_e$  appearance to get information on  $\theta_{13}$  and possibly on leptonic  $CP$  violation.

More detailed descriptions of several of the experiments possible with a superbeam were presented during the remainder of this session. Specific activities at Fermilab (Harris), the JHF to Kamioka experiment planned in Japan (Koichiro Nishikawa), studies being carried out in Europe (Blondel), and Canada (Akira Konaka) were presented. One item of particular interest was the possibility of locating an off-axis detector in Canada where the NuMI beam to Soudan for the MINOS experiment emerges from the ground. The JHF-Kamioka experiment also plans to make use of the off-axis idea by aiming the beam about two degrees away from the detector at Kamioka. These plans were particularly gratifying to the Canadian participants since the off-axis idea originated at TRIUMF [Helmer, Proc. 9<sup>th</sup> Lake Louise Winter Inst., February 20–24, 1994, eds. Astbury *et al.* (World Scientific, Singapore, 1995) 291].

One session was devoted to summaries of past and present activities in Canada where expertise in specific areas had been developed which could be drawn on for some of the possible future experiments. With expertise in high intensity beams developed especially during the KAON proposal era at TRIUMF, Canada is well positioned to make contributions to beam line, target, and accelerator design and construction. In fact, ionization cooling of muons beams, necessary for the operation of a neutrino factory, is being studied now by an international collaboration using beams at TRIUMF (MUSCAT, TRIUMF Expt. 875). Expertise developed in the underground laboratory at SNO leaves Canada well-positioned for the type of physics which can be carried on in this type of environment as well.

The final day began with Barry Barish walking the participants through the history of neutrino physics and offering some glimpses of where it might be headed. He finished by pointing out that within this decade it is expected that gravity wave detectors will

be capable of receiving a signal from a supernova explosion from as far away as the Virgo cluster and he issued a little challenge suggesting that ways of detecting a neutrino signal from that distance ought to be explored. The Canadian participants then held a close-out session during which two working groups were formed. One is charged with helping to flesh out the possible future activities at SNO and the other with possible involvement in accelerator-based experiments. Future workshops are planned in which the areas where Canada might become involved will be narrowed down, with a view to having a well-defined program in place by the end of 2002.

Slides of many of the presentations, as well as other summaries, are available on the workshop Web site <http://www.phys.ualberta.ca/~neutrino/>.

### TRIUMF USERS' GROUP ANNUAL GENERAL MEETING

The TRIUMF Users' Group Annual General Meeting was held on Wednesday, December 12, sandwiched between the Subatomic and Materials Science two-day EEC meetings. The meeting was well attended with 49 paid registrants and much larger audiences for certain talks. For the first time, on a trial basis, the meeting was also available as a live video stream on the Web via <http://video.triumf.ca/> for Users who were unable to travel to TRIUMF.

The very full agenda began with the traditional status reports by the Director and division heads, followed by presentations on the latest plans for the ISAC-II facility. After lunch, John Carr reported on the underwater Antares Neutrino Telescope which is being constructed and deployed in the Mediterranean Sea south of Marseille.

Nate Rodning reported on the efforts of the TRIUMF Users' Executive Committee (TUEC) during the year to promote and sponsor workshops which would lead to the development of proposals for the next five-year plan. Two such workshops had been held during the year; Jess Brewer reported on the Materials Science Workshop, and Rich Helmer on the Neutrino Workshop.

TUEC had been represented on the TRIUMF House task force which was charged with finding a suitable replacement for the present TRIUMF House. TUEC had discussed the matter extensively and polled the Users to get their views, resulting in the formulation of a list of basic requirements. Jim Hanlon presented an overview of the process and the present state of the negotiations with UBC who would donate the land and assist with the architectural designs, while TRIUMF would pay for the construction and maintenance of the building.

Present and future funding of subatomic physics through the GSC-19 envelope was outlined by Ken Ragan, chair of the grant selection committee. The NSERC reallocation exercise and IPP issues were presented by Jean-Michel Poutissou.

Under the business meeting heading, Nate Rodning reported on the activities of TUEC during the year which, in addition to the items covered above, included development of the TUG Web site at <http://www.triumf.ca/tug/> and the full implementation of the new membership database. He announced that, by acclamation, W.D. Ramsay (U. Manitoba) had been elected as chair-elect for 2002; J.E. Sonier (SFU) as a member for 2002; and G.S. Hackman (TRIUMF) and M.M. Pavan (U. Regina/TRIUMF) as members for 2002/2003. TUEC had selected two members to represent the Users on the TRIUMF Operating Committee: G.M. Marshall (TRIUMF) and G.M. Luke (McMaster U.) [replacing E. Mathie (U. Regina)] with alternates S. Yen (TRIUMF) and J.E. Sonier (SFU) [replacing G.M. Luke (McMaster U.)], respectively.

After dinner, a lively discussion ensued regarding TRIUMF's image and how it might best be presented. Many ideas were proposed and discussed. The AGM finally ended on an optimistic note over twelve hours after it had begun.

Welcome	Nate Rodning
State of the Laboratory	Alan Shotter
Science Division Report	Jean-Michel Poutissou
Cyclotron	Gerardo Dutto
ISAC-I	Paul Schmor
ISAC-II – Machine	Bob Laxdal
ISAC-II – Facilities	Greg Hackman
The Antares	John Carr
Neutrino Telescope	<i>CPPM IN2P3 Marseille</i>
Moving Toward	
a Long Range Plan	Nate Rodning
Materials Science Workshop	Jess Brewer
Neutrino Workshop	Rich Helmer
TRIUMF House	Jim Hanlon
GSC-19	Ken Ragan <i>McGill U.</i>
Reallocation / IPP	Jean-Michel Poutissou
Business Meeting	Nate Rodning
Dinner at TRIUMF	

### TUEC Membership for 2001

N. Rodning	U. Alberta	<i>Chair</i>
G.M. Luke	McMaster U.	<i>Chair-elect</i>
J.H. Brewer	UBC	<i>Past-chair</i>
R. Helmer	TRIUMF	2000/2001
A.K. Opper	Ohio U.	2000/2001
G.D. Morris	LANL	2001/2002
W.D. Ramsay	U. Manitoba	2001/2002
M. Comyn	TRIUMF	<i>Liaison Officer</i>

## ORGANIZATION

### Board of Management

The Board of Management of TRIUMF manages the business of the facility and has equal representation from each of the five member universities. At the end of 2001 the Board comprised:

University of Alberta	Dr. W.J. McDonald Dr. A. Noujaim	Chairman
University of British Columbia	Dr. I. Samarasekera Dr. B. Turrell	
Carleton University	Dr. F. Hamdullahpur Dr. P.J.S. Watson	
Simon Fraser University	Dr. W.S. Davidson Dr. C.H.W. Jones	
University of Victoria	Dr. V. Paetkau Dr. M. Taylor	
Private Sector	Ms. G. Gabel Dr. H. Ing	Environmental Sensors Inc. Bubble Technologies Inc.

Towards the end of 1987, Board membership was expanded in anticipation of a broadening of the TRIUMF joint venture to include a more national representation of Canadian universities long associated with the TRIUMF experimental program. The University of Manitoba and Université de Montréal became associate members, and the University of Toronto joined as an observer. At the end of 1988, University of Toronto's status changed from that of observer to associate member. In March, 1989 the University of Regina became an associate member. In December, 1998 Carleton University and Queen's University became associate members. In March, 2000 Carleton University's status changed from that of associate member to full member. In 2001 two private sector positions were added. In October, 2001 McMaster University became an associate member. Associate membership at year-end:

Associate members:	Dr. W.T.H. van Oers	University of Manitoba
	M G. Michaud	Université de Montréal
	Dr. A.B. McDonald	Queen's University
	Dr. K. Bergman	University of Regina
	Dr. R. Orr	University of Toronto
	Dr. A.J. Berlinsky	McMaster University
Non-voting members:	Dr. W. Davidson	National Research Council
	Dr. P. Sinervo	ACOT
	Dr. A. Shotter	Director, TRIUMF
	Dr. J.-M. Poutissou	Associate Director, TRIUMF
	Mr. J. Hanlon	TRIUMF Recording Secretary

The following changes occurred in Board membership during 2001: Ms. G. Gabel and Dr. H. Ing were elected as private sector representatives. Dr. K. Bergman replaced Dr. K. Denford as University of Regina member. Dr. R. Orr replaced Dr. P. Sinervo as University of Toronto member. Dr. A.J. Berlinsky joined as McMaster University member. Dr. W. Davidson replaced Ms. J. Verrett as NRC member. Dr. A. Shotter replaced Dr. A. Astbury as Director of TRIUMF. The Board met 4 times during the year.

### Administration

Under the directorship of Dr. A. Shotter, TRIUMF personnel were grouped into divisions, with division heads as follows:

Division Head, Science Division	J.-M. Poutissou
Division Head, Accelerator Technology Division	E.W. Blackmore
Division Head, Cyclotron Operations Division	G. Dutto
Division Head, Technology Transfer Division	P.L. Gardner
Division Head, ISAC	P.W. Schmor
Division Head, Administration Division	A. Shotter

### Operating Committee

The TRIUMF Operating Committee is responsible for the operation of the facility. It reports to the Board of Management through its chairman, the Director, Dr. A. Shotter. The Operating Committee consists of one voting member from each of the five universities, two voting members representing the interests of the Users, and one representing TRIUMF staff. The Associate Director is a non-voting member. Members of the committee (alternate members in parentheses) at the end of 2001 were:

Dr. A. Shotter	Chairman	Director	
Dr. J.-M. Poutissou	( <i>ex officio</i> )	Associate Director	
Dr. J. Pinfold		University of Alberta	(Dr. N. Rodning)
Dr. G. Oakham		Carleton University	(Dr. D. Karlen)
Dr. K.P. Jackson		Simon Fraser University	(Dr. J.M. D'Auria)
Dr. R. Kowalewski		University of Victoria	(Dr. M. Lefebvre)
Dr. D. Bryman		University of British Columbia	(Dr. T. Mattison)
Dr. G. Luke		Users	(Dr. J. Sonier)
Dr. G. Marshall		Users	(Dr. S. Yen)
Mr. R. Baartman		TRIUMF Employee Group	(Mr. K. Reiniger)
Mr. J. Hanlon	Recording Secretary	TRIUMF	
Dr. W. Davidson	( <i>ex officio</i> )	National Research Council	

Changes in 2001: Dr. A. Shotter replaced Dr. A. Astbury as Director. Dr. J. Pinfold replaced Dr. N. Rodning as University of Alberta member (Dr. Rodning replaced Dr. L.G. Greeniaus as alternate). Dr. K.P. Jackson replaced Dr. P. Percival as Simon Fraser University member, with Dr. J.M. D'Auria replacing Dr. Jackson as alternate. Dr. R. Kowalewski replaced Dr. R. Keeler as University of Victoria member, with Dr. M. Lefebvre replacing Dr. M. Roney as alternate. Dr. D. Bryman replaced Dr. C. Hearty as University of British Columbia member, with Dr. T. Mattison replacing Dr. M.D. Hasinoff as alternate. Dr. G. Luke replaced Dr. E. Mathie as one of the Users members, with Dr. J. Sonier replacing Dr. Luke as alternate. Mr. R. Baartman replaced Mr. K. Reiniger as TRIUMF Employee Group member (Mr. Reiniger remained as alternate). Dr. W. Davidson replaced Ms. J. Verrett as NRC member. The Operating Committee met 11 times in 2001.

### NRC Advisory Committee on TRIUMF

Dr. P. Sinervo	Chairman	University of Toronto
Dr. W. Davidson	Secretary	National Research Council
Dr. J. Äystö		CERN
Dr. A.J. Berlinsky		McMaster University
Dr. R. Boyd		Ohio State University
Dr. A. Fenster		J.P. Robarts Research Institute
Dr. J. Guigné		Guigné International Ltd.
Dr. G. Kalmus		Rutherford Appleton Laboratory
Dr. W. Nazarewicz		University of Tennessee
Dr. J. Siegrist		University of California, Berkeley
Dr. P. Vincett		FairCopy Services Inc.
Dr. R. Keeler	( <i>ex officio</i> )	University of Victoria
Dr. W.J. McDonald	( <i>ex officio</i> )	University of Alberta
Dr. K.J. Ragan	( <i>ex officio</i> )	McGill University

Changes in 2001: Dr. W. Davidson replaced Dr. D. Santry as secretary. Drs. W. Nazarewicz, J. Äystö and J. Siegrist replaced Drs. P.-G. Hansen, R. Taylor and Prof. V. Soergel. Drs. R. Keeler, W.J. McDonald and K.J. Ragan replaced Drs. R. Carnegie, C.H.W. Jones and R. Keeler, respectively, as *ex officio* members.

## Agency Committee on TRIUMF

Dr. A.J. Carty	Chairman	President, National Research Council
Dr. T. Brzustowski		President, Natural Sciences and Engineering Research Council
Mr. V.P. Harder		Deputy Minister, Industry Canada
Dr. W. Davidson	Secretary	National Research Council

Changes in 2001: Mr. V.P. Harder joined the committee. Dr. W. Davidson replaced Ms. J. Verrett as secretary.

## TRIUMF Safety Management Committee

Dr. A. Shotter		Director, TRIUMF
Dr. J.-M. Poutissou		Associate Director/Head, Science Division
Dr. E.W. Blackmore		Head, Accelerator Technology Division
Dr. G. Dutto		Head, Cyclotron Operations Division
Mr. P.L. Gardner		Head, Technology Transfer Division
Dr. P.W. Schmor		Head, ISAC Division
Mr. M. Stenning		Head, Operations Group
Mr. D. Preddy		TAPC Chairman
Mr. G. Wood		Industrial Safety Officer/TAPC
Mr. L. Moritz		Head, Environmental Health & Safety
Mr. J. Hanlon		Manager, Human Resources & Administrative Services
Dr. S. Zeisler		Head, Applied Technology Group
Mrs. K. Gildert	Recording Secretary	

Changes in 2001: Dr. A. Shotter replaced Dr. A. Astbury as Director of TRIUMF. Mr. D. Preddy replaced Dr. M. Adam as TAPC chairman.

## Experiments Evaluation Committees

### Subatomic Committee:

Dr. I.S. Towner	Chairman	Queen's University
Dr. J.-M. Poutissou	Associate Director/ <i>(ex officio)</i>	TRIUMF
Dr. B. Jennings	Secretary	TRIUMF
Dr. H.-O. Meyer		Indiana University
Dr. A. Richter		Technische Universität Darmstadt
Dr. N. Rodning		TUEC Chairman/U. of Alberta/TRIUMF
Dr. B.M. Sherrill		NSCL/Michigan State University
Dr. F.K. Thielemann		Universität Basel
Dr. M.C.T. Wiescher		University of Notre Dame

### Materials Science Committee:

Dr. I.K. Affleck	Chairman	Boston University
Dr. J.-M. Poutissou	Associate Director/ <i>(ex officio)</i>	TRIUMF
Dr. P.W. Percival	Secretary/ <i>(ex officio)</i>	SFU/TRIUMF
Dr. J.H. Brewer		TUEC Past Chairman/UBC
Dr. S.F.J. Cox		Rutherford Appleton Laboratory
Dr. B. Gaulin		McMaster University
Dr. S. Roorda		FOM Inst. for Atomic and Molecular Physics
Dr. G.A. Sawatzky		University of British Columbia
Dr. T.W. Swaddle		University of Calgary

In July, 1994 the Experiments Evaluation Committee was formally split into two committees representing subatomic physics and  $\mu$ SR physics. In 2000 the  $\mu$ SR Committee changed its name to the Materials Science Committee. Changes in membership during the year: on the Subatomic Committee, Dr. B. Jennings replaced Dr. H. Fearing as secretary. Dr. N. Rodning replaced Dr. J.M. D'Auria as TUEC chairman. Drs. W.C. Haxton and K. Langanke completed their terms. The committee welcomed Drs. B.M. Sherrill and F.K. Thielemann. On the Materials Science Committee, Dr. R.E. Wasylshen completed his term. The committee welcomed Dr. T.W. Swaddle.

### Life Sciences Project Evaluation Committee

Dr. A. Fenster	Chairman	J.P. Robarts Research Institute
Dr. J.-M. Poutissou	Associate Director / ( <i>ex officio</i> )	TRIUMF
Dr. L.P. Robertson	Secretary	University of Victoria
Dr. D.C. Price		University of California, San Francisco
Dr. R.L. Wahl		Johns Hopkins Medical Institute
Dr. J.E. van Lier		Université de Sherbrooke
Dr. J. Link		University of Washington
Dr. C.J. Thompson		Montreal Neurological Institute

Changes in 2001: Dr. A. Fenster replaced Dr. T. Lewellen as chairman. Dr. R. Finn completed his term. The committee welcomed Drs. J. Link and C.J. Thompson.

## PUBLICATIONS

This appendix lists publications describing work performed at TRIUMF and also work conducted elsewhere by TRIUMF personnel and TRIUMF users.

## Journal Publications

## Particle, Nuclear and Atomic Physics

A. Lagoyannis, F. Auger, A. Musumarra, N. Alamanos, E.C. Pollacco, A. Pakou, Y. Blumenfeld, F. Braga, M. La Commara, A. Drouart, G. Fioni, A. Gillibert, E. Khan, V. Lapoux, W. Mittig, S. Ottini-Hustache, D. Pierroutsakou, M. Romoli, P. Roussel-Chomaz, M. Sandoli, D. Santonocito, J.A. Scarpaci, J.L. Sida, T. Suomijarvi, S. Karataglidis and K. Amos, *Probing the  ${}^6\text{He}$  halo structure with elastic and inelastic proton scattering*, Phys. Lett. **B518**, 27 (2001) [nucl-ex/0004001].

M.A. Quraan, A. Gaponenko, P. Green, P. Kitching, R. MacDonald, G. Price, N.L. Rodning, J. Schaapman, F. Sobratee, J. Soukup, G. Stinson, A. Khruchinsky, V. Selivanov, V. Torokhov, C.A. Gagliardi, J.C. Hardy, J.R. Musser, R.E. Tribble, M.A. Vasilev, W. Andersson, M. Comyn, Yu. Davydov, J. Doornbos, W. Faszer, D.R. Gill, P. Gumplinger, R. Henderson, J.A. Macdonald, G.M. Marshall, A. Olin, D. Ottewell, R. Openshaw, J.-M. Poutissou, R. Poutissou, G. Sheffer, H.K. Walter, D. Wright, M. Hasinoff, D. Mass, P. Depommier, E. Korkmaz, T.A. Porcelli, T. Mathie, R. Tacik, Y. Shin, D.D. Koetke, R. Manweiler, P. Nord and T.D.S. Stanislaus, *A precision measurement of muon decay*, Int. J. Mod. Phys. **A16S1A**, 296 (2001).

D. Hutcheon, R. Abegg, E.G. Auld, R.M. Churchman, C.A. Davis, R.M. Finlay, P.W. Green, L.G. Greeniaus, R. Henderson, D.V. Jordan, W. Kellner, E. Korkmaz, A.K. Opper, G.V. O'Rielly, T.P. Porcelli, S.D. Reitzner, G. Sheffer, P.L. Walden and S. Yen, *Apparatus for a measurement of charge symmetry breaking in  $np \rightarrow d\pi^0$* , Nucl. Instrum. Methods **A459**, 448 (2001) [TRI-PP-00-55].

A.R. Berdoz, J. Birchall, J.B. Bland, J.D. Bowman, J.R. Campbell, G.H. Coombes, C.A. Davis, P.W. Green, A.A. Hamian, Y. Kuznetsov, L. Lee, C.D.P. Levy, R.E. Mischke, S.A. Page, W.D. Ramsay, S.D. Reitzner, T. Ries, G. Roy, A.M. Sekulovich, J. Soukup, T. Stocki, V. Sum, N.A. Titov, W.T.H. van Oers, R.J. Woo and A.N. Zelenski, *A monitor of beam polarization profiles for the TRIUMF parity experiment*, Nucl. Instrum. Methods **A457**, 288 (2001) [TRI-PP-00-34, physics/0011007].

S. Page and W.T.H. van Oers, *Parity violation in proton-proton scattering*, Nucl. Phys. News **11N3**, 22 (2001) [TRI-PP-00-65].

A.R. Berdoz *et al.* (TRIUMF E497 collaboration), *Parity violation in proton proton scattering at 221 MeV*, Phys. Rev. Lett. **87**, 272301 (2001) [TRI-PP-01-11, nucl-ex/0107014].

F. Merrill, T. Iijima, P. Koran, P.D. Barnes, B. Bassalleck, A.R. Berdoz, T. Bürger, M. Burger, R.E. Chrien, C.A. Davis, G.E. Diebold, H. En'yo, H. Fischer, G.B. Franklin, J. Franz, L. Gan, D.R. Gill, K. Imai, Y. Kondo, M. Landry, L. Lee, J. Lowe, R. Magahiz, A. Masaike, R. McCrady, C.A. Meyer, J.M. Nelson, K. Okada, S.A. Page, K. Paschke, P.H. Pile, B.P. Quinn, W.D. Ramsay, E. Rössle, A. Rusek, R. Sawafta, H. Schmitt, R.A. Schumacher, R.L. Stearns, R.W. Stotzer, I.R. Sukaton, V. Sum, R. Sutter, J.J. Szymanski, F. Takeutchi, W.T.H. van Oers, K. Yamamoto, V.J. Zeps and R. Zybert, *H-dibaryon search via  $\Xi^-$  capture on the deuteron*, Phys. Rev. **C63**, 035206-1 (2001).

J.K. Ahn, S. Ajimura, H. Akikawa, B. Bassalleck, A. Berdoz, D. Carman, R.E. Chrien, C.A. Davis, P. Eugenio, H. Fischer, G.B. Franklin, J. Franz, T. Fukuda, L. Gan, H. Hotchi, A. Ichikawa, K. Imai, S.H. Kahana, P. Khaustov, T. Kishimoto, P. Koran, H. Kohri, A. Kurepin, K. Kubota, M. Landry, M. May, C. Meyer, Z. Meziani, S. Minami, T. Miyachi, T. Nagae, J. Nakano, H. Outa, K. Paschke, P. Pile, M. Prokhvatilov, B.P. Quinn, V. Rasin, A. Rusek, H. Schmitt, R.A. Schumacher, M. Sekimoto, K. Shileev, Y. Shimizu, R. Sutter, T. Tamagawa, L. Tang, K. Tanida, K. Yamamoto and L. Yuan, *Production of  ${}_{\Lambda\Lambda}^4\text{H}$  hypernuclei*, Phys. Rev. Lett. **87**, 132504 (2001).

P. Camerini, E. Fragiaco, N. Grion, R. Rui, J.T. Brack, E.F. Gibson, G.J. Hofman, E.L. Mathie, R. Meier, K. Raymond, M.E. Sevier, G.R. Smith and R. Tacik,  *$\pi \rightarrow \pi\pi$  results in nuclei*, Phys. Rev. **C64**, 067601 (2001) [nucl-ex/0109007].

G.C. Ball, S. Bishop, J.A. Behr, G.C. Boisvert, P. Bricault, J. Cerny, J.M. D'Auria, M. Dombisky, J.C. Hardy, V. Iacob, J.R. Leslie, T. Lindner, J.A. Macdonald, H.-B. Mak, D.M. Moltz, J. Powell, G. Savard and I.S. Towner, *Precise half-life measurement for the superallowed  $0^+ \rightarrow 0^+$   $\beta$  emitter  ${}^{74}\text{Rb}$ : first results from the new radioactive beam facility (ISAC) at TRIUMF*, Phys. Rev. Lett. **86**, 1454 (2001).

N. Bateman, K. Abe, G. Ball, L. Buchmann, J. D'Auria, Y. Fuchi, C. Iliadis, H. Ishiyama, K.P. Jackson, S. Karataglidis, S. Kato, S. Kubono, K. Kumagai, M. Kurokawa, X. Liu, P. Strasser and M.H. Tanaka, *Measurement of the  ${}^{24}\text{Mg}(p,t){}^{22}\text{Mg}$  reaction and implications for the  ${}^{21}\text{Na}(p,\chi){}^{22}\text{Mg}$  stellar reaction rate*, Phys. Rev. **C63**, 035803-1 (2001).

N.S. Kelsall, R. Wadsworth, A.N. Wilson, P. Fallon, A.O. Macchiavelli, R.M. Clark, D.G. Sarantites, D. Seweryniak, C.E. Svensson, S.M. Vincent, S. Frauendorf, J.A. Sheikh and G.C. Ball, *Consequences of neutron proton pairing cor-*



relations for the rotational motion of the  $N = Z$  nucleus  $^{72}\text{Kr}$ , Phys. Rev. **C64**, 024309-1 (2001).

Y. Matsuda, J.D. Bowman, B.E. Crawford, P.P.J. Delheij, T. Haseyama, J.N. Knudsen, L.Y. Lowie, A. Masaïke, Y. Masuda, G.E. Mitchell, S.I. Penttila, H. Postma, N.R. Roberson, S.J. Seestrom, E.I. Sharapov, S.L. Stephenson, Y.-F. Yen and V.W. Yuan, *Parity violation in neutron resonances of antimony and iodine*, Phys. Rev. **C64**, 015501 (2001).

C.E. Svensson, A.O. Macchiavelli, A. Juodagalvis, A. Poves, I. Ragnarsson, S. Aberg, D.E. Appelbe, R.A.E. Austin, G.C. Ball, M.P. Carpenter, E. Caurier, R.M. Clark, M. Cromaz, M.A. Deleplanque, R.M. Diamond, P. Fallon, R.V.F. Janssens, G.J. Lane, I.Y. Lee, F. Nowacki, D.G. Sarantites, F.S. Stephens, K. Vetter and D. Ward, *Lifetimes of superdeformed rotational states in  $^{36}\text{Ar}$* , Phys. Rev. **C63**, 061301 (2001).

M.M. Pavan, J.T. Brack, F. Duncan, A. Feltham, G. Jones, J. Lange, K.J. Raywood, M.E. Sevier, R. Adams, D.F. Otte-well, G.R. Smith, B. Wells, R.L. Helmer, E.L. Mathie, R. Tacik, R.A. Ristinen, I.I. Strakovsky and H-M. Staudenmaier, *Precision pion-proton elastic differential cross sections at energies spanning the  $\Delta$  resonance*, Phys. Rev. **C64**, 064611 (2001) [nucl-ex/0103006].

A. Olin and T.S. Park, *Kaon nucleon scattering and reactions at low energies*, Nucl. Phys. **A691**, 295 (2001).

L. Buchmann, *Radiative cascade transitions and the  $^{12}\text{C}(\alpha, \gamma)^{16}\text{O}$  E2 cross section to the ground state of  $^{16}\text{O}$* , Phys. Rev. **C64**, 022801 (2001).

L. Buchmann, E. Gete, J.C. Chow, J.D. King and D.F. Measday, *Beta delayed particle decay of  $^9\text{C}$  and the  $A = 9$ ,  $T = 1/2$  nuclear system: R-matrix fits, the  $A = 9$  nuclear system, and the stellar reaction rate of  $^4\text{He}(\alpha n, \gamma)^9\text{Be}$* , Phys. Rev. **C63**, 034303 (2001).

T.A. Porcelli, A. Adamczak, J.M. Bailey, G.A. Beer, J.L. Douglas, M.P. Faifman, M.C. Fujiwara, T.M. Huber, P. Kammel, S.K. Kim, P.E. Knowles, A.R. Kunselman, M. Maier, V.E. Markushin, G.M. Marshall, G.R. Mason, F. Mulhauser, A. Olin, C. Petitjean and J. Zmeskal, *Measurement of the resonant  $d\mu t$  molecular formation rate in solid HD*, Phys. Rev. Lett. **86**, 3763 (2001) [TRI-PP-01-01, physics/0104010].

B. Aubert *et al.* (BABAR collaboration), *Measurement of CP-violating asymmetries in  $B^0$  decays to CP eigenstates*, Phys. Rev. Lett. **86**, 2515 (2001) [SLAC-PUB-8777, BABAR-PUB-01-01, hep-ex/0102030].

B. Aubert *et al.* (BABAR collaboration), *Measurement of the  $B \rightarrow J/\psi K^*(892)$  decay amplitudes*, Phys. Rev. Lett. **87**, 241801 (2001) [SLAC-PUB-8898, BABAR-PUB-01-05, hep-ex/0107049].

B. Aubert *et al.* (BABAR collaboration), *Measurement of the  $B^0$  and  $B^+$  meson lifetimes with fully reconstructed*

*hadronic final states*, Phys. Rev. Lett. **87**, 201803 (2001) [SLAC-PUB-8847, BABAR-PUB-01-06, hep-ex/0107019].

B. Aubert *et al.* (BABAR collaboration), *Measurement of branching fractions and search for CP violating charge asymmetries in charmless two-body B decays into pions and kaons*, Phys. Rev. Lett. **87**, 151802 (2001) [SLAC-PUB-8838, BABAR-PUB-01-10, hep-ex/0105061].

B. Aubert *et al.* (BABAR collaboration), *Measurement of  $J/\psi$  production in continuum  $e^+e^-$  annihilations near  $\sqrt{s} = 10.6$  GeV*, Phys. Rev. Lett. **87**, 162002 (2001) [BABAR-PUB-01-12, SLAC-PUB-8854, hep-ex/0106044].

B. Aubert *et al.* (BABAR collaboration), *Measurements of the branching fractions of exclusive charmless B meson decays with  $\eta'$  or  $\omega$  mesons*, Phys. Rev. Lett. **87**, 221802 (2001) [SLAC-PUB-8956, BABAR-PUB-01-15, hep-ex/0108017].

B. Aubert *et al.* (BABAR collaboration), *Observation of CP violation in the  $B^0$  meson system*, Phys. Rev. Lett. **87**, 091801 (2001) [SLAC-PUB-8904, BABAR-PUB-01-18, hep-ex/0107013].

S. Adler *et al.* (BNL E787 collaboration), *Search for the decay  $K^+ \rightarrow \pi^+\pi^0\nu\bar{\nu}$* , Phys. Rev. **D63**, 032004 (2001) [BNL-67631, KEK-PREPRINT-2000-68, PRINCETON-HEP-2000-5, TRI-PP-00-54].

K.A. Aniol *et al.* (HAPPEX collaboration), *New measurement of parity violation in elastic electron-proton scattering and implications for strange form-factors*, Phys. Rev. Lett. **B509**, 211 (2001) [WM-00-107, nucl-ex/0006002].

A. Airapetian *et al.* (HERMES collaboration), *Measurement of longitudinal spin transfer to  $\Lambda$  hyperons in deep inelastic lepton scattering*, Phys. Rev. **D64**, 112005 (2001) [DESY-99-151, hep-ex/9911017].

A. Airapetian *et al.* (HERMES collaboration), *Double-spin asymmetry in the cross section for exclusive  $\rho^0$  production in lepton-proton scattering*, Phys. Lett. **B513**, 301 (2001) [DESY-00-189, hep-ex/0102037].

A. Airapetian *et al.* (HERMES collaboration), *Hadron formation in deep inelastic positron scattering in a nuclear environment*, Eur. Phys. J. **C20**, 479 (2001) [DESY-00-191, hep-ex/0012049].

A. Airapetian *et al.* (HERMES collaboration), *Multiplicity of charged and neutral pions in deep inelastic scattering of 27.5 GeV positrons on hydrogen*, Eur. Phys. J. **C21**, 599 (2001) [DESY-01-037, hep-ex/0104004].

A. Airapetian *et al.* (HERMES collaboration), *Single spin azimuthal asymmetries in electroproduction of neutral pions in semi-inclusive deep inelastic scattering*, Phys. Rev. **D64**, 097101 (2001) [DESY-01-047, hep-ex/0104005].

A. Airapetian *et al.* (HERMES collaboration), *Measurement of the beam spin azimuthal asymmetry associated with deeply virtual Compton scattering*, Phys. Rev. Lett. **87**, 182001 (2001) [DESY-01-091, hep-ex/0106068].

- K. Horie *et al.* (KEK-E246 collaboration), *Measurement of  $\Gamma(K_{\mu 3})/\Gamma(K_{e 3})$  using stopped positive kaons*, Phys. Lett. **B513**, 311 (2001) [hep-ex/0106006].
- G. Abbiendi *et al.* (OPAL collaboration), *Bose-Einstein correlations in  $K^{\pm}K^{\pm}$  pairs from  $Z^0$  decays into two hadronic jets*, Eur. Phys. J. **C21**, 23 (2001) [CERN-EP-99-163, hep-ex/0001045].
- G. Abbiendi *et al.* (OPAL collaboration), *Searches for prompt light gravitino signatures in  $e^+e^-$  collisions at  $\sqrt{s} = 189$  GeV*, Phys. Lett. **B501**, 12 (2001) [CERN-EP-2000-078, hep-ex/0007014].
- G. Abbiendi *et al.* (OPAL collaboration), *A study of one prong  $\tau$  decays with a charged kaon*, Eur. Phys. J. **C19**, 653 (2001) [CERN-EP-2000-091, OPAL-PR-315, hep-ex/0009017].
- G. Abbiendi *et al.* (OPAL collaboration), *Two Higgs doublet model and model independent interpretation of neutral Higgs boson searches*, Eur. Phys. J. **C18**, 425 (2001) [CERN-EP-2000-092, hep-ex/0007040].
- G. Abbiendi *et al.* (OPAL collaboration), *Measurement of  $W$  boson polarizations and  $CP$  violating triple gauge couplings from  $W^+W^-$  production at LEP*, Eur. Phys. J. **C19**, 229 (2001) [CERN-EP-2000-113, hep-ex/0009021].
- G. Abbiendi *et al.* (OPAL collaboration), *Measurement of triple gauge boson couplings from  $W^+W^-$  production at LEP energies up to 189 GeV*, Eur. Phys. J. **C19**, 1 (2001) [CERN-EP-2000-114, hep-ex/0009022].
- G. Abbiendi *et al.* (OPAL collaboration), *Production rates of  $b\bar{b}$  quark pairs from gluons and  $b\bar{b}b\bar{b}$  events in hadronic  $Z^0$  decays*, Eur. Phys. J. **C18**, 447 (2001) [CERN-EP-2000-123, hep-ex/0010029].
- G. Abbiendi *et al.* (OPAL collaboration), *Charged multiplicities in  $Z$  decays into  $u$ ,  $d$  and  $s$  quarks*, Eur. Phys. J. **C19**, 257 (2001) [CERN-EP-2000-128, hep-ex/0011022].
- G. Abbiendi *et al.* (OPAL collaboration), *A study of  $B_s$  meson oscillation using  $D_s^-$  lepton correlations*, Eur. Phys. J. **C19**, 241 (2001) [CERN-EP-2000-136, OPAL-PR-327, hep-ex/0011052].
- G. Abbiendi *et al.* (OPAL collaboration), *Precise determination of the  $Z$  resonance parameters at LEP: 'Zedometry'*, Eur. Phys. J. **C19**, 587 (2001) [CERN-EP-2000-148, OPAL-PR-328, hep-ex/0012018].
- G. Abbiendi *et al.* (OPAL collaboration), *Search for the standard model Higgs boson in  $e^+e^-$  collisions at  $\sqrt{s} \approx 192$ – $209$  GeV*, Phys. Lett. **B499**, 38 (2001) [CERN-EP-2000-156, hep-ex/0101014].
- G. Abbiendi *et al.* (OPAL collaboration), *A simultaneous measurement of the QCD color factors and the strong coupling*, Eur. Phys. J. **C20**, 601 (2001) [CERN-EP-2001-001, hep-ex/0101044].
- G. Abbiendi *et al.* (OPAL collaboration), *A search for a narrow radial excitation of the  $D^{*\pm}$  meson*, Eur. Phys. J. **C20**, 445 (2001) [CERN-EP-2001-003, hep-ex/0101045].
- G. Abbiendi *et al.* (OPAL collaboration), *Precision neutral current asymmetry parameter measurements from the  $\tau$  polarization at LEP*, Eur. Phys. J. **C21**, 1 (2001) [CERN-EP-2001-023, hep-ex/0103045].
- G. Abbiendi *et al.* (OPAL collaboration), *Measurement of  $|V_{ub}|$  using  $b$  hadron semileptonic decay*, Eur. Phys. J. **C21**, 399 (2001) [CERN-EP-2001-044, hep-ex/0107016].
- G. Abbiendi *et al.* (OPAL collaboration), *Angular analysis of the muon pair asymmetry at LEP I*, Phys. Lett. **B516**, 1 (2001) [CERN-EP-2001-052, hep-ex/0107046].
- G. Abbiendi *et al.* (OPAL collaboration), *Measurement of the branching ratio for the process  $b \rightarrow \tau^- \bar{\nu}_\tau X$* , Phys. Lett. **B520**, 1 (2001) [CERN-EP-2001-058, hep-ex/0108031].
- G. Abbiendi *et al.* (OPAL collaboration), *Search for lepton flavor violation in  $e^+e^-$  collisions at  $\sqrt{s} = 189$ – $209$  GeV*, Phys. Lett. **B519**, 23 (2001) [CERN-EP-2001-061, hep-ex/0109011].
- G. Abbiendi *et al.* (OPAL collaboration), *Search for single top quark production at LEP-2*, Phys. Lett. **B521**, 181 (2001) [CERN-EP-2001-066, hep-ex/0110009].
- G. Abbiendi *et al.* (OPAL collaboration), *Genuine correlations of like-sign particles in hadronic  $Z^0$  decays*, Phys. Lett. **B523**, 35 (2001) [CERN-EP-2001-070, hep-ex/0110051].
- Q.R. Ahmad *et al.* (SNO collaboration), *Measurement of the rate of  $\nu_e + d \rightarrow p + p + e^-$  interactions produced by  $^8B$  solar neutrinos at the Sudbury Neutrino Observatory*, Phys. Rev. Lett. **87**, 101301 (2001).

#### Instrumentation/Accelerator Physics/Computing Sciences

S. Koscielniak, S. Hancock and M. Lindroos, *Longitudinal holes in debunched particle beams in storage rings, perpetuated by space-charge forces*, Phys. Rev. ST Accel. Beams **4**, 044201 (2001).

W. Herr, M.P. Zorzano and F. Jones, *A hybrid fast multipole method applied to beam-beam collisions in the strong-strong regime*, Phys. Rev. ST Accel. Beams **4**, 054402 (2001) [CERN-LHC-PROJECT-REPORT-466, CERN-LHC-PROJECT-REPORT-502C].

J.C. Liu, J.S. Bull, J. Drozdoff, R. May and V. Vylet, *Radiation safety system for accelerator facilities*, Radiat. Prot. Dosim. **96**, 429 (2001) [SLAC-PUB-9007].

L.E. Moritz, *Radiation protection at low energy proton accelerators*, Radiat. Prot. Dosim. **96**, 297 (2001).

#### Chemistry and Solid-State Physics

D.R. Noakes, *Toward Monte Carlo simulation of general cases of static muon spin relaxation in disordered magnetic*

materials: long-range magnetic order in alloys, *J. Magn. Mag. Mat.* **236**, 198 (2001).

E. Roduner, P.W. Percival and D.M. Bartels, *Comment on "Evidence for the solvation of hydrogen atoms by water"*, *Magn. Res. Chem.* **39**, 654 (2001).

I. McKenzie, B. Addison-Jones, J.-C. Brodovitch, K. Ghandi and P.W. Percival, *Structure and dynamics of the Mu adduct of diketene*, *Phys. Chem. Comm.* **27**, 1 (2001).

J.E. Sonier, J.H. Brewer, R.F. Kiefl, R.I. Miller, G.D. Morris, C.E. Stronach, J.S. Gardner, S.R. Dunsiger, D.A. Bonn, W.N. Hardy and R. Liang, *Anomalous weak magnetism in superconducting  $YBa_2Cu_3O_{6+x}$* , *Science* **292**, 1692 (2001).

D.H. Ryan, J. van Lierop, M.E. Pumarol, M. Roseman and J.M. Cadogan, *Field dependence of the transverse spin freezing transition*, *Phys. Rev.* **B63** Rapid Comm., 140405 (2001).

J. van Lierop and D.H. Ryan, *Spin dynamics in a frustrated magnet*, *Phys. Rev. Lett.* **86**, 4390 (2001).

D.H. Ryan, J. van Lierop, M.E. Pumarol, M. Roseman and J.M. Cadogan, *Muon spin relaxation examination of transverse spin freezing*, *J. Appl. Phys.* **89**, 7039 (2001).

K.H. Chow, B. Hitti, R.F. Kiefl, R.L. Lichti and T.L. Estle, *Muonium analog of hydrogen passivation: observation of the  $Mu^+ - Zn^-$  reaction in GaAs*, *Phys. Rev. Lett.* **87**, 216403-1 (2001).

#### Life Sciences

A.W. Wong, M.J. Adam and S. Withers, *Synthesis of 2,6-dioxy-2-fluoro-6- $^{18}F$ -fluoro- $\beta$ -D-glucopyranosyl fluoride (2,6FGF) as a potential imaging probe for glucocerebrosidase*, *J. Lab. Compd. Radiopharm.* **44**, 385 (2001).

G. Matte, M.J. Adam and D. Lyster, *Biological evaluation of radioiodinated 2-fluoro-2-iodo-mannose (FIM) and comparison with 18F-FDG and 18F-difluoro-deoxy glucose (DFDG)*, *Nucl. Med. Biol.* **6**, 679 (2001).

L.N. Yatham, P.F. Liddle, I.-S. Shiah, R.W. Lam, M.J. Adam, A.P. Zis and T.J. Ruth, *Effects of a rapid tryptophan depletion on brain 5-HT<sub>2</sub> receptors: A PET study*, *Brit. J. Psychiatry* **178**, 448 (2001).

T.J. Ruth, K.R. Buckley, K.S. Chun, E.T. Hurtado, S. Jivan and S. Zeisler, *A proof of principle for targetry to produce ultra high quantities of 18F-fluoride: a work in progress*, *Appl. Radiat. Isotopes* **55**, 457 (2001).

D.J. Doudet and T.J. Ruth, *Imaging the brain in Parkinson's disease*, *B.C. Med. J.* **43**, 148 (2001).

R. de la Fuente-Fernandez, A.S. Lim, V. Sossi, J.E. Holden, D.B. Calne, T.J. Ruth and A.J. Stoessl, *Apomorphine-induced changes in synaptic dopamine levels: PET evidence for pre-synaptic inhibition*, *J. Cereb. Blood Flow* **21**, 1151 (2001).

R. de la Fuente-Fernandez, T.J. Ruth, V. Sossi, M. Schulzer, D.B. Calne and A.J. Stoessl, *Expectation and dopamine release: mechanism of the placebo effect in Parkinson's disease*, *Science* **293**, 1164 (2001).

R. de la Fuente-Fernandez, Jian-Qiang Lu, V. Sossi, S. Jivan, M. Schulzer, J.E. Holden, C.S. Lee, T.J. Ruth, D.B. Calne and A.J. Stoessl, *Biochemical variations in the synaptic level of dopamine precede motor fluctuations in Parkinson's disease: PET evidence for increased dopamine turnover*, *Ann. Neurol.* **49**, 298 (2001).

P.K. Pal, Z.K. Wszolek, A. Kishore, V. Sossi, R.J. Uitti, T. Dobko, D.B. Calne and A.J. Stoessl, *Positron emission tomography in pallido-ponto-nigral degeneration (PPND) family (frontotemporal dementia with Parkinsonism linked to chromosome 17 and point mutation in tau gene)*, *PARD* **7:2**, 81 (2001).

V. Sossi, J.E. Holden and D.J. Doudet, *A reversible tracer approach to the study of effective dopamine turnover*, *J. Cereb. Blood Flow and Metab.* **21(4)**, 469 (2001).

D.T. Britto, M.Y. Siddiqi, A.D.M. Glass, and H.J. Kronzucker, *Futile membrane ion cycling: a new cellular hypothesis to explain ammonium toxicity in plants*, *PNAS* **98**, 4255 (2001).

D. Britto, A.D.M. Glass, H.J. Kronzucker and M.Y. Siddiqi, *Cytosolic concentrations and transmembrane fluxes of  $NH_4^+/NH_3$ : an analysis of a current controversy*, *Plant Physiol.* **125**, 523 (2001).

A.D.M. Glass, D.J. Britto, B.N. Kaiser, H.J. Kronzucker, A. Kumar, M. Okamoto, S.R. Rawat, M.Y. Siddiqi, S.M. Silim, J.J. Vidmar and D. Zhuo, *Nitrogen transport in plants, with emphasis on the regulation of fluxes to match demand*, *Planzen. Boden.* **164**, 199 (2001).

#### Theoretical Program

S. Ando, T.-S. Park and D.P. Min, *Threshold  $pp \rightarrow pp\pi^0$  up to one loop accuracy*, *Phys. Lett.* **B509**, 253 (2001) [SNU TP-99-052, TRI-PP-00-01, USC-NT-00-1, nucl-th/0003004].

G.C. McLaughlin and J.N. Ng, *The use of nuclear beta decay as a test of bulk neutrinos in extra dimensions*, *Phys. Rev.* **D63**, 053002 (2001) [TRI-PP-00-11, nucl-th/0003023].

W. Schadow, O. Nohadani and W. Sandhas, *Photonuclear reactions of three nucleon systems*, *Phys. Rev.* **C63**, 044006 (2001) [TRI-PP-00-29, nucl-th/0006069].

L. Canton and W. Schadow, *The one pion exchange three nucleon force and the  $A_y$  puzzle*, *Phys. Rev. Lett.* **C64**, 031001 (2001) [DFPD-00-TH-30, TRI-PP-00-32, nucl-th/0006070].

D.H. Wilkinson, *Second-class currents and  $\Delta s$  in  $\nu(\bar{\nu})p$  elastic scattering*, *Nucl. Instrum. Methods* **A469**, 286 (2001) [TRI-PP-00-67].

- S. Kondratyuk, A.D. Lahiff and H.W. Fearing, *The equivalence theorem and the Bethe-Salpeter equation*, Phys. Lett. **B521**, 204 (2001) [TRI-PP-01-07, nucl-th/0106057].
- R. Lewis, N. Mathur and R.M. Woloshyn, *Charmed baryons in lattice QCD*, Phys. Rev. **D64**, 094509 (2001) [TRI-PP-01-08, hep-ph/0107037].
- J. Escher, B.K. Jennings and H.S. Sherif, *Spectroscopic amplitudes and microscopic substructure effects in nucleon capture reactions*, Phys. Rev. **C64**, 065801 (2001) [TRI-PP-01-10, nucl-th/0107011].
- V.E. Shapiro, *Rotating class of parametric resonance processes in coupled oscillators*, Phys. Lett. **A290**, 288 (2001) [TRI-PP-01-20].
- S.W. Hong and B.K. Jennings, *Quark-meson coupling model for a nucleon*, Phys. Rev. **C64**, 038203-1 (2001) [nucl-th/0009089].
- K. Maltman and J. Kambor,  *$m_u + m_d$  from isovector pseudoscalar sum rules*, Phys. Lett. **B517**, 332 (2001) [YU-PP-I-E-KM-2-01, ZU-TH-24-01, hep-ph/0107060].
- S.P. Kim, S. Sengupta and F.C. Khanna, *Multiple scale analysis and renormalization of quenched second order phase transitions*, Phys. Rev. **D64**, 105026-1 (2001) [hep-ph/0105045].
- C.S. Lam and J.N. Ng, *Neutrino oscillations via the bulk*, Phys. Rev. **D64**, 113006 (2001) [hep-ph/0104129].
- D.A. Dicus, H.J. He and J.N. Ng, *Neutrino-lepton masses, Zee scalars and muon  $g - 2$* , Phys. Rev. Lett. **87**, 111803 (2001) [UT-HEP-01-019, hep-ph/0103126].
- S. Kondratyuk and O. Scholten, *Compton scattering on the nucleon at intermediate energies and polarizabilities in a microscopic model*, Phys. Rev. **C64**, 024005 (2001) [nucl-th/0103006].
- S.J.Q. Robinson and L. Zamick, *Degeneracies when  $T = 0$  two body matrix elements are set equal to zero and Regge's  $6j$  symmetry relations*, Phys. Rev. **C63**, 064316 (2001) [nucl-th/0012050].
- S.J.Q. Robinson and L. Zamick, *Degeneracies when  $T = 0$  two body interacting matrix elements are set equal to zero: Talmi's method of calculating coefficients of fractional parentage to states forbidden by the Pauli principle*, Phys. Rev. **C64**, 057302 (2001) [nucl-th/0103064].
- M. Butler, J.-W. Chen and X. Kong, *Neutrino deuteron scattering in effective field theory at next-to-next-to-leading order*, Phys. Rev. **C63**, 035501 (2001) [nucl-th/0008032].
- Y.F. Zhou, Y.L. Wu, J.N. Ng and C.Q. Geng, *The interplay of weak and strong phases and direct CP violation in charmless B meson decays*, Phys. Rev. **D63**, 054011 (2001) [hep-ph/0006225].
- C.H. Hyun, T.S. Park and D.P. Min, *Asymmetry in  $\bar{n} + p \rightarrow d + \gamma$* , Phys. Lett. **B516**, 321 (2001).
- M. de Montigny, F.C. Khanna and A. Santana, *On Galilei-covariant Lagrangian models of fluids*, J. Phys. **A34**, 10921 (2001).
- A. Rakhimov and F.C. Khanna, *Finite temperature amplitudes and reaction rates in thermo field dynamics*, Phys. Rev. **C64**, 064907-1 (2001) [nucl-th/0011039].
- M. de Montigny, F.C. Khanna, A.E. Santana and E.S. Santos, *Galilean covariance and non-relativistic Bhabha equations*, J. Phys. **A34**, 8901 (2001).
- H. Uys, H.G. Miller and F.C. Khanna, *Generalised statistics and high  $T_c$  superconductivity*, Phys. Lett. **A289**, 264 (2001).
- M. de Montigny, F.C. Khanna and A.E. Santana, *Galilean covariance and applications in physics*, Recent Dev. in Physics **1**, 45 (2001).
- R.A. Ritchie, H.G. Miller and F.C. Khanna, *Landau-Ginzberg treatment of nuclear matter at finite temperature*, Eur. Phys. J. **A10**, 97 (2001).
- E. Truhlik, J. Smejkal and F.C. Khanna, *Electromagnetic isoscalar  $\rho\pi\gamma$  exchange currents and the anomalous action*, Nucl. Phys. **A689**, 741 (2001).
- W.C. Haxton, C.P. Liu and M.J. Ramsey-Musolf, *Anapole moment and other constraints on the strangeness conserving hadronic weak interaction*, Phys. Rev. Lett. **86**, 5247 (2001).
- O. Teodorescu, A.K. Dutt-Mazumder and C. Gale, *The effects of meson mixing on dilepton spectra*, Phys. Rev. **C63**, 034903 (2001).
- A.K. Dutt-Mazumder, R. Hofmann and M. Pospelov,  *$\rho - \omega$  mixing in asymmetric nuclear matter via QCD sum rule approach*, Phys. Rev. **C63**, 015204 (2001).
- A. Kurylov, G.C. McLaughlin and M.J. Ramsey-Musolf, *Constraints on T-odd, P-even interactions from electric dipole moments*, Phys. Rev. **D63**, 076007 (2001).
- X. Kong and F. Ravndal, *Proton-proton fusion rate in effective field theory*, Phys. Rev. **C64**, 044002 (2001) [nucl-th/0004038].

## Journal Publications In Press or Submitted

### Particle, Nuclear and Atomic Physics

- B. Dowler *et al.*, *Performance of the ATLAS hadronic end-cap calorimeter in beam tests* (Nucl. Instrum. Methods, in press).
- C. Ruiz, F. Sarazin, L. Buchmann, T. Davinson, R.E. Azuma, A.A. Chen, B.R. Fulton, D. Groombridge, L. Ling, A. Murphy, J. Pearson, I. Roberts, A. Robinson, A.C. Shotton, P. Walden and P.J. Woods, *Strong resonances in elastic scattering of radioactive  $^{21}\text{Na}$  on protons* (submitted to Phys. Rev. C, Rapid Comm.).

- L. Gingras, A. Chernomoretz, Y. Laroche, Z.Y. He, L. Beaulieu, G.C. Ball, F. Greiner, D. Horn, R. Roy, M. Samri, C. St. Pierre, D. Theriault and S. Turbide, *Origins of intermediate velocity particle production in heavy ion reactions* (submitted to Phys. Rev. C).
- N.S. Kelsall, D.P. Balamuth, G.C. Ball, M. Carpenter, R.M. Clark, P. Fallon, S.M. Fischer, R.V.F. Janssens, D.G. Jenkins, C.J. Lister, A.O. Macchiavelli, D.G. Sarantites, D. Seweryniak, C.E. Svensson, S. Vincent, R. Wadsworth, A.N. Wilson, A.V. Afanasjev, S. Frauendorf, I. Ragnarsson and R. Wyss, *Testing mean-field models near the  $N = Z$  line: gamma ray spectroscopy of the  $T_Z = \frac{1}{2}$  nucleus  $^{73}\text{Kr}$*  (submitted to Phys. Rev. C).
- Y. Itow, T. Kajita, K. Kaneyuki, M. Shiozawa, Y. Tot-suka, Y. Hayato, T. Ishida, T. Ishii, T. Kobayashi, T. Maruyama, K. Nakamura, Y. Obayashi, Y. Oyama, M. Sakuda, M. Yoshida, S. Aoki, T. Hara, A. Suzuki, A. Ichikawa, T. Nakaya, K. Nishikawa, T. Hasegawa, K. Ishihara, A. Suzuki and A. Konaka, *The JHF-Kamioka neutrino project* [KEK-REPORT-2001-4, ICRR-REPORT-477-2001-7, TRI-PP-01-05, hep-ex/0106019].
- T. Haseyama, K. Asahi, J.D. Bowman, P.P.J. Delheij, H. Funahashi, S. Ishimoto, G. Jones, A. Masaïke, Y. Masuda, Y. Matsuda, K. Morimoto, S. Muto, S.I. Penttila, V.R. Pomeroy, K. Sakai, E.I. Sharapov, D.A. Smith and V.W. Yuan, *Measurement of parity nonconserving rotation of neutron spin in the 0.734 eV p-wave resonance of  $^{139}\text{La}$*  (Phys. Lett. B, in press) [nucl-ex/0111018].
- A.R. Junghans, E.C. Mohrmann, K.A. Snover, T.D. Steiger, E.G. Adelberger, J.M. Casandjian, H.E. Swanson, L. Buchmann, S.H. Park and A. Zyuzin,  *$^7\text{Be}(p,\gamma)^8\text{B}$  astrophysical S-factor from precision cross section measurements* (submitted to Phys. Rev. Lett.) [nucl-ex/0111014].
- G.M. Huber, G.J. Lolos, Z. Papandreou, J. Hovdebo, S.I.H. Naqvi, D.F. Ottewell, P.L. Walden, G. Jones and X. Aslanoglou, *Study of two step mechanisms in pion absorption on  $^6\text{Li}$ ,  $^{12}\text{C}$  via deuteron emission* [nucl-ex/0009010].
- M. Ellis *et al.* (MuScat collaboration), *Status of the MuScat experiment* (Nucl. Instrum. Methods A, in press).
- B. Aubert *et al.* (BABAR collaboration), *Measurement of  $B^0\bar{B}^0$  flavor oscillations in hadronic  $B^0$  decays* (submitted to Phys. Rev. Lett.) [SLAC-PUB-9061, BABAR-PUB-01-02, hep-ex/0112044].
- B. Aubert *et al.* (BABAR collaboration), *Measurement of  $B \rightarrow K^*\gamma$  branching fractions and charge asymmetries* (submitted to Phys. Rev. Lett.) [SLAC-PUB-8952, BABAR-PUB-01-04, hep-ex/0110065].
- B. Aubert *et al.* (BABAR collaboration), *Measurement of branching fractions for exclusive B decays to charmonium final states* (Phys. Rev. D, in press) [SLAC-PUB-8909, BABAR-PUB-01-07, hep-ex/0107025].
- B. Aubert *et al.*, *The BABAR detector* (submitted to Nucl. Instrum. Methods) [SLAC-PUB-8569, BABAR-PUB-01-08, hep-ex/0105044].
- B. Aubert *et al.* (BABAR collaboration), *Measurement of the branching fractions for  $\psi(2S) \rightarrow e^+e^-$  and  $\psi(2S) \rightarrow \mu^+\mu^-$*  (Phys. Rev. D, in press) [SLAC-PUB-8953, BABAR-PUB-01-13, hep-ex/0109004].
- B. Aubert *et al.* (BABAR collaboration), *Measurement of the ratio of branching fractions  $\mathcal{B}(B^\pm \rightarrow J/\psi\pi^\pm)/\mathcal{B}(B^\pm \rightarrow J/\psi K^\pm)$*  (submitted to Phys. Rev. Lett.) [SLAC-PUB-8942, BABAR-PUB-01-14, hep-ex/0108009].
- B. Aubert *et al.* (BABAR collaboration), *Study of the CP violating asymmetries in  $B^0 \rightarrow \pi^+\pi^-$ ,  $K^+\pi^-$  decays* (Phys. Rev. D, in press) [SLAC-PUB-9012, BABAR-PUB-01-21, hep-ex/0110062].
- B. Aubert *et al.* (BABAR collaboration), *Measurement of the  $B^0\bar{B}^0$  oscillation frequency with inclusive dilepton events* (submitted to Phys. Rev. Lett.) [SLAC-PUB-9096, BABAR-PUB-01-22, hep-ex/0112045].
- B. Aubert *et al.* (BABAR collaboration), *Direct CP violation searches in charmless hadronic B meson decays* (Phys. Rev. D, in press) [SLAC-PUB-9065, BABAR-PUB-01-23, hep-ex/0111087].
- S.C. Adler *et al.* (E787 collaboration), *Further evidence for the decay  $K^+ \rightarrow \pi^+\nu\bar{\nu}$*  (Phys. Rev. Lett., in press) [BNL-68713, KEK-2001-138, PRINCETON-HEP-2001-2, TRI-PP-01-35, hep-ex/0111091].
- S.C. Adler *et al.* (E787 collaboration), *Search for the rare decay  $K^+ \rightarrow \pi^+\gamma$*  (Phys. Rev. D, in press) [BNL-68328, PRINCETON-HEP-2001-1, TRI-PP-01-09, KEK-PREPRINT-2001-26, hep-ex/0108006].
- A. Airapetian *et al.* (HERMES collaboration), *Single spin azimuthal asymmetry in exclusive electroproduction of  $\pi^+$  mesons* (submitted to Phys. Lett. B) [DESY-01-223, hep-ex/0112022].
- G. Abbiendi *et al.* (OPAL collaboration), *Investigation of the decay of orbitally-excited B mesons and first measurement of the branching ratio  $BR(B_J^* \rightarrow B^*\pi(X))$*  (Eur. Phys. J. C, in press) [CERN-EP-2000-125, hep-ex/0010031].
- G. Abbiendi *et al.* (OPAL collaboration), *Search for single leptoquark and squark production in electron photon scattering at  $\sqrt{s_{ee}} = 189$  GeV at LEP* (submitted to Eur. Phys. J. C) [CERN-EP-2001-040, hep-ex/0106031].
- G. Abbiendi *et al.* (OPAL collaboration), *Measurement of  $Z/\gamma^*$  production in Compton scattering of quasi-real photons* (submitted to Eur. Phys. J. C) [CERN-EP-2001-053, hep-ex/0107047].
- G. Abbiendi *et al.* (OPAL collaboration), *Measurement of the hadronic cross section for the scattering of two virtual photons at LEP* (submitted to Eur. Phys. J. C) [CERN-EP-2001-064, hep-ex/0110006].

G. Abbiendi *et al.* (OPAL collaboration), *Particle multiplicity of unbiased gluon jets from  $e^+e^-$  three jet events* (submitted to Eur. Phys. J. C) [CERN-EP-2001-076, hep-ex/0111013].

G. Abbiendi *et al.* (OPAL collaboration), *Search for Yukawa production of a light neutral Higgs boson at LEP* (submitted to Eur. Phys. J. C) [CERN-EP-2001-077, hep-ex/0111010].

G. Abbiendi *et al.* (OPAL collaboration), *Search for doubly charged Higgs bosons with the OPAL detector at LEP* (Phys. Lett. B, in press) [CERN-EP-2001-082, hep-ex/0111059].

G. Abbiendi *et al.* (OPAL collaboration), *Search for leptop-quarks in electron photon scattering at  $\sqrt{s_{ee}}$  up to 209 GeV at LEP* (Phys. Lett. B, in press) [CERN-EP-2001-093, hep-ex/0112024].

#### Chemistry and Solid-State Physics

D.E. MacLaughlin, O.O. Bernal, J.E. Sonier, R.H. Heffner, T. Taniguchi and Y. Miako, *Susceptibility inhomogeneity and non-fermi-liquid behavior in  $Ce(Ru_{0.5}Rh_{0.5})_2Si_2$*  (Phys. Rev. B, in press).

Y.J. Uemura *et al.*, *Muon spin relaxation studies of incommensurate magnetism and superconductivity in stage-4  $La_2CuO_{4.11}$  and  $La_{1.88}Sr_{0.12}CuO_4$*  (submitted to Phys. Rev. B) [cond-mat/0202037].

M.D. Lumsden *et al.*, *Temperature dependence of the magnetic penetration depth in the vortex state of the pyrochlore superconductor,  $Cd_2Re_2O_7$* , (submitted to Phys. Rev. Lett.).

R.I. Miller, R.F. Kiefl, J.H. Brewer, J.E. Sonier, J. Chakhalian, S. Dunsiger, G.D. Morris, A.N. Price, D.A. Bonn, W.H. Hardy and R. Liang, *Evidence for static magnetism in the vortex cores of ortho-II  $YBa_2Cu_3O_{6.50}$*  (Phys. Rev. Lett., in press).

D.R. Noakes, R. Wäppling, G.M. Kalvius, M.F. White and C.E. Stronach, *Singlet ground-state fluctuations in praseodymium observed by muon spin relaxation in  $PrP_x$*  (submitted to J. Phys. Cond. Matter).

D.R. Noakes, G.M. Kalvius and O. Hartmann, *Random anisotropy causes wide distributions of relaxation rates in  $Tb-Mg-Zn$  quasicrystals and amorphous  $DyAg$*  (Phys. Rev. B Brief Reports, in press).

K. Ghandi, B. Addison-Jones, J.-C. Brodovitch, I. McKenzie, P.W. Percival and J. Schüth, *Near-diffusion-controlled reactions of muonium in sub- and supercritical water* (Phys. Chem. Chem. Phys., in press).

D.H. Ryan, J.M. Cadogan and J. van Lierop, *Reply to Comment on the "Field dependence of the transverse spin freezing transition"* (Phys. Rev. B, in press).

J. van Lierop, D.H. Ryan and J.M. Cadogan, *A zero-field muon spin relaxation and selective excitation double*

*Mössbauer study of spin dynamics in the  $a-Fe_{90}Sc_{10}$  spin-glass* (submitted to J. Appl. Phys.).

J. van Lierop, D.H. Ryan and J. Gallego, *Zero-field muon spin relaxation spectra and the dynamic Kubo-Toyabe and spin-glass functions* (submitted to Hyp. Int.).

J. van Lierop and D.H. Ryan, *Dynamics in fine particle magnets* (Phys. Rev. B, in press).

R.L. Lichti, S.F.J. Cox, E.A. Davis, B. Hitti and S.K.L. Sjue, *Positively charged muonium centers in aluminum and gallium nitrides* (Physica B, in press).

S.F.J. Cox, R.L. Lichti and E.A. Davis, *Hydrogen in group III-V nitrides, studied by muon spin resonance* (J. Phys. D, in press).

R.L. Lichti, K.H. Chow, B. Hitti, E.A. Davis, S.K.L. Sjue and S.F.J. Cox, *Motional properties of positive muonium in gallium III-V compounds* (Physica B, in press).

J.E. Sonier, J.H. Brewer, R.F. Kiefl, R.H. Heffner, K. Poon, S.L. Stubbs, G.D. Morris, R.I. Miller, W.N. Hardy, R. Liang, D.A. Bonn, J.S. Gardner and N.J. Curro, *Correlations between charge ordering and local magnetic fields in overdoped  $YBa_2Cu_3O_{6+x}$*  [cond-mat/0108479].

J.E. Sonier, K.F. Poon, G.M. Luke, P. Kyriakou, R.I. Miller, S.L. Stubbs, P. Fournier and R.L. Greene,  *$\mu$ SR study of a  $Pr_{2-x}Ce_xCuO_4$  single crystal* (in preparation).

#### Life Sciences

H. Dougan, J.I. Weitz, A.R. Stafford, K.D. Gillespie, P. Klement, J.B. Hobbs and D.M. Lyster, *Evaluation of DNA aptamers directed towards thrombin as potential thrombus imaging agents* (submitted to Nucl. Med. and Biol.).

J.Q. Lu, J.K. Tsui, T.J. Ruth, D.B. Calne and A.J. Stoessl, *Hypertension alleviates Parkinson's disease: clinical and biochemical evidence* (submitted to Neurology).

D.J. Doudet, S. Jivan, T.J. Ruth and J.E. Holden, *Density and affinity of the dopamine D2 receptors in aged symptomatic and asymptomatic MPTP-treated monkeys: PET studies with [ $^{11}C$ ]raclopride* (Synapse, in press).

D.J. Doudet, J.E. Holden, T.J. Ruth, T.A. Aigner and R.J. Wyatt, *In-vivo PET studies of the dopamine D1 receptors in rhesus monkeys with long-term MPTP-induced Parkinsonism* (Synapse, in press).

L.N. Yatham, P.F. Liddle, I.-S. Shiah, R.W. Lam, E. Ngan, G. Scarrow, M. Imperial, J. Stoessl, V. Sossi and T.J. Ruth, *A positron emission tomography study of  $^{18}F$ -6-fluoro-L-dopa uptake in neuroleptic and mood stabilizer naïve first episode non-psychotic mania: effects of treatment with Divalproex sodium* (Arch. Gen. Psych., in press).

V. Sossi, R. de la Fuente-Fernandez, J.E. Holden, D.J. Doudet, J. McKenzie, A.J. Stoessl and T.J. Ruth,

*Dopamine effective distribution volume: a good discriminator of early Parkinson's disease* (J. Cereb. Blood Flow, in press).

M.E. Daube-Witherspoon, J.S. Karp, M.E. Casey, J. Fernando, H. Hines, G. Muehllehner, V. Simcic, C. Stearns, P. Vernon, L-E. Adam, S. Kohlmyer and V. Sossi, *PET performance measurements using the NU-2-2001 standard* (submitted to J. Nucl. Med.).

V. Sossi, R. de la Fuente-Fernandez, J.E. Holden, D.J. Doudet, J. McKenzie, A.J. Stoessl and T.J. Ruth, *Increase in dopamine turnover occurs early in Parkinson's disease: evidence from a new modeling approach to PET  $^{18}\text{F}$ -fluorodopa data* (J. Cereb. Blood Flow and Metab., in press).

A.D.M. Glass, D.J. Britto, B.N. Kaiser, H.J. Kronzucker, A. Kumar, M. Okamoto, M.Y. Siddiqi, J.J. Vidmar, *The regulation of nitrate and ammonium transport systems in plants* (J. Exp. Bot., in press).

R.A. Hauser, S. Furtado, C.R. Cimino, H. Delgado, S. Eichler, S. Schwartz, D. Scott, G.M. Nauert, E. Soety, V. Sossi, D.A. Holt, P.R. Sanberg, A.J. Stoessl and T.B. Freeman, *Bilateral human fetal striatal transplantation in Huntington's disease* (Neurology, in press).

R. de la Fuente-Fernandez, A.G. Phillips, M. Zamburlini, V. Sossi, D.B. Calne, T.J. Ruth and A.J. Stoessl, *Dopamine release in human ventral striatum and expectation of reward* (submitted to Neuroreport).

### Theoretical Program

S. Ando, H.W. Fearing and D.P. Min, *Polarized photons in radiative muon capture* (Phys. Rev. C, in press) [USC-NT-REPORT-01-1, TRI-PP-01-02, SNUTP-00-037, nucl-th/0104077].

G. Rupak and X. Kong, *Quartet S-wave  $p-d$  scattering in EFT* (submitted to Phys. Rev. C) [TRI-PP-01-13, nucl-th/0108059].

E. Vogt, *Pervasive and extreme neutron halos* (submitted to Phys. Rev. C) [TRI-PP-01-23].

T. Ebertshauser, H.W. Fearing and S. Scherer, *The anomalous chiral perturbation theory meson Lagrangian to order  $p^6$  revisited* (Phys. Rev. D, in press) [MKPH-T-01-22, TRI-PP-01-34, hep-ph/0110261].

E.C.Y. Ho and H.W. Fearing, *Radiative muon capture by  $^3\text{He}$*  (submitted to Phys. Rev. C) [TRI-PP-01-37, nucl-th/0112019].

G. Rupak and N. Shores, *Chiral perturbation theory for the Wilson lattice action* [TRI-PP-01-38, BUHEP-02-04, hep-lat/0201019].

A.Z. Mekjian, *Particle multiplicity distributions: connections with a Feynman-Wilson gas and a Ginzburg-Landau theory* (Phys. Rev. C, in press).

C.Q. Geng and C.-W. Hwang, *Lepton pair decays of the  $K_L$  meson in the light front model* (submitted to Phys. Lett. B) [hep-ph/0112164].

C.Q. Geng, C.-W. Hwang and C.C. Liu, *Study of rare  $B_c^+ \rightarrow D_{d,s}^{*+} \ell \bar{\ell}$  decays* (submitted to Phys. Rev. D) [hep-ph/0110376].

C.-H. Chen and C.Q. Geng, *Long distance contributions in  $B \rightarrow K^* \ell^+ \ell^-$  decays with polarized  $K^*$*  (submitted to Eur. Phys. J. C).

C.-H. Chen and C.Q. Geng,  *$T$  violation in  $B \rightarrow K^* \ell^+ \ell^-$  from SUSY* (submitted to Phys. Rev. D) [hep-ph/0205306].

D. Chang, W.-F. Chang, W.-Y. Keung and N. Sinha, *Squark mixing contributions to  $CP$  violating phase gamma* (Phys. Rev. D, in press) [IMSC-2001-09-50, hep-ph/0109151].

S. Kondratyuk and O. Scholten, *Low-energy Compton scattering on the nucleon and sum rules* (Phys. Rev. C, in press) [nucl-th/0109038].

K. Maltman and J. Kambor, *Decay constants, light quark masses and quark mass bounds from light quark pseudoscalar sum rules* (submitted to Phys. Rev. D) [ZU-TH-26-01, YU-PP-I-E-KM-5-01, hep-ph/0108227].

S.K. Ghosh and B.K. Jennings, *The low energy nuclear density of states and the saddle point approximation* (submitted to Phys. Rev. C) [nucl-th/0107074].

E. Truhlik and F.C. Khanna *On radiative muon capture in hydrogen* (submitted to Phys. Rev. C) [nucl-th/0102006].

T.S. Park, H. Jung and D.P. Min, *In-medium effective pion mass from heavy-baryon chiral perturbation theory* [SNUTP-99-053, USC-NY-01-03, nucl-th/0101064].

J. Escher and A. Leviatan, *Partial dynamical symmetry in the symplectic shell model* (submitted to Phys. Rev. C) [TRI-PP-00-57, nucl-th/0110030].

H.W. Griesshammer and G. Rupak, *Nucleon polarizabilities from Compton scattering on the deuteron* (Phys. Lett., in press) [NT-UW-00-022, TRI-PP-00-62, TUM-T39-00-18, nucl-th/0012096].

F. Khanna, A. Mann, M. Revzen and S. Roy, *Bell's inequality and symmetry* (Phys. Lett. A, in press).

A.E. Santana, F.C. Khanna and M. Revzen, *Entropy of entangled states and  $SU(1,1)$  and  $SU(2)$  symmetries* (Phys. Rev. A, in press).

S. Banerjee, S.K. Ghosh, A. Mazumdar, S. Raha and D. Syam, *Strange quark matter in cosmic ray flux and exotic events* (Astrophys. Space Sci., in press) [astro-ph/0006354].

M. Mitra, S. Bhattacharyya and A.K. Dutt-Mazumder, *Properties of neutron star with delta meson condensate* (submitted to Phys. Rev. C).

O. Teoderescu, A.K. Dutt-Mazumder and C. Gale, *Aspects of meson properties in dense nuclear matter* (submitted to Phys. Rev. C) [nucl-th/0112035].

W.C. Haxton, C.P. Liu and M.J. Ramsey-Musolf, *Nuclear anapole moments* (submitted to Phys. Rev. C) [nucl-th/0109014].

## Conference Publications

### Particle, Nuclear and Atomic Physics

M. Fujiwara, *Using thin film targets for muonic atoms and muon catalyzed fusion studies*, Proc. **KEK Int. Workshop on High Intensity Muon Sources (HIMUS 99)**, Tsukuba, Japan, December 1–4, 1999, Y. Kuno, T. Yokoi, eds. (World Scientific, Singapore, 2001) p.291 [TRI-PP-00-51].

G.C. Ball *et al.* (E823 collaboration), *Tests of the standard model from nuclear beta-decay studies at ISAC*, Proc. **Lake Louise Winter Institute: From Particles to the Universe**, Lake Louise, AB, February 20–26, 2000, A. Astbury, B.A. Campbell, F.C. Khanna and M.G. Vincter, eds. (World Scientific, Singapore, 2001) p.148.

S. Sengupta, S.P. Kim and F.C. Khanna, *Non-equilibrium phase transitions beyond the Gaussian approximation*, *ibid.* 349.

M. Hartig *et al.* (HERMES collaboration), *Diffraction vector meson production at HERMES*, Proc. **Int. Conf. on Quark Nuclear Physics (QNP 2000)**, Adelaide, Australia, February 21–25, 2000, C. Boros, K. Tsushima and A.W. Thomas, eds. (Nucl. Phys. **A680**, 2001) p.264.

A. Ambardar, F. Duncan, A. Feltham, G. Hofman, R.R. Johnson, G. Jones, J.B. Lange, M. Pavan, K.J. Raywood, D. Vetterli, J.T. Brack, D. Ottewell, G.R. Smith and M.E. Seviar, *Measurement of  $\pi p \rightarrow \pi\pi n$  cross-sections near threshold*, Proc. **XVI<sup>th</sup> Int. Conf. on Few-Body Problems in Physics, Taipei, Taiwan, March 6–10, 2000** (Nucl. Phys. **A684**, 2001) p.386.

W. Kühn *et al.* (DISTO collaboration), *Meson production in pp reactions at 2.85 GeV*, *ibid.* 440.

L. Lee, D.E. Alburger, P.D. Barnes, B. Bassalleck, A. Berdoz, A. Biglan, T. Burger, D. Carman, R.E. Chrien, C.A. Davis, H. Fischer, G.B. Franklin, J. Franz, L. Gan, A. Ichikawa, T. Iijima, K. Imai, P. Khaustov, Y. Kondo, P. Koran, M. Landry, J. Lowe, R. Magahiz, M. May, R. McCrady, F. Merrill, C.A. Meyer, S.A. Page, K. Paschke, P.H. Pile, B. Quinn, W.D. Ramsay, A. Rusek, R. Sawafta, H. Schmitt, R.A. Schumacher, R. Stotzer, R. Sutter, F. Takeutchi, W.T.H. van Oers, K. Yamamoto, M. Yosoi and V.J. Zeps, *Search for strangeness  $-2$  hypernuclei*, *ibid.* 598.

P. Depommier *et al.* (KEK-E246 collaboration), *Search for time-reversal violation in the  $K^+ \rightarrow \pi^0 \mu^+ \nu$  decay*, *ibid.* 707.

L. Buchmann, P. Tischhauser, R.E. Azuma, R. Detwiler, U. Giesen, J. Görres, M. Heil, J. Hinnefeld, F. Käppeler,

J.J. Kolata, H. Schatz, A. Shotter, E. Stech, S. Vouzoukas and M. Wiescher, *Restrictions on the stellar  $^{12}C(\alpha, \gamma)^{16}O$  rate from elastic  $\alpha - ^{12}C$  scattering*, Proc. **6<sup>th</sup> Int. Conf. on Nuclei in the Cosmos, Aarhus, Denmark, June 27–July 1, 2000**, J. Christensen-Dalsgaard and K. Langanke, eds. (Nucl. Phys. **A688**, 2001) p.259.

M. Vetterli, *Overview of spin physics*, Proc. **Int. EuroConference in Quantum Chromodynamics: 15 Years of the QCD (QCD 00)**, Montpellier, France, July 6–13, 2000, S. Narison, ed. (Nucl. Phys. **B96**, 2001).

R. Tacik, *The CNI experiment at TRIUMF*, Proc. **3<sup>rd</sup> Workshop on Chiral Dynamics – Chiral Dynamics 2000: Theory and Experiment III**, Newport News, VA, July 17–22, 2000, A.M. Bernstein, J.L. Goity, U.-G. Meissner, eds. (World Scientific, Singapore, 2001).

B. Aubert *et al.* (BABAR collaboration), *Measurement of inclusive production of charmonium states in B meson decays*, Proc. **30<sup>th</sup> Int. Conf. on High-Energy Physics (ICHEP 2000)**, Osaka, Japan, July 27–August 2, 2000, C.S. Lim, T. Yamanaka, eds. (World Scientific, Singapore, 2001) [SLAC-PUB-8526, BABAR-CONF-00-04, hep-ex/0008049].

B. Aubert *et al.* (BABAR collaboration), *Exclusive B decays to charmonium final states*, *ibid.* [SLAC-PUB-8527, BABAR-CONF-00-05, hep-ex/0008050].

B. Aubert *et al.* (BABAR collaboration), *Measurement of the branching fractions for  $B^0 \rightarrow D^{*-}\pi^+$  and  $B^0 \rightarrow D^{*-}\rho^+$* , *ibid.* [SLAC-PUB-8528, BABAR-CONF-00-06, hep-ex/0008051].

B. Aubert *et al.* (BABAR collaboration), *A measurement of the charged and neutral B meson lifetimes using fully reconstructed decays*, *ibid.* [SLAC-PUB-8529, BABAR-CONF-00-07, hep-ex/0008060].

B. Aubert *et al.* (BABAR collaboration), *A measurement of the  $B^0 \bar{B}^0$  oscillation frequency and determination of flavor tagging efficiency using semileptonic and hadronic  $B^0$  decays*, *ibid.* [SLAC-PUB-8530, BABAR-CONF-00-08, hep-ex/0008052].

B. Aubert *et al.* (BABAR collaboration), *Measurement of the  $B^0$  meson properties using partially reconstructed  $B^0 \rightarrow D^{*-}\pi^+$  and  $B^0 \rightarrow D^{*-}\ell^+\nu_\ell$* , *ibid.* [SLAC-PUB-8531, BABAR-CONF-00-09, hep-ex/0008053].

B. Aubert *et al.* (BABAR collaboration), *Measurement of the time dependence of  $B^0 \bar{B}^0$  oscillations using inclusive dilepton events*, *ibid.* [SLAC-PUB-8532, BABAR-CONF-00-10, hep-ex/0008054].

B. Aubert *et al.* (BABAR collaboration), *A measurement of the branching fraction of the exclusive decay  $B^0 \rightarrow K^{*0}\gamma$* , *ibid.* [SLAC-PUB-8534, BABAR-CONF-00-12, hep-ex/0008055].

B. Aubert *et al.* (BABAR collaboration), *Study of inclusive  $D_s^{(*)\pm}$  production in B decays and measurement of*



$B^0 \rightarrow D^{*-} D_s^{(*)+}$  decays using a partial reconstruction technique, *ibid.* [SLAC-PUB-8535, BABAR-CONF-00-13, hep-ex/0008056].

B. Aubert *et al.* (BABAR collaboration), *Measurement of branching fractions for two-body charmless B decays to charged pions and kaons at BABAR*, *ibid.* [SLAC-PUB-8536, BABAR-CONF-00-14, hep-ex/0008057].

B. Aubert *et al.* (BABAR collaboration), *Measurement of charmless three-body and quasi-two-body B decays*, *ibid.* [SLAC-PUB-8537, BABAR-CONF-00-15, hep-ex/0008058].

B. Aubert *et al.* (BABAR collaboration), *Search for  $B^+ \rightarrow K^+ \ell^+ \ell^-$  and  $B^0 \rightarrow K^{*0} \ell^+ \ell^-$* , *ibid.* [SLAC-PUB-8538, BABAR-CONF-00-16, hep-ex/0008059].

B. Aubert *et al.* (BABAR collaboration), *The first year of the BABAR experiment at PEP-II*, *ibid.* [SLAC-PUB-8539, BABAR-CONF-00-17, hep-ex/0012042].

B. Aubert *et al.* (BABAR collaboration), *A study of time dependent CP violating asymmetries in  $B^0 \rightarrow J/\psi K_s^0$  and  $B^0 \rightarrow \psi(2S) K_s^0$  decays*, *ibid.* [SLAC-PUB-8540, BABAR-CONF-00-01, hep-ex/0008048].

C.E. Svensson, A.O. Macchiavelli, A. Juodagalvis, A. Poves, I. Ragnarsson, S. Aberg, D.E. Appelbe, R.A.E. Austin, C. Baktash, G.C. Ball, M.P. Carpenter, E. Caurier, R.M. Clark, M. Cromaz, M.A. Deleplanque, R.M. Diamond, P. Fallon, M. Furlotti, A. Galindo-Uribarri, R.V.F. Janssens, G.J. Lane, I.Y. Lee, M. Lipoglavsek, F. Nowacki, S.D. Paul, D.C. Radford, D.G. Sarantites, D. Seweryniak, F.S. Stephens, V. Tomov, K. Vetter, D. Ward and C.H. Yu, *Collective rotational motion in the  $N = Z$  nucleus  $^{36}\text{Ar}$* , Proc. **Nuclear Structure (NS2000)**, East Lansing, MI, **August 15–19, 2000** (Nucl. Phys. **A682**, 2001) p.1.

G. Suft, W. Beulertz, A. Bock, M. Frank, A. Glombik, J. Hey, B. Kowalzik, W. Kretschmer, S. Merz, H. Meyer, L. Sözüer, R. Weidmann, E. Boschitz, B. Brinkmoller, R. Meier, G. Mertens, B. van den Brandt, P. Hautle, J.A. Konter, S. Mango, L. Mathelitsch, H. Garcilazo, R. Tacik, P. Amaudruz and W. Gruebler, *Measurement of polarization transfer in pion-deuteron elastic scattering*, Proc. **XVII<sup>th</sup> European Conf. on Few-Body Problems in Physics**, Évora, Portugal, **September 11–16, 2000**, A. Stadler *et al.*, eds. (Nucl. Phys. **A689**, 2001) p.406.

D.A. Bryman and L. Littenberg, *Prospects for measuring  $K^+ \rightarrow \pi^+ \nu \bar{\nu}$  and  $K_L^0 \rightarrow \pi^0 \nu \bar{\nu}$  at BNL*, Proc. **Int. Conf. on CP Violation Physics**, Ferrara, Italy, **September 18–22, 2000**, M. Savrie *et al.*, eds. (Nucl. Phys. Proc. Suppl. **99B**, 2001) p.61.

W.T.H. van Oers, *Constraints of a parity-conserving/time-reversal-non-conserving interaction*, Proc. **14<sup>th</sup> Int. Spin Physics Symp. (SPIN 2000)**, Osaka, Japan, **October 16–21, 2000** (AIP Conf. Proc. **570**, New York, 2001) p.331 [TRI-PP-00-66].

G.C. Ball *et al.* (E823 collaboration), *Tests of the standard*

*model from superallowed Fermi  $\beta$ -decay studies at ISAC*, Proc. **16<sup>th</sup> Int. Conf. on the Application of Accelerators in Research and Industry (CAARI 2000)**, Denton, TX, **November 1–4, 2000**, J.L. Duggan and I.L. Morgan, eds. (AIP Conf. Proc. **576**, 2001) p.297.

M.C. Vetterli, *Studies of quark fragmentation at HERMES*, Proc. **Spin Physics at RHIC in Year-1 & Beyond**, RIKEN BNL Research Center Workshop, Upton, NY, **May 14–18, 2001** (BNL-52635, 2001).

M. Khabibullin *et al.* (KEK-PS-E246 collaboration), *New limit on T-violating parameters in kaon decays*, Proc. **Int. Europhysics Conf. on High-Energy Physics (HEP 2001)**, Budapest, Hungary, **July 12–18, 2001** (J. High Energy Physics, Budapest, 2001) [hep2001/061].

B. Aubert *et al.* (BABAR collaboration), *Measurement of the exclusive branching fractions  $B^0 \rightarrow \eta K^{*0}$  and  $B^+ \rightarrow \eta K^{*+}$* , *ibid.* [SLAC-PUB-8914, BABAR-CONF-01-06, hep-ex/0107037].

B. Aubert *et al.* (BABAR collaboration), *Measurement of the  $B^0 \bar{B}^0$  oscillation frequency in hadronic  $B^0$  decays*, *ibid.* [SLAC-PUB-8913, BABAR-CONF-01-23, hep-ex/0107036].

B. Aubert *et al.* (BABAR collaboration), *Search for the rare decays  $B \rightarrow K \ell^+ \ell^-$  and  $B \rightarrow K^*(892) \ell^+ \ell^-$* , *ibid.* [SLAC-PUB-8910, BABAR-CONF-01-24, hep-ex/0107026].

C.E. Covault, L.M. Boone, D. Bramel, E. Chae, P. Fortin, D.M. Gingrich, J.A. Hinton, D.S. Hanna, R. Mukherjee, C. Mueller, R.A. Ong, K. Ragan, R.A. Scalzo, D.R. Schuette, C.G. Theoret and D.A. Williams, *The status of the STACEE Observatory*, Proc. **27<sup>th</sup> Int. Cosmic Ray Conf. (ICRC 2001)**, Hamburg, Germany, **August 7–15, 2001** (Copernicus Gesellschaft, 2001) [astro-ph/0107427].

B. Caron, J. Collot, E. Frank, A. Gupta, P. Loch, H. Ma, F. Merritt, J.P. Mayer, S. Rajagopalan, J. Schwindling, M. Wielers and K. Yip, *Object oriented reconstruction and particle identification in the ATLAS calorimeter*, Proc. **Int. Conf. on Computing in High-Energy Physics and Nuclear Physics (CHEP'01)**, Beijing, China, **September 3–7, 2001** (CHEP, Beijing, 2001) p.182.

C.E. Svensson, A.O. Macchiavelli, A. Juodagalvis, A. Poves, I. Ragnarsson, S. Aberg, D.E. Appelbe, R.A.E. Austin, C. Baktash, G.C. Ball, M.P. Carpenter, E. Caurier, R.M. Clark, M. Cromaz, M.A. Deleplanque, R.M. Diamond, P. Fallon, M. Furlotti, A. Galindo-Uribarri, R.V.F. Janssens, G.J. Lane, I.Y. Lee, M. Lipoglavsek, F. Nowacki, S.D. Paul, D.C. Radford, D.G. Sarantites, D. Seweryniak, F.S. Stephens, V. Tomov, K. Vetter, D. Ward and C.H. Yu, *Fast rotation of the  $N = Z$  nucleus  $^{36}\text{Ar}$* , Proc. **3<sup>rd</sup> Circum-Pan-Pacific Symp. on High Energy Spin Physics (SPIN 2001)**, Beijing, China, **October 8–13, 2001** (Acta Phys. Polon. **B32**, 2001) p.2413 [nucl-th/0104012].

- Yu. Davydov, W. Andersson, M. Comyn, P. Depommier, J. Doornbos, W. Faszer, C.A. Gagliardi, D.R. Gill, P. Green, P. Gumplinger, J.C. Hardy, M. Hasinoff, R. Helmer, R. Henderson, A. Khruchinsky, P. Kitching, D.D. Koetke, E. Korkmaz, Yu. Lachin, D. Maas, J.A. Macdonald, R. MacDonald, R. Manweiler, G.M. Marshall, E.L. Mathie, L. Missoedov, J.R. Musser, P. Nord, A. Olin, R. Openshaw, D. Ottewell, T. Porcelli, J.-M. Poutissou, R. Poutissou, G. Price, M.A. Quraan, N.L. Rodning, J. Schaapman, V. Selivanov, G. Sheffer, B. Shin, F. Sobratee, J. Soukup, T.D.S. Stanislaus, G. Stinson, R. Tacik, V. Torokhov, R.E. Tribble, M.A. Vasilev, H.C. Walter and D. Wright, *Drift chambers for a precision measurement of the Michel parameters in muon decay*, Proc. **8<sup>th</sup> Pisa Meeting on Advanced Detectors: Frontier Detectors for Frontier Physics, La Biodola, Isola d'Elba, Italy, May 21–25, 2000** (Nucl. Instrum. Methods **A461**, 2001) p.468.
- H. Schonauer, B. Autin, R. Cappi, M. Chanel, G. Franchetti, J. Gareyte, R. Garoby, H. Haseroth, M. Martini, E. Metral, D. Mohl, K. Schindl, W. Pirkel, G.H. Rees, C. Prior, I. Hofmann, S. Koscielniak, K. Bongardt and Yu. Senichev, *Proton drivers for neutrino factories: the CERN approach*, Proc. **Int. Workshop, Muon Storage Ring for a Neutrino Factory (NuFACT'00), Monterey, CA, May 22–26, 2000**, S. Chattopadhyay, ed. (Nucl. Instrum. Methods **472**, 2001) p.504 [CERN-PS-2000-065-PP, CERN-NUFACT-NOTE-46].
- R. Helmer *et al.* (SNO collaboration) *First neutrino observations from the Sudbury Neutrino Observatory*, Proc. **6<sup>th</sup> Int. Workshop on Tau Lepton Physics (TAU 2000), Victoria, BC, September 18–21, 2000** (Nucl. Phys. B, Proc. Suppl. **98**, 2001) p.157.
- N.L. Rodning, W. Andersson, Yu. Davydov, P. Depommier, J. Doornbos, W. Faszer, C.A. Gagliardi, A. Gaponenko, D.R. Gill, P.W. Green, P. Gumplinger, J.C. Hardy, M. Hasinoff, R.L. Helmer, R. Henderson, P. Kitching, D.D. Koetke, E. Korkmaz, A. Khruchinsky, D. Maas, J.A. Macdonald, R. MacDonald, R. Manweiler, G.M. Marshall, T. Mathie, J.R. Musser, P. Nord, A. Olin, R. Openshaw, D. Ottewell, T. Porcelli, J.-M. Poutissou, R. Poutissou, G. Price, M. Quraan, J. Schaapman, V. Selivanov, G. Sheffer, B. Shin, F. Sobratee, J. Soukup, T.D.S. Stanislaus, G. Stinson, R. Tacik, V. Torokhov, R.E. Tribble, M.A. Vasilev, H.C. Walter, S.C. Wang and D. Wright, *TWIST – the TRIUMF weak interaction symmetry test: the Michel parameters from  $\mu^+$  decay*, *ibid.* 247.
- P. Bricault, *Status report on the ISAC radioactive beam facility*, Proc. **16<sup>th</sup> Int. Conf. on the Application of Accelerators in Research and Industry (CAARI 2000), Denton, TX, November 1–4, 2000**, J.L. Duggan and I.L. Morgan, eds. (AIP Conf. Proc. **576**, 2001).
- N. van den Elzen, *Applications of beam-line simulators*, Proc. **Workshop on Accelerator Operation (WAO 2001), Villars sur Ollon, Switzerland, January 28–February 2, 2001**, R. Bailey and T. Kehrer, eds. (CERN report CERN-2001-002) p.22.
- J. Kaminski, *A new model for a 500 MeV beam line at TRIUMF*, *ibid.* 34.
- M. Comyn, *Trends over five years of electronic publishing and predictions for the next few conferences*, **Proc. Second Joint Accelerator Conference Website (JACoW) Team Meeting, Frascati, Italy, March 28–29, 2001** (<http://jacow.web.cern.ch/JACoW/TM-2001/Conclusions.pdf>).
- D. Cocq, L. Jensen, R. Jones, J.J. Savioz, D. Bishop, B. Roberts and G. Waters, *First beam tests for the prototype LHC orbit and trajectory system in the CERN-SPS*, Proc. **5<sup>th</sup> European Workshop on Diagnostics and Beam Instrumentation (DIPAC 2001), Grenoble, France, May 13–15, 2001** (ESRF Machine Div., Grenoble, 2001) [CERN-SL-2001-030-BI].
- T. Kuo, R. Baartman, G. Dutto, S. Hahto, J. Ärje and E. Liukkonen, *H<sup>-</sup> source development for Jyväskylä cyclotron*, Proc. **16<sup>th</sup> Int. Conf. on Cyclotrons and Their Applications (CYCLOTRONS 2001), East Lansing, MI, May 12–17, 2001**, F. Marti, ed. (AIP Conf. Proc. **600**, 2001) p.238.
- P. Bricault and M. Domsbky, *The production target at ISAC*, *ibid.* 241.
- M. Olivo, M. Domsbky, K. Jayamanna, M. McDonald, G. Stanford and D. Yuan, *A radiation hard ECR source for ISAC*, *ibid.* 246 [TRI-PP-01-21].
- W.Z. Gelbart, J. Orzechowski, R. Pavan, A. Wong, R. Wong and S. Zeisler, *Turn-key, solid target irradiation system*, *ibid.* 249.
- G. Dutto, K. Fong, R.E. Laxdal, G.H. Mackenzie, R. Poirier and L. Root, *Impact of the cyclotron rf booster on the 500 MeV proton beam production*, *ibid.* 288 [TRI-PP-01-04].
- W.Z. Gelbart, A. Wong, R. Wong and S. Zeisler, *Parallel beams co-extraction*, *ibid.* 440.
- M.K. Craddock, *Cyclotron, psychotron – What's in a name?*, *ibid.* 474 [TRI-PP-01-06].
- R. Baartman, M. D'yachkov and F.W. Jones, *Multi-turn simulation of coherent betatron resonance with space charge*, Proc. **IEEE Particle Accelerator Conf. (PAC 2001), Chicago, IL, June 18–22, 2001**, P. Lucas, S. Webber, eds. (IEEE, New York, 2001) p.267 [TRI-PP-01-27, PAC-2001-TOPB004].
- R. Laxdal, *Completion and operation of ISAC-I and extension to ISAC-II*, *ibid.* 556 [TRI-PP-01-32, PAC-2001-ROPA001].
- S. Fang, K. Fong, M. Laverty, J. Lu and R. Poirier, *Commissioning of the TRIUMF ISAC rf system*, *ibid.* 945 [TRI-PP-01-31, PAC-2001-MPPH077].

S. Fang, K. Fong and M. Laverty, *RF control systems for the TRIUMF ISAC rf structures*, *ibid.* 948 [TRI-PP-01-30, PAC-2001-MPPH078].

A. Vasyuchenko, P. Bricault, K. Fong, R. Laxdal, A. Mitra and R. Poirier, *RF measurement summary of ISAC DTL tanks and DTL bunchers*, *ibid.* 951 [TRI-PP-01-19, PAC-2001-MPPH079].

A. Feschenko, A. Kvasha, A. Menshov, V. Paramonov, A. Vasyuchenko, Y. Bylinsky, G. Dutto, R. Laxdal, A. Mitra and R. Poirier, *Development, fabrication and test of triple gap split-ring bunchers for the TRIUMF ISAC facility*, *ibid.* 978 [TRI-PP-01-26, PAC-2001-MPPH090].

E. Chiaveri, A. Facco, V. Zviagintsev and R. Laxdal, *The superconducting medium beta prototype for radioactive beam acceleration at TRIUMF*, *ibid.* 1092 [PAC-2001-MPPH134].

I. Chiang, J. Glenn, D. Lazarus, M. Sivertz and S. Koscielniak, *Micro-bunching of the AGS slow extracted beam for a rare kaon search*, *ibid.* 1529 [TRI-PP-01-17, PAC-2001-TPAH135].

F. Schmidt, A. Verdier and D. Kalchev, *Robustness of resonance free lattices against gradient errors*, *ibid.* 1690 [CERN-LHC-PROJECT-REPORT-475, PAC-2001-TPPH015].

R. Baartman, P. Bricault, M. Dombisky, G. Dutto, K. Fong, T. Kuo, R. Laxdal, G. Mackenzie, A. Mitra, M. Olivo, R. Poirier, K. Reiniger, L. Root, R. Ruedg, P. Schmor, M. Stenning and G. Stinson, *The TRIUMF facility and cyclotron developments*, *ibid.* 2584 [TRI-PP-01-14, PAC-2001-WPPH059].

S. Hancock, M. Lindroos and S. Koscielniak, *Soliton-like longitudinal holes in debunched beams perpetuated by space-charge forces*, *ibid.* 2967 [TRI-PP-01-15, PAC-2001-RPAH052].

S. Koscielniak, *Longitudinal space-charge geometric factor for an elliptical beam*, *ibid.* 2970 [TRI-PP-01-16, PAC-2001-RPAH053].

S. Dewan, F. Voelker, R. Holmes, K. Reiniger and J. Zeng, *A 250 kW four quadrant switch mode converter for the 1.4 GeV PS-Booster beam transfer lines at CERN*, *ibid.* 3696 [PAC-2001-FPAH015].

R. Laxdal, R. Lee and M. Pasini, *Progress in the conceptual design of the ISAC-II linac at TRIUMF*, *ibid.* 3939 [TRI-PP-01-29, PAC-2001-FPAH111].

G. Dutto, K. Fong, R. Laxdal, G. Mackenzie, M. Pasini, R. Poirier and R. Ruedg, *Beam commissioning and first operation of the ISAC DTL at TRIUMF*, *ibid.* 3942 [TRI-PP-01-28, PAC-2001-FPAH112].

#### Life Sciences

V. Sossi, B. Pointon, C. Boudoux, P. Cohen, K. Hudkins, S. Jivan, K. Nitzek, J. deRosario, C. Stevens and T.J.

Ruth, *NEMA NU 2-2000 performance measurements on an ADAC MCD camera*, Proc. **IEEE Nuclear Science Symp. and Medical Imaging Conf.**, Lyon, France, October 15–20, 2000 (IEEE Trans. Nucl. Sci. **48**(4), 2001) p. 1518.

B. Pointon and V. Sossi, *Monte Carlo investigation of scatter in dual head coincidence imaging*, *ibid.*

T.J. Ruth, *The production of ultra high quantities of  $^{18}\text{F}$ -fluoride: a work in progress*, Proc. **16<sup>th</sup> Int. Conf. on the Application of Accelerators in Research and Industry (CAARI 2000)**, Denton, TX, November 1–4, 2000, J.L. Duggan and I.L. Morgan, eds. (AIP Conf. Proc. **576**, 2001).

#### Theoretical Program

S. Kondratyuk and O. Scholten, *Nucleon dressing from dispersion relations*, Proc. **Int. Conf. on Quark Nuclear Physics (QNP 2000)**, Adelaide, Australia, February 21–25, 2000, C. Boros, K. Tsushima and A.W. Thomas, eds. (Nucl. Phys. **A680**, 2001) p.175.

T.-S. Park, K. Kubodera, D.P. Min and M. Rho, *Effective field theory for nuclei: confronting fundamental questions in astrophysics*, Proc. **XVI<sup>th</sup> Int. Conf. on Few-Body Problems in Physics**, Taipei, Taiwan, March 6–10, 2000 (Nucl. Phys. **A684**, 2001) p.101 [TRI-PP-00-25, nucl-th/0005069].

W.T.H. van Oers, *Symmetries and symmetry breaking*, *ibid.* 266 [TRI-PP-00-27, hep-ph/0006058].

H.W. Fearing, Th.R. Hemmert, R. Lewis and C. Unkmeir, *Charged radiative pion capture on the nucleon in heavy baryon chiral perturbation theory*, *ibid.* 377 [TRI-PP-00-30, hep-ph/0007090].

L. Canton, G. Pisent, W. Schadow and J.P. Svenne, *Spin observables for pion production from pd collisions*, *ibid.* 417 [TRI-PP-00-28, nucl-th/0006027].

E. Truhlik and F.C. Khanna, *Lepton  $U_1$  symmetry and interaction of neutrinos with deuterons at high-energies*, *ibid.* 481 [nucl-th/0007037].

S. Scherer and H.W. Fearing, *A simple model illustrating the impossibility of measuring off-shell effects*, *ibid.* 499 [MKPH-T-00-11, TRI-PP-00-31, nucl-th/0006076].

F.C. Khanna and A.E. Santana, *Topics in thermal field theory*, Proc. **2<sup>nd</sup> Int. School on Field Theory and Gravitation**, Vitoria, Brazil, April 25–28, 2000, C. Pinheiro, A.J. Helayal Neto and G.O. Pires, eds. (Braz. J. Phys. **31**, 2001).

J. Escher, *Partial dynamical symmetry in a fermionic many-body system*, Proc. **Bologna 2000: Structure of the Nucleus at the Dawn of the Century**, Bologna, Italy, May 29–June 3, 2000 (World Scientific, Singapore, 2001) p.350 [TRI-PP-00-56, nucl-th/0008069].

R.M. Woloshyn, *Charmed baryons from lattice QCD*, Proc. **4<sup>th</sup> Int. Conf. on Hyperons, Charm and Beauty Hadrons**, Valencia, Spain, June 27–30, 2000 (Nucl.

Phys. Proc. Suppl. **93**, 2001) p.38 [TRI-PP-00-58, hep-ph/0009332].

R. Lewis and R.M. Woloshyn, *The charmed and bottom meson spectrum from lattice NRQCD*, *ibid.* 192 [hep-ph/0010013].

H.W. Fearing, T.R. Hemmert, R. Lewis and C. Unkmeir, *Radiative pion capture in ChPT*, Proc. **3<sup>rd</sup> Workshop on Chiral Dynamics – Chiral Dynamics 2000: Theory and Experiment**, Newport News, VA, July 17–22, 2000, A.M. Bernstein, J.L. Goity, U.-G. Meissner, eds. (World Scientific, Singapore, 2001) p.380.

J. Escher, *Partial dynamical symmetry in an interacting fermion system*, Proc. **Int. Conf. Symmetries and Spin (PRAHA-SPIN-2000)**, Prague, Czech Republic, July 17–22, 2000 (Czech. J. Phys. **51**, 2001) p.A179 [TRI-PP-00-59].

R. Gupta and K. Maltman, *Light quark masses: A status report at DPF 2000*, Proc. **Meeting of the Division of Particles and Fields of the American Physical Society (DPF 2000)**, Columbus, OH, August 9–12, 2000 (Int. J. Mod. Phys. **A16S1B**, 2001) p.591 [LAUR-00-5684, hep-ph/0101132].

N. Mathur *et al.* (Kentucky Field Theory collaboration), *Strange magnetic moment of the nucleon from lattice QCD*, Proc. **18<sup>th</sup> Int. Symp. on Lattice Field Theory (Lattice 2000)**, Bangalore, India, August 17–22, 2000 (Nucl. Phys. Proc. Suppl. **94**, 2001) p.311 [TRI-PP-00-61, hep-lat/0011015].

R. Lewis and R.M. Woloshyn, *Heavy light meson spectrum with and without NRQCD*, *ibid.* 359 [hep-lat/0010001].

L. Canton, G. Pisent, W. Schadow, T. Melde and J.P. Svenne, *Three-nucleon portrait with pion*, Proc. **8<sup>th</sup> Convegno su Problemi di Fisica Nucleare Teorica**, Cortona, Italy, October 18–21, 2000 (World Scientific, Singapore, 2001) p.249 [TRI-PP-00-63].

E. Truhlik, J. Smejkal and F.C. Khanna, *Electromagnetic isoscalar  $\rho\pi\gamma$  exchange current and the anomalous action*, Proc. **8<sup>th</sup> Meeting On Mesons and Light Nuclei**, Prague, Czech Republic, July 2–6, 2001 (AIP, New York, 2001) p.311.

E. Truhlik and F.C. Khanna, *On radiative muon capture in hydrogen*, *ibid.* 535.

## Conference Presentations

### Particle, Nuclear and Atomic Physics

M. Convery *et al.* (BABAR collaboration), *Charmless B decays from BABAR ( $B^0 \rightarrow K^{*0}\gamma$  and  $B^0 \rightarrow \pi^+\pi^-$ ,  $K^+\pi^-$ ,  $K^+K^-$ )*, Proc. **XV Rencontres de Physique de La Vallée d’Aoste**, La Thuile, Italy, March 4–10, 2001 (Frascati Physics Series, in press) [SLAC-PUB-8848, BABAR-PROC-01/14, hep-ex/0106043].

D.A. Bryman, *Measuring  $K^+ \rightarrow \pi^+\nu\bar{\nu}$  and  $K_L^0 \rightarrow \pi^0\nu\bar{\nu}$  at BNL*, *ibid.* [TRI-PP-01-18].

G.C. Ball, *The physics program at the ISAC radioactive beam facility at TRIUMF: first results and future plans*, Proc. **Int. Conf. on Physics with Radioactive Ion Beams (ISOL’01)**, Oak Ridge, TN, March 11–14, 2001.

V. Brigljevic *et al.* (BABAR collaboration), *Study of charmonium production and electroweak penguins with BABAR*, Proc. **36<sup>th</sup> Rencontres de Moriond on QCD and Hadronic Interactions**, Les Arcs, France, March 17–24, 2001 [SLAC-PUB-9008, BABAR-PROC-01/28, hep-ex/0109043].

A. Miller, *Polarized quark and gluon distributions, and potential of HERMES, COMPASS and RHIC*, Proc. **9<sup>th</sup> Int. Workshop on Deep Inelastic Scattering (DIS 2001)**, Bologna, Italy, April 27 – May 1, 2001 (World Scientific, Singapore, in press).

D.A. Bryman, *KOPIO: measurement of  $K_L^0 \rightarrow \pi^0\nu\bar{\nu}$  at BNL*, Proc. **Int. Conf. on CP Violation (KAON2001)**, Pisa, Italy, June 12–17, 2001 [TRI-PP-01-25].

G.C. Ball *et al.* (E823 collaboration), *Tests of the standard model from superallowed Fermi  $\beta$ -decay studies at ISAC*, Proc. **2001 Gordon Research Conf. on Nuclear Chemistry**, New London, NH, June 17–21, 2001.

A.S. Levchenko *et al.* (KEK-PS E246 collaboration), *Test of exotic scalar and tensor interactions in  $K_{e3}$  decay using stopped positive kaons*, Proc. **3<sup>rd</sup> Int. Conf. on Nonaccelerator New Physics (NANPino 01)**, Dubna, Russia, June 19–23, 2001 (Physics of Atomic Nuclei (Yad. Fiz.), in press) [hep-ex/0111048].

E.F. Zganjar, A. Piechaczek, G.C. Ball, B. Bricault, J.M. D’Auria, J.C. Hardy, D.F. Hodgson, V. Iacob, P. Klages, W.D. Kulp, J.R. Leslie, M. Lipoglavsek, J.A. Macdonald, H.-B. Mak, D.M. Moltz, G. Savard, J. von Schwarzenberg, C.E. Svensson, I.S. Towner and J. Wood, *Tests of the standard model from superallowed Fermi  $\beta$ -decay studies: the  $^{74}\text{Rb}$   $\beta$ -decay*, Proc. **3<sup>rd</sup> Int. Conf. on Exotic Nuclei and Atomic Masses (ENAM 2001)**, Hameenlinna, Finland, July 2–7, 2001 (Eur. Phys. J. A, in press).

M. Vincter, *Future plans for HERMES Run II*, Proc. **Topical Workshop on Transverse Spin Physics**, Zeuthen, Germany, July 9–11, 2001 (in press).

L. De Nardo, *Measurement of the spin structure function  $g_1$  at HERMES*, Proc. **Advanced Study Inst. on Symmetries and Spin (PRAHA SPIN 2001)**, Prague, Czech Republic, July 15–28, 2001 (Czech. J. Phys., in press).

B. Aubert *et al.* (BABAR collaboration), *Investigation of  $B \rightarrow D^{(*)}\bar{D}^{(*)}K$  decays with the BABAR detector*, Proc. **20<sup>th</sup> Int. Symp. on Lepton and Photon Interactions at High Energies (Lepton Photon 01)**, Rome, Italy, July 23–28, 2001 (World Scientific, Singapore, in press) [SLAC-PUB-8924, BABAR-CONF-01-01, hep-ex/0107056].

- B. Aubert *et al.* (BABAR collaboration), *Measurement of the branching fraction for the decay  $B^0 \rightarrow D^{*+}D^{*-}$* , *ibid.* [SLAC-PUB-8925, BABAR-CONF-01-03, hep-ex/0107057].
- B. Aubert *et al.* (BABAR collaboration), *Study of CP violating asymmetries in  $B \rightarrow \pi^{\pm}\pi^{\mp}, K^{\pm}\pi^{\mp}$  decays*, *ibid.* [SLAC-PUB-8929, BABAR-CONF-01-05, hep-ex/0107074].
- B. Aubert *et al.* (BABAR collaboration), *Search for  $B^0 \rightarrow a_0^+(980)\pi^-$* , *ibid.* [SLAC-PUB-8930, BABAR-CONF-01-07, hep-ex/0107075].
- B. Aubert *et al.* (BABAR collaboration), *Measurements of  $B^0$  decays to  $\pi^+\pi^-\pi^0$* , *ibid.* [SLAC-PUB-8926, BABAR-CONF-01-10, hep-ex/0107058].
- B. Aubert *et al.* (BABAR collaboration), *Study of T and CP violation in  $B^0\bar{B}^0$  mixing with inclusive dilepton events*, *ibid.* [SLAC-PUB-8927, BABAR-CONF-01-17, hep-ex/0107059].
- B. Aubert *et al.* (BABAR collaboration), *Measurement of  $D_s^+$  and  $D_s^{*+}$  production in B meson decays and from continuum  $e^+e^-$  annihilations at  $\sqrt{s} = 10.6$  GeV*, *ibid.* [SLAC-PUB-8928, BABAR-CONF-01-27, hep-ex/0107060].
- M.M. Pavan, I.I. Strakovsky, R.L. Workman and R.A. Arndt, *The pion nucleon  $\Sigma$  term is definitely large: results from a G.W.U. analysis of  $\pi N$  scattering data*, Proc. **9<sup>th</sup> Int. Symp. on Meson-Nucleon Physics and the Structure of the Nucleon (MENU 2001)**, Washington, DC, July 26–31, 2001 ( $\pi N$  Newsletter, in press) [hep-ph/0111066].
- B. Seitz, *Single spin asymmetry in hard exclusive electroproduction of  $\pi^+$  and real photons at HERMES*, *ibid.*
- B. Aubert *et al.* (BABAR collaboration), *Search for B decays into  $K^0\bar{K}^0$* , Proc. **9<sup>th</sup> Int. Symp. on Heavy Flavor Physics, Pasadena, CA, September 10–13, 2001** (AIP, New York, in press) [SLAC-PUB-8978, BABAR-CONF-01-04, hep-ex/0109005].
- B. Aubert *et al.* (BABAR collaboration), *Study of semi-inclusive production of  $\eta'$  mesons in B decays*, *ibid.* [SLAC-PUB-8979, BABAR-CONF-01-08, hep-ex/0109034].
- B. Aubert *et al.* (BABAR collaboration), *Search for direct CP violation in quasi two body charmless B decays*, *ibid.* [SLAC-PUB-8980, BABAR-CONF-01-09, hep-ex/0109006].
- B. Aubert *et al.* (BABAR collaboration), *Measurement of the branching fraction for  $B^+ \rightarrow K^{*0}\pi^+$* , *ibid.* [SLAC-PUB-8981, BABAR-CONF-01-12, hep-ex/0109007].
- B. Aubert *et al.* (BABAR collaboration), *Study of  $B \rightarrow D^{(*)}\bar{D}^{(*)}$  decays with the BABAR detector*, *ibid.* [SLAC-PUB-8982, BABAR-CONF-01-28, hep-ex/0109009].
- B. Aubert *et al.* (BABAR collaboration), *Search for a lifetime difference in  $D^0$  decays*, *ibid.* [SLAC-PUB-8983, BABAR-CONF-01-29, hep-ex/0109008].
- G.C. Ball, P. Bricault, M. Domsbky, D.F. Hodgson, P. Klages, J.A. Macdonald, A. Piechaczek, E.F. Zganjar, J.R. Leslie, H.-B. Mak, I.S. Towner, C.E. Svensson, J. D'Auria, D.M. Moltz, J.L. Wood, D. Kulp, J.C. Hardy, V. Iacob, G. Savard and M. Lipoglavsek, *Superallowed  $\beta$ -decay of  $^{74}\text{Rb}$* , Proc. **APS DNP 2001 Fall Meeting and 1<sup>st</sup> Joint Meeting of Nuclear Physicists of the American and Japanese Physical Societies, Maui, HI, October 17–20, 2001**.
- M.A. Caprio, R.F. Casten, N.V. Zamfir, G.C. Ball, K.P. Jackson, P.A. Amaudruz and J.C. Thomas, *Study of collective  $0^+$  excitations in  $^{162}\text{Er}$  at ISAC*, *ibid.*
- 
- Instrumentation/Accelerator Physics/Computing Sciences
- R.E. Laxdal, *ISAC at TRIUMF: status of the post-accelerator*, Proc. **Int. Workshop on Production of Radioactive Ion Beams (PRORIB 2001)**, Puri, India, February 12–17, 2001 [TRI-PP-01-03].
- P.-A. Amaudruz, R. Poutissou *et al.*, *Real time control/monitoring and data acquisition system for nuclear polarization experiments with implanted radioactive ions*, Proc. **12<sup>th</sup> IEEE Real Time Congress on Nuclear and Plasma Sciences, Valencia, Spain, June, 2001**, E. Sanchez, A. Ferrer, eds. (IEEE, in press).
- M. Barnes and G. Wait, *A FET based kicker for a charge booster for the TRIUMF-ISAC project*, Proc. **13<sup>th</sup> IEEE Int. Pulsed Power Conf., Las Vegas, NV, June 17–22, 2001** [TRI-PP-01-12].
- C. Johnstone and S. Koscielniak, *Recent progress on FFAGs for rapid acceleration*, Proc. **APS/DPF/DPB Summer Study on the Future of Particle Physics (Snowmass 2001)**, Snowmass, CO, June 30–July 21, 2001 (SLAC eConf, in press).
- S. Koscielniak, *Review of beamloading and compensation in synchrotrons*, *ibid.* [TRI-PP-01-33].
- G. Dutto, P. Bricault, R. Baartman, K. Fong, R.E. Laxdal, G. Mackenzie, M. Pasini, R. Poirier, P.W. Schmor, G. Stinson and A. Facco, *Completion of the ISAC-I accelerator for radioactive ions and to ISAC-II*, Proc. **2<sup>nd</sup> Asian Particle Accelerator Conf. (APAC01)**, Beijing, China, September 17–21, 2001 (in press) [TRI-PP-01-24].
- R. Assmann, J.B. Jeanneret and D. Kaltchev, *Status of robustness studies for the LHC collimator*, *ibid.*
- K. Fong, M. Laverty and S. Fang, *RF control systems for the TRIUMF ISAC rf*, *ibid.*
- G. Clark, *Construction and measurements of the pre-series twin aperture resistive quadrupole magnet for the LHC beam cleaning insertions*, Proc. **17<sup>th</sup> Int. Conf. on Magnet Technology (MT17)**, Geneva, Switzerland, September 24–28, 2001 (IEEE Trans. Appl. Superconductivity, in press).

G. Clark, *Analysis of lamination measurements for CERN's twin aperture quadrupoles*, *ibid.*

C.D.P. Levy, R. Baartman, J.A. Behr, A. Hatakeyama, Y. Hirayama, R.F. Kiefl, G.D. Morris, R. Nussbaumer, R. Poutissou and G.W. Wight, *A highly polarized  $^8\text{Li}^+$  ion beam at ISAC*, Proc. **Int. Workshop on Polarized Sources and Targets (PST2001)**, Nashville, TN, September 30–October 4, 2001.

A. Hatakeyama, Y. Hirayama, J.A. Behr, H. Izumi, C.D.P. Levy, D. Melconian and T. Shimoda, *Optical pumping at the ISAC polarizer*, *ibid.*

M. Barnes, *Field mapping the TWIST solenoid, detailing the first results and problems of the TWIST magnet mapping*, Proc. **Int. Magnet Measurement Workshop, ESRF Grenoble, France, October 1–4, 2001, held at MT17.**

R. Keitel, *Generating EPICS IOC databases from a relational database: a different approach*, Proc. **8<sup>th</sup> Int. Conf. on Accelerator and Large Experimental Physics Control Systems (ICALEPCS 2001)**, San Jose, CA, November 27–30, 2001 [ICALEPCS-2001-WEAP-071, physics/0111048].

R. Nussbaumer, D. Dale, H. Hui, J. Richards and P. Levy, *Laser stabilization controls for the ISAC beam polarizer*, *ibid.* [ICALEPCS-2001-TUAP-065, physics/0111081].

R. Keitel and R. Nussbaumer, *Automated checking and visualization of interlocks in the ISAC control system*, *ibid.* [ICALEPCS-2001-WEAPO-70, physics/0111094].

R. Keitel, D. Bishop, D. Dale, H. Hui, S. Kadantsev, M. Leross, R. Nussbaumer, J. Richards, E. Tikhomolov and G. Waters, *Status update on the ISAC control system*, *ibid.* [ICALEPCS-2001-TUAP-028, physics/0111095].

#### Chemistry and Solid-State Physics

M.C. Fujiwara *et al.* (Muonic Hydrogen collaboration), *Resonant scattering of muonic hydrogen atoms and dynamics of muonic molecular complex*, Proc. **Int. RIKEN Conf. on Muon Catalyzed Fusion and Related Exotic Atoms, Shimoda, Japan, April 22–26, 2001** (Hyp. Int., in press) [TRI-PP-01-36, nucl-ex/0111019].

D.R. Noakes, G.M. Kalvius, H. Nakotte, E. Schreier and R. Wäppling, *Magnetic ordering in UPdSn and CeCuSn*, Proc. **2001 Strongly Correlated Electron Systems Conf. (SCES 2001)**, Ann Arbor, MI, August 6–10, 2001 (Physica B, in press).

#### Life Sciences

V. Sossi, R. de la Fuente-Fernandez, J.E. Holden, D.J. Doudet, J. McKenzie, T.J. Ruth and A.J. Stoessl, *The dopamine effective distribution volume: a good classifying estimator of early Parkinson's disease*, Proc. **48<sup>th</sup> Annual Society of Nuclear Medicine Conf.**, Toronto, ON, June 23–27, 2001.

V. Sossi, R. de la Fuente-Fernandez, J.E. Holden, D.J. Doudet, J. McKenzie, T.J. Ruth and A.J. Stoessl, *Changes in effective dopamine turnover due to PD are measurable earlier than changes in FD uptake rate using PET*, Proc. **XIV Int. Congress on Parkinson's Disease, Helsinki, Finland, July 27 – August 1, 2001.**

#### Theoretical Program

A.D. Lahiff and I.R. Afnan, *Pion-nucleon scattering in a Bethe-Salpeter approach*, Proc. **9<sup>th</sup> Int. Symp. on Meson-Nucleon Physics and the Structure of the Nucleon (MENU 2001)**, Washington, DC, July 26–31, 2001 ( $\pi N$  Newsletter, in press) [nucl-th/0109054].

A.D. Lahiff, *Covariant meson exchange model of the  $\bar{K}N$  interaction*, *ibid.* [nucl-th/0110028].

R. Lewis, N. Mathur and R.M. Woloshyn, *Spin splittings among charmed hadrons*, Proc. **19<sup>th</sup> Int. Symp. on Lattice Field Theory (Lattice 2001)**, Berlin, Germany, August 19–24, 2001 (Nucl. Phys. B, proc. suppl., in press) [hep-lat/0109014].

N. Mathur, R. Lewis and R.M. Woloshyn, *Heavy baryons from lattice NRQCD*, *ibid.* [TRI-PP-01-22, hep-lat/0110031].

#### **Books**

M.K. Craddock, *Cyclotrons*, in McGraw-Hill Encyclopedia of Science and Technology, 9<sup>th</sup> Edition (McGraw-Hill, New York, in press).

G.M. Kalvius, D.R. Noakes and O. Hartmann,  *$\mu\text{SR}$  studies of rare-earth and actinide magnetic materials*, in Handbook on the Physics and Chemistry of Rare Earths, Vol. 32, K.A. Gschneider Jr., L. Eyring and G.H. Lander, eds. (Elsevier Science B.V., 2001) p.55.

#### **Theses**

A. May, *An investigation of muon scattering off low Z materials* (B.Sc., Physics, University of Birmingham).

K. Babcock, *Third order low energy constants of heavy baryon chiral perturbation theory* (M.Sc., Physics, University of Regina).

J. Bland, *The TRIUMF E497 parity violation experiment in the 221 MeV  $\bar{p}p$  system: a complete analysis of the Feb97, Jul98 and May99 data runs* (M.Sc., Physics, University of Manitoba).

W. Liu, *Charge state studies of heavy ions passing through gas* (M.Sc., Physics, Simon Fraser University).

R.P. MacDonald, *Backgrounds for TWIST at TRIUMF* (M.Sc., Physics, University of Alberta).

M.F. White, Jr., *Numerical investigations of novel observed muon spin relaxation functions* (M.Sc., Chemistry and Physics, Virginia State University).

K. Horie, *Measurement of  $\Gamma(K_{\mu 3})/\Gamma(K_{e 3})$  using stopped positive kaons* (Ph.D., Graduate School of Science, Osaka University).

M. Milek, *Measurement of inclusive production of charmonium states at BaBar* (Ph.D., Physics, McGill University).

A.C. Morton, *The beta-delayed particle decay of  $^{17}\text{Ne}$*  (Ph.D., Physics, University of Toronto).

M.C. Trinczek, *Limits on heavy neutrino mixing from the beta decay of  $^{38m}\text{K}$  confined in a magneto-optical trap* (Ph.D., Chemistry, Simon Fraser University).

J. van Lierop, *Separation of static and dynamic disorder in magnetic materials* (Ph.D., Physics, McGill University).

**SEMINARS\***

The following seminars were presented at TRIUMF this year.

- 12/01 *The Strange World of the  $\pi$ -N Sigma Term*, Marcello Pavan, TRIUMF.  
 18/01 *Cold Neutrino Dark Matter*, Kev Abazajian, U. California, San Diego.  
 24/01 *Nucleon Dressing and Causality Constraints*, Sergey Kondratyuk, TRIUMF.  
 30/01 *Neutrino Flavour Transformation and Prospects for the r-Process in Core-Collapse Supernovae*, Mitesh Patel, U. California, San Diego.  
 31/01 *Next Linear Collider. The Path to Subnanometer Beams*, Andrei Seryi, SLAC.  
 01/02 *Hadrons in Nuclear Matter*, Abhee Dutt-Mazumder, McGill U.  
 08/02 *Determining Radioisotope Production in Novae from Laboratory Measurements Made at the ORNL HRIBF*, Dan Bardayan, ORNL.  
 12/02 *The Strong Isospin-Breaking (IB) Correction for  $\epsilon'/\epsilon$  at Next-to-Leading Order (NLO) in the Chiral Expansion*, Carl E. Wolfe, Indiana U.  
 15/02 *Extra Dimensions, SN1987a, and Nucleon-Nucleon Scattering Data*, Daniel Phillips, Ohio U.  
 20/02 *Nuclear Anapole Moment – A Manifestation of Nuclear Parity Nonconservation*, Cheng-Pang Liu, U. Washington.  
 22/02 *Mass Measurements at ISOLDE for Nuclear (Astro)physics*, David Lunney, CSNSM, U. de Paris Sud, Orsay.  
 26/02 *Recent Result from K2K Experiment, and a Proposal of the Second Generation Neutrino Oscillation Experiment with New JHF 50 GeV PS and Super-Kamiokande*, Tsuyoshi Nakaya, Kyoto U.  
 27/02 *Direct Mass Measurements of Exotic Nuclides with ISOLTRAP and SHIPTRAP*, Jens Dilling, GSI Darmstadt.  
 01/03 *Muon Properties and the Search for “New Physics”*, Andrzej Czarnecki, U. Alberta.  
 02/03 *Exotic Beam Coulomb Excitation*, Greg Hackman, U. Kansas.  
 08/03 *Breakup of Radioactive  $^{17}\text{F}$* , Felix Liang, ORNL.  
 13/03 *Explosive Nucleosynthesis Through  $^{22}\text{Mg}$* , Alan Chen, TRIUMF.  
 15/03 *Hard Virtual Photons: For Never a Dull Moment*, Andy Miller, TRIUMF.  
 20/03 *Electric Dipole Moments and the Mass Scale of T-Violating, P-Conserving New Physics*, Michael Ramsey-Musolf, U. Connecticut.  
 29/03 *A Precision Measurement of the Anomalous Magnetic Moment of the Muon: A Search for Physics Beyond the Standard Model*, Paul Debevec, U. Illinois at Urbana-Champaign.  
 05/04 *Fundamental Symmetries and Nuclear Beta Decay*, Andrew Hime, LANL.  
 19/04 *Variations on a Theme by Dirac: Magnetic Monopoles in Gauge Field Theories*, Ioan Popescu, U. Kentucky.  
 25/04 *Nuclear Astrophysics Program in the CNS-RIKEN Joint Venture*, Shigeru Kubono, CNS, U. Tokyo.  
 26/04 *Quark Matter in Neutron Stars*, Sanjay Reddy, INT, Seattle.  
 03/05 *Neutrino-Induced Muon Results from SNO*, Chris Waltham, UBC.  
 14/05 *Laser Spectroscopy of Long-Lived Lanthanum Isotopes*, Hans Schuessler, Texas A&M U.  
 22/05 *Does a Deeply Bound Kaonic State Exist?*, Masahiko Iwasaki, Tokyo Inst. Tech.  
 24/05 *Modelling of the Dopaminergic System with Positron Emission Tomography (PET)*, Vesna Sossi, TRIUMF.  
 21/06 *Solar Neutrino Results from SNO*, Richard Helmer, TRIUMF.  
 28/06 *Classical Novae: A Laboratory for Nuclear Astrophysics*, Jordi Jose, Polytechnical U. Catalonia/Inst. for Spatial Studies of Catalonia, Barcelona.  
 05/07 *Status of REX/ISOLDE*, Oliver Kester, CERN.  
 05/07 *The  $4\pi$  Detector for RIB Facility: Fragment Spectrometer FOBOS and its Applications*, Dmitri Kamanin, JINR, Dubna.  
 10/07 *Who, What, Where, When, Why, and How of Patent Law for Scientists and Engineers*, Donald Daley and Hrayr Sayadian, Birch, Stewart, Kolasch and Birch, LLP.  
 18/07 *MELPOMENE, a Measurement of Positron Longitudinal Polarization from Muon Decay*, Jules Deutsch, U. Catholique de Louvain.  
 19/07 *Detection of Short-Lived Nuclides as Probes of Nucleosynthesis*, Michael Paul, Hebrew U.  
 24/07 *Kaon Condensation in QCD*, Thomas Schaefer, SUNY at Stony Brook/RIKEN-BNL.  
 26/07 *Quasiparticle Excitation in the Mixed State of  $\text{MgB}_2$  Probed by  $\mu\text{SR}$* , Ryosuke Kadono, Inst. Materials Structure Science, KEK.  
 27/07 *Nickel, Iron and Gamma Ray Bursts*, Gail McLaughlin, SUNY at Stony Brook.  
 30/07 *Measurement of  $V_{ub}$  Using b Semileptonic Decay*, Jiansen Lu, UBC.  
 02/08 *Coulomb Gauge QCD, Confinement, and the Constituent Quark Model*, Eric Swanson, Pittsburg U./TJNAF.  
 23/08 *The Casimir Effect at Finite Temperature*, Ademir E. Santana, IF/UFBA, U. Federal da Bahia/Theoretical Phys. Inst., U. Alberta.



- 24/08 *The RIB Project at VECC Calcutta: A Status Report*, Alok Chakrabarti, VECC, Calcutta.  
 28/08  *$^8\text{Li}$ -NMR on  $^8\text{Li}$  Adsorbed on Metal and Semiconductor Single Crystal Surfaces*, Dieter Fick, Philipps U., Marburg.  
 06/09 *CP Violation from Compactification*, Darwin Chang, National Tsing Hua U., Taiwan/LBNL.  
 07/09 *Searching for Strangeness -2 Hypernuclei at BNL*, Charles Davis, TRIUMF.  
 13/09 *Recent Results from the Microscopic Schrödinger Optical Model*, Steven Karataglidis, LANL.  
 18/09 *Linear-Geometry Ion Traps: From Atomic Collisions to Sympathetic Laser Cooling of Molecules*, Robert I. Thompson, U. Calgary.  
 21/09 *Ultra-Trace Isotope Analysis by High-Resolution Triple-Resonance Ionization Mass Spectroscopy*, Bruce Bushaw, Pacific Northwest National Lab.  
 24/09 *The Status of Colour Transparency Below  $Q^2 \sim 10 \text{ GeV}^2/c^2$* , Ken Garrow, TJNAF.  
 03/10 *Heavy-Ion Linac Development for the U.S. RIA Project*, Peter N. Ostroumov, ANL.  
 05/10 *New Predictions with a Microscopic Model of p-Nucleus Scattering*, Ken Amos, U. Melbourne.  
 11/10 *Next Generation Long Baseline Neutrino Experiment*, Akira Konaka, TRIUMF.  
 15/10 *Doubly Strange Nuclear Systems and Beyond*, Avraham Gal, Hebrew U., Jerusalem.  
 17/10 *Nuclear Astrophysics: Observations – Stellar Models – Nucleosynthesis*, Falk Herwig, U. Victoria.  
 22/10 *The Past and Future of QCD*, Harry Lipkin, Weizmann Institute.  
 25/10 *Recent Results from Belle*, Asish Satpathy, U. Cincinnati.  
 06/11 *Latest Results on the Measurement of  $K^+ \rightarrow \pi^+ \nu \bar{\nu}$* , Joe Mildener, TRIUMF.  
 22/11 *Radiative Corrections to Polarized Muon Decay Spectrum*, Andrej Arbuzov, U. Alberta.  
 29/11 *Radioactive Beams and the Synthesis of Super-Heavy Elements*, Mark Stoyer, LLNL.  
 06/12 *Rare Weak K and B Decays*, Chao-Qiang Geng, National Tsing Hua U., Taiwan.

The following joint UBC/TRIUMF seminars were presented this year.

- 19/01 *Top Physics at the Tevatron*, Pierre Savard, U. Toronto.  
 25/01 *Tests of the Electroweak Gauge Theory at LEP2*, Alain Bellerive, U. Chicago.  
 02/02 *New Physics Searches with Photonic Final States at LEP2*, Peter Krieger, Carleton U.  
 08/11 *CP Violation: la Belle Époque*, Steve Olsen, U. Hawaii.

The following lunchtime seminars were presented at TRIUMF this year.

- 08/01 *TWISTING with F90*, Art Olin, TRIUMF.  
 09/03 *Developing an  $^{15}\text{O}$  Beam at TRIUMF*, Alex Zyuzin, TRIUMF.  
 02/04 *NALTA: A Vast Network of Cosmic Ray Air Shower Arrays*, Jim Pinfold, U. Alberta.  
 07/05 *The ATLAS Trigger: Challenges and Expected Performance*, Monika Wielers, TRIUMF.  
 26/06 *Neutron Spectra Unfolding Using a Genetic Algorithm*, Bhaskar Mukherjee, National Medical Cyclotron, Australia.  
 06/07 *Neutron Detection for Diagnosing Tokamak Plasmas*, Vitaly Kovaltchouk, Troitsk.

---

\* All matters concerning TRIUMF seminars should be referred via e-mail to seminar@triumf.ca

The latest listing of TRIUMF seminars can be seen at <http://www.triumf.ca/seminars/>

## USERS GROUPS

### TRIUMF USERS' GROUP

*From the TRIUMF Users' Group Charter:*

The TRIUMF Users' Group is an organization of scientists and engineers with special interest in the use of the TRIUMF facility. Its purpose is:

- (a) to provide a formal means for exchange of information relating to the development and use of the facility;
- (b) to advise members of the entire TRIUMF organization of projects and facilities available;
- (c) to provide an entity responsive to the representations of its members for offering advice and counsel to the TRIUMF management on operating policy and facilities.

Membership of the TRIUMF Users' Group (TUG) is open to all scientists and engineers interested in the TRIUMF program. At the end of 2001 the TUG had 265 members from 12 countries.

### TRIUMF Users' Executive Committee (TUEC)

The TRIUMF Users' Executive Committee (TUEC) is a committee of elected members whose role is to represent the interests of the TUG to the TRIUMF administration.

Among other things, TUEC maintains the TUG Web site at <http://www.triumf.ca/tug/> where detailed information is available about its membership, that of related committees, and various TUG activities.

### TUEC Membership for 2001

N. Rodning	U. Alberta	<i>Chair</i>
G.M. Luke	McMaster U.	<i>Chair-elect</i>
J.H. Brewer	UBC	<i>Past-chair</i>
R. Helmer	TRIUMF	2000/2001
A.K. Opper	Ohio U.	2000/2001
G.D. Morris	LANL	2001/2002
W.D. Ramsay	U. Manitoba	2001/2002
M. Comyn	TRIUMF	<i>Liaison Officer</i>

W.D. Ramsay (U. Manitoba) was elected as chair-elect for 2002. J.E. Sonier (SFU) was elected as a member for 2002; G.S. Hackman (TRIUMF) and M.M. Pavan (U. Regina/TRIUMF) were elected as members for 2002/2003.

In addition, TUEC selected two members to represent the Users on the TRIUMF Operating Committee: G.M. Marshall (TRIUMF) and G.M. Luke (McMaster U.) [replacing E. Mathie (U. Regina)] with alternates S. Yen (TRIUMF) and J.E. Sonier (SFU) [replacing G.M. Luke (McMaster U.)], respectively.

### $\mu$ SR USERS GROUP

Full details regarding the  $\mu$ SR Users Group and  $\mu$ SR facilities can be obtained via the WWW at <http://musr.triumf.ca/>.

## EXPERIMENT PROPOSALS

The following lists experiment proposals received up to the end of 2001 (missing numbers cover proposals that have been withdrawn or replaced by later versions, rejected, or combined with another proposal). Experiments 1–699 are omitted from this listing (except for those reporting results in this Annual Report). Please refer to the 1999 Annual Report or see <http://www.triumf.ca/annrep/experiments.html> for a full listing of these earlier experiments. Page numbers are given for those experiments which are included in this Annual Report.

- |      |  |           |
|------|--|-----------|
| 497. | Measurement of the flavour-conserving hadronic weak interaction [completed], A.R. Berdoz, J. Birchall, J. Bland, J.R. Campbell, A.A. Green, A.A. Hamian, L. Lee, S.A. Page, W.D. Ramsay, S.D. Reitzner, A.M. Sekulovich, V. Sum, W.T.H. van Oers, R.J. Woo ( <i>U. Manitoba</i> ), G.H. Coombes, C.A. Davis, R. Helmer, S. Kadantsev, C.D.P. Levy, T. Ries ( <i>TRIUMF</i> ), P.W. Green, G. Roy, J. Soukup, T. Stocki, G.M. Stinson ( <i>U. Alberta</i> ), J.D. Bowman, R.E. Mischke ( <i>Los Alamos Nat. Lab</i> ), Y. Kuznetsov, N.A. Titov, S. Zadorozhny, A.N. Zelenski ( <i>INR Moscow</i> )   | Page<br>5 |
| 614. | Precise measurement of the $\rho$ , $\sigma$ and $(P_{\mu\xi})$ parameters in muon decay [active], W. Andersson, C. Ballard, J. Doornbos, W. Faszer, A. Gaponenko, D.R. Gill, P. Gumplinger, R. Helmer, R. Henderson, B. Jamieson, D. Maas, J.A. Macdonald, G. Marshall, A. Olin, R. Openshaw, D. Ottewell, J.-M. Poutissou, R. Poutissou, G. Price, J. Schaapman, G. Sheffer, S.-C. Wang ( <i>TRIUMF</i> ), P. Depommier ( <i>U. Montréal</i> ), P. Green, P. Kitching, M. Quraan, R. MacDonald, N. Rodning, J. Soukup, G.M. Stinson ( <i>U. Alberta</i> ), M. Hasinoff ( <i>UBC</i> ), E.L. Mathie, R. Tacik ( <i>U. Regina</i> ), W. Shin ( <i>U. Saskatchewan</i> ), E. Korkmaz, T. Porcelli ( <i>UNBC</i> ) C. Gagliardi, J. Hardy, J. Musser, R. Tribble, M. Vasiliev ( <i>Texas A&amp;M U.</i> ), D. Koetke, P. Nord, S. Stanislaus ( <i>Valparaiso U.</i> ), Y. Davydov, A. Khurchinsky, V. Selivanov, V. Torokhov ( <i>KIAE, Moscow</i> )   | 11        |
| 700. | Measuring cross sections of long-lived radionuclides produced by 200–500 MeV protons in elements found in meteorites and lunar rocks [completed], J. Vincent ( <i>TRIUMF</i> ), J.M. Sisterson ( <i>Harvard U.</i> ), K. Kim ( <i>San Jose State U.</i> ), A.J.T. Jull ( <i>U. Arizona</i> ), M.W. Caffee ( <i>Lawrence Livermore National Lab</i> ), R.C. Reedy ( <i>Los Alamos Nat. Lab</i> )  |           |
| 702. | Measurement of kaon-nucleon elastic scattering at 16 MeV [active], G.A. Beer, P. Knowles, G.R. Mason, A. Olin, L.P. Robertson ( <i>U. Victoria</i> ), P. Amaudruz, D.R. Gill, G. Smith, S. Yen ( <i>TRIUMF</i> ), L. Lee ( <i>U. Manitoba</i> ), G. Tagliente ( <i>UBC</i> )   |           |
| 703. | Study of the decay $\pi^+ \rightarrow e^+ \nu$ phase I – lifetime measurement of the pion [completed], D.A. Bryman, T. Numaou, A. Olin ( <i>TRIUMF</i> )   |           |
| 704. | Charge symmetry breaking in $np \rightarrow d\pi^0$ close to threshold [completed data-taking], R. Abegg*, P.W. Green, D.A. Hutcheon ( <i>TRIUMF–U. Alberta</i> ), L.G. Greeniaus ( <i>U. Alberta–TRIUMF</i> ), R.W. Finlay, A.K. Opper, S.D. Reitzner ( <i>Ohio U.</i> ), E. Korkmaz, T.A. Porcelli ( <i>UNBC</i> ), J.A. Niskanen ( <i>U. Helsinki</i> ), P. Walden ( <i>TRIUMF–UBC</i> ), S. Yen ( <i>TRIUMF</i> ), C.A. Davis ( <i>TRIUMF–U. Manitoba</i> ), D.V. Jordan ( <i>Ohio U.–U. Alberta</i> ), E. Auld ( <i>UBC</i> )   | 38        |
| 705. | Development of modular gas microstrip chambers as in-target tracking devices for an experiment to detect $\Lambda\Lambda$ hypernuclei at the BNL AGS (BNL885) [completed data-taking], C.A. Davis ( <i>TRIUMF–U. Manitoba</i> ), B. Bassalleck, R. Stotzer ( <i>U. New Mexico</i> ), A.R. Berdoz, A. Biglan, D.S. Carman, G.B. Franklin, P. Khaustov, P. Koran, R. Magahiz, R. McCrady, C.A. Meyer, K. Paschke, B. Quinn, R.A. Schumacher, ( <i>Carnegie-Mellon U.</i> ), J. Birchall, L. Gan, M.R. Landry, L. Lee, S.A. Page, W.D. Ramsay, W.T.H. van Oers ( <i>U. Manitoba</i> ), T. Bürger, H. Fischer, J. Franz, H. Schmitt ( <i>U. Freiburg</i> ), D.E. Alburger, R.E. Chrien, M. May, P.H. Pile, A. Rusek, R. Sawafta, R. Sutter ( <i>Brookhaven National Lab</i> ), A. Ichikawa, K. Imai, Y. Kondo, K. Yamamoto, M. Yosoi ( <i>Kyoto U.</i> ), F. Takeuchi ( <i>Kyoto Sangyo U.</i> ), V.J. Zeps ( <i>U. Kentucky</i> ), P.D. Barnes, F. Merrill ( <i>Los Alamos Nat. Lab</i> ), V.J. Zeps ( <i>U. Kentucky</i> ), T. Iijima ( <i>KEK</i> ), J. Lowe ( <i>U. Birmingham</i> ) |           |
| 706. | $\mu$ SR studies of spin fluctuations in CePt <sub>2</sub> Sn <sub>2</sub> and other Kondo spin systems [completed], A. Keren, K. Kojima, G.M. Luke, Y.J. Uemura, W.D. Wu ( <i>Columbia U.</i> ), K. Andres, G.M. Kalvius ( <i>Tech. U. Munich</i> ), H. Fujii, G. Nakamoto, T. Takabatake, H. Tanaka ( <i>Hiroshima U.</i> ), M. Ishikawa ( <i>ISSP, U. Tokyo</i> ), B. Andraka ( <i>U. Florida</i> ), D.L. Cox ( <i>Ohio State U.</i> )  |           |
| 707. | $\mu$ SR measurements on two-dimensional site-diluted antiferromagnets [active], K. Kojima ( <i>Columbia U.–U. Tokyo</i> ), A. Keren, G.M. Luke, Y.J. Uemura, W.D. Wu ( <i>Columbia U.</i> ), H. Ikeda ( <i>KEK–KENS</i> ), R.J. Birgeneau ( <i>MIT</i> ), K. Nagamine ( <i>U. Tokyo</i> )   |           |
| 708. | The spin relaxation and chemical reactivity of muonium-substituted organic radicals in the gas phase [completed], D.G. Fleming, J.J. Pan, M. Shelley ( <i>UBC</i> ), D.J. Arseneau ( <i>TRIUMF–UBC</i> ), M. Senba ( <i>TRIUMF</i> ), J.C. Brodovitch, P.W. Percival ( <i>SFU</i> ), H. Dilger, E. Roduner ( <i>U. Zürich</i> ), S.F.J. Cox ( <i>Rutherford Appleton Lab</i> )   |           |

709.  $^{90,92,94,96}\text{Zr}(n,p)^{90,92,94,96}\text{Y}$  reaction at 200 MeV [completed data-taking], A.G. Ling, P.L. Walden (*TRIUMF*), J. Rapaport (*Ohio U.*), D.A. Cooper, D.L. Prout, E.R. Sugarbaker (*Ohio State U.*), M. Halbert (*Oak Ridge National Lab*), D. Mercer (*U. Colorado*), J. Campbell (*U. Manitoba-TRIUMF*), M. Hartig (*U. Muenster*)
710. Dynamics of muonium in Ge and GaAs [completed], R.L. Lichti (*Texas Tech. U.*), S.F.J. Cox (*Rutherford Appleton Lab*), R.F. Kiefl (*UBC*), K.H. Chow (*Lehigh U.*), T.L. Estle (*Rice U.*), B. Hitti (*TRIUMF*), E.A. Davis (*Leicester U.*), C.R. Schwab (*CNRS, Strasbourg*)
712.  $\mu\text{SR}$  study of superconducting spin glasses [completed], V. McMullen, D.R. Noakes, C.E. Stronach (*Virginia State U.*), E.J. Ansaldò (*U. Saskatchewan*), J.H. Brewer (*UBC*), G. Cao, J.E. Crow (*NHMFL*), S. McCall (*Florida State U.-NHMFL*)
713. Muonium chemistry in supercritical water [completed], B. Addison-Jones, J.-C. Brodovitch, K. Ghandi, I. McKenzie, P. Percival (*SFU*), J. Schüth (*U. Bonn*)
714. Atomic PNC in francium: preparations [inactive], J.A. Behr, L. Buchmann, M. Dombisky, P. Jackson, C.D.P. Levy (*TRIUMF*), J.M. D’Auria, P. Dubé, A. Gorelov, D. Melconian, T. Swanson, M. Trinczek (*SFU*), O. Häusser (*SFU-TRIUMF*), U. Giesen (*U. Alberta*), I. Kelson, A.I. Yavin (*Tel Aviv U.*), J. Deutsch (*U. Catholique de Louvain*), J. Dilling (*SFU-Heidelberg*)
715. Weak interaction symmetries in  $\beta^+$  decay of optically trapped  $^{37,38\text{m}}\text{K}$  [active], J.M. D’Auria, A. Gorelov, D. Melconian, M. Trinczek (*SFU*), G. Ball, J.A. Behr, P. Bricault, M. Dombisky, K.P. Jackson, B.K. Jennings (*TRIUMF*), S. Gu, M. Pearson (*UBC*), U. Giesen (*U. Notre Dame*), W.P. Alford (*U. Western Ontario*), J. Deutsch (*U. Catholique de Louvain*), D.A. Ashery, O. Aviv (*Tel Aviv U.*)
716. Complete beta-delayed particle emission study of  $^{31}\text{Ar}$  [deferred], J. Cerny, D.M. Moltz, T. Ognibene, M.W. Rowe, R.J. Tighe (*Lawrence Berkeley Lab*), L. Buchmann (*TRIUMF*), J. D’Auria (*SFU*), M. Dombisky (*SFU-U. Alberta*), G. Roy (*U. Alberta*)
717. Muon hyperfine transition rates in light nuclei [completed], J.H. Brewer, E. Gete, M.C. Fujiwara, J. Lange, D.F. Measday, B.A. Moftah, M.A. Saliba, T. Stocki (*UBC*), T.P. Gorringer (*U. Kentucky*)
718. Superconductivity and magnetism in quaternary boron carbides [completed], A. Keren, G.M. Luke, Y.J. Uemura, W.D. Wu (*Columbia U.*), K. Kojima (*Columbia U.-U. Tokyo*), S. Uchida (*U. Tokyo*)
719.  $^4\text{He}(\pi^+, \pi^- pp)$  invariant mass measurement with CHAOS [completed data-taking], P. Amaudruz, L. Felawka, D. Ottewell, G. Smith (*TRIUMF*), E.T. Mathie, R. Tacik, D.M. Yeomans (*U. Regina*), H. Clement, J. Gräter, R. Meier, G.J. Wagner (*U. Tübingen*), J. Clark, M. Seviør (*U. Melbourne*), A. Ambardar, G.J. Hofman, M. Kermani, G. Tagliente (*UBC*), F. Bonutti, P. Camerini, N. Grion, R. Rui (*U. di Trieste*), J. Brack, R. Ristinen (*U. Colorado*), E. Gibson (*California State U., Sacramento*), M. Schepkin (*ITEP Moscow*)
720. Muonium’s nucleophilicity [active], G.B. Porter, D.C. Walker (*UBC*), J.M. Stadlbauer\* (*Hood Coll.*), K. Venkateswaran (*Hindustan Lever Ltd.*), M.V. Barnabas (*Proctor & Gamble Ltd.*)
721. The delta nucleon reaction in CHAOS [completed data-taking], F. Farzanpay, P. Hong, E.L. Mathie, N. Mobed (*U. Regina*), R. Tacik (*TRIUMF-U. Regina*), P.A. Amaudruz, L. Felawka, R. Meier, D. Ottewell, G.R. Smith (*TRIUMF*), N. Grion (*INFN, Trieste*), P. Camerini, R. Rui (*U. di Trieste*), E. Gibson (*California State U., Sacramento*), G. Hofman, G. Jones, M. Kermani (*UBC*), M.E. Seviør (*U. Melbourne*), J.T. Brack, R.A. Ristinen (*U. Colorado*)
722. Pion initial state interactions in the  $^{12}\text{C}(\pi^+, ppp)$  reaction [completed data-taking], T. Mathie, R. Tacik (*U. Regina*), P.A. Amaudruz, L. Felawka, D. Ottewell, K. Raywood, G.R. Smith (*TRIUMF*), M. Kermani, S. McFarland (*UBC*), F. Bonutti, P. Camerini, R. Rui (*U. di Trieste*), N. Grion (*INFN, Trieste*), E.F. Gibson (*California State U., Sacramento*), M. Seviør (*U. Melbourne*), J. Brack, G. Hofman (*U. Colorado*), R. Meier (*U. Tübingen*)
723. Study of pion-nucleus double-scattering reactions [completed data-taking], R. Tacik (*TRIUMF-U. Regina*), T. Mathie (*U. Regina*), P. Amaudruz, L. Felawka, D. Ottewell, K. Raywood, G. Smith (*TRIUMF*), M. Kermani, S. McFarland (*UBC*), F. Bonutti, P. Camerini, R. Rui (*U. di Trieste*), N. Grion (*INFN, Trieste*), J. Brack, G. Hofman (*U. Colorado*), R. Meier (*U. Tübingen*), M. Seviør (*U. Melbourne*), E. Gibson (*California State U. Sacramento*)
724.  $\mu\text{SR}$  measurements on spin ladder systems [completed], A. Keren, G.M. Luke, Y.J. Uemura, W.D. Wu (*Columbia U.*), K. Kojima (*Columbia U.-U. Tokyo*), M. Takano (*Kyoto U.*), K. Nagamine (*U. Tokyo*)
725. Pion double charge exchange reactions on  $^3,4\text{He}$  in the energy range 50–100 MeV [completed], P. Amaudruz, L. Felawka, R. Meier, D. Ottewell, G. Smith (*TRIUMF*), T. Mathie, R. Tacik, M. Yeomans (*U. Regina*), J. Graeter, G. Wagner (*U. Tübingen*), J. Clark, M. Seviør (*U. Melbourne*), G. Hofman, M. Kermani, P. Tagliente (*UBC*), F. Bonutti, P. Camerini, N. Grion, R. Rui (*U. di Trieste*), J. Brack, R. Ristinen (*U. Colorado*), E. Gibson (*California State U., Sacramento*), O. Patarakin (*Kurchatov Inst.*), E. Friedman (*Hebrew U. Jerusalem*)

726. Beta-delayed proton and  $\gamma$ -decay of  $^{65}\text{Se}$ ,  $^{69}\text{Kr}$  and  $^{73}\text{Sr}$  [active], D. Anthony, J. D'Auria, M. Trinczek (*SFU*), R.E. Azuma, J.D. King (*U. Toronto*), L. Buchmann, K.P. Jackson, J. Vincent (*TRIUMF*), M. Domsbky (*SFU-U. Alberta*), U. Giesen (*TRIUMF-U. Alberta*), J. Görres, H. Schatz, M. Wiescher (*U. Notre Dame*), C. Iliadis (*TRIUMF-U. Toronto*), G. Roy (*U. Alberta*)
728. Search for population and de-excitation of low-spin superdeformed states in Po-Hg region via  $\beta^+$  and  $\alpha$  decays [completed data-taking], Y.A. Akovali, M. Brinkman (*Oak Ridge National Lab*), J.M. D'Auria (*TRIUMF-SFU*), J.A. Becker, E.A. Henry (*Lawrence Livermore National Lab*), M. Domsbky (*SFU*), P.F. Mantica (*UNISOR*), W. Nazarewicz (*Joint Inst. for Heavy Ion*), J. Rikowska, N.J. Stone (*Oxford U.*), M.A. Stoyer (*Lawrence Berkeley National Lab*), R.A. Wyss (*MSI, Sweden*)
729. Gamow-Teller and spin-dipole strengths from  $^{17,18}\text{O}(n,p)$  [completed data-taking], D.P. Beatty, H.T. Fortune, P.P. Hui, R.B. Ivie, Z.Q. Mao, M.G. McKinzie, D.A. Smith (*U. Pennsylvania*), W.P. Alford (*U. Western Ontario*), K.P. Jackson, A.G. Ling, C.A. Miller, P. Walden, S. Yen (*TRIUMF*)
730. The solar neutrino problem and a new measurement of  $^7\text{Be}(p,\gamma)^8\text{B}$  [deferred], R.E. Azuma, J.D. King (*U. Toronto*), P. Bricault, L. Buchmann, T. Ruth, H. Schneider, J. Vincent, S. Zeisler (*TRIUMF*), J. D'Auria, R. Korteling (*SFU*), M. Domsbky (*SFU-U. Alberta*), U. Giesen (*TRIUMF-U. Alberta*), C. Iliadis (*TRIUMF-U. Toronto*), G. Roy (*U. Alberta*), M. Wiescher (*U. Notre Dame*)
731. Investigation of spin-polarized muonium in metallic semiconductors [completed], K.H. Chow, S. Dunsiger, R.F. Kiefl, W.A. MacFarlane, J. Sonier (*UBC*), S.F.J. Cox (*Rutherford Appleton Lab*), E.A. Davis, A. Singh (*Leicester U.*), T.L. Estle, B. Hitti (*Rice U.*), R.L. Lichti (*Texas Tech. U.*), P. Mendels (*Orsay U.*), C. Schwab (*CRN, Strasbourg*)
732. Quantum impurities in one dimensional spin 1/2 chains [completed], I. Affleck, J.H. Brewer, K. Chow, S. Dunsiger, S. Eggert, R.F. Kiefl, A. MacFarlane, J. Sonier (*UBC*), A. Keren, Y.J. Uemura (*Columbia U.*)
733. Probing high  $T_c$  superconductor with “paramagnetic” ( $\mu^- \text{O}$ ) system [active], H. Kojima, I. Tanaka, E. Torikai (*Yamanashi U.*), K. Nishiyama (*U. Tokyo*), K. Nagamine (*U. Tokyo-RIKEN*), I. Watanabe (*RIKEN*), T.P. Das (*State U. New York*), S. Maekawa (*Nagoya U.*)
734. Radiative muon capture on nickel isotopes [completed], D.S. Armstrong, P. McKenzie (*Coll. of William & Mary*), G. Azuelos, P. Depommier (*U. de Montréal*), P. Bergbusch, P. Gumpfinger, M. Hasinoff, E. Saettler (*UBC*), B. Doyle, T.P. Gorringer, R. Sedlar (*U. Kentucky*), M. Blecher, C. Sigler (*Virginia Polytechnic Inst.*), J.A. MacDonald, J.-M. Poutissou, R. Poutissou, D. Wright (*TRIUMF*)
735. Studies of single layer cuprate superconductors [completed], G.M. Luke, B. Nachumi, Y.J. Uemura (*Columbia U.*), K. Kojima (*Columbia U.-U. Tokyo*), S. Uchida (*U. Tokyo*), R.H. Heffner, L.P. Le (*Los Alamos Nat. Lab*), R. MacLaughlin (*U. California, Riverside*), M.B. Maple (*U. California, San Diego*)
736. Tests of electro-weak theory using  $^{14}\text{O}$  beam [deferred], M. Bahtacharya, A. Garcia, R. Rutchi, M. Wayne (*U. Notre Dame*), L. Buchmann (*TRIUMF*), C. Iliadis (*TRIUMF-U. Toronto*), B. Fujikawa (*Lawrence Berkeley Lab.*), S.J. Freedman, J. Mortara (*U. California, Berkeley*)
737. Magnetic and superconducting behaviour in selected oxide materials [completed], R.H. Heffner, L.P. Le (*Los Alamos Nat. Lab*), D.E. Maclaughlin (*U. California, Riverside*), G. Luke, B. Nachuma, Y.J. Uemura (*Columbia U.*), K. Kojima (*Columbia U.-U. Tokyo*)
740. Irradiation of silicon tracker components [completed], R. Lipton, L. Spiegel (*Fermilab*), K.F. O'Shaughnessy (*U. California, Santa Cruz*), B. Barnett, J. Cameratta, J. Skarha (*Johns Hopkins U.*), N. Brunner, M. Frautschi, M. Gold, Y. Ling, J. Matthews, S. Seidel (*U. New Mexico*), D. Bortoletto, A. Garfinkel, A. Hardman, K. Hoffman, T. Keaffaber, N.M. Shaw (*Purdue U.*)
741. Beta-delayed proton decay of  $^{17}\text{Ne}$  to  $\alpha$ -emitting states in  $^{16}\text{O}$  [completed], R.E. Azuma, J. Chow, J.D. King, A.C. Morton (*U. Toronto*), L. Buchmann, M. Domsbky (*TRIUMF*), U. Giesen (*U. Notre Dame*), T. Davinson, A.C. Shotter (*U. Edinburgh*), R.N. Boyd (*Ohio State U.*), C. Iliadis (*U. North Carolina*), J. Powell (*U. California, Berkeley*),
742. Scattering of muonic hydrogen isotopes [completed], V.M. Bystritsky, V.A. Stolupin (*JINR*), R. Jacot-Guillarmod, P.E. Knowles, F. Mulhauser (*U. Fribourg*), G.M. Marshall (*TRIUMF*), M. Filipowicz, J. Wozniak (*Fac. Phys., Nucl. Tech., Krakow*), A. Adamczak (*Inst. Nucl. Physics, Krakow*), A.R. Kunselman (*U. Wyoming*), V.E. Markushin, C. Petitjean (*PSI*), T.M. Huber (*Gustavus Adolphus Coll.*), G.A. Beer, M. Maier, A. Olin, T.A. Porcelli (*U. Victoria*), P. Kammel (*U. California, Berkeley*), M.C. Fujiwara (*UBC*), J. Zmeskal (*IMEP Vienna*), S.K. Kim (*Jeonbuk National U.*)
743. Gamow-Teller strength in  $^{64,66,68}\text{Zn}$  and  $^{63,65}\text{Cu}(n,p)$  [completed data-taking], W.P. Alford (*U. Western Ontario*), D. Beatty, H.T. Fortune, P.P. Hui, R.B. Ivie, Z. Mao, M.G. McKinzie, D.A. Smith (*U. Pennsylvania*), S. Yen (*TRIUMF*)

744. Hadronic weak and electromagnetic form factors via  $\pi^- p \rightarrow e^+ e^- n$  [active], P. Gumplinger, M.D. Hasinoff (*UBC*), E. Christy, B.C. Doyle, T.P. Gorringer, M.A. Kovash, S. Tripathi, P. Zolnierchuk (*U. Kentucky*), D.H. Wright (*SLAC*)
745.  $\mu^-$ SR measurements on one-dimensional spin systems [active], K. Kojima (*Columbia U.-U. Tokyo*), K. Nagamine, K. Nishiyama, S. Uchida (*U. Tokyo*), G.M. Luke, B. Nachumi, Y.J. Uemura (*Columbia U.*), I. Affleck, S. Dunsiger, S. Eggert, R.F. Kiefl (*UBC*)
746. Muonium dynamics in Si, Ge and GaAs studied by RF- $\mu$ SR and  $\mu$ W- $\mu$ SR [active], S.R. Kreitzman (*TRIUMF*), T.L. Estle, B. Hitti (*Rice U.*), R. Lichti (*Texas Tech.*), K. Chow (*UBC*), S.F.J. Cox (*Rutherford Appleton Lab*), E.A. Davis (*Leicester U.*), C. Schwab (*CRN Strasbourg*)
747.  $\mu$ SR study of re-entrant spin glasses a-FeMn, AuFe, and Fe<sub>70</sub>Al<sub>30</sub> [completed], I.A. Campbell (*U. Paris Sud Orsay*), S. Dunsiger, R.F. Kiefl (*UBC*), M.J.P. Gingras (*TRIUMF*), M. Hennion, I. Mirebeau (*Saclay, LLB*), K. Kojima, G.M. Luke, B. Nachumi, Y.J. Uemura, W.D. Wu (*Columbia U.*)
749. Muonium-substituted free radicals [completed], B. Addison-Jones, J.C. Brodovitch, K. Ghandi, I. McKenzie, P.W. Percival (*SFU*), J. Schüth (*U. Bonn*)
750. Liquid chemistry  $\mu$ SR [completed], G.B. Porter, D.C. Walker (*UBC*), J.M. Stadlbauer\* (*Hood Coll.*), K. Venkateswaran (*Lever Hindustan Ltd.*), M.V. Barnabas *Procter & Gamble Ltd.*)
751. Tests in preparation for  $\mu$ SR measurements of off-axis internal magnetic fields in anisotropic superconductors [active], E. Csomortani, W.J. Kossler, X. Wan (*Coll. of William & Mary*), D.R. Harshman (*Physikon Research Inc.*), A. Greer (*Gonzaga U.*), E. Koster, D.L. Williams (*UBC*), C.E. Stronach (*Virginia State U.*)
752. Muonium centres in Si and GaAs [completed], K.H. Chow (*Oxford U.*), S.F.J. Cox (*Rutherford Appleton Lab*), E.A. Davis (*Leicester U.*), S. Dunsiger, R.F. Kiefl, W.A. MacFarlane (*UBC*), T.L. Estle (*Rice U.*), B. Hitti (*TRIUMF*), R.L. Lichti (*Texas Tech.*), C. Schwab (*CRN Strasbourg*)
753. Studies of magnetic correlations in planar oxides [completed], K. Kojima (*Columbia U.-U. Tokyo*), M. Larkin, G.M. Luke, J. Merrin, B. Nachumi, Y.J. Uemura (*Columbia U.*), B.J. Sternlieb (*Brookhaven Nat. Lab*), S. Uchida (*U. Tokyo*)
754. A search for the muonium substituted hydroxyl radical [deferred], T.A. Claxton, G. Marston (*Leicester U.*), S.F.J. Cox (*Rutherford Appleton Lab*), D. Arseneau, D. Fleming, M. Senba, P. Wassell (*UBC*), J.-C. Brodovitch, P.W. Percival (*SFU*)
755. Muonium formation in Zn-spinels [deferred], G.M. Kalvius, A. Kratzer, W. Potzel (*Tech. U. Munich*), R. Wäppling (*U. Uppsala*), D.R. Noakes (*Virginia State U.*), S.R. Kreitzman (*TRIUMF*), A. Martin (*U. Jena*), M.K. Krause (*U. Leipzig*)
756. Mu+NO spin relaxation: electron exchange or paramagnetism? [deferred], D.G. Fleming, J.J. Pan, M. Senba, M. Shelley (*UBC*), D.J. Arseneau (*TRIUMF*), E. Roduner (*U. Zürich*)
757. Study of muon dynamics in ferroelectric materials and proton ionic conductors – comparison with proton dynamics [completed], W.K. Dawson, K. Nishiyama, S. Ohira, K. Shimomura (*U. Tokyo*), K. Nagamine (*U. Tokyo-RIKEN*), S. Ikeda (*KEK*), S. Shin (*U. Tokyo-ISSP*), N. Sata (*Tohoku U.*)
758. Electronic structure of muonium and muonium-lithium complexes in graphite and related compounds [completed], J. Brewer, J. Chakhalian, S. Dunsiger, R.F. Kiefl, W.A. MacFarlane, R. Miller, J. Sonier (*UBC*), J. Dahn (*Dalhousie U.*), J. Fischer (*U. Pennsylvania*), B. Hitti, S.R. Kreitzman (*TRIUMF*)
759. Study of the isotropic hyperfine coupling constant of muonium at high temperature and under uniaxial pressure [completed], W.K. Dawson, K. Nishiyama, S. Ohira, K. Shimomura (*U. Tokyo*), K. Nagamine (*U. Tokyo-RIKEN*), T.P. Das (*U. New York, Albany*)
761. Parity violation in  $p-p$  scattering at 450 MeV [deferred], J. Birchall, C.A. Davis, L. Lee, S.A. Page, W.D. Ramsay, A.W. Rauf, G. Rutledge, W.T.H. van Oers (*U. Manitoba*), R. Helmer, R. Laxdal, C.D.P. Levy (*TRIUMF*), P.W. Green, G. Roy, G.M. Stinson (*U. Alberta*), N.A. Titov, S. Zadorozhny, A.N. Zelenski (*INR, Moscow*), J.D. Bowman, R.E. Mischke, S. Penttila, W.S. Wilburn (*Los Alamos Nat. Lab*), E. Korkmaz, (*UNBC*), M. Simonius (*ETH Zürich*), J. Bisplinghoff, P.D. Eversheim, F. Hinterberger (*U. Bonn*), W. Kretschmer, G. Morgenroth (*U. Erlangen*), H. Schieck (*U. Cologne*), P. von Rossen (*KFA Jülich*)
762. Gamow-Teller and spin-flip dipole strengths near  $A=90$  [completed data-taking], W.P. Alford (*U. Western Ontario*), D.P. Beat-ty, H.T. Fortune, P.P. Hui, R.B. Ivie, D. Koltenuk, J. Yu (*U. Pennsylvania*), A. Ling, S. Yen (*TRIUMF*), S. El-Kateb (*King Fahd U.*)
763. Muon cooling and acceleration in an undulating crystal channel [deferred], S.A. Bogacz, D.B. Cline, D.A. Sanders (*UCLA*), L.M. Cremaldi, B. Denardo, Q. Jie, D.J. Summers (*U. Mississippi-Oxford*), G.M. Marshall (*TRIUMF*)

764. Calibration of a segmented neutron detector [completed], E. Korkmaz, G. O’Rielly (*UNBC*), D.A. Hutcheon (*TRIUMF*), A.K. Opper (*U. Alberta*), G. Feldman, N.R. Kolb (*U. Saskatchewan*)
766. The ortho-para transition rate in muonic molecular hydrogen [completed data-taking], D.S. Armstrong, J.H.D. Clark, P. King (*Coll. of William & Mary*), T.P. Gorringer, S. Tripathi, P.A. Żolnierczuk (*U. Kentucky*), M.D. Hasinoff, T. Stocki (*UBC*), D.H. Wright (*TRIUMF*)
767. Direct measurement of sticking in muon catalyzed  $d - t$  fusion [inactive], J.M. Bailey (*Chester Technology, UK*), G.A. Beer, M. Maier, G.R. Mason, T.A. Porcelli (*U. Victoria*), K.M. Crowe, P. Kammel (*U. California, Berkeley-LBL*), M.C. Fujiwara, E. Gete, T.J. Stocki (*UBC*), T.M. Huber (*Gustavus Adolphus Coll.*), S.K. Kim (*Jeonbuk National U.*), A.R. Kunselman (*U. Wyoming*), G.M. Marshall, A. Olin (*TRIUMF*), C.J. Martoff (*Temple U.*), V.S. Melezhik (*JINR, Dubna*), F. Mulhauser (*U. Fribourg*), C. Petitjean (*PSI*), J. Zmeskal (*IMEP Vienna*)
768. Generalized Fulde-Ferrell-Larkin-Ovchinnikov state in heavy fermion and intermediate valence systems [active], J. Akimitsu, K. Oishi, H. Takagiwa, T. Yokoo (*Aoyama Gakuin U.*), W. Higemoto, R. Kadono, A. Koda (*KEK-IMSS*), M. Nohara (*U. Tokyo*), M. Hedo (*Ryukyuu U.*), Y. Onuki (*Osaka U.*)
769. Effects of uniaxial stress on muonium in semiconductors [completed], K.H. Chow (*Oxford*), B. Hitti (*TRIUMF*), R.F. Kiefl (*UBC*), T.L. Estle (*Rice U.*), R. Lichti (*Texas Tech. U.*)
770.  $\mu$ SR studies of organic conductors:  $(\text{BEDT-TTF})_2\text{-X}$  and  $(\text{TMTTF})_2\text{Br}$  [completed], K. Kojima, M. Larkin, G.M. Luke, J. Merrin, B. Nachumi, Y.J. Uemura (*Columbia U.*), P.M. Chaikin (*Princeton U.*), G. Saito (*Kyoto U.*)
771.  $\mu$ SR studies of geometrically frustrated  $S = 1/2$  spin systems [completed], K. Kojima, M. Larkin, G.M. Luke, J. Merrin, B. Nachumi, Y.J. Uemura (*Columbia U.*), M.J.P. Gingras (*TRIUMF*), S. Dunsiger, R.F. Kiefl (*UBC*), D.C. Johnston, S. Kondo (*Iowa State U.*), S. Uchida (*U. Tokyo*), R.J. Cava (*AT&T Bell Labs*)
772. Search for the  $\Delta - \Delta$  dibaryon [inactive], R. Abegg\*, C.A. Miller, P. Walden, S. Yen (*TRIUMF*), R. Bent (*Indiana U.*), T.Y. Chen, F. Wang, C.H. Ye (*Nanjing U.*), W. Falk (*U. Manitoba*), D. Frekers, M. Hartig (*U. Muenster*), T. Goldman (*Los Alamos Nat. Lab*), M. Heyrat, C.W. Wong (*UCLA*), G. Jones (*UBC*), E. Korkmaz, G. O’Rielly (*UNBC*), C. Rangacharyulu (*U. Saskatchewan*), I. Strakovsky (*Virginia Tech. Inst.*), Z.X. Sun, J.C. Xu (*Inst. Atomic Energy, China*), T. Walton (*Cariboo U. Coll.*)
773. Muon-electron interaction in  $n$ -type silicon [completed], D. Arseneau, B. Hitti, S.R. Kreitzman (*TRIUMF*), J.H. Brewer, R.F. Kiefl, G. Morris (*UBC*), K. Chow (*Oxford U.*), S.F.J. Cox (*Rutherford Appleton Lab*), D.G. Eshchenko (*INR, Moscow*), T.L. Estle (*Rice U.*), R. Lichti (*Texas Tech. U.*), V.G. Storchak, (*Kurchatov Inst.*)
774. Muonium dynamics in GaAs studied by rf and  $\mu$ -wave  $\mu$ SR [active], B. Hitti, S.R. Kreitzman (*TRIUMF*), T.L. Estle (*Rice U.*), R. Lichti (*Texas Tech. U.*)
775. Electron transport in insulators, semiconductors and magnetic materials [active], J.H. Brewer, A. Izadi, D.M.C. Liu, K.M. Nichol, S. Sivanandam, A.T. Warkentin (*UBC*), G.D. Morris (*TRIUMF*), V.G. Storchak (*Kurchatov Inst.*), D.G. Eshchenko (*INR, Moscow*), J.D. Brewer (*SFU*)
776. Rare earth materials with disordered spin structures [completed], J.H. Brewer (*UBC*), K. Fukamichi (*Tohoku U.*), G.M. Kalvius (*Tech. U. Munich*), D.R. Noakes, C.E. Stronach (*Virginia State U.*), R. Wäppling (*Uppsala U.*)
777. Vortex state of  $s$ -wave superconductors investigated by muon spin rotation [active], J.C. Chakhalian, K. Chow, R. Miller, A.N. Price (*UBC*), J.H. Brewer, R.F. Kiefl (*UBC-TRIUMF*), G.M. Luke (*McMaster U.*), J.E. Sonier (*SFU*)
778.  $\pi^\pm p$  differential cross sections in the Coulomb-nuclear interference region [completed data-taking], P. Amaudruz, D. Ottewell, (*TRIUMF*), P. Camerini, E. Fragiaco, N. Grion, S. Piano, R. Rui (*U. di Trieste*), K. Babcock, E. Mathie, H. Xu, D.M. Yeomans (*U. Regina*), G. Hofman, M.M. Pavan, K.J. Raywood, R. Tacik (*Regina-TRIUMF*), J. Breitschopf, H. Denz, R. Meier, F. von Wrochem, G. Wagner (*U. Tübingen*), G. Moloney, M. Sevir (*U. Melbourne*), J. Brack, J. Patterson, R. Ristinen (*U. Colorado*), E. Gibson (*California State U., Sacramento*), O. Patarakin (*Kurchatov Inst.*), G. Smith (*Jefferson Lab*)
779. Accelerator mass spectrometry experiments at ISAC [inactive], S. Calvert, A. Glass, R.R. Johnson, T. Petersen (*UBC*), Z. Gelbart, D. Ottewell (*TRIUMF*), R. Schubank (*unaffiliated*), C.S. Wong (*Inst. of Ocean Sciences*), J. Clague (*Geological Survey Canada*), M. Paul (*Hebrew U. Jerusalem*)
780. Deeply bound pionic states through  $^{208}\text{Pb}(p, ^3\text{He})^{206}\text{Pb} \otimes \pi^-$  [completed], D. Frekers, W. Garske, K. Grewer, M. Hartig, H. Wörtche (*U. Muenster*), H. Machner (*KFA, Jülich*), D. Hutcheon, P. Walden, S. Yen (*TRIUMF*), A. Opper (*U. Ohio*)

63

65

45

781. Investigations of the  $\pi\pi$  invariant mass distributions of nuclear ( $\pi^+$ ,  $\pi^-\pi^+$ ) reactions with the CHAOS detector [completed data-taking], J. Clark, G. Moloney, M.E. Seviour (*U. Melbourne*), G. Hofman (*UBC-U. Colorado*), M. Kermani, S. McFarland, K. Raywood (*UBC*), P. Amaudruz, L. Felawka, D.F. Ottewell, G.R. Smith (*TRIUMF*), R. Meier (*TRIUMF-U. Tübingen*), F. Bonutti, P. Camerini, E. Fragiaco, R. Rui (*INFN, Trieste-U. Trieste*), N. Grion (*INFN, Trieste*), E.L. Mathie, R. Tacik, (*U. Regina*), J. Brack (*TRIUMF-U. Colorado*), R.A. Ristinen (*U. Colorado*), E. Gibson (*California State U., Sacramento*), J. Graeter, G. Wagner (*U. Tübingen*), V. Mayorov, O. Patarakin, V. Tikhonov (*Kurchatov Inst.*)
782. Non-fermi-liquid behaviour and other novel phenomena in heavy-fermion alloys [active], D.E. MacLaughlin (*U. California, Riverside*), R.H. Heffner (*Los Alamos Nat. Lab*), Y.J. Uemura (*Columbia U.*), M.B. Maple (*U. California, San Diego*), O.O. Bernal (*Cal. State U., Los Angeles*), G.M. Luke (*McMaster U.*), J.E. Sonier (*SFU*), B. Andraka, G.R. Stewart (*U. Florida*) 66
783. Paramagnetic frequency shifts in unconventional superconductors [active], R.H. Heffner, G.D. Morris (*Los Alamos Nat. Lab*), D.E. MacLaughlin (*U. California, Riverside*), G.J. Nieuwenhuys (*U. Leiden*), O.O. Bernal (*Cal. State U., Los Angeles*), J.E. Sonier (*SFU*) 68
784.  $\mu$ SR studies of spin singlet states in oxides [active], A. Fukaya, I. Gat, M. Larkin, A. Savici, Y.J. Uemura (*Columbia U.*), T. Ito (*Columbia U.-ETL*), H. Kageyama, K. Ueda, Y. Ueda (*U. Tokyo*), P.P. Kyriakou, G.M. Luke, M.T. Rovers (*McMaster U.*) 69
785. Pion double charge exchange on  $^3\text{He}$  with CHAOS [completed data-taking], R. Tacik (*TRIUMF-U. Regina*), E.L. Mathie, M. Yeomans (*U. Regina*), H. Clement, J. Graeter, R. Meier, J. Petzold, G.J. Wagner (*U. Tübingen*), E. Friedman (*Hebrew U. Jerusalem*), N. Grion (*INFN Trieste*), P. Camerini, E. Fragiaco, R. Rui (*U. Trieste*), L. Felawka, D. Ottewell, K. Raywood, G.R. Smith (*TRIUMF*), G. Hofman, B. Jamieson, G. Tagliente (*UBC*), J. Clark, G. Molony, M.E. Seviour (*U. Melbourne*), E. Gibson (*California State U. Sacramento*), H. Staudenmeyer (*U. Karlsruhe*), S. Filippov, Y. Gavrillov, T. Karavicheva (*Moscow Meson Factory*)
786. Low energy structures in the  $\beta$ -delayed particle decays of  $^9\text{C}$ ,  $^{12}\text{N}$  and  $^{17}\text{Ne}$  [completed data-taking], N. Bateman (*TRIUMF-SFU-U. Toronto*), L. Buchmann, K.P. Jackson, T. Shoppa (*TRIUMF*), J. Chow, J.D. King, C. Mortin (*U. Toronto*), T. Davison, A. Ostrowski, A. Shotter (*U. Edinburgh*), J. D'Auria (*SFU*), E. Gete, D. Measday (*UBC*), U. Giesen (*U. Alberta*)
788. Nuclear and atomic physics with the CPT spectrometer [inactive], B. Barber, K.S. Sharma (*U. Manitoba*), X. Feng (*U. Manitoba-McGill U.*), F. Buchinger, J. Crawford, S. Gulick, J. Lee, B. Moore (*McGill U.*), E. Hagberg, J. Hardy, V. Koslowsky, G. Savard (*Chalk River Nuclear Lab*)
789.  $\mu$ SR studies of magnetic fluctuations in hydronium jarosites, model Kagomé antiferromagnets [completed], A. Harrison, A.S. Wills (*U. Edinburgh*), Y. Fudamoto, K. Kojima, M. Larkin, G.M. Luke, J. Merrin, B. Nachumi, Y.J. Uemura (*Columbia U.*), T. Mason (*U. Toronto*)
790.  $\mu$ SR studies of stripe order in  $\text{La}_{1.6-x}\text{Sr}_x\text{Nd}_{0.4}\text{CuO}_4$  modified cuprate superconductors [completed], Y. Fudamoto, K. Kojima, M. Larkin, G.M. Luke, J. Merrin, B. Nachumi, Y.J. Uemura (*Columbia U.*), M. Crawford (*Du Pont*), A. Moodenbaugh (*Brookhaven National Lab*), S. Uchida (*U. Tokyo*)
791. Electronic structure and dynamics of charged muonium and muonium-dopant centers in semiconductors [active], K.H. Chow (*Oxford U.*), R.F. Kiefl (*UBC*), B. Hitti (*TRIUMF*), T.L. Estle (*Rice U.*), R. Lichti (*Texas Tech. U.*), S.F.J. Cox (*Rutherford Appleton Lab*), C. Schwab (*CRN, Strasbourg*) 69
792. Muonium in III-V semiconductors: identification of states and transitions [completed], K.H. Chow (*Oxford U.*), S.F.J. Cox (*Rutherford Appleton Lab*), B. Hitti (*TRIUMF*), T.L. Estle (*Rice U.*), R.L. Lichti (*Texas Tech. U.*), C. Schwab (*CRN, Strasbourg*)
793. Production of an intense  $^{15}\text{O}$  beam for ISAC [completed], J. D'Auria, R. Lange (*SFU*), M. Domsbky, T. Ruth, J. Vincent (*TRIUMF*), K. Carter (*Oak Ridge National Lab*), B. Zhuikov (*INR, Moscow*)
794.  $\mu^+$ SR study on the magnetic properties of  $\text{LaCoO}_3$  and  $\text{La}_{1-x}\text{Sr}_x\text{CoO}_3$  [completed], V.V. Krishnamurthy, I. Watanabe (*RIKEN*), K. Asai, N. Yamada (*U. Electro-communications*), K. Nagamine (*U. Tokyo-RIKEN*)
795.  $\mu$ SR study on non fermi liquid behaviour [completed], Y. Miyako, Y. Yamamoto (*Osaka U.*), S. Murayama (*Muroran Inst. Tech.*), K. Nagamine (*U. Tokyo*), K. Nishiyama (*U. Tokyo-RIKEN*)
796.  $\mu$ SR studies in ionic crystals doped with either colour centres or impurity [deferred], Y. Miyake, K. Nagamine, K. Nishiyama, K. Shimomura (*U. Tokyo*), A. Matsusita (*RIKEN*)
797. Magnetic correlations in the ternary equiatomic Ce compounds  $\text{CeTSn}$  [completed], G. Grosse, G.M. Kalvius A. Kratzner (*Tech. U. Munich*), R. Wäppling (*U. Uppsala*), T. Takabatake (*Hiroshima U.*), D.R. Noakes, C.R. Stronach (*Virginia State U.*), Y. Echizen (*Hiroshima U.*), H. Nakotte (*New Mexico State U.*), H.v. Löhneysen (*U. Karlsruhe*)



798.  $\mu$ SR studies on the competition of RKKY exchange and Kondo effect in  $\text{CeT}_2\text{X}_2$  compounds (T=transition metal, X=Si,Ge) [completed], H.-H. Klauss, W. Kopmann, F.J. Litterst, W. Wagener, H. Walf (*Tech. U. Braunschweig*), E. Baggio Saitovitch, M.B. Fontes (*CBPF Rio de Janeiro*), A. Krimmel, A. Loidl (*U. Augsburg*)
799. Hyperfine structure and site determination of ( $\mu^-$ O) system in  $\text{LaSuCuO}$  high  $T_c$  superconductors [completed], H. Kojima, I. Tanaka, E. Torikai (*Yamanashi U.*), K. Nishiyama (*U. Tokyo-RIKEN*), K. Nagamine, K. Shimomura (*U. Tokyo*), I. Watanabe (*RIKEN*), T.P. Das (*State U. New York*)
801. Studies of multi-phonon states via  $\beta$ -decay [completed data-taking], C.J. Barton, M.A. Caprio, R.F. Casten, N.V. Zamfir (*Yale U.*), D.S. Brenner (*Clark U.*), G.C. Ball, K.P. Jackson (*TRIUMF*)
802. Superdeformation and smooth band termination on and near the  $N = Z$  line: Part 1  $^{60}\text{Zn}$  [active], J.A. Cameron, S. Flibotte, D.S. Haslip, J. Nieminen, C. Svensson, J.C. Waddington, J.N. Wilson (*McMaster U.*), G. Ball (*TRIUMF*), A. Galindo-Uribarri, D.C. Radford (*Oak Ridge National Lab*), D. Ward (*Lawrence Berkeley National Lab*)
803. Experimental studies of interaction and properties of neutron-rich nuclei at ISAC [inactive], A.S. Iljinov, A.V. Klyachko, E.S. Konobeevsky, M.V. Morodovskoy, M.A. Prohvatilov, A.I. Reshetin, Yu.V. Ryabov, K.A. Shileev, V.A. Simonov, V.M. Skorkin, S.V. Zuyev (*INR, Moscow*)
804. Muonium in gallium nitride [active], B.A. Bailey, R.L. Lichti (*Texas Tech. U.*), K.H. Chow (*U. Alberta*), B. Hitti (*TRIUMF*), S.F.J. Cox (*Rutherford Appleton Lab*), E.A. Davis (*Leicester U.*)
805. A study of the  $^{13}\text{N}(p,\gamma)^{14}\text{O}$  reaction with a  $^{13}\text{N}$  beam [active], R.E. Azuma, J. Chow, J.D. King, A.C. Morton (*U. Toronto*), N. Bateman (*TRIUMF-Toronto*), L. Buchmann, K.P. Jackson, T. Shoppa (*TRIUMF*), J.M. D'Auria (*SFU*), U. Giesen (*SFU-TRIUMF*), G. Roy (*U. Alberta*), W. Galster (*U. Catholique de Louvain*), A.C. Shotter (*U. Edinburgh*), R.N. Boyd (*Ohio State U.*), U. Greife, C. Rolfs, F. Strieder, H.-P. Trautvetter (*Ruhr U. Bochum*)
806. Excitation of high-spin isomeric states and compound nucleus formation by intermediate energy protons and stopped pions [completed data-taking], A.S. Iljinov, V.M. Kokhanyuk, B.L. Zhuikov (*INR, Moscow*), I. Liu, J. Vincent, A.Z. Zyuzin (*TRIUMF*)
808. Spin glass order in magnets frustrated by competing ferro- and antiferromagnetic exchange [completed], G.M. Kalvius, A. Kratzer, E. Schreier (*Techn. U. Munich*), R. Wäppling (*U. Uppsala*), D.R. Noakes (*Virginia State U.*), J. Gal (*Beer Sheva U.*), W. Schäfer (*Bonn U.*)
809. Quantum diffusion of muonium in crystals with orientational degrees of freedom [completed], D. Arseneau, B. Hitti, S.R. Kreitzman (*TRIUMF*), J.H. Brewer, A. Izadi, G.D. Morris (*UBC*), D.G. Eshchenko (*INR, Moscow*), V.G. Storchak (*Kurchatov Inst.*), J.D. Brewer (*SFU*)
810. First direct study of the  $^{23}\text{Mg}(p,\gamma)^{24}\text{Al}$  reaction with a recoil mass separator (DRAGON) [active], N.P.T. Bateman, J.M. D'Auria, D. Hunter, R. Korteling (*SFU*), R.N. Boyd (*Ohio State U.*), L. Buchmann, R. Helmer, D. Hutcheon, K.P. Jackson, A. Olin, J. Rogers (*TRIUMF*), U. Giesen, G. Roy (*U. Alberta*), L. Gialanella, U. Greife, C. Rolfs, F. Strieder, H.-P. Trautvetter (*Ruhr U. Bochum*), A. Hussein (*UNBC*), M. Junker (*INFN Gran Sasso*), J.D. King (*U. Toronto*), P.D. Parker (*Yale U.*), A. Shotter (*U. Edinburgh*), M. Wiescher (*U. Notre Dame*)
811. A direct study of the  $^{19}\text{Ne}(p,\gamma)^{20}\text{Na}$  reaction with a recoil mass separator (DRAGON) [active], N.P.T. Bateman, J.M. D'Auria, D. Hunter, R. Korteling (*SFU*), R.N. Boyd (*Ohio State U.*), L. Buchmann, R. Helmer, D. Hutcheon, K.P. Jackson, A. Olin, J. Rogers (*TRIUMF*), U. Giesen, G. Roy (*U. Alberta*), L. Gialanella, U. Greife, C. Rolfs, F. Strieder, H.-P. Trautvetter (*Ruhr U. Bochum*), A. Hussein (*UNBC*), M. Junker (*INFN Gran Sasso*), J.D. King (*U. Toronto*), P.D. Parker (*Yale U.*), A. Shotter (*U. Edinburgh*), M. Wiescher (*U. Notre Dame*)
812. Proposed study of the  $^8\text{Li}(\alpha,n)^{11}\text{B}$  reaction [active], R.N. Boyd, A. Murphy, L. Sahin, E. Smith, M. Zahar (*Ohio State U.*), L. Buchmann, P. Walden (*TRIUMF*), J.M. D'Auria (*SFU*), J.D. King (*U. Toronto*), M. Nishimura, S. Nishimura, I. Tanihata (*RIKEN*)
813. A study of the  $^{15}\text{O}(\alpha,\gamma)^{19}\text{Ne}$  reaction at the astrophysically important energy [active], N.P.T. Bateman, J.M. D'Auria, D. Hunter, R. Korteling (*SFU*), R.N. Boyd (*Ohio State U.*), L. Buchmann, R. Helmer, D. Hutcheon, K.P. Jackson, A. Olin, J. Rogers (*TRIUMF*), U. Giesen, G. Roy (*U. Alberta*), U. Greife, C. Rolfs, F. Strieder, H.-P. Trautvetter (*Ruhr U. Bochum*), A. Hussein (*UNBC*), J.D. King (*U. Toronto*), P.D. Parker (*Yale U.*), A. Shotter (*U. Edinburgh*), M. Wiescher (*U. Notre Dame*)
814.  $\mu$ SR studies of unconventional superconductivity in  $\text{Sr}_2\text{RuO}_4$  [active], Y. Fudamoto, K.M. Kojima, M. Larkin, G.M. Luke, J. Merrin, B. Nachumi, Y.J. Uemura (*Columbia U.*), Y. Maeno (*Kyoto U.*), R.J. Cava (*Princeton U.*)

46

70

815.  $\beta$ -NMR investigation of magnetic multilayers and giant magnetoresistance [active], W.A. MacFarlane, R. Miller, (UBC), J.H. Brewer, R.F. Kiefl (UBC-TRIUMF), P. Amaudruz, R. Baartman, T.R. Beals, J. Behr, S. Daviel, S.R. Kreitzmann, T. Kuo, C.D.P. Levy, M. Olivo, R. Poutissou, G.D. Wight (TRIUMF) S.R. Dunsiger, R. Heffner, G.D. Morris (Los Alamos Nat. Lab), C. Bommas (U. Bonn), A. Hatakeyama, Y. Hirayama, T. Shimoda (Osaka U.), K.H. Chow (U. Alberta), L.H. Greene (U. Illinois-Urbana-Champaign) 72
816. Semiconductor quantum wells investigated by  $\beta$ -NMR [active], J.H. Brewer, J.C. Chakhalian, S. Dunsiger, R. Miller, T. Tiedje (UBC), M. Gingras (U. Waterloo), B. Ittermann (U. Marburg), B. Hitti, P. Levy, S.R. Kreitzman, A. Zelenski (TRIUMF), R.F. Kiefl (TRIUMF-UBC) 72
817.  $\beta$ -NMR investigation of type II superconductors [active], D. Bonn, J.H. Brewer, J.C. Chakhalian, S. Dunsiger, W. Hardy, R. Liang, R.F. Kiefl, W.A. MacFarlane, R. Miller, J. Sonier (UBC), M. Gingras (U. Waterloo), R. Heffner (Los Alamos Nat. Lab), B. Ittermann (U. Marburg), B. Hitti, P. Levy, S.R. Kreitzman, A. Zelenski (TRIUMF), G.M. Luke (Columbia U.), J.W. Brill (U. Kentucky) 72
818.  $\mu^+$ SR study of magnetic ordering in the one-dimensional spin-1/2 antiferromagnet copper benzoate [completed], J.C. Chakhalian, S. Dunsiger, R.F. Kiefl, W.A. MacFarlane, R. Miller, J. Sonier (UBC), C. Broholm, D.C. Dender, P. Hammar, D. Reich (Johns-Hopkins U.), G. Luke, T. Uemura (Columbia U.)
819.  $\mu^+$ SR studies of the antiferromagnetic instability and metastable state in colossal magnetoresistance system  $(\text{Nd}_{1-y}\text{Sm}_y)_{1/2}\text{Sr}_{1/2}\text{MnO}_3$  ( $y = 0.875$ ) [completed], W. Higemoto, I. Watanabe (RIKEN), K. Nishiyama (KEK), K. Nagamine (RIKEN-KEK), A. Asamitsu, H. Kuwahara, Y. Tokura (JRCAT, U. Tokyo)
821. Shape coexistence and shape mixing in neutron-deficient platinum isotopes: on-line nuclear orientation studies of the decays of  $^{182}\text{Au}$  and  $^{186}\text{Au}$  [active], K.S. Krane (Oregon State U.), J.L. Wood (Georgia Inst. Tech.), J. D'Auria (SFU)
822. Effect of disorder on quantum spin liquid state [active], J. Akimitsu, K. Ishii, K. Oishi, T. Yokoo (Aoyama Gakuin U.), R. Kadono, K. Nagamine (RIKEN), K. Nishiyama (KEK)
823. Pure fermi decay in medium mass nuclei [active], G.C. Ball, R. Beaton, P. Bricault, G. Hackman, P. Klages, J.A. Macdonald, E. Vandervoort (TRIUMF), D.F. Hodgson (U. Surrey-TRIUMF), J. Cerny, D.M. Moltz, J. Powell (Lawrence Berkeley Lab), G. Savard (Argonne National Lab), J.C. Hardy, V. Iacob (Texas A&M U.), S. Bishop, J. D'Auria (SFU), J.R. Leslie, H.-B. Mak, I.S. Towner (Queen's U.), D. Kulp, J.L. Wood (Georgia Inst. Tech.), E.F. Zganjar, A. Piechaczek (Louisiana State U.) 47
824. Measurement of the astrophysical rate of the  $^{21}\text{Na}(p, \gamma)^{22}\text{Mg}$  reaction [active], S. Bishop, A. Chen, J.M. D'Auria, D. Hunter, M. Lamey, W. Liu, C. Wrede, (SFU), L. Buchmann, D. Hutcheon, D. Ottewell, J. Rogers (TRIUMF), S. Engel (Ruhr U.), D. Gigliotti, A. Hussein (UNBC), R. Azuma, J.D. King, A. Olin (U. Toronto), R. Lewis, P.D. Parker (Yale U.), M. Wiescher (U. Notre Dame), S. Kubono, S. Mitimasa (U. Tokyo), M. Chatterjee (U. Calcutta), U. Greife, C. Jewett (ColSchMines) 49
825. Equilibrium defects and order in intermetallic compounds studied using isomeric probes [active], G.S. Collins (Washington State U.)
826. Studies of ultrathin magnetic films with implanted isotopes [active], R. Kiefl, J. Pond, B.G. Turrell (UBC), C.A. Davis, P.P.J. Delheij (TRIUMF), K.S. Krane, J. Loats, P. Schmelzenbach, C. Stapels (Oregon State U.), D. Groh, W. Kumarasiri, P. Mantica (Michigan State U.), D. Kulp, J.L. Wood, (Georgia Inst. Tech.)
827. Parity violation in  $^{182}\text{W}$  [active], J. D'Auria (TRIUMF-SFU), C.A. Davis, P.P.J. Delheij (TRIUMF), R. Kiefl, A. Kotlicki, J. Pond, B. Turrell (UBC), K.S. Krane (Oregon State U.)
828. Nuclear moments in the mass-100 region [active], K.S. Krane, J. Loats, P. Schmelzenbach, C. Stapels (Oregon State U.), D. Kulp, J.L. Wood (Georgia Inst. Tech.), C.A. Davis, P.P.J. Delheij (TRIUMF), D. Groh, W. Kumarasiri, P. Mantica (Michigan State U.), R. Kiefl, J. Pond, B.G. Turrell (UBC)
829. Muonium as a hydrogen isotope: reactions in solution [completed], D.P. Chong, G.B. Porter, D.C. Walker (UBC), K. Venkateswaran (Hindustan Lever Ltd.), H.A. Gillis (St. Francis Xavier U.)
830. The hot entropy bubble and the decay of  $^9\text{Li}$  [active], N. Bateman (TRIUMF-SFU-Toronto), L. Buchmann, K.P. Jackson, S. Karataglidis, T. Shoppa, E. Vogt (TRIUMF), J. Chow, J.D. King, C. Mortin (U. Toronto), T. Davison, A. Ostrowski, A. Shotter (U. Edinburgh), J. D'Auria, U. Giesen (SFU), E. Gete, D. Measday (UBC)
831. Magnetic properties of  $\text{REBa}_2\text{Cu}_3\text{O}_x$  [completed data-taking], D. Andreica, F.N. Gyax, M. Pinkpank, A. Schenck (ETH Zürich), B. Hitti (TRIUMF), A. Amato (PSI), J.H. Brewer (UBC-TRIUMF)
832. Study of the non-magnetic-magnetic transition in the  $\text{Yb}(\text{Cu}_{1-x}\text{Ni}_x)_2\text{Si}_2$  system [completed data-taking], D. Andreica, F. Gyax, M. Pinkpank, A. Schenck (ETH Zürich-PSI), A. Amato (PSI), B. Hitti (TRIUMF)

833.  $\mu$ SR studies of doped MnSi and  $V_{2-y}O_3$ : non-fermi-liquid behaviour, spin fluctuations and itinerant magnetism [active], A. Fukaya, I.M. Gat, M. Larkin, A.J. Millis, P.L. Russo, A.T. Savici, Y.J. Uemura (*Columbia U.*), P.P. Kyriakou, G.M. Luke, C.R. Wiebe (*McMaster U.*), Y.V. Sushko (*U. Kentucky*), R.H. Heffner (*Los Alamos Nat. Lab*), D.E. MacLaughlin (*U. California, Riverside*), D. Andreika, A. Schenck (*PSI*), M. Kalvius (*Tech. U. Munich*) 75
834.  $\mu$ SR study of transverse spin freezing in bond-frustrated magnets [active], A.D. Beath, D.H. Ryan, (*McGill U.*), J.M. Cadogan (*U. New South Wales*), J. van Lierop (*Brookhaven National Lab*) 75
835.  $\mu$ SR studies of intercalated HfN and Bi2212 superconductors [active], R. Breslow, Y. Fudamoto, A. Fukaya, I.M. Gat, K. Groves, M.I. Larkin, A. Savici, Y.J. Uemura (*Columbia U.*), P. Kyriakou, G.M. Luke, M. Rovers (*McMaster U.*), K.M. Kojima (*U. Tokyo*), S. Yamanaka (*Hiroshima U.*), T. Ito (*Columbia U.-CERC*) 77
836. Elasticks [active], R.E. Azuma, J.D. King (*U. Toronto*), G. Ball, L. Buchmann, K.P. Jackson, B. Jennings, S. Karataglidis, E. Vogt (*TRIUMF*), N. Bateman (*TRIUMF-SFU-U. Toronto*), T. Davison, A. Ostrowski, A. Shotter (*U. Edinburgh*), J. D’Auria (*SFU*), W. Galster (*U. Catholique de Louvain*), G. Roy (*U. Alberta*)
837. Pion-induced errors in memory chips [completed], J.T. Brack, G. Hofman, J. Patterson R.J. Peterson, R.A. Ristinen (*U. Colorado*), J.F. Ziegler (*IBM*), M.E. Nelson (*US Naval Academy*), G. Smith (*TRIUMF*)
838. Measurement of the  $\pi^-p \rightarrow \gamma\gamma n$  capture mode of pionic hydrogen [completed data-taking], T. Gorringe, M. Kovash, S. Tripathi, P. Żolnierczuk (*U. Kentucky*), D. Armstrong, J. Clark (*Coll. of William & Mary*), M. Hasinoff (*UBC*), D. Healey, D. Wright (*TRIUMF*) 52
839. Thermal test of prototype high power ISAC target [completed], D. Drake, D. Liska, W.L. Talbert, M. Wilson (*Amparo Corp.*), P. Bricault, M. Dombisky, P. Schmor (*TRIUMF*), E. Dalder, C. Landram, K. Sale, D. Slaughter (*Lawrence Livermore National Lab*), J. Nolen, G. Savard (*Argonne National Lab*), G. Alton (*Oak Ridge National Lab*)
840. Muon transfer from excited states of muonic hydrogen with x-ray measurement [active], S. Sakamoto, K. Shimomura (*KEK*), K. Nagamine (*KEK-RIKEN*), K. Ishida, N. Kawamura, Y. Matsuda, T. Matsuzaki, S.N. Nakamura, P. Strasser (*RIKEN*)
841. ISAC beam and target development [active], P. Bricault, M. Dombisky (*TRIUMF*)
842. Muonium-substituted free radicals in sub- and supercritical water [active], J.-C. Brodovitch, K. Ghandi, S. Kecman, I. McKenzie, P.W. Percival (*SFU*), J. Schüth (*U. Bonn*), B. Addison-Jones (*UCC Kamloops*) 77
843. Quadrupole ordering in dense Kondo system studied by  $\mu$ LCR [active], J. Akimitsu, K. Kakuta, K. Ohishi (*Aoyama Gakuin U.*), W. Higemoto, R. Kadono (*KEK-IMSS*), T. Yokoo (*CREST*)
844. Quantum impurities in one dimensional spin 1/2 chains [completed], I. Affleck, J. Brewer, J. Chakhalian, S. Dunsiger, R.F. Kiefl, R. Miller, A. Price (*UBC*), S. Eggert (*Chalmers U.*), B. Hitti (*TRIUMF*), A.A. Keren (*Israel Inst. Tech.*), W.A. MacFarlane (*U. Paris-Sud*), G. Morris (*UBC-TRIUMF*), Y.J. Uemura (*Columbia U.*), M. Verdagner (*CNRS*), I. Yamada (*Chiba U.*)
845.  $\mu$ SR studies of vortex phases in (Ba,K)BiO<sub>3</sub> [completed], G.M. Luke, M.A. Lumsden (*McMaster U.*), Y. Fudamoto, M.I. Larkin, Y.J. Uemura (*Columbia U.*), K.M. Kojima (*U. Tokyo*), M. Gingras (*U. Waterloo*), I. Joumard, T. Klein, J. Marcus (*U. Grenoble*)
846. Complex order parameter symmetry in YB<sub>2</sub>Cu<sub>3</sub>O<sub>7- $\delta$</sub>  at low  $T$  and high magnetic field [active], D.A. Bonn, J.H. Brewer, W.N. Hardy, R.F. Kiefl, R.-X. Liang, R.I. Miller (*UBC*), R.H. Heffner, G.D. Morris (*Los Alamos Nat. Lab*), J.S. Gardner (*NRC*), K.F. Poon, J.E. Sonier (*SFU*), C.E. Stronach (*Virginia State U.*), S.L. Stubbs (*U. Alberta*) 79
847. Electron-doped high- $T_c$  superconductors [active], P. Kyriakou, G.M. Luke (*McMaster U.*), P. Fournier (*U. de Sherbrooke*), K.F. Poon, J.E. Sonier (*SFU*), R.L. Greene (*U. Maryland*), R.I. Miller (*UBC*), 80
848.  $\mu$ SR investigation of the vortex state of YBa<sub>2</sub>Cu<sub>3</sub>O<sub>6+x</sub> [active], D.A. Bonn, J.C. Chakhalian, K. Chow, W.N. Hardy, R.X. Liang, R. Miller, A.N. Price (*UBC*), J.H. Brewer, R.F. Kiefl (*UBC-TRIUMF*), J. Sonier (*SFU*) 81
849. Spin structure and magnetic volume fraction of La214 systems: revisiting “1/8”, “stripes”, “spin glass”, and “swiss cheese” [completed], K.M. Kojima (*U. Tokyo*), Y. Fudamoto, I.M. Gat, M.I. Larkin, A.T. Savici, Y.J. Uemura (*Columbia U.*), G.M. Luke (*McMaster U.*), M.A. Kastner, Y.S. Lee (*MIT*), R.J. Birgeneau (*MIT-U. Toronto*), K. Yamada (*Kyoto U.*) 82
850. Effects of dilute (Cu,Zn) substitution in spin gap systems SrCu<sub>2</sub>O<sub>3</sub> and CuGeO<sub>3</sub> [completed], Y. Fudamoto, I. Gat, M.I. Larkin, Y.J. Uemura (*Columbia U.*), K.M. Kojima, K. Manabe, K. Uchinokura (*U. Tokyo*), G.M. Luke (*McMaster U.*), M. Azuma, M. Takano (*Kyoto U.*)

851.  $\mu$ SR in ruthenate and cuprate high- $T$  compounds [active], D.R. Harshman (*Physikon Research Inc.*), H.A. Blackstead (*U. Notre Dame*), D.Y. Chen, M.K. Wu (*Nat. Tsing Hua U.*), F.Z. Chien (*Tamkang U.*), J.D. Dow (*Arizona State U.*), A.J. Greer (*Gonzaga U.*), B. Hitti (*TRIUMF*), W.J. Kossler (*Coll. of William & Mary*), E. Koster (*UBC*), C.E. Stronach (*Virginia State U.*)
852. Magnetic phases in geometrically frustrated rare earth pyrochlores [active], R. Kiefl (*UBC-TRIUMF*), B.D. Gaulin, G. Luke (*McMaster U.*), M.J.P. Gingras (*U. Waterloo*), S. Dunsiger, G.D. Morris (*Los Alamos Nat. Lab*), R. Miller, A.N. Price (*UBC*), J.S. Gardner (*NRC*), S.T. Bramwell (*U. College London*), K. Chow (*U. Alberta*), R. Jin, M.D. Lumsden, D. Mandrus (*Oak Ridge Nat. Lab*), J.E. Sonier (*SFU*)
856.  $\mu$ SR study on CuO [active], W. Higemoto, K. Nishiyama, K. Shimomura (*KEK*), M. Suzuki, S. Tanaka, N. Tsutsumi, X.G. Zheng (*Saga U.*)
857. Investigation of the magnetic properties of the cerium compound probed by negative muon [active], W. Higemoto, K. Nagamine, K. Nishiyama, K. Shimomura (*KEK*), V.V. Krishnamurthy (*RIKEN*)
858. Repolarization of muonic atom in semiconductors by laser optical pumping in solids [active], W. Higemoto, R. Kadono, K. Nagamine, K. Nishiyama K. Shimomura (*KEK*)
859. A search for non-Markovian  $\mu^+$  diffusion in solids:  $\mu^+$  spectral spin hopping in high transverse field [inactive], G. Alexandrowicz, A. Grayevsky, N. Kaplan, T. Tashma (*Racah Inst. Physics*), A. Schenck (*ETH Zürich*)
860. Mass and charge transport in disordered media: orientational glasses [active], J.H. Brewer, A. Izadi, D.M.C. Liu, K.M. Nichol, S. Sivanandam, A.T. Warkentin (*UBC*), G.D. Morris (*TRIUMF*), V.G. Storchak (*Kurchatov Inst.*), D.G. Eshchenko (*INR, Moscow*), J.D. Brewer (*SFU*)
862. Polarization observables in the  $\bar{p}(\pi^\pm, \pi^+, \pi^\pm)$  reactions: a test of chiral perturbation theory [active], P. Amaudruz, D. Ottewell (*TRIUMF*), K. Craig, G. Hofman, M.M. Pavan, K.J. Raywood, R. Tacik (*Regina-TRIUMF*), K. Babcock, E. Mathie, H. Xu, M. Yeomans (*U. Regina*), P. Camerini, E. Fragiacomio, N. Grion, R. Rui (*U. di Trieste*), J. Breitschopf, H. Denz, R. Meier, G. Wagner (*U. Tübingen*), G. Smith (*Jefferson Lab*), E. Gibson (*California State U. Sacramento*), C. Riedel (*Montana State U. Bozeman*)
863. Magnetic dipole moments measurements of  $^{75,77,79}\text{Ga}$  using low temperature nuclear orientation and  $\beta$ -NMR [active], A. Davies, D. Groh, P.F. Mantica, A.C. Morton (*Michigan State U.*), C.A. Davis, P.P.J. Delheij (*TRIUMF*), B. Turrell (*UBC*)
864. Measurement of the two-photon capture mode of the pionic deuterium atom [completed data-taking], S. Arole, T. Goringe, C. Nenkov, S. Tripathi, P. Żołnierczuk (*U. Kentucky*), D. Armstrong, J. Clark (*Coll. of William & Mary*), M. Hasinoff (*UBC*), D. Wright (*TRIUMF*)
865. Electronic structure and diffusion kinetics of muonium in group III nitrides [active], W. Higemoto, R. Kadono, K. Nishiyama, K. Shimomura (*KEK-IMSS*), M. Mizuta (*NEC Corp.*), M. Saito (*NEC Inf. Syst. Ltd.*)
866.  $S = 0$  doping to the  $1d$  spin chain: comparison between the  $S = 1/2$  and  $S = 1$  chains [active], I. Eisaki, K.M. Kojima, T. Masuda, S. Uchida, K. Uchinokura (*U. Tokyo*), Y. Fudamoto, I. Gat, M.I. Larkin, Y.J. Uemura (*Columbia U.*), G.M. Luke (*McMaster U.*)
867.  $\mu$ SR studies of magnetic properties of strontium/calcium ruthenates [active], Y. Fudamoto, I. Gat, M. Larkin, A. Savici, Y.J. Uemura (*Columbia U.*), G.M. Luke (*McMaster U.*), K. Kojima (*U. Tokyo*), S. Ikeda, Y. Maeno (*Kyoto U.*)
868. Magnetic correlations in impurity doped one dimensional spin systems [active], D. Baabe, H.-H. Klauss, W. Kopmann, F.J. Litterst, D. Mienert (*Tech. U. Braunschweig*), U. Ammerahl, B. Büchner (*U. Köln*), C. Geibel (*MPI Dresden*)
869. Measurement of the  $^1\text{H}(\pi^-, \pi^0)n$  differential cross section at 100–140 MeV/c and forward angles [completed data-taking], S. Arole, T. Goringe, M. Kovash, S. Tripathi, P. Żołnierczuk (*U. Kentucky*), M. Hasinoff (*UBC*), D. Armstrong (*Coll. of William & Mary*), M. Pavan (*TRIUMF*)
870. Breakout from the hot CNO cycle via the  $^{18}\text{Ne}(\alpha, p)^{21}\text{Na}$  reaction [active], T. Davinson, A. Ostrowski, F. Sarazin, A. Shotter, P. Woods (*U. Edinburgh*), L. Buchmann, J. D'Auria (*TRIUMF*), J. Daly, J. Görres, M. Wiescher (*U. Notre Dame*), P. Leleux (*U. Catholique de Louvain*)
871. Meson and quark effects in nuclear  $\beta$ -decay of  $^{20}\text{Na}$  [active], M. Fukuda, K. Matsuta, M. Mihara, K. Minamisono, T. Minamisono, T. Sumikama (*Osaka U.*), J. Behr, P. Bricault, M. Dombbsky, K.P. Jackson, P. Levy (*TRIUMF*), R. Kiefl (*UBC-TRIUMF*), K. Koshigiri (*Osaka Kyoiku U.*), M. Morita (*Josai Int. U.*)
872. Weak interaction studies with trapped radioactive ions [active], J. Dilling, D. Melconian (*SFU*), G. Savard (*Argonne National Lab-U. Chicago*), G.C. Ball, J.A. Behr, P. Bricault, K.P. Jackson (*TRIUMF*), F. Büchinger, J.E. Crawford, J.K.P. Lee, R.B. Moore (*McGill U.*), K.S. Sharma (*U. Manitoba*)

83

52

53

54

874. Study of  $^{19}\text{Ne}$   $\alpha$ -decay properties related to the hot-CNO breakout reaction  $^{15}\text{O}(\alpha, \gamma)^{19}\text{Ne}$  [active], T. Davinson, D. Groombridge, A.M. Laird, A.N. Ostrowski, F. Sarazin, K. Schmidt, A.C. Shotter, P.J. Woods (*U. Edinburgh*), L. Buchmann (*TRIUMF*), S. Cherubini, P. Leleux (*U. Catholique de Louvain*), J. Hinnefeld (*U. South Bend*)
875. Muon scattering in low  $Z$  materials for muon cooling studies [active], M. Curtis-Rouse, T.R. Edgecock, M. Ellis, J. Lidbury, W. Murray, P.R. Norton, K.J. Peach (*Rutherford Appleton Lab*), K. Ishida, Y. Matsuda, K. Nagamine (*RIKEN*), T. McMahon, J.A. Wilson (*U. Birmingham*), G. Barber, A. Jamdagni, K. Long, E. McKigney (*Imp. Coll., London*), W. Allison (*U. Oxford*), S. Benveniste, D. Cline, Y. Fukui, K. Lee, Y. Pischalnikov (*UCLA*), R. Fernow (*Brookhaven National Lab*), P. Gruber, B. Holzer, C. Johnson, A. Lombardi (*CERN*), S.N. Nakamura (*U. Tohoku*), G. Marshall (*TRIUMF*) 55
876. Disordered magnetism near magnetic instabilities in  $f$ -electron materials [active], B. Kessler, D.R. Noakes, C.E. Stronach (*Virginia State U.*), G.M. Kalvius (*Tech. U. Munich*), A. Loidl (*Augsburg U.*), H. Nakotte (*New Mexico State U.*), R. Wäppling (*Uppsala U.*) 86
877.  $\mu\text{SR}$  studies of strongly correlated electron systems under a high pressure [active], W. Higemoto, R. Kadono, A. Koda, K. Nishiyama (*KEK-MSL*), K. Satoh (*Saitama U.*), Y. Kitaoka, K. Ishida (*Osaka U.*), K. Nagamine (*RIKEN-KEK-MSL*)
878.  $\mu^+\text{SR}$  studies on magnetism of layered compounds  $\text{Cu}_2(\text{OH})_3\text{X}$  ( $\text{X}=\text{Cl}, \text{Br}, \text{I}$ ) [active], G. Maruta, K. Nishiyama (*KEK-MSL*), S. Takeda (*Gunma U.*)
879. Proton- $^{21}\text{Na}$  elastic scattering at astrophysical energies [active], L. Buchmann (*TRIUMF*), T. Davinson, A. Ostrowski, F. Sarazin, A. Shotter, P. Woods (*U. Edinburgh*), R.E. Azuma, J.D. King (*U. Toronto*), A. Chen (*TRIUMF-SFU*), J. Daly, J. Görres, M. Wiescher (*U. Notre Dame*), J. D'Auria (*SFU*), E.S. Konobeevsky, M.V. Mordovskoy, V.A. Simonov, A.V. Stepanov, V.P. Zavarzina (*INR, Moscow*) 58
880. Ortho-para effect of muon catalyzed fusion in solid deuterium [completed data-taking], K. Ishida (*RIKEN-KEK*), K. Nagamine (*KEK-RIKEN*), A. Toyoda (*U. Tokyo-RIKEN-KEK*), K. Shimomura (*KEK*), S.N. Nakamura (*RIKEN-Tohoku U.*), Y. Matsuda (*RIKEN*)
881. Magnetism of Ce-based heavy fermion superconductor [active], W. Higemoto, R. Kadono, A. Koda (*KEK-IMSS*), K. Ishida, Y. Kitaoka (*Osaka U.*), C. Geibel, F. Steglich (*Max-Planck Inst.*)
882.  $\mu\text{SR}$  studies of unconventional superconductivity in an organic superconductor  $(\text{TMTSF})_2\text{ClO}_4$  [active], I.M. Gat, M.I. Larkin, A. Savici, Y.J. Uemura (*Columbia U.*), T. Ito (*Columbia U.-ETL*), P. Kyriakou, G.M. Luke, M. Rovers (*McMaster U.*), K.M. Kojima (*U. Tokyo*), P.M. Chaikin, I.J. Lee (*Princeton U.*), M.J. Naughton (*Boston Coll.*)
883. Muonium-substituted methyl and associated free radicals [active], J.-C. Brodovitch, K. Ghandi, S. Kecman, I. McKenzie, P.W. Percival (*SFU*), B. Addison-Jones (*UCC Kamloops*) 87
884.  $\mu\text{SR}$  studies on magnetic ground state of  $S = 1/2$  kagomé spin system  $\text{Cu}_3\text{V}_2\text{O}_7(\text{OH})\cdot 2.2\text{H}_2\text{O}$  [active], A. Fukaya, I.M. Gat, M.I. Larkin, A. Savici, Y.J. Uemura (*Columbia U.*), T. Ito (*CERC-AIST*), A. Keren (*Technion-Israel Inst. of Tech.*), P.P. Kyriakou, G.M. Luke, M.T. Rovers (*McMaster U.*), Z. Hiroi (*U. Tokyo*) 89
885. High-TF line-shape measurement of impurity-doped high- $T_c$  cuprates [active], K.M. Kojima, Y. Kojima, Y. Maeda, T. Okamura, S. Uchida (*U. Tokyo*), I. Gat, T. Itoh, A. Kinkhabwala, M.I. Larkin, Y.J. Uemura (*Columbia U.*), G.M. Luke (*McMaster U.*), S.R. Dunsiger, R.F. Kiefl, R. Miller (*UBC*), J.E. Sonier (*Los Alamos Nat. Lab*)
886. Study of field dependent  $T_1$  relaxation and coexistence of order parameters in the (anti)ferromagnetic ruthenate-cuprate superconductors  $\text{RuSr}_2(\text{Gd}, \text{Eu}, \text{Y})\text{Cu}_2\text{O}_8$  [active], C. Bernhard (*Max Planck Inst.*), C. Niedermayer, V. Oehmichen (*U. Konstanz*), E.J. Ansaldo (*U. Saskatoon*), J.L. Tallon (*NZIIIRD*)
887. Search for broken time reversal symmetry in high temperature superconductors [active], P. Kyriakou, G.M. Luke, M. Rovers (*McMaster U.*), R.H. Heffner (*Los Alamos Nat. Lab*), M.I. Larkin, Y.J. Uemura (*Columbia U.*), J. Sonier (*SFU*), K.M. Kojima (*U. Tokyo*)
888. Test of delayed-muonium model for hydrocarbon liquids [active], D.C. Walker (*UBC*), K. Venkateswaran (*Hindustan Lever Ltd.*), H.A. Gillis (*St. Francis Xavier U.*), G.B. Porter (*UBC*)
889. Study of field induced gap in Cu benzoate [active], Y. Ajiro, T. Asano, Y. Inagaki (*Kyushu U.*), H. Nojiri (*Tohoku U.*), W. Higemoto, R. Kadono, A. Koda (*KEK-IMSS*)
890. Anisotropic Kondo effect in  $\text{Ce}_{0.8}\text{La}_{0.2}\text{Al}_3$ ? [active], D.E. MacLaughlin (*U. California, Riverside*), O.O. Bernal (*Cal. State U., Los Angeles*), R.H. Heffner (*Los Alamos Nat. Lab*), G.M. Luke (*McMaster U.*), G.J. Nieuwenhuys (*U. Leiden*), J.E. Sonier (*SFU*), B. Andraka (*U. Florida*) 89

891. Superconductivity and magnetism in  $Ce_nT_mIn_{3n+2m}$  [active], R.H. Heffner, G.D. Morris, J. Sarrao (*Los Alamos Nat. Lab*), J.E. Sonier (*SFU*), D.E. MacLaughlin (*U. California, Riverside*), G.J. Nieuwenhuys (*U. Leiden*), O.O. Bernal (*Cal. State U., Los Angeles*)
892. Resonance ionization spectroscopy of stable and radioactive nuclides at TISOL [deferred] F. Buchinger, J.E. Crawford, S. Gulick, J.K.P. Lee (*McGill U.*), K. Sharma (*U. Manitoba*), J. Pinard (*Lab. Aimé Cotton, Orsay*)
893. Hyperfine field of Rb in the ferromagnets Fe, Ni, Co [active], C.A. Davis, P.P.J. Delheij (*TRIUMF*), S. Cottenier (*K.U. Leuven*), H. Haas (*Hahn Meitner Inst.*), K.S. Krane (*Oregon State U.*), B. Turrell (*UBC*), J. Wood (*Georgia Inst. Tech.*)
894. Muonium kinetics and free radical formation in solutions of fullerenes [active], B. Addison-Jones (*UCC Kamloops*), J.-C. Brodovitch, K. Ghandi, S. Kecman, I. McKenzie, P.W. Percival (*SFU*)
895. The vortex structure and magnetism of electron-doped cuprate superconductors [active], K.M. Kojima, S. Uchida (*U. Tokyo*), W. Higemoto, R. Kadono, A. Koda (*KEK*), M. Azuma, M. Fujita, M. Takano, K. Yamada (*Kyoto U.*), K. Ishida, Y. Kawasaki, Y. Kitaoka (*Osaka U.*), M.I. Larkin, Y.J. Uemura (*Columbia U.*)
896. Investigation of spin liquid behaviour in chromium and manganese spinels [active], H. Dabkowska, J. Greedan, P.P. Kyriakou, G.M. Luke, M.T. Rovers (*McMaster U.*), I.M. Gat, M.I. Larkin, A.T. Savici, Y.J. Uemura (*Columbia U.*), K.M. Kojima (*U. Tokyo*)
897. Absolute magnetic penetration depth in the Meissner state of superconductors measured with low frequency beta-NMR [active], D. Bonn, J.H. Brewer, K.H. Chow, W. Hardy, R. Liang, R. Miller, G. Morris (*UBC*), S. Dunsiger, B. Heffner (*Los Alamos Nat. Lab*), R.F. Kiefl (*UBC-TRIUMF*), S. Kreitzman, P. Levy (*TRIUMF*), G. Luke (*McMaster U.*), J. Sonier (*SFU*), C. Stronach (*Virginia State U.*)
898. MULTI development with applications in superconductors and semiconductors [active], P. Amadruz, D. Arseneau, S. Chan, K.H. Chow, B. Hitti, G. Morris, R. Poutissou (*TRIUMF*), J. Chakhalian, S. Dunsiger, R.F. Kiefl, R. Miller (*UBC*)
900. A determination of the  $\alpha+^{15}\text{O}$  radiative capture rate by a measurement of the  $^{15}\text{O}(^6\text{Li},d)^{19}\text{Ne}$  reaction [active], B.R. Fulton, B. Greenhalgh, J. Pearson, D.L. Watson (*U. York*), N.M. Clarke (*U. Birmingham*), T. Davinson, N. Farrington, P. Monroe, C. Ruiz, F. Sarazin, K. Schmidt, A.C. Shotter, P.J. Woods (*U. Edinburgh*), L. Buchmann, P. Walden (*TRIUMF*), J. D'Auria (*SFU*)
902. Muon capture on  $^{45}\text{Sc}$ ,  $^{51}\text{V}$ ,  $^{55}\text{Mn}$  and  $^{59}\text{Co}$  [active], D.F. Measday (*UBC*), T.P. Gorringer (*U. Kentucky*)
903. Spectroscopic study of  $^{11}\text{Be}$  with polarized  $^{11}\text{Li}$  beam [active], Y. Hirayama, H. Izumi, M. Kawabata, K. Matsuta, K. Minamisono, T. Minamisono, S. Shimizu, T. Shimoda (*Osaka U.*), H. Ishiyama, S.C. Jeong, H. Miyatake (*IPNS, KEK*), K.P. Jackson, C.D.P. Levy (*TRIUMF*)
907. Improving  $S_{E1}(300)$ : the  $\beta - \alpha$  branching ratio of  $^{16}\text{N}$  [deferred] R.E. Azuma, J.D. King (*U. Toronto*), L. Buchmann (*TRIUMF*)
909. Isospin symmetry breaking in superallowed Fermi beta decays [active], C.E. Svensson (*Guelph U.*), R.A.E. Austin, J.A. Cameron, J.C. Waddington (*McMaster U.*), G.C. Ball, P. Bricault, N. Kintz, J.A. Macdonald (*TRIUMF*), J.C. Hardy, V. Iacob (*TAMU*), J.R. Leslie (*Queen's U.*), D.M. Moltz (*Lawrence Berkeley National Lab*), G. Savard (*Argonne National Lab-U. Chicago*)
910. Study of the ground state proton emitter  $^{73}\text{Rb}$  and implications for the astrophysical rp-process [active], A. Piechaczek, E.F. Zganjar (*Louisiana State U.*), G.C. Ball (*TRIUMF*), J.C. Batchelder (*Oak Ridge Assoc. U.*), D. Kulp, B.D. MacDonald, J.L. Wood (*Georgia Inst. Tech.*)
911. Test of aerogel proto-type detector for  $G\theta$  phase II [active], J. Birchall, W. Falk, L. Lee, S. Page, W.D. Ramsay, A. Rauf, G. Rutledge, W.T.H. van Oers (*U. Manitoba*), C. Davis (*TRIUMF*), L. Hannelius, J. Martin (*Caltech*), E. Korkmaz, T. Porcelli (*UNBC*), S. Kox, G. Quemener, R. Tieulent (*ISN Grenoble*), D. Beck (*U. Illinois, Urbana*)
912. Formation, structure, and dynamics of muonium in GaAs studied by EF-ALC-RF  $\mu^+\text{SR}$  [active], B. Hitti, S.R. Kreitzman (*TRIUMF*), K.H. Chow (*U. Alberta*), J.H. Brewer, R.F. Kiefl (*UBC*), T.L. Estle (*Rice U.*), R.L. Lichti (*Texas Tech. U.*), D.G. Eshchenko (*INR, Moscow*), V.G. Storchak (*Kurchatov Inst.*)
913. Photo-induced dynamics and reactivity of spin polarized  $^8\text{Li}$  in semiconductors [active], K.H. Chow (*U. Alberta*), T. Beals, R.F. Kiefl, R.I. Miller (*UBC*), P. Amadruz, D. Arseneau, S. Daviel, B. Hitti, S.R. Kreitzman, P. Levy, R. Poutissou (*TRIUMF*), R.L. Lichti (*Texas Tech. U.*), G.D. Morris (*Los Alamos National Lab*), C. Bommas (*U. Bonn*)
914. Zero-field  $\mu\text{SR}$  in Bi2212 and Bi2201 searching for effects related to the pseudo-gap [active], Y. Ching, M. Greven, N. Kaneko, P.K. Mang (*Stanford U.*), A. Fukaya, I.M. Gat, M.I. Larkin, P.L. Russo, A. Savici, Y.J. Uemura, J. Zhang (*Columbia U.*), H. Dabkowska, P. Kilyakui, G.M. Luke, M. Rovers (*McMaster U.*)

91

92

93

915. Muonium in semiconductor alloys [active], B.A. Bailey, R.L. Lichti (*Texas Tech. U.*), K.H. Chow (*U. Alberta*), S.F.J. Cox, P.J.C. King (*Rutherford Appleton Lab*), E.A. Davis (*U. Leicester*), J.M. Gil (*U. Coimbra*), B. Hitti (*TRIUMF*) 94
916. QLCR of diamagnetic states in GaP [active], B.A. Bailey, R.L. Lichti (*Texas Tech. U.*), K.H. Chow (*U. Alberta*), S.F.J. Cox (*Rutherford Appleton Lab*), E.A. Davis (*U. Leicester*), B. Hitti (*TRIUMF*) 95
917. Correlation between magnetism and transport properties of thermoelectric oxides [active], R. Asahi, S. Hirano, H. Itahara, J. Sugiyama, T. Tani (*Toyota Central R&D Labs Inc.*), J.H. Brewer (*UBC*) 96
918. High field study of  $\text{La}_2\text{CuO}_4$  based superconductors [active], A. Fukaya, I.M. Gat, M.I. Larkin, P.L. Russo, A. Savici, Y.J. Uemura, J. Zhang (*Columbia U.*), P. Kyriakou, G.M. Luke, M. Rovers (*McMaster U.*), K.M. Kojima, S. Uchida (*U. Tokyo*), T. Ito (*ETL, Tsukuba*), Y.S. Lee (*National Inst. Standards Technology*), M.A. Kastner (*MIT*), R.J. Birgeneau (*U. Toronto*)
919. Proton irradiation effects in SOI devices [active], P. Dodd, G. Hash, R. Loemker, J. Schwank, M. Shaneyfelt (*Sandia National Lab*), V. Ferlet-Cavrois, P. Paillet (*CEA*)
920. Nuclear charge radii and moments of short lived neutron deficient Lanthanum isotopes [active], H.A. Schuessler (*Texas A&M U.*), P. Levy (*TRIUMF*), H. Iimura (*Japan Atomic Energy Res. Inst.*), F. Buchinger, J. Crawford, J. Lee (*McGill U.*), R.I. Thompson (*U. Calgary*)
921. High-K isomers in neutron-rich  $A = 170\text{--}190$  nuclei [active], A.A. Hill, Z. Podolyák, P.H. Regan, P.M. Walker, C. Wheldon, R. Wood (*U. Surrey*), G.C. Ball, P. Bricault, G. Hackman (*TRIUMF*), C.E. Svensson (*U. Guelph*), R. Austin, J.C. Waddington (*McMaster U.*), A. Piechaczek, E.F. Zganjar (*Louisiana State U.*)
922. On the production of  $^{26}\text{Al}$  in novae: measurement of the  $^{25}\text{Al}(p,\gamma)^{26}\text{Si}$  reaction rate [pending], S. Bishop, A.A. Chen, J.M. D'Auria, D. Hunter, M. Lamey, C. Wrede (*SFU*), L. Buchmann, D.A. Hutcheon, K.P. Jackson, A. Olin, J. Rogers (*TRIUMF*), S. Engel (*Ruhr-U. Bochum*), C.S. Galovich (*U. Northern Colorado*), D. Gigliotti, A. Hussein (*UNBC*), U. Greife, C.C. Jewett (*Colorado School of Mines*), J. José (*UPC/IEEC Barcelona*), P.D. Parker (*Yale U.*)
923. Measurement of  $^{25}\text{Al} + p$  resonances through elastic scattering [active], A.A. Chen, J.M. D'Auria (*SFU*), L. Buchmann, F. Sarazin, A. Shotter, P. Walden (*TRIUMF*), T. Davinson, A. Murphy, I. Roberts, A. Robinson, C. Ruiz, P. Woods (*U. Edinburgh*), B. Fulton, D. Groombridge, J. Pearson (*U. York*), P.D. Parker (*Yale U.*)
924. The hot CNO cycle and the  $^{14}\text{O}(\alpha,p)^{17}\text{F}$  reaction [active], M. Aliotta, T. Davinson, A. Murphy, I. Roberts, A. Robinson, P.J. Woods (*U. Edinburgh*), L. Buchmann, A. Chen, P. Walden (*TRIUMF*), B. Fulton, D. Groombridge, J. Pearson (*U. York*), P. Leleux (*U. Catholique de Louvain*), R. Azuma (*U. Toronto*)
925. Isospin mixing in  $^{36}\text{Ar}$  via spin-polarized observables in  $^{36}\text{K}$   $\beta^+$  decay [active], J.M. D'Auria, D. Melconian (*SFU*), G.C. Ball, J.A. Behr, P. Bricault, M. Dombisky, K.P. Jackson (*TRIUMF*), S. Gu, M. Pearson (*UBC*), W.P. Alford (*U. Western Ontario*), D. Ashery, O. Aviv (*Tel Aviv U.*), I.A. Towner (*Queen's U.*), S. Karataglidis (*Los Alamos National Lab*), B.A. Brown (*Michigan State U.*)
926. Measurement of charge radius and  $\beta^+$ -decay Q-value of laser-trapped  $^{74}\text{Rb}$  [active], S. Gu, M. Pearson (*UBC*), J.A. Behr, P. Bricault, M. Dombisky, K.P. Jackson (*TRIUMF*), D. Melconian (*SFU*), D. Ashery, O. Aviv (*Tel Aviv U.*)
927. Using ( $^3\text{He},p$ ): spectroscopy of proton unbound  $^{19}\text{Na}$  [active], G.C. Ball, L. Buchmann, G. Hackman, A. Laird, F. Sarazin, A. Shotter, P. Walden (*TRIUMF*), A.A. Chen (*SFU*), T. Davinson, I. Roberts, A. Robinson, C. Ruiz, P. Woods (*U. Edinburgh*), B. Fulton, D. Groombridge, J. Pearson (*U. York*), C.E. Svensson (*U. Guelph*), J. Waddington (*McMaster U.*)
928. Level structure of  $^{21}\text{Mg}$ : nuclear and astrophysical implications [active], M. Aliotta, T. Davinson, A.St.J. Murphy, A. Robinson, P.J. Woods (*U. Edinburgh*), J.M. D'Auria (*SFU*), R. Azuma (*U. Toronto*), R. Boyd (*Ohio State U.*), L. Buchmann, A. Chen, D. Hutcheon, A. Laird, P. Walden (*TRIUMF*), B. Fulton (*U. York*)
929. Octupole deformation and spin-exchange polarization of odd- $A$  radon isotopes: toward radon electric dipole moment measurements at ISAC [active], C.E. Svensson (*U. Guelph*), S.B. Bayram, T.E. Chupp, K. Coulter, W. Lorenzen (*U. Michigan*), D.E. Appelbe (*Daresbury*), R.A.E. Austin, J.C. Waddington (*McMaster U.*), G.C. Ball, J.A. Behr, P. Bricault, G.S. Hackman, K.P. Jackson, J.A. Macdonald (*TRIUMF*), P. Garrett (*Lawrence Livermore National Lab*), M.E. Hayden (*SFU*), D. Kulp, J.L. Wood (*Georgia Tech. U.*), M.R. Pearson (*UBC*), A. Piechaczek, E.F. Zganjar (*Louisiana State U.*)
930. Measurement of  $\pi^-$  absorption in water [active], T. Awes, V. Cianciolo, G. Young (*Oak Ridge National Lab*), W. Bugg, Yu. Efremenko, Yu. Kamyshkov, S. Ovchinnikov (*U. Tennessee*), Yu. Davydov, T. Numaou, J.-M. Poutissou (*TRIUMF*)

931. Magnetic properties of multinuclear, open-shell coordination complexes and polymers probed by  $\mu$ SR [active], N. Draper, A. Gabert, D.B. Leznoff, G. Mund, K.F. Poon, C. Shorrock, J.E. Sonier (*SFU*)
932. Improving  $\mu^-$  SR performance [active], M.A. Bayer, J.H. Brewer, D.F. Measday (*UBC*), G.M. Marshall, M.M. Pavan (*TRIUMF*)
933. Effects of nonlocality in superconductors [active], R. Miller, R. Kiefl (*UBC-TRIUMF*), S.L. Bud'ko, P. Canfield, V. Kogan (*Iowa State U.*), P. Poon, J.E. Sonier (*SFU*)
934. MuSR study of polymerized C<sub>60</sub> [active], A. Fukaya, I.M. Gat, P.L. Russo, A. Savici, Y.J. Uemura (*Columbia U.*), P. Kyriakou, G.M. Luke (*McMaster U.*), T. Makarova, B. Sundqvist (*Umea U. Sweden*)
935. High pressure study of URu<sub>2</sub>Si<sub>2</sub> [active], J. Garrett, P. Kyriakou, G.M. Luke, C. Wiebe (*McMaster U.*), I.M. Gat, A. Savici, Y.J. Uemura (*Columbia U.*), Y. Sushko (*U. Kentucky*), K.M. Kojima (*U. Tokyo*)
936. Magnetic dynamics in spin ice systems [active], S.T. Bramwell, J. Lago (*U. College London*), S.R. Dunsiger (*Los Alamos National Lab*), J.S. Gardner (*NRC*), M.J.P. Gingras (*U. Waterloo*), R. Kiefl (*UBC-TRIUMF*), G.M. Luke (*McMaster U.*)
937. Muonium in hexagonal semiconductors [active], B.A. Bailey, R.L. Lichti (*Texas Tech. U.*), K.H. Chow (*U. Alberta*), S.F.J. Cox (*Rutherford Appleton Lab*), E.A. Davis (*U. Leicester*), J.M. Gil (*U. Coimbra*), B. Hitti (*TRIUMF*)

\*deceased



## LIFE SCIENCES PROJECT PROPOSALS

	Page
The following lists life sciences project proposals received up to the end of 2001 (missing numbers cover proposals that have been withdrawn or replaced by later versions, rejected, or combined with another proposal). Page numbers are given for those experiments which are included in this Annual Report.	
LS0. PET facilities [active], <u>K.R. Buckley</u> , E.T. Hurtado, E. Piccioni ( <i>TRIUMF</i> ), D. Becker, C. English, S. Jivan, C. Williams ( <i>UBC-TRIUMF</i> )	98
LS1. Attenuation maps for quantitative SPECT [completed], <u>A. Celler</u> ( <i>UBC-VH&amp;HSC</i> ), S. McFarland ( <i>UBC</i> ), S. Barney, M. Limber ( <i>SFU</i> )	
LS2. Synthesis of <sup>18</sup> F-glycosides as potential imaging agents for the study of glycosidase activity in the brain [completed], <u>M.J. Adam</u> ( <i>TRIUMF</i> ), D. Lyster ( <i>VH&amp;HSC</i> ), G. Matte ( <i>Halifax H.</i> )	99
LS3. Synthesis of radiopharmaceuticals for positron emission tomography [active], <u>M.J. Adam</u> , K.R. Buckley, E.T. Hurtado, J. Huser, S. Jivan, J.-M. Lu, T.J. Ruth ( <i>TRIUMF</i> )	100
LS4. TR13 targets for PET radioisotope production [active], K. Buckley, T. Hurtado, <u>T.J. Ruth</u> , S.K. Zeisler ( <i>TRIUMF</i> )	101
LS5. Production and on-line separation of <sup>124</sup> I from enriched tellurium [inactive], W.Z. Gelbart, E.T. Hurtado, <u>T.J. Ruth</u> , N.R. Stevenson, S.K. Zeisler ( <i>TRIUMF</i> ), R.R. Johnson ( <i>UBC</i> )	
LS6. Bone calcium resorption studies in pre- and peri-menopausal women using accelerator mass spectrometry [completed], <u>R.R. Johnson</u> , A. Priestman, J.C. Prior ( <i>UBC</i> ), A. Altman, W.Z. Gelbart, V. Sossi ( <i>TRIUMF</i> ), D. Berkovits, S. Ghelberg, M. Paul ( <i>Racah Inst., Hebrew U. Jerusalem</i> ), L.M. Shulman ( <i>Chaim Sheba Med. Centre</i> ), R. Chechik ( <i>Weizmann Inst.</i> ), E. Venzel ( <i>SFU</i> )	
LS7. PET 3D data quantification and integration into a research clinical environment [completed], K.S. Morrison, T.J. Ruth, V. Sossi, M.W. Stazyk ( <i>UBC-TRIUMF</i> ), K.R. Buckley ( <i>TRIUMF</i> ), J.S. Barney ( <i>VH&amp;HSC</i> ), D. Sirota, B.J. Snow ( <i>UBC</i> )	
LS8. Radiotracers for the physical and biosciences [active], L. Buchmann, T.J. Ruth, S.K. Zeisler ( <i>TRIUMF</i> ), A.D.M. Glass, R.R. Johnson, M. Lowe, C.E.R. Orvig ( <i>UBC</i> ), T.F. Budinger ( <i>Lawrence Berkeley National Lab</i> )	101
LS10. Biological evaluation of radiohalogenated DNA aptamers [completed], <u>H. Dougan</u> ( <i>TRIUMF</i> ), J.B. Hobbs, D.M. Lyster ( <i>UBC</i> ), J.I. Weitz ( <i>McMaster U.</i> )	103
LS11. Development of single photon imaging agents [inactive], <u>D. Lyster</u> ( <i>UBC-VH&amp;HSC</i> ), L. Alcorn, M. Hampong, T. Lutz, C. Vo ( <i>UBC</i> )	
LS12. A simulation platform for the design of position encoding multicrystal detectors [completed], A. Altman, <u>C. Moisan</u> , <u>J.G. Rogers</u> ( <i>TRIUMF</i> ), E. Hoskinson, G. Tsang ( <i>UBC</i> )	
LS13. Utility of 2-[F-18]-fluoro-2-deoxy-d-glucose SPECT imaging in the evaluation of patients with solitary pulmonary nodules [completed], A. Celler, D. Lyster, <u>D. Worsley</u> ( <i>UBC</i> ), M. Adam ( <i>TRIUMF</i> )	
LS14. Production of <sup>127</sup> Xe from cesium with 90–110 MeV protons [inactive], D. Pearce, <u>J. Vincent</u> ( <i>TRIUMF</i> )	
LS15. Investigation of frame realignment on the reproducibility of <sup>18</sup> F-6-fluorodopa positron emission tomography [inactive], K.S. Morrison, T.J. Ruth ( <i>UBC-TRIUMF</i> ), B.J. Snow ( <i>UBC</i> )	
LS17. Table-top radiocarbon facility [inactive], W. Gelbart, <u>R.B. Schubank</u> ( <i>TRIUMF</i> ), E. Venzel ( <i>UBC-SFU</i> ), S. Calvert, R.R. Johnson, J. Nagel, T. Peterson, V. Sossi ( <i>UBC</i> ), D.E. Nelson ( <i>SFU</i> ), J. Prior, K. Schoenholzer, R. Sutton, V. Walker ( <i>UBC-VH&amp;HSC</i> ), R. Middleton ( <i>U. Pennsylvania</i> ), M. Paul ( <i>Hebrew U. Jerusalem</i> ), J. Clague, L. Jackson, J. Lutenuer, D. Templeman-Kluit ( <i>Geological Survey of Canada</i> ), R.N. McNeely, J.-S. Vincent ( <i>GSC Ottawa</i> ), V. Barrie ( <i>Pacific Geoscience Center</i> ), D. Prior, K.R. Robertson, G. Vilks ( <i>Bedford Inst. Oceanography</i> ), R. Brown, S. Wang ( <i>Elemental Research Inc.</i> ), J. Vogel ( <i>Lawrence Livermore National Lab</i> ), A.E. Litherland ( <i>U. Toronto</i> ), S. Dias, S. Sood ( <i>Ontario Hydro</i> ), H.R. Andrews, R.M. Brown, R.J. Cornett ( <i>AECL</i> ), D.B. Carlisle ( <i>Environment Canada</i> ), J. Carron, A. Kabir, R.C.J. Wilkinson ( <i>Canadian Centre for Inland Waters</i> ), R. Gephart, P. Molton, D. Robertson ( <i>Batelle Pacific Northwest Labs</i> )	
LS18. Cooperative development of <sup>82</sup> Sr-Rb generators for human use in Canada [completed], <u>J. Vincent</u> ( <i>TRIUMF</i> ), R. Beanlands ( <i>U. Ottawa Heart Inst.</i> ), B. Bowen ( <i>McMaster U.</i> ), W. Dickie ( <i>Nordion Int.</i> )	
LS19. An <sup>15</sup> O-water generator: a feasibility study [inactive], K.R. Buckley, <u>T.J. Ruth</u> ( <i>TRIUMF</i> )	
LS20. Prototype heat-pipe water target for <sup>18</sup> F-production [inactive], K.R. Buckley, E.T. Hurtado, <u>T.J. Ruth</u> ( <i>TRIUMF</i> ), J.W. Lenz ( <i>private consultant</i> )	

- LS21. Aluminum kinetics in plants [inactive], A. Glass, R.R. Johnson, L. Oliveira (*UBC*), K. Buckley, Z. Gelbart (*TRIUMF*), D. Berkovitz, M. Paul (*Hebrew U. Jerusalem*), E. Venczel (*SFU*)
- LS22. Virtual national biomedical tracer facility [inactive], T.J. Ruth, J.S. Vincent (*TRIUMF*), E.J. Peterson, D. Phillips (*Los Alamos National Lab*)
- LS24. Scanning for early detection and staging of breast cancer: a comparative study using FDG PET and MIBI SPECT [deferred], P.F. Cohen, P. Klimo (*Lions Gate H.-UBC*), M. Cackette (*EBCO Industries Ltd.*), J. Whiffen (*JALORN*), V. Sossi (*TRIUMF-UBC*), J. Porter (*Nordion Int.*), R.R. Johnson (*UBC*)
- LS25. 3D PET in human neuroreceptor studies: quantification and reconstruction [completed], K.S. Morrison, T. Oakes, T.J. Ruth, V. Sossi (*UBC-TRIUMF*), K.R. Buckley (*TRIUMF*), M. Krzywinski, M. Schulzer, J. Stoessl (*UBC*)
- LS26. A gaseous planar positron source for routine 3D PET normalization [completed], T. Oakes, T.J. Ruth, V. Sossi (*UBC-TRIUMF*), K. Buckley, S. Jivan, R. MacDonald (*TRIUMF*)
- LS27. The feasibility and efficacy of using 2-(F-18)-fluoro-2-deoxy-D-glucose (18-FDG) to evaluate children with musculoskeletal neoplasm [deferred], R. Anderson, J. Davis, D. Lyster, H.R. Nadel, T.J. Ruth, M. Stilwell, D. Worsley (*UBC*)
- LS28. Evaluation of potentially viable myocardium with dobutamine myocardial SPECT imaging [completed], H. Abbey, A.-Y. Fung, L. Hook, D.M. Lyster, D.F. Worsley (*VH&HSC*), M. Adam, S. Jivan (*TRIUMF*)
- LS29. Production and distribution of FDG for clinical studies [active], D. Lyster, D. Worsley (*VH&HSC*), P. Cohen (*Lions Gate H.*), H. Nadel (*Children's H.*), M.J. Adam, S. Jivan, T.J. Ruth, V. Sossi (*TRIUMF*) 103
- LS31. Auger electron emitters for therapy-physics and chemistry [inactive], D. Pearce, T.J. Ruth, J. Vincent, A. Zyuzin (*TRIUMF*), V. Kokhanyuk, V. Kravchuk, B.L. Zhuikov (*INR Moscow*)
- LS32.  $^{18}\text{F-H}_2^{18}\text{O}$  supply to the University of Alberta [active], S.A. McQuarrie, J.R. Mercer (*U. Alberta*), A.J.B. McEwan (*CCI*), R.R. Johnson (*UBC-EBCO*), T.J. Ruth (*UBC-TRIUMF*)
- LS33. Evaluation and improvement of a dual head coincidence camera [active], K.S. Morrison, T.J. Ruth, V. Sossi (*UBC-TRIUMF*), M. Krzywinski (*UBC*), P. Cohen (*Lions Gate H.*), P. Klimo (*Lions Gate H.-UBC*), T.K. Lewellen, D.A. Mankoff (*U. Washington*) 103
- LS34. Production of  $^{103}\text{Pd}$  [inactive], R.R. Johnson, R. Pavan (*UBC*), M. Cackette, K.L. Erdman (*EBCO Industries Ltd.*), Z. Gelbart (*TRIUMF*)
- LS35. Development of F-18 labelled nitroimidazole PET imaging agents for tissue hypoxia [active], M.J. Adam (*TRIUMF*), K. Skov (*BCCRC-UBC*), S. Evans, C. Koch, A. Kachera (*U. Pennsylvania*), I. Baird, B. James (*UBC*) 104
- LS37. Feasibility of  $^{125}\text{Xe}$  implantation as a  $^{125}\text{I}$  brachytherapy source [completed], D. Ottewell, T. Ruth, J. Vincent, A. Zyuzin (*TRIUMF*)
- LS38. Dopaminergic tracers kinetic modeling with minimally invasive scanning procedures [completed], G. Chan, M. Krzywinski, T.J. Ruth, V. Sossi (*UBC-TRIUMF*), J. Holden (*U. Wisconsin*), D. Doudet, J. Stoessl (*UBC*) 104
- LS39. Positron emission profiling (PEP) for pulp and paper fluid dynamic studies [active], M. Martinez, J. Olson (*UBC*), M.J. Adam, K. Buckley, S. Jivan, T.J. Ruth, V. Sossi (*TRIUMF*) 106
- LS40. F-18 FDG cardiac PET scans using a coincidence PET/SPECT camera to assess myocardial viability in patients with fixed abnormalities and low ejection fractions on gated sestamibi stress tests [deferred], P.F. Cohen, J. Imrie, K. Woo (*Lions Gate H.*), D. Worsley (*Vancouver General H.*), V. Sossi (*TRIUMF-UBC*), T. Ruth (*UBC-TRIUMF*), R.R. Johnson (*UBC*)
- LS41. Impact of the ADAC coincidence PET camera in the management of selected cancer patients [deferred], P.F. Cohen, J. Imrie, K. Woo (*Lions Gate H.*), J. Powe (*Vancouver General H.*), V. Sossi (*TRIUMF-UBC*), T. Ruth (*UBC-TRIUMF*), R.R. Johnson (*UBC*)
- LS42. Configuration modeling and image reconstruction studies on a depth encoding research tomograph [active], T. Ruth, V. Sossi (*UBC-TRIUMF*), V. Astakhov (*UBC*), K. Buckley (*TRIUMF*), S. Houle (*Centre Addiction & Mental Health, Toronto*), C. Moisan (*U. Laval*) 106
- LS43. Positron emission mammography system (PEM) [deferred], K. Buckley, S. Jivan, T.J. Ruth, V. Sossi (*TRIUMF*), M. Stilwell (*B.C. Women's H.*), P. Gordon (*UBC*), H. Nadel (*Children's H.*)
- LS44. Development of a high-speed formation (areal density) measurement system for paper [active], M. Avikainen, S. Heath, M. Martinez, J. Olson (*UBC*), K. Buckley, T.J. Ruth, M. Salomon (*TRIUMF*) 107
- LS45. Modelling genetic risk for ionizing radiation exposure in space [deferred], J.G. de Boer, J. Holcroft, S. Zhang (*U. Victoria*)

- LS46. Modelling of the dopaminergic system in more severely affected PD patients [active], T.J. Ruth, V. Sossi (*UBC-TRIUMF*), J. Holden (*U. Wisconsin*), R. de la Fuente-Fernandez, D. Doudet, C.S. Lee, M. Schulzer, J. Stoessl (*UBC*) 107
- LS47. PET imaging of recurrent prostate cancer with 2-F-18-fluoromethy-dimethy-2-hydroxyethylammonia (FCH), [active], M. Gleave, D. Lyster, J. Powe, D. Worsley (*Vancouver General H.-UBC*), M. Adam (*TRIUMF*), H. Abbey (*Vancouver General H.*)
- LS48. Anorexia nervosa: autonomic dysfunction, the brain and the heart [deferred], A.S. Belzberg, C.L. Birmingham, C. Kerr, G.P. Sexsmith, M. Stilwell (*St. Paul's H.*), M.J. Stock (*St. George's H.*), P. Beumont (*U. Sydney, Aust.*), V. Sossi (*UBC-TRIUMF*)
- LS49.  $^{18}\text{F}$  FDG cardiac PET scans using a third generation coincidence camera to assess myocardial viability in patients who are candidates for cardiac transplantation [deferred], A.S. Belzberg, S. Chan, A. Ignaszewski, M. Kiess, G. Sexsmith, M. Stilwell (*St. Paul's H.*), V. Sossi (*TRIUMF-UBC*)
- LS50. Antisense imaging nucleic acids for Parkinson's disease [active], M. Adam, H. Dougan, T.J. Ruth (*TRIUMF*), J.B. Hobbs, D.M. Lyster, J. Stoessl (*UBC*), A.I. Kassis (*Harvard U.*) 108
- LS51. Auger therapy for prostate cancer [active], H. Dougan, T.J. Ruth, J.S. Vincent (*TRIUMF*), C.C. Nelson, P.S. Rennie (*Prostate Centre*), C.M. Ludgate (*UBC-U. Victoria*), D.M. Lyster (*UBC*) 108
- LS52. Comparison of commercial FDG synthesis systems [active], T.J. Ruth (*UBC/TRIUMF*), M. Adam, K. Buckley, S. Jivan (*TRIUMF*), D. Lyster (*UBC*), R. McDonald (*IPET*) 108
- LS53. Synthesis of  $^{99\text{m}}\text{Tc}$  and  $^{186,188}\text{Re}$  sugar derivatives [active], M.J. Adam (*TRIUMF*), C. Orvig (*UBC*), S. Bayly, C. Fisher (*TRIUMF/UBC*), M. Abrams (*AnorMED*) 109